

# Summary for Policymakers

**A Report of Working Group I of the Intergovernmental Panel on Climate Change**

***Based on a draft prepared by:***

Daniel L. Albritton, Myles R. Allen, Alfons P. M. Baede, John A. Church, Ulrich Cubasch, Dai Xiaosu, Ding Yihui, Dieter H. Ehhalt, Christopher K. Folland, Filippo Giorgi, Jonathan M. Gregory, David J. Griggs, Jim M. Haywood, Bruce Hewitson, John T. Houghton, Joanna I. House, Michael Hulme, Ivar Isaksen, Victor J. Jaramillo, Achuthan Jayaraman, Catherine A. Johnson, Fortunat Joos, Sylvie Joussaume, Thomas Karl, David J. Karoly, Haroon S. Kheshgi, Corrine Le Quéré, Kathy Maskell, Luis J. Mata, Bryant J. McAvaney, Mack McFarland, Linda O. Mearns, Gerald A. Meehl, L. Gylvan Meira-Filho, Valentin P. Meleshko, John F. B. Mitchell, Berrien Moore, Richard K. Mugara, Maria Noguer, Buruhani S. Nyenzi, Michael Oppenheimer, Joyce E. Penner, Steven Pollonais, Michael Prather, I. Colin Prentice, Venkatchalam Ramaswamy, Armando Ramirez-Rojas, Sarah C. B. Raper, M. Jim Salinger, Robert J. Scholes, Susan Solomon, Thomas F. Stocker, John M. R. Stone, Ronald J. Stouffer, Kevin E. Trenberth, Ming-Xing Wang, Robert T. Watson, Kok S. Yap, John Zillman with contributions from many authors and reviewers.

# Summary for Policymakers

The Third Assessment Report of Working Group I of the Intergovernmental Panel on Climate Change (IPCC) builds upon past assessments and incorporates new results from the past five years of research on climate change<sup>1</sup>. Many hundreds of scientists<sup>2</sup> from many countries participated in its preparation and review.

This Summary for Policymakers (SPM), which was approved by IPCC member governments in Shanghai in January 2001<sup>3</sup>, describes the current state of understanding of the climate system and provides estimates of its projected future evolution and their uncertainties. Further details can be found in the underlying report, and the appended Source Information provides cross references to the report's chapters.

## An increasing body of observations gives a collective picture of a warming world and other changes in the climate system.

Since the release of the Second Assessment Report (SAR)<sup>4</sup>, additional data from new studies of current and palaeoclimates, improved analysis of data sets, more rigorous evaluation of their quality, and comparisons among data from different sources have led to greater understanding of climate change.

### ***The global average surface temperature has increased over the 20th century by about 0.6°C.***

- The global average surface temperature (the average of near surface air temperature over land, and sea surface temperature)

has increased since 1861. Over the 20th century the increase has been  $0.6 \pm 0.2^\circ\text{C}$ <sup>5,6</sup> (Figure 1a). This value is about  $0.15^\circ\text{C}$  larger than that estimated by the SAR for the period up to 1994, owing to the relatively high temperatures of the additional years (1995 to 2000) and improved methods of processing the data. These numbers take into account various adjustments, including urban heat island effects. The record shows a great deal of variability; for example, most of the warming occurred during the 20th century, during two periods, 1910 to 1945 and 1976 to 2000.

- Globally, it is very likely<sup>7</sup> that the 1990s was the warmest decade and 1998 the warmest year in the instrumental record, since 1861 (see Figure 1a).
- New analyses of proxy data for the Northern Hemisphere indicate that the increase in temperature in the 20th century is likely<sup>7</sup> to have been the largest of any century during the past 1,000 years. It is also likely<sup>7</sup> that, in the Northern Hemisphere, the 1990s was the warmest decade and 1998 the warmest year (Figure 1b). Because less data are available, less is known about annual averages prior to 1,000 years before present and for conditions prevailing in most of the Southern Hemisphere prior to 1861.
- On average, between 1950 and 1993, night-time daily minimum air temperatures over land increased by about  $0.2^\circ\text{C}$  per decade. This is about twice the rate of increase in daytime daily maximum air temperatures ( $0.1^\circ\text{C}$  per decade). This has lengthened the freeze-free season in many mid- and high latitude regions. The increase in sea surface temperature over this period is about half that of the mean land surface air temperature.

<sup>1</sup> Climate change in IPCC usage refers to any change in climate over time, whether due to natural variability or as a result of human activity. This usage differs from that in the Framework Convention on Climate Change, where climate change refers to a change of climate that is attributed directly or indirectly to human activity that alters the composition of the global atmosphere and that is in addition to natural climate variability observed over comparable time periods.

<sup>2</sup> In total 122 Co-ordinating Lead Authors and Lead Authors, 515 Contributing Authors, 21 Review Editors and 420 Expert Reviewers.

<sup>3</sup> Delegations of 99 IPCC member countries participated in the Eighth Session of Working Group I in Shanghai on 17 to 20 January 2001.

<sup>4</sup> The IPCC Second Assessment Report is referred to in this Summary for Policymakers as the SAR.

<sup>5</sup> Generally temperature trends are rounded to the nearest  $0.05^\circ\text{C}$  per unit time, the periods often being limited by data availability.

<sup>6</sup> In general, a 5% statistical significance level is used, and a 95% confidence level.

<sup>7</sup> In this Summary for Policymakers and in the Technical Summary, the following words have been used where appropriate to indicate judgmental estimates of confidence: *virtually certain* (greater than 99% chance that a result is true); *very likely* (90–99% chance); *likely* (66–90% chance); *medium likelihood* (33–66% chance); *unlikely* (10–33% chance); *very unlikely* (1–10% chance); *exceptionally unlikely* (less than 1% chance). The reader is referred to individual chapters for more details.

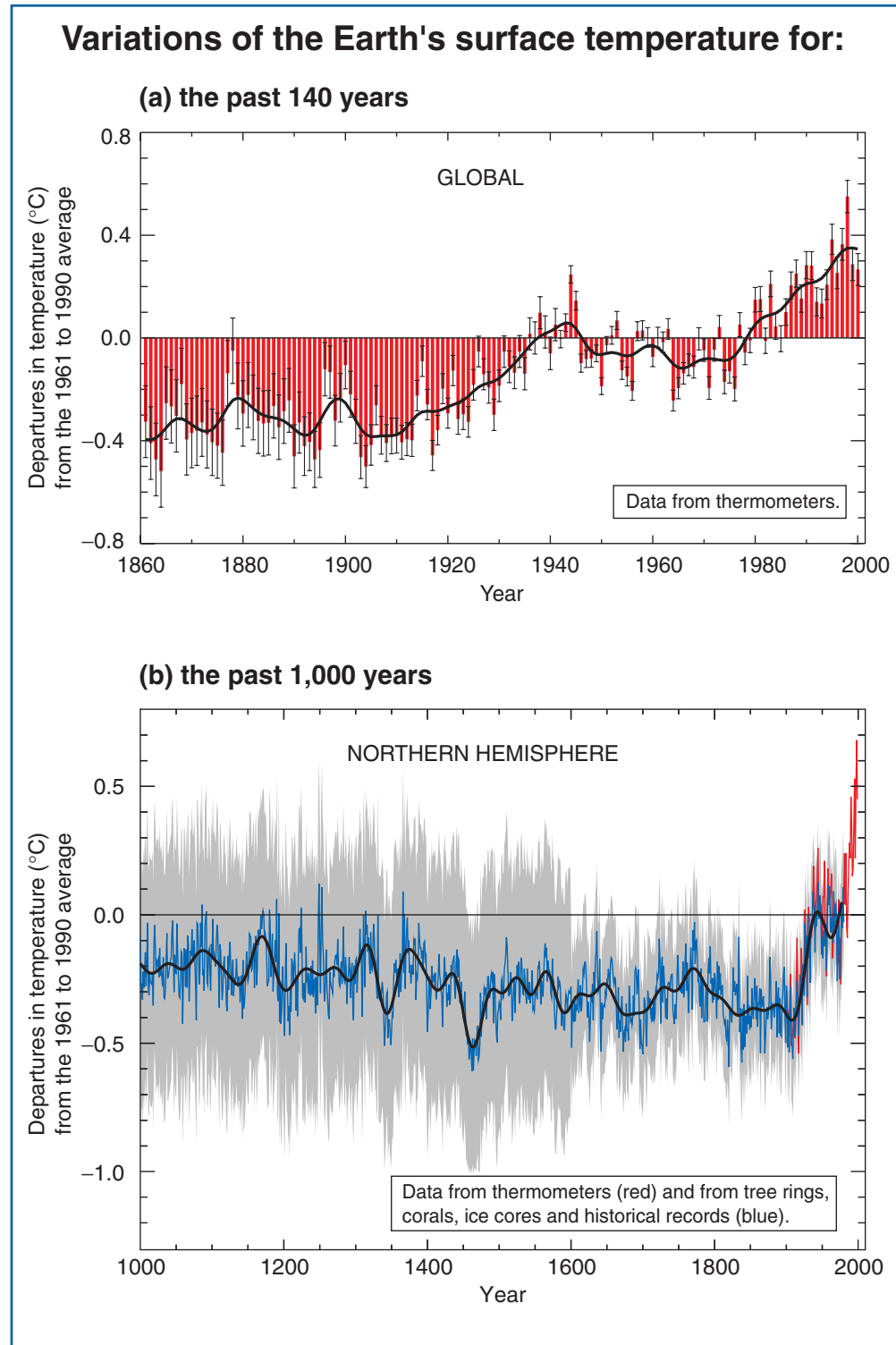


**Figure 1: Variations of the Earth's surface temperature over the last 140 years and the last millennium.**

(a) The Earth's surface temperature is shown year by year (red bars) and approximately decade by decade (black line, a filtered annual curve suppressing fluctuations below near decadal time-scales). There are uncertainties in the annual data (thin black whisker bars represent the 95% confidence range) due to data gaps, random instrumental errors and uncertainties, uncertainties in bias corrections in the ocean surface temperature data and also in adjustments for urbanisation over the land. Over both the last 140 years and 100 years, the best estimate is that the global average surface temperature has increased by  $0.6 \pm 0.2^{\circ}\text{C}$ .

(b) Additionally, the year by year (blue curve) and 50 year average (black curve) variations of the average surface temperature of the Northern Hemisphere for the past 1000 years have been reconstructed from "proxy" data calibrated against thermometer data (see list of the main proxy data in the diagram). The 95% confidence range in the annual data is represented by the grey region. These uncertainties increase in more distant times and are always much larger than in the instrumental record due to the use of relatively sparse proxy data. Nevertheless the rate and duration of warming of the 20th century has been much greater than in any of the previous nine centuries. Similarly, it is likely<sup>7</sup> that the 1990s have been the warmest decade and 1998 the warmest year of the millennium.

[Based upon (a) Chapter 2, Figure 2.7c and (b) Chapter 2, Figure 2.20]

### **Temperatures have risen during the past four decades in the lowest 8 kilometres of the atmosphere.**

- Since the late 1950s (the period of adequate observations from weather balloons), the overall global temperature increases in the lowest 8 kilometres of the atmosphere and in surface temperature have been similar at 0.1°C per decade.
- Since the start of the satellite record in 1979, both satellite and weather balloon measurements show that the global average temperature of the lowest 8 kilometres of the atmosphere has changed by  $+0.05 \pm 0.10^\circ\text{C}$  per decade, but the global average surface temperature has increased significantly by  $+0.15 \pm 0.05^\circ\text{C}$  per decade. The difference in the warming rates is statistically significant. This difference occurs primarily over the tropical and sub-tropical regions.
- The lowest 8 kilometres of the atmosphere and the surface are influenced differently by factors such as stratospheric ozone depletion, atmospheric aerosols, and the El Niño phenomenon. Hence, it is physically plausible to expect that over a short time period (e.g., 20 years) there may be differences in temperature trends. In addition, spatial sampling techniques can also explain some of the differences in trends, but these differences are not fully resolved.

### **Snow cover and ice extent have decreased.**

- Satellite data show that there are very likely<sup>7</sup> to have been decreases of about 10% in the extent of snow cover since the late 1960s, and ground-based observations show that there is very likely<sup>7</sup> to have been a reduction of about two weeks in the annual duration of lake and river ice cover in the mid- and high latitudes of the Northern Hemisphere, over the 20th century.
- There has been a widespread retreat of mountain glaciers in non-polar regions during the 20th century.
- Northern Hemisphere spring and summer sea-ice extent has decreased by about 10 to 15% since the 1950s. It is likely<sup>7</sup> that there has been about a 40% decline in Arctic sea-ice thickness during late summer to early autumn in recent decades and a considerably slower decline in winter sea-ice thickness.

### **Global average sea level has risen and ocean heat content has increased.**

- Tide gauge data show that global average sea level rose between 0.1 and 0.2 metres during the 20th century.
- Global ocean heat content has increased since the late 1950s, the period for which adequate observations of sub-surface ocean temperatures have been available.

### **Changes have also occurred in other important aspects of climate.**

- It is very likely<sup>7</sup> that precipitation has increased by 0.5 to 1% per decade in the 20th century over most mid- and high latitudes of the Northern Hemisphere continents, and it is likely<sup>7</sup> that rainfall has increased by 0.2 to 0.3% per decade over the tropical ( $10^\circ\text{N}$  to  $10^\circ\text{S}$ ) land areas. Increases in the tropics are not evident over the past few decades. It is also likely<sup>7</sup> that rainfall has decreased over much of the Northern Hemisphere sub-tropical ( $10^\circ\text{N}$  to  $30^\circ\text{N}$ ) land areas during the 20th century by about 0.3% per decade. In contrast to the Northern Hemisphere, no comparable systematic changes have been detected in broad latitudinal averages over the Southern Hemisphere. There are insufficient data to establish trends in precipitation over the oceans.
- In the mid- and high latitudes of the Northern Hemisphere over the latter half of the 20th century, it is likely<sup>7</sup> that there has been a 2 to 4% increase in the frequency of heavy precipitation events. Increases in heavy precipitation events can arise from a number of causes, e.g., changes in atmospheric moisture, thunderstorm activity and large-scale storm activity.
- It is likely<sup>7</sup> that there has been a 2% increase in cloud cover over mid- to high latitude land areas during the 20th century. In most areas the trends relate well to the observed decrease in daily temperature range.
- Since 1950 it is very likely<sup>7</sup> that there has been a reduction in the frequency of extreme low temperatures, with a smaller increase in the frequency of extreme high temperatures.

- Warm episodes of the El Niño-Southern Oscillation (ENSO) phenomenon (which consistently affects regional variations of precipitation and temperature over much of the tropics, sub-tropics and some mid-latitude areas) have been more frequent, persistent and intense since the mid-1970s, compared with the previous 100 years.
- Over the 20th century (1900 to 1995), there were relatively small increases in global land areas experiencing severe drought or severe wetness. In many regions, these changes are dominated by inter-decadal and multi-decadal climate variability, such as the shift in ENSO towards more warm events.
- In some regions, such as parts of Asia and Africa, the frequency and intensity of droughts have been observed to increase in recent decades.

***Some important aspects of climate appear not to have changed.***

- A few areas of the globe have not warmed in recent decades, mainly over some parts of the Southern Hemisphere oceans and parts of Antarctica.
- No significant trends of Antarctic sea-ice extent are apparent since 1978, the period of reliable satellite measurements.
- Changes globally in tropical and extra-tropical storm intensity and frequency are dominated by inter-decadal to multi-decadal variations, with no significant trends evident over the 20th century. Conflicting analyses make it difficult to draw definitive conclusions about changes in storm activity, especially in the extra-tropics.
- No systematic changes in the frequency of tornadoes, thunder days, or hail events are evident in the limited areas analysed.

**Emissions of greenhouse gases and aerosols due to human activities continue to alter the atmosphere in ways that are expected to affect the climate.**

Changes in climate occur as a result of both internal variability within the climate system and external factors (both natural and anthropogenic). The influence of external factors on climate can be broadly compared using the concept of radiative forcing<sup>8</sup>. A positive radiative forcing, such as that produced by increasing concentrations of greenhouse gases, tends to warm the surface. A negative radiative forcing, which can arise from an increase in some types of aerosols (microscopic airborne particles) tends to cool the surface. Natural factors, such as changes in solar output or explosive volcanic activity, can also cause radiative forcing.

Characterisation of these climate forcing agents and their changes over time (see Figure 2) is required to understand past climate changes in the context of natural variations and to project what climate changes could lie ahead. Figure 3 shows current estimates of the radiative forcing due to increased concentrations of atmospheric constituents and other mechanisms.

<sup>8</sup> Radiative forcing is a measure of the influence a factor has in altering the balance of incoming and outgoing energy in the Earth-atmosphere system, and is an index of the importance of the factor as a potential climate change mechanism. It is expressed in Watts per square metre ( $\text{Wm}^{-2}$ ).

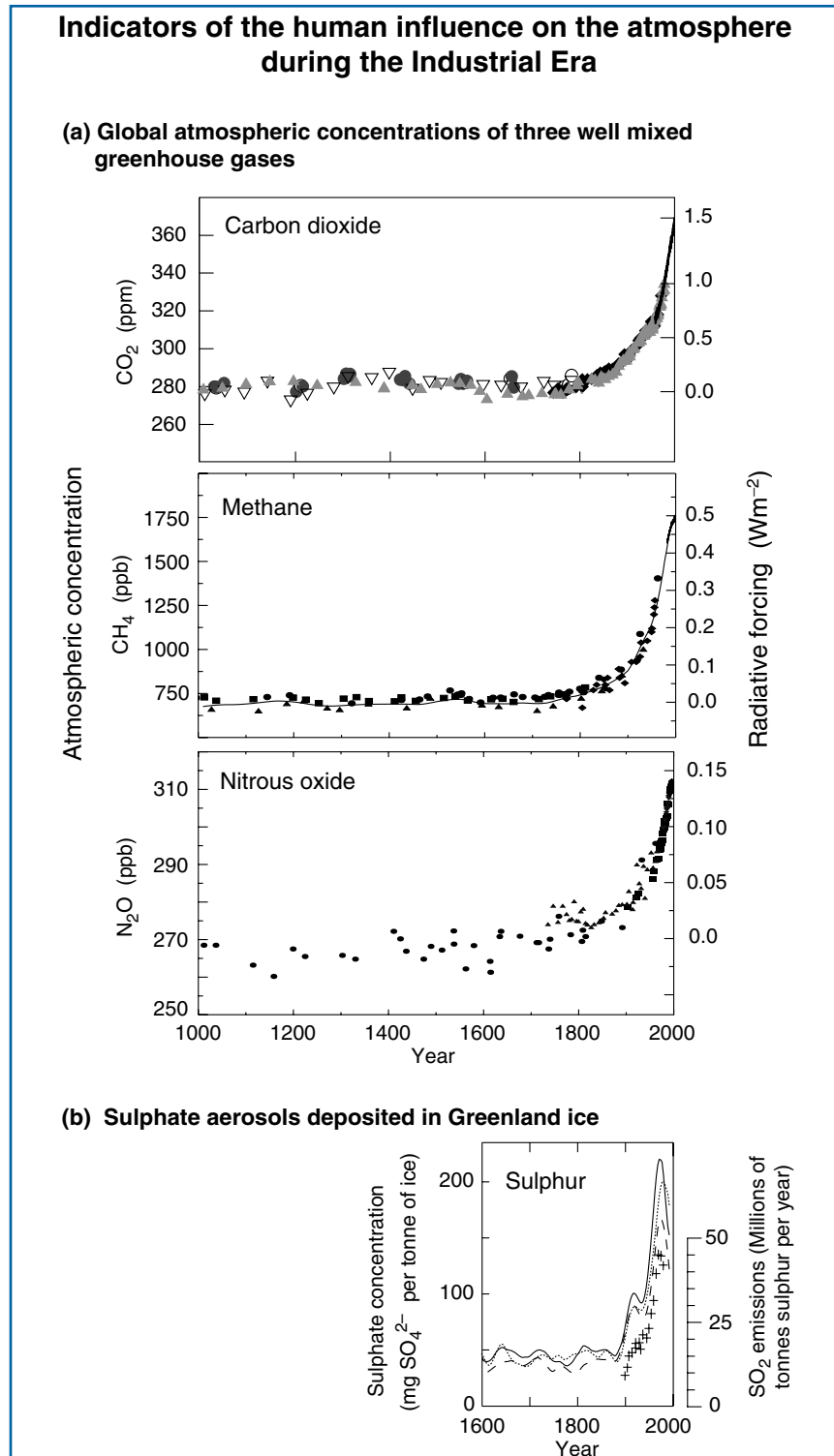


**Figure 2: Long records of past changes in atmospheric composition provide the context for the influence of anthropogenic emissions.**

(a) shows changes in the atmospheric concentrations of carbon dioxide (CO<sub>2</sub>), methane (CH<sub>4</sub>), and nitrous oxide (N<sub>2</sub>O) over the past 1000 years. The ice core and firn data for several sites in Antarctica and Greenland (shown by different symbols) are supplemented with the data from direct atmospheric samples over the past few decades (shown by the line for CO<sub>2</sub> and incorporated in the curve representing the global average of CH<sub>4</sub>). The estimated positive radiative forcing of the climate system from these gases is indicated on the right-hand scale. Since these gases have atmospheric lifetimes of a decade or more, they are well mixed, and their concentrations reflect emissions from sources throughout the globe. All three records show effects of the large and increasing growth in anthropogenic emissions during the Industrial Era.

(b) illustrates the influence of industrial emissions on atmospheric sulphate concentrations, which produce negative radiative forcing. Shown is the time history of the concentrations of sulphate, not in the atmosphere but in ice cores in Greenland (shown by lines; from which the episodic effects of volcanic eruptions have been removed). Such data indicate the local deposition of sulphate aerosols at the site, reflecting sulphur dioxide (SO<sub>2</sub>) emissions at mid-latitudes in the Northern Hemisphere. This record, albeit more regional than that of the globally-mixed greenhouse gases, demonstrates the large growth in anthropogenic SO<sub>2</sub> emissions during the Industrial Era. The pluses denote the relevant regional estimated SO<sub>2</sub> emissions (right-hand scale).

[Based upon (a) Chapter 3, Figure 3.2b (CO<sub>2</sub>); Chapter 4, Figure 4.1a and b (CH<sub>4</sub>) and Chapter 4, Figure 4.2 (N<sub>2</sub>O) and (b) Chapter 5, Figure 5.4a]

***Concentrations of atmospheric greenhouse gases and their radiative forcing have continued to increase as a result of human activities.***

- The atmospheric concentration of carbon dioxide ( $\text{CO}_2$ ) has increased by 31% since 1750. The present  $\text{CO}_2$  concentration has not been exceeded during the past 420,000 years and likely<sup>7</sup> not during the past 20 million years. The current rate of increase is unprecedented during at least the past 20,000 years.
- About three-quarters of the anthropogenic emissions of  $\text{CO}_2$  to the atmosphere during the past 20 years is due to fossil fuel burning. The rest is predominantly due to land-use change, especially deforestation.
- Currently the ocean and the land together are taking up about half of the anthropogenic  $\text{CO}_2$  emissions. On land, the uptake of anthropogenic  $\text{CO}_2$  very likely<sup>7</sup> exceeded the release of  $\text{CO}_2$  by deforestation during the 1990s.
- The rate of increase of atmospheric  $\text{CO}_2$  concentration has been about 1.5 ppm<sup>9</sup> (0.4%) per year over the past two decades. During the 1990s the year to year increase varied from 0.9 ppm (0.2%) to 2.8 ppm (0.8%). A large part of this variability is due to the effect of climate variability (e.g., El Niño events) on  $\text{CO}_2$  uptake and release by land and oceans.
- The atmospheric concentration of methane ( $\text{CH}_4$ ) has increased by 1060 ppb<sup>9</sup> (151%) since 1750 and continues to increase. The present  $\text{CH}_4$  concentration has not been exceeded during the past 420,000 years. The annual growth in  $\text{CH}_4$  concentration slowed and became more variable in the 1990s, compared with the 1980s. Slightly more than half of current  $\text{CH}_4$  emissions are anthropogenic (e.g., use of fossil fuels, cattle, rice agriculture and landfills). In addition, carbon monoxide (CO) emissions have recently been identified as a cause of increasing  $\text{CH}_4$  concentration.
- The atmospheric concentration of nitrous oxide ( $\text{N}_2\text{O}$ ) has increased by 46 ppb (17%) since 1750 and continues to increase. The present  $\text{N}_2\text{O}$  concentration has not been exceeded during at least the past thousand years. About a third of current  $\text{N}_2\text{O}$  emissions are anthropogenic (e.g., agricultural soils, cattle feed lots and chemical industry).
- Since 1995, the atmospheric concentrations of many of those halocarbon gases that are both ozone-depleting and greenhouse gases (e.g.,  $\text{CFCl}_3$  and  $\text{CF}_2\text{Cl}_2$ ), are either increasing more slowly or decreasing, both in response to reduced emissions under the regulations of the Montreal Protocol and its Amendments. Their substitute compounds (e.g.,  $\text{CHF}_2\text{Cl}$  and  $\text{CF}_3\text{CH}_2\text{F}$ ) and some other synthetic compounds (e.g., perfluorocarbons (PFCs) and sulphur hexafluoride ( $\text{SF}_6$ )) are also greenhouse gases, and their concentrations are currently increasing.
- The radiative forcing due to increases of the well-mixed greenhouse gases from 1750 to 2000 is estimated to be  $2.43 \text{ W m}^{-2}$ :  $1.46 \text{ W m}^{-2}$  from  $\text{CO}_2$ ;  $0.48 \text{ W m}^{-2}$  from  $\text{CH}_4$ ;  $0.34 \text{ W m}^{-2}$  from the halocarbons; and  $0.15 \text{ W m}^{-2}$  from  $\text{N}_2\text{O}$ . (See Figure 3, where the uncertainties are also illustrated.)
- The observed depletion of the stratospheric ozone ( $\text{O}_3$ ) layer from 1979 to 2000 is estimated to have caused a negative radiative forcing ( $-0.15 \text{ W m}^{-2}$ ). Assuming full compliance with current halocarbon regulations, the positive forcing of the halocarbons will be reduced as will the magnitude of the negative forcing from stratospheric ozone depletion as the ozone layer recovers over the 21st century.
- The total amount of  $\text{O}_3$  in the troposphere is estimated to have increased by 36% since 1750, due primarily to anthropogenic emissions of several  $\text{O}_3$ -forming gases. This corresponds to a positive radiative forcing of  $0.35 \text{ W m}^{-2}$ .  $\text{O}_3$  forcing varies considerably by region and responds much more quickly to changes in emissions than the long-lived greenhouse gases, such as  $\text{CO}_2$ .

<sup>9</sup> ppm (parts per million) or ppb (parts per billion, 1 billion = 1,000 million) is the ratio of the number of greenhouse gas molecules to the total number of molecules of dry air. For example: 300 ppm means 300 molecules of a greenhouse gas per million molecules of dry air.

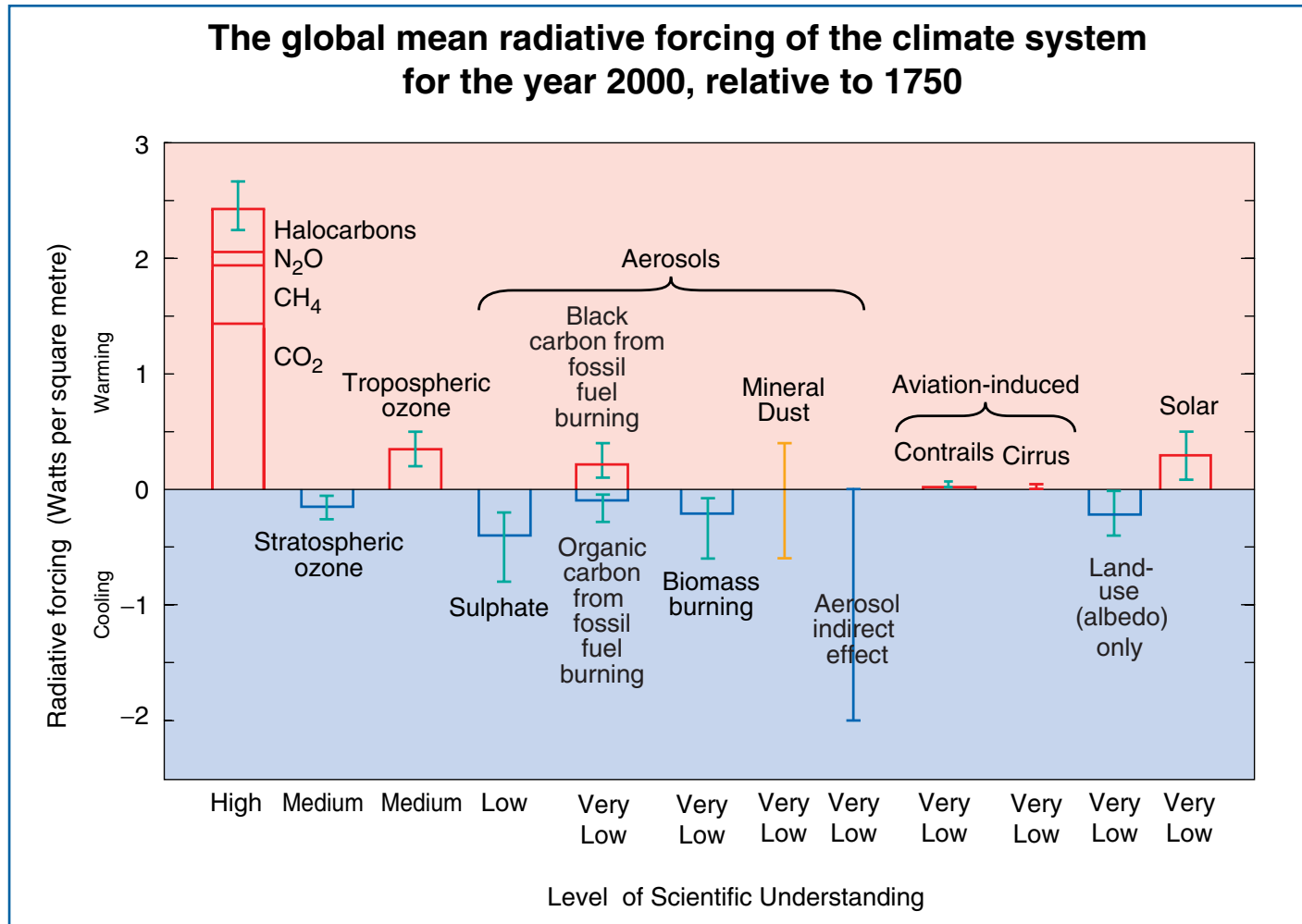


Figure 3: Many external factors force climate change.

These radiative forcings arise from changes in the atmospheric composition, alteration of surface reflectance by land use, and variation in the output of the sun. Except for solar variation, some form of human activity is linked to each. The rectangular bars represent estimates of the contributions of these forcings – some of which yield warming, and some cooling. Forcing due to episodic volcanic events, which lead to a negative forcing lasting only for a few years, is not shown. The indirect effect of aerosols shown is their effect on the size and number of cloud droplets. A second indirect effect of aerosols on clouds, namely their effect on cloud lifetime, which would also lead to a negative forcing, is not shown. Effects of aviation on greenhouse gases are included in the individual bars. The vertical line about the rectangular bars indicates a range of estimates, guided by the spread in the published values of the forcings and physical understanding. Some of the forcings possess a much greater degree of certainty than others. A vertical line without a rectangular bar denotes a forcing for which no best estimate can be given owing to large uncertainties. The overall level of scientific understanding for each forcing varies considerably, as noted. Some of the radiative forcing agents are well mixed over the globe, such as  $\text{CO}_2$ , thereby perturbing the global heat balance. Others represent perturbations with stronger regional signatures because of their spatial distribution, such as aerosols. For this and other reasons, a simple sum of the positive and negative bars cannot be expected to yield the net effect on the climate system. The simulations of this assessment report (for example, Figure 5) indicate that the estimated net effect of these perturbations is to have warmed the global climate since 1750. [Based upon Chapter 6, Figure 6.6]

***Anthropogenic aerosols are short-lived and mostly produce negative radiative forcing.***

- The major sources of anthropogenic aerosols are fossil fuel and biomass burning. These sources are also linked to degradation of air quality and acid deposition.
- Since the SAR, significant progress has been achieved in better characterising the direct radiative roles of different types of aerosols. Direct radiative forcing is estimated to be  $-0.4 \text{ Wm}^{-2}$  for sulphate,  $-0.2 \text{ Wm}^{-2}$  for biomass burning aerosols,  $-0.1 \text{ Wm}^{-2}$  for fossil fuel organic carbon and  $+0.2 \text{ Wm}^{-2}$  for fossil fuel black carbon aerosols. There is much less confidence in the ability to quantify the total aerosol direct effect, and its evolution over time, than that for the gases listed above. Aerosols also vary considerably by region and respond quickly to changes in emissions.
- In addition to their direct radiative forcing, aerosols have an indirect radiative forcing through their effects on clouds. There is now more evidence for this indirect effect, which is negative, although of very uncertain magnitude.

***Natural factors have made small contributions to radiative forcing over the past century.***

- The radiative forcing due to changes in solar irradiance for the period since 1750 is estimated to be about  $+0.3 \text{ Wm}^{-2}$ , most of which occurred during the first half of the 20th century. Since the late 1970s, satellite instruments have observed small oscillations due to the 11-year solar cycle. Mechanisms for the amplification of solar effects on climate have been proposed, but currently lack a rigorous theoretical or observational basis.
- Stratospheric aerosols from explosive volcanic eruptions lead to negative forcing, which lasts a few years. Several major eruptions occurred in the periods 1880 to 1920 and 1960 to 1991.
- The combined change in radiative forcing of the two major natural factors (solar variation and volcanic aerosols) is estimated to be negative for the past two, and possibly the past four, decades.

***Confidence in the ability of models to project future climate has increased.***

Complex physically-based climate models are required to provide detailed estimates of feedbacks and of regional features. Such models cannot yet simulate all aspects of climate (e.g., they still cannot account fully for the observed trend in the surface-troposphere temperature difference since 1979) and there are particular uncertainties associated with clouds and their interaction with radiation and aerosols. Nevertheless, confidence in the ability of these models to provide useful projections of future climate has improved due to their demonstrated performance on a range of space and time-scales.

- Understanding of climate processes and their incorporation in climate models have improved, including water vapour, sea-ice dynamics, and ocean heat transport.
- Some recent models produce satisfactory simulations of current climate without the need for non-physical adjustments of heat and water fluxes at the ocean-atmosphere interface used in earlier models.
- Simulations that include estimates of natural and anthropogenic forcing reproduce the observed large-scale changes in surface temperature over the 20th century (Figure 4). However, contributions from some additional processes and forcings may not have been included in the models. Nevertheless, the large-scale consistency between models and observations can be used to provide an independent check on projected warming rates over the next few decades under a given emissions scenario.
- Some aspects of model simulations of ENSO, monsoons and the North Atlantic Oscillation, as well as selected periods of past climate, have improved.

### **There is new and stronger evidence that most of the warming observed over the last 50 years is attributable to human activities.**

The SAR concluded: “The balance of evidence suggests a discernible human influence on global climate”. That report also noted that the anthropogenic signal was still emerging from the background of natural climate variability. Since the SAR, progress has been made in reducing uncertainty, particularly with respect to distinguishing and quantifying the magnitude of responses to different external influences. Although many of the sources of uncertainty identified in the SAR still remain to some degree, new evidence and improved understanding support an updated conclusion.

- There is a longer and more closely scrutinised temperature record and new model estimates of variability. The warming over the past 100 years is very unlikely<sup>7</sup> to be due to internal variability alone, as estimated by current models. Reconstructions of climate data for the past 1,000 years (Figure 1b) also indicate that this warming was unusual and is unlikely<sup>7</sup> to be entirely natural in origin.
- There are new estimates of the climate response to natural and anthropogenic forcing, and new detection techniques have been applied. Detection and attribution studies consistently find evidence for an anthropogenic signal in the climate record of the last 35 to 50 years.
- Simulations of the response to natural forcings alone (i.e., the response to variability in solar irradiance and volcanic eruptions) do not explain the warming in the second half of the 20th century (see for example Figure 4a). However, they indicate that natural forcings may have contributed to the observed warming in the first half of the 20th century.
- The warming over the last 50 years due to anthropogenic greenhouse gases can be identified despite uncertainties in forcing due to anthropogenic sulphate aerosol and natural factors (volcanoes and solar irradiance). The anthropogenic sulphate aerosol forcing, while uncertain, is negative over this period and therefore cannot explain the warming. Changes in natural forcing during most of this period are also estimated to be negative and are unlikely<sup>7</sup> to explain the warming.
- Detection and attribution studies comparing model simulated changes with the observed record can now take into account uncertainty in the magnitude of modelled response to external forcing, in particular that due to uncertainty in climate sensitivity.
- Most of these studies find that, over the last 50 years, the estimated rate and magnitude of warming due to increasing concentrations of greenhouse gases alone are comparable with, or larger than, the observed warming. Furthermore, most model estimates that take into account both greenhouse gases and sulphate aerosols are consistent with observations over this period.
- The best agreement between model simulations and observations over the last 140 years has been found when all the above anthropogenic and natural forcing factors are combined, as shown in Figure 4c. These results show that the forcings included are sufficient to explain the observed changes, but do not exclude the possibility that other forcings may also have contributed.

In the light of new evidence and taking into account the remaining uncertainties, most of the observed warming over the last 50 years is likely<sup>7</sup> to have been due to the increase in greenhouse gas concentrations.

Furthermore, it is very likely<sup>7</sup> that the 20th century warming has contributed significantly to the observed sea level rise, through thermal expansion of sea water and widespread loss of land ice. Within present uncertainties, observations and models are both consistent with a lack of significant acceleration of sea level rise during the 20th century.

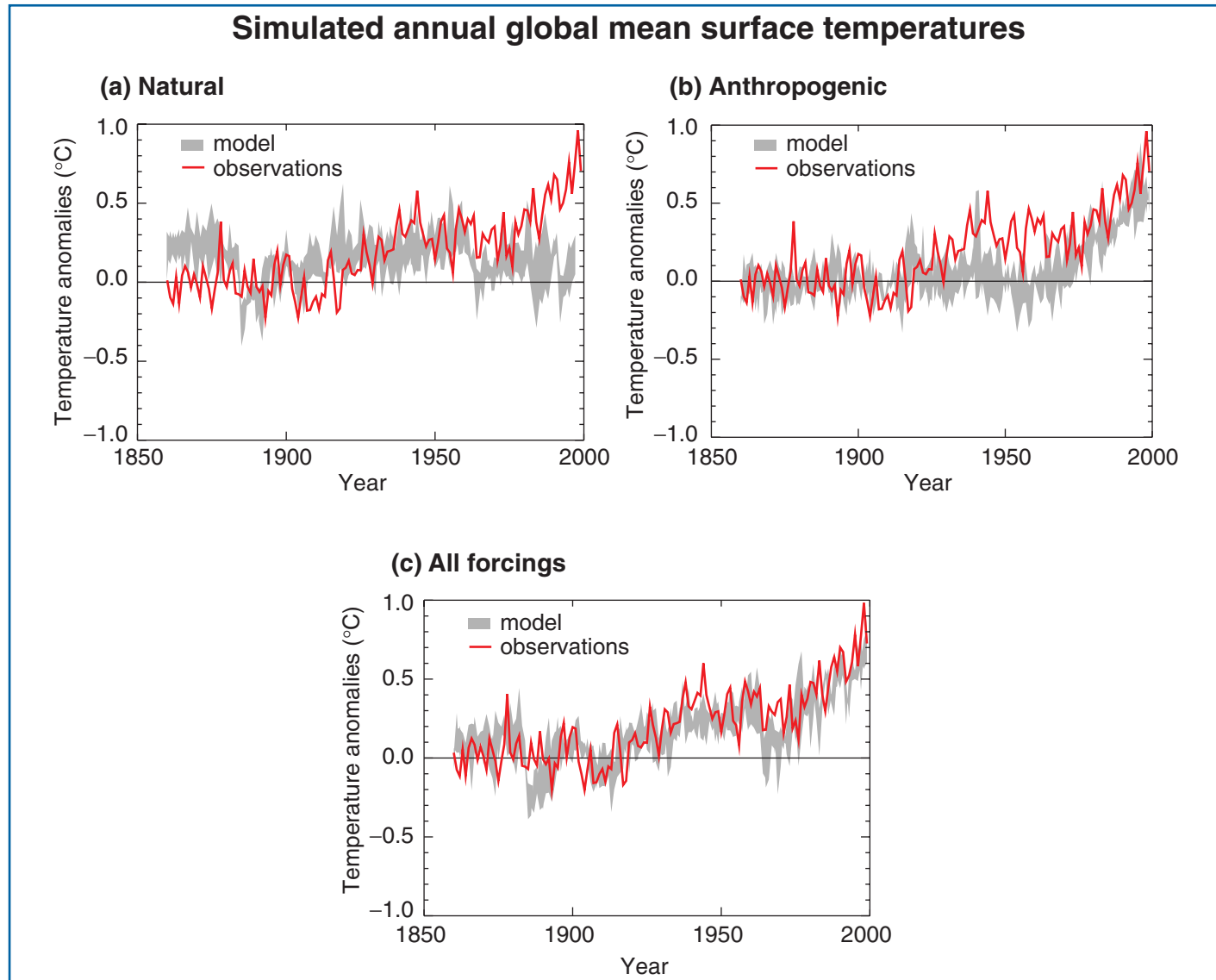


**Figure 4:** Simulating the Earth's temperature variations, and comparing the results to measured changes, can provide insight into the underlying causes of the major changes.

A climate model can be used to simulate the temperature changes that occur both from natural and anthropogenic causes. The simulations represented by the band in (a) were done with only natural forcings: solar variation and volcanic activity. Those encompassed by the band in (b) were done with anthropogenic forcings: greenhouse gases and an estimate of sulphate aerosols, and those encompassed by the band in (c) were done with both natural and anthropogenic forcings included. From (b), it can be seen that inclusion of anthropogenic forcings provides a plausible explanation for a substantial part of the observed temperature changes over the past century, but the best match with observations is obtained in (c) when both natural and anthropogenic factors are included. These results show that the forcings included are sufficient to explain the observed changes, but do not exclude the possibility that other forcings may also have contributed. The bands of model results presented here are for four runs from the same model. Similar results to those in (b) are obtained with other models with anthropogenic forcing. [Based upon Chapter 12, Figure 12.7]

### Human influences will continue to change atmospheric composition throughout the 21st century.

Models have been used to make projections of atmospheric concentrations of greenhouse gases and aerosols, and hence of future climate, based upon emissions scenarios from the IPCC Special Report on Emission Scenarios (SRES) (Figure 5). These scenarios were developed to update the IS92 series, which were used in the SAR and are shown for comparison here in some cases.

#### Greenhouse gases

- Emissions of CO<sub>2</sub> due to fossil fuel burning are virtually certain<sup>7</sup> to be the dominant influence on the trends in atmospheric CO<sub>2</sub> concentration during the 21st century.
- As the CO<sub>2</sub> concentration of the atmosphere increases, ocean and land will take up a decreasing fraction of anthropogenic CO<sub>2</sub> emissions. The net effect of land and ocean climate feedbacks as indicated by models is to further increase projected atmospheric CO<sub>2</sub> concentrations, by reducing both the ocean and land uptake of CO<sub>2</sub>.
- By 2100, carbon cycle models project atmospheric CO<sub>2</sub> concentrations of 540 to 970 ppm for the illustrative SRES scenarios (90 to 250% above the concentration of 280 ppm in the year 1750), Figure 5b. These projections include the land and ocean climate feedbacks. Uncertainties, especially about the magnitude of the climate feedback from the terrestrial biosphere, cause a variation of about –10 to +30% around each scenario. The total range is 490 to 1260 ppm (75 to 350% above the 1750 concentration).
- Changing land use could influence atmospheric CO<sub>2</sub> concentration. Hypothetically, if all of the carbon released by historical land-use changes could be restored to the terrestrial biosphere over the course of the century (e.g., by reforestation), CO<sub>2</sub> concentration would be reduced by 40 to 70 ppm.
- Model calculations of the concentrations of the non-CO<sub>2</sub> greenhouse gases by 2100 vary considerably across the SRES illustrative scenarios, with CH<sub>4</sub> changing by –190 to +1,970 ppb (present concentration 1,760 ppb), N<sub>2</sub>O changing

by +38 to +144 ppb (present concentration 316 ppb), total tropospheric O<sub>3</sub> changing by –12 to +62%, and a wide range of changes in concentrations of HFCs, PFCs and SF<sub>6</sub>, all relative to the year 2000. In some scenarios, total tropospheric O<sub>3</sub> would become as important a radiative forcing agent as CH<sub>4</sub> and, over much of the Northern Hemisphere, would threaten the attainment of current air quality targets.

- Reductions in greenhouse gas emissions and the gases that control their concentration would be necessary to stabilise radiative forcing. For example, for the most important anthropogenic greenhouse gas, carbon cycle models indicate that stabilisation of atmospheric CO<sub>2</sub> concentrations at 450, 650 or 1,000 ppm would require global anthropogenic CO<sub>2</sub> emissions to drop below 1990 levels, within a few decades, about a century, or about two centuries, respectively, and continue to decrease steadily thereafter. Eventually CO<sub>2</sub> emissions would need to decline to a very small fraction of current emissions.

#### Aerosols

- The SRES scenarios include the possibility of either increases or decreases in anthropogenic aerosols (e.g., sulphate aerosols (Figure 5c), biomass aerosols, black and organic carbon aerosols) depending on the extent of fossil fuel use and policies to abate polluting emissions. In addition, natural aerosols (e.g., sea salt, dust and emissions leading to the production of sulphate and carbon aerosols) are projected to increase as a result of changes in climate.

#### Radiative forcing over the 21st century

- For the SRES illustrative scenarios, relative to the year 2000, the global mean radiative forcing due to greenhouse gases continues to increase through the 21st century, with the fraction due to CO<sub>2</sub> projected to increase from slightly more than half to about three quarters. The change in the direct plus indirect aerosol radiative forcing is projected to be smaller in magnitude than that of CO<sub>2</sub>.

## Global average temperature and sea level are projected to rise under all IPCC SRES scenarios.

In order to make projections of future climate, models incorporate past, as well as future emissions of greenhouse gases and aerosols. Hence, they include estimates of warming to date and the commitment to future warming from past emissions.<sup>7</sup>

### Temperature

- The globally averaged surface temperature is projected to increase by 1.4 to 5.8°C (Figure 5d) over the period 1990 to 2100. These results are for the full range of 35 SRES scenarios, based on a number of climate models<sup>10,11</sup>.
- Temperature increases are projected to be greater than those in the SAR, which were about 1.0 to 3.5°C based on the six IS92 scenarios. The higher projected temperatures and the wider range are due primarily to the lower projected sulphur dioxide emissions in the SRES scenarios relative to the IS92 scenarios.
- The projected rate of warming is much larger than the observed changes during the 20th century and is very likely<sup>7</sup> to be without precedent during at least the last 10,000 years, based on palaeoclimate data.
- By 2100, the range in the surface temperature response across the group of climate models run with a given scenario is comparable to the range obtained from a single model run with the different SRES scenarios.
- On timescales of a few decades, the current observed rate of warming can be used to constrain the projected response to a given emissions scenario despite uncertainty in climate sensitivity. This approach suggests that anthropogenic

warming is likely<sup>7</sup> to lie in the range of 0.1 to 0.2°C per decade over the next few decades under the IS92a scenario, similar to the corresponding range of projections of the simple model used in Figure 5d.

- Based on recent global model simulations, it is very likely<sup>7</sup> that nearly all land areas will warm more rapidly than the global average, particularly those at northern high latitudes in the cold season. Most notable of these is the warming in the northern regions of North America, and northern and central Asia, which exceeds global mean warming in each model by more than 40%. In contrast, the warming is less than the global mean change in south and southeast Asia in summer and in southern South America in winter.
- Recent trends for surface temperature to become more El Niño-like in the tropical Pacific, with the eastern tropical Pacific warming more than the western tropical Pacific, with a corresponding eastward shift of precipitation, are projected to continue in many models.

### Precipitation

- Based on global model simulations and for a wide range of scenarios, global average water vapour concentration and precipitation are projected to increase during the 21st century. By the second half of the 21st century, it is likely<sup>7</sup> that precipitation will have increased over northern mid- to high latitudes and Antarctica in winter. At low latitudes there are both regional increases and decreases over land areas. Larger year to year variations in precipitation are very likely<sup>7</sup> over most areas where an increase in mean precipitation is projected.

<sup>10</sup> Complex physically based climate models are the main tool for projecting future climate change. In order to explore the full range of scenarios, these are complemented by simple climate models calibrated to yield an equivalent response in temperature and sea level to complex climate models. These projections are obtained using a simple climate model whose climate sensitivity and ocean heat uptake are calibrated to each of seven complex climate models. The climate sensitivity used in the simple model ranges from 1.7 to 4.2°C, which is comparable to the commonly accepted range of 1.5 to 4.5°C.

<sup>11</sup> This range does not include uncertainties in the modelling of radiative forcing, e.g. aerosol forcing uncertainties. A small carbon-cycle climate feedback is included.

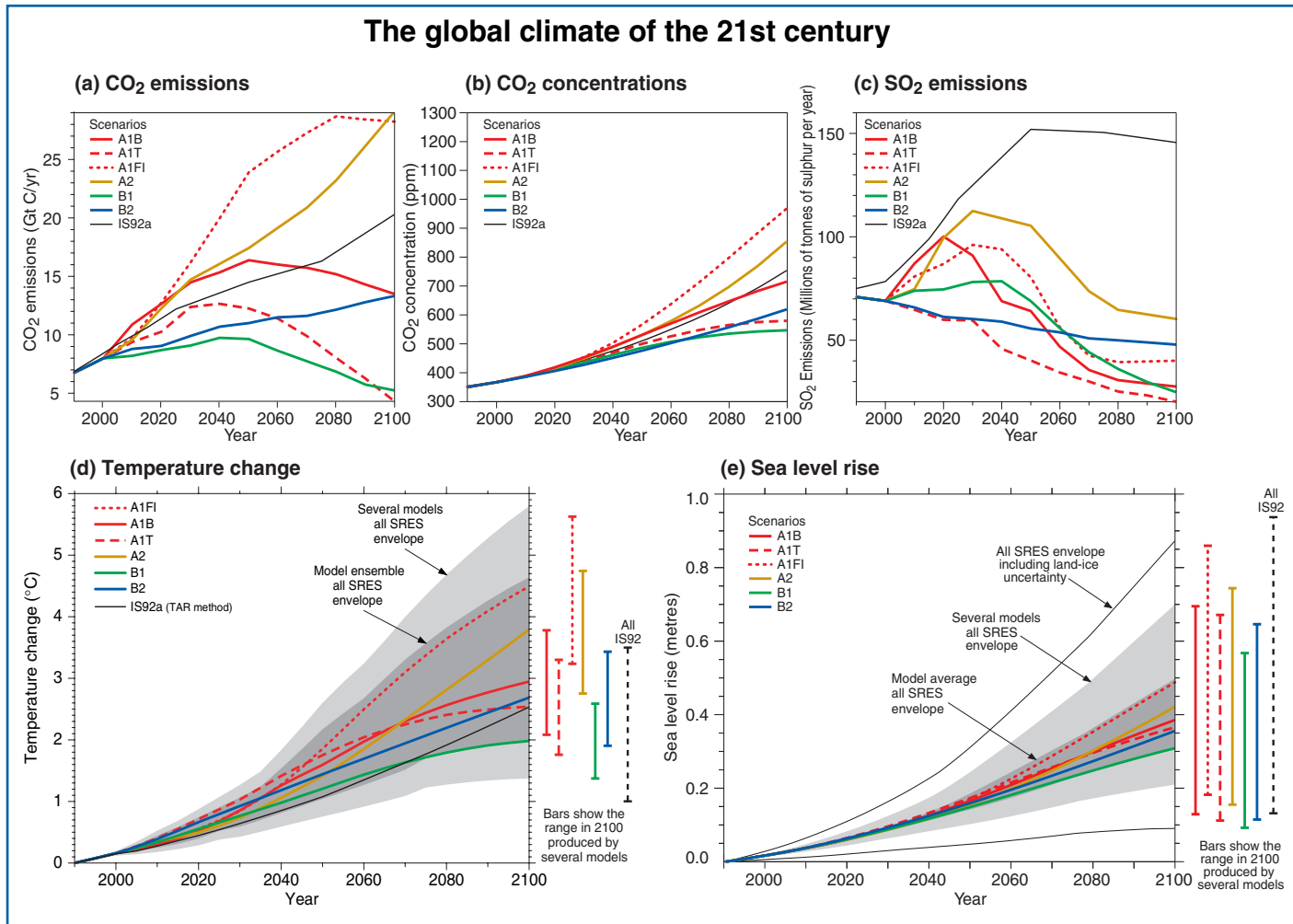


**Figure 5: The global climate of the 21st century will depend on natural changes and the response of the climate system to human activities.**

Climate models project the response of many climate variables – such as increases in global surface temperature and sea level – to various scenarios of greenhouse gas and other human-related emissions. (a) shows the CO<sub>2</sub> emissions of the six illustrative SRES scenarios, which are summarised in the box on page 18, along with IS92a for comparison purposes with the SAR. (b) shows projected CO<sub>2</sub> concentrations. (c) shows anthropogenic SO<sub>2</sub> emissions. Emissions of other gases and other aerosols were included in the model but are not shown in the figure. (d) and (e) show the projected temperature and sea level responses, respectively. The “several models all SRES envelope” in (d) and (e) shows the temperature and sea level rise, respectively, for the simple model when tuned to a number of complex models with a range of climate sensitivities. All SRES envelopes refer to the full range of 35 SRES scenarios. The “model average all SRES envelope” shows the average from these models for the range of scenarios. Note that the warming and sea level rise from these emissions would continue well beyond 2100. Also note that this range does not allow for uncertainty relating to ice dynamical changes in the West Antarctic ice sheet, nor does it account for uncertainties in projecting non-sulphate aerosols and greenhouse gas concentrations. [Based upon (a) Chapter 3, Figure 3.12, (b) Chapter 3, Figure 3.12, (c) Chapter 5, Figure 5.13, (d) Chapter 9, Figure 9.14, (e) Chapter 11, Figure 11.12, Appendix II]

## Extreme Events

Table 1 depicts an assessment of confidence in observed changes in extremes of weather and climate during the latter half of the 20th century (left column) and in projected changes during the 21st century (right column)<sup>a</sup>. This assessment relies on observational and modelling studies, as well as the physical plausibility of future projections across all commonly-used scenarios and is based on expert judgement<sup>7</sup>.

- For some other extreme phenomena, many of which may have important impacts on the environment and society, there is currently insufficient information to assess recent trends, and climate models currently lack the spatial detail required to make confident projections. For example, very small-scale phenomena, such as thunderstorms, tornadoes, hail and lightning, are not simulated in climate models.

**Table 1:** Estimates of confidence in observed and projected changes in extreme weather and climate events.

Confidence in observed changes (latter half of the 20th century)	Changes in Phenomenon	Confidence in projected changes (during the 21st century)
Likely <sup>7</sup>	<b>Higher maximum temperatures and more hot days over nearly all land areas</b>	Very likely <sup>7</sup>
Very likely <sup>7</sup>	<b>Higher minimum temperatures, fewer cold days and frost days over nearly all land areas</b>	Very likely <sup>7</sup>
Very likely <sup>7</sup>	<b>Reduced diurnal temperature range over most land areas</b>	Very likely <sup>7</sup>
Likely <sup>7</sup> , over many areas	<b>Increase of heat index<sup>12</sup> over land areas</b>	Very likely <sup>7</sup> , over most areas
Likely <sup>7</sup> , over many Northern Hemisphere mid- to high latitude land areas	<b>More intense precipitation events<sup>b</sup></b>	Very likely <sup>7</sup> , over many areas
Likely <sup>7</sup> , in a few areas	<b>Increased summer continental drying and associated risk of drought</b>	Likely <sup>7</sup> , over most mid-latitude continental interiors. (Lack of consistent projections in other areas)
Not observed in the few analyses available	<b>Increase in tropical cyclone peak wind intensities<sup>c</sup></b>	Likely <sup>7</sup> , over some areas
Insufficient data for assessment	<b>Increase in tropical cyclone mean and peak precipitation intensities<sup>c</sup></b>	Likely <sup>7</sup> , over some areas

<sup>a</sup> For more details see Chapter 2 (observations) and Chapter 9, 10 (projections).

<sup>b</sup> For other areas, there are either insufficient data or conflicting analyses.

<sup>c</sup> Past and future changes in tropical cyclone location and frequency are uncertain.

<sup>12</sup> Heat index: A combination of temperature and humidity that measures effects on human comfort.

### El Niño

- Confidence in projections of changes in future frequency, amplitude, and spatial pattern of El Niño events in the tropical Pacific is tempered by some shortcomings in how well El Niño is simulated in complex models. Current projections show little change or a small increase in amplitude for El Niño events over the next 100 years.
- Even with little or no change in El Niño amplitude, global warming is likely<sup>7</sup> to lead to greater extremes of drying and heavy rainfall and increase the risk of droughts and floods that occur with El Niño events in many different regions.

### Monsoons

- It is likely<sup>7</sup> that warming associated with increasing greenhouse gas concentrations will cause an increase of Asian summer monsoon precipitation variability. Changes in monsoon mean duration and strength depend on the details of the emission scenario. The confidence in such projections is also limited by how well the climate models simulate the detailed seasonal evolution of the monsoons.

### Thermohaline circulation

- Most models show weakening of the ocean thermohaline circulation which leads to a reduction of the heat transport into high latitudes of the Northern Hemisphere. However, even in models where the thermohaline circulation weakens, there is still a warming over Europe due to increased greenhouse gases. The current projections using climate models do not exhibit a complete shut-down of the thermohaline circulation by 2100. Beyond 2100, the thermohaline circulation could completely, and possibly irreversibly, shut-down in either hemisphere if the change in radiative forcing is large enough and applied long enough.

### Snow and ice

- Northern Hemisphere snow cover and sea-ice extent are projected to decrease further.
- Glaciers and ice caps are projected to continue their widespread retreat during the 21st century.
- The Antarctic ice sheet is likely<sup>7</sup> to gain mass because of greater precipitation, while the Greenland ice sheet is likely<sup>7</sup> to lose mass because the increase in runoff will exceed the precipitation increase.
- Concerns have been expressed about the stability of the West Antarctic ice sheet because it is grounded below sea level. However, loss of grounded ice leading to substantial sea level rise from this source is now widely agreed to be very unlikely<sup>7</sup> during the 21st century, although its dynamics are still inadequately understood, especially for projections on longer time-scales.

### Sea level

- Global mean sea level is projected to rise by 0.09 to 0.88 metres between 1990 and 2100, for the full range of SRES scenarios. This is due primarily to thermal expansion and loss of mass from glaciers and ice caps (Figure 5e). The range of sea level rise presented in the SAR was 0.13 to 0.94 metres based on the IS92 scenarios. Despite the higher temperature change projections in this assessment, the sea level projections are slightly lower, primarily due to the use of improved models, which give a smaller contribution from glaciers and ice sheets.

## **Anthropogenic climate change will persist for many centuries.**

- Emissions of long-lived greenhouse gases (i.e., CO<sub>2</sub>, N<sub>2</sub>O, PFCs, SF<sub>6</sub>) have a lasting effect on atmospheric composition, radiative forcing and climate. For example, several centuries after CO<sub>2</sub> emissions occur, about a quarter of the increase in CO<sub>2</sub> concentration caused by these emissions is still present in the atmosphere.
- After greenhouse gas concentrations have stabilised, global average surface temperatures would rise at a rate of only a few tenths of a degree per century rather than several degrees per century as projected for the 21st century without stabilisation. The lower the level at which concentrations are stabilised, the smaller the total temperature change.
- Global mean surface temperature increases and rising sea level from thermal expansion of the ocean are projected to continue for hundreds of years after stabilisation of greenhouse gas concentrations (even at present levels), owing to the long timescales on which the deep ocean adjusts to climate change.
- Ice sheets will continue to react to climate warming and contribute to sea level rise for thousands of years after climate has been stabilised. Climate models indicate that the local warming over Greenland is likely<sup>7</sup> to be one to three times the global average. Ice sheet models project that a local warming of larger than 3°C, if sustained for millennia, would lead to virtually a complete melting of the Greenland ice sheet with a resulting sea level rise of about 7 metres. A local warming of 5.5°C, if sustained for 1,000 years, would be likely<sup>7</sup> to result in a contribution from Greenland of about 3 metres to sea level rise.
- Current ice dynamic models suggest that the West Antarctic ice sheet could contribute up to 3 metres to sea level rise over the next 1,000 years, but such results are strongly dependent on model assumptions regarding climate change scenarios, ice dynamics and other factors.

## **Further action is required to address remaining gaps in information and understanding.**

Further research is required to improve the ability to detect, attribute and understand climate change, to reduce uncertainties and to project future climate changes. In particular, there is a need for additional systematic and sustained observations, modelling and process studies. A serious concern is the decline of observational networks. The following are high priority areas for action.

- Systematic observations and reconstructions:
  - Reverse the decline of observational networks in many parts of the world.
  - Sustain and expand the observational foundation for climate studies by providing accurate, long-term, consistent data including implementation of a strategy for integrated global observations.
  - Enhance the development of reconstructions of past climate periods.
  - Improve the observations of the spatial distribution of greenhouse gases and aerosols.
- Modelling and process studies:
  - Improve understanding of the mechanisms and factors leading to changes in radiative forcing.
  - Understand and characterise the important unresolved processes and feedbacks, both physical and biogeochemical, in the climate system.
  - Improve methods to quantify uncertainties of climate projections and scenarios, including long-term ensemble simulations using complex models.
  - Improve the integrated hierarchy of global and regional climate models with a focus on the simulation of climate variability, regional climate changes and extreme events.
  - Link more effectively models of the physical climate and the biogeochemical system, and in turn improve coupling with descriptions of human activities.

Cutting across these foci are crucial needs associated with strengthening international co-operation and co-ordination in order to better utilise scientific, computational and observational resources. This should also promote the free exchange of data among scientists. A special need is to increase the observational and research capacities in many regions, particularly in developing countries. Finally, as is the goal of this assessment, there is a continuing imperative to communicate research advances in terms that are relevant to decision making.

### The Emissions Scenarios of the Special Report on Emissions Scenarios (SRES)

A1. The A1 storyline and scenario family describes a future world of very rapid economic growth, global population that peaks in mid-century and declines thereafter, and the rapid introduction of new and more efficient technologies. Major underlying themes are convergence among regions, capacity building and increased cultural and social interactions, with a substantial reduction in regional differences in per capita income. The A1 scenario family develops into three groups that describe alternative directions of technological change in the energy system. The three A1 groups are distinguished by their technological emphasis: fossil intensive (A1FI), non-fossil energy sources (A1T), or a balance across all sources (A1B) (where balanced is defined as not relying too heavily on one particular energy source, on the assumption that similar improvement rates apply to all energy supply and end use technologies).

A2. The A2 storyline and scenario family describes a very heterogeneous world. The underlying theme is self-reliance and preservation of local identities. Fertility patterns across regions converge very slowly, which results in continuously increasing population. Economic development is primarily regionally oriented and per capita economic growth and technological change more fragmented and slower than other storylines.

B1. The B1 storyline and scenario family describes a convergent world with the same global population, that peaks in mid-century and declines thereafter, as in the A1 storyline, but with rapid change in economic structures toward a service and information economy, with reductions in material intensity and the introduction of clean and resource-efficient technologies. The emphasis is on global solutions to economic, social and environmental sustainability, including improved equity, but without additional climate initiatives.

B2. The B2 storyline and scenario family describes a world in which the emphasis is on local solutions to economic, social and environmental sustainability. It is a world with continuously increasing global population, at a rate lower than A2, intermediate levels of economic development, and less rapid and more diverse technological change than in the B1 and A1 storylines. While the scenario is also oriented towards environmental protection and social equity, it focuses on local and regional levels.

An illustrative scenario was chosen for each of the six scenario groups A1B, A1FI, A1T, A2, B1 and B2. All should be considered equally sound.

The SRES scenarios do not include additional climate initiatives, which means that no scenarios are included that explicitly assume implementation of the United Nations Framework Convention on Climate Change or the emissions targets of the Kyoto Protocol.

## Source Information: Summary for Policymakers

This appendix provides the cross-reference of the topics in the Summary for Policymakers (page and bullet point topic) to the sections of the chapters of the full report that contain expanded information about the topic.

***An increasing body of observations gives a collective picture of a warming world and other changes in the climate system.***

**SPM Page Cross-Reference: SPM Topic – Chapter Section**

2	<i>The global average surface temperature has increased over the 20th century by about 0.6°C.</i> ● Chapter 2.2.2 ● Chapter 2.2.2 ● Chapter 2.3 ● Chapter 2.2.2
4	<i>Temperatures have risen during the past four decades in the lowest 8 kilometres of the atmosphere.</i> ● Chapter 2.2.3 and 2.2.4 ● Chapter 2.2.3 and 2.2.4 ● Chapter 2.2.3, 2.2.4 and Chapter 12.3.2
4	<i>Snow cover and ice extent have decreased.</i> All three bullet points: Chapter 2.2.5 and 2.2.6
4	<i>Global average sea level has risen and ocean heat content has increased.</i> ● Chapter 11.3.2 ● Chapter 2.2.2 and Chapter 11.2.1
4 – 5	<i>Changes have also occurred in other important aspects of climate.</i> ● Chapter 2.5.2 ● Chapter 2.7.2 ● Chapter 2.2.2 and 2.5.5 ● Chapter 2.7.2 ● Chapter 2.6.2 and 2.6.3 ● Chapter 2.7.3 ● Chapter 2.7.3
5	<i>Some important aspects of climate appear not to have changed.</i> ● Chapter 2.2.2 ● Chapter 2.2.5 ● Chapter 2.7.3 ● Chapter 2.7.3

***Emissions of greenhouse gases and aerosols due to human activities continue to alter the atmosphere in ways that are expected to affect the climate system.***

**SPM Page Cross-Reference: SPM Topic – Chapter Section**

5	<i>Chapeau:</i> “Changes in climate occur ...” Chapter 1, Chapter 3.1, Chapter 4.1, Chapter 5.1, Chapter 6.1, 6.2, 6.9, 6.11 and 6.13
7	<i>Concentrations of atmospheric greenhouse gases and their radiative forcing have continued to increase as a result of human activities.</i>  Carbon dioxide: ● Chapter 3.3.1, 3.3.2, 3.3.3 and 3.5.1 ● Chapter 3.5.1 ● Chapter 3.2.2, 3.2.3, 3.5.1 and Table 3.1 ● Chapter 3.5.1 and 3.5.2  Methane: ● Chapter 4.2.1  Nitrous oxide: ● Chapter 4.2.1  Halocarbons: ● Chapter 4.2.2  Radiative forcing of well-mixed gases: ● Chapter 4.2.1 and Chapter 6.3  Stratospheric ozone: ● Chapter 4.2.2 and Chapter 6.4  Tropospheric ozone: ● Chapter 4.2.4 and Chapter 6.5  <i>Anthropogenic aerosols are short-lived and mostly produce negative radiative forcing.</i> ● Chapter 5.2 and 5.5.4 ● Chapter 5.1, 5.2 and Chapter 6.7 ● Chapter 5.3.2, 5.4.3 and Chapter 6.8
9	<i>Natural factors have made small contributions to radiative forcing over the past century.</i> ● Chapter 6.11 and 6.15.1 ● Chapter 6.9 and 6.15.1 ● Chapter 6.15.1

***Confidence in the ability of models to project future climate has increased.***

SPM Page	Cross-Reference: SPM Topic – Chapter Section
9	Chapeau: “Complex physically-based …” Chapter 8.3.2, 8.5.1, 8.6.1, 8.10.3 and Chapter 12.3.2 ● Chapter 7.2.1, 7.5.2 and 7.6.1 ● Chapter 8.4.2 ● Chapter 8.6.3 and Chapter 12.3.2 ● Chapter 8.5.5, 8.7.1 and 8.7.5
9	

***There is new and stronger evidence that most of the warming observed over the last 50 years is attributable to human activities.***

SPM Page	Cross-Reference: SPM Topic – Chapter Section
10	Chapeau: “The SAR concluded: The balance of evidence suggests …” Chapter 12.1.2 and 12.6 ● Chapter 12.2.2, 12.4.3 and 12.6 ● Chapter 12.4.1, 12.4.2, 12.4.3 and 12.6 ● Chapter 12.2.3, 12.4.1, 12.4.2, 12.4.3 and 12.6 ● Chapter 12.4.3 and 12.6. ● Chapter 12.6 ● Chapter 12.4.3 ● Chapter 12.4.3 and 12.6
10	
10	“In the light of new evidence and taking into account the …” Chapter 12.4 and 12.6
10	“Furthermore, it is very likely that the 20th century warming has …” Chapter 11.4

***Human influences will continue to change atmospheric composition throughout the 21st century.***

SPM Page	Cross-Reference: SPM Topic – Chapter Section
12	Chapeau: “Models have been used to make projections …” Chapter 4.4.5 and Appendix II
12	<i>Greenhouse gases</i> ● Chapter 3.7.3 and Appendix II ● Chapter 3.7.1, 3.7.2, 3.7.3 and Appendix II ● Chapter 3.7.3 and Appendix II ● Chapter 3.2.2 and Appendix II ● Chapter 4.4.5, 4.5, 4.6 and Appendix II ● Chapter 3.7.3
12	
12	<i>Aerosols</i> ● Chapter 5.5.2, 5.5.3 and Appendix II
12	<i>Radiative forcing over the 21st century</i> ● Chapter 6.15.2 and Appendix II

***Global average temperature and sea level are projected to rise under all IPCC SRES scenarios.***

SPM Page	Cross-Reference: SPM Topic – Chapter Section
13	<i>Temperature</i> ● Chapter 9.3.3 ● Chapter 9.3.3 ● Chapter 2.2.2, 2.3.2 and 2.4 ● Chapter 9.3.3 and Chapter 10.3.2 ● Chapter 8.6.1, Chapter 12.4.3, Chapter 13.5.1 and 13.5.2 ● Chapter 10.3.2 and Box 10.1 ● Chapter 9.3.2
13	
15	<i>Precipitation</i> ● Chapter 9.3.1, 9.3.6, Chapter 10.3.2 and Box 10.1
16	<i>Extreme events</i> Table 1: Chapter 2.1, 2.2, 2.5, 2.7.2, 2.7.3, Chapter 9.3.6 and Chapter 10.3.2 ● Chapter 2.7.3 and Chapter 9.3.6
16	<i>El Niño</i> ● Chapter 9.3.5 ● Chapter 9.3.5
16	<i>Monsoons</i> ● Chapter 9.3.5
16	<i>Thermohaline circulation</i> ● Chapter 9.3.4
16	<i>Snow and ice</i> ● Chapter 9.3.2 ● Chapter 11.5.1 ● Chapter 11.5.1 ● Chapter 11.5.4
16	<i>Sea level</i> ● Chapter 11.5.1

***Anthropogenic climate change will persist for many centuries.***

SPM Page	Cross-Reference: SPM Topic – Chapter Section
17	● Chapter 3.2.3, Chapter 4.4 and Chapter 6.15 ● Chapter 9.3.3 and 9.3.4 ● Chapter 11.5.4 ● Chapter 11.5.4 ● Chapter 11.5.4

***Further work is required to address remaining gaps in information and understanding.***

SPM Page	Cross-Reference: SPM Topic – Chapter Section
17 – 18	All bullet points: Chapter 14, Executive Summary

# Technical Summary

**A report accepted by Working Group I of the IPCC  
but not approved in detail**

“Acceptance” of IPCC Reports at a Session of the Working Group or Panel signifies that the material has not been subject to line by line discussion and agreement, but nevertheless presents a comprehensive, objective and balanced view of the subject matter.

## **Co-ordinating Lead Authors**

D.L. Albritton (USA), L.G. Meira Filho (Brazil)

## **Lead Authors**

U. Cubasch (Germany), X. Dai (China), Y. Ding (China), D.J. Griggs (UK), B. Hewitson (South Africa), J.T. Houghton (UK), I. Isaksen (Norway), T. Karl (USA), M. McFarland (USA), V.P. Meleshko (Russia), J.F.B. Mitchell (UK), M. Noguer (UK), B.S. Nyenzi (Tanzania), M. Oppenheimer (USA), J.E. Penner (USA), S. Pollonais (Trinidad and Tobago), T. Stocker (Switzerland), K.E. Trenberth (USA)

## **Contributing Authors**

M.R. Allen, (UK), A.P.M. Baede (Netherlands), J.A. Church (Australia), D.H. Ehhalt (Germany), C.K. Folland (UK), F. Giorgi (Italy), J.M. Gregory (UK), J.M. Haywood (UK), J.I. House (Germany), M. Hulme (UK), V.J. Jaramillo (Mexico), A. Jayaraman (India), C.A. Johnson (UK), S. Joussaume (France), D.J. Karoly (Australia), H. Kheshgi (USA), C. Le Quéré (France), L.J. Mata (Germany), B.J. McAvaney (Australia), L.O. Mearns (USA), G.A. Meehl (USA), B. Moore III (USA), R.K. Mugara (Zambia), M. Prather (USA), C. Prentice (Germany), V. Ramaswamy (USA), S.C.B. Raper (UK), M.J. Salinger (New Zealand), R. Scholes (S. Africa), S. Solomon (USA), R. Stouffer (USA), M-X. Wang (China), R.T. Watson (USA), K-S. Yap (Malaysia)

## **Review Editors**

F. Joos (Switzerland), A. Ramirez-Rojas (Venezuela), J.M.R. Stone (Canada), J. Zillman (Australia)

# Technical Summary of the Working Group I Report

## A. Introduction

### A.1 The IPCC and its Working Groups

The Intergovernmental Panel on Climate Change (IPCC) was established by the World Meteorological Organisation (WMO) and the United Nations Environment Programme (UNEP) in 1988. The aim was, and remains, to provide an assessment of the understanding of all aspects of climate change<sup>1</sup>, including how human activities can cause such changes and can be impacted by them. It had become widely recognised that human-influenced emissions of greenhouse gases have the potential to alter the climate system (see Box 1), with possible deleterious or beneficial effects. It was also recognised that addressing such global issues required organisation on a global scale, including assessment of the understanding of the issue by the worldwide expert communities.

At its first session, the IPCC was organised into three Working Groups. The current remits of the Working Groups are for Working Group I to address the scientific aspects of the climate system and climate change, Working Group II to address the impacts of and adaptations to climate change, and Working Group III to address the options for the mitigation of climate change. The IPCC provided its first major assessment report in 1990 and its second major assessment report in 1996.

The IPCC reports are (i) up-to-date descriptions of the knowns and unknowns of the climate system and related factors, (ii) based on the knowledge of the international expert communities, (iii) produced by an open and peer-reviewed professional process, and (iv) based upon scientific publications whose findings are summarised in terms useful to decision makers. While the assessed information is policy relevant, the IPCC does not establish or advocate public policy.

The scope of the assessments of Working Group I includes observations of the current changes and trends in the climate

system, a reconstruction of past changes and trends, an understanding of the processes involved in those changes, and the incorporation of this knowledge into models that can attribute the causes of changes and that can provide simulation of natural and human-induced future changes in the climate system.

### A.2 The First and Second Assessment Reports of Working Group I

In the First Assessment Report in 1990, Working Group I broadly described the status of the understanding of the climate system and climate change that had been gained over the preceding decades of research. Several major points were emphasised. The greenhouse effect is a natural feature of the planet, and its fundamental physics is well understood. The atmospheric abundances of greenhouse gases were increasing, due largely to human activities. Continued future growth in greenhouse gas emissions was predicted to lead to significant increases in the average surface temperature of the planet, increases that would exceed the natural variation of the past several millennia and that could be reversed only slowly. The past century had, at that time, seen a surface warming of nearly 0.5°C, which was broadly consistent with that predicted by climate models for the greenhouse gas increases, but was also comparable to what was then known about natural variation. Lastly, it was pointed out that the current level of understanding at that time and the existing capabilities of climate models limited the prediction of changes in the climate of specific regions.

Based on the results of additional research and Special Reports produced in the interim, IPCC Working Group I assessed the new state of understanding in its Second Assessment Report (SAR<sup>2</sup>) in 1996. The report underscored that greenhouse gas abundances continued to increase in the atmosphere and that very substantial cuts in emissions would be required for stabilisation of greenhouse gas concentrations in the atmosphere (which is the ultimate goal of Article 2 of the Framework Convention on Climate Change). Further, the general increase in

<sup>1</sup> Climate change in IPCC usage refers to any change in climate over time, whether due to natural variability or as a result of human activity. This usage differs from that in the Framework Convention on Climate Change, where climate change refers to a change of climate that is attributed directly or indirectly to human activity that alters the composition of the global atmosphere and that is in addition to natural climate variability observed over comparable time periods. For a definition of scientific and technical terms: see the Glossary in Appendix I.

<sup>2</sup> The IPCC Second Assessment Report is referred to in this Technical Summary as the SAR.

global temperature continued, with recent years being the warmest since at least 1860. The ability of climate models to simulate observed events and trends had improved, particularly with the inclusion of sulphate aerosols and stratospheric ozone as radiative forcing agents in climate models. Utilising this simulative capability to compare to the observed patterns of regional temperature changes, the report concluded that the ability to quantify the human influence on global climate was limited. The limitations arose because the expected signal was still emerging from the noise of natural variability and because of uncertainties in other key factors. Nevertheless, the report also concluded that “the balance of evidence suggests a discernible human influence on global climate”. Lastly, based on a range of scenarios of future greenhouse gas abundances, a set of responses of the climate system was simulated.

### A.3 The Third Assessment Report: This Technical Summary

The third major assessment report of IPCC Working Group I builds upon these past assessments and incorporates the results of the past five years of climate research. This Technical Summary is based on the underlying information of the chapters, which is cross-referenced in the Source Notes in the Appendix. This Summary aims to describe the major features (see Figure 1) of the understanding of the climate system and climate change at the outset of the 21st century. Specifically:

- What does the observational record show with regard to past climate changes, both globally and regionally and both on the average and in the extremes? (Section B)

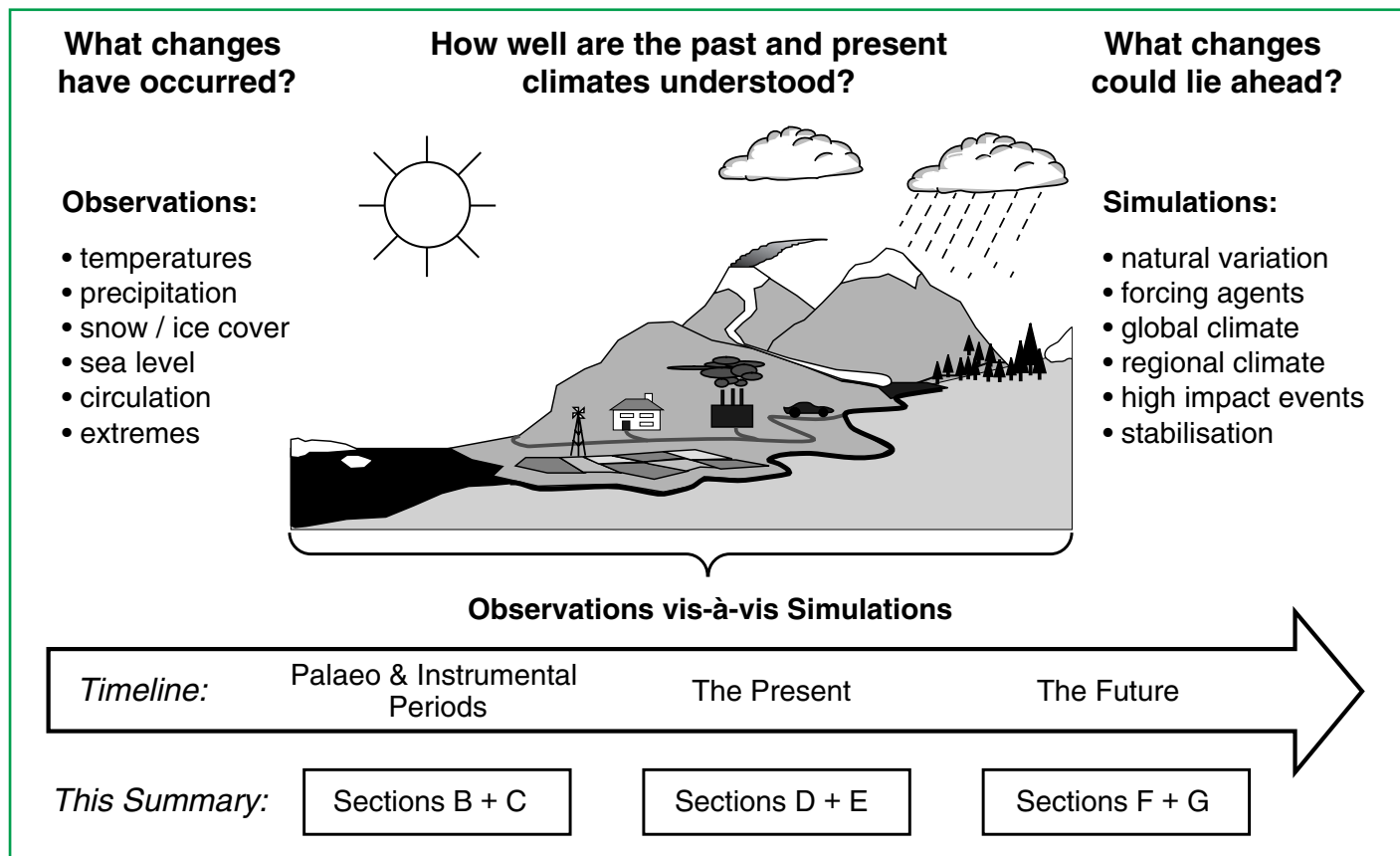


**Figure 1:** Key questions about the climate system and its relation to humankind. This Technical Summary, which is based on the underlying information in the chapters, is a status report on the answers, presented in the structure indicated.

- How quantitative is the understanding of the agents that cause climate to change, including both those that are natural (e.g., solar variation) and human-related (e.g., greenhouse gases) phenomena? (Section C)
- What is the current ability to simulate the responses of the climate system to these forcing agents? In particular, how well are key physical and biogeochemical processes described by present global climate models? (Section D)
- Based on today's observational data and today's climate predictive capabilities, what does the comparison show regarding a human influence on today's climate? (Section E)
- Further, using current predictive tools, what could the possible climate future be? Namely, for a wide spectrum of projections for several climate-forcing agents, what does current understanding project for global temperatures, regional patterns of precipitation, sea levels, and changes in extremes? (Section F)

*Finally, what are the most urgent research activities that need to be addressed to improve our understanding of the climate system and to reduce our uncertainty regarding future climate change?*

The Third Assessment Report of IPCC Working Group I is the product of hundreds of scientists from the developed and developing world who contributed to its preparation and review. What follows is a summary of their understanding of the climate system.

### Box 1: What drives changes in climate?

The Earth absorbs radiation from the Sun, mainly at the surface. This energy is then redistributed by the atmospheric and oceanic circulations and radiated back to space at longer (infrared) wavelengths. For the annual mean and for the Earth as a whole, the incoming solar radiation energy is balanced approximately by the outgoing terrestrial radiation. Any factor that alters the radiation received from the Sun or lost to space, or that alters the redistribution of energy within the atmosphere and between the atmosphere, land, and ocean, can affect climate. A change in the net radiative energy available to the global Earth-atmosphere system is termed here, and in previous IPCC reports, a radiative forcing. Positive radiative forcings tend to warm the Earth's surface and lower atmosphere. Negative radiative forcings tend to cool them.

Increases in the concentrations of greenhouse gases will reduce the efficiency with which the Earth's surface radiates to space. More of the outgoing terrestrial radiation from the surface is absorbed by the atmosphere and re-emitted at higher altitudes and lower temperatures. This results in a positive radiative forcing that tends to warm the lower atmosphere and surface. Because less heat escapes to space, this is the enhanced greenhouse effect – an enhancement of an effect that has operated in the Earth's atmosphere for billions of years due to the presence of naturally occurring greenhouse gases: water vapour, carbon dioxide, ozone, methane and nitrous oxide. The amount of radiative forcing depends on the size of the increase in concentration of each greenhouse gas, the radiative properties of the gases involved, and the concentrations of other greenhouse gases already present in the atmosphere. Further, many greenhouse gases reside in the atmosphere for centuries after being emitted, thereby introducing a long-term commitment to positive radiative forcing.

Anthropogenic aerosols (microscopic airborne particles or droplets) in the troposphere, such as those derived from fossil fuel and biomass burning, can reflect solar radiation, which leads to a cooling tendency in the climate system. Because it can absorb solar radiation, black carbon (soot) aerosol tends to warm the climate system. In addition, changes in aerosol concentrations can alter cloud amount and cloud reflectivity through their effect on cloud properties and lifetimes. In most cases, tropospheric aerosols tend to produce a negative radiative forcing and a cooler climate. They have a much shorter lifetime (days to weeks) than most greenhouse

gases (decades to centuries), and, as a result, their concentrations respond much more quickly to changes in emissions.

Volcanic activity can inject large amounts of sulphur-containing gases (primarily sulphur dioxide) into the stratosphere, which are transformed into sulphate aerosols. Individual eruptions can produce a large, but transitory, negative radiative forcing, tending to cool the Earth's surface and lower atmosphere over periods of a few years.

The Sun's output of energy varies by small amounts (0.1%) over an 11-year cycle and, in addition, variations over longer periods may occur. On time-scales of tens to thousands of years, slow variations in the Earth's orbit, which are well understood, have led to changes in the seasonal and latitudinal distribution of solar radiation. These changes have played an important part in controlling the variations of climate in the distant past, such as the glacial and inter-glacial cycles.

When radiative forcing changes, the climate system responds on various time-scales. The longest of these are due to the large heat capacity of the deep ocean and dynamic adjustment of the ice sheets. This means that the transient response to a change (either positive or negative) may last for thousands of years. Any changes in the radiative balance of the Earth, including those due to an increase in greenhouse gases or in aerosols, will alter the global hydrological cycle and atmospheric and oceanic circulation, thereby affecting weather patterns and regional temperatures and precipitation.

Any human-induced changes in climate will be embedded in a background of natural climatic variations that occur on a whole range of time- and space-scales. Climate variability can occur as a result of natural changes in the forcing of the climate system, for example variations in the strength of the incoming solar radiation and changes in the concentrations of aerosols arising from volcanic eruptions. Natural climate variations can also occur in the absence of a change in external forcing, as a result of complex interactions between components of the climate system, such as the coupling between the atmosphere and ocean. The El Niño-Southern Oscillation (ENSO) phenomenon is an example of such natural "internal" variability on interannual time-scales. To distinguish anthropogenic climate changes from natural variations, it is necessary to identify the anthropogenic "signal" against the background "noise" of natural climate variability.

## B. The Observed Changes in the Climate System

Is the Earth's climate changing? The answer is unequivocally "Yes". A suite of observations supports this conclusion and provides insight about the rapidity of those changes. These data are also the bedrock upon which to construct the answer to the more difficult question: "*Why* is it changing?", which is addressed in later Sections.

This Section provides an updated summary of the observations that delineate how the climate system has changed in the past. Many of the variables of the climate system have been measured directly, i.e., the "instrumental record". For example, widespread direct measurements of surface temperature began around the middle of the 19th century. Near global observations of other surface "weather" variables, such as precipitation and winds, have been made for about a hundred years. Sea level measurements have been made for over 100 years in some places, but the network of tide gauges with long records provides only limited global coverage. Upper air observations have been made systematically only since the late 1940s. There are also long records of surface oceanic observations made from ships since the mid-19th century and by dedicated buoys since about the late 1970s. Sub-surface oceanic temperature measurements with near global coverage are now available from the late 1940s. Since the late 1970s, other data from Earth-observation satellites have been used to provide a wide range of global observations of various components of the climate system. In addition, a growing set of palaeoclimatic data, e.g., from trees, corals, sediments, and ice, are giving information about the Earth's climate of centuries and millennia before the present.

This Section places particular emphasis on current knowledge of past changes in key climate variables: temperature, precipitation and atmospheric moisture, snow cover, extent of land and sea ice, sea level, patterns in atmospheric and oceanic circulation, extreme weather and climate events, and overall features of the climate variability. The concluding part of this Section compares the observed trends in these various climate indicators to see if a collective picture emerges. The degree of this internal consistency is a critical factor in assessing the level of confidence in the current understanding of the climate system.

## B.1 Observed Changes in Temperature

### Temperatures in the instrumental record for land and oceans

The global average surface temperature has increased by  $0.6 \pm 0.2^\circ\text{C}$ <sup>3</sup> since the late 19th century. It is very likely that the 1990s was the warmest decade and 1998 the warmest year in the instrumental record since 1861 (see Figure 2). The main cause of the increased estimate of global warming of  $0.15^\circ\text{C}$  since the SAR is related to the record warmth of the additional six years (1995 to 2000) of data. A secondary reason is related to improved methods of estimating change. The current, slightly larger uncertainty range ( $\pm 0.2^\circ\text{C}$ , 95% confidence interval) is also more objectively based. Further, the scientific basis for confidence in the estimates of the increase in global

1910 to 1945 and since 1976. The rate of increase of temperature for both periods is about  $0.15^\circ\text{C}/\text{decade}$ . Recent warming has been greater over land compared to oceans; the increase in sea surface temperature over the period 1950 to 1993 is about half that of the mean land-surface air temperature. The high global temperature associated with the 1997 to 1998 El Niño event stands out as an extreme event, even taking into account the recent rate of warming.

The regional patterns of the warming that occurred in the early part of the 20th century were different than those that occurred in the latter part. Figure 3 shows the regional patterns of the warming that have occurred over the full 20th century, as well as for three component time periods. The most recent period of warming (1976 to 1999) has been almost global, but the largest

increases in temperature have occurred over the mid- and high latitudes of the continents in the Northern Hemisphere. Year-round cooling is evident in the north-western North Atlantic and the central North Pacific Oceans, but the North Atlantic cooling trend has recently reversed. The recent regional patterns of temperature change have been shown to be related, in part, to various phases of atmospheric-oceanic oscillations, such as the North Atlantic-Arctic Oscillation and possibly the Pacific Decadal Oscillation. Therefore, regional temperature trends over a few decades can be strongly influenced by regional variability in the climate system and can depart

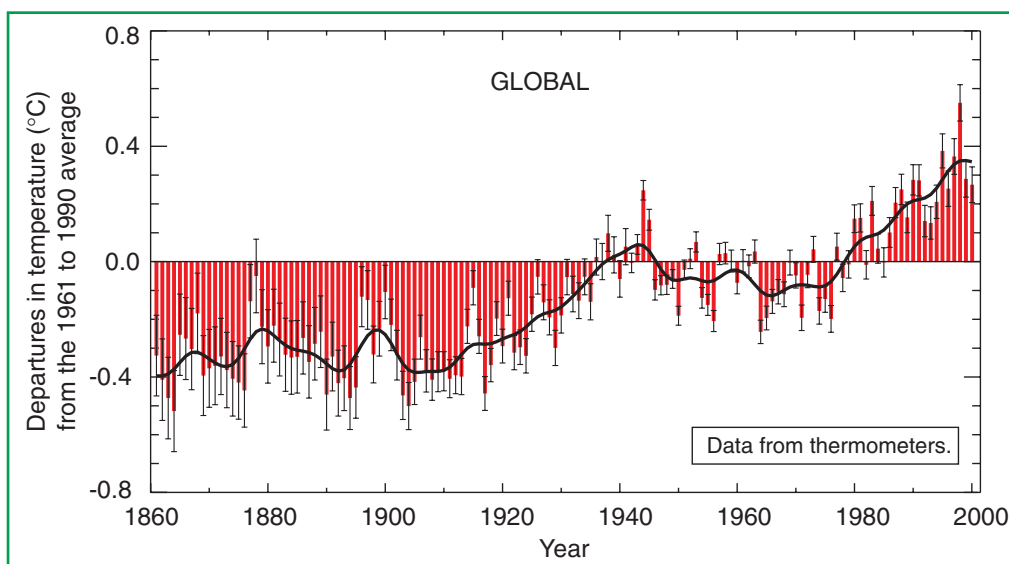


Figure 2: Combined annual land-surface air and sea surface temperature anomalies ( $^\circ\text{C}$ ) 1861 to 2000, relative to 1961 to 1990. Two standard error uncertainties are shown as bars on the annual number.

[Based on Figure 2.7c]

temperature since the late 19th century has been strengthened since the SAR. This is due to the improvements derived from several new studies. These include an independent test of the corrections used for time-dependent biases in the sea surface temperature data and new analyses of the effect of urban “heat island” influences on global land-temperature trends. As indicated in Figure 2, most of the increase in global temperature since the late 19th century has occurred in two distinct periods:

appreciably from a global average. The 1910 to 1945 warming was initially concentrated in the North Atlantic. By contrast, the period 1946 to 1975 showed significant cooling in the North Atlantic, as well as much of the Northern Hemisphere, and warming in much of the Southern Hemisphere.

New analyses indicate that global ocean heat content has increased significantly since the late 1950s. More than half of the increase in heat content has occurred in the upper 300 m

<sup>3</sup> Generally, temperature trends are rounded to the nearest  $0.05^\circ\text{C}$  per unit of time, the periods often being limited by data availability.

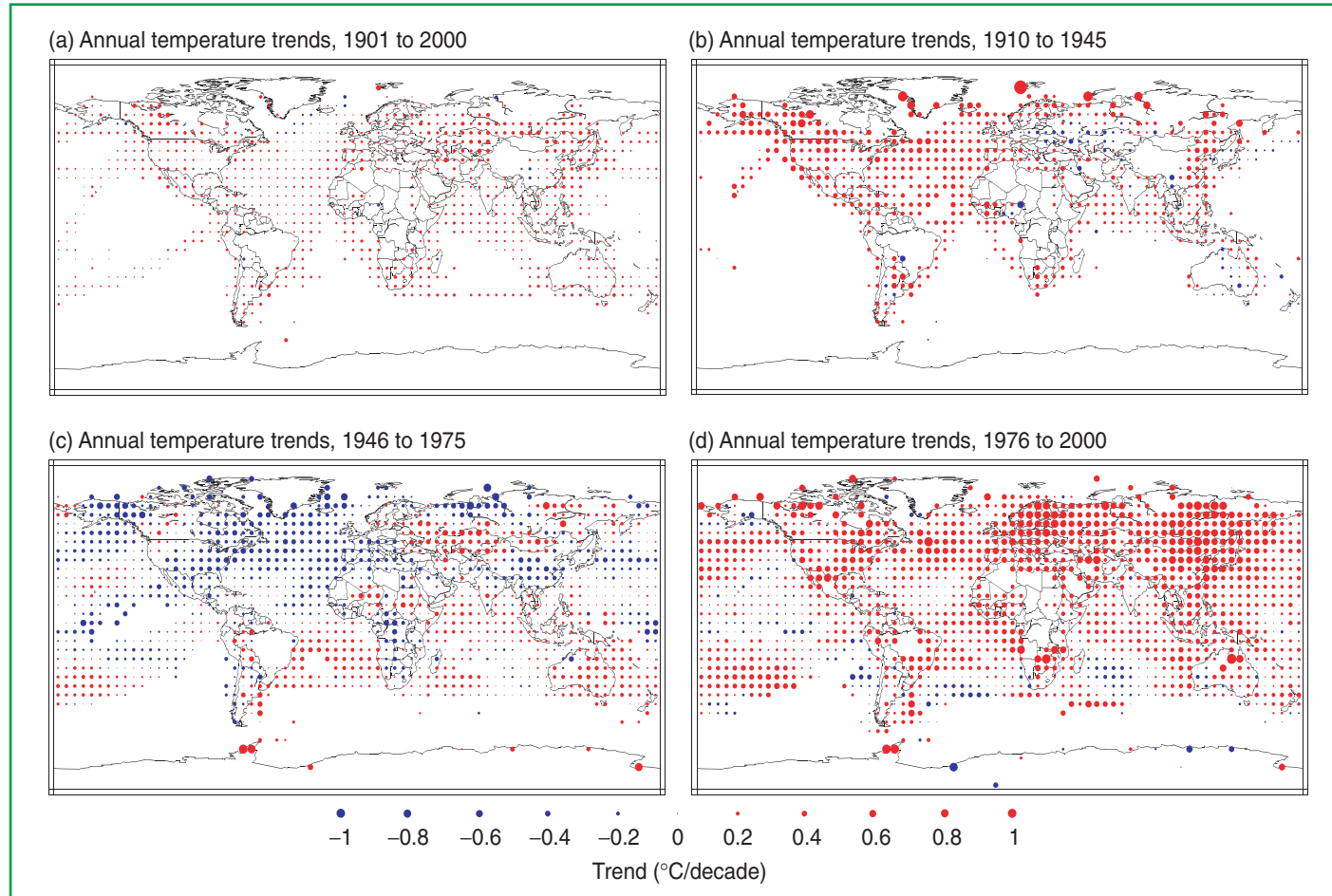


**Figure 3:** Annual temperature trends for the periods 1901 to 1999, 1910 to 1945, 1946 to 1975 and 1976 to 1999 respectively. Trends are represented by the area of the circle with red representing increases, blue representing decreases, and green little or no change. Trends were calculated from annually averaged gridded anomalies with the requirement that the calculation of annual anomalies include a minimum of 10 months of data. For the period 1901 to 1999, trends were calculated only for those grid boxes containing annual anomalies in at least 66 of the 100 years. The minimum number of years required for the shorter time periods (1910 to 1945, 1946 to 1975, and 1976 to 1999) was 24, 20, and 16 years respectively. [Based on Figure 2.9]

of the ocean, equivalent to a rate of temperature increase in this layer of about  $0.04^{\circ}\text{C}/\text{decade}$ .

New analyses of daily maximum and minimum land-surface temperatures for 1950 to 1993 continue to show that this measure of diurnal temperature range is decreasing very widely, although not everywhere. On average, minimum temperatures are increasing at about twice the rate of maximum temperatures ( $0.2$  versus  $0.1^{\circ}\text{C}/\text{decade}$ ).

#### Temperatures above the surface layer from satellite and weather balloon records

Surface, balloon and satellite temperature measurements show that the troposphere and Earth's surface have warmed and that the stratosphere has cooled. Over the shorter time period for which there have been both satellite and weather balloon data (since 1979), the balloon and satellite records show significantly less lower-tropospheric warming than observed at the surface. Analyses of temperature trends since 1958 for the lowest 8 km of the atmosphere and at the surface are in

good agreement, as shown in Figure 4a, with a warming of about  $0.1^{\circ}\text{C}$  per decade. However, since the beginning of the satellite record in 1979, the temperature data from both satellites and weather balloons show a warming in the global middle-to-lower troposphere at a rate of approximately  $0.05 \pm 0.10^{\circ}\text{C}$  per decade. The global average surface temperature has increased significantly by  $0.15 \pm 0.05^{\circ}\text{C}/\text{decade}$ . The difference in the warming rates is statistically significant. By contrast, during the period 1958 to 1978, surface temperature trends were near zero, while trends for the lowest 8 km of the atmosphere were near  $0.2^{\circ}\text{C}/\text{decade}$ . About half of the observed difference in warming since 1979 is likely<sup>4</sup> to be due to the combination of the differences in spatial coverage of the surface and tropospheric observations and the physical effects of the sequence of volcanic eruptions and a substantial El Niño (see Box 4 for a general description of ENSO) that occurred within this period. The remaining difference is very likely real and not an observing bias. It arises primarily due to differences in the rate of temperature change over the tropical and sub-tropical regions, which were faster in the lowest 8 km of the atmosphere before about 1979, but which have been slower since then. There are no significant differences in warming rates over mid-latitude continental regions in the Northern Hemisphere. In the upper troposphere, no significant global temperature trends have been detected since the early 1960s. In the stratosphere, as shown in Figure 4b, both satellites and balloons show substantial cooling, punctuated by sharp warming episodes of one to two years long that are due to volcanic eruptions.

### Surface temperatures during the pre-instrumental period from the proxy record

*It is likely that the rate and duration of the warming of the 20th century is larger than any other time during the last 1,000 years. The 1990s are likely to have been the warmest decade of the millennium in the Northern Hemisphere, and 1998 is likely to have been the warmest year. There has been a considerable advance in understanding of temperature change that occurred over the last millennium, especially from the synthesis of individual temperature reconstructions. This new detailed temperature record for the Northern Hemisphere is shown in*

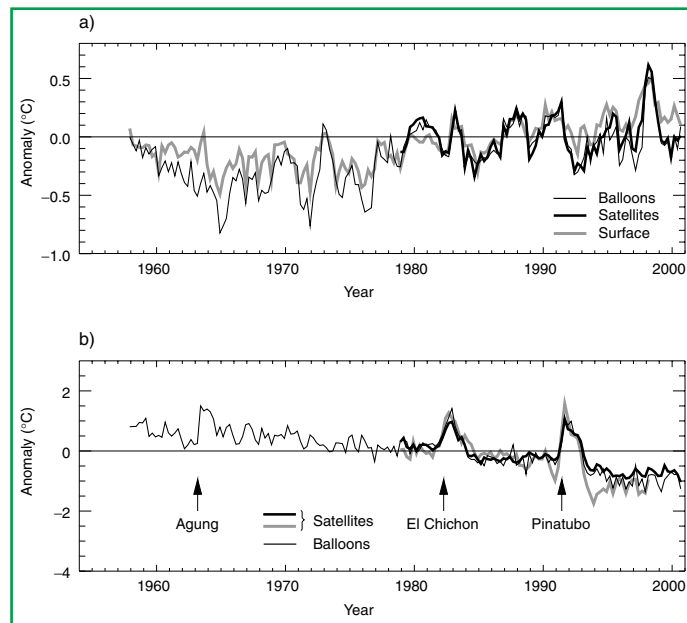


**Figure 4:** (a) Time-series of seasonal temperature anomalies of the troposphere based on balloons and satellites in addition to the surface. (b) Time-series of seasonal temperature anomalies of the lower stratosphere from balloons and satellites. [Based on Figure 2.12]

Figure 5. The data show a relatively warm period associated with the 11th to 14th centuries and a relatively cool period associated with the 15th to 19th centuries in the Northern Hemisphere. However, evidence does not support these “Medieval Warm Period” and “Little Ice Age” periods, respectively, as being globally synchronous. As Figure 5 indicates, the rate and duration of warming of the Northern Hemisphere in the 20th century appears to have been unprecedented during the millennium, and it cannot simply be considered as a recovery from the “Little Ice Age” of the 15th to 19th centuries. These analyses are complemented by sensitivity analysis of the spatial representativeness of available palaeoclimatic data, indicating that the warmth of the recent decade is outside the 95% confidence interval of temperature uncertainty, even during the warmest periods of the last millennium. Moreover, several different analyses have now been completed, each suggesting

<sup>4</sup> In this Technical Summary and in the Summary for Policymakers, the following words have been used to indicate approximate judgmental estimates of confidence: *virtually certain* (greater than 99% chance that a result is true); *very likely* (90–99% chance); *likely* (66–90% chance); *medium likelihood* (33–66% chance); *unlikely* (10–33% chance); *very unlikely* (1–10% chance); *exceptionally unlikely* (less than 1% chance). The reader is referred to individual chapters for more details.

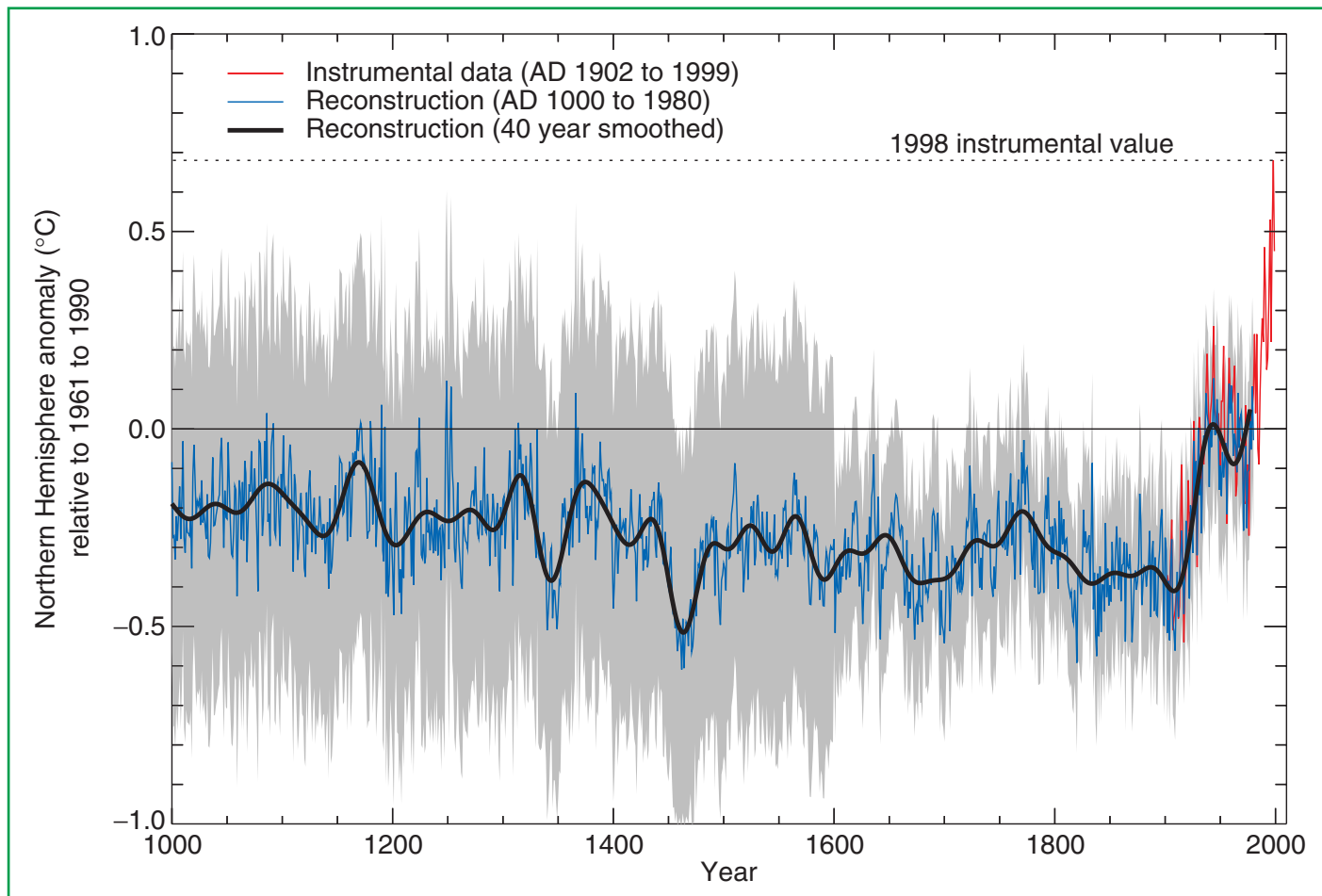


**Figure 5:** Millennial Northern Hemisphere (NH) temperature reconstruction (blue – tree rings, corals, ice cores, and historical records) and instrumental data (red) from AD 1000 to 1999. Smoother version of NH series (black), and two standard error limits (gray shaded) are shown. [Based on Figure 2.20]

that the Northern Hemisphere temperatures of the past decade have been warmer than any other time in the past six to ten centuries. This is the time-span over which temperatures with annual resolution can be calculated using hemispheric-wide tree-ring, ice-cores, corals, and other annually-resolved proxy data. Because less data are available, less is known about annual averages prior to 1,000 years before the present and for conditions prevailing in most of the Southern Hemisphere prior to 1861.

*It is likely that large rapid decadal temperature changes occurred during the last glacial and its deglaciation (between about 100,000 and 10,000 years ago), particularly in high latitudes of the Northern Hemisphere. In a few places during the deglaciation, local increases in temperature of 5 to 10°C are likely to have occurred over periods as short as a few decades. During the last 10,000 years, there is emerging evidence of significant rapid regional temperature changes, which are part of the natural variability of climate.*

### B.2 Observed Changes in Precipitation and Atmospheric Moisture

Since the time of the SAR, annual land precipitation has continued to increase in the middle and high latitudes of the Northern Hemisphere (very likely to be 0.5 to 1%/decade), except over Eastern Asia. Over the sub-tropics (10°N to 30°N), land-surface rainfall has decreased on average (likely to be about 0.3%/decade), although this has shown signs of recovery in recent years. Tropical land-surface precipitation measurements indicate that precipitation likely has increased by about 0.2 to 0.3%/decade over the 20th century, but increases are not evident over the past few decades and the amount of tropical land (versus ocean) area for the latitudes 10°N to 10°S is relatively small. Nonetheless, direct measurements of precipitation and model reanalyses of inferred precipitation indicate that rainfall has also increased over large parts of the tropical oceans. Where and when available, changes in annual streamflow often relate well to changes in total precipitation. The increases in precipitation over Northern Hemisphere mid- and high latitude land areas have a strong correlation to long-term increases in total cloud amount. In contrast to the Northern Hemisphere, no comparable systematic changes in precipitation have been detected in broad latitudinal averages over the Southern Hemisphere.

*It is likely that total atmospheric water vapour has increased several per cent per decade over many regions of the Northern Hemisphere.* Changes in water vapour over approximately the past 25 years have been analysed for selected regions using *in situ* surface observations, as well as lower-tropospheric measurements from satellites and weather balloons. A pattern of overall surface and lower-tropospheric water vapour increases over the past few decades is emerging from the most reliable data sets, although there are likely to be time-dependent biases in these data and regional variations in the trends. Water vapour in the lower stratosphere is also likely to have increased by about 10% per decade since the beginning of the observational record (1980).

*Changes in total cloud amounts over Northern Hemisphere mid- and high latitude continental regions indicate a likely increase in cloud cover of about 2% since the beginning of the 20th century, which has now been shown to be positively correlated with decreases in the diurnal temperature range.*

Similar changes have been shown over Australia, the only Southern Hemisphere continent where such an analysis has been completed. Changes in total cloud amount are uncertain both over sub-tropical and tropical land areas, as well as over the oceans.

### B.3 Observed Changes in Snow Cover and Land- and Sea-Ice Extent

*Decreasing snow cover and land-ice extent continue to be positively correlated with increasing land-surface temperatures.* Satellite data show that there are very likely to have been decreases of about 10% in the extent of snow cover since the late 1960s. There is a highly significant correlation between increases in Northern Hemisphere land temperatures and the decreases. There is now ample evidence to support a major retreat of alpine and continental glaciers in response to 20th century warming. In a few maritime regions, increases in precipitation due to regional atmospheric circulation changes have overshadowed increases in temperature in the past two decades, and glaciers have re-advanced. Over the past 100 to 150 years, ground-based observations show that there is very likely to have been a reduction of about two weeks in the annual duration of lake and river ice in the mid- to high latitudes of the Northern Hemisphere.

*Northern Hemisphere sea-ice amounts are decreasing, but no significant trends in Antarctic sea-ice extent are apparent.* A retreat of sea-ice extent in the Arctic spring and summer of 10 to 15% since the 1950s is consistent with an increase in spring temperatures and, to a lesser extent, summer temperatures in the high latitudes. There is little indication of reduced Arctic sea-ice extent during winter when temperatures have increased in the surrounding region. By contrast, there is no readily apparent relationship between decadal changes of Antarctic temperatures and sea-ice extent since 1973. After an initial decrease in the mid-1970s, Antarctic sea-ice extent has remained stable, or even slightly increased.

*New data indicate that there likely has been an approximately 40% decline in Arctic sea-ice thickness in late summer to early autumn between the period of 1958 to 1976 and the mid-1990s, and a substantially smaller decline in winter.* The relatively short record length and incomplete sampling limit the interpretation of these data. Interannual variability and inter-decadal variability could be influencing these changes.

## B.4 Observed Changes in Sea Level

### Changes during the instrumental record

*Based on tide gauge data, the rate of global mean sea level rise during the 20th century is in the range 1.0 to 2.0 mm/yr, with a central value of 1.5 mm/yr (the central value should not be interpreted as a best estimate). (See Box 2 for the factors that influence sea level.) As Figure 6 indicates, the longest instrumental records (two or three centuries at most) of local sea level come from tide gauges. Based on the very few long tide-gauge records, the average rate of sea level rise has been larger during the 20th century than during the 19th century. No significant acceleration*

*in the rate of sea level rise during the 20th century has been detected. This is not inconsistent with model results due to the possibility of compensating factors and the limited data.*

### Changes during the pre-instrumental record

*Since the last glacial maximum about 20,000 years ago, the sea level in locations far from present and former ice sheets has risen by over 120 m as a result of loss of mass from these ice sheets. Vertical land movements, both upward and downward, are still occurring in response to these large transfers of mass from ice sheets to oceans. The most rapid rise in global sea level was between 15,000 and 6,000 years*

### Box 2: What causes sea level to change?

The level of the sea at the shoreline is determined by many factors in the global environment that operate on a great range of time-scales, from hours (tidal) to millions of years (ocean basin changes due to tectonics and sedimentation). On the time-scale of decades to centuries, some of the largest influences on the average levels of the sea are linked to climate and climate change processes.

Firstly, as ocean water warms, it expands. On the basis of observations of ocean temperatures and model results, thermal expansion is believed to be one of the major contributors to historical sea level changes. Further, thermal expansion is expected to contribute the largest component to sea level rise over the next hundred years. Deep ocean temperatures change only slowly; therefore, thermal expansion would continue for many centuries even if the atmospheric concentrations of greenhouse gases were to stabilise.

The amount of warming and the depth of water affected vary with location. In addition, warmer water expands

more than colder water for a given change in temperature. The geographical distribution of sea level change results from the geographical variation of thermal expansion, changes in salinity, winds, and ocean circulation. The range of regional variation is substantial compared with the global average sea level rise.

Sea level also changes when the mass of water in the ocean increases or decreases. This occurs when ocean water is exchanged with the water stored on land. The major land store is the water frozen in glaciers or ice sheets. Indeed, the main reason for the lower sea level during the last glacial period was the amount of water stored in the large extension of the ice sheets on the continents of the Northern Hemisphere. After thermal expansion, the melting of mountain glaciers and ice caps is expected to make the largest contribution to the rise of sea level over the next hundred years. These glaciers and ice caps make up only a few per cent of the world's land-ice area, but they are more sensitive to climate change than the larger ice sheets in Greenland and Antarctica, because the ice sheets are in colder climates with low precipitation

and low melting rates. Consequently, the large ice sheets are expected to make only a small net contribution to sea level change in the coming decades.

Sea level is also influenced by processes that are not explicitly related to climate change. Terrestrial water storage (and hence, sea level) can be altered by extraction of ground water, building of reservoirs, changes in surface runoff, and seepage into deep aquifers from reservoirs and irrigation. These factors may be offsetting a significant fraction of the expected acceleration in sea level rise from thermal expansion and glacial melting. In addition, coastal subsidence in river delta regions can also influence local sea level. Vertical land movements caused by natural geological processes, such as slow movements in the Earth's mantle and tectonic displacements of the crust, can have effects on local sea level that are comparable to climate-related impacts. Lastly, on seasonal, interannual, and decadal time-scales, sea level responds to changes in atmospheric and ocean dynamics, with the most striking example occurring during El Niño events.

ago, with an average rate of about 10 mm/yr. Based on geological data, eustatic sea level (i.e., corresponding to a change in ocean volume) may have risen at an average rate of 0.5 mm/yr over the past 6,000 years and at an average rate of 0.1 to 0.2 mm/yr over the last 3,000 years. This rate is about one tenth of that occurring during the 20th century. Over the past 3,000 to 5,000 years, oscillations in global sea level on time-scales of 100 to 1,000 years are unlikely to have exceeded 0.3 to 0.5 m.

### B.5 Observed Changes in Atmospheric and Oceanic Circulation Patterns

The behaviour of ENSO (see Box 4 for a general description), has been unusual since the mid-1970s compared with the previous 100 years, with warm phase ENSO episodes being relatively more frequent, persistent, and intense than the opposite cool phase. This recent behaviour of ENSO is reflected in variations in precipitation and temperature over much of the global tropics and sub-tropics. The overall effect

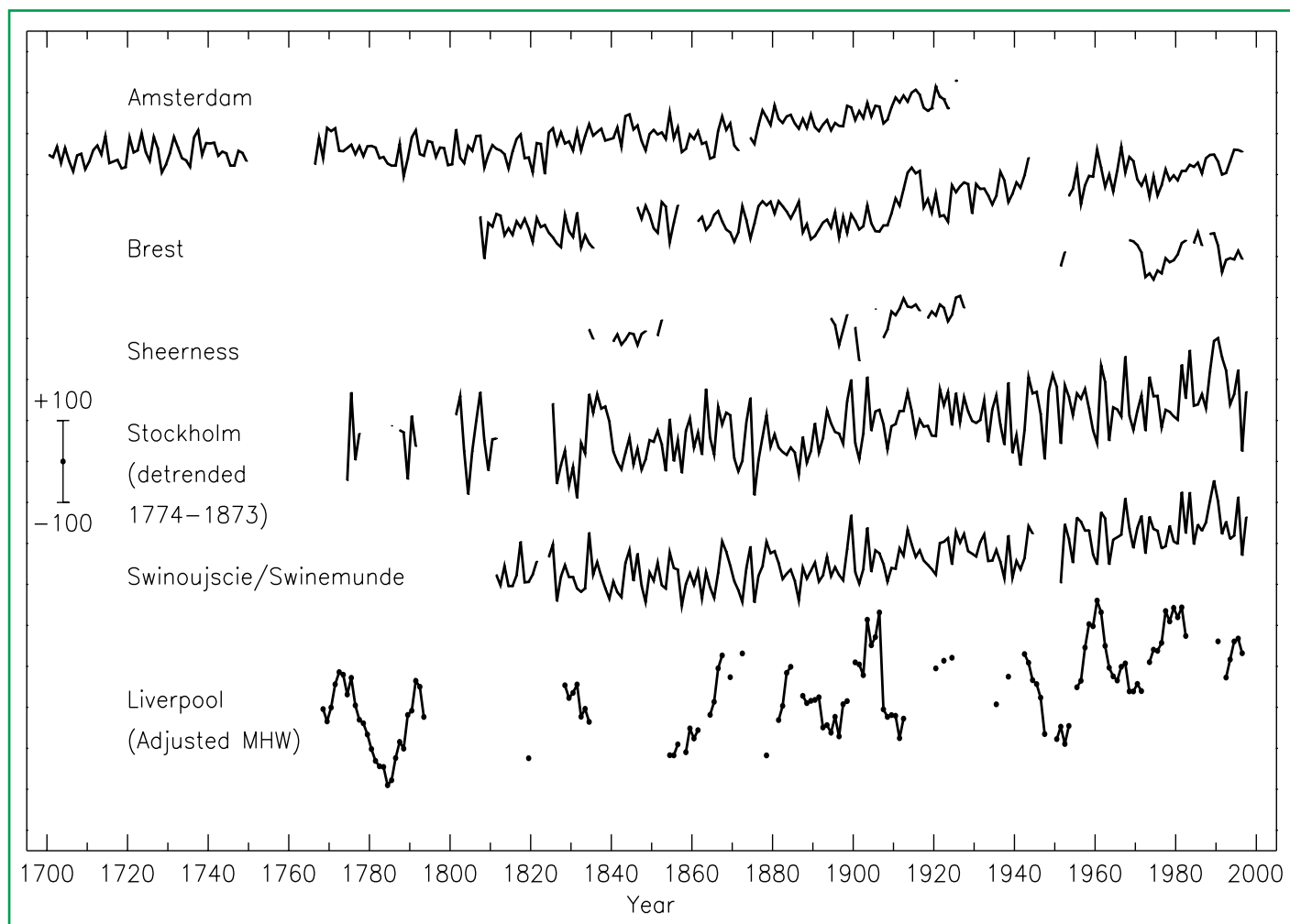


**Figure 6:** Time-series of relative sea level for the past 300 years from Northern Europe: Amsterdam, Netherlands; Brest, France; Sheerness, UK; Stockholm, Sweden (detrended over the period 1774 to 1873 to remove the contribution of post-glacial rebound); Swinoujscie, Poland (formerly Swinemunde, Germany); and Liverpool, UK. Data for the latter are of “Adjusted Mean High Water” rather than Mean Sea Level and include a nodal (18.6 year) term. The scale bar indicates  $\pm 100$  mm. [Based on Figure 11.7]

is likely to have been a small contribution to the increase in global temperatures during the last few decades. The Inter-decadal Pacific Oscillation and the Pacific Decadal Oscillation are associated with decadal to multidecadal climate variability over the Pacific basin. It is likely that these oscillations modulate ENSO-related climate variability.

*Other important circulation features that affect the climate in large regions of the globe are being characterised.* The North Atlantic Oscillation (NAO) is linked to the strength of the westerlies over the Atlantic and extra-tropical Eurasia. During winter the NAO displays irregular oscillations on interannual to multi-decadal time-scales. Since the 1970s, the winter NAO has often been in a phase that contributes to stronger westerlies, which correlate with cold season warming over Eurasia. New evidence indicates that the NAO and changes in Arctic sea ice are likely to be closely coupled. The NAO is now believed to be part of a wider scale atmospheric Arctic Oscillation that affects much of the extratropical Northern Hemisphere. A similar Antarctic Oscillation has been in an enhanced positive phase during the last 15 years, with stronger westerlies over the Southern Oceans.

### B.6 Observed Changes in Climate Variability and Extreme Weather and Climate Events

*New analyses show that in regions where total precipitation has increased, it is very likely that there have been even more pronounced increases in heavy and extreme precipitation events. The converse is also true.* In some regions, however, heavy and extreme events (i.e., defined to be within the upper or lower ten percentiles) have increased despite the fact that total precipitation has decreased or remained constant. This is attributed to a decrease in the frequency of precipitation events. Overall, it is likely that for many mid- and high latitude areas, primarily in the Northern Hemisphere, statistically significant increases have occurred in the proportion of total annual precipitation derived from heavy and extreme precipitation events; it is likely that there has been a 2 to 4% increase in the frequency of heavy precipitation events over the latter half of the 20th century. Over the 20th century (1900 to 1995), there were relatively small increases in global land areas experiencing severe drought or severe wetness. In some regions, such as parts of

Asia and Africa, the frequency and intensity of drought have been observed to increase in recent decades. In many regions, these changes are dominated by inter-decadal and multi-decadal climate variability, such as the shift in ENSO towards more warm events. In many regions, inter-daily temperature variability has decreased, and increases in the daily minimum temperature are lengthening the freeze-free period in most mid- and high latitude regions. Since 1950 it is very likely that there has been a significant reduction in the frequency of much-below-normal seasonal mean temperatures across much of the globe, but there has been a smaller increase in the frequency of much-above-normal seasonal temperatures.

*There is no compelling evidence to indicate that the characteristics of tropical and extratropical storms have changed.* Changes in tropical storm intensity and frequency are dominated by interdecadal to multidecadal variations, which may be substantial, e.g., in the tropical North Atlantic. Owing to incomplete data and limited and conflicting analyses, it is uncertain as to whether there have been any long-term and large-scale increases in the intensity and frequency of extra-tropical cyclones in the Northern Hemisphere. Regional increases have been identified in the North Pacific, parts of North America, and Europe over the past several decades. In the Southern Hemisphere, fewer analyses have been completed, but they suggest a decrease in extra-tropical cyclone activity since the 1970s. Recent analyses of changes in severe local weather (e.g., tornadoes, thunderstorm days, and hail) in a few selected regions do not provide compelling evidence to suggest long-term changes. In general, trends in severe weather events are notoriously difficult to detect because of their relatively rare occurrence and large spatial variability.

### B.7 The Collective Picture: A Warming World and Other Changes in the Climate System

As summarised above, a suite of climate changes is now well-documented, particularly over the recent decades to century time period, with its growing set of direct measurements. Figure 7 illustrates these trends in temperature indicators (Figure 7a) and hydrological and storm-related indicators (Figure 7b), as well as also providing an indication of certainty about the changes.

### Taken together, these trends illustrate a collective picture of a warming world:

- Surface temperature measurements over the land and oceans (with two separate estimates over the latter) have been measured and adjusted independently. All data sets show quite similar upward trends globally, with two major warming periods globally: 1910 to 1945 and since 1976. There is an emerging tendency for global land-surface air temperatures to warm faster than the global ocean-surface temperatures.
- Weather balloon measurements show that lower-tropospheric temperatures have been increasing since 1958, though only slightly since 1979. Since 1979, satellite data are available and show similar trends to balloon data.
- The decrease in the continental diurnal temperature range coincides with increases in cloud amount, precipitation, and increases in total water vapour.
- The nearly worldwide decrease in mountain glacier extent and ice mass is consistent with worldwide surface temperature increases. A few recent exceptions in coastal regions are consistent with atmospheric circulation variations and related precipitation increases.
- The decreases in snow cover and the shortening seasons of lake and river ice relate well to increases in Northern Hemispheric land-surface temperatures.
- The systematic decrease in spring and summer sea-ice extent and thickness in the Arctic is consistent with increases in temperature over most of the adjacent land and ocean.
- Ocean heat content has increased, and global average sea level has risen.
- The increases in total tropospheric water vapour in the last 25 years are qualitatively consistent with increases in tropospheric temperatures and an enhanced hydrologic cycle, resulting in more extreme and heavier precipitation events in many areas with increasing precipitation, e.g., middle and high latitudes of the Northern Hemisphere.

### Some important aspects of climate appear not to have changed.

- A few areas of the globe have not warmed in recent decades, mainly over some parts of the Southern Hemisphere oceans and parts of Antarctica.
- No significant trends in Antarctic sea-ice extent are apparent over the period of systematic satellite measurements (since 1978).
- Based on limited data, the observed variations in the intensity and frequency of tropical and extra-tropical cyclones and severe local storms show no clear trends in the last half of the 20th century, although multi-decadal fluctuations are sometimes apparent.

The variations and trends in the examined indicators imply that it is virtually certain that there has been a generally increasing trend in global surface temperature over the 20th century, although short-term and regional deviations from this trend occur.

(a) Temperature Indicators

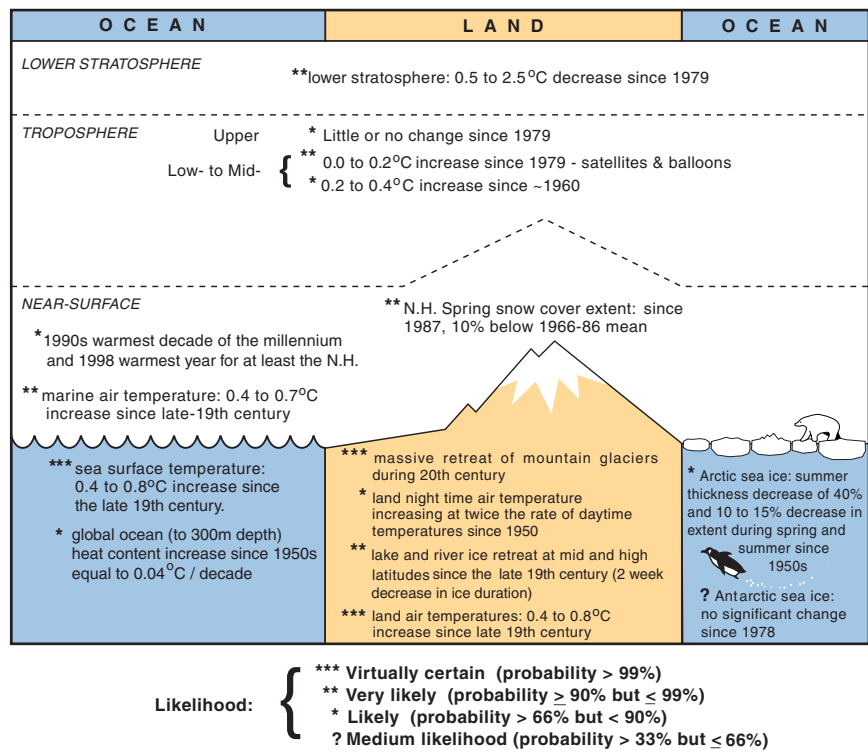


**Figure 7a:** Schematic of observed variations of the temperature indicators. [Based on Figure 2.39a]

(b) Hydrological and Storm related Indicators

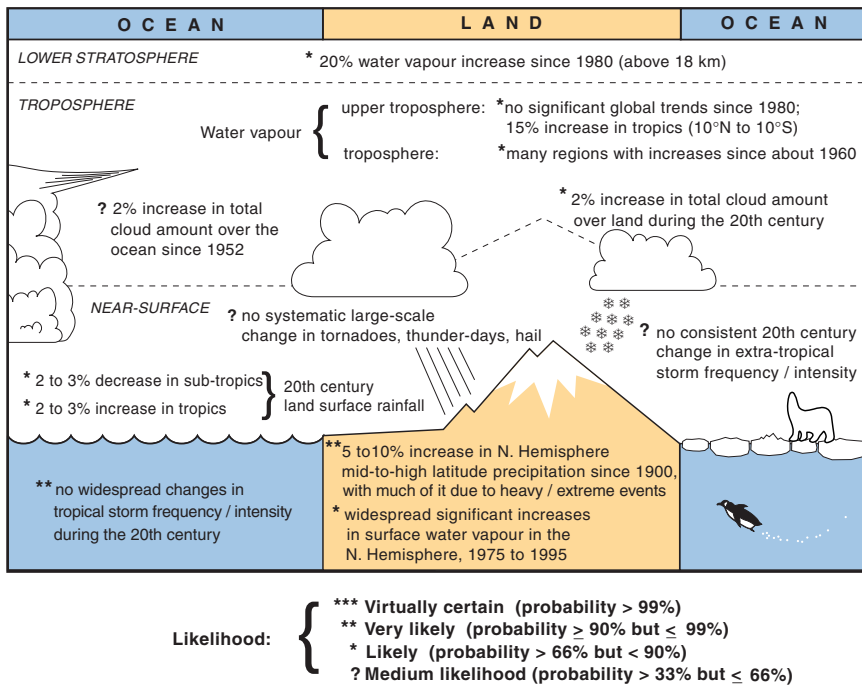


**Figure 7b:** Schematic of observed variations of the hydrological and storm-related indicators. [Based on Figure 2.39b]

## C. The Forcing Agents That Cause Climate Change

In addition to the past variations and changes in the Earth's climate, observations have also documented the changes that have occurred in agents that can cause climate change. Most notable among these are increases in the atmospheric concentrations of greenhouse gases and aerosols (microscopic airborne particles or droplets) and variations in solar activity, both of which can alter the Earth's radiation budget and hence climate. These observational records of climate-forcing agents are part of the input needed to understand the past climate changes noted in the preceding Section and, very importantly, to predict what climate changes could lie ahead (see Section F).

Like the record of past climate changes, the data sets for forcing agents are of varying length and quality. Direct measurements of solar irradiance exist for only about two decades. The sustained direct monitoring of the atmospheric concentrations of carbon dioxide ( $\text{CO}_2$ ) began about the middle of the 20th century and, in later years, for other long-lived, well-mixed gases such as methane. Palaeo-atmospheric data from ice cores reveal the concentration changes occurring in earlier millennia for some greenhouse gases. In contrast, the time-series measurements for the forcing agents that have relatively short residence times in the atmosphere (e.g., aerosols) are more recent and are far less complete, because they are harder to measure and are spatially heterogeneous. Current data sets show the human influence on atmospheric concentrations of both the long-lived greenhouse gases and short-lived forcing agents during the last part of the past millennium. Figure 8 illustrates the effects of the large growth over the Industrial Era in the anthropogenic emissions of greenhouse gases and sulphur dioxide, the latter being a precursor of aerosols.

A change in the energy available to the global Earth-atmosphere system due to changes in these forcing agents is termed radiative forcing ( $\text{W m}^{-2}$ ) of the climate system (see Box 1). Defined in this manner, radiative forcing of climate change constitutes an index of the relative global mean impacts on the surface-troposphere system due to different natural and anthropogenic causes. This Section updates the knowledge of the radiative forcing of climate change that has occurred from pre-industrial times to the present. Figure 9 shows the estimated radiative forcings from the beginning of the Industrial Era (1750) to 1999 for the quantifiable natural and anthropogenic

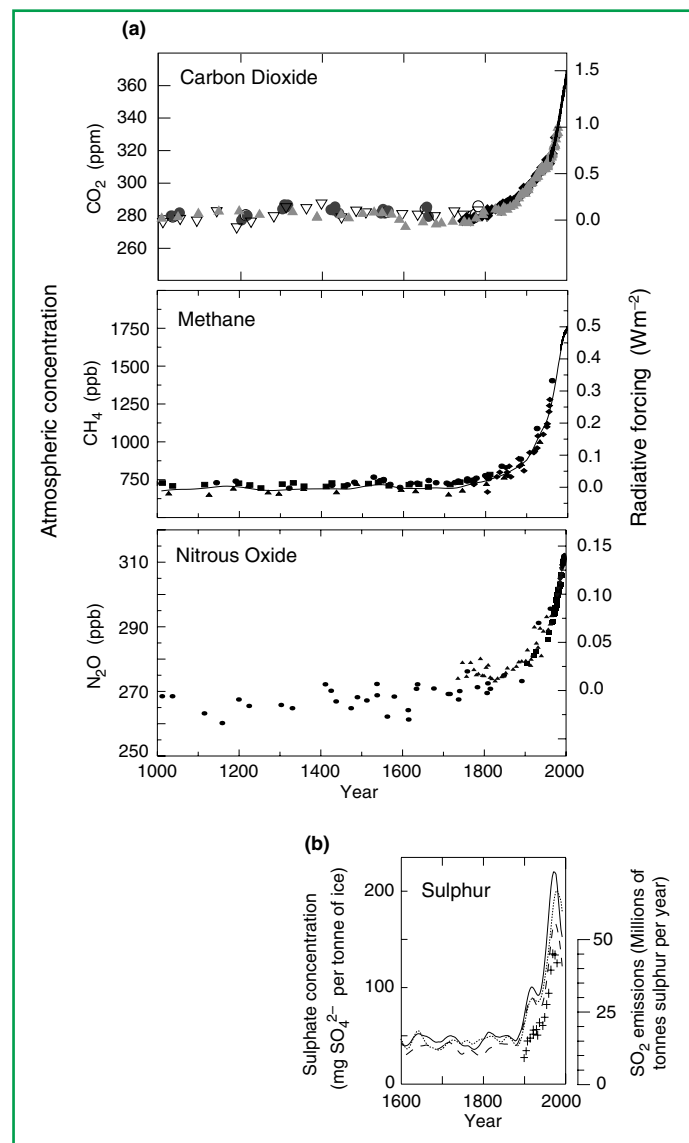


**Figure 8:** Records of changes in atmospheric composition. (a) Atmospheric concentrations of  $\text{CO}_2$ ,  $\text{CH}_4$  and  $\text{N}_2\text{O}$  over the past 1,000 years. Ice core and firn data for several sites in Antarctica and Greenland (shown by different symbols) are supplemented with the data from direct atmospheric samples over the past few decades (shown by the line for  $\text{CO}_2$  and incorporated in the curve representing the global average of  $\text{CH}_4$ ). The estimated radiative forcing from these gases is indicated on the right-hand scale. (b) Sulphate concentration in several Greenland ice cores with the episodic effects of volcanic eruptions removed (lines) and total  $\text{SO}_2$  emissions from sources in the US and Europe (crosses). [Based on (a) Figure 3.2b ( $\text{CO}_2$ ), Figure 4.1a and b ( $\text{CH}_4$ ) and Figure 4.2 ( $\text{N}_2\text{O}$ ) and (b) Figure 5.4a]

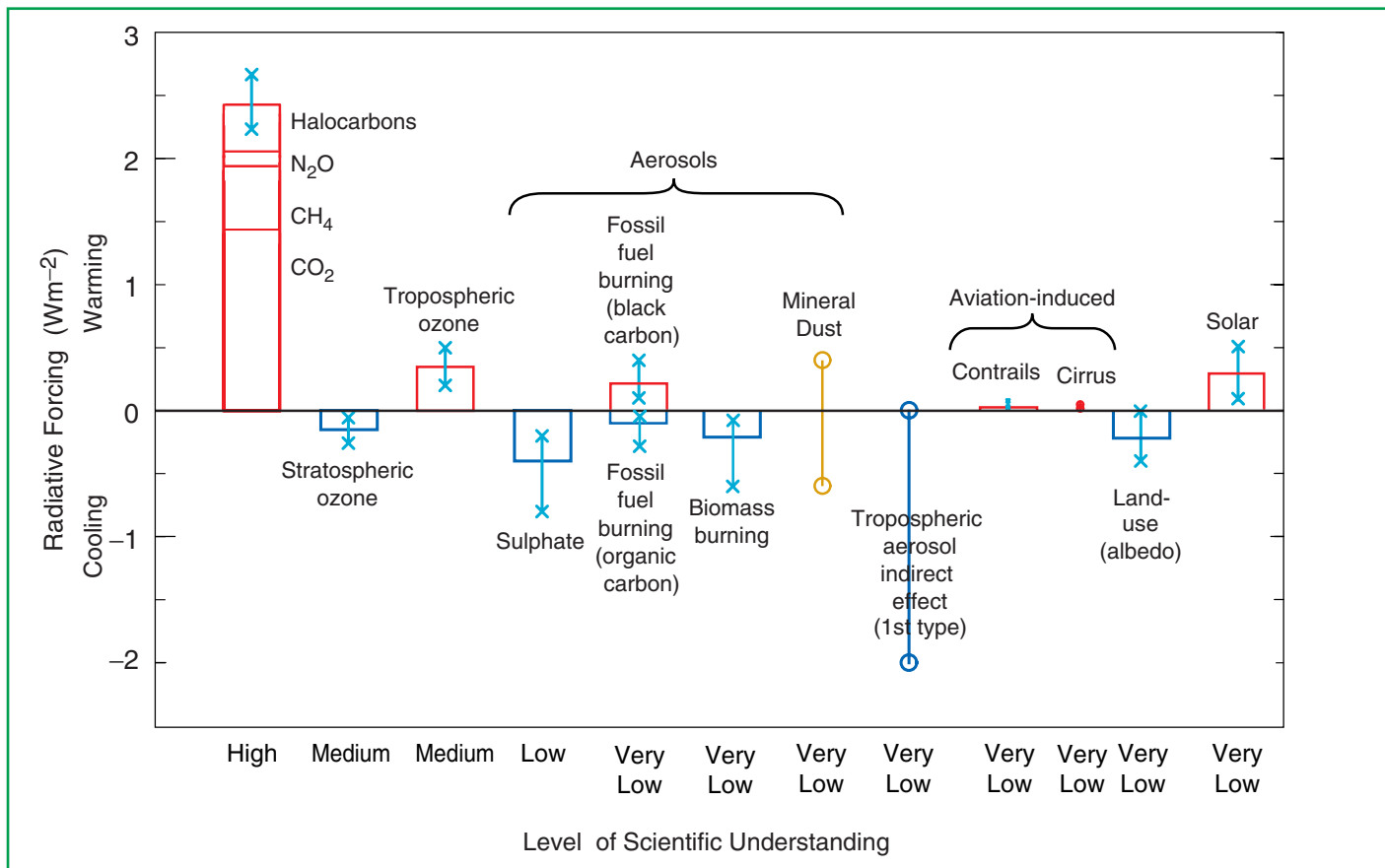


**Figure 9:** Global, annual-mean radiative forcings ( $\text{Wm}^{-2}$ ) due to a number of agents for the period from pre-industrial (1750) to present (late 1990s; about 2000) (numerical values are also listed in Table 6.11 of Chapter 6). For detailed explanations, see Chapter 6.13. The height of the rectangular bar denotes a central or best estimate value, while its absence denotes no best estimate is possible. The vertical line about the rectangular bar with “x” delimiters indicates an estimate of the uncertainty range, for the most part guided by the spread in the published values of the forcing. A vertical line without a rectangular bar and with “o” delimiters denotes a forcing for which no central estimate can be given owing to large uncertainties. The uncertainty range specified here has no statistical basis and therefore differs from the use of the term elsewhere in this document. A “level of scientific understanding” index is accorded to each forcing, with high, medium, low and very low levels, respectively. This represents the subjective judgement about the reliability of the forcing estimate, involving factors such as the assumptions necessary to evaluate the forcing, the degree of knowledge of the physical/chemical mechanisms determining the forcing, and the uncertainties surrounding the quantitative estimate of the forcing (see Table 6.12). The well-mixed greenhouse gases are grouped together into a single rectangular bar with the individual mean contributions due to CO<sub>2</sub>, CH<sub>4</sub>, N<sub>2</sub>O and halocarbons shown (see Tables 6.1 and 6.11). Fossil fuel burning is separated into the “black carbon” and “organic carbon” components with its separate best estimate and range. The sign of the effects due to mineral dust is itself an uncertainty. The indirect forcing due to tropospheric aerosols is poorly understood. The same is true for the forcing due to aviation via its effects on contrails and cirrus clouds. Only the “first” type of indirect effect due to aerosols as applicable in the context of liquid clouds is considered here. The “second” type of effect is conceptually important, but there exists very little confidence in the simulated quantitative estimates. The forcing associated with stratospheric aerosols from volcanic eruptions is highly variable over the period and is not considered for this plot (however, see Figure 6.8). All the forcings shown have distinct spatial and seasonal features (Figure 6.7) such that the global, annual means appearing on this plot do not yield a complete picture of the radiative perturbation. They are only intended to give, in a relative sense, a first-order perspective on a global, annual mean scale and cannot be readily employed to obtain the climate response to the total natural and/or anthropogenic forcings. As in the SAR, it is emphasised that the positive and negative global mean forcings cannot be added up and viewed *a priori* as providing offsets in terms of the complete global climate impact. [Based on Figure 6.6]

forcing agents. Although not included in the figure due to their episodic nature, volcanic eruptions are the source of another important natural forcing. Summaries of the information about each forcing agent follow in the sub-sections below.

The forcing agents included in Figure 9 vary greatly in their form, magnitude and spatial distribution. Some of the greenhouse gases are emitted directly into the atmosphere; some are chemical products from other emissions. Some greenhouse gases have long atmospheric residence times and, as a result, are well-mixed throughout the atmosphere. Others are short-lived and have heterogeneous regional concentrations. Most of the gases originate from both natural and anthropogenic sources. Lastly, as shown in Figure 9, the radiative forcings of individual agents can be positive (i.e., a tendency to warm the Earth's surface) or negative (i.e., a tendency to cool the Earth's surface).

### C.1 Observed Changes in Globally Well-Mixed Greenhouse Gas Concentrations and Radiative Forcing

Over the millennium before the Industrial Era, the atmospheric concentrations of greenhouse gases remained relatively constant. Since then, however, the concentrations of many greenhouse gases have increased directly or indirectly because of human activities.

Table 1 provides examples of several greenhouse gases and summarises their 1750 and 1998 concentrations, their change during the 1990s, and their atmospheric lifetimes. The contribution of a species to radiative forcing of climate change depends on the molecular radiative properties of the gas, the size of the increase in atmospheric concentration, and the residence time of the species in the atmosphere, once emitted. *The latter – the atmospheric residence time of the greenhouse gas – is a highly policy relevant characteristic. Namely, emissions of a greenhouse gas that has a long atmospheric residence time is a quasi-irreversible commitment to sustained radiative forcing over decades, centuries, or millennia, before natural processes can remove the quantities emitted.*

**Table 1:** Examples of greenhouse gases that are affected by human activities. [Based upon Chapter 3 and Table 4.1]

	CO <sub>2</sub> (Carbon Dioxide)	CH <sub>4</sub> (Methane)	N <sub>2</sub> O (Nitrous Oxide)	CFC-11 (Chlorofluoro -carbon-11)	HFC-23 (Hydrofluoro -carbon-23)	CF <sub>4</sub> (Perfluoro- methane)
Pre-industrial concentration	about 280 ppm	about 700 ppb	about 270 ppb	zero	zero	40 ppt
Concentration in 1998	365 ppm	1745 ppb	314 ppb	268 ppt	14 ppt	80 ppt
Rate of concentration change <sup>b</sup>	1.5 ppm/yr <sup>a</sup>	7.0 ppb/yr <sup>a</sup>	0.8 ppb/yr	-1.4 ppt/yr	0.55 ppt/yr	1 ppt/yr
Atmospheric lifetime	5 to 200 yr <sup>c</sup>	12 yr <sup>d</sup>	114 yr <sup>d</sup>	45 yr	260 yr	>50,000 yr

<sup>a</sup> Rate has fluctuated between 0.9 ppm/yr and 2.8 ppm/yr for CO<sub>2</sub> and between 0 and 13 ppb/yr for CH<sub>4</sub> over the period 1990 to 1999.

<sup>b</sup> Rate is calculated over the period 1990 to 1999.

<sup>c</sup> No single lifetime can be defined for CO<sub>2</sub> because of the different rates of uptake by different removal processes.

<sup>d</sup> This lifetime has been defined as an “adjustment time” that takes into account the indirect effect of the gas on its own residence time.

## Carbon dioxide ( $\text{CO}_2$ )

The atmospheric concentration of  $\text{CO}_2$  has increased from 280 ppm<sup>5</sup> in 1750 to 367 ppm in 1999 (31%, Table 1). Today's  $\text{CO}_2$  concentration has not been exceeded during the past 420,000 years and likely not during the past 20 million years. The rate of increase over the past century is unprecedented, at least during the past 20,000 years (Figure 10). The  $\text{CO}_2$  isotopic composition and the observed decrease in Oxygen ( $\text{O}_2$ ) demonstrates that the observed increase in  $\text{CO}_2$  is predominately due to the oxidation of organic carbon by fossil-fuel combustion and deforestation. An expanding set of palaeo-atmospheric data from air trapped in ice over hundreds of millennia provide a context for the increase in  $\text{CO}_2$  concentrations during the Industrial Era (Figure 10). Compared to the relatively stable  $\text{CO}_2$  concentrations (280 ± 10 ppm) of the preceding several thousand years, the increase during the Industrial Era is dramatic. The average rate of increase since 1980 is 0.4%/yr. The increase is a consequence of  $\text{CO}_2$  emissions. Most of the emissions during the past 20 years are due to fossil fuel burning, the rest (10 to 30%) is predominantly due to land-use change, especially deforestation. As shown in Figure 9,  $\text{CO}_2$  is the dominant human-influenced greenhouse gas, with a current radiative forcing of 1.46  $\text{W m}^{-2}$ , being 60% of the total from the changes in concentrations of all of the long-lived and globally mixed greenhouse gases.

*Direct atmospheric measurements of  $\text{CO}_2$  concentrations made over the past 40 years show that year to year fluctuations in the rate of increase of atmospheric  $\text{CO}_2$  are large. In the 1990s, the annual rates of  $\text{CO}_2$  increase in the atmosphere varied from 0.9 to 2.8 ppm/yr, equivalent to 1.9 to 6.0 PgC/yr. Such annual changes can be related statistically to short-term climate variability, which alters the rate at which atmospheric  $\text{CO}_2$  is taken up and released by the oceans and land. The highest rates of increase in atmospheric  $\text{CO}_2$  have typically been in strong El Niño years (Box 4). These higher rates of increase can be plausibly explained by reduced terrestrial uptake (or terrestrial outgassing) of  $\text{CO}_2$  during El Niño years, overwhelming the tendency of the ocean to take up more  $\text{CO}_2$  than usual.*

*Partitioning of anthropogenic  $\text{CO}_2$  between atmospheric increases and land and ocean uptake for the past two decades can now be calculated from atmospheric observations. Table 2 presents a global  $\text{CO}_2$  budget for the 1980s (which proves to be similar to the one constructed with the help of ocean model results in the SAR) and for the 1990s. Measurements of the decrease in atmospheric oxygen ( $\text{O}_2$ ) as well as the increase in  $\text{CO}_2$  were used in the construction of these new budgets. Results from this approach are consistent with other analyses based on the isotopic composition of atmospheric  $\text{CO}_2$  and with independent estimates based on measurements of  $\text{CO}_2$  and  $^{13}\text{CO}_2$  in seawater. The 1990s budget is based on newly available measurements and updates the budget for*

**Table 2:** Global  $\text{CO}_2$  budgets (in PgC/yr) based on measurements of atmospheric  $\text{CO}_2$  and  $\text{O}_2$ . Positive values are fluxes to the atmosphere; negative values represent uptake from the atmosphere. [Based upon Tables 3.1 and 3.3]

	SAR <sup>a,b</sup>	This Report <sup>a</sup>	
	1980 to 1989	1980 to 1989	1990 to 1999
Atmospheric increase	3.3 ± 0.1	3.3 ± 0.1	3.2 ± 0.1
Emissions (fossil fuel, cement) <sup>c</sup>	5.5 ± 0.3	5.4 ± 0.3	6.3 ± 0.4
Ocean-atmosphere flux	-2.0 ± 0.5	-1.9 ± 0.6	-1.7 ± 0.5
Land-atmosphere flux <sup>d</sup>	-0.2 ± 0.6	-0.2 ± 0.7	-1.4 ± 0.7

<sup>a</sup> Note that the uncertainties cited in this table are ±1 standard error. The uncertainties cited in the SAR were ±1.6 standard error (i.e., approximately 90% confidence interval). Uncertainties cited from the SAR were adjusted to ±1 standard error. Error bars denote uncertainty, not interannual variability, which is substantially greater.

<sup>b</sup> Previous IPCC carbon budgets calculated ocean uptake from models and the land-atmosphere flux was inferred by difference.

<sup>c</sup> The fossil fuel emissions term for the 1980s has been revised slightly downward since the SAR.

<sup>d</sup> The land-atmosphere flux represents the balance of a positive term due to land-use change and a residual terrestrial sink. The two terms cannot be separated on the basis of current atmospheric measurements. Using independent analyses to estimate the land-use change component for 1980 to 1989, the residual terrestrial sink can be inferred as follows: Land-use change 1.7 PgC/yr (0.6 to 2.5); Residual terrestrial sink -1.9 PgC/yr (-3.8 to 0.3). Comparable data for the 1990s are not yet available.

<sup>5</sup> Atmospheric abundances of trace gases are reported here as the mole fraction (molar mixing ratio) of the gas relative to dry air (ppm =  $10^{-6}$ , ppb =  $10^{-9}$ , ppt =  $10^{-12}$ ). Atmospheric burden is reported as the total mass of the gas (e.g., Mt = Tg =  $10^{12}$  g). The global carbon cycle is expressed in PgC = GtC.

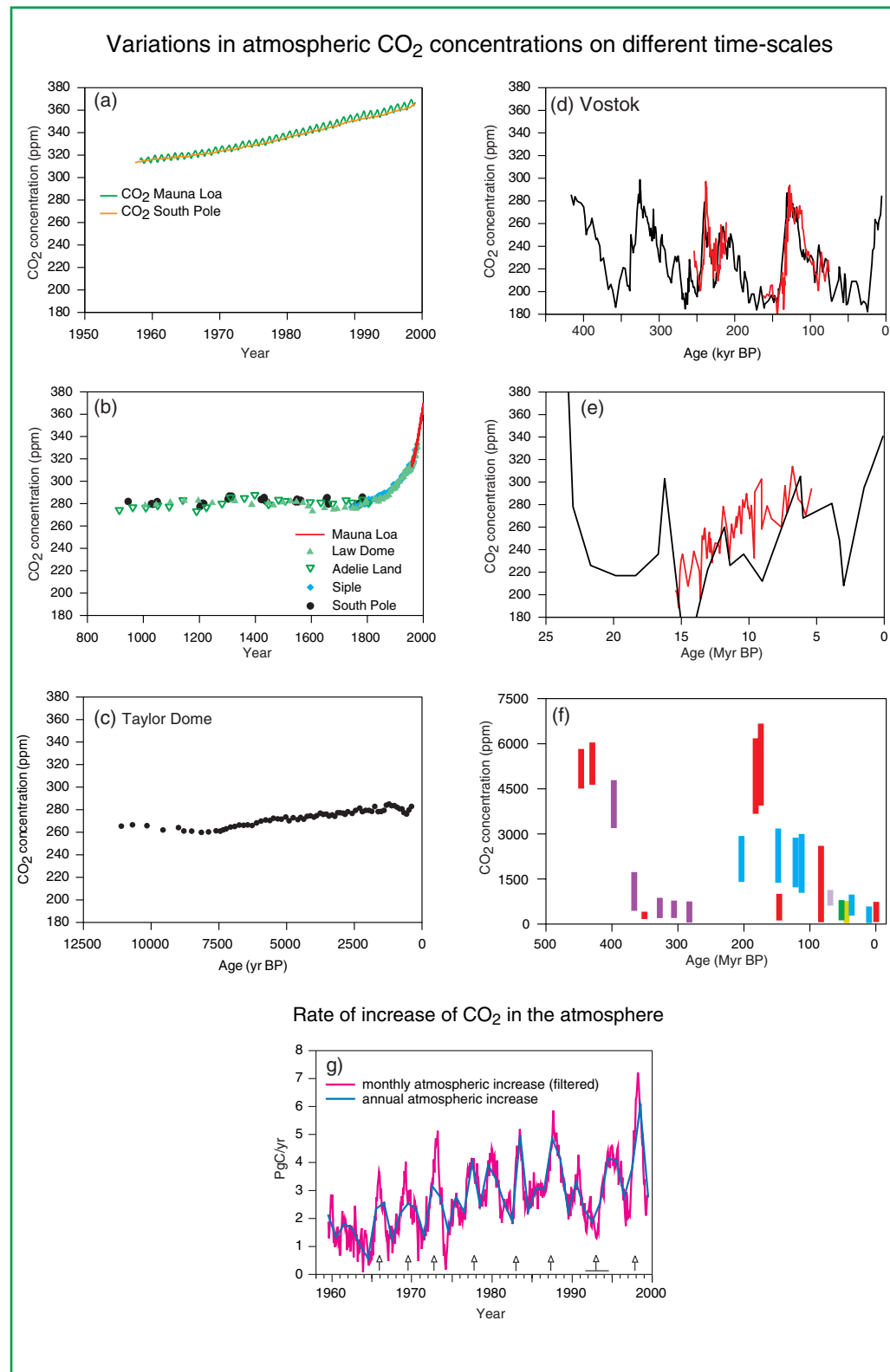


**Figure 10:** Variations in atmospheric CO<sub>2</sub> concentration on different time-scales. (a) Direct measurements of atmospheric CO<sub>2</sub>. (b) CO<sub>2</sub> concentration in Antarctic ice cores for the past millenium. Recent atmospheric measurements (Mauna Loa) are shown for comparison. (c) CO<sub>2</sub> concentration in the Taylor Dome Antarctic ice core. (d) CO<sub>2</sub> concentration in the Vostok Antarctic ice core. (Different colours represent results from different studies.) (e to f) Geochemically inferred CO<sub>2</sub> concentrations. (Coloured bars and lines represent different published studies) (g) Annual atmospheric increases in CO<sub>2</sub>. Monthly atmospheric increases have been filtered to remove the seasonal cycle. Vertical arrows denote El Niño events. A horizontal line defines the extended El Niño of 1991 to 1994. [Based on Figures 3.2 and 3.3]

1989 to 1998 derived using SAR methodology for the IPCC Special Report on Land Use, Land-Use Change and Forestry (2000). The terrestrial biosphere as a whole has gained carbon during the 1980s and 1990s; i.e., the  $\text{CO}_2$  released by land-use change (mainly tropical deforestation) was more than compensated by other terrestrial sinks, which are likely located in both the northern extra-tropics and in the tropics. There remain large uncertainties associated with estimating the  $\text{CO}_2$  release due to land-use change (and, therefore, with the magnitude of the residual terrestrial sink).

*Process-based modelling (terrestrial and ocean carbon models) has allowed preliminary quantification of mechanisms in the global carbon cycle.* Terrestrial model results indicate that enhanced plant growth due to higher  $\text{CO}_2$  ( $\text{CO}_2$  fertilisation) and anthropogenic nitrogen deposition contribute significantly to  $\text{CO}_2$  uptake, i.e., are potentially responsible for the residual terrestrial sink described above, along with other proposed mechanisms, such as changes in land-management practices. The modelled effects of climate change during the 1980s on the terrestrial sink are small and of uncertain sign.

### Methane ( $\text{CH}_4$ )

Atmospheric methane ( $\text{CH}_4$ ) concentrations have increased by about 150% (1,060 ppb) since 1750. The present  $\text{CH}_4$  concentration has not been exceeded during the past 420,000 years. Methane ( $\text{CH}_4$ ) is a greenhouse gas with both natural (e.g., wetlands) and human-influenced sources (e.g., agriculture, natural gas activities, and landfills). Slightly more than half of current  $\text{CH}_4$  emissions are anthropogenic. It is removed from the atmosphere by chemical reactions. As Figure 11 shows, systematic, globally representative measurements of the concentration of  $\text{CH}_4$  in the atmosphere have been made since 1983, and the record of atmospheric concentrations has been extended to earlier times from air extracted from ice cores and firn layers. The current direct radiative forcing of  $0.48 \text{ W m}^{-2}$  from  $\text{CH}_4$  is 20% of the total from all of the long-lived and globally mixed greenhouse gases (see Figure 9).

The atmospheric abundance of  $\text{CH}_4$  continues to increase, from about 1,610 ppb in 1983 to 1,745 ppb in 1998, but the observed annual increase has declined during this period. The increase was highly variable during the 1990s; it was near zero in 1992 and as large as 13 ppb during 1998. There is no clear quantitative explanation for this variability. Since

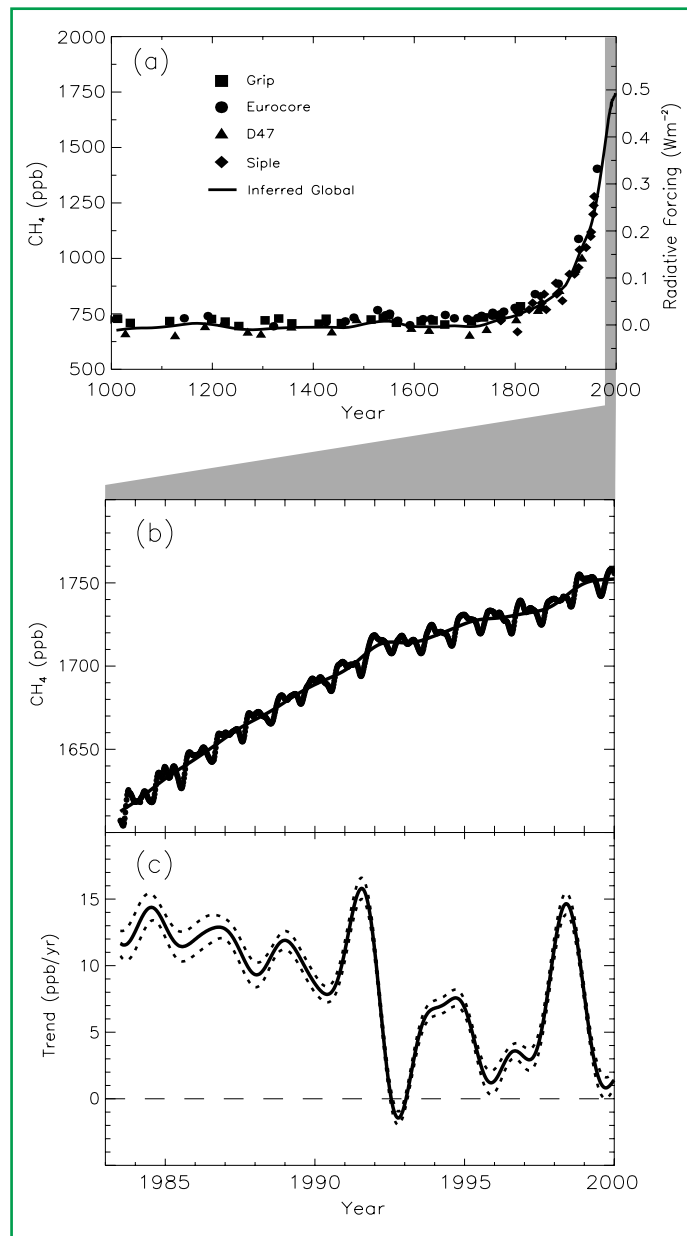


**Figure 11:** (a) Change in  $\text{CH}_4$  abundance (mole fraction, in  $\text{ppb} = 10^{-9}$ ) determined from ice cores, firn, and whole air samples plotted for the last 1000 years. Radiative forcing, approximated by a linear scale since the pre-industrial era, is plotted on the right axis. (b) Globally averaged  $\text{CH}_4$  (monthly varying) and deseasonalised  $\text{CH}_4$  (smooth line) abundance plotted for 1983 to 1999. (c) Instantaneous annual growth rate ( $\text{ppb/yr}$ ) in global atmospheric  $\text{CH}_4$  abundance from 1983 through 1999 calculated as the derivative of the deseasonalised trend curve above. Uncertainties (dotted lines) are  $\pm 1$  standard deviation. [Based on Figure 4.1.]

the SAR, quantification of certain anthropogenic sources of  $\text{CH}_4$ , such as that from rice production, has improved.

*The rate of increase in atmospheric  $\text{CH}_4$  is due to a small imbalance between poorly characterised sources and sinks, which makes the prediction of future concentrations problematic.* Although the major contributors to the global  $\text{CH}_4$  budget likely have been identified, most of them are quite uncertain quantitatively because of the difficulty in assessing emission rates of highly variable biospheric sources. The limitations of poorly quantified and characterised  $\text{CH}_4$  source strengths inhibit the prediction of future  $\text{CH}_4$  atmospheric concentrations (and hence its contribution to radiative forcing) for any given anthropogenic emission scenario, particularly since both natural emissions and the removal of  $\text{CH}_4$  can be influenced substantially by climate change.

### Nitrous oxide ( $\text{N}_2\text{O}$ )

*The atmospheric concentration of nitrous oxide ( $\text{N}_2\text{O}$ ) has steadily increased during the Industrial Era and is now 16% (46 ppb) larger than in 1750.* The present  $\text{N}_2\text{O}$  concentration has not been exceeded during at least the past thousand years. Nitrous oxide is another greenhouse gas with both natural and anthropogenic sources, and it is removed from the atmosphere by chemical reactions. Atmospheric concentrations of  $\text{N}_2\text{O}$  continue to increase at a rate of 0.25%/yr (1980 to 1998). Significant interannual variations in the upward trend of  $\text{N}_2\text{O}$  concentrations are observed, e.g., a 50% reduction in annual growth rate from 1991 to 1993. Suggested causes are several-fold: a decrease in use of nitrogen-based fertiliser, lower biogenic emissions, and larger stratospheric losses due to volcanic-induced circulation changes. Since 1993, the growth of  $\text{N}_2\text{O}$  concentrations has returned to rates closer to those observed during the 1980s. While this observed multi-year variance has provided some potential insight into what processes control the behaviour of atmospheric  $\text{N}_2\text{O}$ , the multi-year trends of this greenhouse gas remain largely unexplained.

*The global budget of nitrous oxide is in better balance than in the SAR, but uncertainties in the emissions from individual sources are still quite large.* Natural sources of  $\text{N}_2\text{O}$  are estimated to be approximately 10 TgN/yr (1990), with soils being about 65% of the sources and oceans about 30%. New, higher estimates of the emissions from anthropogenic sources (agriculture, biomass burning, industrial activities, and livestock management) of approximately 7 TgN/yr have

brought the source/sink estimates closer in balance, compared with the SAR. However, the predictive understanding associated with this significant, long-lived greenhouse gas has not improved significantly since the last assessment. The radiative forcing is estimated at  $0.15 \text{ W m}^{-2}$ , which is 6% of the total from all of the long-lived and globally mixed greenhouse gases (see Figure 9).

### Halocarbons and related compounds

*The atmospheric concentrations of many of those gases that are both ozone-depleting and greenhouse gases are either decreasing (CFC-11, CFC-113,  $\text{CH}_3\text{CCl}_3$  and  $\text{CCl}_4$ ) or increasing more slowly (CFC-12) in response to reduced emissions under the regulations of the Montreal Protocol and its Amendments. Many of these halocarbons are also radiatively effective, long-lived greenhouse gases.*

Halocarbons are carbon compounds that contain fluorine, chlorine, bromine or iodine. For most of these compounds, human activities are the sole source. Halocarbons that contain chlorine (e.g., chlorofluorocarbons - CFCs) and bromine (e.g., halons) cause depletion of the stratospheric ozone layer and are controlled under the Montreal Protocol. The combined tropospheric abundance of ozone-depleting gases peaked in 1994 and is slowly declining. The atmospheric abundances of some of the major greenhouse halocarbons have peaked, as shown for CFC-11 in Figure 12. The concentrations of CFCs and chlorocarbons in the troposphere are consistent with reported emissions. Halocarbons contribute a radiative forcing of  $0.34 \text{ W m}^{-2}$ , which is 14% of the radiative forcing from all of the globally mixed greenhouse gases (Figure 9).

*The observed atmospheric concentrations of the substitutes for the CFCs are increasing, and some of these compounds are greenhouse gases.* The abundances of the hydrochlorofluorocarbons (HCFCs) and hydrofluorocarbons (HFCs) are increasing as a result of continuation of earlier uses and of their use as substitutes for the CFCs. For example, the concentration of HFC-23 has increased by more than a factor of three between 1978 and 1995. Because current concentrations are relatively low, the present contribution of HFCs to radiative forcing is relatively small. The present contribution of HCFCs to radiative forcing is also relatively small, and future emissions of these gases are limited by the Montreal Protocol.

*The perfluorocarbons (PFCs, e.g.,  $\text{CF}_4$  and  $\text{C}_2\text{F}_6$ ) and sulphur hexafluoride ( $\text{SF}_6$ ) have anthropogenic sources, have extremely*

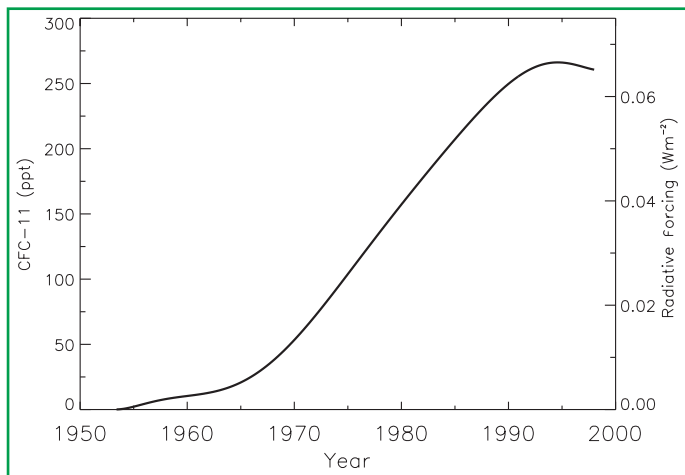


**Figure 12:** Global mean CFC-11 ( $\text{CFCl}_3$ ) tropospheric abundance (ppt) from 1950 to 1998 based on smoothed measurements and emission models. CFC-11's radiative forcing is shown on the right axis. [Based on Figure 4.6]

long atmospheric residence times, and are strong absorbers of infrared radiation. Therefore, these compounds, even with relatively small emissions, have the potential to influence climate far into the future. Perfluoromethane ( $\text{CF}_4$ ) resides in the atmosphere for at least 50,000 years. It has a natural background; however, current anthropogenic emissions exceed natural ones by a factor of 1,000 or more and are responsible for the observed increase. Sulphur hexafluoride ( $\text{SF}_6$ ) is 22,200 times more effective a greenhouse gas than  $\text{CO}_2$  on a per-kg basis. The current atmospheric concentrations are very small (4.2 ppt), but have a significant growth rate (0.24 ppt/yr). There is good agreement between the observed atmospheric growth rate of  $\text{SF}_6$  and the emissions based on revised sales and storage data.

## C.2 Observed Changes in Other Radiatively Important Gases

### Atmospheric ozone ( $\text{O}_3$ )

Ozone ( $\text{O}_3$ ) is an important greenhouse gas present in both the stratosphere and troposphere. The role of ozone in the atmospheric radiation budget is strongly dependent on the altitude at which changes in ozone concentrations occur. The changes in ozone concentrations are also spatially variable.

Further, ozone is not a directly emitted species, but rather it is formed in the atmosphere from photochemical processes involving both natural and human-influenced precursor species. Once formed, the residence time of ozone in the atmosphere is relatively short, varying from weeks to months. As a result, estimation of ozone's radiative role is more complex and much less certain than for the above long-lived and globally well-mixed greenhouse gases.

The observed losses of stratospheric ozone layer over the past two decades have caused a negative forcing of  $0.15 \pm 0.1 \text{ Wm}^{-2}$  (i.e., a tendency toward cooling) of the surface troposphere system. It was reported in Climate Change 1992: The Supplementary Report to the IPCC Scientific Assessment, that depletion of the ozone layer by anthropogenic halocarbons introduces a negative radiative forcing. The estimate shown in Figure 9 is slightly larger in magnitude than that given in the SAR, owing to the ozone depletion that has continued over the past five years, and it is more certain as a result of an increased number of modelling studies. Studies with General Circulation Models indicate that, despite the inhomogeneity in ozone loss (i.e., lower stratosphere at high latitudes), such a negative forcing does relate to a surface temperature decrease in proportion to the magnitude of the negative forcing. Therefore, this negative forcing over the past two decades has offset some of the positive forcing that is occurring from the long-lived and globally well-mixed greenhouse gases (Figure 9). A major source of uncertainty in the estimation of the negative forcing is due to incomplete knowledge of ozone depletion near the tropopause. Model calculations indicate that increased penetration of ultraviolet radiation to the troposphere, as a result of stratospheric ozone depletion, leads to enhanced removal rates of gases like  $\text{CH}_4$ , thus amplifying the negative forcing due to ozone depletion. As the ozone layer recovers in future decades because of the effects of the Montreal Protocol, relative to the present, future radiative forcing associated with stratospheric ozone is projected to become positive.

The global average radiative forcing due to increases in tropospheric ozone since pre-industrial times is estimated to have enhanced the anthropogenic greenhouse gas forcing by  $0.35 \pm 0.2 \text{ Wm}^{-2}$ . This makes tropospheric ozone the third most important greenhouse gas after  $\text{CO}_2$  and  $\text{CH}_4$ . Ozone is formed by photochemical reactions and its future change will be determined by, among other things, emissions of  $\text{CH}_4$  and

pollutants (as noted below). Ozone concentrations respond relatively quickly to changes in the emissions of pollutants. On the basis of limited observations and several modelling studies, tropospheric ozone is estimated to have increased by about 35% since the Pre-industrial Era, with some regions experiencing larger and some with smaller increases. There have been few observed increases in ozone concentrations in the global troposphere since the mid-1980s at most of the few remote locations where it is regularly measured. The lack of observed increase over North America and Europe is related to the lack of a sustained increase in ozone-precursor emissions from those continents. However, some Asian stations indicate a possible rise in tropospheric ozone, which could be related to the increase in East Asian emissions. As a result of more modelling studies than before, there is now an increased confidence in the estimates of tropospheric ozone forcing. The confidence, however, is still much less than that for the well-mixed greenhouse gases, but more so than that for aerosol forcing. Uncertainties arise because of limited information on pre-industrial ozone distributions and limited information to evaluate modelled global trends in the modern era (i.e., post-1960).

### Gases with only indirect radiative influences

Several chemically reactive gases, including reactive nitrogen species ( $\text{NO}_x$ ), carbon monoxide (CO), and the volatile organic compounds (VOCs), control, in part, the oxidising capacity of the troposphere, as well as the abundance of ozone. These pollutants act as indirect greenhouse gases through their influence not only on ozone, but also on the lifetimes of  $\text{CH}_4$  and other greenhouse gases. The emissions of  $\text{NO}_x$  and CO are dominated by human activities.

*Carbon monoxide is identified as an important indirect greenhouse gas.* Model calculations indicate that emission of 100 Mt of CO is equivalent in terms of greenhouse gas perturbations to the emission of about 5 Mt of  $\text{CH}_4$ . The abundance of CO in the Northern Hemisphere is about twice that in the Southern Hemisphere and has increased in the second half of the 20th century along with industrialisation and population.

*The reactive nitrogen species NO and  $\text{NO}_2$ , (whose sum is denoted  $\text{NO}_x$ ), are key compounds in the chemistry of the troposphere, but their overall radiative impact remains difficult to quantify.* The importance of  $\text{NO}_x$  in the radiation budget is because increases in  $\text{NO}_x$  concentrations perturb several greenhouse gases; for example, decreases in methane and the HFCs and increases in tropospheric ozone. Deposition

of the reaction products of  $\text{NO}_x$  fertilises the biosphere, thereby decreasing atmospheric  $\text{CO}_2$ . While difficult to quantify, increases in  $\text{NO}_x$  that are projected to the year 2100 would cause significant changes in greenhouse gases.

### C.3 Observed and Modelled Changes in Aerosols

Aerosols (very small airborne particles and droplets) are known to influence significantly the radiative budget of the Earth/atmosphere. Aerosol radiative effects occur in two distinct ways: (i) the direct effect, whereby aerosols themselves scatter and absorb solar and thermal infrared radiation, and (ii) the indirect effect, whereby aerosols modify the microphysical and hence the radiative properties and amount of clouds. Aerosols are produced by a variety of processes, both natural (including dust storms and volcanic activity) and anthropogenic (including fossil fuel and biomass burning). The atmospheric concentrations of tropospheric aerosols are thought to have increased over recent years due to increased anthropogenic emissions of particles and their precursor gases, hence giving rise to radiative forcing. Most aerosols are found in the lower troposphere (below a few kilometres), but the radiative effect of many aerosols is sensitive to the vertical distribution. Aerosols undergo chemical and physical changes while in the atmosphere, notably within clouds, and are removed largely and relatively rapidly by precipitation (typically within a week). Because of this short residence time and the inhomogeneity of sources, aerosols are distributed inhomogeneously in the troposphere, with maxima near the sources. The radiative forcing due to aerosols depends not only on these spatial distributions, but also on the size, shape, and chemical composition of the particles and various aspects (e.g., cloud formation) of the hydrological cycle as well. As a result of all of these factors, obtaining accurate estimates of this forcing has been very challenging, from both the observational and theoretical standpoints.

*Nevertheless, substantial progress has been achieved in better defining the direct effect of a wider set of different aerosols.* The SAR considered the direct effects of only three anthropogenic aerosol species: sulphate aerosols, biomass-burning aerosols, and fossil fuel black carbon (or soot). Observations have now shown the importance of organic materials in both fossil fuel carbon aerosols and biomass-burning carbon aerosols. Since

the SAR, the inclusion of estimates for the abundance of fossil fuel organic carbon aerosols has led to an increase in the predicted total optical depth (and consequent negative forcing) associated with industrial aerosols. Advances in observations and in aerosol and radiative models have allowed quantitative estimates of these separate components, as well as an estimate for the range of radiative forcing associated with mineral dust, as shown in Figure 9. Direct radiative forcing is estimated to be  $-0.4 \text{ Wm}^{-2}$  for sulphate,  $-0.2 \text{ Wm}^{-2}$  for biomass-burning aerosols,  $-0.1 \text{ Wm}^{-2}$  for fossil fuel organic carbon, and  $+0.2 \text{ Wm}^{-2}$  for fossil fuel black carbon aerosols. Uncertainties remain relatively large, however. These arise from difficulties in determining the concentration and radiative characteristics of atmospheric aerosols and the fraction of the aerosols that are of anthropogenic origin, particularly the knowledge of the sources of carbonaceous aerosols. This leads to considerable differences (i.e., factor of two to three range) in the burden and substantial differences in the vertical distribution (factor of ten). Anthropogenic dust aerosol is also poorly quantified. Satellite observations, combined with model calculations, are enabling the identification of the spatial signature of the total aerosol radiative effect in clear skies; however, the quantitative amount is still uncertain.

*Estimates of the indirect radiative forcing by anthropogenic aerosols remain problematic, although observational evidence points to a negative aerosol-induced indirect forcing in warm clouds.* Two different approaches exist for estimating the indirect effect of aerosols: empirical methods and mechanistic methods. The former have been applied to estimate the effects of industrial aerosols, while the latter have been applied to estimate the effects of sulphate, fossil fuel carbonaceous aerosols, and biomass aerosols. In addition, models for the indirect effect have been used to estimate the effects of the initial change in droplet size and concentrations (a first indirect effect), as well as the effects of the subsequent change in precipitation efficiency (a second indirect effect). The studies represented in Figure 9 provide an expert judgement for the range of the first of these; the range is now slightly wider than in the SAR; the radiative perturbation associated with the second indirect effect is of the same sign and could be of similar magnitude compared to the first effect.

*The indirect radiative effect of aerosols is now understood to also encompass effects on ice and mixed-phase clouds, but the*

*magnitude of any such indirect effect is not known, although it is likely to be positive.* It is not possible to estimate the number of anthropogenic ice nuclei at the present time. Except at cold temperatures (below  $-45^\circ\text{C}$ ) where homogeneous nucleation is expected to dominate, the mechanisms of ice formation in these clouds are not yet known.

#### C.4 Observed Changes in Other Anthropogenic Forcing Agents

##### Land-use (albedo) change

*Changes in land use, deforestation being the major factor, appear to have produced a negative radiative forcing of  $-0.2 \pm 0.2 \text{ Wm}^{-2}$  (Figure 8).* The largest effect is estimated to be at the high latitudes. This is because deforestation has caused snow-covered forests with relatively low albedo to be replaced with open, snow-covered areas with higher albedo. The estimate given above is based on simulations in which pre-industrial vegetation is replaced by current land-use patterns. However, the level of understanding is very low for this forcing, and there have been far fewer investigations of this forcing compared to investigations of other factors considered in this report.

#### C.5 Observed and Modelled Changes in Solar and Volcanic Activity

*Radiative forcing of the climate system due to solar irradiance change is estimated to be  $0.3 \pm 0.2 \text{ Wm}^{-2}$  for the period 1750 to the present (Figure 8), and most of the change is estimated to have occurred during the first half of the 20th century.* The fundamental source of all energy in the Earth's climate system is radiation from the Sun. Therefore, variation in solar output is a radiative forcing agent. The absolute value of the spectrally integrated total solar irradiance (TSI) incident on the Earth is not known to better than about  $4 \text{ Wm}^{-2}$ , but satellite observations since the late 1970s show relative variations over the past two solar 11-year activity cycles of about 0.1%, which is equivalent to a variation in radiative forcing of about  $0.2 \text{ Wm}^{-2}$ . Prior to these satellite observations, reliable direct measurements of solar irradiance are not available. Variations over longer periods may have been larger, but the techniques used to reconstruct historical values of TSI from proxy observations (e.g., sunspots) have not been adequately verified. Solar variation varies more substantially in the ultraviolet region, and studies with climate models suggest that inclusion of spectrally resolved solar irradiance variations and solar-

induced stratospheric ozone changes may improve the realism of model simulations of the impact of solar variability on climate. Other mechanisms for the amplification of solar effects on climate have been proposed, but do not have a rigorous theoretical or observational basis.

Stratospheric aerosols from explosive volcanic eruptions lead to negative forcing that lasts a few years. Several explosive eruptions occurred in the periods 1880 to 1920 and 1960 to 1991, and no explosive eruptions since 1991. Enhanced stratospheric aerosol content due to volcanic eruptions, together with the small solar irradiance variations, result in a net negative natural radiative forcing over the past two, and possibly even the past four, decades.

### C.6 Global Warming Potentials

*Radiative forcings and Global Warming Potentials (GWPs) are presented in Table 3 for an expanded set of gases.* GWPs are a measure of the relative radiative effect of a given substance compared to CO<sub>2</sub>, integrated over a chosen time horizon. New categories of gases in Table 3 include fluorinated organic molecules, many of which are ethers that are proposed as halocarbon substitutes. Some of the GWPs have larger uncertainties than that of others, particularly for those gases where detailed laboratory data on lifetimes are not yet available. The direct GWPs have been calculated relative to CO<sub>2</sub> using an improved calculation of the CO<sub>2</sub> radiative forcing, the SAR response function for a CO<sub>2</sub> pulse, and new values for the radiative forcing and lifetimes for a number of halocarbons. Indirect GWPs, resulting from indirect radiative forcing effects, are also estimated for some new gases, including carbon monoxide. The direct GWPs for those species whose lifetimes are well characterised are estimated to be accurate within ±35%, but the indirect GWPs are less certain.

## D. The Simulation of the Climate System and its Changes

The preceding two Sections reported on the climate from the distant past to the present day through the observations of climate variables and the forcing agents that cause climate to change. This Section bridges to the climate of the future by describing the only tool that provides quantitative estimates of future climate changes, namely, numerical models. The basic understanding of the energy balance of the Earth system means that quite simple models can provide a broad quantitative estimate of some globally averaged variables, but more accurate estimates of feedbacks and of regional detail can only come from more elaborate climate models. The complexity of the processes in the climate system prevents the use of extrapolation of past trends or statistical and other purely empirical techniques for projections. Climate models can be used to simulate the climate responses to different input scenarios of future forcing agents (Section F). Similarly, projection of the fate of emitted CO<sub>2</sub> (i.e., the relative sequestration into the various reservoirs) and other greenhouse gases requires an understanding of the biogeochemical processes involved and incorporating these into a numerical carbon cycle model.

A climate model is a simplified mathematical representation of the Earth's climate system (see Box 3). The degree to which the model can simulate the responses of the climate system hinges to a very large degree on the level of understanding of the physical, geophysical, chemical and biological processes that govern the climate system. Since the SAR, researchers have made substantial improvements in the simulation of the Earth's climate system with models. First, the current understanding of some of the most important processes that govern the climate system and how well they are represented in present climate models are summarised here. Then, this Section presents an assessment of the overall ability of present models to make useful projections of future climate.

### D.1 Climate Processes and Feedbacks

Processes in the climate system determine the natural variability of the climate system and its response to perturbations, such as the increase in the atmospheric concentrations of greenhouse gases. Many basic climate processes of importance are well-known and modelled exceedingly well. Feedback processes amplify (a positive feedback) or reduce (a negative

**Table 3:** Direct Global Warming Potentials (GWPs) relative to carbon dioxide (for gases for which the lifetimes have been adequately characterised). GWPs are an index for estimating relative global warming contribution due to atmospheric emission of a kg of a particular greenhouse gas compared to emission of a kg of carbon dioxide. GWPs calculated for different time horizons show the effects of atmospheric lifetimes of the different gases. [Based upon Table 6.7]

Gas		Lifetime (years)	Global Warming Potential (Time Horizon in years)		
			20 yrs	100 yrs	500 yrs
Carbon dioxide	CO <sub>2</sub>		1	1	1
Methane <sup>a</sup>	CH <sub>4</sub>	12.0 <sup>b</sup>	62	23	7
Nitrous oxide	N <sub>2</sub> O	114 <sup>b</sup>	275	296	156
<b>Hydrofluorocarbons</b>					
HFC-23	CHF <sub>3</sub>	260	9400	12000	10000
HFC-32	CH <sub>2</sub> F <sub>2</sub>	5.0	1800	550	170
HFC-41	CH <sub>3</sub> F	2.6	330	97	30
HFC-125	CHF <sub>2</sub> CF <sub>3</sub>	29	5900	3400	1100
HFC-134	CHF <sub>2</sub> CHF <sub>2</sub>	9.6	3200	1100	330
HFC-134a	CH <sub>2</sub> FCF <sub>3</sub>	13.8	3300	1300	400
HFC-143	CHF <sub>2</sub> CH <sub>2</sub> F	3.4	1100	330	100
HFC-143a	CF <sub>3</sub> CH <sub>3</sub>	52	5500	4300	1600
HFC-152	CH <sub>2</sub> FCH <sub>2</sub> F	0.5	140	43	13
HFC-152a	CH <sub>3</sub> CHF <sub>2</sub>	1.4	410	120	37
HFC-161	CH <sub>3</sub> CH <sub>2</sub> F	0.3	40	12	4
HFC-227ea	CF <sub>3</sub> CHFCF <sub>3</sub>	33	5600	3500	1100
HFC-236cb	CH <sub>2</sub> FCF <sub>2</sub> CF <sub>3</sub>	13.2	3300	1300	390
HFC-236ea	CHF <sub>2</sub> CHFCF <sub>3</sub>	10	3600	1200	390
HFC-236fa	CF <sub>3</sub> CH <sub>2</sub> CF <sub>3</sub>	220	7500	9400	7100
HFC-245ca	CH <sub>2</sub> FCF <sub>2</sub> CHF <sub>2</sub>	5.9	2100	640	200
HFC-245fa	CHF <sub>2</sub> CH <sub>2</sub> CF <sub>3</sub>	7.2	3000	950	300
HFC-365mfc	CF <sub>3</sub> CH <sub>2</sub> CF <sub>2</sub> CH <sub>3</sub>	9.9	2600	890	280
HFC-43-10mee	CF <sub>3</sub> CHFCF <sub>2</sub> CF <sub>3</sub>	15	3700	1500	470
<b>Fully fluorinated species</b>					
SF <sub>6</sub>		3200	15100	22200	32400
CF <sub>4</sub>		50000	3900	5700	8900
C <sub>2</sub> F <sub>6</sub>		10000	8000	11900	18000
C <sub>2</sub> F <sub>8</sub>		2600	5900	8600	12400
C <sub>4</sub> F <sub>10</sub>		2600	5900	8600	12400
c-C <sub>4</sub> F <sub>8</sub>		3200	6800	10000	14500
C <sub>5</sub> F <sub>12</sub>		4100	6000	8900	13200
C <sub>6</sub> F <sub>14</sub>		3200	6100	9000	13200
<b>Ethers and Halogenated Ethers</b>					
CH <sub>3</sub> OCH <sub>3</sub>		0.015	1	1	<<1
HFE-125	CF <sub>3</sub> OCHF <sub>2</sub>	150	12900	14900	9200
HFE-134	CHF <sub>2</sub> OCHF <sub>2</sub>	26.2	10500	6100	2000
HFE-143a	CH <sub>3</sub> OCF <sub>3</sub>	4.4	2500	750	230
HCFE-235da2	CF <sub>3</sub> CHClOCHF <sub>2</sub>	2.6	1100	340	110
HFE-245fa2	CF <sub>3</sub> CH <sub>2</sub> OCHF <sub>2</sub>	4.4	1900	570	180
HFE-254cb2	CHF <sub>2</sub> CF <sub>2</sub> OCH <sub>3</sub>	0.22	99	30	9
HFE-7100	C <sub>4</sub> F <sub>9</sub> OCH <sub>3</sub>	5.0	1300	390	120
HFE-7200	C <sub>4</sub> F <sub>9</sub> OC <sub>2</sub> H <sub>5</sub>	0.77	190	55	17
H-Galden 1040x	CHF <sub>2</sub> OCF <sub>2</sub> OC <sub>2</sub> F <sub>4</sub> OCHF <sub>2</sub>	6.3	5900	1800	560
HG-10	CHF <sub>2</sub> OCF <sub>2</sub> OCHF <sub>2</sub>	12.1	7500	2700	850
HG-01	CHF <sub>2</sub> OCF <sub>2</sub> CF <sub>2</sub> OCHF <sub>2</sub>	6.2	4700	1500	450

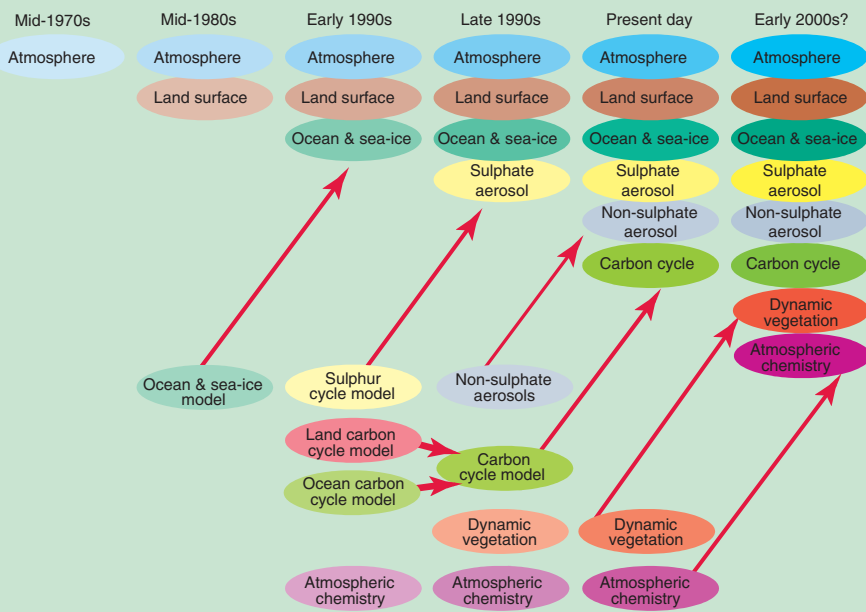
<sup>a</sup> The methane GWPs include an indirect contribution from stratospheric H<sub>2</sub>O and O<sub>3</sub> production.

<sup>b</sup> The values for methane and nitrous oxide are adjustment times, which incorporate the indirect effects of emission of each gas on its own lifetime.

### Box 3: Climate Models: How are they built and how are they applied?

Comprehensive climate models are based on physical laws represented by mathematical equations that are solved using a three-dimensional grid over the globe. For climate simulation, the major components of the climate system must be represented in sub-models (atmosphere, ocean, land surface, cryosphere and biosphere), along with the processes that go on within and between them. Most results in this report are derived from the results of models, which include some representation of all these components. Global climate models in which the atmosphere and ocean components have been coupled together are also known as Atmosphere-Ocean General Circulation Models (AOGCMs). In the atmospheric module, for example, equations are solved that describe the large-scale evolution of momentum, heat and moisture. Similar equations are solved for the ocean. Currently, the resolution of the atmospheric part of a typical model is about 250 km in the horizontal and about 1 km in the vertical above the boundary layer. The resolution of a typical ocean model is about 200 to 400 m in the vertical, with a horizontal resolution of about 125 to 250 km. Equations are typically solved for every half hour of a model integration. Many physical processes, such as those related to clouds or ocean convection, take place on much smaller spatial scales than the model grid and therefore cannot be modelled and resolved explicitly. Their average effects are approximately included in a simple way by taking advantage of

### The Development of Climate models, Past, Present and Future



**Box 3, Figure 1:** The development of climate models over the last 25 years showing how the different components are first developed separately and later coupled into comprehensive climate models.

physically based relationships with the larger-scale variables. This technique is known as parametrization.

In order to make quantitative projections of future climate change, it is necessary to use climate models that simulate all the important processes governing the future evolution of the climate. Climate models have developed over the past few decades as computing power has increased. During that time, models of the main components, atmosphere, land, ocean and sea ice have been developed separately and then gradually integrated. This coupling of the various components is a difficult process. Most recently, sulphur cycle components

have been incorporated to represent the emissions of sulphur and how they are oxidised to form aerosol particles.

Currently in progress, in a few models, is the coupling of the land carbon cycle and the ocean carbon cycle. The atmospheric chemistry component currently is modelled outside the main climate model. The ultimate aim is, of course, to model as much as possible of the whole of the Earth's climate system so that all the components can interact and, thus, the predictions of climate change will continuously take into account the effect of feedbacks among components. The Figure above shows the past, present and possible future evolution of climate models.

Some models offset errors and surface flux imbalances through “flux adjustments”, which are empirically determined systematic adjustments at the atmosphere-ocean interface held fixed in time in order to bring the simulated climate closer to the observed state. A strategy has been designed for carrying out climate experiments that removes much of the effects of some model errors on results. What is often done is that first a “control” climate simulation is run with the model. Then, the climate change experiment simulation is run, for example, with increased CO<sub>2</sub> in the model atmosphere. Finally, the difference is taken to provide an estimate of the change in climate due to the perturbation. The differencing technique removes most of the effects of any artificial adjustments in the model, as well as systematic errors that are common to both runs. However, a comparison of different model results makes it apparent that the nature of some errors still influences the outcome.

Many aspects of the Earth’s climate system are chaotic – its evolution is sensitive to small perturbations in initial conditions. This sensitivity limits predictability of the detailed evolution of weather to about two weeks. However, predictability of climate is not so limited because of the systematic influences on the atmosphere of the more slowly varying components of the climate system. Nevertheless, to be able to make reliable forecasts in the presence of both initial condition and model uncertainty, it is desirable to repeat the prediction many times from different perturbed initial states and using different global models. These ensembles are the basis of probability forecasts of the climate state.

Comprehensive AOGCMs are very complex and take large computer resources to run. To explore different scenarios of emissions of greenhouse gases and the effects of assumptions or approximations in parameters in the model more thoroughly, simpler models are also widely used. The simplifications may include coarser resolution and simplified dynamics and physical processes. Together, simple, intermediate, and comprehensive models form a “hierarchy of climate models”, all of which are necessary to explore choices made in parametrizations and assess the robustness of climate changes.

feedback) changes in response to an initial perturbation and hence are very important for accurate simulation of the evolution of climate.

### Water vapour

*A major feedback accounting for the large warming predicted by climate models in response to an increase in CO<sub>2</sub> is the increase in atmospheric water vapour.* An increase in the temperature of the atmosphere increases its water-holding capacity; however, since most of the atmosphere is undersaturated, this does not automatically mean that water vapour, itself, must increase. Within the boundary layer (roughly the lowest 1 to 2 km of the atmosphere), water vapour increases with increasing temperature. In the free troposphere above the boundary layer, where the water vapour greenhouse effect is most important, the situation is harder to quantify. Water vapour feedback, as derived from current models, approximately doubles the warming from what it would be for fixed water vapour. Since the SAR, major improvements have occurred in the treatment of water vapour in models, although detrainment of moisture from clouds remains quite uncertain and discrepancies exist between model water vapour distributions and those observed. Models are capable of simulating the moist and very dry regions observed in the tropics and sub-tropics and how they evolve with the seasons and from year to year. While reassuring, this does not provide a check of the feedbacks, although the balance of evidence favours a positive clear-sky water vapour feedback of the magnitude comparable to that found in simulations.

### Clouds

As has been the case since the first IPCC Assessment Report in 1990, probably the greatest uncertainty in future projections of climate arises from clouds and their interactions with radiation. Clouds can both absorb and reflect solar radiation (thereby cooling the surface) and absorb and emit long wave radiation (thereby warming the surface). The competition between these effects depends on cloud height, thickness and radiative properties. The radiative properties and evolution of clouds depend on the distribution of atmospheric water vapour, water drops, ice particles, atmospheric aerosols and cloud thickness. The physical basis of cloud parametrizations is greatly improved in models through inclusion of bulk representation of cloud microphysical properties in a cloud water budget equation, although considerable uncertainty remains. Clouds represent a significant source of potential error in climate simulations. The possibility that models underestimate systematically solar

absorption in clouds remains a controversial matter. The sign of the net cloud feedback is still a matter of uncertainty, and the various models exhibit a large spread. Further uncertainties arise from precipitation processes and the difficulty in correctly simulating the diurnal cycle and precipitation amounts and frequencies.

### Stratosphere

*There has been a growing appreciation of the importance of the stratosphere in the climate system because of changes in its structure and recognition of the vital role of both radiative and dynamical processes.* The vertical profile of temperature change in the atmosphere, including the stratosphere, is an important indicator in detection and attribution studies. Most of the observed decreases in lower-stratospheric temperatures have been due to ozone decreases, of which the Antarctic “ozone hole” is a part, rather than increased CO<sub>2</sub> concentrations. Waves generated in the troposphere can propagate into the stratosphere where they are absorbed. As a result, stratospheric changes alter where and how these waves are absorbed, and the effects can extend downward into the troposphere. Changes in solar irradiance, mainly in the ultraviolet (UV), lead to photochemically-induced ozone changes and, hence, alter the stratospheric heating rates, which can alter the tropospheric circulation. Limitations in resolution and relatively poor representation of some stratospheric processes adds uncertainty to model results.

### Ocean

*Major improvements have taken place in modelling ocean processes, in particular heat transport. These improvements, in conjunction with an increase in resolution, have been important in reducing the need for flux adjustment in models and in producing realistic simulations of natural large-scale circulation patterns and improvements in simulating El Niño (see Box 4).* Ocean currents carry heat from the tropics to higher latitudes. The ocean exchanges heat, water (through evaporation and precipitation) and CO<sub>2</sub> with the atmosphere. Because of its huge mass and high heat capacity, the ocean slows climate change and influences the time-scales of variability in the ocean-atmosphere system. Considerable progress has been made in the understanding of ocean processes relevant for climate change. Increases in resolution, as well as improved representation (parametrization) of important sub-grid scale processes (e.g., mesoscale eddies), have increased the realism of simulations. Major uncertainties

still exist with the representation of small-scale processes, such as overflows (flow through narrow channels, e.g., between Greenland and Iceland), western boundary currents (i.e., large-scale narrow currents along coastlines), convection and mixing. Boundary currents in climate simulations are weaker and wider than in nature, although the consequences of this for climate are not clear.

### Cryosphere

*The representation of sea-ice processes continues to improve, with several climate models now incorporating physically based treatments of ice dynamics. The representation of land-ice processes in global climate models remains rudimentary.* The cryosphere consists of those regions of Earth that are seasonally or perennially covered by snow and ice. Sea ice is important because it reflects more incoming solar radiation than the sea surface (i.e., it has a higher albedo), and it insulates the sea from heat loss during the winter. Therefore, reduction of sea ice gives a positive feedback on climate warming at high latitudes. Furthermore, because sea ice contains less salt than sea water, when sea ice is formed the salt content (salinity) and density of the surface layer of the ocean is increased. This promotes an exchange of water with deeper layers of the ocean, affecting ocean circulation. The formation of icebergs and the melting of ice shelves returns fresh water from the land to the ocean, so that changes in the rates of these processes could affect ocean circulation by changing the surface salinity. Snow has a higher albedo than the land surface; hence, reductions in snow cover lead to a similar positive albedo feedback, although weaker than for sea ice. Increasingly complex snow schemes and sub-grid scale variability in ice cover and thickness, which can significantly influence albedo and atmosphere-ocean exchanges, are being introduced in some climate models.

### Land surface

*Research with models containing the latest representations of the land surface indicates that the direct effects of increased CO<sub>2</sub> on the physiology of plants could lead to a relative reduction in evapotranspiration over the tropical continents, with associated regional warming and drying over that predicted for conventional greenhouse warming effects.* Land surface changes provide important feedbacks as anthropogenic climate changes (e.g., increased temperature, changes in precipitation, changes in net radiative heating, and the direct effects of CO<sub>2</sub>) will influence the state of the land surface (e.g., soil moisture, albedo, roughness and vegetation). Exchanges of

energy, momentum, water, heat and carbon between the land surface and the atmosphere can be defined in models as functions of the type and density of the local vegetation and the depth and physical properties of the soil, all based on land-surface data bases that have been improved using satellite observations. Recent advances in the understanding of vegetation photosynthesis and water use have been used to couple the terrestrial energy, water and carbon cycles within a new generation of land surface parametrizations, which have been tested against field observations and implemented in a few GCMs, with demonstrable improvements in the simulation of land-atmosphere fluxes. However, significant problems remain to be solved in the areas of soil moisture processes, runoff prediction, land-use change and the treatment of snow and sub-grid scale heterogeneity.

Changes in land-surface cover can affect global climate in several ways. Large-scale deforestation in the humid tropics (e.g., South America, Africa, and Southeast Asia) has been identified as the most important ongoing land-surface process, because it reduces evaporation and increases surface temperature. These effects are qualitatively reproduced by most models. However, large uncertainties still persist on the quantitative impact of large-scale deforestation on the hydrological cycle, particularly over Amazonia.

### **Carbon cycle**

*Recent improvements in process-based terrestrial and ocean carbon cycle models and their evaluation against observations have given more confidence in their use for future scenario studies.* CO<sub>2</sub> naturally cycles rapidly among the atmosphere, oceans and land. However, the removal of the CO<sub>2</sub> perturbation added by human activities from the atmosphere takes far longer. This is because of processes that limit the rate at which ocean and terrestrial carbon stocks can increase. Anthropogenic CO<sub>2</sub> is taken up by the ocean because of its high solubility (caused by the nature of carbonate chemistry), but the rate of uptake is limited by the finite speed of vertical mixing. Anthropogenic CO<sub>2</sub> is taken up by terrestrial ecosystems through several possible mechanisms, for example, land management, CO<sub>2</sub> fertilisation (the enhancement of plant growth as a result of increased atmospheric CO<sub>2</sub> concentration) and increasing anthropogenic inputs of nitrogen. This uptake is limited by the relatively small fraction of plant carbon that can enter long-term storage (wood and humus). The fraction of emitted CO<sub>2</sub> that can be taken up by the oceans and land is expected to decline with increasing CO<sub>2</sub>

concentrations. Process-based models of the ocean and land carbon cycles (including representations of physical, chemical and biological processes) have been developed and evaluated against measurements pertinent to the natural carbon cycle. Such models have also been set up to mimic the human perturbation of the carbon cycle and have been able to generate time-series of ocean and land carbon uptake that are broadly consistent with observed global trends. There are still substantial differences among models, especially in how they treat the physical ocean circulation and in regional responses of terrestrial ecosystem processes to climate. Nevertheless, current models consistently indicate that when the effects of climate change are considered, CO<sub>2</sub> uptake by oceans and land becomes smaller.

### **D.2 The Coupled Systems**

As noted in Section D.1, many feedbacks operate within the individual components of the climate system (atmosphere, ocean, cryosphere and land surface). However, many important processes and feedbacks occur through the coupling of the climate system components. Their representation is important to the prediction of large-scale responses.

#### **Modes of natural variability**

*There is an increasing realisation that natural circulation patterns, such as ENSO and NAO, play a fundamental role in global climate and its interannual and longer-term variability.* The strongest natural fluctuation of climate on interannual time-scales is the ENSO phenomenon (see Box 4). It is an inherently coupled atmosphere-ocean mode with its core activity in the tropical Pacific, but with important regional climate impacts throughout the world. Global climate models are only now beginning to exhibit variability in the tropical Pacific that resembles ENSO, mainly through increased meridional resolution at the equator. Patterns of sea surface temperature and atmospheric circulation similar to those occurring during ENSO on interannual time-scales also occur on decadal and longer time-scales.

*The North Atlantic Oscillation (NAO) is the dominant pattern of northern wintertime atmospheric circulation variability and is increasingly being simulated realistically.* The NAO is closely related to the Arctic Oscillation (AO), which has an additional annular component around the Arctic. There is strong evidence that the NAO arises mainly from internal atmospheric processes involving the entire troposphere-stratosphere system.

### Box 4: The El Niño-Southern Oscillation (ENSO)

The strongest natural fluctuation of climate on interannual time-scales is the El Niño-Southern Oscillation (ENSO) phenomenon. The term “El Niño” originally applied to an annual weak warm ocean current that ran southwards along the coast of Peru about Christmas-time and only subsequently became associated with the unusually large warmings. The coastal warming, however, is often associated with a much more extensive anomalous ocean warming to the International Dateline, and it is this Pacific basinwide phenomenon that forms the link with the anomalous global climate patterns. The atmospheric component tied to “El Niño” is termed the “Southern Oscillation”. Scientists often call this phenomenon, where the atmosphere and ocean collaborate together, ENSO (El Niño-Southern Oscillation).

ENSO is a natural phenomenon, and there is good evidence from cores of coral and glacial ice in the Andes that it has been going on for millennia. The ocean and atmospheric conditions in the tropical Pacific are seldom average, but instead fluctuate somewhat irregularly between El Niño events and the opposite “La Niña” phase, consisting of a basinwide cooling of the tropical Pacific, with a preferred period of about three to six years. The most intense phase of each event usually lasts about a year.

A distinctive pattern of sea surface temperatures in the Pacific Ocean sets the stage for ENSO events. Key features are the “warm pool” in the tropical western Pacific, where the warmest ocean waters in the world reside, much colder waters in the eastern Pacific, and a cold tongue along the equator that is most pronounced about October and weakest in March. The atmospheric easterly trade winds in the tropics pile up the warm waters in the west, producing an upward slope of sea level along the equator of 0.60 m from east to west. The winds drive the surface ocean currents, which determine where the surface waters flow and diverge. Thus, cooler nutrient-rich waters upwell from below along the equator and western coasts of the Americas, favouring development of phytoplankton, zooplankton, and hence fish. Because convection and thunderstorms preferentially occur over warmer waters, the pattern of sea surface temperatures determines the distribution of rainfall in the tropics, and this in turn determines the atmospheric heating patterns through the release of latent heat. The heating drives the large-scale monsoonal-type circulations in the tropics, and consequently determines the winds. This strong coupling between the atmosphere and ocean in the tropics gives rise to the El Niño phenomenon.

During El Niño, the warm waters from the western tropical Pacific migrate eastward as the trade winds weaken, shifting the pattern of tropical rainstorms, further weakening the trade winds, and thus reinforcing the changes in sea temperatures. Sea level drops in the west, but rises in the east by as much as 0.25 m, as warm waters surge eastward along the equator. However, the changes in atmospheric circulation are not confined to the tropics, but extend globally and influence the jet streams and storm tracks in mid-latitudes. Approximately reverse patterns occur during the opposite La Niña phase of the phenomenon.

Changes associated with ENSO produce large variations in weather and climate around the world from year to year. These often have a profound impact on humanity and society because of associated droughts, floods, heat waves and other changes that can severely disrupt agriculture, fisheries, the environment, health, energy demand, air quality and also change the risks of fire. ENSO also plays a prominent role in modulating exchanges of CO<sub>2</sub> with the atmosphere. The normal upwelling of cold nutrient-rich and CO<sub>2</sub>-rich waters in the tropical Pacific is suppressed during El Niño.

Fluctuations in Atlantic Sea Surface Temperatures (SSTs) are related to the strength of the NAO, and a modest two-way interaction between the NAO and the Atlantic Ocean, leading to decadal variability, is emerging as important in projecting climate change.

*Climate change may manifest itself both as shifting means, as well as changing preference of specific climate regimes, as*

*evidenced by the observed trend toward positive values for the last 30 years in the NAO index and the climate “shift” in the tropical Pacific about 1976. While coupled models simulate features of observed natural climate variability, such as the NAO and ENSO, which suggests that many of the relevant processes are included in the models, further progress is needed to depict these natural modes accurately. Moreover,*

because ENSO and NAO are key determinants of regional climate change and can possibly result in abrupt and counter intuitive changes, there has been an increase in uncertainty in those aspects of climate change that critically depend on regional changes.

#### **The thermohaline circulation (THC)**

*The thermohaline circulation (THC) is responsible for the major part of the meridional heat transport in the Atlantic Ocean.* The THC is a global-scale overturning in the ocean driven by density differences arising from temperature and salinity effects. In the Atlantic, heat is transported by warm surface waters flowing northward and cold saline waters from the North Atlantic returning at depth. Reorganisations in the Atlantic THC can be triggered by perturbations in the surface buoyancy, which is influenced by precipitation, evaporation, continental runoff, sea-ice formation, and the exchange of heat, processes that could all change with consequences for regional and global climate. Interactions between the atmosphere and the ocean are also likely to be of considerable importance on decadal and longer time-scales, where the THC is involved. The interplay between the large-scale atmospheric forcing, with warming and evaporation in low latitudes and cooling and increased precipitation at high latitudes, forms the basis of a potential instability of the present Atlantic THC. ENSO may also influence the Atlantic THC by altering the fresh water balance of the tropical Atlantic, therefore providing a coupling between low and high latitudes. Uncertainties in the representation of small-scale flows over sills and through narrow straits and of ocean convection limit the ability of models to simulate situations involving substantial changes in the THC. The less saline North Pacific means that a deep THC does not occur in the Pacific.

#### **Non-linear events and rapid climate change**

*The possibility for rapid and irreversible changes in the climate system exists, but there is a large degree of uncertainty about the mechanisms involved and hence also about the likelihood or time-scales of such transitions.* The climate system involves many processes and feedbacks that interact in complex non-linear ways. This interaction can give rise to thresholds in the climate system that can be crossed if the system is perturbed sufficiently. There is evidence from polar ice cores suggesting that atmospheric regimes can change within a few years and that large-scale hemispheric changes can evolve as fast as a few decades. For example, the possibility of a threshold for a rapid transition of the Atlantic THC to a collapsed state has been

demonstrated with a hierarchy of models. It is not yet clear what this threshold is and how likely it is that human activity would lead it to being exceeded (see Section F.6). Atmospheric circulation can be characterised by different preferred patterns; e.g., arising from ENSO and the NAO/AO, and changes in their phase can occur rapidly. Basic theory and models suggest that climate change may be first expressed in changes in the frequency of occurrence of these patterns. Changes in vegetation, through either direct anthropogenic deforestation or those caused by global warming, could occur rapidly and could induce further climate change. It is supposed that the rapid creation of the Sahara about 5,500 years ago represents an example of such a non-linear change in land cover.

#### **D.3 Regionalisation Techniques**

*Regional climate information was only addressed to a limited degree in the SAR. Techniques used to enhance regional detail have been substantially improved since the SAR and have become more widely applied.* They fall into three categories: high and variable resolution AOGCMs; regional (or nested limited area) climate models (RCMs); and empirical/statistical and statistical/dynamical methods. The techniques exhibit different strengths and weaknesses and their use at the continental scale strongly depends on the needs of specific applications.

*Coarse resolution AOGCMs simulate atmospheric general circulation features well in general.* At the regional scale, the models display area-average biases that are highly variable from region to region and among models, with sub-continental area averaged seasonal temperature biases typically  $\pm 4^{\circ}\text{C}$  and precipitation biases between  $-40$  and  $+80\%$ . These represent an important improvement compared to AOGCMs evaluated in the SAR.

*The development of high resolution/variable resolution Atmospheric General Circulation Models (AGCMs) since the SAR generally shows that the dynamics and large-scale flow in the models improves as resolution increases.* In some cases, however, systematic errors are worsened compared to coarser resolution models, although only very few results have been documented.

*High resolution RCMs have matured considerably since the SAR.* Regional models consistently improve the spatial detail of simulated climate compared to AGCMs. RCMs driven by

observed boundary conditions evidence area-averaged temperature biases (regional scales of  $10^5$  to  $10^6 \text{ km}^2$ ) generally below  $2^\circ\text{C}$ , while precipitation biases are below 50%. Regionalisation work indicates at finer scales that the changes can be substantially different in magnitude or sign from the large area-average results. A relatively large spread exists among models, although attribution of the cause of these differences is unclear.

## D.4 Overall Assessment of Abilities

*Coupled models have evolved and improved significantly since the SAR. In general, they provide credible simulations of climate, at least down to sub-continental scales and over temporal scales from seasonal to decadal. Coupled models, as a class, are considered to be suitable tools to provide useful projections of future climates.* These models cannot yet simulate all aspects of climate (e.g., they still cannot account fully for the observed trend in the surface-troposphere temperature differences since 1979). Clouds and humidity also remain sources of significant uncertainty, but there have been incremental improvements in simulations of these quantities. No single model can be considered “best”, and it is important to utilise results from a range of carefully evaluated coupled models to explore effects of different formulations. The rationale for increased confidence in models arises from model performance in the following areas.

### Flux adjustment

*The overall confidence in model projections is increased by the improved performance of several models that do not use flux adjustment. These models now maintain stable, multi-century simulations of surface climate that are considered to be of sufficient quality to allow their use for climate change projections.* The changes whereby many models can now run without flux adjustment have come from improvements in both the atmospheric and oceanic components. In the model atmosphere, improvements in convection, the boundary layer, clouds, and surface latent heat fluxes are most notable. In the model ocean, the improvements are in resolution, boundary layer mixing, and in the representation of eddies. The results from climate change studies with flux adjusted and non-flux adjusted models are broadly in agreement; nonetheless, the development of stable non-flux adjusted models increases confidence in their ability to simulate future climates.

## Climate of the 20th century

*Confidence in the ability of models to project future climates is increased by the ability of several models to reproduce warming trends in the 20th century surface air temperature when driven by increased greenhouse gases and sulphate aerosols.* This is illustrated in Figure 13. However, only idealized scenarios of sulphate aerosols have been used and contributions from some additional processes and forcings may not have been included in the models. Some modelling studies suggest that inclusion of additional forcings like solar variability and volcanic aerosols may improve some aspects of the simulated climate variability of the 20th century.

### Extreme events

*Analysis of and confidence in extreme events simulated within climate models are still emerging, particularly for storm tracks and storm frequency.* “Tropical-cyclone-like” vortices are being simulated in climate models, although enough uncertainty remains over their interpretation to warrant caution in projections of tropical cyclone changes. However, in general, the analysis of extreme events in both observations (see Section B.6) and coupled models is underdeveloped.

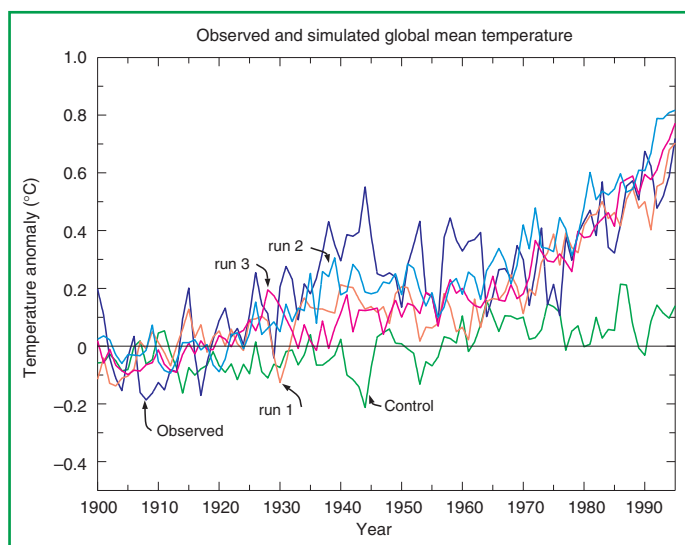


**Figure 13:** Observed and modelled global annual mean temperature anomalies ( $^\circ\text{C}$ ) relative to the average of the observations over the period 1900 to 1930. The control and three independent simulations with the same greenhouse gas plus aerosol forcing and slightly different initial conditions are shown from an AOGCM. The three greenhouse gas plus aerosol simulations are labeled ‘run 1’, ‘run 2’, and ‘run 3’ respectively. [Based on Figure 8.15]

### **Interannual variability**

*The performance of coupled models in simulating ENSO has improved; however, its variability is displaced westward and its strength is generally underestimated.* When suitably initialised with surface wind and sub-surface ocean data, some coupled models have had a degree of success in predicting ENSO events.

### **Model intercomparisons**

*The growth in systematic intercomparisons of models provides the core evidence for the growing capabilities of climate models.* For example, the Coupled Model Intercomparison Project (CMIP) is enabling a more comprehensive and systematic evaluation and intercomparison of coupled models run in a standardised configuration and responding to standardised forcing. Some degree of quantification of improvements in coupled model performance has now been demonstrated. The Palaeoclimate Model Intercomparison Project (PMIP) provides intercomparisons of models for the mid-Holocene (6,000 years before present) and for the Last Glacial Maximum (21,000 years before present). The ability of these models to simulate some aspects of palaeoclimates, compared to a range of palaeoclimate proxy data, gives confidence in models (at least the atmospheric component) over a range of different forcings.

## **E. The Identification of a Human Influence on Climate Change**

Sections B and C characterised the observed past changes in climate and in forcing agents, respectively. Section D examined the capabilities of climate models to predict the response of the climate system to such changes in forcing. This Section uses that information to examine the question of whether a human influence on climate change to date can be identified.

This is an important point to address. The SAR concluded that “the balance of evidence suggests that there is a discernible human influence on global climate”. It noted that the detection and attribution of anthropogenic climate change signals will be accomplished through a gradual accumulation of evidence. The SAR also noted uncertainties in a number of factors, including internal variability and the magnitude and patterns of forcing and response, which prevented them from drawing a stronger conclusion.

### **E.1 The Meaning of Detection and Attribution**

**Detection** is the process of demonstrating that an observed change is significantly different (in a statistical sense) than can be explained by natural variability. **Attribution** is the process of establishing cause and effect with some defined level of confidence, including the assessment of competing hypotheses. The response to anthropogenic changes in climate forcing occurs against a backdrop of natural internal and externally forced climate variability. Internal climate variability, i.e., climate variability not forced by external agents, occurs on all time-scales from weeks to centuries and even millennia. Slow climate components, such as the ocean, have particularly important roles on decadal and century time-scales because they integrate weather variability. Thus, the climate is capable of producing long time-scale variations of considerable magnitude without external influences. Externally forced climate variations (signals) may be due to changes in natural forcing factors, such as solar radiation or volcanic aerosols, or to changes in anthropogenic forcing factors, such as increasing concentrations of greenhouse gases or aerosols. The presence of this natural climate variability means that the detection and attribution of anthropogenic climate change is a statistical “signal to noise” problem. **Detection** studies demonstrate whether or not an observed change is highly unusual in a statistical sense, but this does not necessarily

imply that we understand its causes. The *attribution* of climate change to anthropogenic causes involves statistical analysis and the careful assessment of multiple lines of evidence to demonstrate, within a pre-specified margin of error, that the observed changes are:

- unlikely to be due entirely to internal variability;
- consistent with the estimated responses to the given combination of anthropogenic and natural forcing; and
- not consistent with alternative, physically plausible explanations of recent climate change that exclude important elements of the given combination of forcings.

## **E.2 A Longer and More Closely Scrutinised Observational Record**

Three of the last five years (1995, 1997 and 1998) were the warmest globally in the instrumental record. The impact of observational sampling errors has been estimated for the global and hemispheric mean temperature record. There is also a better understanding of the errors and uncertainties in the satellite-based (Microwave Sounding Unit, MSU) temperature record. Discrepancies between MSU and radiosonde data have largely been resolved, although the observed trend in the difference between the surface and lower tropospheric temperatures cannot fully be accounted for (see Section B). New reconstructions of temperature over the last 1,000 years indicate that the temperature changes over the last hundred years are unlikely to be entirely natural in origin, even taking into account the large uncertainties in palaeo-reconstructions (see Section B).

## **E.3 New Model Estimates of Internal Variability**

The warming over the past 100 years is very unlikely to be due to internal variability alone, as estimated by current models. The instrumental record is short and covers the period of human influence and palaeo-records include natural forced variations, such as those due to variations in solar irradiance and in the frequency of major volcanic eruptions. These limitations leave few alternatives to using long “control” simulations with coupled models for the estimation of internal climate variability. Since the SAR, more models have been used to estimate the magnitude of internal climate variability, a representative sample of which is given in Figure 14. As can be seen, there is a wide range of global scale internal

variability in these models. Estimates of the longer time-scale variability relevant to detection and attribution studies is uncertain, but, on interannual and decadal time-scales, some models show similar or larger variability than observed, even though models do not include variance from external sources. Conclusions on detection of an anthropogenic signal are insensitive to the model used to estimate internal variability, and recent changes cannot be accounted for as pure internal variability, even if the amplitude of simulated internal variations is increased by a factor of two or perhaps more. Most recent detection and attribution studies find no evidence that model-estimated internal variability at the surface is inconsistent with the residual variability that remains in the observations after removal of the estimated anthropogenic signals on the large spatial and long time-scales used in detection and attribution studies. Note, however, the ability to detect inconsistencies is limited. As Figure 14 indicates, no model control simulation shows a trend in surface air temperature as large as the observed trend over the last 1,000 years.

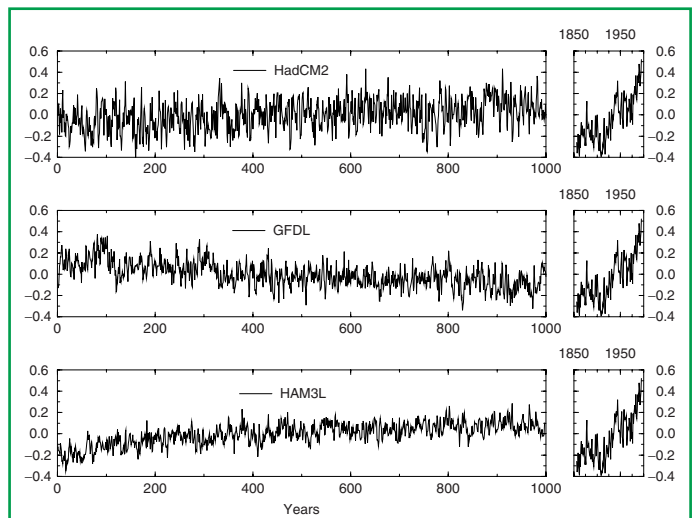


**Figure 14:** Global mean surface air temperature anomalies from 1,000 year control simulations with three different climate models, – Hadley, Geophysical Fluid Dynamics Laboratory and Hamburg, compared to the recent instrumental record. No model control simulation shows a trend in surface air temperature as large as the observed trend. If internal variability is correct in these models, the recent warming is likely not due to variability produced within the climate system alone. [Based on Figure 12.1]

## **E.4 New Estimates of Responses to Natural Forcing**

*Assessments based on physical principles and model simulations indicate that natural forcing alone is unlikely to explain the recent observed global warming or the observed changes in vertical temperature structure of the atmosphere.* Fully coupled ocean-atmosphere models have used reconstructions of solar and volcanic forcings over the last one to three centuries to estimate the contribution of natural forcing to climate variability and change. Although the reconstruction of natural forcings is uncertain, including their effects produces an increase in variance at longer (multi-decadal) time-scales. This brings the low-frequency variability closer to that deduced from palaeo-reconstructions. It is likely that the net natural forcing (i.e., solar plus volcanic) has been negative over the past two decades, and possibly even the past four decades. Statistical assessments confirm that simulated natural variability, both internal and naturally forced, is unlikely to explain the warming in the latter half of the 20th century (see Figure 15). However, there is evidence for a detectable volcanic influence on climate and evidence that suggests a detectable solar influence, especially in the early part of the 20th century. Even if the models underestimate the magnitude of the response to solar or volcanic forcing, the spatial and temporal patterns are such that these effects alone cannot explain the observed temperature changes over the 20th century.

## **E.5 Sensitivity to Estimates of Climate Change Signals**

*There is a wide range of evidence of qualitative consistencies between observed climate changes and model responses to anthropogenic forcing.* Models and observations show increasing global temperature, increasing land-ocean temperature contrast, diminishing sea-ice extent, glacial retreat, and increases in precipitation at high latitudes in the Northern Hemisphere. Some qualitative inconsistencies remain, including the fact that models predict a faster rate of warming in the mid- to upper troposphere than is observed in either satellite or radiosonde tropospheric temperature records.

*All simulations with greenhouse gases and sulphate aerosols that have been used in detection studies have found that a significant anthropogenic contribution is required to account for surface and tropospheric trends over at least the last 30 years.* Since the SAR, more simulations with increases in

greenhouse gases and some representation of aerosol effects have become available. Several studies have included an explicit representation of greenhouse gases (as opposed to an equivalent increase in CO<sub>2</sub>). Some have also included tropospheric ozone changes, an interactive sulphur cycle, an explicit radiative treatment of the scattering of sulphate aerosols, and improved estimates of the changes in stratospheric ozone. Overall, while detection of the climate response to these other anthropogenic factors is often ambiguous, detection of the influence of greenhouse gases on the surface temperature changes over the past 50 years is robust. In some cases, ensembles of simulations have been run to reduce noise in the estimates of the time-dependent response. Some studies have evaluated seasonal variation of the response. Uncertainties in the estimated climate change signals have made it difficult to attribute the observed climate change to one specific combination of anthropogenic and natural influences, but all studies have found a significant anthropogenic contribution is required to account for surface and tropospheric trends over at least the last thirty years.

## **E.6 A Wider Range of Detection Techniques**

### **Temperature**

*Evidence of a human influence on climate is obtained over a substantially wider range of detection techniques.* A major advance since the SAR is the increase in the range of techniques used and the evaluation of the degree to which the results are independent of the assumptions made in applying those techniques. There have been studies using pattern correlations, optimal detection studies using one or more fixed patterns and time-varying patterns, and a number of other techniques. The increase in the number of studies, breadth of techniques, increased rigour in the assessment of the role of anthropogenic forcing in climate, and the robustness of results to the assumptions made using those techniques, has increased the confidence in these aspects of detection and attribution.

*Results are sensitive to the range of temporal and spatial scales that are considered.* Several decades of data are necessary to separate forced signals from internal variability. Idealised studies have demonstrated that surface temperature changes are detectable only on scales in the order of 5,000 km. Such studies show that the level of agreement found between simulations and observations in pattern correlation studies is close to what one would expect in theory.

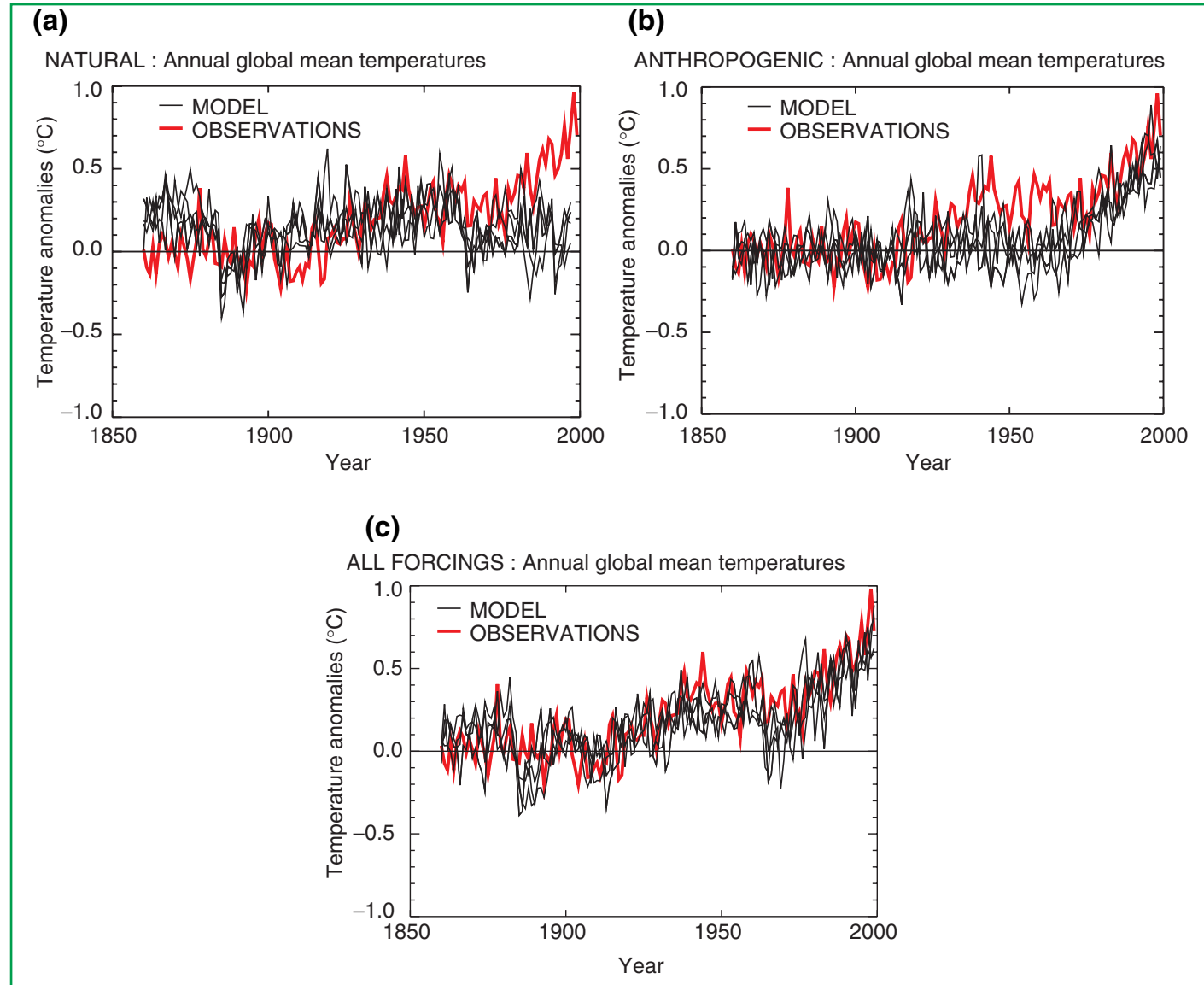


**Figure 15:** Global mean surface temperature anomalies relative to the 1880 to 1920 mean from the instrumental record compared with ensembles of four simulations with a coupled ocean-atmosphere climate model forced (a) with solar and volcanic forcing only, (b) with anthropogenic forcing including well mixed greenhouse gases, changes in stratospheric and tropospheric ozone and the direct and indirect effects of sulphate aerosols, and (c) with all forcings, both natural and anthropogenic. The thick line shows the instrumental data while the thin lines show the individual model simulations in the ensemble of four members. Note that the data are annual mean values. The model data are only sampled at the locations where there are observations. The changes in sulphate aerosol are calculated interactively, and changes in tropospheric ozone were calculated offline using a chemical transport model. Changes in cloud brightness (the first indirect effect of sulphate aerosols) were calculated by an off line simulation and included in the model. The changes in stratospheric ozone were based on observations. The volcanic and solar forcing were based on published combinations of measured and proxy data. The net anthropogenic forcing at 1990 was  $1.0 \text{ Wm}^{-2}$  including a net cooling of  $1.0 \text{ Wm}^{-2}$  due to sulphate aerosols. The net natural forcing for 1990 relative to 1860 was  $0.5 \text{ Wm}^{-2}$ , and for 1992 was a net cooling of  $2.0 \text{ Wm}^{-2}$  due to Mount Pinatubo. Other models forced with anthropogenic forcing give similar results to those shown in (b). [Based on Figure 12.7]

*Most attribution studies find that, over the last 50 years, the estimated rate and magnitude of global warming due to increasing concentrations of greenhouse gases alone are comparable with or larger than the observed warming.* Attribution studies address the question of “whether the magnitude of the simulated response to a particular forcing agent is consistent with observations”. The use of multi-signal techniques has enabled studies that discriminate between the effects of different factors on climate. The inclusion of the time dependence of signals has helped to distinguish between natural and anthropogenic forcings. As more response patterns are included, the problem of degeneracy (different combinations of patterns yielding near identical fits to the observations) inevitably arises. Nevertheless, even with all the major responses that have been included in the analysis, a distinct greenhouse gas signal remains detectable.

Furthermore, most model estimates that take into account both greenhouse gases and sulphate aerosols are consistent with observations over this period. The best agreement between model simulations and observations over the last 140 years is found when both anthropogenic and natural factors are included (see Figure 15). These results show that the forcings included are sufficient to explain the observed changes, but do not exclude the possibility that other forcings have also contributed. Overall, the magnitude of the temperature response to increasing concentrations of greenhouse gases is found to be consistent with observations on the scales considered (see Figure 16), but there remain discrepancies between modelled and observed response to other natural and anthropogenic factors.

*Uncertainties in other forcings that have been included do not prevent identification of the effect of anthropogenic greenhouse gases over the last 50 years.* The sulphate forcing, while uncertain, is negative over this period. Changes in natural forcing during most of this period are also estimated to be negative. Detection of the influence of anthropogenic greenhouse gases therefore cannot be eliminated either by the uncertainty in sulphate aerosol forcing or because natural forcing has not been included in all model simulations. Studies that distinguish the separate responses to greenhouse gas, sulphate aerosol and natural forcing produce uncertain estimates of the amplitude of the sulphate aerosol and natural signals, but almost all studies are nevertheless able to detect the presence of the anthropogenic greenhouse gas signal in the recent climate record.

*The detection and attribution methods used should not be sensitive to errors in the amplitude of the global mean response to individual forcings.* In the signal-estimation methods used in this report, the amplitude of the signal is estimated from the observations and not the amplitude of the simulated response. Hence the estimates are independent of those factors determining the simulated amplitude of the response, such as the climate sensitivity of the model used. In addition, if the signal due to a given forcing is estimated individually, the amplitude is largely independent of the magnitude of the forcing used to derive the response. Uncertainty in the amplitude of the solar and indirect sulphate aerosol forcing should not affect the magnitude of the estimated signal.

#### **Sea level**

*It is very likely that the 20th century warming has contributed significantly to the observed sea level rise, through thermal expansion of sea water and widespread loss of land ice.* Within present uncertainties, observations and models are both consistent with a lack of significant acceleration of sea level rise during the 20th century.

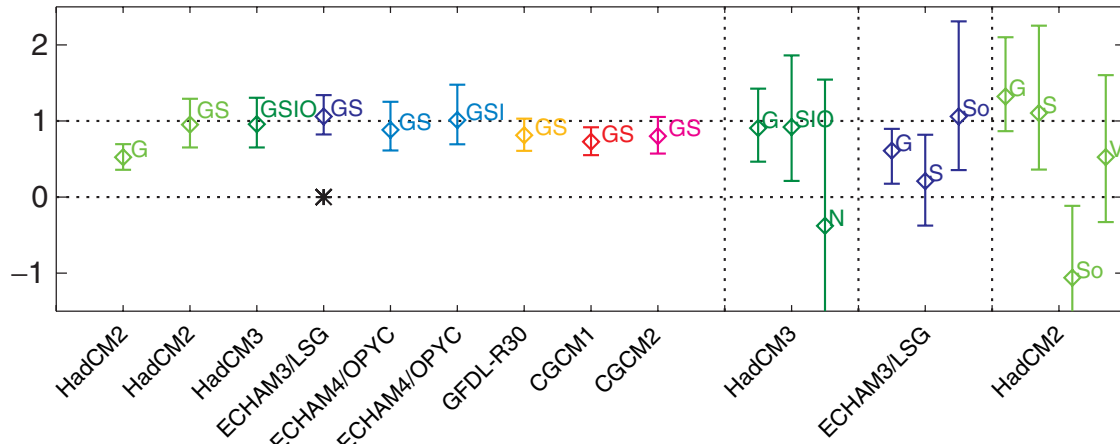
#### **E.7 Remaining Uncertainties in Detection and Attribution**

*Some progress has been made in reducing uncertainty, though many of the sources of uncertainty identified in the SAR still exist. These include:*

- *Discrepancies between the vertical profile of temperature change in the troposphere seen in observations and models.* These have been reduced as more realistic forcing histories have been used in models, although not fully resolved. Also, the difference between observed surface and lower-tropospheric trends over the last two decades cannot be fully reproduced by model simulations.
- *Large uncertainties in estimates of internal climate variability from models and observations.* Although as noted above, these are unlikely (bordering on very unlikely) to be large enough to nullify the claim that a detectable climate change has taken place.
- *Considerable uncertainty in the reconstructions of solar and volcanic forcing which are based on proxy or limited observational data for all but the last two decades.* Detection of the influence of greenhouse gases on climate

(a)

Scaling required on model-simulated signals



(b)

Estimated contributions to 20th century warming ( $^{\circ}\text{C}/\text{century}$ )

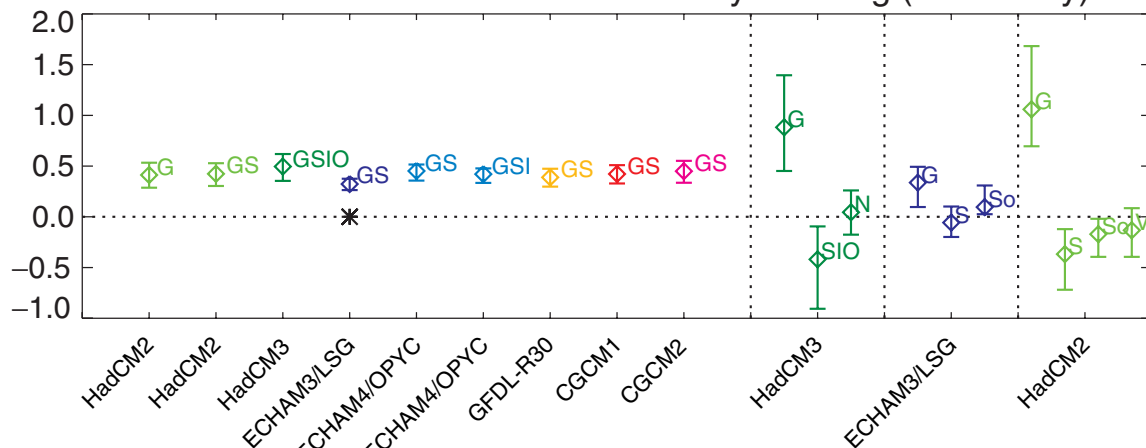


**Figure 16:** (a) Estimates of the “scaling factors” by which the amplitude of several model-simulated signals must be multiplied to reproduce the corresponding changes in the observed record. The vertical bars indicate the 5 to 95% uncertainty range due to internal variability. A range encompassing unity implies that this combination of forcing amplitude and model-simulated response is consistent with the corresponding observed change, while a range encompassing zero implies that this model-simulated signal is not detectable. Signals are defined as the ensemble mean response to external forcing expressed in large-scale ( $>5,000 \text{ km}$ ) near-surface temperatures over the 1946 to 1996 period relative to the 1896 to 1996 mean. The first entry (G) shows the scaling factor and 5 to 95% confidence interval obtained with the assumption that the observations consist only of a response to greenhouse gases plus internal variability. The range is significantly less than one (consistent with results from other models), meaning that models forced with greenhouse gases alone significantly over predict the observed warming signal. The next eight entries show scaling factors for model-simulated responses to greenhouse and sulphate forcing (GS), with two cases including indirect sulphate and tropospheric ozone forcing, one of these also including stratospheric ozone depletion (GSI and GSIO, respectively). All but one (CGCM1) of these ranges is consistent with unity. Hence there is little evidence that models are

appears to be robust to possible amplification of the solar forcing by ozone-solar or solar-cloud interactions, provided these do not alter the pattern or time-dependence of the response to solar forcing. Amplification of the solar signal by these processes, which are not yet included in models, remains speculative.

- *Large uncertainties in anthropogenic forcing are associated with the effects of aerosols.* The effects of some anthropogenic factors, including organic carbon, black carbon, biomass aerosols, and changes in land use, have not been included in detection and attribution studies. Estimates of the size and geographic pattern of the effects of these forcings vary considerably, although individually their global effects are estimated to be relatively small.

- Large differences in the response of different models to the same forcing. These differences, which are often greater than the difference in response in the same model with and without aerosol effects, highlight the large uncertainties in climate change prediction and the need to quantify uncertainty and reduce it through better observational data sets and model improvement.

### E.8 Synopsis

*In the light of new evidence and taking into account the remaining uncertainties, most of the observed warming over the last 50 years is likely to have been due to the increase in greenhouse gas concentrations.*

systematically over- or under predicting the amplitude of the observed response under the assumption that model-simulated GS signals and internal variability are an adequate representation (i.e., that natural forcing has had little net impact on this diagnostic). Observed residual variability is consistent with this assumption in all but one case (ECHAM3, indicated by the asterisk). One is obliged to make this assumption to include models for which only a simulation of the anthropogenic response is available, but uncertainty estimates in these single signal cases are incomplete since they do not account for uncertainty in the naturally forced response. These ranges indicate, however, the high level of confidence with which internal variability, as simulated by these various models, can be rejected as an explanation of recent near-surface temperature change. A more complete uncertainty analysis is provided by the next three entries, which show corresponding scaling factors on individual greenhouse (G), sulphate (S), solar-plus-volcanic (N), solar-only (So) and volcanic-only (V) signals for those cases in which the relevant simulations have been performed. In these cases, multiple factors are estimated simultaneously to account for uncertainty in the amplitude of the naturally forced response. The uncertainties increase but the greenhouse signal remains consistently detectable. In one case (ECHAM3) the model appears to be overestimating the greenhouse response (scaling range in the G signal inconsistent with unity), but this result is sensitive to which component of the control is used to define the detection space. It is also not known how it would respond to the inclusion of a volcanic signal. In cases where both solar and volcanic forcing is included (HadCM2 and HadCM3), G and S signals remain detectable and consistent with unity independent of whether natural signals are estimated jointly or separately (allowing for different errors in S and V responses).

(b) Estimated contributions to global mean warming over the 20th century, based on the results shown in (a), with 5 to 95% confidence intervals. Although the estimates vary depending on which model's signal and what forcing is assumed, and are less certain if more than one signal is estimated, all show a significant contribution from anthropogenic climate change to 20th century warming. [Based on Figure 12.12]

### F. The Projections of the Earth's Future Climate

The tools of climate models are used with future scenarios of forcing agents (e.g., greenhouse gases and aerosols) as input to make a suite of projected future climate changes that illustrates the possibilities that could lie ahead. Section F.1 provides a description of the future scenarios of forcing agents given in the IPCC Special Report on Emission Scenarios (SRES) on which, wherever possible, the future changes presented in this section are based. Sections F.2 to F.9 present the resulting projections of changes to the future climate. Finally, Section F.10 presents the results of future projections based on scenarios of a future where greenhouse gas concentrations are stabilised.

#### *F.1 The IPCC Special Report on Emissions Scenarios (SRES)*

In 1996, the IPCC began the development of a new set of emissions scenarios, effectively to update and replace the well-known IS92 scenarios. The approved new set of scenarios is described in the IPCC Special Report on Emission Scenarios (SRES). Four different narrative storylines were developed to describe consistently the relationships between the forces driving emissions and their evolution and to add context for the scenario quantification. The resulting set of 40 scenarios (35 of which contain data on the full range of gases required to force climate models) cover a wide range of the main demographic, economic and technological driving forces of future greenhouse gas and sulphur emissions. Each scenario represents a specific quantification of one of the four storylines. All the scenarios based on the same storyline constitute a scenario "family" (See Box 5, which briefly describes the main characteristics of the four SRES storylines and scenario families). The SRES scenarios do not include additional climate initiatives, which means that no scenarios are included that explicitly assume implementation of the United Nations Framework Convention on Climate Change or the emissions targets of the Kyoto Protocol. However, greenhouse gas emissions are directly affected by non-climate change policies designed for a wide range of other purposes (e.g., air quality). Furthermore, government policies can, to varying degrees, influence the greenhouse gas emission drivers, such as

demographic change, social and economic development, technological change, resource use, and pollution management. This influence is broadly reflected in the storylines and resulting scenarios.

Since the SRES was not approved until 15 March 2000, it was too late for the modelling community to incorporate the final approved scenarios in their models and have the results available in time for this Third Assessment Report. However, draft scenarios were released to climate modellers earlier to facilitate their input to the Third Assessment Report, in accordance with a decision of the IPCC Bureau in 1998. At that time, one marker scenario was chosen from each of four of the scenario groups based directly on the storylines (A1B, A2, B1, and B2). The choice of the markers was based on which of the initial quantifications best reflected the storyline and features of specific models. Marker scenarios are no more or less likely than any other scenarios, but are considered illustrative of a particular storyline. Scenarios were also selected later to illustrate the other two scenario groups (A1FI and A1T) within the A1 family, which specifically explore alternative technology developments, holding the other driving forces constant. Hence there is an illustrative scenario for each of the six scenario groups, and all are equally plausible. Since the latter two illustrative scenarios were selected at a late stage in the process, the AOGCM modelling results presented in this report only use two of the four draft marker scenarios. At present, only scenarios A2 and B2 have been integrated by more than one AOGCM. The AOGCM results have been augmented by results from simple climate models that cover all six illustrative scenarios. The IS92a scenario is also presented in a number of cases to provide direct comparison with the results presented in the SAR.

The final four marker scenarios contained in the SRES differ in minor ways from the draft scenarios used for the AOGCM experiments described in this report. In order to ascertain the likely effect of differences in the draft and final SRES scenarios, each of the four draft and final marker scenarios were studied using a simple climate model. For three of the four marker scenarios (A1B, A2, and B2) temperature change from the draft and marker scenarios are very similar. The primary difference is a change to the standardised values for 1990 to 2000, which is common to all these scenarios. This results in a higher forcing early in the period.

**Box 5: The Emissions Scenarios of the Special Report on Emissions Scenarios (SRES)**

A1. The A1 storyline and scenario family describes a future world of very rapid economic growth, global population that peaks in mid-century and declines thereafter, and the rapid introduction of new and more efficient technologies. Major underlying themes are convergence among regions, capacity building and increased cultural and social interactions, with a substantial reduction in regional differences in per capita income. The A1 scenario family develops into three groups that describe alternative directions of technological change in the energy system. The three A1 groups are distinguished by their technological emphasis: fossil intensive (A1FI), non-fossil energy sources (A1T), or a balance across all sources (A1B) (where balanced is

defined as not relying too heavily on one particular energy source, on the assumption that similar improvement rates apply to all energy supply and end-use technologies).

A2. The A2 storyline and scenario family describes a very heterogeneous world. The underlying theme is self-reliance and preservation of local identities. Fertility patterns across regions converge very slowly, which results in continuously increasing population. Economic development is primarily regionally oriented and per capita economic growth and technological change more fragmented and slower than other storylines.

B1. The B1 storyline and scenario family describes a convergent world with the same global population, that peaks in mid-century and declines thereafter, as in the A1 storyline, but with rapid change in economic

structures toward a service and information economy, with reductions in material intensity and the introduction of clean and resource-efficient technologies. The emphasis is on global solutions to economic, social and environmental sustainability, including improved equity, but without additional climate initiatives.

B2. The B2 storyline and scenario family describes a world in which the emphasis is on local solutions to economic, social and environmental sustainability. It is a world with continuously increasing global population, at a rate lower than A2, intermediate levels of economic development, and less rapid and more diverse technological change than in the A1 and B1 storylines. While the scenario is also oriented towards environmental protection and social equity, it focuses on local and regional levels.

There are further small differences in net forcing, but these decrease until, by 2100, differences in temperature change in the two versions of these scenarios are in the range 1 to 2%. For the B1 scenario, however, temperature change is significantly lower in the final version, leading to a difference in the temperature change in 2100 of almost 20%, as a result of generally lower emissions across the full range of greenhouse gases.

Anthropogenic emissions of the three main greenhouse gases, CO<sub>2</sub>, CH<sub>4</sub> and N<sub>2</sub>O, together with anthropogenic sulphur dioxide emissions, are shown for the six illustrative SRES scenarios in Figure 17. It is evident that these scenarios encompass a wide range of emissions. For comparison, emissions are also shown for IS92a. Particularly noteworthy are the much lower future sulphur dioxide emissions for the six SRES scenarios, compared to the IS92 scenarios, due to structural changes in the energy system as well as concerns about local and regional air pollution.

## F.2 Projections of Future Changes in Greenhouse Gases and Aerosols

Models indicate that the illustrative SRES scenarios lead to very different CO<sub>2</sub> concentration trajectories (see Figure 18). By 2100, carbon cycle models project atmospheric CO<sub>2</sub> concentrations of 540 to 970 ppm for the illustrative SRES scenarios (90 to 250% above the concentration of 280 ppm in 1750). The net effect of land and ocean climate feedbacks as indicated by models is to further increase projected atmospheric CO<sub>2</sub> concentrations by reducing both the ocean and land uptake of CO<sub>2</sub>. These projections include the land and ocean climate feedbacks. Uncertainties, especially about the magnitude of the climate feedback from the terrestrial biosphere, cause a variation of about -10 to +30% around each scenario. The total range is 490 to 1260 ppm (75 to 350% above the 1750 concentration).

Measures to enhance carbon storage in terrestrial ecosystems could influence atmospheric CO<sub>2</sub> concentration, but the upper bound for reduction of CO<sub>2</sub> concentration by such means is 40

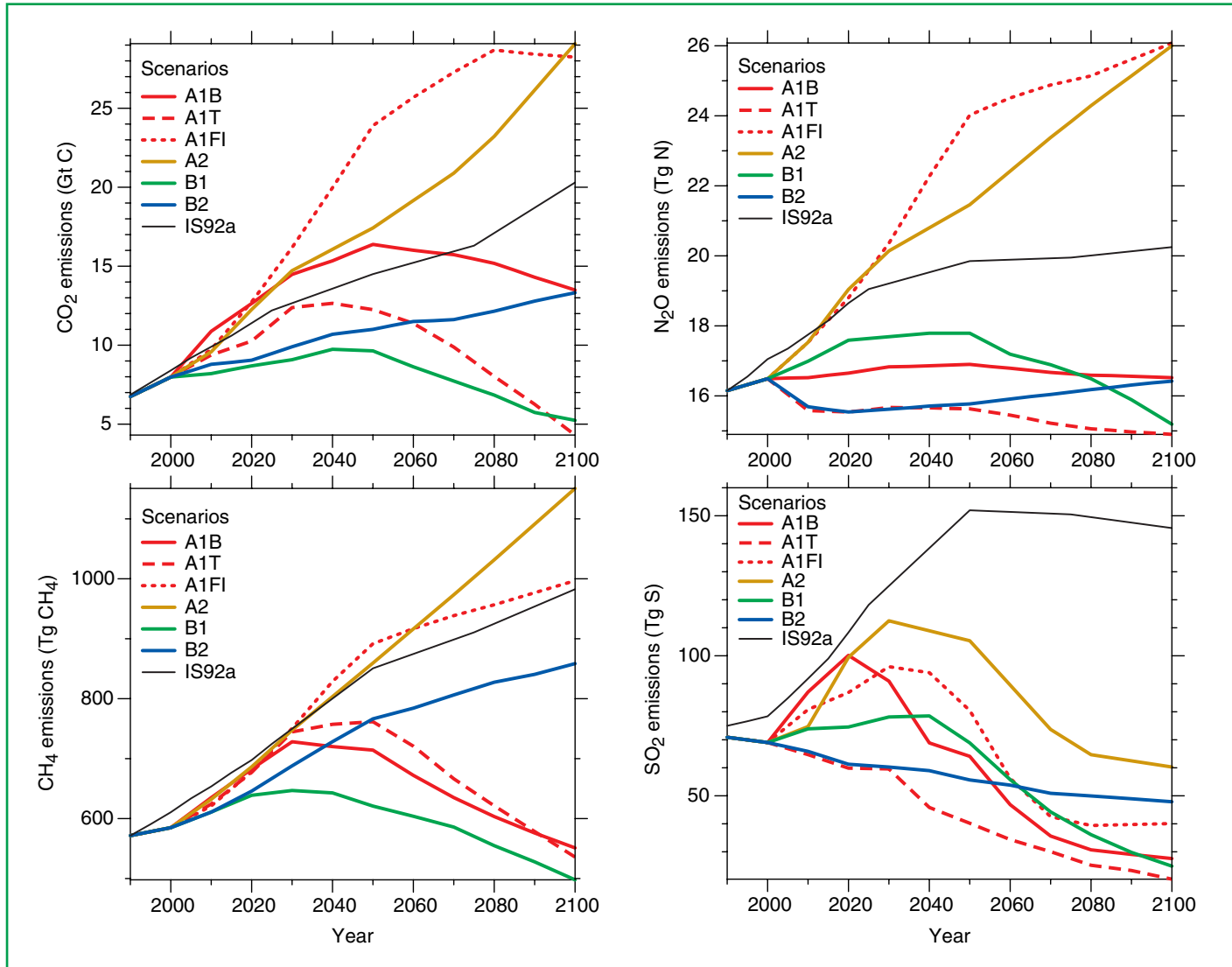


**Figure 17:** Anthropogenic emissions of CO<sub>2</sub>, CH<sub>4</sub>, N<sub>2</sub>O and sulphur dioxide for the six illustrative SRES scenarios, A1B, A2, B1 and B2, A1FI and A1T. For comparison the IS92a scenario is also shown. [Based on IPCC Special Report on Emissions Scenarios.]

to 70 ppm. If all the carbon released by historic land-use changes could be restored to the terrestrial biosphere over the course of the century (e.g., by reforestation), CO<sub>2</sub> concentration would be reduced by 40 to 70 ppm. Thus, fossil fuel CO<sub>2</sub> emissions are virtually certain to remain the dominant control over trends in atmospheric CO<sub>2</sub> concentration during this century.

*Model calculations of the abundances of the primary non-CO<sub>2</sub> greenhouse gases by the year 2100 vary considerably across*

*the six illustrative SRES scenarios.* In general A1B, A1T and B1 have the smallest increases, and A1FI and A2, the largest. The CH<sub>4</sub> changes from 1998 to 2100 range from -190 to +1970 ppb (-11 to +112%), and N<sub>2</sub>O increases from +38 to +144 ppb (+12 to +46%) (see Figures 17b and c). The HFCs (134a, 143a, and 125) reach abundances of a few hundred to a thousand ppt from negligible levels today. The PFC CF4 is projected to increase to 200 to 400 ppt, and SF<sub>6</sub> is projected to increase to 35 to 65 ppt.

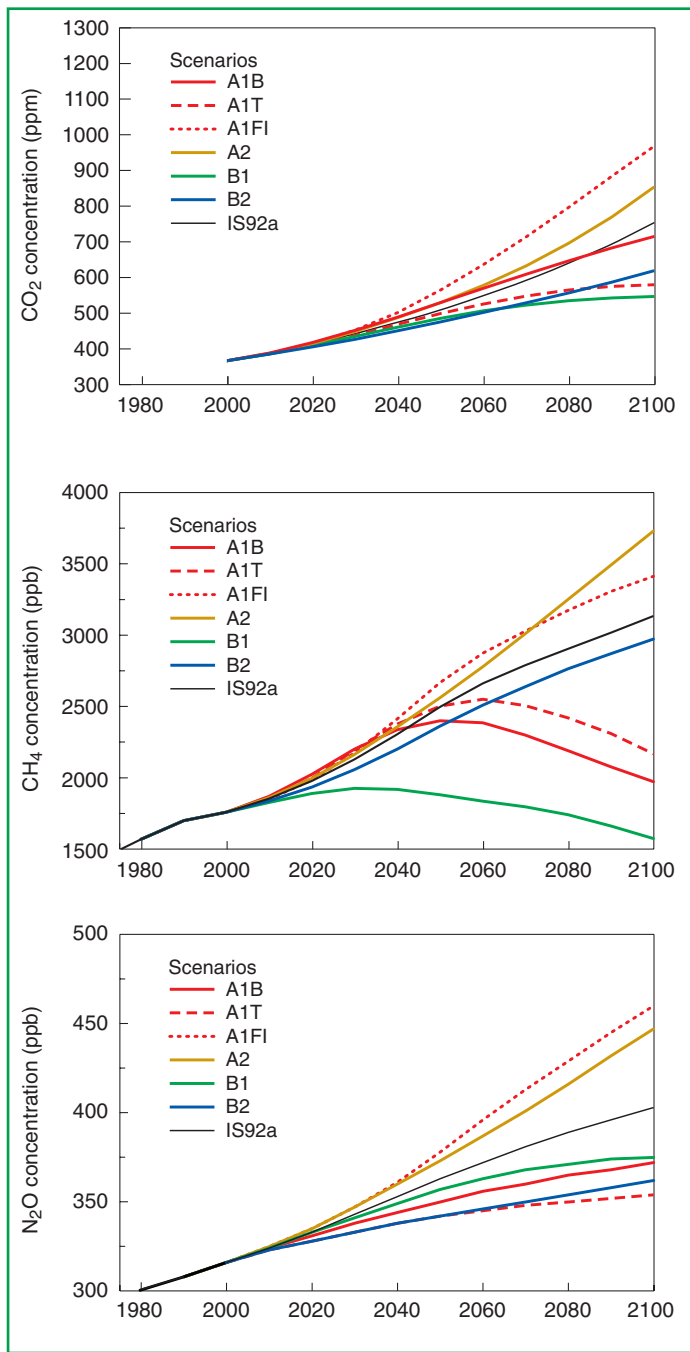


**Figure 18:** Atmospheric concentrations of  $\text{CO}_2$ ,  $\text{CH}_4$  and  $\text{N}_2\text{O}$  resulting from the six SRES scenarios and from the IS92a scenario computed with current methodology. [Based on Figures 3.12 and 4.14]

For the six illustrative SRES emissions scenarios, projected emissions of indirect greenhouse gases ( $\text{NO}_x$ ,  $\text{CO}$ , VOC), together with changes in  $\text{CH}_4$ , are projected to change the global mean abundance of the tropospheric hydroxyl radical ( $\text{OH}$ ), by  $-20\%$  to  $+6\%$  over the next century. Because of the importance of  $\text{OH}$  in tropospheric chemistry, comparable, but opposite sign, changes occur in the atmospheric lifetimes of the greenhouse gases  $\text{CH}_4$  and HFCs. This impact depends in large part on the magnitude of and the balance between  $\text{NO}_x$  and  $\text{CO}$  emissions. Changes in tropospheric  $\text{O}_3$  of  $-12$  to  $+62\%$  are calculated from 2000 until 2100. The largest increase predicted for the 21st century is for scenarios A1FI and A2 and would be more than twice as large as that experienced since the Pre-industrial Era. These  $\text{O}_3$  increases are attributable to the concurrent and large increases in anthropogenic  $\text{NO}_x$  and  $\text{CH}_4$  emissions.

The large growth in emissions of greenhouse gases and other pollutants as projected in some of the six illustrative SRES scenarios for the 21st century will degrade the global environment in ways beyond climate change. Changes projected in the SRES A2 and A1FI scenarios would degrade air quality over much of the globe by increasing background levels of tropospheric  $\text{O}_3$ . In northern mid-latitudes during summer, the zonal average of  $\text{O}_3$  increases near the surface are about 30 ppb or more, raising background levels to about 80 ppb, threatening the attainment of current air quality standards over most metropolitan and even rural regions and compromising crop and forest productivity. This problem reaches across continental boundaries and couples emissions of  $\text{NO}_x$  on a hemispheric scale.

Except for sulphate and black carbon, models show an approximately linear dependence of the abundance of aerosols on emissions. The processes that determine the removal rate for black carbon differ substantially between the models, leading to major uncertainty in the future projections of black carbon. Emissions of natural aerosols such as sea salt, dust, and gas phase precursors of aerosols such as terpenes, sulphur dioxide ( $\text{SO}_2$ ), and dimethyl sulphide oxidation may increase as a result of changes in climate and atmospheric chemistry.

The six illustrative SRES scenarios cover nearly the full range of forcing that results from the full set of SRES scenarios. Estimated total historical anthropogenic radiative forcing from 1765 to 1990 followed by forcing resulting from the six

SRES scenarios are shown in Figure 19. The forcing from the full range of 35 SRES scenarios is shown on the figure as a shaded envelope, since the forcings resulting from individual scenarios cross with time. The direct forcing from biomass-burning aerosols is scaled with deforestation rates. The SRES scenarios include the possibility of either increases or decreases in anthropogenic aerosols (e.g., sulphate aerosols, biomass aerosols, and black and organic carbon aerosols), depending on the extent of fossil fuel use and policies to abate polluting emissions. The SRES scenarios do not include emissions estimates for non-sulphate aerosols. Two methods for projecting these emissions were considered in this report: the first scales the emissions of fossil fuel and biomass aerosols with CO while the second scales the emissions with SO<sub>2</sub> and deforestation. Only the second method was used for climate projections. For comparison, radiative forcing is also shown for the IS92a scenario. It is evident that the range for the new SRES scenarios is shifted higher compared to the IS92 scenarios. This is mainly due to the reduced future SO<sub>2</sub> emissions of the SRES scenarios compared to the IS92 scenarios, but also to the slightly larger cumulative carbon emissions featured in some SRES scenarios.

*In almost all SRES scenarios, the radiative forcing due to CO<sub>2</sub>, CH<sub>4</sub>, N<sub>2</sub>O and tropospheric O<sub>3</sub> continue to increase, with the fraction of the total radiative forcing due to CO<sub>2</sub> projected to increase from slightly more than half to about*

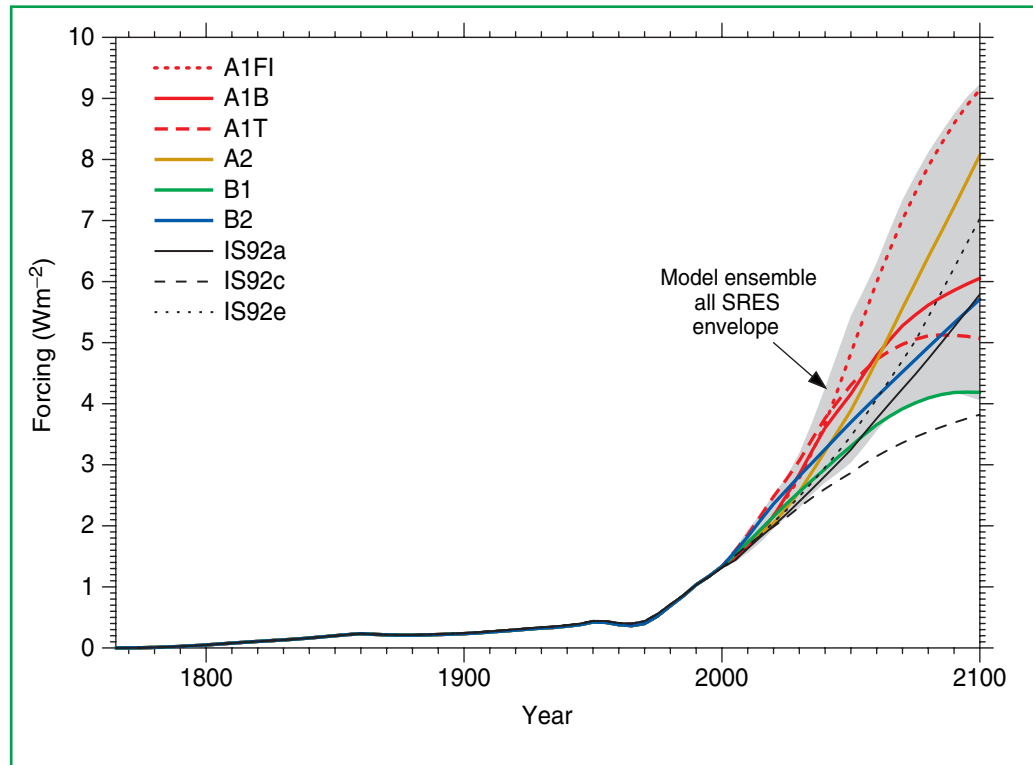


**Figure 19:** Simple model results: estimated historical anthropogenic radiative forcing up to the year 2000 followed by radiative forcing for the six illustrative SRES scenarios. The shading shows the envelope of forcing that encompasses the full set of thirty five SRES scenarios. The method of calculation closely follows that explained in the chapters. The values are based on the radiative forcing for a doubling of CO<sub>2</sub> from seven AOGCMs. The IS92a, IS92c, and IS92e forcing is also shown following the same method of calculation. [Based on Figure 9.13a]

*three-quarters of the total.* The radiative forcing due to O<sub>3</sub>-depleting gases decreases due to the introduction of emission controls aimed at curbing stratospheric ozone depletion. The direct aerosol (sulphate and black and organic carbon components taken together) radiative forcing (evaluated relative to present day, 2000) varies in sign for the different scenarios. The direct plus indirect aerosol effects are projected to be smaller in magnitude than that of CO<sub>2</sub>. No estimates are made for the spatial aspects of the future forcings. The indirect effect of aerosols on clouds is included in simple climate model calculations and scaled non-linearly with SO<sub>2</sub> emissions, assuming a present day value of  $-0.8 \text{ Wm}^{-2}$ , as in the SAR.

### F.3 Projections of Future Changes in Temperature

#### AOGCM results

*Climate sensitivity is likely to be in the range of 1.5 to 4.5°C. This estimate is unchanged from the first IPCC Assessment Report in 1990 and the SAR.* The climate sensitivity is the equilibrium response of global surface temperature to a doubling of equivalent CO<sub>2</sub> concentration. The range of estimates arises from uncertainties in the climate models and their internal feedbacks, particularly those related to clouds and related processes. Used for the first time in this IPCC report is the Transient Climate Response (TCR). The TCR is defined as the globally averaged surface air temperature change, at the time of doubling of CO<sub>2</sub>, in a 1%/yr CO<sub>2</sub>-increase experiment. This rate of CO<sub>2</sub> increase is assumed to represent the radiative forcing from all greenhouse gases. The TCR combines elements of model sensitivity and factors that affect response (e.g., ocean heat uptake). The range of the TCR for current AOGCMs is 1.1 to 3.1°C.

*Including the direct effect of sulphate aerosols reduces global mean mid-21st century warming.* The surface temperature response pattern for a given model, with and without sulphate aerosols, is more similar than the pattern between two models using the same forcing.

*Models project changes in several broad-scale climate variables.* As the radiative forcing of the climate system changes, the land warms faster and more than the ocean, and there is greater relative warming at high latitudes. Models project a smaller surface air temperature increase in the North Atlantic and circumpolar southern ocean regions relative to the global mean. There is projected to be a decrease in diurnal temperature range in many areas, with night-time lows increasing more than daytime highs. A number of models show a general decrease of daily variability of surface air temperature in winter and increased daily variability in summer in the Northern Hemisphere land areas. As the climate warms, the Northern Hemisphere snow cover and sea-ice extent are projected to decrease. Many of these changes are consistent with recent observational trends, as noted in Section B.

*Multi-model ensembles of AOGCM simulations for a range of scenarios are being used to quantify the mean climate change and uncertainty based on the range of model results.* For the end of the 21st century (2071 to 2100), the mean change in global

average surface air temperature, relative to the period 1961 to 1990, is 3.0°C (with a range of 1.3 to 4.5°C) for the A2 draft marker scenario and 2.2°C (with a range of 0.9 to 3.4°C) for the B2 draft marker scenario. The B2 scenario produces a smaller warming that is consistent with its lower rate of increased CO<sub>2</sub> concentration.

*On time-scales of a few decades, the current observed rate of warming can be used to constrain the projected response to a given emissions scenario despite uncertainty in climate sensitivity.* Analysis of simple models and intercomparisons of AOGCM responses to idealised forcing scenarios suggest that, for most scenarios over the coming decades, errors in large-scale temperature projections are likely to increase in proportion to the magnitude of the overall response. The estimated size of and uncertainty in current observed warming rates attributable to human influence thus provides a relatively model-independent estimate of uncertainty in multi-decade projections under most scenarios. To be consistent with recent observations, anthropogenic warming is likely to lie in the range 0.1 to 0.2°C/decade over the next few decades under the IS92a scenario. This is similar to the range of responses to this scenario based on the seven versions of the simple model used in Figure 22.

*Most of the features of the geographical response in the SRES scenario experiments are similar for different scenarios (see Figure 20) and are similar to those for idealised 1% CO<sub>2</sub>-increase integrations.* The biggest difference between the 1% CO<sub>2</sub>-increase experiments, which have no sulphate aerosol, and the SRES experiments is the regional moderating of the warming over industrialised areas, in the SRES experiments, where the negative forcing from sulphate aerosols is greatest. This regional effect was noted in the SAR for only two models, but this has now been shown to be a consistent response across the greater number of more recent models.

*It is very likely that nearly all land areas will warm more rapidly than the global average, particularly those at northern high latitudes in the cold season.* Results (see Figure 21) from recent AOGCM simulations forced with SRES A2 and B2 emissions scenarios indicate that in winter the warming for all high-latitude northern regions exceeds the global mean warming in each model by more than 40% (1.3 to 6.3°C for the range of models and scenarios considered). In summer, warming is in excess of 40% above the global mean change in central and northern Asia. Only in south Asia and southern South America in June/July/August, and Southeast Asia for both seasons, do the models consistently show warming less than the global average.

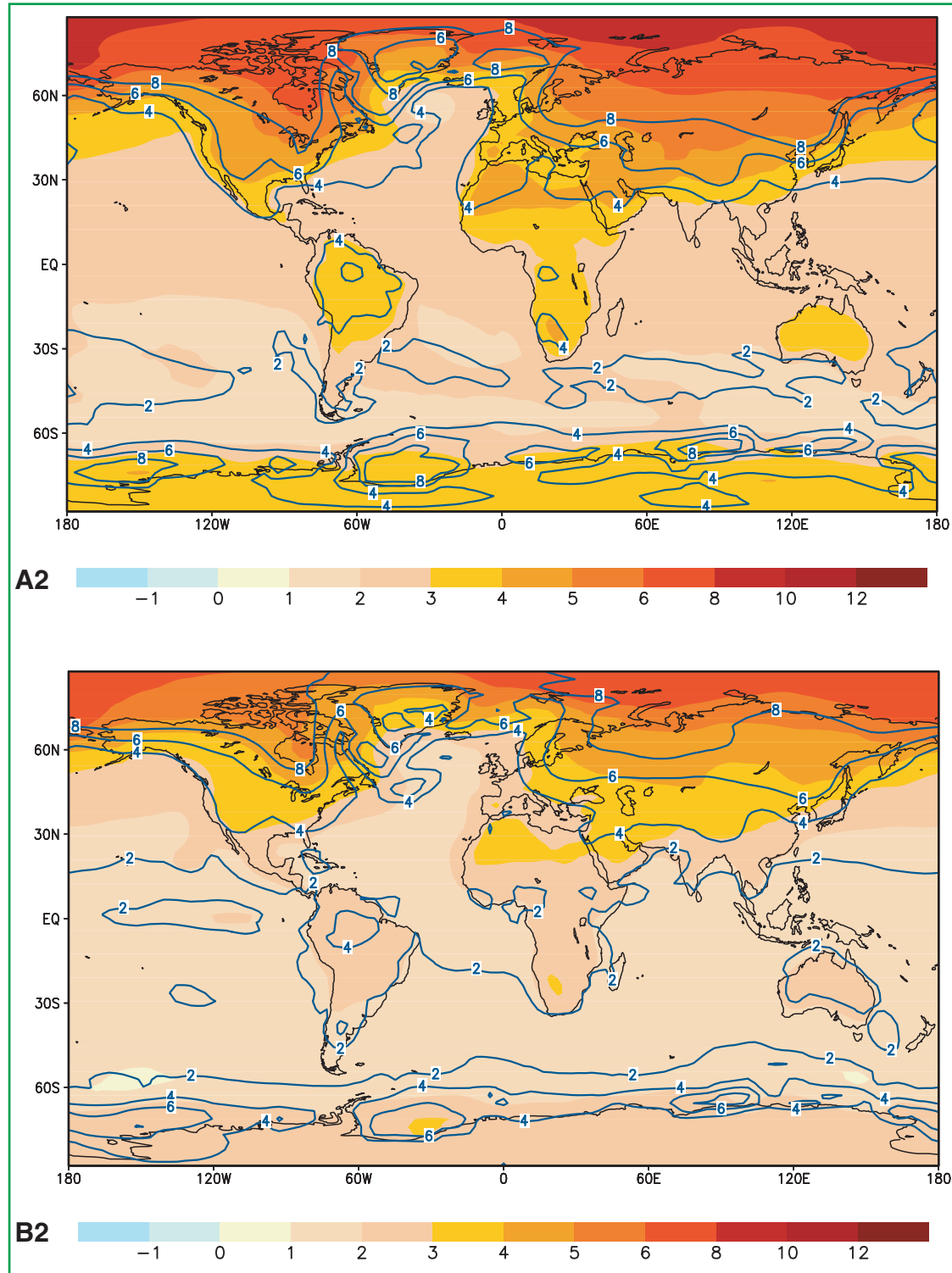


**Figure 20:** The annual mean change of the temperature (colour shading) and its range (isolines) (Unit: °C) for the SRES scenario A2 (upper panel) and the SRES scenario B2 (lower panel). Both SRES scenarios show the period 2071 to 2100 relative to the period 1961 to 1990 and were performed by OAGCMs. [Based on Figures 9.10d and 9.10e]

### Simple climate model results

*Due to computational expense, AOGCMs can only be run for a limited number of scenarios.* A simple model can be calibrated to represent globally averaged AOGCM responses and run for a much larger number of scenarios.

*The globally averaged surface temperature is projected to increase by 1.4 to 5.8°C (Figure 22(a)) over the period 1990 to 2100.* These results are for the full range of 35 SRES scenarios, based on a number of climate models.<sup>6,7</sup> Temperature increases are projected to be greater than those in the SAR, which were about 1.0 to 3.5°C based on six IS92 scenarios. The higher

projected temperatures and the wider range are due primarily to the lower projected SO<sub>2</sub> emissions in the SRES scenarios relative to the IS92 scenarios. The projected rate of warming is much larger than the observed changes during the 20th century and is very likely to be without precedent during at least the last 10,000 years, based on palaeoclimate data.

*The relative ranking of the SRES scenarios in terms of global mean temperature changes with time.* In particular, for scenarios with higher fossil fuel use (hence, higher carbon dioxide emissions, e.g., A2), the SO<sub>2</sub> emissions are also higher. In the near term (to around 2050), the cooling effect of

<sup>6</sup> Complex physically based climate models are the main tool for projecting future climate change. In order to explore the range of scenarios, these are complemented by simple climate models calibrated to yield an equivalent response in temperature and sea level to complex climate models. These projections are obtained using a simple climate model whose climate sensitivity and ocean heat uptake are calibrated to each of 7 complex climate models. The climate sensitivity used in the simple model ranges from 1.7 to 4.2°C, which is comparable to the commonly accepted range of 1.5 to 4.5°C.

<sup>7</sup> This range does not include uncertainties in the modelling of radiative forcing, e.g. aerosol forcing uncertainties. A small carbon cycle climate feedback is included.

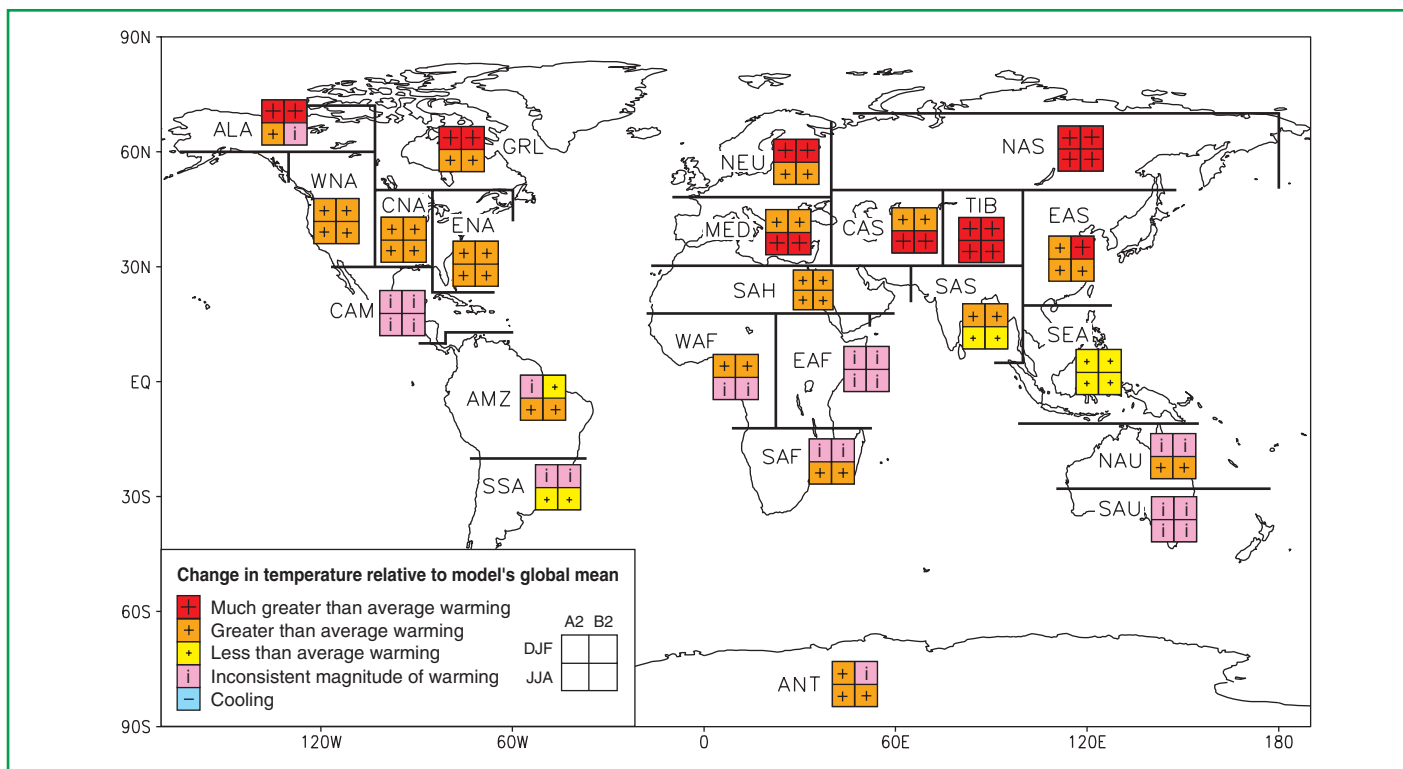


**Figure 21:** Analysis of inter-model consistency in regional relative warming (warming relative to each model's global average warming). Regions are classified as showing either agreement on warming in excess of 40% above the global average ('Much greater than average warming'), agreement on warming greater than the global average ('Greater than average warming'), agreement on warming less than the global average ('Less than average warming'), or disagreement amongst models on the magnitude of regional relative warming ('Inconsistent magnitude of warming'). There is also a category for agreement on cooling (which never occurs). A consistent result from at least seven of the nine models is deemed necessary for agreement. The global annual average warming of the models used span 1.2 to 4.5°C for A2 and 0.9 to 3.4°C for B2, and therefore a regional 40% amplification represents warming ranges of 1.7 to 6.3°C for A2 and 1.3 to 4.7°C for B2. [Based on Chapter 10, Box 1, Figure 1]

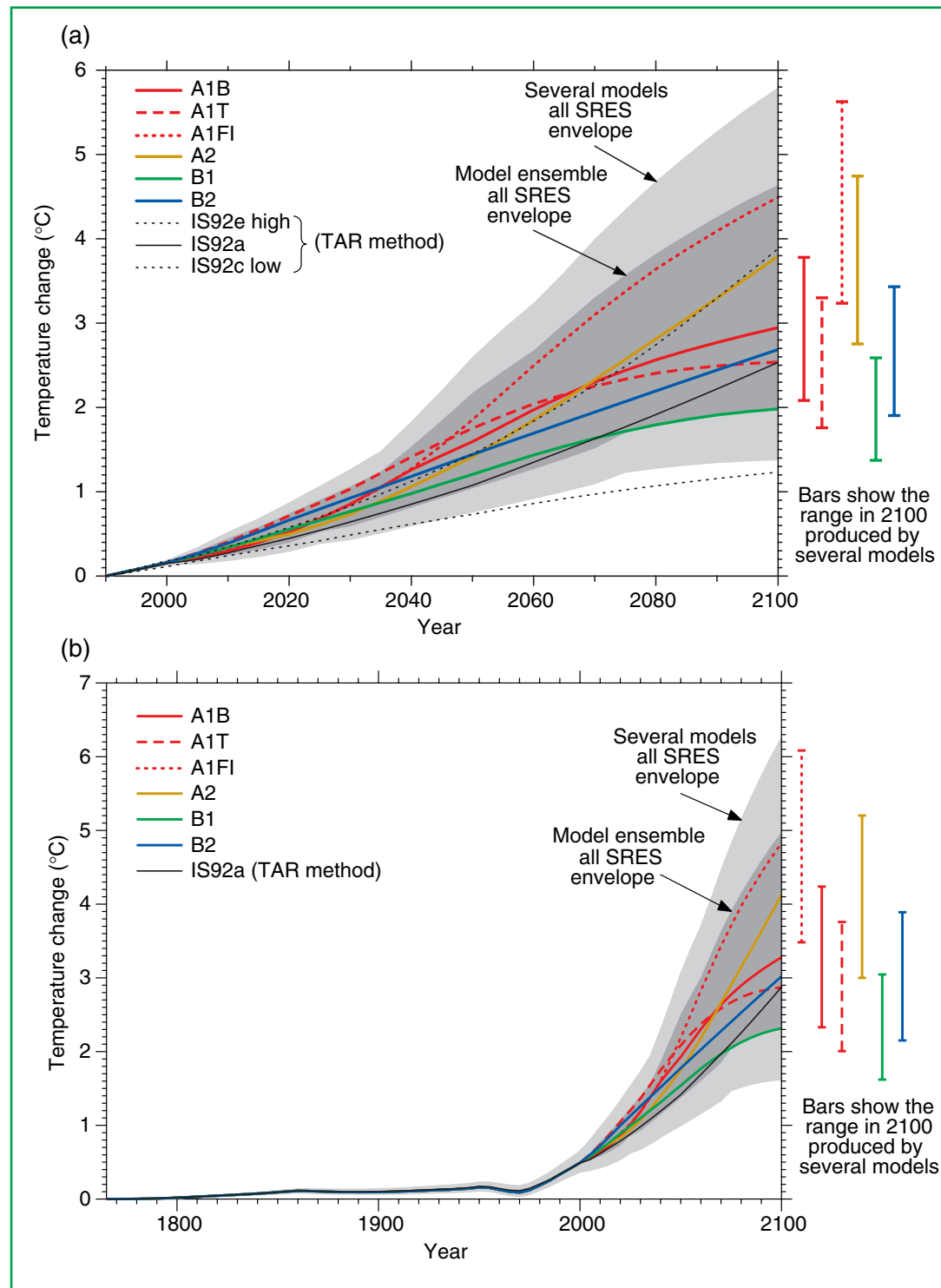


**Figure 22:** Simple model results: (a) global mean temperature projections for the six illustrative SRES scenarios using a simple climate model tuned to a number of complex models with a range of climate sensitivities. Also for comparison, following the same method, results are shown for IS92a. The darker shading represents the envelope of the full set of thirty-five SRES scenarios using the average of the model results (mean climate sensitivity is  $2.8^{\circ}\text{C}$ ). The lighter shading is the envelope based on all seven model projections (with climate sensitivity in the range  $1.7$  to  $4.2^{\circ}\text{C}$ ). The bars show, for each of the six illustrative SRES scenarios, the range of simple model results in 2100 for the seven AOGCM model tunings. (b) Same as (a) but results using estimated historical anthropogenic forcing are also used. [Based on Figures 9.14 and 9.13b]

higher sulphur dioxide emissions significantly reduces the warming caused by increased emissions of greenhouse gases in scenarios such as A2. The opposite effect is seen for scenarios B1 and B2, which have lower fossil fuel emissions as well as lower SO<sub>2</sub> emissions, and lead to a larger near-term warming. In the longer term, however, the level of emissions of long-lived greenhouse gases such as CO<sub>2</sub> and N<sub>2</sub>O become the dominant determinants of the resulting climate changes.

*By 2100, differences in emissions in the SRES scenarios and different climate model responses contribute similar uncertainty to the range of global temperature change. Further uncertainties arise due to uncertainties in the radiative forcing. The largest forcing uncertainty is that due to the sulphate aerosols.*

#### F.4 Projections of Future Changes in Precipitation

*Globally averaged water vapour, evaporation and precipitation are projected to increase. At the regional scale both increases and decreases in precipitation are seen. Results (see Figure 23) from recent AOGCM simulations forced with SRES A2 and B2 emissions scenarios indicate that it is likely for precipitation to increase in both summer and winter over high-latitude regions. In winter, increases are also seen over northern mid-latitudes, tropical Africa and Antarctica, and in summer in southern and eastern Asia. Australia, central America, and southern Africa show consistent decreases in winter rainfall.*

*Based on patterns emerging from a limited number of studies with current AOGCMs, older GCMs, and regionalisation studies, there is a strong correlation between precipitation*

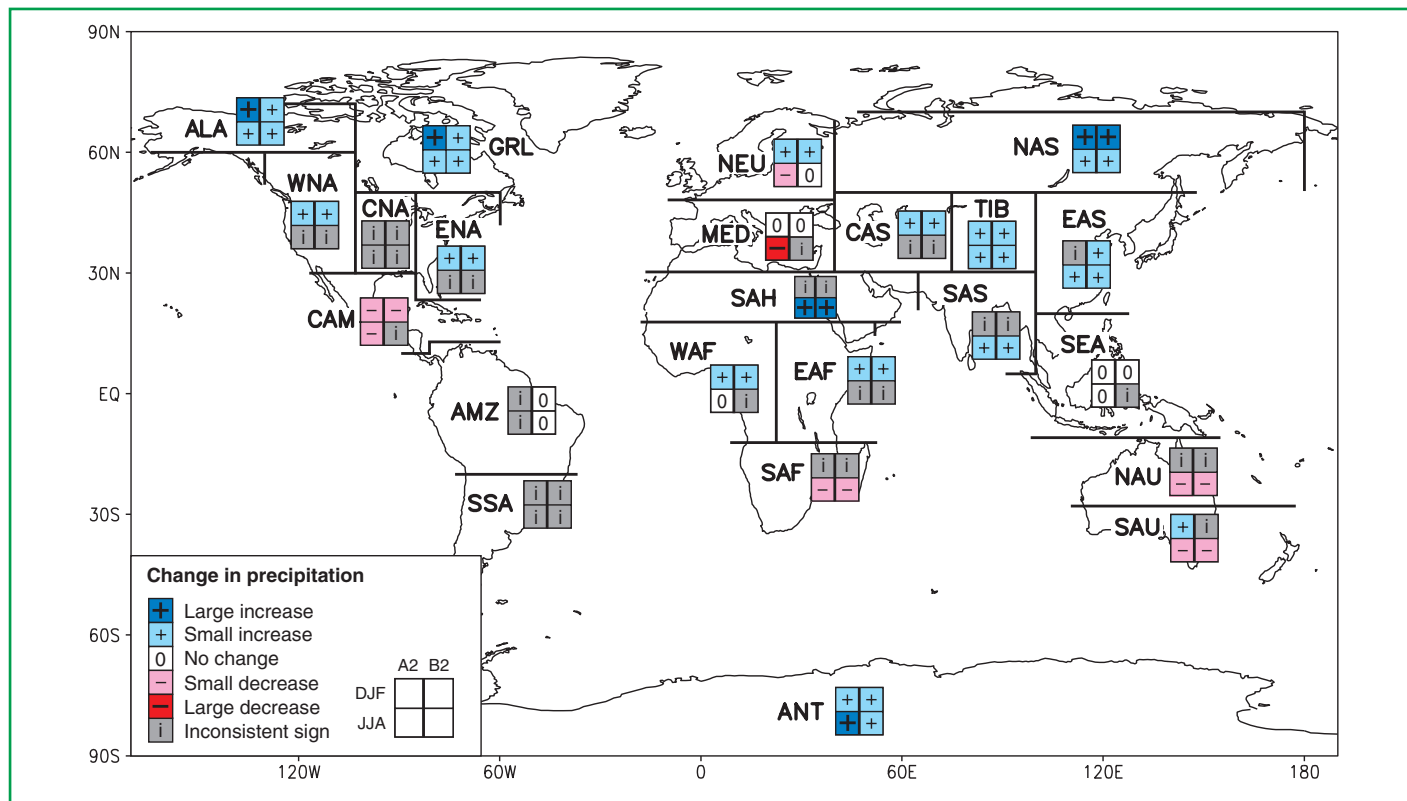


**Figure 23:** Analysis of inter-model consistency in regional precipitation change. Regions are classified as showing either agreement on increase with an average change of greater than 20% ('Large increase'), agreement on increase with an average change between 5 and 20% ('Small increase'), agreement on a change between -5 and +5% or agreement with an average change between -5 and 5% ('No change'), agreement on decrease with an average change between -5 and -20% ('Small decrease'), agreement on decrease with an average change of less than -20% ('Large decrease'), or disagreement ('Inconsistent sign'). A consistent result from at least seven of the nine models is deemed necessary for agreement. [Based on Chapter 10, Box 1, Figure 2]

*interannual variability and mean precipitation.* Future increases in mean precipitation will likely lead to increases in variability. Conversely, precipitation variability will likely decrease only in areas of reduced mean precipitation.

## F.5 Projections of Future Changes in Extreme Events

*It is only recently that changes in extremes of weather and climate observed to date have been compared to changes projected by models (Table 4).* More hot days and heat waves are very likely over nearly all land areas. These increases are projected to be largest mainly in areas where soil moisture decreases occur. Increases in daily minimum temperature are

projected to occur over nearly all land areas and are generally larger where snow and ice retreat. Frost days and cold waves are very likely to become fewer. The changes in surface air temperature and surface absolute humidity are projected to result in increases in the heat index (which is a measure of the combined effects of temperature and moisture). The increases in surface air temperature are also projected to result in an increase in the “cooling degree days” (which is a measure of the amount of cooling required on a given day once the temperature exceeds a given threshold) and a decrease in “heating degree days”. Precipitation extremes are projected to increase more than the mean and the intensity of precipitation events are projected to increase. The frequency of extreme

**Table 4:** Estimates of confidence in observed and projected changes in extreme weather and climate events. The table depicts an assessment of confidence in observed changes in extremes of weather and climate during the latter half of the 20th century (left column) and in projected changes during the 21st century (right column)<sup>a</sup>. This assessment relies on observational and modelling studies, as well as physical plausibility of future projections across all commonly used scenarios and is based on expert judgement (see Footnote 4). [Based upon Table 9.6]

Confidence in observed changes (latter half of the 20th century)	Changes in Phenomenon	Confidence in projected changes (during the 21st century)
Likely	<b>Higher maximum temperatures and more hot days over nearly all land areas</b>	Very likely
Very likely	<b>Higher minimum temperatures, fewer cold days and frost days over nearly all land areas</b>	Very likely
Very likely	<b>Reduced diurnal temperature range over most land areas</b>	Very likely
Likely, over many areas	<b>Increase of heat index<sup>8</sup> over land areas</b>	Very likely, over most areas
Likely, over many Northern Hemisphere mid- to high latitude land areas	<b>More intense precipitation events<sup>b</sup></b>	Very likely, over many areas
Likely, in a few areas	<b>Increased summer continental drying and associated risk of drought</b>	Likely, over most mid-latitude continental interiors (Lack of consistent projections in other areas)
Not observed in the few analyses available	<b>Increase in tropical cyclone peak wind intensities<sup>c</sup></b>	Likely, over some areas
Insufficient data for assessment	<b>Increase in tropical cyclone mean and peak precipitation intensities<sup>c</sup></b>	Likely, over some areas

<sup>a</sup> For more details see Chapter 2 (observations) and Chapters 9, 10 (projections).

<sup>b</sup> For other areas there are either insufficient data or conflicting analyses.

<sup>c</sup> Past and future changes in tropical cyclone location and frequency are uncertain.

<sup>8</sup> Heat index: A combination of temperature and humidity that measures effects on human comfort

precipitation events is projected to increase almost everywhere. There is projected to be a general drying of the mid-continental areas during summer. This is ascribed to a combination of increased temperature and potential evaporation that is not balanced by increases of precipitation. There is little agreement yet among models concerning future changes in mid-latitude storm intensity, frequency, and variability. There is little consistent evidence that shows changes in the projected frequency of tropical cyclones and areas of formation. However, some measures of intensities show projected increases, and some theoretical and modelling studies suggest that the upper limit of these intensities could increase. Mean and peak precipitation intensities from tropical cyclones are likely to increase appreciably.

*For some other extreme phenomena, many of which may have important impacts on the environment and society, there is currently insufficient information to assess recent trends, and confidence in models and understanding is inadequate to make firm projections.* In particular, very small-scale phenomena such as thunderstorms, tornadoes, hail, and lightning are not simulated in global models. Insufficient analysis has occurred of how extra-tropical cyclones may change.

### F.6 Projections of Future Changes in Thermohaline Circulation

Most models show weakening of the Northern Hemisphere Thermohaline Circulation (THC), which contributes to a reduction of the surface warming in the northern North Atlantic. Even in models where the THC weakens, there is still a warming over Europe due to increased greenhouse gases. In experiments where the atmospheric greenhouse gas concentration is stabilised at twice its present day value, the North Atlantic THC is projected to recover from initial weakening within one to several centuries. The THC could collapse entirely in either hemisphere if the rate of change in radiative forcing is large enough and applied long enough. Models indicate that a decrease of the THC reduces its resilience to perturbations, i.e., a once reduced THC appears to be less stable and a shut-down can become more likely. However, it is too early to say with confidence whether an irreversible collapse in the THC is likely or not, or at what threshold it might occur and what the climate implications could be. None of the current projections with coupled models exhibits a complete shut-down of the THC by 2100. Although the North

Atlantic THC weakens in most models, the relative roles of surface heat and fresh water fluxes vary from model to model. Wind stress changes appear to play only a minor role in the transient response.

### F.7 Projections of Future Changes in Modes of Natural Variability

Many models show a mean El Niño-like response in the tropical Pacific, with the central and eastern equatorial Pacific sea surface temperatures projected to warm more than the western equatorial Pacific and with a corresponding mean eastward shift of precipitation. Although many models show an El Niño-like change of the mean state of tropical Pacific sea surface temperatures, the cause is uncertain. It has been related to changes in the cloud radiative forcing and/or evaporative damping of the east-west sea surface temperature gradient in some models. Confidence in projections of changes in future frequency, amplitude, and spatial pattern of El Niño events in the tropical Pacific is tempered by some shortcomings in how well El Niño is simulated in complex models. Current projections show little change or a small increase in amplitude for El Niño events over the next 100 years. However, even with little or no change in El Niño amplitude, global warming is likely to lead to greater extremes of drying and heavy rainfall and increase the risk of droughts and floods that occur with El Niño events in many regions. It also is likely that warming associated with increasing greenhouse gas concentrations will cause an increase of Asian summer monsoon precipitation variability. Changes in monsoon mean duration and strength depend on the details of the emission scenario. The confidence in such projections is limited by how well the climate models simulate the detailed seasonal evolution of the monsoons. There is no clear agreement on changes in frequency or structure of naturally occurring modes of variability, such as the North Atlantic Oscillation, i.e., the magnitude and character of the changes vary across the models.

### F.8 Projections of Future Changes in Land Ice (Glaciers, Ice Caps and Ice Sheets), Sea Ice and Snow Cover

Glaciers and ice caps will continue their widespread retreat during the 21st century and Northern Hemisphere snow cover and sea ice are projected to decrease further. Methods have been developed recently for estimating glacier melt from

seasonally and geographically dependent patterns of surface air temperature change, that are obtained from AOGCM experiments. Modelling studies suggest that the evolution of glacial mass is controlled principally by temperature changes, rather than precipitation changes, on the global average.

*The Antarctic ice sheet is likely to gain mass because of greater precipitation, while the Greenland ice sheet is likely to lose mass because the increase in runoff will exceed the precipitation increase.* The West Antarctic Ice Sheet (WAIS)

has attracted special attention because it contains enough ice to raise sea level by 6 m and because of suggestions that instabilities associated with its being grounded below sea level may result in rapid ice discharge when the surrounding ice shelves are weakened. However, loss of grounded ice leading to substantial sea level rise from this source is now widely agreed to be very unlikely during the 21st century, although its dynamics are still inadequately understood, especially for projections on longer time-scales.

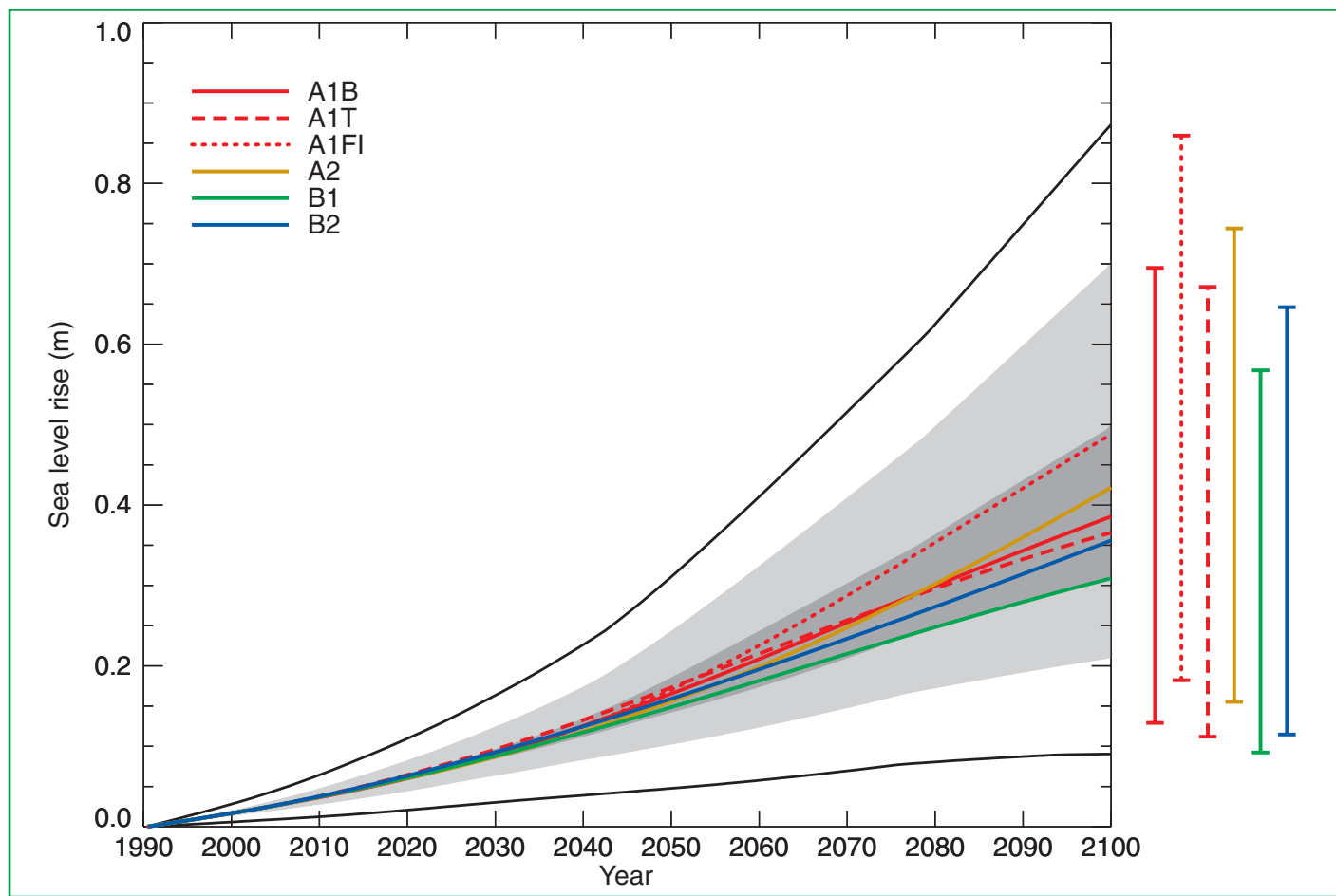


**Figure 24:** Global average sea level rise 1990 to 2100 for the SRES scenarios. Thermal expansion and land ice changes were calculated using a simple climate model calibrated separately for each of seven AOGCMs, and contributions from changes in permafrost, the effect of sediment deposition and the long-term adjustment of the ice sheets to past climate change were added. Each of the six lines appearing in the key is the average of AOGCMs for one of the six illustrative scenarios. The region in dark shading shows the range of the average of AOGCMs for all thirty five SRES scenarios. The region in light shading shows the range of all AOGCMs for all thirty five scenarios. The region delimited by the outermost lines shows the range of all AOGCMs and scenarios including uncertainty in land-ice changes, permafrost changes and sediment deposition. Note that this range does not allow for uncertainty relating to ice-dynamic changes in the West Antarctic ice sheet. [Based on Figure 11.12]

## F.9 Projections of Future Changes in Sea Level

*Projections of global average sea level rise from 1990 to 2100, using a range of AOGCMs following the IS92a scenario (including the direct effect of sulphate aerosol emissions), lie in the range 0.11 to 0.77 m. This range reflects the systematic uncertainty of modelling. The main contributions to this sea level rise are:*

- a thermal expansion of 0.11 to 0.43 m, accelerating through the 21st century;
- a glacier contribution of 0.01 to 0.23 m;
- a Greenland contribution of –0.02 to 0.09 m; and
- an Antarctic contribution of –0.17 to +0.02 m.

Also included in the computation of the total change are smaller contributions from thawing of permafrost, deposition of sediment, and the ongoing contributions from ice sheets as a result of climate change since the Last Glacial Maximum. To establish the range of sea level rise resulting from the choice of different SRES scenarios, results for thermal expansion and land-ice change from simple models tuned to several AOGCMs are used (as in Section F.3 for temperature).

*For the full set of SRES scenarios, a sea level rise of 0.09 to 0.88 m is projected for 1990 to 2100 (see Figure 24), primarily from thermal expansion and loss of mass from glaciers and ice caps. The central value is 0.48 m, which corresponds to an average rate of about two to four times the rate over the 20th century. The range of sea level rise presented in the SAR was 0.13 to 0.94 m based on the IS92 scenarios. Despite higher temperature change projections in this assessment, the sea level projections are slightly lower, primarily due to the use of improved models which give a smaller contribution from glaciers and ice sheets. If terrestrial storage continues at its current rates, the projections could be changed by –0.21 to 0.11 m. For an average of the AOGCMs, the SRES scenarios give results that differ by 0.02 m or less for the first half of the 21st century. By 2100, they vary over a range amounting to about 50% of the central value. Beyond the 21st century, sea level rise depends strongly on the emissions scenario.*

Models agree on the qualitative conclusion that the range of regional variation in sea level change is substantial

compared to global average sea level rise. However, confidence in the regional distribution of sea level change from AOGCMs is low because there is little similarity between models, although nearly all models project greater than average rise in the Arctic Ocean and less than average rise in the Southern Ocean. Further, land movements, both isostatic and tectonic, will continue through the 21st century at rates that are unaffected by climate change. It can be expected that by 2100, many regions currently experiencing relative sea level fall will instead have a rising relative sea level. Lastly, extreme high water levels will occur with increasing frequency as a result of mean sea level rise. Their frequency may be further increased if storms become more frequent or severe as a result of climate change.

## F.10 Projections of Future Changes in Response to CO<sub>2</sub> Concentration Stabilisation Profiles

### Greenhouse gases and aerosols

*All of the stabilisation profiles studied require CO<sub>2</sub> emissions to eventually drop well below current levels. Anthropogenic CO<sub>2</sub> emission rates that arrive at stable CO<sub>2</sub> concentration levels from 450 to 1,000 ppm were deduced from the prescribed CO<sub>2</sub> profiles (Figure 25a). The results (Figure 25b) are not substantially different from those presented in the SAR; however, the range is larger, mainly due to the range of future terrestrial carbon uptake caused by different assumptions in the models. Stabilisation at 450, 650 or 1,000 ppm would require global anthropogenic emissions to drop below 1990 levels within a few decades, about a century, or about two centuries, respectively, and continue to steadily decrease thereafter. Although there is sufficient uptake capacity in the ocean to incorporate 70 to 80% of foreseeable anthropogenic CO<sub>2</sub> emissions to the atmosphere, this process takes centuries due to the rate of ocean mixing. As a result, even several centuries after emissions occurred, about a quarter of the increase in concentration caused by these emissions is still present in the atmosphere. To maintain constant CO<sub>2</sub> concentration beyond 2300 requires emissions to drop to match the rate of carbon sinks at that time. Natural land and ocean sinks with the capacity to persist for hundreds or thousands of years are small (<0.2 PgC/yr).*

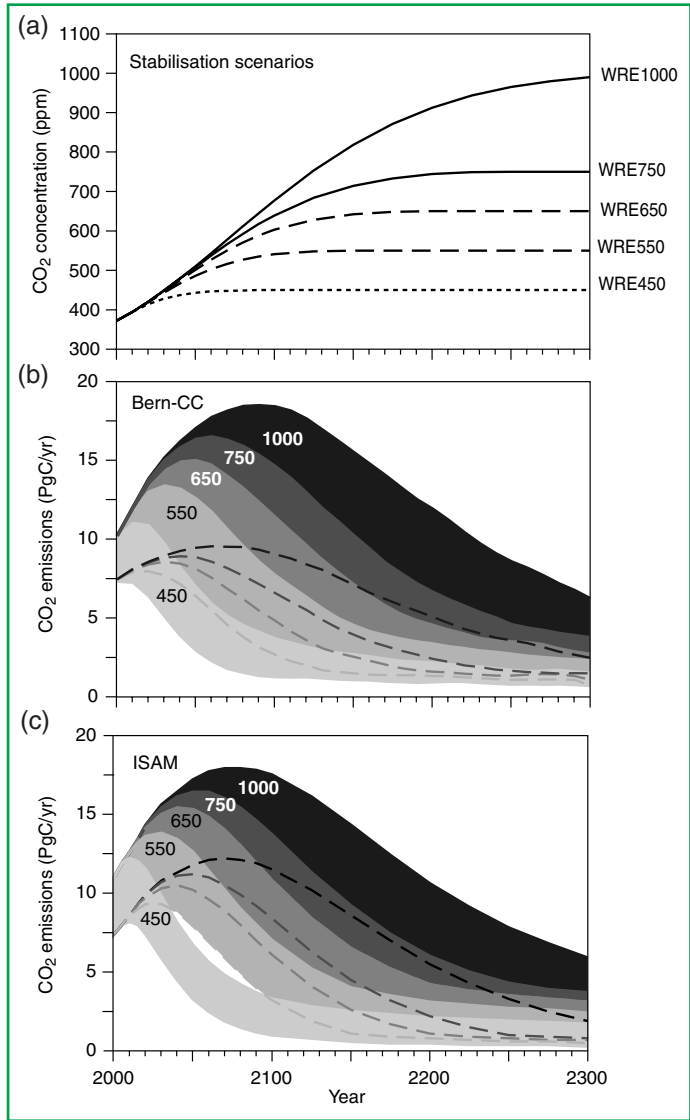


**Figure 25:** Projected CO<sub>2</sub> emissions permitting stabilisation of atmospheric CO<sub>2</sub> concentrations at different final values. Panel (a) shows the assumed trajectories of CO<sub>2</sub> concentration (WRE scenarios) and panels (b) and (c) show the implied CO<sub>2</sub> emissions, as projected with two fast carbon cycle models, Bern-CC and ISAM. The model ranges for ISAM were obtained by tuning the model to approximate the range of responses to CO<sub>2</sub> and climate from model intercomparisons. This approach yields a lower bound on uncertainties in the carbon cycle response. The model ranges for Bern-CC were obtained by combining different bounding assumptions about the behaviour of the CO<sub>2</sub> fertilization effect, the response of heterotrophic respiration to temperature and the turnover time of the ocean, thus approaching an upper bound on uncertainties in the carbon cycle response. For each model, the upper and lower bounds are indicated by the top and bottom of the shaded area. Alternatively, the lower bound (where hidden) is indicated by a hatched line. [Based on Figure 3.13]

### Temperature

Global mean temperature continues to increase for hundreds of years at a rate of a few tenths of a degree per century after concentrations of CO<sub>2</sub> have been stabilised, due to long time-scales in the ocean. The temperature implications of CO<sub>2</sub> concentration profiles leading to stabilisation from 450 ppm to 1,000 ppm were studied using a simple climate model tuned to seven AOGCMs with a mean climate sensitivity of 2.8°C. For all the pathways leading to stabilisation, the climate system shows considerable warming during the 21st century and beyond (see Figure 26). The lower the level at which concentrations stabilise, the smaller the total temperature change.

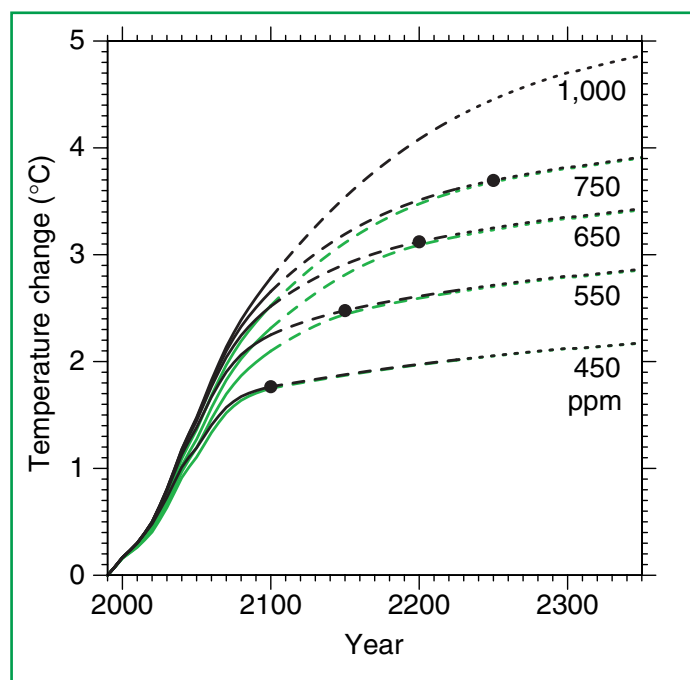


**Figure 26:** Simple model results: Projected global mean temperature changes when the concentration of CO<sub>2</sub> is stabilised following the WRE profiles (see Chapter 9 Section 9.3.3). For comparison, results based on the S profiles in the SAR are also shown in green (S1000 not available). The results are the average produced by a simple climate model tuned to seven AOGCMs. The baseline scenario is scenario A1B, this is specified only to 2100. After 2100, the emissions of gases other than CO<sub>2</sub> are assumed to remain constant at their A1B 2100 values. The projections are labelled according to the level of CO<sub>2</sub> stabilisation. The broken lines after 2100 indicate increased uncertainty in the simple climate model results beyond 2100. The black dots indicate the time of CO<sub>2</sub> stabilisation. The stabilisation year for the WRE1000 profile is 2375. [Based on Figure 9.16]

## Sea level

*If greenhouse gas concentrations were stabilised (even at present levels), sea level would nonetheless continue to rise for hundreds of years.* After 500 years, sea level rise from thermal expansion may have reached only half of its eventual level, which models suggest may lie within a range of 0.5 to 2.0 m and 1 to 4 m for CO<sub>2</sub> levels of twice and four times pre-industrial, respectively. The long time-scale is characteristic of the weak diffusion and slow circulation processes that transport heat into the deep ocean.

*The loss of a substantial fraction of the total glacier mass is likely.* Areas that are currently marginally glaciated are most likely to become ice-free.

*Ice sheets will continue to react to climatic change during the next several thousand years, even if the climate is stabilised.* Together, the present Antarctic and Greenland ice sheets contain enough water to raise sea level by almost 70 m if they were to melt, so that only a small fractional change in their volume would have a significant effect.

*Models project that a local annual average warming of larger than 3°C, sustained for millennia, would lead to virtually a complete melting of the Greenland ice sheet with a resulting sea level rise of about 7 m.* Projected temperatures over Greenland are generally greater than globally averaged temperatures by a factor of 1.2 to 3.1 for the range of models

used in Chapter 11. For a warming over Greenland of 5.5°C, consistent with mid-range stabilisation scenarios (see Figure 26), the Greenland ice sheet is likely to contribute about 3 m in 1,000 years. For a warming of 8°C, the contribution is about 6 m, the ice sheet being largely eliminated. For smaller warmings, the decay of the ice sheet would be substantially slower (see Figure 27).

*Current ice dynamic models project that the West Antarctic ice sheet (WAIS) will contribute no more than 3 mm/yr to sea level rise over the next thousand years, even if significant changes were to occur in the ice shelves.* Such results are strongly dependent on model assumptions regarding climate change scenarios, ice dynamics and other factors. Apart from the possibility of an internal ice dynamic instability, surface melting will affect the long-term viability of the Antarctic ice sheet. For warmings of more than 10°C, simple runoff models predict that a zone of net mass loss would develop on the ice sheet surface. Irreversible disintegration of the WAIS would result because the WAIS cannot retreat to higher ground once its margins are subjected to surface melting and begin to recede. Such a disintegration would take at least a few millennia. Thresholds for total disintegration of the East Antarctic ice sheet by surface melting involve warmings above 20°C, a situation that has not occurred for at least 15 million years and which is far more than predicted by any scenario of climate change currently under consideration.

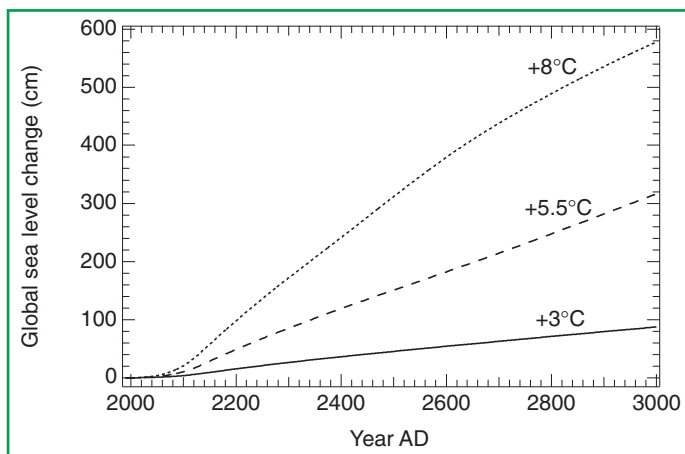


**Figure 27:** Response of the Greenland ice sheet to three climatic warming scenarios during the third millennium expressed in equivalent changes of global sea level. The curve labels refer to the mean annual temperature rise over Greenland by 3000 AD as predicted by a two-dimensional climate and ocean model forced by greenhouse gas concentration rises until 2130 AD and kept constant after that. Note that projected temperatures over Greenland are generally greater than globally averaged temperatures by a factor of 1.2 to 3.1 for the range of models used in Chapter 11. [Based on Figure 11.16]

### G. Advancing Understanding

The previous sections have contained descriptions of the current state of knowledge of the climate of the past and present, the current understanding of the forcing agents and processes in the climate system and how well they can be represented in climate models. Given the knowledge possessed today, the best assessment was given whether climate change can be detected and whether that change can be attributed to human influence. With the best tools available today, projections were made of how the climate could change in the future for different scenarios of emissions of greenhouse gases.

This Section looks into the future in a different way. Uncertainties are present in each step of the chain from emissions of greenhouse gases and aerosols, through to the impacts that they have on the climate system and society (see Figure 28). Many factors continue to limit the ability to detect, attribute, and understand current climate change and to project what future climate changes may be. Further work is needed in nine broad areas.

#### G.1 Data

*Arrest the decline of observational networks in many parts of the world.* Unless networks are significantly improved, it may be difficult or impossible to detect climate change in many areas of the globe.

*Expand the observational foundation for climate studies to provide accurate, long-term data with expanded temporal and spatial coverage.* Given the complexity of the climate system and the inherent multi-decadal time-scale, there is a need for long-term consistent data to support climate and environmental change investigations and projections. Data from the present and recent past, climate-relevant data for the last few centuries, and for the last several millennia are all needed. There is a particular shortage of data in polar regions and data for the quantitative assessment of extremes on the global scale.

#### G.2 Climate Processes and Modelling

*Estimate better future emissions and concentrations of greenhouse gases and aerosols.* It is particularly important that improvements are realised in deriving concentrations from emissions of gases and particularly aerosols, in addressing biogeochemical sequestration and cycling, and specifically, and in determining the spatial-temporal distribution of CO<sub>2</sub> sources and sinks, currently and in the future.

*Understand and characterise more completely dominant processes (e.g., ocean mixing) and feedbacks (e.g., from clouds and sea ice) in the atmosphere, biota, land and ocean surfaces, and deep oceans.* These sub-systems, phenomena, and processes are important and merit increased attention to improve prognostic capabilities generally. The interplay of observation and models will be the key for progress. The rapid forcing of a non-linear system has a high prospect of producing surprises.

*Address more completely patterns of long-term climate variability.* This topic arises both in model calculations and in the climate system. In simulations, the issue of climate drift within model calculations needs to be clarified better in part because it compounds the difficulty of distinguishing signal and noise. With respect to the long-term natural variability in the climate system per se, it is important to understand this variability and to expand the emerging capability of predicting patterns of organised variability such as ENSO.

*Explore more fully the probabilistic character of future climate states by developing multiple ensembles of model calculations.* The climate system is a coupled non-linear chaotic system, and therefore the long-term prediction of future exact climate states is not possible. Rather the focus must be upon the prediction of the probability distribution of the system's future possible states by the generation of ensembles of model solutions.

*Improve the integrated hierarchy of global and regional climate models with emphasis on improving the simulation of regional impacts and extreme weather events.* This will require improvements in the understanding of the coupling between the major atmospheric, oceanic, and terrestrial systems, and extensive diagnostic modelling and observational studies that evaluate and improve simulative performance. A particularly important issue is the adequacy of data needed to attack the question of changes in extreme events.

### G.3 Human Aspects

*Link more formally physical climate-biogeochemical models with models of the human system and thereby provide the basis for expanded exploration of possible cause-effect-cause patterns linking human and non-human components of the Earth system.* At present, human influences generally are treated only through emission scenarios that provide external forcings to the climate system. In future more comprehensive models are required in which human activities need to begin to interact with the dynamics of physical, chemical, and biological sub-systems through a diverse set of contributing activities, feedbacks and responses.

### G.4 International Framework

*Accelerate internationally progress in understanding climate change by strengthening the international framework that is needed to co-ordinate national and institutional efforts so that research, computational, and observational resources may be used to the greatest overall advantage.* Elements of this framework exist in the international programmes supported by the International Council of Scientific Unions (ICSU), the World Meteorological Organization (WMO), the United Nations Environment Programme (UNEP), and the United Nations Education, Scientific and Cultural Organisation (UNESCO). There is a corresponding need for strengthening the co-operation within the international research community, building research capacity in many regions and, as is the goal of this assessment, effectively describing research advances in terms that are relevant to decision making.

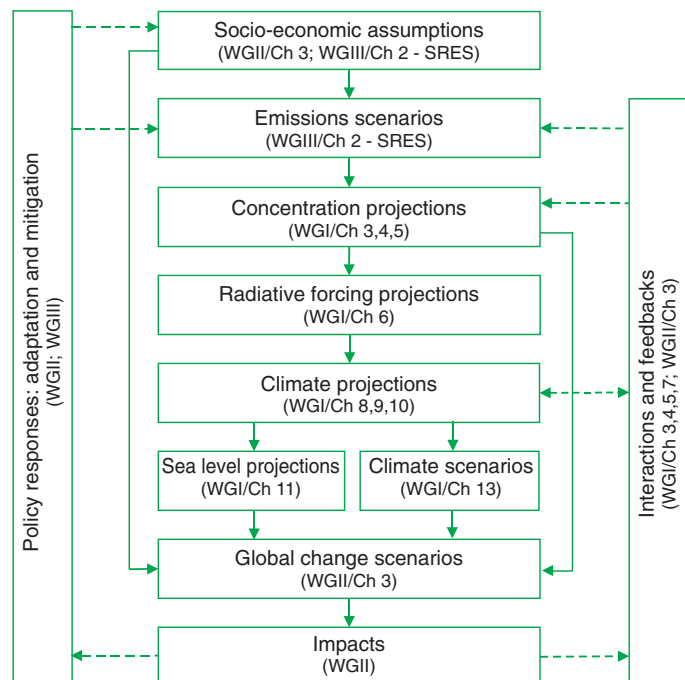


**Figure 28:** The cascade of uncertainties in projections to be considered in developing climate and related scenarios for climate change impact, adaptation, and mitigation assessment. [Based on Figure 13.2]

## Source Information: Technical Summary

This Appendix provides the cross-reference of the topics in the Technical Summary (page and section) to the sections of the chapters that contain expanded information about the topic.

### **Section A: Introduction**

<b>TS Page</b>	<b>Technical Summary Section and Topic – Chapter Section</b>
22	<b>A.1 The IPCC and its Working Groups</b> Introduction to the Intergovernmental Panel on Climate Change (from the IPCC Secretariat, Geneva) or the IPCC web page at <a href="http://www.ipcc.ch">http://www.ipcc.ch</a>
22 – 23	<b>A.2 The First and Second Assessment Reports of Working Group I</b> IPCC, 1990a: Climate Change: The IPCC Scientific Assessment. J.T. Houghton, G.J. Jenkins and J.J. Ephraums (eds.), Cambridge University Press, Cambridge, United Kingdom, 365 pp.  IPCC, 1992: Climate Change 1992: The Supplementary Report to the IPCC Scientific Assessment. J.T. Houghton, B.A. Callander and S.K. Varney (eds.), Cambridge University Press, Cambridge, United Kingdom, 198 pp.  IPCC, 1994: Climate Change 1994: Radiative Forcing of Climate Change and an Evaluation of the IPCC IS92 Emission Scenarios. J.T. Houghton, L.G. Meira Filho, J. Bruce, Hoesung Lee, B.A. Callander, E. Haites, N. Harris and K. Maskell (eds.), Cambridge University Press, Cambridge, United Kingdom, 339 pp.  IPCC, 1996a: Climate Change 1995: The Science of Climate Change. Contribution of Working Group I to the Second Assessment Report of the Intergovernmental Panel on Climate Change [Houghton, J.T., L.G. Meira Filho, B.A. Callander, N Harris, A. Kattenberg, and K. Maskell (eds.)]. Cambridge University Press, Cambridge, United Kingdom and New York, NY, USA, 572 pp.
23 – 24	<b>A.3 The Third Assessment Report: This Technical Summary</b> Background to these questions is in Chapter 1. Box 1: What drives changes in climate? – Chapter 1.

### **Section B: The Observed Changes in the Climate System**

<b>TS Page</b>	<b>Technical Summary Section and Topic – Chapter Section</b>
26 – 29	<b>B.1 Observed Changes in Temperature</b> Temperatures in the instrumental record for land and oceans – Chapter 2.2.2 and 2.3. Temperatures above the surface layer from satellite and weather balloon records – Chapter 2.2.3 and 2.2.4. Surface temperatures during the pre-instrumental record from the proxy record Last 1,000 years – Chapter 2.3. Last glacial and deglaciation – Chapter 2.4.
30	<b>B.2 Observed Changes in Precipitation and Atmospheric Moisture</b> Annual land-surface precipitation – Chapter 2.5.2. Water vapour – Chapter 2.5.3. Cloud amounts – Chapter 2.5.5.
30	<b>B.3 Observed Changes in Snow Cover and Land- and Sea-Ice Extent</b> Snow cover and land-ice extent – Chapter 2.2.5. Sea-ice extent – Chapter 2.2.5. Arctic sea-ice thickness – Chapter 2.2.5.
31 – 32	<b>B.4 Observed Changes in Sea Level</b> Changes During the Instrumental Record Tide gauge data for the 20th century – Chapter 11.3.2. Box 2: What causes sea level to change? – Chapter 11.2. Changes during the pre-instrumental record – Chapter 11.3.1.
32 – 33	<b>B.5 Observed Changes in Atmospheric and Oceanic Circulation Patterns</b> El Niño-Southern Oscillation (ENSO) – Chapter 2.6.2 and 2.6.3. North Atlantic, Arctic, and Antarctic oscillations – Chapter 2.6.5 and 2.6.6.
33	<b>B.6 Observed Changes in Climate Variability and Extreme Weather and Climate Events</b> Heavy and extreme precipitation – Chapter 2.7.2. Tropical and extra-tropical storms – Chapter 2.7.3.
33	<b>B.7 The Collective Picture: A Warming World and Other Changes in the Climate System</b> A warming world – Chapter 2.8. Little or no change – Chapter 2.2.5 and 2.7.3.

**Section C: The Forcing Agents That Cause Climate Change**

<b>TS Page</b>	<b>Technical Summary Section and Topic – Chapter Section</b>
38 – 43	<p><i>C.1 Observed Changes in Globally Well-Mixed Greenhouse Gas Concentrations and Radiative Forcing.</i>            Carbon dioxide – Chapter 3.2.2, 3.2.3, 3.3.1, 3.3.2, and 3.5, Chapter 6.13            Methane – Chapter 4.2.1, Chapter 6.13.            Nitrous Oxide – Chapter 4.2, Chapter 6.13.            Halocarbons and Related Compounds – Chapter 4.2.2, Chapter 6.13.</p>
43 – 44	<p><i>C.2 Observed Changes in Other Radiatively Important Gases</i>            Atmospheric ozone – Chapter 4.2.2 and 4.2.4, Chapter 6.13.            Gases with only indirect radiative influence – Chapter 4.2.3, Chapter 6.13</p>
44 – 45	<p><i>C.3 Observed and Modelled Changes in Aerosols</i>            Observed and modelled changes in aerosols – Chapter 5.1, 5.2, 5.3 and 5.4, Chapter 6.7 and 6.8.</p>
45	<p><i>C.4 Observed Changes in Other Anthropogenic Forcing Agents</i>            Land-use (albedo) change – Chapter 6.13.</p>
45 – 46	<p><i>C.5 Observed and Modelled Changes in Solar Activity</i>            Observed and modelled changes in solar activity – Chapter 6.10.</p>
46	<p><i>C.6 Global Warming Potentials</i>            Global warming potentials - Chapter 6.12</p>

**Section D: The Simulation of the Climate System and Its Changes**

<b>TS Page</b>	<b>Technical Summary Section and Topic – Chapter Section</b>
46 – 51	<p><i>D.1 Climate Processes and Feedbacks</i>            Box 3: Climate Models: How are they built and how are they applied? – Chapter 8.3.            Water vapour – Chapter 7.2.1.            Clouds – Chapter 7.2.2 and 7.2.3, Chapter 8.5.1.            Stratosphere – Chapter 7.2.4 and 7.2.5, Chapter 8.5.1.            Ocean – Chapter 7.3, Chapter 8.5.2.            Cryosphere – Chapter 7.5, Chapter 8.5.3.            Land surface – Chapter 7.4, Chapter 8.5.4.            Carbon cycle – Chapter 3.6.</p>
51 – 53	<p><i>D.2 The Coupled Systems</i>            Modes of natural variability – Chapter 7.6, Chapter 8.7.            Box 4: The El Niño/Southern Oscillation (ENSO) – Chapter 7.6.5, Chapter 8.7.1            The thermohaline circulation – Chapter 7.3.7 and 7.7, Chapter 9.3.4.            Non-linear events and rapid climate change – Chapter 7.7.</p>
53 – 54	<p><i>D.3 Regionalisation Techniques</i>            Categories of techniques – Chapter 10.1, 10.2, Chapter 13.            Coarse resolution AOGCMs – Chapter 10.3, Chapter 13.            High resolution RCMs – Chapter 10.5, Chapter 13.</p>
54 – 55	<p><i>D.4 Overall Assessment of Abilities</i>            Flux adjustment – Chapter 7.2, 7.3 and 7.6, Chapter 8.4 and 8.9.            Climate of the 20th century – Chapter 8.6.            Extreme events – Chapter 8.8.            Interannual variability – Chapter 8.7.            Model intercomparisons – Chapter 8.6.2 and 8.10.</p>

### **Section E: The Identification of a Human Influence on Climate Change**

<b>TS Page</b>	<b>Technical Summary Section and Topic – Chapter Section</b>
55 – 56	<i>E.1 The Meaning of Detection and Attribution</i> Detection/Attribution – Chapter 12.1.1 and 12.2.
56	<i>E.2 A Longer and More Closely Scrutinised Observational Record</i> Three of last five years – Chapter 12.2.1.
56	<i>E.3 New Model Estimates of Internal Variability</i> The warming over the past 100 years – Chapter 12.2.2.
57	<i>E.4 New Estimates of Responses to Natural Forcing</i> Natural forcing alone – Chapter 12.2.3.
57	<i>E.5 Sensitivity to Estimates of Climate Changes Signals</i> Responses to anthropogenic forcing – Chapter 12.2.3. Significant anthropogenic forcing contribution – Chapter 12.2.3.
57 – 59	<i>E.6 A Wider Range of Detection Techniques</i> Temperature – Chapter 12.3 and 12.4. Sea level – Chapter 11.4.
59 – 61	<i>E.7 Remaining Uncertainties in Detection and Attribution</i> Summary – Chapter 12.5.
61	<i>E.8 Synopsis</i> Most of the observed warming over the past 50 years – Chapter 12.6.

### **Section F: The Projections of the Earth's Future Climate**

<b>TS Page</b>	<b>Technical Summary Section and Topic – Chapter Section</b>
62 – 63	<i>F.1 The IPCC Special Report on Emissions Scenarios (SRES)</i> SRES scenarios – Chapter 6.15.2, SRES Report. Box 5: The Emission Scenarios of the Special Report on Emission Scenarios (SRES) – Chapter 6.15.2, SRES Report, Appendix II.
63 – 66	<i>F.2 Projections of Future Changes in Greenhouse Gases and Aerosols</i> CO <sub>2</sub> concentration trajectories – Chapter 3.3 and 3.7, Appendix II. Carbon storage in terrestrial ecosystems – Chapter 3.2 and 3.6. Abundance of the non-CO <sub>2</sub> greenhouse gases – Chapter 4.3, Chapter 6.15, Appendix II. Emissions of indirect greenhouse gases and atmospheric chemistry – Chapter 4.4.4 and 4.4.5, Chapter 6.15. Emissions of indirect greenhouse gases and air quality – Chapter 4.4.5 Dependence of the abundance of aerosols on emissions – Chapter 5.5, Chapter 6.15, Appendix II.
67 – 71	<i>F.3 Projections of Future Changes in Temperature</i> AOGCM Results – Chapter 9.3 Simple Climate Model Results – Chapter 9.3
71 – 72	<i>F.4 Projections of Future Changes in Precipitation</i> Globally averaged precipitation and variability – Chapter 9.3.
72 – 73	<i>F.5 Projections of Future Changes in Extreme Events</i> Changes in extreme events – Chapter 9.3.6.
73	<i>F.6 Projections of Future Changes in Thermohaline Circulation</i> Weakening of Thermohaline Circulation – Chapter 9.3.4.

	<b><i>Section G: Advancing Understanding</i></b>	
	<b>TS Page</b>	<b>Technical Summary Section and Topic – Chapter Section</b>
73	<i>F.7 Projections of Future Changes in Modes of Natural Variability</i> Changes in modes of natural variability – Chapter 9.3.5.	
73 – 74	<i>F.8 Projections of Future Changes in Land Ice (Glaciers, Ice Caps and Ice Sheets), Sea Ice and Snow Cover</i> Glaciers, ice caps, and ice sheets – Chapter 11.5.4.	
75	<i>F.9 Projections of Future Changes in Sea Level</i> Global average sea level change – Chapter 11.5.1. Regional sea level change – Chapter 11.5.2. Extremes of sea level – Chapter 11.5.3.	
75 – 77	<i>F.10 Projections of Future Changes in Response to CO<sub>2</sub> Concentration Stabilisation Profiles</i> Greenhouse gases and aerosols – Chapter 3.7.3. Temperature – Chapter 9.3.3. Sea level – Chapter 11.5.4.	
	78	<i>G.1 Data</i> Decline of observational networks and the observing system – Chapter 14.2.1.
	78	<i>G.2 Climate Processes and Modelling</i> Greenhouse gases and aerosols – Chapter 14.2.6. Processes – Chapter 14.2.3. Patterns of variability – Chapter 14.2.2. Ensembles of model results – Chapter 14.2.2. Hierarchy of models – Chapter 14.2.2
	79	<i>G.3 Human Aspects</i> Physical system/human system – Chapter 14.3, Chapter 13.1
	79	<i>G.4 International Framework</i> Co-ordination – Chapter 14.4.



# 1

---

## The Climate System: an Overview

---

### **Co-ordinating Lead Author**

A.P.M. Baede

### **Lead Authors**

E. Ahlonsou, Y. Ding, D. Schimel

### **Review Editors**

B. Bolin, S. Pollonais

# Contents

---

<b>1.1</b>	<b>Introduction to the Climate System</b>	87	<b>1.3</b>	<b>Human-induced Climate Variations</b>	92
1.1.1	Climate	87	1.3.1	Human Influence on the Climate System	92
1.1.2	The Climate System	87	1.3.2	Modelling and Projection of Anthropogenic Climate Change	94
<b>1.2</b>	<b>Natural Climate Variations</b>	89	1.3.3	Observing Anthropogenic Climate Change	96
1.2.1	Natural Forcing of the Climate System	89	<b>1.4</b>	<b>A ‘Road-map’ to this Report</b>	97
1.2.2	Natural Variability of Climate	91			
1.2.3	Extreme Events	92		<b>References</b>	98

## 1.1 Introduction to the Climate System

### 1.1.1 Climate

#### *Weather and climate*

Weather and climate have a profound influence on life on Earth. They are part of the daily experience of human beings and are essential for health, food production and well-being. Many consider the prospect of human-induced climate change as a matter of concern. The IPCC Second Assessment Report (IPCC, 1996) (hereafter SAR) presented scientific evidence that human activities may already be influencing the climate. If one wishes to understand, detect and eventually predict the human influence on climate, one needs to understand the system that determines the climate of the Earth and of the processes that lead to climate change.

In common parlance the notions “weather” and “climate” are loosely defined<sup>1</sup>. The “weather”, as we experience it, is the fluctuating state of the atmosphere around us, characterised by the temperature, wind, precipitation, clouds and other weather elements. This weather is the result of rapidly developing and decaying weather systems such as mid-latitude low and high pressure systems with their associated frontal zones, showers and tropical cyclones. Weather has only limited predictability. Mesoscale convective systems are predictable over a period of hours only; synoptic scale cyclones may be predictable over a period of several days to a week. Beyond a week or two individual weather systems are unpredictable. “Climate” refers to the average weather in terms of the mean and its variability over a certain time-span and a certain area. Classical climatology provides a classification and description of the various climate regimes found on Earth. Climate varies from place to place, depending on latitude, distance to the sea, vegetation, presence or absence of mountains or other geographical factors. Climate varies also in time; from season to season, year to year, decade to decade or on much longer time-scales, such as the Ice Ages. Statistically significant variations of the mean state of the climate or of its variability, typically persisting for decades or longer, are referred to as “climate change”. The Glossary gives definitions of these important and central notions of “climate variability” and “climate change”.

Climate variations and change, caused by external forcings, may be partly predictable, particularly on the larger, continental and global, spatial scales. Because human activities, such as the emission of greenhouse gases or land-use change, do result in external forcing, it is believed that the large-scale aspects of human-induced climate change are also partly predictable. However the ability to actually do so is limited because we cannot accurately predict population change, economic change, technological development, and other relevant characteristics of future human activity. In practice, therefore, one has to rely on carefully constructed scenarios of human behaviour and determine climate projections on the basis of such scenarios.

#### *Climate variables*

The traditional knowledge of weather and climate focuses on those variables that affect daily life most directly: average, maximum and minimum temperature, wind near the surface of the Earth, precipitation in its various forms, humidity, cloud type and amount, and solar radiation. These are the variables observed hourly by a large number of weather stations around the globe.

However this is only part of the reality that determines weather and climate. The growth, movement and decay of weather systems depend also on the vertical structure of the atmosphere, the influence of the underlying land and sea and many other factors not directly experienced by human beings. Climate is determined by the atmospheric circulation and by its interactions with the large-scale ocean currents and the land with its features such as albedo, vegetation and soil moisture. The climate of the Earth as a whole depends on factors that influence the radiative balance, such as for example, the atmospheric composition, solar radiation or volcanic eruptions. To understand the climate of our planet Earth and its variations and to understand and possibly predict the changes of the climate brought about by human activities, one cannot ignore any of these many factors and components that determine the climate. We must understand the *climate system*, the complicated system consisting of various components, including the dynamics and composition of the atmosphere, the ocean, the ice and snow cover, the land surface and its features, the many mutual interactions between them, and the large variety of physical, chemical and biological processes taking place in and among these components. “Climate” in a wider sense refers to the state of the climate system as a whole, including a statistical description of its variations. This chapter provides the reader with an overview of the climate system and the climate in this wider sense, and acts as an introduction to the Report.

### 1.1.2 The Climate System

#### *Its components*

The climate system, as defined in this Report, is an interactive system consisting of five major components: the atmosphere, the hydrosphere, the cryosphere, the land surface and the biosphere, forced or influenced by various external forcing mechanisms, the most important of which is the Sun (see Figure 1.1). Also the direct effect of human activities on the climate system is considered an external forcing.

The *atmosphere* is the most unstable and rapidly changing part of the system. Its composition, which has changed with the evolution of the Earth, is of central importance to the problem assessed in this Report. The Earth’s dry atmosphere is composed mainly of nitrogen ( $N_2$ , 78.1% volume mixing ratio), oxygen ( $O_2$ , 20.9% volume mixing ratio), and argon ( $Ar$ , 0.93% volume mixing ratio). These gases have only limited interaction with the incoming solar radiation and they do not interact with the infrared radiation emitted by the Earth. However there are a number of trace gases, such as carbon dioxide ( $CO_2$ ), methane ( $CH_4$ ), nitrous oxide ( $N_2O$ ) and ozone ( $O_3$ ), which do absorb and emit infrared radiation. These so called greenhouse gases, with a total volume mixing ratio in dry air of less than 0.1% by volume, play an essential role in the Earth’s energy budget. Moreover the

<sup>1</sup> For a definition of scientific and technical terms used in this Report: see Appendix I: Glossary.

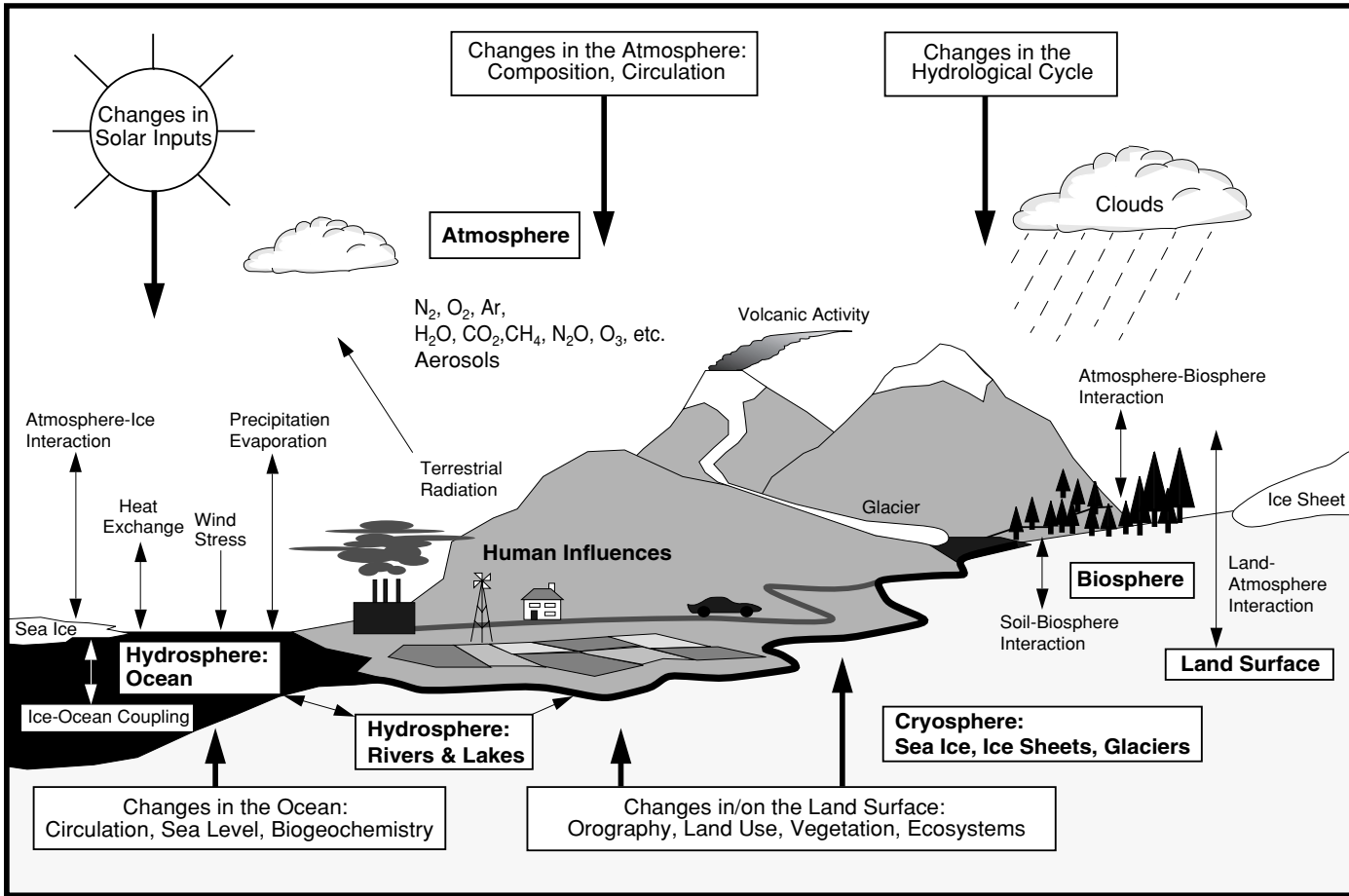


**Figure 1.1:** Schematic view of the components of the global climate system (bold), their processes and interactions (thin arrows) and some aspects that may change (bold arrows).

atmosphere contains water vapour ( $H_2O$ ), which is also a natural greenhouse gas. Its volume mixing ratio is highly variable, but it is typically in the order of 1%. Because these greenhouse gases absorb the infrared radiation emitted by the Earth and emit infrared radiation up- and downward, they tend to raise the temperature near the Earth's surface. Water vapour,  $CO_2$  and  $O_3$  also absorb solar short-wave radiation.

The atmospheric distribution of ozone and its role in the Earth's energy budget is unique. Ozone in the lower part of the atmosphere, the troposphere and lower stratosphere, acts as a greenhouse gas. Higher up in the stratosphere there is a natural layer of high ozone concentration, which absorbs solar ultra-violet radiation. In this way this so-called ozone layer plays an essential role in the stratosphere's radiative balance, at the same time filtering out this potentially damaging form of radiation.

Beside these gases, the atmosphere also contains solid and liquid particles (aerosols) and clouds, which interact with the incoming and outgoing radiation in a complex and spatially very variable manner. The most variable component of the atmosphere is water in its various phases such as vapour, cloud droplets, and ice crystals. Water vapour is the strongest greenhouse gas. For these reasons and because the transition between the various phases absorb and release much energy, water vapour is central to the climate and its variability and change.

The *hydrosphere* is the component comprising all liquid surface and subterranean water, both fresh water, including rivers, lakes and aquifers, and saline water of the oceans and seas. Fresh water runoff from the land returning to the oceans in rivers influences the ocean's composition and circulation. The oceans cover approximately 70% of the Earth's surface. They store and transport a large amount of energy and dissolve and store great quantities of carbon dioxide. Their circulation, driven by the wind and by density contrasts caused by salinity and thermal gradients (the so-called thermohaline circulation), is much slower than the atmospheric circulation. Mainly due to the large thermal inertia of the oceans, they damp vast and strong temperature changes and function as a regulator of the Earth's climate and as a source of natural climate variability, in particular on the longer time-scales.

The *cryosphere*, including the ice sheets of Greenland and Antarctica, continental glaciers and snow fields, sea ice and permafrost, derives its importance to the climate system from its high reflectivity (albedo) for solar radiation, its low thermal conductivity, its large thermal inertia and, especially, its critical role in driving deep ocean water circulation. Because the ice sheets store a large amount of water, variations in their volume are a potential source of sea level variations (Chapter 11).

Vegetation and soils at the *land surface* control how energy received from the Sun is returned to the atmosphere. Some is returned as long-wave (infrared) radiation, heating the atmosphere as the land surface warms. Some serves to evaporate water, either in the soil or in the leaves of plants, bringing water back into the atmosphere. Because the evaporation of soil moisture requires energy, soil moisture has a strong influence on the surface temperature. The texture of the land surface (its roughness) influences the atmosphere dynamically as winds blow over the land's surface. Roughness is determined by both topography and vegetation. Wind also blows dust from the surface into the atmosphere, which interacts with the atmospheric radiation.

The marine and terrestrial *biospheres* have a major impact on the atmosphere's composition. The biota influence the uptake and release of greenhouse gases. Through the photosynthetic process, both marine and terrestrial plants (especially forests) store significant amounts of carbon from carbon dioxide. Thus, the biosphere plays a central role in the carbon cycle, as well as in the budgets of many other gases, such as methane and nitrous oxide. Other biospheric emissions are the so-called volatile organic compounds (VOC) which may have important effects on atmospheric chemistry, on aerosol formation and therefore on climate. Because the storage of carbon and the exchange of trace gases are influenced by climate, feedbacks between climate change and atmospheric concentrations of trace gases can occur. The influence of climate on the biosphere is preserved as fossils, tree rings, pollen and other records, so that much of what is known of past climates comes from such biotic indicators.

#### *Interactions among the components*

Many physical, chemical and biological interaction processes occur among the various components of the climate system on a wide range of space and time scales, making the system extremely complex. Although the components of the climate system are very different in their composition, physical and chemical properties, structure and behaviour, they are all linked by fluxes of mass, heat and momentum: all subsystems are open and interrelated.

As an example, the atmosphere and the oceans are strongly coupled and exchange, among others, water vapour and heat through evaporation. This is part of the hydrological cycle and leads to condensation, cloud formation, precipitation and runoff, and supplies energy to weather systems. On the other hand, precipitation has an influence on salinity, its distribution and the thermohaline circulation. Atmosphere and oceans also exchange, among other gases, carbon dioxide, maintaining a balance by dissolving it in cold polar water which sinks into the deep ocean and by outgassing in relatively warm upwelling water near the equator.

Some other examples: sea ice hinders the exchanges between atmosphere and oceans; the biosphere influences the carbon dioxide concentration by photosynthesis and respiration, which in turn is influenced by climate change. The biosphere also affects the input of water in the atmosphere through evapotranspiration, and the atmosphere's radiative balance through the amount of sunlight reflected back to the sky (albedo).

These are just a few examples from a virtually inexhaustible list of complex interactions some of which are poorly known or perhaps even unknown. Chapter 7 provides an assessment of the present knowledge of physical climate processes and feedbacks, whilst Chapter 3 deals with biological feedbacks.

Any change, whether natural or anthropogenic, in the components of the climate system and their interactions, or in the external forcing, may result in climate variations. The following sections introduce various aspects of natural climate variations, followed by an introduction to the human influence on the climate system.

## 1.2 Natural Climate Variations

### 1.2.1 Natural Forcing of the Climate System

#### *The Sun and the global energy balance*

The ultimate source of energy that drives the climate system is radiation from the Sun. About half of the radiation is in the visible short-wave part of the electromagnetic spectrum. The other half is mostly in the near-infrared part, with some in the ultraviolet part of the spectrum. Each square metre of the Earth's spherical surface outside the atmosphere receives an average throughout the year of 342 Watts of solar radiation, 31% of which is immediately reflected back into space by clouds, by the atmosphere, and by the Earth's surface. The remaining  $235 \text{ Wm}^{-2}$  is partly absorbed by the atmosphere but most ( $168 \text{ Wm}^{-2}$ ) warms the Earth's surface: the land and the ocean. The Earth's surface returns that heat to the atmosphere, partly as infrared radiation, partly as sensible heat and as water vapour which releases its heat when it condenses higher up in the atmosphere. This exchange of energy between surface and atmosphere maintains under present conditions a global mean temperature near the surface of  $14^\circ\text{C}$ , decreasing rapidly with height and reaching a mean temperature of  $-58^\circ\text{C}$  at the top of the troposphere.

For a stable climate, a balance is required between incoming solar radiation and the outgoing radiation emitted by the climate system. Therefore the climate system itself must radiate on average  $235 \text{ Wm}^{-2}$  back into space. Details of this energy balance can be seen in Figure 1.2, which shows on the left hand side what happens with the incoming solar radiation, and on the right hand side how the atmosphere emits the outgoing infrared radiation. Any physical object radiates energy of an amount and at wavelengths typical for the temperature of the object: at higher temperatures more energy is radiated at shorter wavelengths. For the Earth to radiate  $235 \text{ Wm}^{-2}$ , it should radiate at an effective emission temperature of  $-19^\circ\text{C}$  with typical wavelengths in the infrared part of the spectrum. This is  $33^\circ\text{C}$  lower than the average temperature of  $14^\circ\text{C}$  at the Earth's surface. To understand why this is so, one must take into account the radiative properties of the atmosphere in the infrared part of the spectrum.

#### *The natural greenhouse effect*

The atmosphere contains several trace gases which absorb and emit infrared radiation. These so-called greenhouse gases absorb infrared radiation, emitted by the Earth's surface, the atmosphere

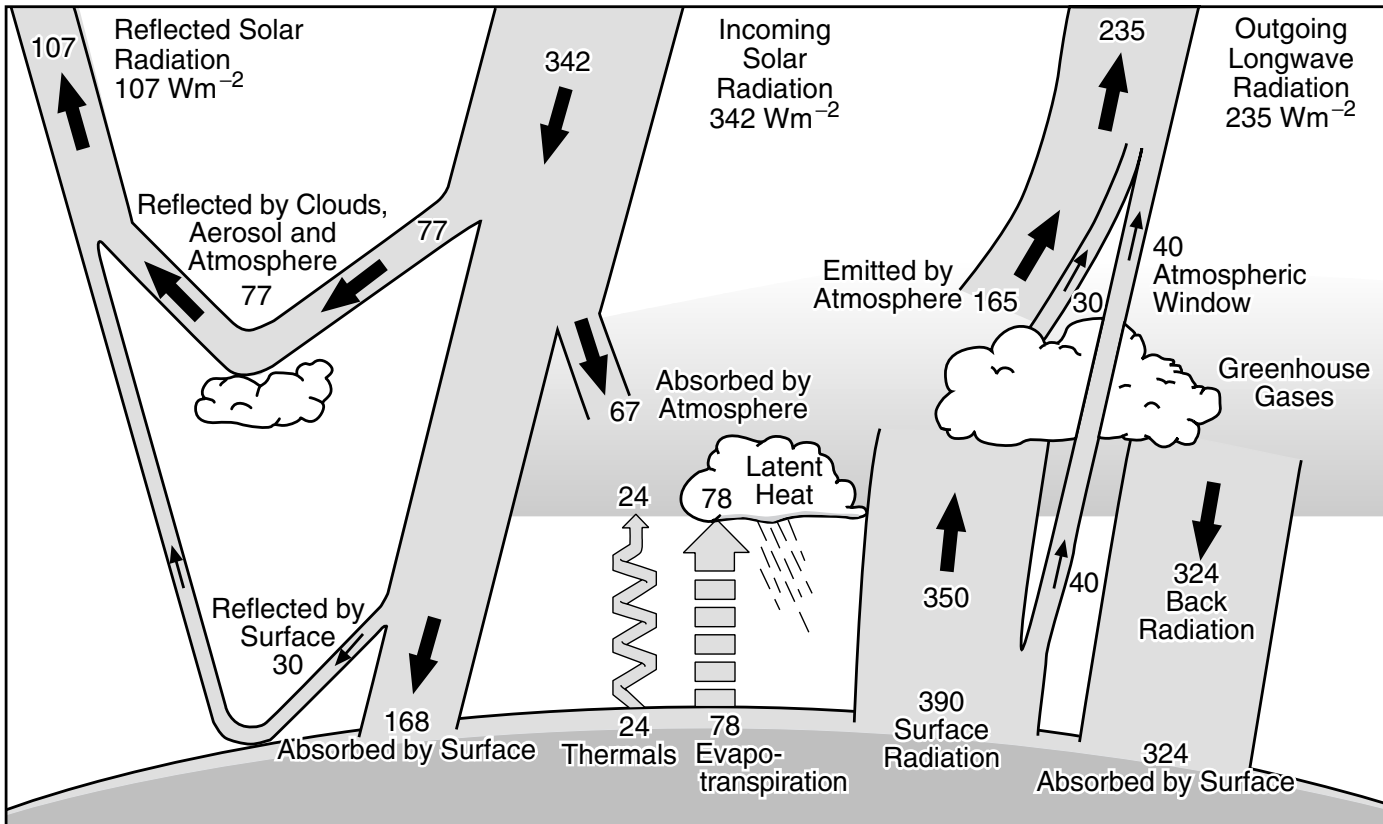


**Figure 1.2:** The Earth's annual and global mean energy balance. Of the incoming solar radiation, 49% ( $168 \text{ W m}^{-2}$ ) is absorbed by the surface. That heat is returned to the atmosphere as sensible heat, as evapotranspiration (latent heat) and as thermal infrared radiation. Most of this radiation is absorbed by the atmosphere, which in turn emits radiation both up and down. The radiation lost to space comes from cloud tops and atmospheric regions much colder than the surface. This causes a greenhouse effect. Source: Kiehl and Trenberth, 1997: Earth's Annual Global Mean Energy Budget, *Bull. Am. Met. Soc.* 78, 197-208.

and clouds, except in a transparent part of the spectrum called the “atmospheric window”, as shown in Figure 1.2. They emit in turn infrared radiation in all directions including downward to the Earth’s surface. Thus greenhouse gases trap heat within the atmosphere. This mechanism is called the natural greenhouse effect. The net result is an upward transfer of infrared radiation from warmer levels near the Earth’s surface to colder levels at higher altitudes. The infrared radiation is effectively radiated back into space from an altitude with a temperature of, on average,  $-19^\circ\text{C}$ , in balance with the incoming radiation, whereas the Earth’s surface is kept at a much higher temperature of on average  $14^\circ\text{C}$ . This effective emission temperature of  $-19^\circ\text{C}$  corresponds in mid-latitudes with a height of approximately 5 km. Note that it is essential for the greenhouse effect that the temperature of the lower atmosphere is not constant (isothermal) but decreases with height. The natural greenhouse effect is part of the energy balance of the Earth, as can be seen schematically in Figure 1.2.

Clouds also play an important role in the Earth’s energy balance and in particular in the natural greenhouse effect. Clouds absorb and emit infrared radiation and thus contribute to warming the Earth’s surface, just like the greenhouse gases. On the other hand, most clouds are bright reflectors of solar radiation and tend to cool the climate system. The net average effect of the Earth’s cloud cover in the present climate is a slight cooling: the

reflection of radiation more than compensates for the greenhouse effect of clouds. However this effect is highly variable, depending on height, type and optical properties of clouds.

This introduction to the global energy balance and the natural greenhouse effect is entirely in terms of the global mean and in radiative terms. However, for a full understanding of the greenhouse effect and of its impact on the climate system, dynamical feedbacks and energy transfer processes should also be taken into account. Chapter 7 presents a more detailed analysis and assessment.

#### Radiative forcing and forcing variability

In an equilibrium climate state the average net radiation at the top of the atmosphere is zero. A change in either the solar radiation or the infrared radiation changes the net radiation. The corresponding imbalance is called “radiative forcing”. In practice, for this purpose, the top of the troposphere (the tropopause) is taken as the top of the atmosphere, because the stratosphere adjusts in a matter of months to changes in the radiative balance, whereas the surface-troposphere system adjusts much more slowly, owing principally to the large thermal inertia of the oceans. The radiative forcing of the surface troposphere system is then the change in net irradiance at the tropopause after allowing for stratospheric temperatures to re-adjust to radiative equilibrium, but with surface and tropospheric temperatures and state held

fixed at the unperturbed values. A detailed explanation and discussion of the radiative forcing concept may be found in Appendix 6.1 to Chapter 6.

External forcings, such as the solar radiation or the large amounts of aerosols ejected by volcanic eruption into the atmosphere, may vary on widely different time-scales, causing natural variations in the radiative forcing. These variations may be negative or positive. In either case the climate system must react to restore the balance. A positive radiative forcing tends to warm the surface on average, whereas a negative radiative forcing tends to cool it. Internal climate processes and feedbacks may also cause variations in the radiative balance by their impact on the reflected solar radiation or emitted infrared radiation, but such variations are not considered part of radiative forcing. Chapter 6 assesses the present knowledge of radiative forcing and its variations, including the anthropogenic change of the atmospheric composition.

### **1.2.2 Natural Variability of Climate**

#### *Internally and externally induced climate variability*

Climate variations, both in the mean state and in other statistics such as, for example, the occurrence of extreme events, may result from radiative forcing, but also from internal interactions between components of the climate system. A distinction can therefore be made between externally and internally induced natural climate variability and change.

When variations in the external forcing occur, the response time of the various components of the climate system is very different. With regard to the atmosphere, the response time of the troposphere is relatively short, from days to weeks, whereas the stratosphere comes into equilibrium on a time-scale of typically a few months. Due to their large heat capacity, the oceans have a much longer response time, typically decades but up to centuries or millennia. The response time of the strongly coupled surface-troposphere system is therefore slow compared with that of the stratosphere, and is mainly determined by the oceans. The biosphere may respond fast, e.g. to droughts, but also very slowly to imposed changes. Therefore the system may respond to variations in external forcing on a wide range of space- and time-scales. The impact of solar variations on the climate provides an example of such externally induced climate variations.

But even without changes in external forcing, the climate may vary naturally, because, in a system of components with very different response times and non-linear interactions, the components are never in equilibrium and are constantly varying. An example of such internal climate variation is the El Niño-Southern Oscillation (ENSO), resulting from the interaction between atmosphere and ocean in the tropical Pacific.

#### *Feedbacks and non-linearities*

The response of the climate to the internal variability of the climate system and to external forcings is further complicated by feedbacks and non-linear responses of the components. A process is called a feedback when the result of the process affects its origin thereby intensifying (positive feedback) or reducing (negative feedback) the original effect. An important example of a positive

feedback is the water vapour feedback in which the amount of water vapour in the atmosphere increases as the Earth warms. This increase in turn may amplify the warming because water vapour is a strong greenhouse gas. A strong and very basic negative feedback is radiative damping: an increase in temperature strongly increases the amount of emitted infrared radiation. This limits and controls the original temperature increase.

A distinction is made between physical feedbacks involving physical climate processes, and biogeochemical feedbacks often involving coupled biological, geological and chemical processes. An example of a physical feedback is the complicated interaction between clouds and the radiative balance. Chapter 7 provides an overview and assessment of the present knowledge of such feedbacks. An important example of a biogeochemical feedback is the interaction between the atmospheric CO<sub>2</sub> concentration and the carbon uptake by the land surface and the oceans. Understanding this feedback is essential for an understanding of the carbon cycle. This is discussed and assessed in detail in Chapter 3.

Many processes and interactions in the climate system are non-linear. That means that there is no simple proportional relation between cause and effect. A complex, non-linear system may display what is technically called chaotic behaviour. This means that the behaviour of the system is critically dependent on very small changes of the initial conditions. This does not imply, however, that the behaviour of non-linear chaotic systems is entirely unpredictable, contrary to what is meant by “chaotic” in colloquial language. It has, however, consequences for the nature of its variability and the predictability of its variations. The daily weather is a good example. The evolution of weather systems responsible for the daily weather is governed by such non-linear chaotic dynamics. This does not preclude successful weather prediction, but its predictability is limited to a period of at most two weeks. Similarly, although the climate system is highly non-linear, the quasi-linear response of many models to present and predicted levels of external radiative forcing suggests that the large-scale aspects of human-induced climate change may be predictable, although as discussed in Section 1.3.2 below, unpredictable behaviour of non-linear systems can never be ruled out. The predictability of the climate system is discussed in Chapter 7.

#### *Global and hemispheric variability*

Climate varies naturally on all time-scales. During the last million years or so, glacial periods and interglacials have alternated as a result of variations in the Earth's orbital parameters. Based on Antarctic ice cores, more detailed information is available now about the four full glacial cycles during the last 500,000 years. In recent years it was discovered that during the last glacial period large and very rapid temperature variations took place over large parts of the globe, in particular in the higher latitudes of the Northern Hemisphere. These abrupt events saw temperature changes of many degrees within a human lifetime. In contrast, the last 10,000 years appear to have been relatively more stable, though locally quite large changes have occurred.

Recent analyses suggest that the Northern Hemisphere climate of the past 1,000 years was characterised by an irregular but steady cooling, followed by a strong warming during the 20th

century. Temperatures were relatively warm during the 11th to 13th centuries and relatively cool during the 16th to 19th centuries. These periods coincide with what are traditionally known as the medieval Climate Optimum and the Little Ice Age, although these anomalies appear to have been most distinct only in and around the North Atlantic region. Based on these analyses, the warmth of the late 20th century appears to have been unprecedented during the millennium. A comprehensive review and assessment of observed global and hemispheric variability may be found in Chapter 2.

The scarce data from the Southern Hemisphere suggest temperature changes in past centuries markedly different from those in the Northern Hemisphere, the only obvious similarity being the strong warming during the 20th century.

#### *Regional patterns of climate variability*

Regional or local climate is generally much more variable than climate on a hemispheric or global scale because regional or local variations in one region are compensated for by opposite variations elsewhere. Indeed a closer inspection of the spatial structure of climate variability, in particular on seasonal and longer time-scales, shows that it occurs predominantly in preferred large-scale and geographically anchored spatial patterns. Such patterns result from interactions between the atmospheric circulation and the land and ocean surfaces. Though geographically anchored, their amplitude can change in time as, for example, the heat exchange with the underlying ocean changes.

A well-known example is the quasi-periodically varying ENSO phenomenon, caused by atmosphere-ocean interaction in the tropical Pacific. The resulting El Niño and La Niña events have a worldwide impact on weather and climate.

Another example is the North Atlantic Oscillation (NAO), which has a strong influence on the climate of Europe and part of Asia. This pattern consists of opposing variations of barometric pressure near Iceland and near the Azores. On average, a westerly current, between the Icelandic low pressure area and the Azores high-pressure area, carries cyclones with their associated frontal systems towards Europe. However the pressure difference between Iceland and the Azores fluctuates on time-scales of days to decades, and can be reversed at times. The variability of NAO has considerable influence on the regional climate variability in Europe, in particular in wintertime. Chapter 7 discusses the internal processes involved in NAO variability.

Similarly, although data are scarcer, leading modes of variability have been identified over the Southern Hemisphere. Examples are a North-South dipole structure over the Southern Pacific, whose variability is strongly related to ENSO variability, and the Antarctic Oscillation, a zonal pressure fluctuation between middle and high latitudes of the Southern Hemisphere. A detailed account of regional climate variability may be found in Chapter 2.

#### **1.2.3 Extreme Events**

Climate as defined is associated with a certain probability distribution of weather events. Weather events with values far away from the mean (such as heat waves, droughts and flooding) are by definition less likely to occur. The least likely events in a statis-

tical sense are called “extreme events”. Extreme weather in one region (e.g. a heat wave) may be normal in another. In both regions nature and society are adapted to the regional weather averaged over longer periods, but much less to extremes. For example, tropical African temperatures could severely damage vegetation or human health if they occurred in Northern Europe. Impacts of extreme events are felt strongly by ecosystems and society and may be destructive.

Small changes in climate may, but will not necessarily, have a large impact on the probability distribution of weather events in space and time, and on the intensity of extremes. Nature and society are often particularly ill prepared and vulnerable for such changes. This is the reason why since the SAR much more attention has been paid to observed and projected variations of extremes. Chapter 2 gives an assessment of the present knowledge.

### **1.3 Human-induced Climate Variations**

#### *1.3.1 Human Influence on the Climate System*

Human beings, like other living organisms, have always influenced their environment. It is only since the beginning of the Industrial Revolution, mid-18th century, that the impact of human activities has begun to extend to a much larger scale, continental or even global. Human activities, in particular those involving the combustion of fossil fuels for industrial or domestic usage, and biomass burning, produce greenhouse gases and aerosols which affect the composition of the atmosphere. The emission of chlorofluorocarbons (CFCs) and other chlorine and bromine compounds has not only an impact on the radiative forcing, but has also led to the depletion of the stratospheric ozone layer. Land-use change, due to urbanisation and human forestry and agricultural practices, affect the physical and biological properties of the Earth’s surface. Such effects change the radiative forcing and have a potential impact on regional and global climate.

#### *Anthropogenic perturbation of the atmospheric composition*

For about a thousand years before the Industrial Revolution, the amount of greenhouse gases in the atmosphere remained relatively constant. Since then, the concentration of various greenhouse gases has increased. The amount of carbon dioxide, for example, has increased by more than 30% since pre-industrial times and is still increasing at an unprecedented rate of on average 0.4% per year, mainly due to the combustion of fossil fuels and deforestation. We know that this increase is anthropogenic because the changing isotopic composition of the atmospheric CO<sub>2</sub> betrays the fossil origin of the increase. The concentration of other natural radiatively active atmospheric components, such as methane and nitrous oxide, is increasing as well due to agricultural, industrial and other activities. The concentration of the nitrogen oxides (NO and NO<sub>2</sub>) and of carbon monoxide (CO) are also increasing. Although these gases are not greenhouse gases, they play a role in the atmospheric chemistry and have led to an increase in tropospheric ozone, a greenhouse gas, by 40% since pre-industrial times (Chapter 4). Moreover,

$\text{NO}_2$  is an important absorber of visible solar radiation. Chlorofluorocarbons and some other halogen compounds do not occur naturally in the atmosphere but have been introduced by human activities. Beside their depleting effect on the stratospheric ozone layer, they are strong greenhouse gases. Their greenhouse effect is only partly compensated for by the depletion of the ozone layer which causes a negative forcing of the surface-troposphere system. All these gases, except tropospheric ozone and its precursors, have long to very long atmospheric lifetimes and therefore become well-mixed throughout the atmosphere.

Human industrial, energy related, and land-use activities also increase the amount of aerosol in the atmosphere, in the form of mineral dust, sulphates and nitrates and soot. Their atmospheric lifetime is short because they are removed by rain. As a result their concentrations are highest near their sources and vary substantially regionally, with global consequences. The increases in greenhouse gas concentrations and aerosol content in the atmosphere result in a change in the radiative forcing to which the climate system must act to restore the radiative balance.

#### *The enhanced greenhouse effect*

The increased concentration of greenhouse gases in the atmosphere enhances the absorption and emission of infrared radiation. The atmosphere's opacity increases so that the altitude from which the Earth's radiation is effectively emitted into space becomes higher. Because the temperature is lower at higher altitudes, less energy is emitted, causing a positive radiative forcing. This effect is called the enhanced greenhouse effect, which is discussed in detail in Chapter 6.

If the amount of carbon dioxide were doubled instantaneously, with everything else remaining the same, the outgoing infrared radiation would be reduced by about  $4 \text{ Wm}^{-2}$ . In other words, the radiative forcing corresponding to a doubling of the  $\text{CO}_2$  concentration would be  $4 \text{ Wm}^{-2}$ . To counteract this imbalance, the temperature of the surface-troposphere system would have to increase by  $1.2^\circ\text{C}$  (with an accuracy of  $\pm 10\%$ ), in the absence of other changes. In reality, due to feedbacks, the response of the climate system is much more complex. It is believed that the overall effect of the feedbacks amplifies the temperature increase to  $1.5$  to  $4.5^\circ\text{C}$ . A significant part of this uncertainty range arises from our limited knowledge of clouds and their interactions with radiation. To appreciate the magnitude of this temperature increase, it should be compared with the global mean temperature difference of perhaps  $5$  or  $6^\circ\text{C}$  from the middle of the last Ice Age to the present interglacial.

The so-called water vapour feedback, caused by an increase in atmospheric water vapour due to a temperature increase, is the most important feedback responsible for the amplification of the temperature increase. Concern has been expressed about the strength of this feedback, in particular in relation to the role of upper tropospheric humidity. Since the SAR, thinking about this feedback has become increasingly sophisticated thanks both to modelling and to observational studies. Feedbacks are discussed and assessed in Chapter 7. In particular, the present state of knowledge of the water vapour feedback is examined in Section 7.2.1.

It has been suggested that the absorption by  $\text{CO}_2$  is already saturated so that an increase would have no effect. This, however,

is not the case. Carbon dioxide absorbs infrared radiation in the middle of its  $15 \mu\text{m}$  band to the extent that radiation in the middle of this band cannot escape unimpeded: this absorption is saturated. This, however, is not the case for the band's wings. It is because of these effects of partial saturation that the radiative forcing is not proportional to the increase in the carbon dioxide concentration but shows a logarithmic dependence. Every further doubling adds an additional  $4 \text{ Wm}^{-2}$  to the radiative forcing.

The other human-made greenhouse gases add to the effect of increased carbon dioxide. Their total effect at the surface is often expressed in terms of the effect of an equivalent increase in carbon dioxide.

#### *The effect of aerosols*

The effect of the increasing amount of aerosols on the radiative forcing is complex and not yet well known. The direct effect is the scattering of part of the incoming solar radiation back into space. This causes a negative radiative forcing which may partly, and locally even completely, offset the enhanced greenhouse effect. However, due to their short atmospheric lifetime, the radiative forcing is very inhomogeneous in space and in time. This complicates their effect on the highly non-linear climate system. Some aerosols, such as soot, absorb solar radiation directly, leading to local heating of the atmosphere, or absorb and emit infrared radiation, adding to the enhanced greenhouse effect.

Aerosols may also affect the number, density and size of cloud droplets. This may change the amount and optical properties of clouds, and hence their reflection and absorption. It may also have an impact on the formation of precipitation. As discussed in Chapter 5, these are potentially important indirect effects of aerosols, resulting probably in a negative radiative forcing of as yet very uncertain magnitude.

#### *Land-use change*

The term "land-use change" refers to a change in the use or management of land. Such change may result from various human activities such as changes in agriculture and irrigation, deforestation, reforestation and afforestation, but also from urbanisation or traffic. Land-use change results in changing the physical and biological properties of the land surface and thus the climate system.

It is now recognized that land-use change on the present scale may contribute significantly to changing the local, regional or even global climate and moreover has an important impact on the carbon cycle. Physical processes and feedbacks caused by land-use change, that may have an impact on the climate, include changes in albedo and surface roughness, and the exchange between land and atmosphere of water vapour and greenhouse gases. These climatic consequences of land-use change are discussed and evaluated in Section 4 of Chapter 7. Land-use change may also affect the climate system through biological processes and feedbacks involving the terrestrial vegetation, which may lead to changes in the sources and sinks of carbon in its various forms. Chapter 3 reviews the consequences for the carbon cycle. Obviously the combined effect of these physical and biogeochemical processes and feedbacks is complex, but new data sets and models start to shed light on this.

Urbanisation is another kind of land-use change. This may affect the local wind climate through its influence on the surface roughness. It may also create a local climate substantially warmer than the surrounding countryside by the heat released by densely populated human settlements, by changes in evaporation characteristics and by modifying the outgoing long-wave radiation through interception by tall buildings etc. This is known as an “urban heat island”. The influence on the regional climate may be noticeable but small. It may however have a significant influence on long instrumental temperature records from stations affected by expanding urbanisation. The consequences of this urbanisation effect for the global surface temperature record has been the subject of debate. It is discussed in Section 2.2.2 of Chapter 2.

#### *Climate response*

The increase in greenhouse gas and aerosol concentrations in the atmosphere and also land-use change produces a radiative forcing or affects processes and feedbacks in the climate system. As discussed in Chapter 7, the response of the climate to these human-induced forcings is complicated by such feedbacks, by the strong non-linearity of many processes and by the fact that the various coupled components of the climate system have very different response times to perturbations. Qualitatively, an increase of atmospheric greenhouse gas concentrations leads to an average increase of the temperature of the surface-troposphere system. The response of the stratosphere is entirely different. The stratosphere is characterised by a radiative balance between absorption of solar radiation, mainly by ozone, and emission of infrared radiation mainly by carbon dioxide. An increase in the carbon dioxide concentration therefore leads to an increase of the emission and thus to a cooling of the stratosphere.

The only means available to quantify the non-linear climate response is by using numerical models of the climate system based on well-established physical, chemical and biological principles, possibly combined with empirical and statistical methods.

### **1.3.2 Modelling and Projection of Anthropogenic Climate Change**

#### *Climate models*

The behaviour of the climate system, its components and their interactions, can be studied and simulated using tools known as climate models. These are designed mainly for studying climate processes and natural climate variability, and for projecting the response of the climate to human-induced forcing. Each component or coupled combination of components of the climate system can be represented by models of varying complexity.

The nucleus of the most complex atmosphere and ocean models, called General Circulation Models (Atmospheric General Circulation Models (AGCMs) and Ocean General Circulation Models (OGCMs)) is based upon physical laws describing the dynamics of atmosphere and ocean, expressed by mathematical equations. Since these equations are non-linear, they need to be solved numerically by means of well-established mathematical techniques. Current atmosphere models are solved spatially on a three-dimensional grid of points on the globe with

a horizontal resolution typically of 250 km and some 10 to 30 levels in the vertical. A typical ocean model has a horizontal resolution of 125 to 250 km and a resolution of 200 to 400 m in the vertical. Their time-dependent behaviour is computed by taking time steps typically of 30 minutes. The impact of the spatial resolution on the model simulations is discussed in Section 8.9 of Chapter 8.

Models of the various components of the climate system may be coupled to produce increasingly complex models. The historical development of such coupled climate models is shown in Box 3 of the Technical Summary. Processes taking place on spatial and temporal scales smaller than the model’s resolution, such as individual clouds or convection in atmosphere models, or heat transport through boundary currents or mesoscale eddies in ocean models, are included through a parametric representation in terms of the resolved basic quantities of the model. Coupled atmosphere-ocean models, including such parametrized physical processes, are called Atmosphere-Ocean General Circulation Models (AOGCMs). They are combined with mathematical representations of other components of the climate system, sometimes based on empirical relations, such as the land surface and the cryosphere. The most recent models may include representations of aerosol processes and the carbon cycle, and in the near future perhaps also the atmospheric chemistry. The development of these very complex coupled models goes hand in hand with the availability of ever larger and faster computers to run the models. Climate simulations require the largest, most capable computers available.

A realistic representation of the coupling between the various components of the climate system is essential. In particular the coupling between the atmosphere and the oceans is of central importance. The oceans have a huge heat capacity and a decisive influence on the hydrological cycle of the climate system, and store and exchange large quantities of carbon dioxide. To a large degree the coupling between oceans and atmosphere determines the energy budget of the climate system. There have been difficulties modelling this coupling with enough accuracy to prevent the model climate unrealistically drifting away from the observed climate. Such climate drift may be avoided by adding an artificial correction to the coupling, the so-called “flux adjustment”. The evaluation in Chapter 8 of recent model results identifies improvements since the SAR, to the point that there is a reduced reliance on such corrections, with some recent models operating with minimal or no adjustment.

For various reasons, discussed in Section 8.3 of Chapter 8, it is important to also develop and use simpler models than the fully coupled comprehensive AOGCMs, for example to study only one or a specific combination of components of the climate system or even single processes, or to study many different alternatives, which is not possible or is impractical with comprehensive models. In IPCC (1997) a hierarchy of models used in the IPCC assessment process was identified and described, differing in such aspects as the number of spatial dimensions, the extent to which physical processes are explicitly represented, the level to which empirical parametrization is involved, and the computational costs of running the models. In the IPCC context, simple models are also used to compute the consequences of greenhouse

gas emission scenarios. Such models are tuned to the AOGCMs to give similar results when globally averaged.

#### *Projections of climate change*

Climate models are used to simulate and quantify the climate response to present and future human activities. The first step is to simulate the present climate for extended simulation periods, typically many decades, under present conditions without any change in external climate forcing.

The quality of these simulations is assessed by systematically comparing the simulated climate with observations of the present climate. In this way the model is evaluated and its quality established. A range of diagnostic tools has been developed to assist the scientists in carrying out the evaluation. This step is essential to gain confidence in and provide a baseline for projections of human-induced climate change. Models may also be evaluated by running them under different palaeoclimate (e.g. Ice Age) conditions. Chapter 8 of this report presents a detailed assessment of the latest climate models of various complexity, in particular the AOGCMs. Once the quality of the model is established, two different strategies have been applied to make projections of future climate change.

The first, so-called equilibrium method is to change, e.g. double, the carbon dioxide concentration and to run the model again to a new equilibrium. The differences between the climate statistics of the two simulations provide an estimate of the climate change corresponding to the doubling of carbon dioxide, and of the sensitivity of the climate to a change in the radiative forcing. This method reduces systematic errors present in both simulations. If combined with simple slab ocean models, this strategy is relatively cheap because it does not require long runs to reach equilibrium. However it does not provide insight in to the time dependence of climate change.

The second, so-called transient, method, common nowadays with improved computer resources, is to force the model with a greenhouse gas and aerosol scenario. The difference between such simulation and the original baseline simulation provides a time-dependent projection of climate change.

This transient method requires a time-dependent profile of greenhouse gas and aerosol concentrations. These may be derived from so-called emission scenarios. Such scenarios have been developed, among others by IPCC, on the basis of various internally coherent assumptions concerning future socio-economic and demographic developments. In the SAR the IPCC Scenarios IS92 were used (IPCC, 1994). The most recent IPCC emission scenarios are described in the IPCC Special Report on Emission Scenarios (Nakićenović *et al.*, 2000). Different assumptions concerning e.g. the growth of the world population, energy intensity and efficiency, and economic growth, lead to considerably different emission scenarios. For example the two extreme estimates in the IPCC IS92 scenarios of the carbon dioxide emission by 2100 differ by a factor of 7. Because scenarios by their very nature should not be used and regarded as predictions, the term "climate projections" is used in this Report.

Transient simulations may also be based on artificially constructed, so-called idealised, scenarios. For example, scenarios have been constructed, assuming a gradual increase of

greenhouse gas concentrations followed by stabilisation at various levels. Climate simulations based on such idealised scenarios may provide insight in to the climate response to potential policy measures leading to a stabilisation of the GHG concentrations, which is the ultimate objective of the United Nations Framework Convention on Climate Change (UNFCCC) as formulated in its Article 2. See Section 3 of Chapter 9 for an assessment.

Projections from present models show substantial agreement, but at the same time there is still a considerable degree of ambiguity and difference between the various models. All models show an increase in the globally averaged equilibrium surface temperature and global mean precipitation. In Chapter 9 the results of various models and intercomparison projects are assessed. Model results are more ambiguous about the spatial patterns of climate change than about the global response. Regional patterns depend significantly on the time dependence of the forcing, the spatial distribution of aerosol concentrations and details of the modelled climate processes. Research tools have been developed to generate more reliable regional climate information. These tools and their results are presented and assessed in Chapter 10.

To study the impact of climate change, a plausible and consistent description of a possible future climate is required. The construction of such climate change scenarios relies mainly on results from model projections, although sometimes information from past climates is used. The basis for and development of such scenarios is assessed in Chapter 13. Global and regional sea-level change scenarios are reviewed in Chapter 11.

#### *Predictability, global and regional*

In trying to quantify climate change, there is a fundamental question to be answered: is the evolution of the state of the climate system predictable? Since the pioneering work by Lorenz in the 1960s, it is well known that complex non-linear systems have limited predictability, even though the mathematical equations describing the time evolution of the system are perfectly deterministic.

The climate system is, as we have seen, such a non-linear complex system with many inherent time scales. Its predictability may depend on the type of climate event considered, the time and space scales involved and whether internal variability of the system or variability from changes in external forcing is involved. Internal variations caused by the chaotic dynamics of the climate system may be predictable to some extent. Recent experience has shown that the ENSO phenomenon may possess a fair degree of predictability for several months or even a year ahead. The same may be true for other events dominated by the long oceanic time-scales, such as perhaps the NAO. On the other hand, it is not known, for example, whether the rapid climate changes observed during the last glacial period are at all predictable or are unpredictable consequences of small changes resulting in major climatic shifts.

There is evidence to suggest that climate variations on a global scale resulting from variations in external forcing are partly predictable. Examples are the mean annual cycle and short-term climate variations from individual volcanic eruptions,

which models simulate well. Regularities in past climates, in particular the cyclic succession of warm and glacial periods forced by geometrical changes in the Sun-Earth orbit, are simulated by simple models with a certain degree of success. The global and continental scale aspects of human-induced climate change, as simulated by the models forced by increasing greenhouse gas concentration, are largely reproducible. Although this is not an absolute proof, it provides evidence that such externally forced climate change may be predictable, if their forcing mechanisms are known or can be predicted.

Finally, global or continental scale climate change and variability may be more predictable than regional or local scale change, because the climate on very large spatial scales is less influenced by internal dynamics, whereas regional and local climate is much more variable under the influence of the internal chaotic dynamics of the system. See Chapter 7 for an assessment of the predictability of the climate system.

#### *Rapid climate change*

A non-linear system such as the climate system may exhibit rapid climate change as a response to internal processes or rapidly changing external forcing. Because the probability of their occurrence may be small and their predictability limited, they are colloquially referred to as “unexpected events” or “surprises”. The abrupt events that took place during the last glacial cycle are often cited as an example to demonstrate the possibility of such rapid climate change. Certain possible abrupt events as a result of the rapidly increasing anthropogenic forcing could be envisioned. Examples are a possible reorganization of the thermohaline ocean circulation in the North Atlantic resulting in a more southerly course of the Gulf Stream, which would have a profound influence on the climate of Western Europe, a possible reduction of upper-level ocean cycling in the Southern Ocean, or a possible but unlikely rapid disintegration of part of the Antarctic ice sheet with dramatic consequences for the global sea level.

More generally, with a rapidly changing external forcing, the non-linear climate system may experience as yet unenvisionable, unexpected, rapid change. Chapter 7, in particular Section 7.7, of this Report reviews and assesses the present knowledge of non-linear events and rapid climate change. Potential rapid changes in sea level are assessed in Chapter 11.

### **1.3.3 Observing Anthropogenic Climate Change**

#### *Observing the climate*

The question naturally arises whether the system has already undergone human-induced climate change. To answer this question, accurate and detailed observations of climate and climate variability are required. Instrumental observations of land and ocean surface weather variables and sea surface temperature have been made increasingly widely since the mid-19th century. Recently, ships' observations have been supplemented by data from dedicated buoys. The network of upper-air observations, however, only became widespread in the late 1950s. The density of observing stations always has been and still is extremely inhomogeneous, with many stations in densely populated areas and virtually none in huge oceanic areas. In recent times special

earth-observation satellites have been launched, providing a wide range of observations of various components of the climate system all over the globe. The correct interpretation of such data still requires high quality *in situ* and surface data. The longer observational records suffer from changes in instrumentation, measurement techniques, exposure and gaps due to political circumstances or wars. Satellite data also require compensation for orbital and atmospheric transmission effects and for instrumental biases and instabilities. Earlier the problems related to urbanisation were mentioned. To be useful for the detection of climate change, observational records have to be adjusted carefully for all these effects.

Concern has been expressed about the present condition of the observational networks. The number of upper-air observations, surface stations and observations from ships is declining, partly compensated for by an increasing number of satellite observations. An increasing number of stations are being automated, which may have an impact on the quality and homogeneity of the observations. Maintaining and improving the quality and density of existing observational networks is essential for necessary high standard information. In order to implement and improve systematic observations of all components of the climate system, the World Meteorological Organization and the International Oceanographic Commission have established a Global Climate Observing System (GCOS). Initially GCOS uses existing atmospheric, oceanic and terrestrial networks. Later GCOS will aim to amplify and improve the observational networks where needed and possible.

Observations alone are not sufficient to produce a coherent and global picture of the state of the climate system. So-called data assimilation systems have been developed, which combine observations and their temporal and spatial statistics with model information to provide a coherent quantitative estimate in space and time of the state of the climate system. Data assimilation also allows the estimation of properties which cannot easily be observed directly but which are linked to the observations through physical laws. Some institutions have recently reanalysed several decades of data by means of the most recent and most sophisticated version of their data assimilation system, avoiding in this way inhomogeneities due to changes in their system. However inhomogeneities in these reanalyses may still exist due to changing sources of information, such as the introduction of new satellite systems.

#### *The 20th century*

Historically, human activities such as deforestation may have had a local or regional impact, but there is no reason to expect any large human influence on the global climate before the 20th century. Observations of the global climate system during the 20th century are therefore of particular importance. Chapter 2 presents evidence that there has been a mean global warming of 0.4 to 0.8°C of the atmosphere at the surface since the late 19th century. Figure 2.1 of Chapter 2 shows that this increase took place in two distinct phases, the first one between 1910 and 1945, and recently since 1976. Recent years have been exceptionally warm, with a larger increase in minimum than in maximum temperatures possibly related, among other factors, to an increase

in cloud cover. Surface temperature records indicate that the 1990s are likely to have been the warmest decade of the millennium in the Northern hemisphere, and 1998 is likely to have been the warmest year. For instrumentally recorded history, 1998 has been the warmest year globally. Concomitant with this temperature increase, sea level has risen during the 20th century by 10 to 20 cm and there has been a general retreat of glaciers worldwide, except in a few maritime regions, e.g. Norway and New Zealand (Chapter 11).

Regional changes are also apparent. The observed warming has been largest over the mid- and high-latitude continents in winter and spring. Precipitation trends vary considerably geographically and, moreover, data in most of the Southern Hemisphere and over the oceans are scarce. From the data available, it appears that precipitation has increased over land in mid- and high latitudes of the Northern Hemisphere, especially during winter and early spring, and over most Southern Hemisphere land areas. Over the tropical and the Northern Hemisphere subtropical land areas, particularly over the Mediterranean region during winter, conditions have become drier. In contrast, over large parts of the tropical oceans rainfall has increased.

There is considerable variability of the atmospheric circulation at long time-scales. The NAO for example, with its strong influence on the weather and climate of extratropical Eurasia, fluctuates on multi-annual and multi-decadal time-scales, perhaps influenced by varying temperature patterns in the Atlantic Ocean. Since the 1970s the NAO has been in a phase that gives stronger westerly winds in winter. Recent ENSO behaviour seems to have been unusual compared to that of previous decades: there is evidence that El Niño episodes since the mid-1970s have been relatively more frequent than the opposite La Niña episodes.

There are suggestions that the occurrence of extreme weather events has changed in certain areas, but a global pattern is not yet apparent. For example, it is likely that in many regions of the world, both in the Northern and Southern Hemisphere, there has been a disproportionate increase in heavy and extreme precipitation rates in areas where the total precipitation has increased. Across most of the globe there has been a decrease in the frequency of much below-normal seasonal temperatures.

A detailed assessment of observed climate variability and change may be found in Chapter 2, and of observed sea level change in Chapter 11. Figure 2.39 of Chapter 2 summarises observed variations in temperature and the hydrological cycle.

#### *Detection and attribution*

The fact that the global mean temperature has increased since the late 19th century and that other trends have been observed does not necessarily mean that an anthropogenic effect on the climate system has been identified. Climate has always varied on all time-scales, so the observed change may be natural. A more detailed analysis is required to provide evidence of a human impact.

Identifying human-induced climate change requires two steps. First it must be demonstrated that an observed climate change is unusual in a statistical sense. This is the detection problem. For this to be successful one has to know quantitatively

how climate varies naturally. Although estimates have improved since the SAR, there is still considerable uncertainty in the magnitude of this natural climate variability. The SAR concluded nevertheless, on the basis of careful analyses, that “the observed change in global mean, annually averaged temperature over the last century is unlikely to be due entirely to natural fluctuations of the climate system”.

Having detected a climatic change, the most likely cause of that change has to be established. This is the attribution problem. Can one attribute the detected change to human activities, or could it also be due to natural causes? Also attribution is a statistical process. Neither detection nor attribution can ever be “certain”, but only probable in a statistical sense. The attribution problem has been addressed by comparing the temporal and spatial patterns of the observed temperature increase with model calculations based on anthropogenic forcing by greenhouse gases and aerosols, on the assumption that these patterns carry a fingerprint of their cause. In this way the SAR found that “there is evidence of an emerging pattern of climate response to forcing by greenhouse gases and sulphate aerosols in the observed climate record”. Since the SAR new results have become available which tend to support this conclusion. The present status of the detection of climate change and attribution of its causes is assessed in Chapter 12.

#### **1.4 A ‘Road-map’ to this Report**

This Report, the third IPCC Working Group I Assessment Report since 1990, assesses the state of scientific understanding of the climate system and its variability and change, in particular human-induced climate change. This section provides a ‘road map’ to the 14 chapters of this report and the major issues they are designed to address. Each chapter provides an initial summary of the Working Group I Second Assessment Report (IPCC, 1996) and then goes on to emphasise the progress made since then. The chapters can be viewed as covering the following three broad areas: *past* changes and the factors that can force climate change (Chapters 2 to 6), our *present* understanding and ability to model the climate system (Chapters 7, 8 and 14) and possible *future* climate change (Chapters 9 to 13).

In order to understand, assess and quantify the possible human influence on climate, an analysis of past climate variability and change is required (Chapter 2). The chapter tackles such questions as: how much is the world warming and is the recent global warming unusual? It looks in detail at trends and variability during the recent instrumental period (the last 100 years or so) and draws on palaeo-data to put them into the context of climate over much longer periods.

There are many factors that are known to influence climate, both natural and human-induced. The increase in concentrations of greenhouse gases and aerosols through human activity is of particular concern. Chapters 3 to 5 examine how well the three most important human contributions to the changing composition of the atmosphere; carbon dioxide, other greenhouse gases and aerosols, are understood, including the physical, chemical and biological processes which determine the atmospheric concentrations of these components. The next step, taken in Chapter 6, is

to evaluate how this change in atmospheric composition has affected radiative forcing within the context of other factors such as land-use change, volcanic eruptions and solar variations.

Understanding the climate response to these various radiative forcings and projecting how they could affect future climate requires an understanding of the physical processes and feedbacks in the climate system and an ability to model them (Chapter 7). The only tools available for such projections of future climate are numerical models of the climate system of various complexity. An evaluation of such models against observations of the present and past climate and model intercomparisons provide the basis for confidence in such tools (Chapter 8).

Climate models together with scenarios of future emissions of radiatively active atmospheric components, as for example the SRES scenarios (Nakićenović *et al.*, 2000), recently developed by IPCC specifically for this purpose, are used to project future climate change. State-of-the-art projections for the next 100 years are assessed in Chapter 9, mainly at a global level, but also including large-scale patterns, their spatial and temporal variability and extreme events. Partly in response to the need for more details of climate change at a regional level, research in this area has been particularly active over the last 5 years. A new chapter, compared to previous assessments, has been included which examines the various techniques available to derive regional climate projections and, as far as is currently possible, assesses regional climate change information (Chapter 10). Chapter 11 assesses the current state of knowledge of the rate of change of global average and regional sea level in response to climate change.

A key conclusion from the SAR was that “the balance of evidence suggests that there is a discernible human influence on global climate”. Chapter 12 assesses research over the last 5 years on the detection and attribution of climate change drawing on the developments in observational research (Chapters 2 to 6) and modelling (Chapters 7 to 10) to consider how this conclusion has changed.

Data derived directly from projections with climate models are often inappropriate for assessing the impacts of climate change which can require detailed, regional or local information as well as observational data describing current (or baseline) climate. Climate change scenarios are plausible representations of future climate constructed explicitly for impact assessment and form a key link between IPCC Working Groups I and II. For the first time, Working Group I have included a chapter dedicated to climate scenarios (Chapter 13) – this is intended to provide an assessment of scenario generation techniques, rather than to present scenarios themselves.

All chapters of the report highlight areas of certainty and uncertainty, and gaps in current knowledge. Chapter 14 draws together this information to present key areas that need to be addressed to advance understanding and reduce uncertainty in the science of climate change.

A comprehensive and integrated summary of all results of this assessment report may be found in the Technical Summary in this volume. A brief summary highlighting points of particular policy relevance is presented in the Summary for Policymakers.

## References

- IPCC**, 1994: *Climate Change 1994: Radiative Forcing of Climate Change and an Evaluation of the IPCC IS92 Emission Scenarios*, [J.T. Houghton, L.G. Meira Filho, J. Bruce, Hoesung Lee, B.A. Callander, E. Haites, N. Harris and K. Maskell (eds.)]. Cambridge University Press, Cambridge, UK and New York, NY, USA, 339 pp.
- IPCC**, 1996: *Climate Change 1995: The Science of Climate Change. Contribution of Working Group I to the Second Assessment Report of the Intergovernmental Panel on Climate Change* [Houghton, J.T., L.G. Meira Filho, B.A. Callander, N. Harris, A. Kattenberg, and K. Maskell (eds.)]. Cambridge University Press, Cambridge, United Kingdom and New York, NY, USA, 572 pp.
- IPCC**, 1997: *IPCC Technical Paper II: An introduction to simple climate models used in the IPCC Second Assessment Report*, [J.T. Houghton, L.G. Meira Filho, D.J. Griggs and K. Maskell (eds.)].
- Nakićenović, N., J. Alcamo, G. Davis, B. de Vries, J. Fenner, S. Gaffin, K. Gregory, A. Grübler, T. Y. Jung, T. Kram, E. L. La Rovere, L. Michaelis, S. Mori, T. Morita, W. Pepper, H. Pitcher, L. Price, K. Raihi, A. Roehrl, H-H. Rogner, A. Sankovski, M. Schlesinger, P. Shukla, S. Smith, R. Swart, S. van Rooijen, N. Victor, Z. Dadi, 2000: *IPCC Special Report on Emissions Scenarios*, Cambridge University Press, Cambridge, United Kingdom and New York, NY, USA, 599 pp.

# 2

---

## Observed Climate Variability and Change

---

### Co-ordinating Lead Authors

C.K. Folland, T.R. Karl

### Lead Authors

J.R. Christy, R.A. Clarke, G.V. Gruza, J. Jouzel, M.E. Mann, J. Oerlemans, M.J. Salinger, S.-W. Wang

### Contributing Authors

J. Bates, M. Crowe, P. Frich, P. Groisman, J. Hurrell, P. Jones, D. Parker, T. Peterson, D. Robinson, J. Walsh, M. Abbott, L. Alexander, H. Alexandersson, R. Allan, R. Alley, P. Ambenje, P. Arkin, L. Bajuk, R. Balling, M.Y. Bardin, R. Bradley, R. Brázdil, K.R. Briffa, H. Brooks, R.D. Brown, S. Brown, M. Brunet-India, M. Cane, D. Changnon, S. Changnon, J. Cole, D. Collins, E. Cook, A. Dai, A. Douglas, B. Douglas, J.C. Duplessy, D. Easterling, P. Englehart, R.E. Eskridge, D. Etheridge, D. Fisher, D. Gaffen, K. Gallo, E. Genikhovich, D. Gong, G. Gutman, W. Haeberli, J. Haigh, J. Hansen, D. Hardy, S. Harrison, R. Heino, K. Hennessy, W. Hogg, S. Huang, K. Hughen, M.K. Hughes, M. Hulme, H. Iskenderian, O.M. Johannessen, D. Kaiser, D. Karoly, D. Kley, R. Knight, K.R. Kumar, K. Kunkel, M. Lal, C. Landsea, J. Lawrimore, J. Lean, C. Leovy, H. Lins, R. Livezey, K.M. Lugina, I. Macadam, J.A. Majorowicz, B. Manighetti, J. Marengo, E. Mekis, M.W. Miles, A. Moberg, I. Mokhov, V. Morgan, L. Mysak, M. New, J. Norris, L. Ogallo, J. Overpeck, T. Owen, D. Paillard, T. Palmer, C. Parkinson, C.R. Pfister, N. Plummer, H. Pollack, C. Prentice, R. Quayle, E.Y. Rankova, N. Rayner, V.N. Razuvayev, G. Ren, J. Renwick, R. Reynolds, D. Rind, A. Robock, R. Rosen, S. Rösner, R. Ross, D. Rothrock, J.M. Russell, M. Serreze, W.R. Skinner, J. Slack, D.M. Smith, D. Stahle, M. Stendel, A. Sterin, T. Stocker, B. Sun, V. Swail, V. Thapliyal, L. Thompson, W.J. Thompson, A. Timmermann, R. Toumi, K. Trenberth, H. Tuomenvirta, T. van Ommen, D. Vaughan, K.Y. Vinnikov, U. von Grafenstein, H. von Storch, M. Vuille, P. Wadhams, J.M. Wallace, S. Warren, W. White, P. Xie, P. Zhai

### Review Editors

R. Hallgren, B. Nyenzi

# Contents

---

<b>Executive Summary</b>	101	<b>2.5 How have Precipitation and Atmospheric Moisture Changed?</b>	142
<b>2.1 Introduction</b>	105	2.5.1 Background	142
<b>2.2 How Much is the World Warming?</b>	105	2.5.2 Changes in Precipitation and Related Variables	142
2.2.1 Background	105	2.5.2.1 Land	142
2.2.2 Temperature in the Instrumental Record for Land and Oceans	105	2.5.2.2 Palaeo-drought	143
2.2.2.1 Land-surface air temperature	105	2.5.2.3 Ocean	145
2.2.2.2 Sea surface temperature and ocean air temperature	110	2.5.3 Water Vapour	146
2.2.2.3 Land and sea combined	112	2.5.3.1 Surface water vapour	146
2.2.2.4 Are the land and ocean surface temperature changes mutually consistent?	116	2.5.3.2 Lower-tropospheric water vapour	147
2.2.2.5 Sub-surface ocean temperatures and salinities	118	2.5.3.3 Upper-tropospheric and lower-stratospheric water vapour	147
2.2.3 Temperature of the Upper Air	119	2.5.4 Evaporation	148
2.2.4 How do Surface and Upper Air Temperature Variations Compare?	121	2.5.4.1 Land	148
2.2.5 Changes in the Cryosphere	123	2.5.5 Clouds	148
2.2.5.1 Snow cover, including snowfall	123	2.5.5.1 Land	149
2.2.5.2 Sea-ice extent and thickness	124	2.5.5.2 Ocean	149
2.2.5.3 Permafrost	127	2.5.5.3 Global	149
2.2.5.4 Mountain glaciers	127	2.5.6 Summary	149
2.2.5.5 Lake and river ice	129		
2.2.6 Are the Retreat of Glaciers, Sea Ice, and Snow Cover Consistent with the Surface Temperature Trends?	129	<b>2.6 Are the Atmospheric/Oceanic Circulations Changing?</b>	150
2.2.7 Summary	129	2.6.1 Background	150
<b>2.3 Is the Recent Warming Unusual?</b>	130	2.6.2 El Niño-Southern Oscillation and Tropical/Extra-tropical Interaction	150
2.3.1 Background	130	2.6.3 Decadal to Inter-decadal Pacific Oscillation, and the North Pacific Oscillation	151
2.3.2 Temperature of the Past 1,000 Years	130	2.6.4 Monsoons	152
2.3.2.1 Palaeoclimate proxy indicators	130	2.6.5 The Northern Hemisphere, excluding the North Pacific Ocean	152
2.3.2.2 Multi-proxy synthesis of recent temperature change	133	2.6.6 The Southern Hemisphere	153
2.3.3 Was there a “Little Ice Age” and a “Medieval Warm Period”?	133	2.6.7 Summary	154
2.3.4 Volcanic and Solar Effects in the Recent Record	136		
2.3.5 Summary	136	<b>2.7 Has Climate Variability, or have Climate Extremes, Changed?</b>	155
<b>2.4 How Rapidly did Climate Change in the Distant Past?</b>	136	2.7.1 Background	155
2.4.1 Background	136	2.7.2 Is There Evidence for Changes in Variability or Extremes?	155
2.4.2 How Stable was the Holocene Climate?	138	2.7.2.1 Temperature	156
2.4.3 How Fast did Climate Change during the Glacial Period?	140	2.7.2.2 Precipitation	157
2.4.4 How Stable was the Previous Inter-glacial?	141	2.7.3 Is There Evidence for Changes in Extreme Weather or Climate Events?	160
2.4.5 Summary	142	2.7.3.1 Tropical cyclones	160
		2.7.3.2 Extra-tropical cyclones	160
		2.7.3.3 Droughts and wet spells	162
		2.7.3.4 Tornadoes, hail and other severe local weather	163
		2.7.4 Summary	163
		<b>2.8 Are the Observed Trends Internally Consistent?</b>	163
		<b>References</b>	165

## Executive Summary

### Overview

The best estimate of global surface temperature change is a  $0.6^{\circ}\text{C}$  increase since the late 19th century with a 95% confidence interval of  $0.4$  to  $0.8^{\circ}\text{C}$ . The increase in temperature of  $0.15^{\circ}\text{C}$  compared to that assessed in the IPCC WGI Second Assessment Report (IPCC, 1996) (hereafter SAR) is partly due to the additional data for the last five years, together with improved methods of analysis and the fact that the SAR decided not to update the value in the First Assessment Report, despite slight additional warming. It is likely that there have been real differences between the rate of warming in the troposphere and the surface over the last twenty years, which are not fully understood. New palaeoclimate analyses for the last 1,000 years over the Northern Hemisphere indicate that the magnitude of 20th century warming is likely to have been the largest of any century during this period. In addition, the 1990s are likely to have been the warmest decade of the millennium. New analyses indicate that the global ocean has warmed significantly since the late 1940s: more than half of the increase in heat content has occurred in the upper 300 m, mainly since the late 1950s. The warming is superimposed on strong global decadal variability. Night minimum temperatures are continuing to increase, lengthening the freeze-free season in many mid- and high latitude regions. There has been a reduction in the frequency of extreme low temperatures, without an equivalent increase in the frequency of extreme high temperatures. Over the last twenty-five years, it is likely that atmospheric water vapour has increased over the Northern Hemisphere in many regions. There has been quite a widespread reduction in daily and other sub-monthly time-scales of temperature variability during the 20th century. New evidence shows a decline in Arctic sea-ice extent, particularly in spring and summer. Consistent with this finding are analyses showing a near 40% decrease in the average thickness of summer Arctic sea ice over approximately the last thirty years, though uncertainties are difficult to estimate and the influence of multi-decadal variability cannot yet be assessed. Widespread increases are likely to have occurred in the proportion of total precipitation derived from heavy and extreme precipitation events over land in the mid- and high latitudes of the Northern Hemisphere.

### Changes in Temperature and Related Variables

#### *Changes in near-surface temperature from the instrumental record*

- Average global surface temperature has increased by approximately  $0.6^{\circ}\text{C}$  since the late 19th century, with 95% confidence limits of close to  $0.4$  and  $0.8^{\circ}\text{C}$ . Most of this increase has occurred in two periods, from about 1910 to 1945 and since 1976, and the largest recent warming is in the winter extra-tropical Northern Hemisphere. The warming rate since 1976,  $0.17^{\circ}\text{C}/\text{decade}$ , has been slightly larger than the rate of warming during the 1910 to 1945 period ( $0.14^{\circ}\text{C}/\text{decade}$ ), although the total increase in temperature is larger for the 1910 to 1945 period. The most recent warming period also has a faster rate of warming over land compared with the oceans. The high global

temperature associated with the 1997/98 El Niño event stands out in both surface and tropospheric temperatures as an extreme event, even after consideration of the recent rate of warming.

- Confidence in the magnitude of global warming since the late 19th century has increased since the SAR due to new analyses, including model simulations of land-surface temperature changes and new studies of the effect of urbanisation on global land temperature trends. There is a high level of consistency between changes in sea surface temperatures (SSTs) and near-surface land air temperatures across the land-ocean boundary over the 20th century, despite independent observing systems and independent bias correction factors for SSTs before 1942. The assessed warming is considerably larger than the total contributions of the plausible sources of error.
- Twentieth century temperature trends show a broad pattern of tropical warming, while extra-tropical trends have been more variable. Warming from 1910 to 1945 was initially concentrated in the North Atlantic and nearby regions. The Northern Hemisphere shows cooling during the period 1946 to 1975 while the Southern Hemisphere shows warming. The recent 1976 to 2000 warming was largely globally synchronous, but emphasised in the Northern Hemisphere continents during winter and spring, with year-round cooling in parts of the Southern Hemisphere oceans and Antarctica. North Atlantic cooling between about 1960 and 1985 has recently reversed. Overall, warming over the Southern Hemisphere has been more uniform during the instrumental record than that over the Northern Hemisphere.
- The patterns of global temperature change since the 1970s are related in part to the positive westerly phase of the North Atlantic/Arctic Oscillation and possibly to decadal to multi-decadal variability in the Pacific.
- A multi-decadal fluctuation of SST in the North Atlantic has been in a rising phase since about the mid-1980s. Warming in many regions of this ocean has accelerated over the last five years and is likely to have contributed to quite rapid parallel increases of near-surface air temperature in much of Europe.
- New analysis shows that the global ocean heat content has increased since the late 1950s. This increase is superimposed on substantial global decadal variability. More than half the heating is contained in the uppermost 300 m where it is equivalent to an average temperature increase of  $0.037^{\circ}\text{C}/\text{decade}$ .
- Analyses of mean daily maximum and minimum land surface air temperatures continue to support a reduction in the diurnal temperature range in many parts of the world, with, globally, minimum temperatures increasing at nearly twice the rate of maximum temperatures between about 1950 and 1993. The rate of temperature increase during this time has been  $0.1^{\circ}\text{C}$  and  $0.2^{\circ}\text{C}$  for the maximum and minimum, respectively. This is about half of the rate of temperature increase over the oceans during this time.

### *Changes in temperature-related variables*

- Alpine and continental glaciers have extensively retreated in response to 20th century warming. Glaciers in a few maritime regions are advancing, mainly due to increases in precipitation related to atmospheric circulation changes, e.g., Norway, New Zealand.
- The duration of Northern Hemisphere lake-ice and river-ice cover over the past century, or more, shows widespread decreases averaging to about two fewer weeks of ice cover.
- There is a highly significant interannual (+0.6) and multi-decadal correlation between increases in the Northern Hemisphere spring land temperature and a reduction in the Northern Hemisphere spring snow cover since data have been available (1966). Snow cover extent has decreased by about 10% since 1966.
- A 10 to 15% reduction in sea-ice extent in the Arctic spring and summer since the 1950s is consistent with an increase in spring, and to a lesser extent, summer temperatures in the high latitudes. There is little indication of reduced Arctic sea-ice extent during winter when temperatures have increased in the surrounding region.
- New data from submarines indicate that there has been about a 40% decline in Arctic sea-ice thickness in summer or early autumn between the period 1958 to 1976 and the mid-1990s, an average of near 4 cm per year. Other independent observations show a much slower decrease in winter sea-ice thickness of about 1 cm per year. The influence of substantial interannual and inter-decadal variability on these changes cannot be assessed because of restricted sampling.
- By contrast, there is no readily apparent relationship between decadal changes in Antarctic temperatures and sea-ice extent since 1973. Satellite data indicate that after a possible initial decrease in the mid-1970s, Antarctic sea-ice extent has stayed almost stable or even increased since 1978.

### *Changes in temperature above the surface layer*

- Analysis of global temperature trends since 1958 in the low to mid-troposphere from balloons shows a warming of about  $+0.1^{\circ}\text{C}/\text{decade}$ , which is similar to the average rate of warming at the surface. Since the early 1960s no significant trends have been detected for the global mean temperature in the uppermost troposphere.
- Satellites have only been available since 1979. Between 1979 and 2000, based on satellites and balloons, the lower-tropospheric trend has been  $+0.04 \pm 0.11^{\circ}\text{C}/\text{decade}$  and  $0.03 \pm 0.10^{\circ}\text{C}/\text{decade}$ , respectively. By contrast, surface temperature trends for 1979 to 2000 were greater, at  $0.16 \pm 0.06^{\circ}\text{C}/\text{decade}$ . The trend in the difference of the surface and lower-tropospheric series of  $0.13 \pm 0.06^{\circ}\text{C}/\text{decade}$  is clearly statistically significant. This is in contrast to near zero surface temperature trends over 1958 to 1978 when the global lower-tropospheric temperature warmed by  $0.03^{\circ}\text{C}/\text{decade}$  relative to the surface.

- It is very likely that these significant differences in trends between the surface and lower troposphere are real and not solely an artefact of measurement bias, though differences in spatial and temporal sampling are likely to contribute. The differences are particularly apparent in many parts of the tropics and sub-tropics where the surface has warmed faster than the lower troposphere. In some other regions, e.g., North America, Europe and Australia, lower-tropospheric and surface trends are very similar.
- Throughout the stratosphere, negative temperature trends have been observed since 1979, ranging from a decrease of 0.5 or  $0.6^{\circ}\text{C}/\text{decade}$  in the lower stratosphere to  $2.5^{\circ}\text{C}/\text{decade}$  in the upper stratosphere.

### *Changes in temperature during the pre-instrumental period*

#### *The past millennium*

- New analyses indicate that the magnitude of Northern Hemisphere warming over the 20th century is likely to have been the largest of any century in the last 1,000 years.
- The 1990s are likely to have been the warmest decade of the millennium in the Northern Hemisphere and 1998 is likely to have been the warmest year. Because less data are available, less is known about annual averages prior to 1,000 years before the present and for conditions prevailing in most of the Southern Hemisphere prior to 1861.
- Evidence does not support the existence of globally synchronous periods of cooling or warming associated with the ‘Little Ice Age’ and ‘Medieval Warm Period’. However, reconstructed Northern Hemisphere temperatures do show a cooling during the 15th to 19th centuries and a relatively warm period during the 11th to 14th centuries, though the latter period is still cooler than the late 20th century.
- Analyses of borehole temperatures indicate a non-linear increase in global average ground surface temperature over land of  $1.0 \pm 0.3^{\circ}\text{C}$  over the last 500 years, with most of the increase occurring since the late 19th century. There may be additional uncertainties due to the assumptions used in this technique, and decreasing resolution back in time limits confidence in the exact timing of the warming.

### *Changes across the last 500,000 years*

- It is very likely that large and rapid decadal temperature changes occurred during the last glacial and its deglaciation (between about 100,000 and 10,000 years ago), particularly in higher latitudes of the Northern Hemisphere. During the last deglaciation, local increases in temperature are likely to have been as large as 5 to  $10^{\circ}\text{C}$  over a few decades. Over the same period there is evidence of less pronounced but nearly synchronous changes worldwide, except in high southern latitudes.
- Antarctic ice cores have provided new evidence of almost in-phase changes of temperature, carbon dioxide and methane through the ice age cycles over the past 420,000 years.

- There is emerging evidence for significant, rapid (time-scales of several decades or more), regional temperature changes during the last 10,000 years. However, the evidence does not indicate that any such events were global in scale.

### **Changes in Precipitation and Related Variables**

#### *Precipitation*

- Instrumental records of land-surface precipitation continue to show an increase of 0.5 to 1%/decade in much of the Northern Hemisphere mid- and high latitudes. A notable exception includes parts of eastern Russia. In contrast, over much of the sub-tropical land areas rainfall has decreased during the 20th century (by  $-0.3\%/\text{decade}$ ), but this trend has weakened in recent decades. Other precipitation indicators suggest that large parts of the tropical oceans have had more precipitation in recent decades, and that precipitation has significantly increased over tropical land areas during the 20th century ( $2.4\%/\text{century}$ ). The increase in precipitation over the tropics is not evident during the past few decades.
- In the Southern Hemisphere, the pattern of island rainfall in parts of the South Pacific has changed since the mid-1970s, associated with the more frequent occurrence of the warm phase of the El Niño-Southern Oscillation (ENSO).
- Where data are available, changes in annual streamflow usually relate well to changes in total precipitation.

#### *Water vapour*

- Changes in water vapour mixing ratio have been analysed for selected regions using *in situ* surface observations as well as lower-tropospheric measurements based on satellites and weather balloons. A pattern of overall surface and lower-tropospheric water vapour mixing ratio increases over the past few decades is emerging, although there are likely to be some time-dependent biases in these data and regional variations in trends. The more reliable data sets show that it is likely that total atmospheric water vapour has increased several per cent per decade over many regions of the Northern Hemisphere since the early 1970s. Changes over the Southern Hemisphere cannot yet be assessed.
- Satellite observations of upper-tropospheric humidity from 1980 to 1997 show statistically significant positive trends of  $0.1\%/\text{year}$  for the zone  $10^\circ\text{N}$  to  $10^\circ\text{S}$ . Other trends are not statistically significant, but include a  $0.04\%/\text{year}$  positive trend for the zone  $60^\circ\text{N}$  to  $60^\circ\text{S}$  but a negative trend of  $-0.1\%/\text{year}$  over the region  $30^\circ\text{S}$  to  $60^\circ\text{S}$ .
- Balloon observations of stratospheric water vapour above 18 km show an increase of about  $1\%/\text{year}$  for the period from 1981 to 2000. Shorter satellite records show a similar positive trend, suggesting that the change is global in character, but they also indicate a slowing of the positive trend after 1996.

#### *Clouds*

- It is likely that there has been an increase in total cloud cover of about 2% over many mid- to high latitude land areas since the beginning of the 20th century. The increases in total cloud amount are positively correlated with decreases in the diurnal temperature range. Changes in total cloud amount are uncertain both over sub-tropical and tropical land areas as well as over the oceans.

### **Changes in Atmospheric/Oceanic Circulation**

#### *El Niño-Southern Oscillation (ENSO)*

- The frequency and intensity of ENSO has been unusual since the mid-1970s compared with the previous 100 years. Warm phase ENSO episodes have been relatively more frequent, persistent, or intense than the opposite cold phase during this period.
- This recent behaviour of ENSO is related to variations in precipitation and temperature over much of the global tropics and subtropics and some mid-latitude areas. The overall effect is likely to have made a small contribution to the increase in global surface temperature during the last few decades.

#### *Other Oscillations*

- The Inter-decadal Pacific Oscillation is likely to be a Pacific-wide manifestation of the Pacific Decadal Oscillation. Both are associated with decadal climate variability over the Pacific basin. It is likely that these related phenomena modulate ENSO-related climate variability.
- The winter North Atlantic Oscillation (NAO) and the associated Arctic Oscillation (AO), which appear to be largely the same phenomenon, show decadal to multi-decadal variability. Since the 1970s these oscillations have been in a phase that gives stronger westerly winds over much of extra-tropical Eurasia in the winter half year. This is associated with cold season warming over extra-tropical Eurasia, but cooling in some regions further south.
- The High Latitude Mode (HLM) or Antarctic Oscillation (AAO) in the Southern Hemisphere has been in an enhanced positive phase in the last fifteen years, with stronger westerly winds over the Southern Ocean.
- It is likely that rapid (time-scales of several decades or more) changes of atmospheric and ocean circulation occurred during inter-glacial periods, affecting regional climate, without human interference.

### **Changes in Extreme (within the upper or lower ten percentiles) Weather and Climate Events**

#### *Precipitation*

- New analyses show that in regions where total precipitation has increased it is very likely that there have been even more pronounced increases in heavy and extreme precipitation events. The converse is also true.

- In some regions, heavy and extreme precipitation events have increased despite the fact that total precipitation has decreased or remained constant. This is attributed to a decrease in the frequency of precipitation events. Changes in the frequency of heavy precipitation events can arise from several causes, e.g., changes in atmospheric moisture or circulation.
- Over the latter half of the 20th century it is likely that there has been a 2 to 4% increase in the frequency of heavy precipitation events reported by the available observing stations in the mid- and high latitudes of the Northern Hemisphere.
- Trends for severe drought and wet area statistics for 1900 to 1995 are relatively small over global land areas. However, during the last two or three decades there have been some increases in the globally combined severe dry and wet areas.

#### *Temperature*

- In many regions inter-daily temperature variability has decreased. Increases in the daily minimum temperatures are

lengthening the freeze-free season in most mid- and high latitude regions.

- A significant reduction in the frequency of extreme low monthly and seasonal average temperatures across much of the globe has occurred since the late 19th century. However, a relatively smaller increase in the frequency of extreme high monthly and seasonal average temperatures has been observed.

#### *Storms*

- Changes in tropical and extra-tropical storm intensity and frequency are dominated by inter-decadal to multi-decadal variations, with no significant trends over the 20th century evident. Conflicting analyses make it difficult to draw definitive conclusions about changes in storm activity, especially in the extra-tropics.
- No systematic changes in the frequency of tornadoes, thunder days, or hail events are evident in the limited areas analysed.

## 2.1 Introduction

Observed climate change and variability (for definitions, see the IPCC Glossary, Appendix I) are considered in this chapter by addressing seven commonly asked questions related to the detection of climate change and sensitivity of the climate to anthropogenic activity. The questions are:

- How much is the world warming?*
- Is the recent warming unusual?*
- How rapidly did climate change in the distant past?*
- Have precipitation and atmospheric moisture changed?*
- Are the atmospheric/oceanic circulations changing?*
- Has climate variability, or have climate extremes, changed?*
- Are the observed trends internally consistent?*

This chapter emphasises change against a background of variability. The certainty of conclusions that can be drawn about climate from observations depends critically on the availability of accurate, complete and consistent series of observations. For many variables important in documenting, detecting, and attributing climate change, Karl *et al.* (1995a) demonstrate that the data are still not good enough for really firm conclusions to be reached, as noted in the IPCC WGI Second Assessment Report (IPCC, 1996) (hereafter SAR). This especially applies to global trends in variables that have large regional variations, such as precipitation, whereas conclusions about temperature changes are often considerably more firmly based. The recently designated Global Climate Observing System (GCOS) upper air network (Wallis, 1998) and a GCOS surface network (Peterson *et al.*, 1997), maintained and reporting to higher standards, may have had a limited positive impact on the quality and availability of some of our results. New data sets e.g., on surface humidity, sea-ice thickness and sub-surface ocean temperature, have widened the range of conclusions than can be drawn since the SAR, albeit tentatively. However, a wider range of analytical techniques and tests of the data have increased our confidence in areas such as surface temperature changes.

Throughout the chapter we try to consistently indicate the degree of our confidence in trends and other results. Sometimes we provide quantitative estimates of uncertainty, as far as possible the value of twice the standard error, or we estimate statistical significance at the 0.05 (5%) level. This is the appropriate terminology and implies that what we see is very unusual, given the null hypothesis. We use the word "trend" to designate a generally progressive change in the level of a variable. Where numerical values are given, they are equivalent linear trends, though more complex changes in the variable will often be clear from the description. We use the word "consistent" to imply similarity between results or data sets that are expected to be related on physical grounds. Where this is not possible, we use the following words to indicate judgmental estimates of confidence: virtually certain (>99% chance that a result is true); very likely (>90% but ≤99% chance); likely (>66% but <90% chance); medium likelihood (>33% but ≤66% chance), unlikely (>10% but ≤33% chance); very unlikely (>1% but ≤10% chance) and exceptionally unlikely (<1% chance).

## 2.2 How Much is the World Warming?

### 2.2.1 Background

The SAR concluded that, on a global average, land-surface air and sea surface temperature rose by between 0.3°C and 0.6°C between the late 19th century and 1994. In this section, the recent warming is re-examined, using updated data. We include recent analyses of the diurnal asymmetry of the warming and its geographical structure. Conventional temperature observations are supplemented by indirect evidence and by satellite-based data. For the first time, we make objective estimates of uncertainties in the surface temperature data, though these are preliminary. We also assess recent work in compiling hemispheric and global temperature records from palaeoclimatic data, especially for the most recent millennium.

### 2.2.2 Temperature in the Instrumental Record for Land and Oceans

Note that all data sets are adjusted to have zero anomaly when averaged over the period 1961 to 1990.

#### 2.2.2.1 Land-surface air temperature

The SAR reviewed the three databases of land-surface air temperature due to Jones (1994), Hansen and Lebedeff (1988) and Vinnikov *et al.* (1990). The first and second databases have been updated by Jones *et al.* (2001) and Hansen *et al.* (1999), respectively, and a further analysis has become available (Peterson and Vose, 1997; Peterson *et al.*, 1998a, 1999). The last paper also separates rural temperature stations in the Global Historical Climatology Network (GHCN) (Peterson and Vose, 1997) from the full set of stations which, in common with the other three analyses, have been screened for urbanisation effects. While there is little difference in the long-term (1880 to 1998) rural (0.70°C/century) and full set of station temperature trends (actually less at 0.65°C/century), more recent data (1951 to 1989), as cited in Peterson *et al.* (1999), do suggest a slight divergence in the rural (0.80°C/century) and full set of station trends (0.92°C/century). However, neither pair of differences is statistically significant. In addition, while not reported in Peterson *et al.*, the 1951 to 1989 trend for urban stations alone was 0.10°C/decade. We conclude that estimates of long-term (1880 to 1998) global land-surface air temperature variations and trends are relatively little affected by whether the station distribution typically used by the four global analyses is used, or whether a special effort is made to concentrate on rural stations using elaborate criteria to identify them. Part of the reason for this lack of sensitivity is that the average trends in available worldwide *urban* stations for 1951 to 1989 are not greatly more than those for all land stations (0.09°C/decade). The differences in trend between rural and all stations are also virtually unaffected by elimination of areas of largest temperature change, like Siberia, because such areas are well represented in both sets of stations.

These results confirm the conclusions of Jones *et al.* (1990) and Easterling *et al.* (1997) that urban effects on 20th century globally and hemispherically averaged land air temperature time-

**Box 2.1:** Urban Heat Island and the Observed Increases in Land Air Temperature.

There are two primary reasons why urban heat islands have been suspected as being partially responsible for the observed increases in land air temperatures over the last few decades. The first is related to the observed decrease in the diurnal temperature range and the second is related to a lower rate of warming observed over the past twenty years in the lower troposphere compared with the surface.

Since the 1950s both daily maximum and minimum temperatures are available over more than 50% of the global land area. These data indicate that on average the mean minimum temperature has increased at nearly twice the rate of the maximum temperature, reducing the daily temperature range by about  $0.8^{\circ}\text{C}$  over these areas. This has raised questions related to whether the growth of urban heat islands may be responsible for a substantial portion of the observed mean temperature increase, because it is well-known that compared to non-urban areas urban heat islands raise night-time temperatures more than daytime temperatures. Nonetheless, the relatively strong correlation between observed decreases in the daily temperature range with increases of both precipitation (leading to more moist surface conditions) and total cloud amount support the notion that the reduction in diurnal temperature range is in response to these physical changes.

Since 1979 satellite observations and weather balloons (which generally agree well) show substantially less warming of the global lower troposphere (around 2 km) than surface temperatures ( $0.03$  and  $0.04^{\circ}\text{C}/\text{decade}$ , respectively, compared to  $0.16^{\circ}\text{C}/\text{decade}$  at the surface). However, over the Northern Hemisphere land areas where urban heat islands are most apparent, both the trends of lower-tropospheric temperature and surface air temperature show no significant differences. In fact, the lower-tropospheric temperatures warm at a slightly greater rate over North America (about  $0.28^{\circ}\text{C}/\text{decade}$  using satellite data) than do the surface temperatures ( $0.27^{\circ}\text{C}/\text{decade}$ ), although again the difference is not statistically significant. In the global average, the trend differences arise largely from the tropical and sub-tropical oceans. In many such regions, the near-surface marine air temperatures tend to be cool and dense compared with conditions aloft, allowing for the lapse rate with height, disconnecting near-surface (up to about 1 km) conditions from higher layers in the atmosphere. Thus the surface marine layer and the troposphere above can have differing variations and trends.

Clearly, the urban heat island effect is a real climate change in urban areas, but is not representative of larger areas. Extensive tests have shown that the urban heat island effects are no more than about  $0.05^{\circ}\text{C}$  up to 1990 in the global temperature records used in this chapter to depict climate change. Thus we have assumed an uncertainty of zero in global land-surface air temperature in 1900 due to urbanisation, linearly increasing to  $0.06^{\circ}\text{C}$  (two standard deviations  $0.12^{\circ}\text{C}$ ) in 2000.

series do not exceed about  $0.05^{\circ}\text{C}$  over the period 1900 to 1990 (assumed here to represent one standard error in the assessed non-urban trends). However, greater urbanisation influences in future cannot be discounted. Note that changes in borehole temperatures (Section 2.3.2), the recession of the glaciers (Section 2.2.5.4), and changes in marine temperature (Section 2.2.2.2), which are not subject to urbanisation, agree well with the instrumental estimates of surface warming over the last century. Reviews of the homogeneity and construction of current surface air temperature databases appear in Peterson *et al.* (1998b) and Jones *et al.* (1999a). The latter shows that global temperature anomalies can be converted into absolute temperature values with only a small extra uncertainty.

Figure 2.1a shows the Jones *et al.* (2001) CRU (Climatic Research Unit) annual averages, together with an approximately decadally smoothed curve, to highlight decadal and longer changes. This is compared with smoothed curves from the other three analyses in Figure 2.1b. We do not show standard errors for the CRU land data using the Jones *et al.* (1997b) method as tests suggest that these may not be reliable for land data on its own. Instead we use an optimum averaging method (Folland *et al.*, 2001) where the calculated uncertainties are centred on the simple CRU average. We have added an estimate of the additional, independent, uncertainty (twice the standard error)

due to urbanisation increasing from zero in 1900 to  $0.12^{\circ}\text{C}$  in 2000. (The Jones *et al.* (1990) estimates can be interpreted as one standard error equal to 10% of the global warming to that time of about  $0.05^{\circ}\text{C}$ , see also Box 2.1 on urbanisation.) Note that the warming substantially exceeds the calculated uncertainties. (We have not included the possible refinement of assuming urbanisation uncertainties to apply to the cold side of the trend line only, which would reduce the total uncertainty range in Figure 2.1.)

Over global land, a further warming of surface air temperature has occurred since the SAR. The Peterson and Vose (1997) NCDC (National Climate Data Center) series gives distinctly more warming than does the CRU series since the mid-1980s. The former series is a straightforward average of local land areas, weighted according to their size, whereas the CRU series is a simple average of the two hemispheres which gives more weight to the relatively small area of the Southern Hemisphere land. Because the Northern Hemisphere land has warmed considerably faster than the Southern Hemisphere land since the mid-1980s (reflected in Table 2.1), the simple average results in less warming. The Hansen *et al.* (1999) GISS (Goddard Institute for Space Studies) series has recently been revised and shows a little less warming than the CRU series since the late 1980s. One reason for this behaviour lies in the way that the Hansen series is constructed. Among other differences, this series gives much more

weight to oceanic islands and Antarctica. Because the oceans and Antarctica have warmed less than the rest of the global land in the last fifteen years (see below), the Hansen series can be expected to show less warming. Some of these considerations apply to the Vinnikov *et al.* (1990) SHI (State Hydrological Institute) series, though this excludes areas south of 60°S.

A new record was set in all four series in 1998 (anomalies relative to 1961 to 1990 of CRU, 0.68°C; NCDC, 0.87°C; GISS, 0.58°C; and SHI, 0.58°C). 1998 was influenced by the strong 1997/98 El Niño; the warming influence of El Niño on global temperature is empirically well attested (e.g., Jones, 1994) and the physical causes are starting to be uncovered (Meehl *et al.*, 1998). However, 1998 was considerably warmer than 1983, a year warmed by the comparable 1982/83 El Niño. In fact 1998 was between 0.34 and 0.54°C warmer than 1983 over land, depending on the temperature series used, though there was some offsetting cooling from volcanic aerosols from the 1982 El Chichón eruption in 1983. 1999 was globally much cooler than 1998, with an anomaly of 0.40°C in the CRU series, as it was cooled by the strongest La Niña since 1988/89. Despite its relative coolness, 1999 was still the fifth warmest year in the CRU record. Depending on the record used, 1999 was between 0.11°C and 0.33°C warmer than the last comparable La Niña year, 1989. It is noteworthy, however, that north of 20°N, 1999 was nearly as warm as 1998. Mitigation of the warming trend in the early 1990s was short-lived and was mainly due to the cooling influence of the eruption of Mount Pinatubo in 1991 (Parker *et al.*, 1996), highlighted in the SAR. The ten warmest years in all four records have occurred after 1980, six or seven of them in the 1990s in each series.

Based on the CRU series, equivalent linear trends in global, Northern and Southern Hemisphere land-surface air temperature are shown in Table 2.1. Because warming may not persist at the rates shown, all trends are shown in °C/decade. The two main periods of warming in all three series are between about 1910 to 1945 and between 1976 to 2000 (updated from Karl *et al.*, 2000). Trends have been calculated using a restricted maximum likelihood method (Diggle *et al.*, 1999) that allows for serial correlation in the data. It gives larger standard errors than ordinary least squares methods when data have a complex temporal structure, as is true here. Table 2.1 and Figure 2.1 show that the rate of global and hemispheric warming in land-surface air temperature from 1976 to 2000 was about twice as fast (but interannually more variable) than that for the period 1910 to 1945. However, trends over such short periods are very susceptible to end effects so the values in Table 2.1, and Table 2.2 below, should be viewed with caution for these periods. Both periods of warming are statistically significant, as is (easily) the warming since 1861 or 1901. Uncertainties in the annual values due to data gaps, including an additional estimate of uncertainties due to urbanisation, are included for land-surface air temperature but equivalent uncertainties are not currently available for the marine data alone. Thus estimates in Table 2.1 for the marine data may be conservative, though the effect of adding the influence of annual uncertainties to the land-surface air temperature data trends was small. The period 1946 to 1975 had no significant change of temperature, though there was a small non-significant, but regionally more marked, cooling over the Northern Hemisphere, as discussed by Parker *et al.* (1994).

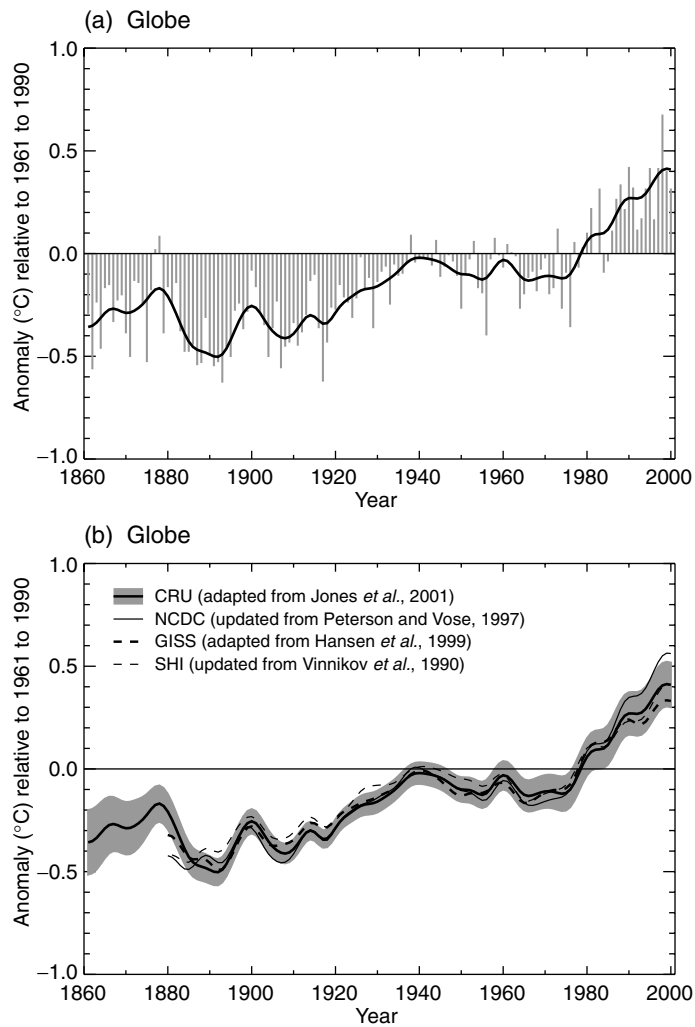


**Figure 2.1:** (a) Annual anomalies of global average land-surface air temperature (°C), 1861 to 2000, relative to 1961 to 1990 values. Bars and solid curve are from CRU (Jones *et al.*, 2001). Values are the simple average of the anomalies for the two hemispheres. The smoothed curve was created using a 21-point binomial filter giving near decadal averages. (b) As (a) but smoothed curves only from NCDC (updated from Peterson and Vose, 1997) – thin solid curve; GISS (adapted from Hansen *et al.*, 1999) – thick dashed curve; SHI (updated from Vinnikov *et al.*, 1990) – thin dashed curve to 1999 only; Peterson and Vose (1997) – thin solid curve. Thick solid curve – as in (a). Two standard error uncertainties are centred on the CRU curve and are estimated using an optimum averaging method (Folland *et al.*, 2001) and include uncertainties due to urbanisation but not due to uncertainties in thermometer exposures. The NCDC curve is the weighted average of the two hemispheres according to the area sampled, which accounts for most of the differences from the CRU curve.

The equivalent linear changes in global average CRU land-surface air temperature over 1861 to 2000 and 1901 to 2000 that take into account annual sampling errors and uncertainties due to urbanisation are  $0.63 \pm 0.24^\circ\text{C}$  and  $0.61 \pm 0.18^\circ\text{C}$  respectively. Corresponding Northern and Southern Hemisphere changes for 1901 to 2000 are  $0.71 \pm 0.31^\circ\text{C}$  and  $0.52 \pm 0.13^\circ\text{C}$ , respectively. Marine surface temperatures are discussed further in Section 2.2.2.

**Table 2.1:** Restricted maximum likelihood linear trends in annual average land-surface air temperature (LSAT) anomalies from CRU and sea surface temperature (SST) and night marine air temperature (NMAT) anomalies from the UK Met Office (UKMO). Twice the standard errors of the trends are shown in brackets. Trends significant at the 5% level or better, according to calculations made using an appropriate form of the *t* test, are shown in bold type. The significances of the trends are indicated beneath their twice standard errors. The method for calculating the trends, standard errors and significances allows for serial correlation and can result in a trend for the globe that is not exactly equal to the average of the trends for the hemispheres, consistent with uncertainties in the trends. The estimates of trends and errors for the land data account for uncertainties in the annual anomalies due to data gaps and urbanisation. Uncertainties in annual marine anomalies are not available. Trends are given in °C/decade.

	1861 to 2000	1901 to 2000	1910 to 1945	1946 to 1975	1976 to 2000
Northern Hemisphere	<b>0.06</b> (0.02) 1%	<b>0.07</b> (0.03) 1%	<b>0.14</b> (0.05) 1%	-0.04 (0.06)	<b>0.31</b> (0.11) 1%
CRU LSAT (Jones <i>et al.</i> , 2001)					
Southern Hemisphere	<b>0.03</b> (0.01) 1%	<b>0.05</b> (0.01) 1%	<b>0.08</b> (0.04) 1%	0.02 (0.05)	<b>0.13</b> (0.08) 1%
CRU LSAT (Jones <i>et al.</i> , 2001)					
Global	<b>0.05</b> (0.02) 1%	<b>0.06</b> (0.02) 1%	<b>0.11</b> (0.03) 1%	-0.01 (0.05)	<b>0.22</b> (0.08) 1%
CRU LSAT (Jones <i>et al.</i> , 2001)					
Northern Hemisphere	<b>0.03</b> (0.01) 1%	<b>0.05</b> (0.02) 1%	<b>0.15</b> (0.04) 1%	-0.05 (0.10)	<b>0.18</b> (0.05) 1%
UKMO SST (Jones <i>et al.</i> , 2001)					
Southern Hemisphere	<b>0.04</b> (0.01) 1%	<b>0.06</b> (0.01) 1%	<b>0.13</b> (0.05) 1%	0.06 (0.07)	<b>0.10</b> (0.05) 1%
UKMO SST (Jones <i>et al.</i> , 2001)					
Global	<b>0.04</b> (0.01) 1%	<b>0.06</b> (0.01) 1%	<b>0.15</b> (0.04) 1%	0.01 (0.06)	<b>0.14</b> (0.04) 1%
UKMO SST (Jones <i>et al.</i> , 2001)					
Global		<b>0.05</b> (0.02) 1%	<b>0.14</b> (0.04) 1%	-0.01 (0.06)	<b>0.11</b> (0.05) 1%
UKMO NMAT (Parker <i>et al.</i> , 1995)					

#### Maximum and minimum temperature

As reported in the SAR, and updated by Easterling *et al.* (1997), the increase in temperature in recent decades has involved a faster rise in daily minimum than daily maximum temperature in many continental regions. This gives a decrease in the diurnal temperature range (DTR) in many parts of the world. The analysis by Easterling *et al.* (1997) increased total global coverage from 37% to 54% of global land area. Large parts of the world have still not been analysed due to a lack of observations or inaccessible data, particularly in the tropics. Updating all the data remains a problem, so the analysis ends in 1993.

The overall global trend for the maximum temperature during 1950 to 1993 is approximately 0.1°C/decade and the trend for the minimum temperature is about 0.2°C/decade. Consequently, the trend in the DTR is about -0.1°C/decade. The rate of temperature increase for both maximum and minimum temperature over this period is greater than for the mean temperature over the entire 20th century, reflecting the strong warming in recent decades. Note that these trends for 1950 to 1993 will differ from the global trends due to the restricted data coverage so we only quote trends to 0.1°C.

Since the DTR is the maximum temperature minus the minimum temperature, the DTR can decrease when the trend in the maximum or minimum temperature is downward, upward, or unchanging. This contributes to less spatial coherence on the DTR map than on maps of mean temperature trend. Maximum temperatures have increased over most areas with the notable exception of eastern Canada, the southern United States, portions of Eastern

and southern Europe (Brunetti *et al.*, 2000a), southern China, and parts of southern South America. Minimum temperatures, however, increased almost everywhere except in eastern Canada and small areas of Eastern Europe and the Middle East. The DTR decreased in most areas, except over middle Canada, and parts of southern Africa, south-west Asia, Europe, and the western tropical Pacific Islands. In some areas the pattern of temperature change has been different. In both New Zealand (Salinger, 1995) and central Europe (Weber *et al.*, 1994; Brázdil *et al.*, 1996) maximum and minimum temperatures have increased at similar rates. In India the DTR has increased due to a decrease in the minimum temperature (Kumar *et al.*, 1994). Eastern Canada also shows a slight increase in DTR due to a stronger cooling in maximum temperatures relative to minimum temperatures (Easterling *et al.*, 1997). However, recently annual mean maximum and minimum temperatures for Canada have been analysed using newly homogenised data (Vincent, 1998; Vincent and Gullet, 1999); these have increased by 0.3 and 0.4°C, respectively, over the last fifty years (Zhang *et al.*, 1999). Central England temperature also shows no decrease in DTR since 1878 (Parker and Horton, 1999). Similarly, a new temperature data set for north-east Spain (not available on Figure 2.2 below, Brunet-India *et al.*, 1999a,b), shows an increase in maximum temperature over 1913 to 1998 to be about twice as fast as that of minimum temperature. Recent analyses by Quintana-Gomez (1999) reveal a large reduction in the DTR over Venezuela and Colombia, primarily due to increasing minimum temperatures (up to 0.5°C/decade). In northern China, the decrease in DTR is due to a stronger warming

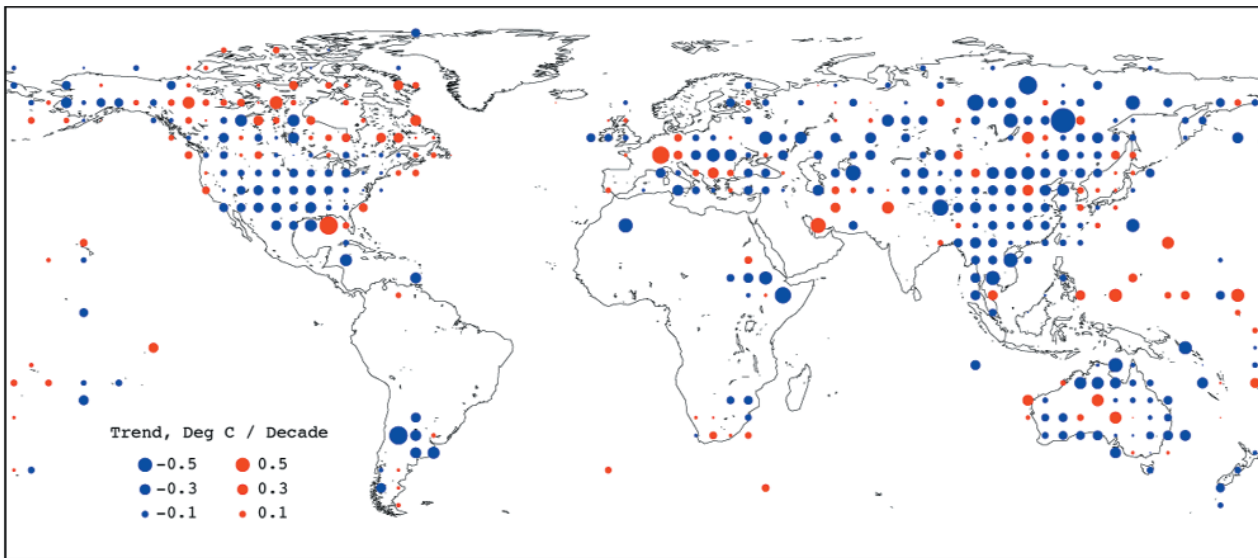


**Figure 2.2:** Trends in annual diurnal temperature range (DTR,  $^{\circ}\text{C}/\text{decade}$ ), from 1950 to 1993, for non-urban stations only, updated from Easterling *et al.* (1997). Decreases are in blue and increases in red. This data set of maximum and minimum temperature differs from and has more restricted coverage than those of mean temperature used elsewhere in Section 2.2.

in minimum temperature compared with maximum temperatures. However, in southern China the decreased DTR is due to a cooling in maximum with a slight warming in minimum temperature (Zhai and Ren, 1999).

The DTR is particularly susceptible to urban effects. Gallo *et al.* (1996) examined differences in DTR between stations based on predominant land use in the vicinity of the observing site. Results show statistically significant differences in DTR between stations associated with predominantly rural land use/land cover and those associated with more urban land use/land cover, with rural settings generally having larger DTR than urban settings. Although this shows that the distinction between urban and rural land use is important as one of the factors that can influence the trends observed in temperatures, Figure 2.2 shows annual mean trends in diurnal temperature range in worldwide non-urban stations over the period 1950 to 1993 (from Easterling *et al.*, 1997). The trends for both the maximum and minimum temperatures are about  $0.005^{\circ}\text{C}/\text{decade}$  smaller than the trends for the full network including urban sites, which is consistent with earlier estimated urban effects on global temperature anomaly time-series (Jones *et al.*, 1990).

Minimum temperature for both hemispheres increased abruptly in the late 1970s, coincident with an apparent change in the character of the El Niño-Southern Oscillation (ENSO) phenomenon, giving persistently warmer sea temperatures in the tropical central and east Pacific (see Section 2.6.2). Seasonally, the strongest changes in the DTR were in the boreal winter ( $-0.13^{\circ}\text{C}/\text{decade}$  for rural stations) and the smallest changes were during boreal summer ( $-0.065^{\circ}\text{C}/\text{decade}$ ), indicating some seasonality in the changes. Preliminary extensions of the Easterling *et al.* (1997) analysis to 1997 show that the declining trends in DTR have continued in much of North America and Asia.

Figure 2.3 shows the relationship between cloudiness and the DTR for a number of regions where long-term cloud cover data are available (Dai *et al.*, 1997a). For each region there was an increase in cloud cover over the 20th century and generally a

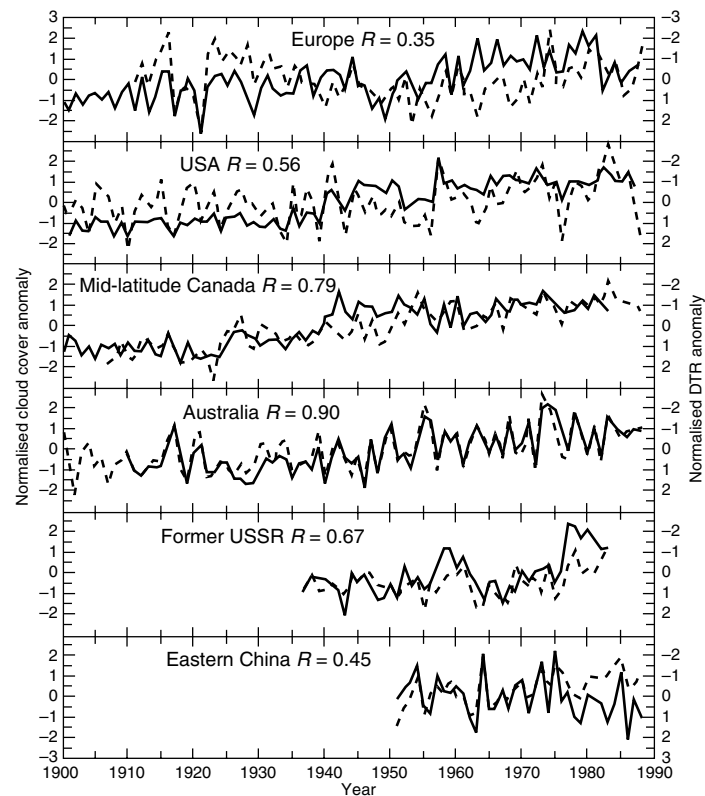


**Figure 2.3:** Cloud cover (solid line) and DTR ( $^{\circ}\text{C}$ , dashed line) for Europe, USA, Canada, Australia, the former Soviet Union, and eastern China (from Dai *et al.*, 1997a). Note that the axis for DTR has been inverted. Therefore, a positive correlation of cloud cover with inverted DTR indicates a negative cloud cover/DTR correlation.

decrease in DTR. In some instances the correlation between annual cloud cover and annual DTR is remarkably strong, suggesting a distinct relationship between cloud cover and DTR. This would be expected since cloud dampens the diurnal cycle of radiation balance at the surface. Anthropogenically-caused

increases in tropospheric aerosol loadings have been implicated in some of these cloud cover changes, while the aerosols themselves can cause small changes in DTR without cloud changes (Hansen *et al.*, 1998 and Chapter 6).

#### 2.2.2.2 Sea surface temperature and ocean air temperature

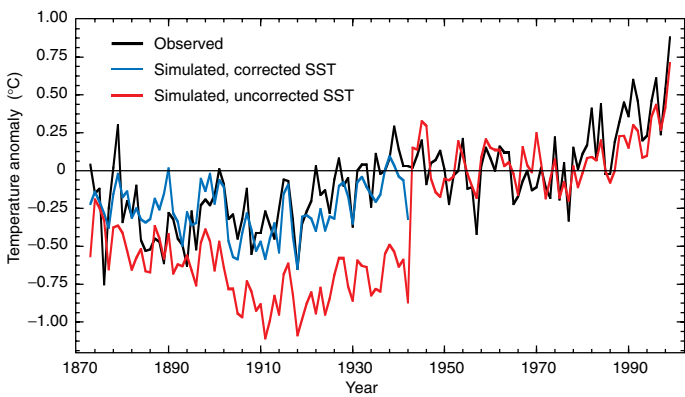
The analyses of SST described here all estimate the sub-surface bulk temperature, (i.e. the temperature in the first few metres of the ocean) not the skin temperature. Thus the Reynolds and Smith (1994) and Smith *et al.* (1996) data, which incorporate polar orbiting satellite temperatures, utilise skin temperatures that have been adjusted to estimate bulk SST values through a calibration procedure.

Many historical *in situ* marine data still remain to be digitised and incorporated into the database, to improve coverage and reduce the uncertainties in our estimates of marine climatic variations. A combined physical-empirical method (Folland and Parker, 1995) is used, as in the SAR, to estimate adjustments to ships' SST data obtained up to 1941 to compensate for heat losses from uninsulated (mainly canvas) or partly-insulated (mainly wooden) buckets (see Box 2.2). The corrections are independent of the land-surface air temperature data. Confirmation that these spatially and temporally complex adjustments are quite realistic globally is emerging from simulations of the Jones (1994) land-surface air temperature anomalies using the Hadley Centre atmospheric climate model HadAM3 forced with observed SST and sea-ice extents since 1871, updated from Rayner *et al.* (1996). Figure 2.4 (Folland *et al.*, 2001) shows simulations of global land-surface air temperature anomalies in model runs forced with SST, with and without bias adjustments to the SST data before 1942. All runs with uncorrected SST (only the average is shown) give too cold a simulation of land-surface air temperature for much of the period before 1941 relative to the 1946 to 1965 base period, with a dramatic increase in 1942. All

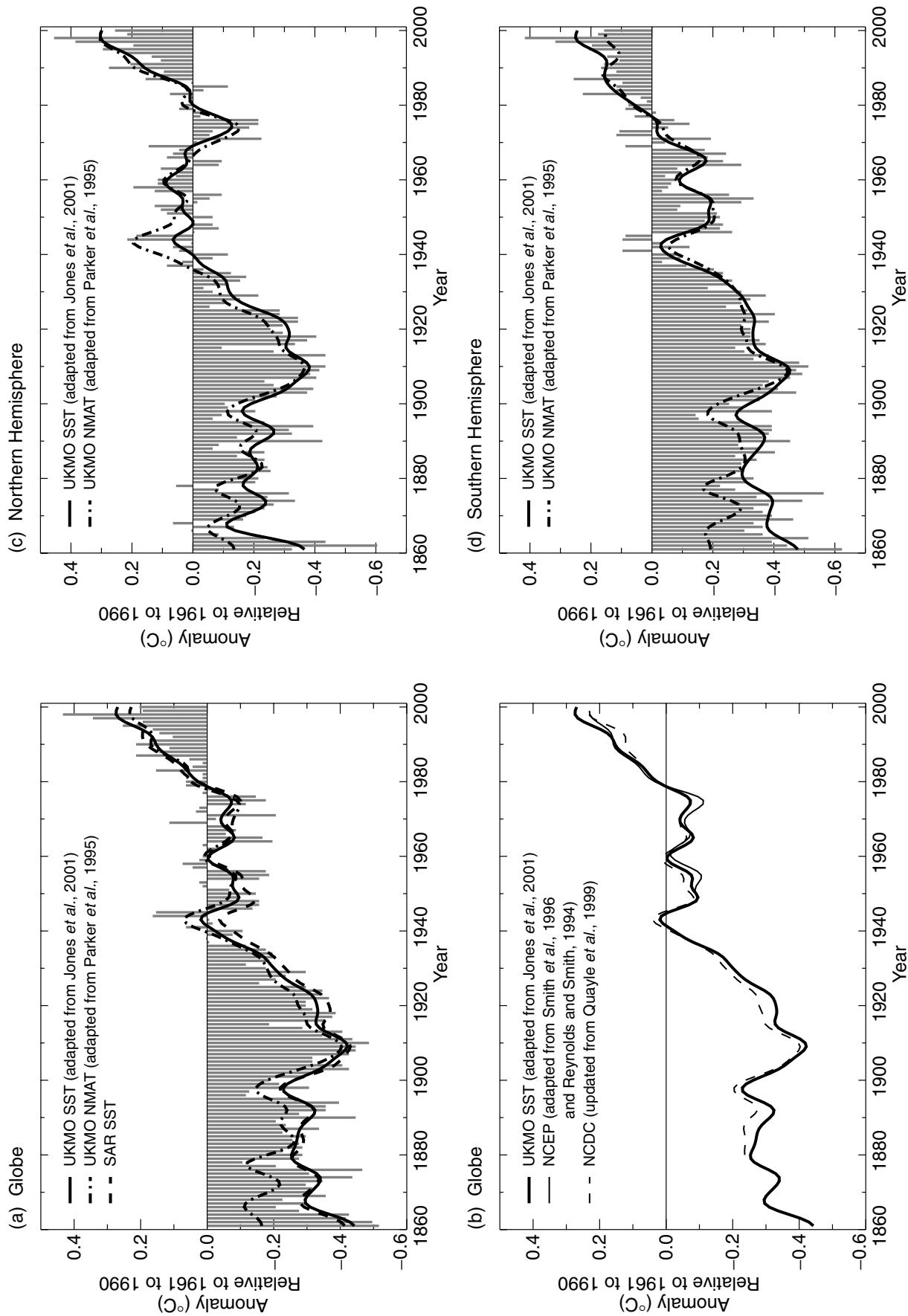
six individual runs with bias-adjusted SST (only the average is shown) give simulated land air temperatures close to those observed so that internal model variability is small on decadal time-scales compared to the signal being sought. These global results are mostly confirmed by ten similar large regional land-surface air temperature analyses (not shown). Hanawa *et al.* (2000) have provided independent confirmation of the SST bias corrections around Japan. Therefore, our confidence in the SST data sets has increased. Marine data issues are discussed further in Box 2.2, in Trenberth *et al.* (1992) and Folland *et al.* (1993).

Figure 2.5a shows annual values of global SST, using a recently improved UKMO analysis that does not fill regions of missing data (Jones *et al.*, 2001), together with decadally smoothed values of SST from the same analysis. NMAT is also shown. These generally agree well after 1900, but NMAT data are warmer before that time with a slow cooling trend from 1860 not seen in the SSTs, though the minimum around 1910 is seen in both series. The SST analysis from the SAR is also shown. The changes in SST since the SAR are generally fairly small, though the peak warmth in the early 1940s is more evident in the more recent analysis, supported by the NMAT analysis. A contribution to decadally averaged global warmth at that time is likely to have arisen from closely spaced multiple El Niño events centred near 1939 to 1941 and perhaps 1942 to 1944 (Bigg and Inoue, 1992; and Figure 2.29). The NMAT data largely avoid daytime heating of ships' decks (Bottomley *et al.*, 1990; Folland and Parker, 1995). Although NMAT data have been corrected for warm biases in World War II they may still be too warm in the Northern Hemisphere at that time (Figure 2.5c), though there is good agreement in the Southern Hemisphere (Figure 2.5d). The NMAT analysis is based on that in Parker *et al.* (1995) but differs from that used in the SAR in that it incorporates optimal interpolated data using orthogonal spatial patterns (eigenvectors). This is similar to the technique described by Kaplan *et al.* (1997, 1998) but with additional allowance for non-stationarity of the data (Parker *et al.*, 1995). Great care is needed in making these reconstructions in a changing climate, as pointed out by Hurrell and Trenberth (1999). This NMAT analysis has been chosen because of the often very sparse data. NMAT confirms the SST trends in the 20th century until 1991 (see also Table 2.1). After 1991, NMAT warmed at a slower rate than SST in parts of the Southern Hemisphere, notably the South Indian and the tropical South Pacific Oceans. Overall, however, the SST data should be regarded as more reliable, though the relative changes in NMAT since 1991 may be partly real (Christy *et al.*, 2001). The similar trends in SST and island air temperature found by Folland *et al.* (1997) for four regions of the tropical and extra-tropical South Pacific over much of the last century support the generally greater reliability of the SST data.

Figure 2.5b shows three time-series of changes in global SST. The UKMO series (as in Figure 2.5a) does not include polar orbiting satellite data because of possible time-varying biases in them that remain difficult to correct fully (Reynolds, 1993) though the NCEP (National Centers for Environmental Prediction) data (adapted from Smith *et al.*, 1996 and Reynolds and Smith, 1994), starting in 1950, do include satellite data after 1981. The NCDC series (updated from Quayle *et al.*, 1999) starts in 1880 and



**Figure 2.4:** Tests of bias adjustments to sea surface temperature (SST) using a climate model (Folland *et al.*, 2001). Black line - annual mean observed land surface air temperature (SAT) anomaly ( $^{\circ}$ C) from a 1946 to 1965 average (Jones, 1994), a period before major anthropogenic warming. Red line - annual averages of four simulations of SAT anomalies using uncorrected SST data, 1872 to 1941, and an average of six simulations for 1941 to 1998. Blue line - average of six simulations of SAT, forced with SST data corrected up to 1941 (Folland and Parker, 1995). Simulated data are collocated with available observations.



**Figure 2.5:** (a) Annual anomalies of global SST (bars and solid curve) and global night marine air temperature (NMAT, dotted curve), 1861 to 2000, relative to 1961 to 1990 ( $^{\circ}\text{C}$ ) from UK Met Office analyses (NMAT updated from Parker *et al.*, 1995). Smoothed curves were created using a 21-point binomial filter to give near-decadal averages. Also shown are the equivalent SST anomalies from the SAR – dashed curve. (b) Smoothed annual global SST ( $^{\circ}\text{C}$ ), 1861 to 2000, relative to 1961 to 1990, from USA National Climate Data Centre, Quayle *et al.* (1999) (thin dashed line, includes satellite data); USA National Centres for Environmental Prediction, Reynolds and Smith (1994) and Smith *et al.* (1996) (thin solid line, includes satellite data, to 1999 only), and UK Met Office (Jones *et al.*, 2001) (thick line). (c) UKMO SST and NMAT anomaly time-series from a 1961 to 1990 average for the Northern Hemisphere. (d) As (c) but for the Southern Hemisphere. Both for 1861 to 2000.

**Box 2.2:** Adjustments and Corrections to Marine Observations.

The SST data used here comprise over 80 million observations from the UK Main Marine Data Bank, the United States Comprehensive Ocean Atmosphere Data Set (COADS) and recent information telecommunicated from ships and buoys from the World Weather Watch. These observations have been carefully checked for homogeneity and carefully corrected for the use of uninsulated wooden and canvas buckets for collecting seawater prior to 1942. However, corrections prior to about 1900 are less well known because of uncertainties in the mix of wooden and canvas buckets. Nevertheless, Figure 2.4 provides good evidence that even in the 1870s, SST was little biased relative to land-surface air temperatures globally. Since 1941, observations mainly come from ship engine intake measurements, better insulated buckets and, latterly, from buoys. SST anomalies (from a 1961 to 1990 average) are first averaged into  $1^{\circ}$  latitude by  $1^{\circ}$  longitude boxes for five-day periods; the anomaly for a given observation is calculated from a  $1^{\circ}$  box climatology that changes each day throughout the year. The five-day  $1^{\circ}$  box anomalies are then aggregated into  $5^{\circ}$  boxes for the whole month with outlying values rejected, and monthly average anomalies calculated. Further adjustments are made to monthly SST anomalies for the varying numbers of observations in each  $5^{\circ}$  box because when observations are few, random errors tend to increase the variance of the monthly mean. NMAT data are treated similarly and have quite similar characteristics. However, a variance adjustment to NMAT data is not yet made. NMAT data are also corrected for the progressive increase in the height of thermometer screens on ships above the ocean surface, though no corrections have been made since 1930. Because there are only about half as many NMAT as SST data and NMAT have smaller temporal persistence, monthly NMAT anomalies may be less representative than SST anomalies even on quite large space scales. On longer time-scales, and over the majority of large ocean regions in the 20th century, there is good agreement between NMAT and SST. 19th century NMAT anomaly time-series should be viewed cautiously because of the sparse character of the constituent observations, and regionally varying biases, only some of which have been corrected.

includes satellite data to provide nearly complete global coverage. Up to 1981, the Quayle *et al.* series is based on the UKMO series, adjusted by linear regression to match the NCEP series after 1981. It has a truly global coverage based on the optimally interpolated Reynolds and Smith data. The Kaplan *et al.* (1998) global analysis is not shown because it makes no allowance for non-stationarity (here the existence of global warming) in its optimum interpolation procedures, as noted by Hurrell and Trenberth (1999). The warmest year globally in each SST record was 1998 (UKMO,  $0.43^{\circ}\text{C}$ , NCDC,  $0.39^{\circ}\text{C}$ , and NCEP,  $0.34^{\circ}\text{C}$ , above the 1961 to 1990 average). The latter two analyses are in principle affected by artificially reduced trends in the satellite data (Hurrell and Trenberth, 1999), though the data we show include recent attempts to reduce this. The global SST show mostly similar trends to those of the land-surface air temperature until 1976, but the trend since 1976 is markedly less (Table 2.1). NMAT trends are not calculated from 1861, as they are too unreliable. The difference in trend between global SST and global land air temperature since 1976 does not appear to be significant, but the trend in NMAT (despite any residual data problems) does appear to be less than that in the land air temperature since 1976. Figures 2.5c and d show that NMAT and SST trends remain very similar in the Northern Hemisphere to the end of the record, but diverge rather suddenly in the Southern Hemisphere from about 1991, as mentioned above. The five warmest years in each of the UKMO, NCDC and NCEP SST analyses have occurred after 1986, four of them in the 1990s in the UKMO analysis.

Particularly strong warming has occurred in the extra-tropical North Atlantic since the mid-1980s (approximately  $35^{\circ}$  to  $65^{\circ}\text{N}$ ,  $0^{\circ}$  to  $35^{\circ}\text{W}$  not shown). This warming appears to be related in part to the warming phase of a multi-decadal fluctuation (Folland *et al.*, 1986, 1999a; Delworth and Mann, 2000; see Section 2.6), perhaps not confined to the North Atlantic (Minobe, 1997; Chao *et al.*, 2000), though global warming is likely to be

contributing too. In addition, the cooling in the north-western North Atlantic south of Greenland, reported in the SAR, has ceased. These features were noted by Hansen *et al.* (1999).

#### 2.2.2.3 Land and sea combined

Figure 2.6 summarises the relative changes of UKMO SST, UKMO NMAT and CRU land-surface air temperature. The greater warming of the land in recent years is clear, but otherwise all three curves have a generally similar shape except that modest cooling of NMAT in the late 19th century is not seen in the SST data as noted for Figure 2.5. The relative coldness of the land around 1885 to 1895 comes from the Northern Hemisphere continental interiors, particularly in winter, as global coastal land air temperature and adjacent SST anomalies agree well at this time (Parker *et al.*, 1995), confirmed by the Jones *et al.* (2001) data. Note that there are some systematic compensating differences between the land and SST in the late 19th century in both hemispheres (not shown). The CRU land data are generally about  $0.1$  to  $0.2^{\circ}\text{C}$  colder in the Northern Hemisphere except at the beginning of the record (early 1860s), when they agree, and rather colder than this in 1885 to 1890. The opposite is seen in the Southern Hemisphere before 1885 when SST is generally  $0.1$  to  $0.2^{\circ}\text{C}$  colder and  $0.3^{\circ}\text{C}$  colder around 1875. Overall the SST data are less variable in each hemisphere in these rather poorly observed periods. The Southern Hemisphere land temperature at this time can actually represent a very small observed area of the hemisphere while the SST data, though sparse, are generally considerably more widespread. The sharp cooling in SST around 1903/4 in Figures 2.5 and 2.6, seen in the land as well as the two ocean surface data sets, was discussed for the North Atlantic and Indian Oceans by Helland-Hansen and Nansen (1920) not long after the event. The reduced warming of the NMAT in the last decade reflects differences in the Southern Hemisphere discussed above. Slightly greater warming of the global ocean than the

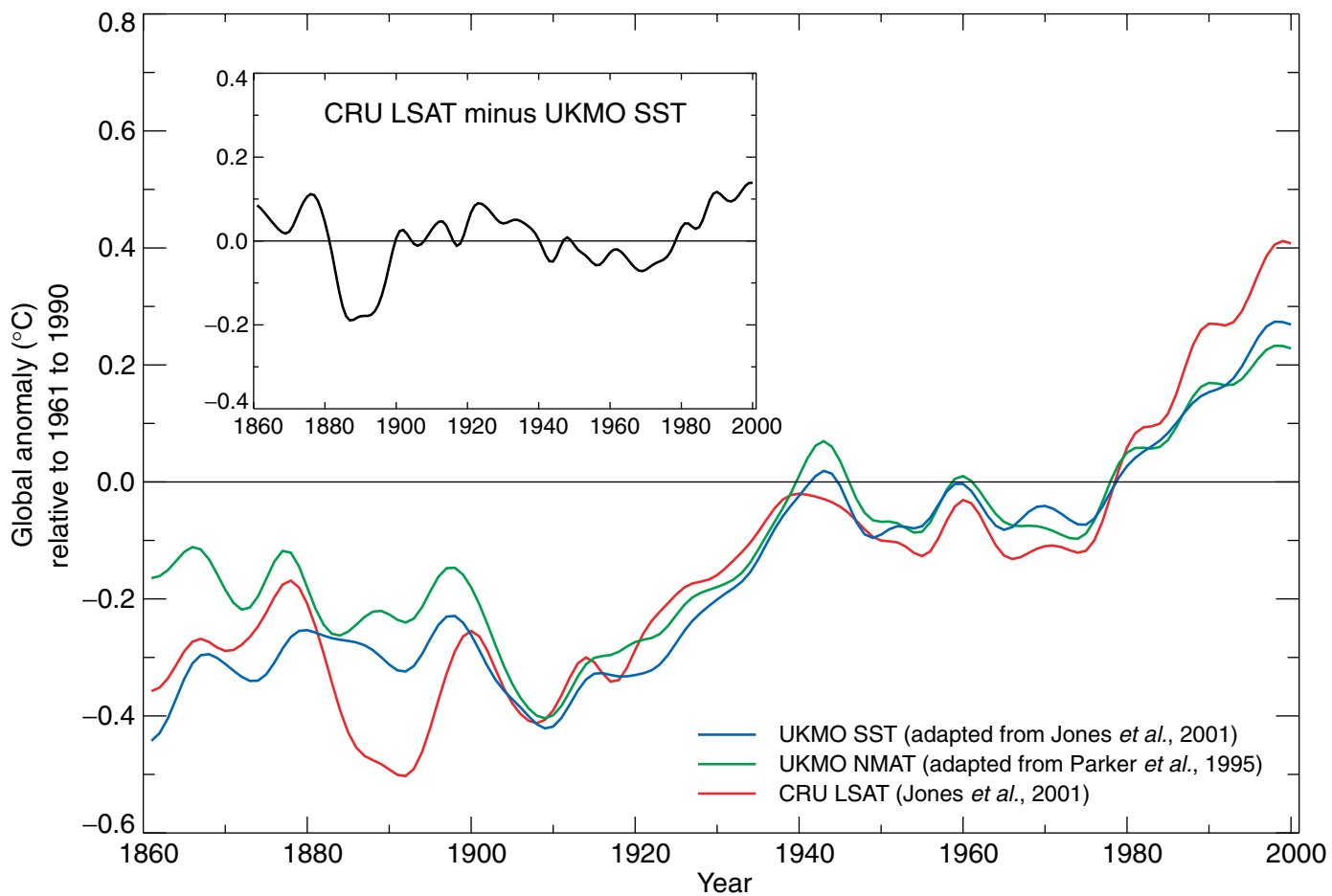


**Figure 2.6:** Smoothed annual anomalies of global average sea surface temperature ( $^{\circ}\text{C}$ ) 1861 to 2000, relative to 1961 to 1990 (blue curve), night marine air temperature (green curve), and land-surface air temperature (red curve). The data are from UK Met Office and CRU analyses (adapted from Jones *et al.*, 2001, and Parker *et al.*, 1995). The smoothed curves were created using a 21-point binomial filter giving near-decadal averages. Also shown (inset) are the smoothed differences between the land-surface air and sea surface temperature anomalies.

global land in 1910 to 1945 (seen in Table 2.1) is within the uncertainties of either data set, as a slightly slower warming of the ocean might be expected on physical grounds.

Figures 2.7a to c show annual time-series of anomalies of combined land-surface air temperature and SST for the hemispheres and globe since 1861, based on the latest CRU land air temperature data and the UKMO SST data. Jones *et al.* (2001) temperature data have been averaged by both a standard weighting method, used in the SAR, as shown by the dashed smoothed curves, and by an optimum averaging method (Shen *et al.*, 1998; Folland *et al.*, 2001) as shown by the bars and solid smoothed curves. The latter method uses the variance-covariance matrix instead of correlation functions (Kagan, 1997). The calculated uncertainties (twice the standard error) in the annual values are also shown (including the independent urbanisation and SST bias correction uncertainties). Optimum averaging gives less weight to areas of high data uncertainty than do ordinary averaging methods, and it takes much better account of data gaps. It also gives more weight to Antarctica, the great bulk of which (away from the Antarctic Peninsula) has warmed little in the last two decades (Comiso, 2000). Optimum averages can affect individual

years markedly when data are sparse. Thus extra warmth of the warm year 1878 (strongly affected by the 1877/78 El Niño) in the Northern relative to the Southern Hemisphere in the area weighted average (not shown) disappears when optimum averages are used. In the Northern Hemisphere, the optimum averages are little different from area weighted averages, but they are consistently warmer in the sparsely sampled Southern Hemisphere before 1940, often by more than one tenth of a degree. The overall effect on global temperature is small, however (Figure 2.7c).

The five warmest global optimally averaged years since the beginning of the record in 1861 all occurred in the 1990s with 1998 having the warmest anomaly ( $0.55^{\circ}\text{C}$ ). This year was significantly warmer than the second warmest year, 1995 ( $0.38^{\circ}\text{C}$ ), while 1999 was fourth warmest year, despite the strong La Niña event. The remarkably consistent monthly global warmth of 1998 is discussed in Karl *et al.* (2000).

Table 2.2 shows linear trends of the annual optimum averages, and twice their standard errors, for the globe and hemispheres using the restricted maximum likelihood method as in Table 2.1 and allowing for the annual uncertainties due to data gaps, urbanisation over land, and bias corrections to SST. Since

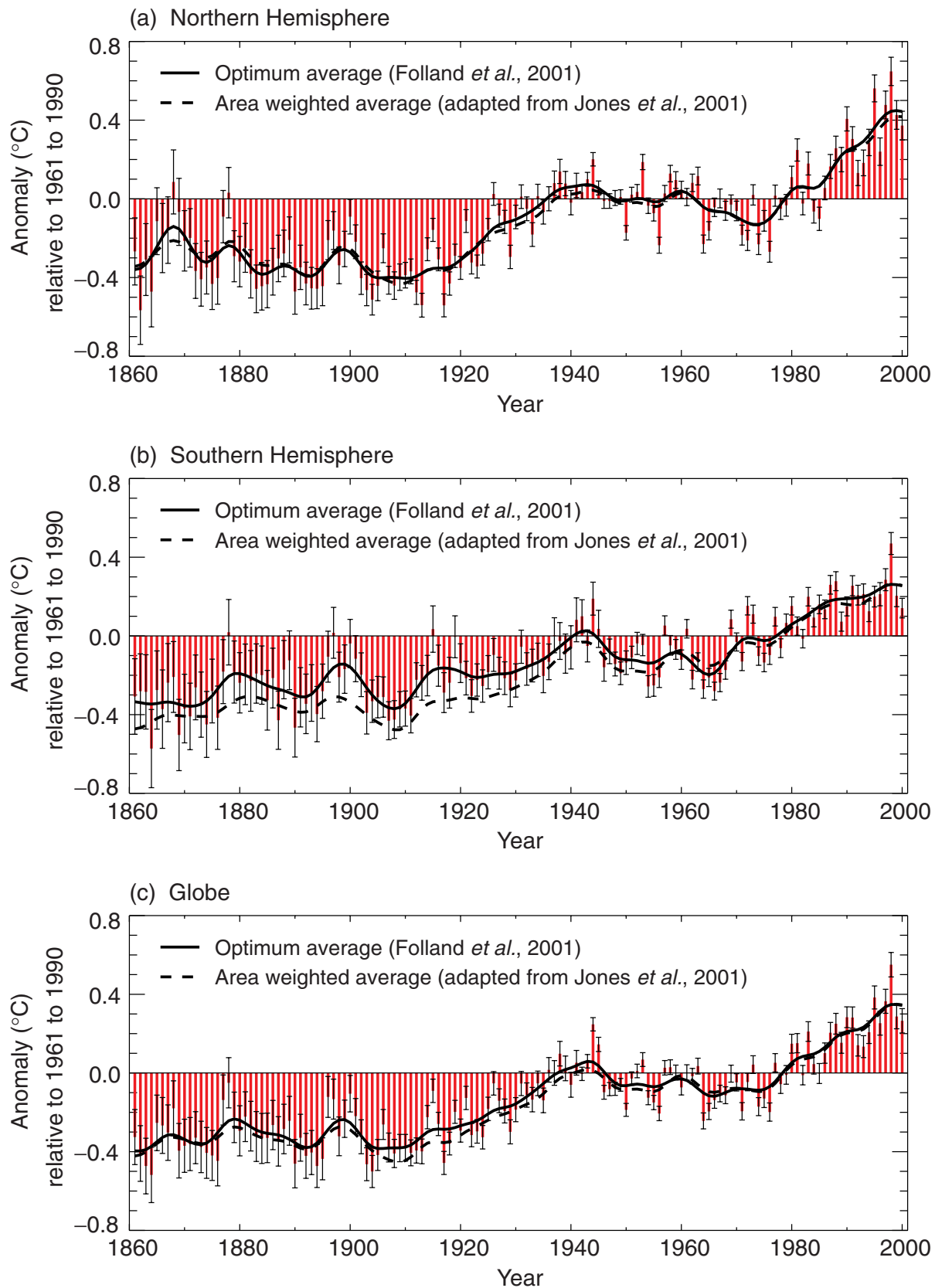


**Figure 2.7:** Smoothed annual anomalies of combined land-surface air and sea surface temperatures ( $^{\circ}\text{C}$ ), 1861 to 2000, relative to 1961 to 1990, for (a) Northern Hemisphere; (b) Southern Hemisphere; and (c) Globe. The smoothed curves were created using a 21-point binomial filter giving near-decadal averages. Optimally averaged anomalies (Folland *et al.*, 2001) – solid curves; standard area weighted anomalies (adapted from Jones *et al.*, 2001) – dashed curves. Also shown are the unsmoothed optimum averages – red bars, and twice their standard errors – width denoted by black “T”. Note that optimum averages for the Southern Hemisphere are a little warmer before 1940, when the data are sparse, than the area-weighted averages. However, the two types of averaging give similar results in the Northern Hemisphere.

**Table 2.2:** As Table 2.1 but for annual optimally averaged combined CRU land-surface air temperature anomalies and UKMO sea surface temperature anomalies (CRU LSAT + UKMO SST). All of the estimates of trends and errors in the table account for uncertainties in the annual anomalies due to data gaps, urbanisation over land, and bias corrections to SST.

	1861 to 2000	1901 to 2000	1910 to 1945	1946 to 1975	1976 to 2000
Northern Hemisphere	<b>0.05</b>	<b>0.06</b>	<b>0.17</b>	-0.05	<b>0.24</b>
CRU LSAT + UKMO SST (Folland <i>et al.</i> , 2001)	(0.02)	(0.02)	(0.03)	(0.05)	(0.07)
<b>1%</b>	<b>1%</b>	<b>1%</b>	<b>1%</b>		<b>1%</b>
Southern Hemisphere	<b>0.04</b>	<b>0.05</b>	<b>0.09</b>	0.03	<b>0.11</b>
CRU LSAT + UKMO SST (Folland <i>et al.</i> , 2001)	(0.01)	(0.02)	(0.05)	(0.07)	(0.05)
<b>1%</b>	<b>1%</b>	<b>1%</b>	<b>1%</b>		<b>1%</b>
Global	<b>0.04</b>	<b>0.06</b>	<b>0.14</b>	-0.01	<b>0.17</b>
CRU LSAT + UKMO SST (Folland <i>et al.</i> , 2001)	(0.01)	(0.02)	(0.04)	(0.04)	(0.05)
<b>1%</b>	<b>1%</b>	<b>1%</b>	<b>1%</b>		<b>1%</b>

1861 the hemispheres have warmed by approximately the same amount. However both the earlier period of warming (1910 to 1945) and the more recent one (1976 to 1999) saw rates of warming about twice as great in the Northern Hemisphere. There was continued (non-significant) warming in the Southern Hemisphere, though at a reduced rate, in 1946 to 1975, which partially offset (non-significant) cooling in the Northern Hemisphere over the same period to give a (non-significant) 0.03°C cooling globally. The global trend from 1861 to 2000 can be cautiously interpreted as an equivalent linear warming of 0.61°C over the 140-year period, with a 95% confidence level uncertainty of  $\pm 0.16^\circ\text{C}$ . From 1901 an equivalent warming of 0.57°C has occurred, with an uncertainty of  $\pm 0.17^\circ\text{C}$ .

Figure 2.8 shows a smoothed optimally averaged annual global time-series with estimates of uncertainty at  $\pm$  twice the standard error of the smoothed (near decadal) estimate. Note that the optimum average uncertainties increase in earlier years mainly because of the much larger data gaps. Also shown are uncertainties estimated by Jones *et al.* (1997b) using a different method centred on the Jones *et al.* (2001) land and sea surface temperature series. This series uses the average of anomalies from all available grid boxes, weighted according to grid box area. Therefore, in contrast to the Jones *et al.* (2001) global land-surface air temperature data, the global land and sea surface temperature data are not a simple average of the hemispheres. The optimally averaged uncertainties vary from about 15 to 65% less than those given by Jones *et al.* (1997b). This is reasonable as optimum averages have minimum variance amongst the range of unbiased estimates of the average. Not surprisingly, there is relatively little difference in the decadal averages themselves. However unlike the Jones *et al.* estimates of uncertainty, the optimum average also includes uncertainties in bias corrections to SST up to 1941 (Folland and Parker, 1995) and the uncertainties (as included in Figure 2.1) in the land data component that are due to urbanisation. Cessation of the SST component of uncertainty after 1941 is the reason for a lack of increase in uncertainties in the fairly poorly observed period 1942 to 1945. Uncertainties due to changes in thermometer screens are poorly known but could be 0.1°C globally in the 19th and early 20th centuries (Parker, 1994); they are not included here, but a preliminary analysis appears in Folland *et al.* (2001). For further discussion of changes in land and ocean surface temperature, see Jones *et al.* (1999a).

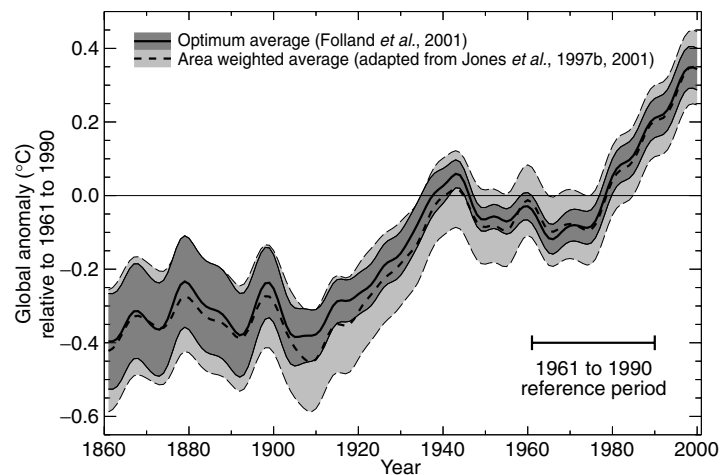
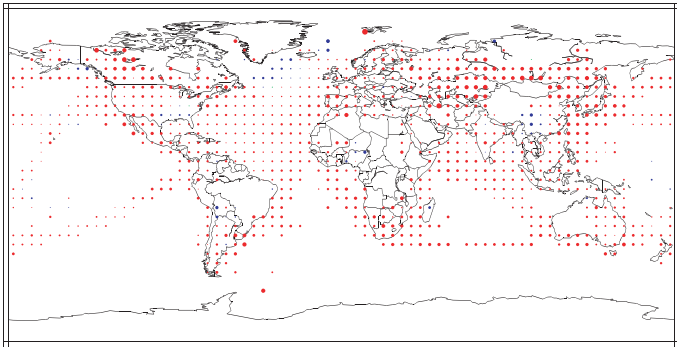


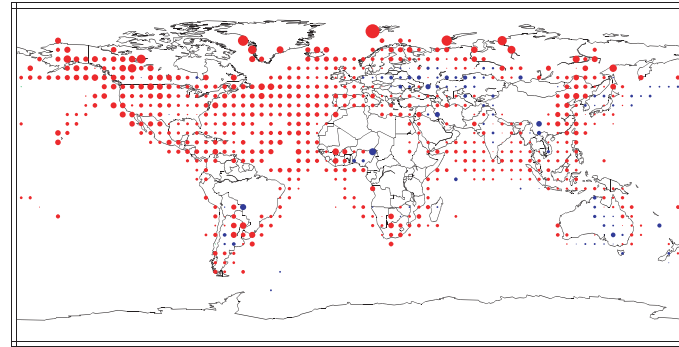
**Figure 2.8:** Smoothed annual anomalies of global combined land-surface air and sea surface temperatures (°C), 1861 to 2000, relative to 1961 to 1990, and twice their standard errors. The smoothed curves and shaded areas were created using a 21-point binomial filter giving near-decadal averages, with appropriate errors. Optimally averaged anomalies and uncertainties (Folland *et al.*, 2001) – solid curve and dark shading; standard area weighted anomalies and uncertainties (adapted from Jones *et al.*, 1997b, 2001) – dashed curve and light shading. Note that uncertainties decrease after 1941 due to the cessation of uncertainties due to bias corrections in sea surface temperature. On the other hand, uncertainties due to urbanisation of the land component, assessed as zero in 1900, continue to increase after 1941 to a maximum in 2000.

Referring back to Table 2.2 and including the second decimal place, our best estimate of the equivalent linear rate of global land and ocean surface warming between 1861 to 2000 is 0.044°C/decade, or a warming of  $0.61 \pm 0.16^\circ\text{C}$ . Over the period 1901 to 2000, the equivalent values are 0.058°C/decade or a warming of  $0.57 \pm 0.17^\circ\text{C}$ . These values include the modifying effects of the annual uncertainties. So we calculate that since the late 19th or the beginning of the 20th century, up to 2000, global warming has been  $0.6 \pm 0.2^\circ\text{C}$ . This is  $0.15^\circ\text{C}$  more warming than the 0.3 to  $0.6^\circ\text{C}$  estimated more subjectively up to 1994 by the SAR. This relatively large increase is explained by the increase in temperature since the SAR was completed, improved

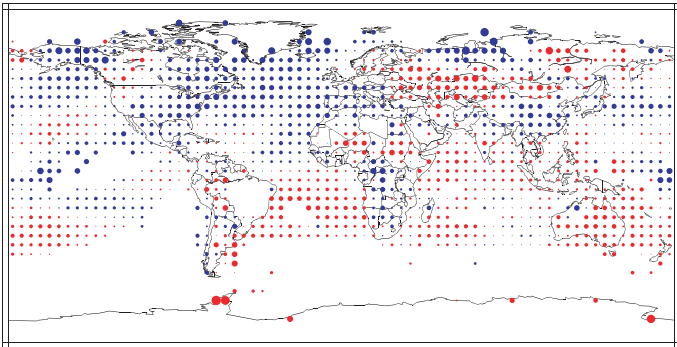
(a) Annual temperature trends, 1901 to 2000



(b) Annual temperature trends, 1910 to 1945



(c) Annual temperature trends, 1946 to 1975



(d) Annual temperature trends, 1976 to 2000

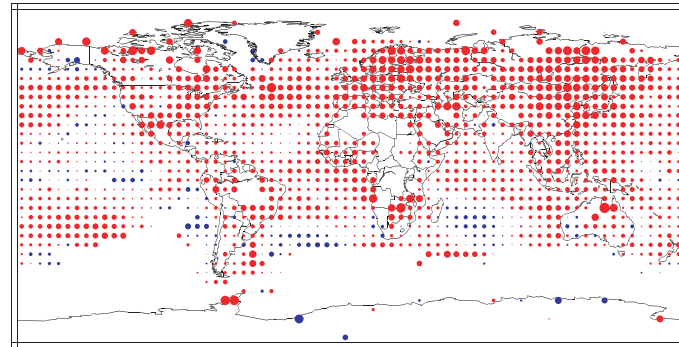


**Figure 2.9:** (a) to (d) Annual surface temperature trends for the periods 1901 to 2000, 1910 to 1945, 1946 to 1975, and 1976 to 2000, respectively ( $^{\circ}\text{C}/\text{decade}$ ), calculated from combined land-surface air and sea surface temperatures adapted from Jones *et al.* (2001). The red, blue and green circles indicate areas with positive trends, negative trends and little or no trend respectively. The size of each circle reflects the size of the trend that it represents. Trends were calculated from annually averaged gridded anomalies with the requirement that annual anomalies include a minimum of 10 months of data. For the period 1901 to 2000, trends were calculated only for those grid boxes containing annual anomalies in at least 66 of the 100 years. The minimum number of years required for the shorter time periods (1910 to 1945, 1946 to 1975, and 1976 to 2000) was 24, 20, and 16 years, respectively.

methods of analysis and the fact that the SAR decided not update the value in the First Assessment Report, despite slight additional warming. The latter decision was likely to have been due to a cautious interpretation of overall uncertainties which had at that time to be subjectively assessed.

#### 2.2.2.4 Are the land and ocean surface temperature changes mutually consistent?

Most of the warming in the 20th century occurred in two distinct periods separated by several decades of little overall globally averaged change, as objectively identified by Karl *et al.* (2000) and discussed in IPCC (1990, 1992, 1996) and several references quoted therein. Figures 2.9 and 2.10 highlight the worldwide behaviour of temperature change in the three periods. These linear trends have been calculated from the Jones *et al.* (2001) gridded combination of UKMO SST and CRU land-surface air temperature, from which the trends in Table 2.2 were calculated. Optimum averaging has not been used for Figures 2.9 and 2.10, and only trends for grid boxes where reasonably complete time-series of data exist are shown. The periods chosen are 1910 to 1945 (first

warming period), 1946 to 1975 (period of little global temperature change), 1976 to 2000 (second warming period, where all four seasons are shown in Figure 2.10) and the 20th century, 1901 to 2000. It can be seen that there is a high degree of local consistency between the SST and land air temperature across the land-ocean boundary, noting that the corrections to SST (Folland and Parker, 1995) are independent of the land data. The consistency with which this should be true locally is not known physically, but is consistent with the similarity of larger-scale coastal land and ocean surface temperature anomalies on decadal time-scales found by Parker *et al.* (1995). The warming observed in the period from 1910 to 1945 was greatest in the Northern Hemisphere high latitudes, as discussed in Parker *et al.* (1994). By contrast, the period from 1946 to 1975 shows widespread cooling in the Northern Hemisphere relative to much of the Southern, consistent with Tables 2.1 and 2.2 and Parker *et al.* (1994). Much of the cooling was seen in the Northern Hemisphere regions that showed most warming in 1910 to 1945 (Figure 2.9 and Parker *et al.*, 1994). In accord with the results in the SAR, recent warming (1976 to 2000) has been greatest over the mid-latitude Northern

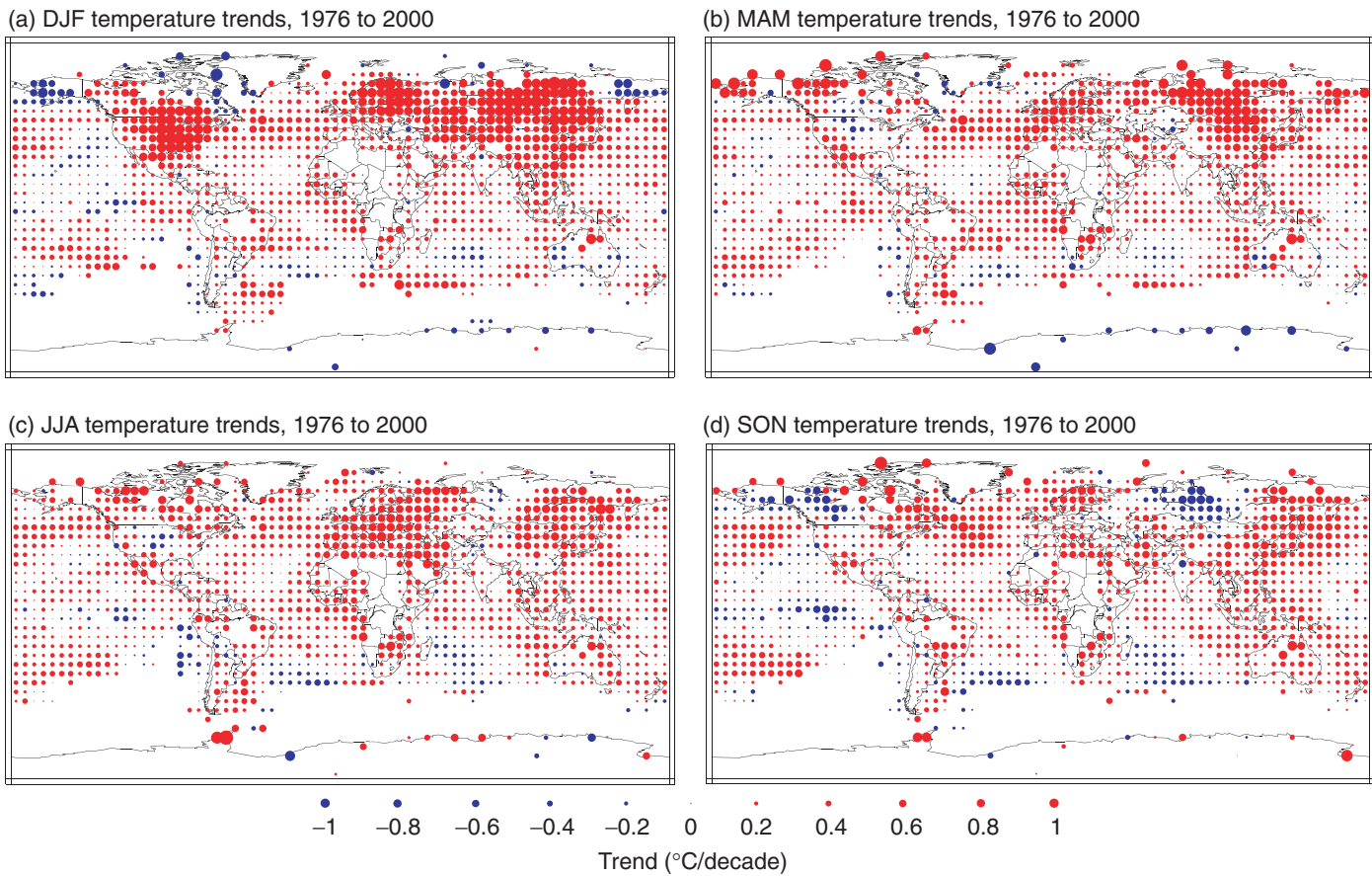


**Figure 2.10:** (a) to (d) Seasonal surface temperature trends for the period 1976 to 2000 ( $^{\circ}\text{C}/\text{decade}$ ), calculated from combined land-surface air and sea surface temperatures adapted from Jones *et al.* (2001). The red, blue and green circles indicate areas with positive trends, negative trends and little or no trend respectively. The size of each circle reflects the size of the trend that it represents. Trends were calculated from seasonally averaged gridded anomalies with the requirement that the calculation of seasonal anomalies should include all three months. Trends were calculated only for those grid boxes containing seasonal anomalies in at least 16 of the 24 years.

Hemisphere continents in winter. However, the updated data shows only very limited areas of year-round cooling in the north-west North Atlantic and mid-latitude North Pacific. Over 1901 to 2000 as a whole, noting the strong consistency across the land-ocean boundary, most warming is observed over mid- and high latitude Asia and parts of western Canada. The only large areas of observed cooling are just south and east of Greenland and in a few scattered continental regions in the tropics and sub-tropics.

Faster warming of the land-surface temperature than the ocean surface temperature in the last two decades, evident in Figure 2.6, could in part be a signal of anthropogenic warming (see Chapters 9 and 12). However, a component, at least in the Northern Hemisphere north of  $40$  to  $45^{\circ}\text{N}$ , may result from the sharp increase in the positive phase of the winter half year North Atlantic Oscillation (NAO)/Arctic Oscillation (AO) since about 1970 (Section 2.6.5), though this itself might have an anthropogenic component (Chapter 7). There has also been a strong bias to the warm phase of El Niño since about 1976 (Section 2.6.2). In particular, Hurrell and van Loon (1997) and Thompson *et al.* (2000a) show that the positive phase of the NAO advects additional warm air over extra-tropical Eurasia north of about  $45^{\circ}\text{N}$ . The positive phase of the NAO or AO is therefore likely to be a major cause of

the winter half-year warming in Siberia and northern Europe in Figure 2.10, as also quantified by Hurrell (1996). Cooling over the western North Atlantic Ocean also occurs, partly due to advection of cold air in an enhanced north to north-west airflow. Hurrell (1996) also shows that the warm phase of El Niño is associated with widespread extra-tropical continental warming, particularly over North America and parts of Siberia, with cooling over the North Pacific Ocean. Both effects are consistent with the strong warming over Siberia in winter in 1976 to 2000 (Figure 2.10), warming over much of North America and cooling over the Davis Strait region. Note that some regional details of the seasonal trends for 1976 to 2000 in Figure 2.10 may be sensitive to small changes in record length. A test for the shorter period 1980 to 1997 showed the same general worldwide pattern of (generally somewhat reduced) seasonal warming trends as in Figure 2.10, but with some regional changes, particularly over North America, almost certainly related to atmospheric circulation fluctuations. However, Siberian trends were considerably more robust.

We conclude that in the 20th century we have seen a consistent large-scale warming of the land and ocean surface. Some regional details can be explained from accompanying atmospheric circulation changes.

### 2.2.2.5 Sub-surface ocean temperatures and salinities

While the upper ocean temperature and salinity are coupled to the atmosphere on diurnal and seasonal time-scales, the deep ocean responds on much longer time-scales. During the last decade, data set development, rescue, declassification and new global surveys have made temperature and salinity profile data more readily available (Levitus *et al.*, 1994, 2000a).

#### Global

Levitus *et al.* (1997, 2000b) made annual estimates of the heat content of the upper 300 m of the world ocean from 1948 through to 1998 (Figure 2.11). The Atlantic and Indian Oceans each show a similar change from relatively cold to relatively warm conditions around 1976. The Pacific Ocean exhibits more of a bidecadal signal in heat storage. In 1998, the upper 300 m of the world ocean contained  $(1.0 \pm 0.5) \times 10^{23}$  Joules more heat than it did in the mid-1950s, which represents a warming of  $0.3 \pm 0.15^\circ\text{C}$ . A least squares linear regression to the annual temperature anomalies from 1958 to 1998 gives a warming of  $0.037^\circ\text{C}/\text{decade}$ . White *et al.* (1997, 1998b) computed changes in diabatic heat storage within the seasonal mixed layer from 1955 to 1996 between  $20^\circ\text{S}$  and  $60^\circ\text{N}$  and observed a warming of  $0.15 \pm 0.02^\circ\text{C}$  or  $0.036^\circ\text{C}/\text{decade}$ .

Extension of the analysis to the upper 3,000 m shows that similar changes in heat content have occurred over intermediate and deep waters in all the basins, especially in the North and South Atlantic and the South Indian Oceans. The change in global ocean heat content from the 1950s to the 1990s is equivalent to a net downwards surface heat flux of  $0.3 \text{ W m}^{-2}$  over the whole period.

#### Pacific

The winter and spring mixed-layer depths over the sub-tropical gyre of the North Pacific deepened 30 to 80% over the period 1960 to 1988 (Polovina *et al.*, 1995). Over the sub-polar gyre, mixed-layer depths reduced by 20 to 30% over the same period. The surface layer of the sub-polar gyre in the north-east Pacific has both warmed and freshened, resulting in a lower surface density (Freeland *et al.*, 1997). Wong *et al.* (1999) compared trans-Pacific data from the early 1990s to historical data collected about twenty years earlier. The changes in temperature and salinity are consistent with surface warming and freshening at mid- and higher latitudes and the subsequent subduction (downward advection) of these changes into the thermocline. From 1968/69 and 1990/91, the South Pacific waters beneath the base of the thermocline have cooled and freshened (Johnson and Orsi, 1997); the greatest cooling and freshening of  $-1.0^\circ\text{C}$  and 0.25, respectively, occurred near  $48^\circ\text{S}$  and were still observed at  $20^\circ\text{S}$ . All the deep water masses show a cooling and freshening at these high southern latitudes.

#### Arctic

Recent surveys of the Arctic Ocean (Quadfasel *et al.*, 1993; Carmack *et al.*, 1995; Jones *et al.*, 1996) have revealed a sub-surface Atlantic-derived warm water layer that is up to  $1^\circ\text{C}$  warmer and whose temperature maximum is up to 100 dbar shallower than observed from ice camps from the 1950s to the

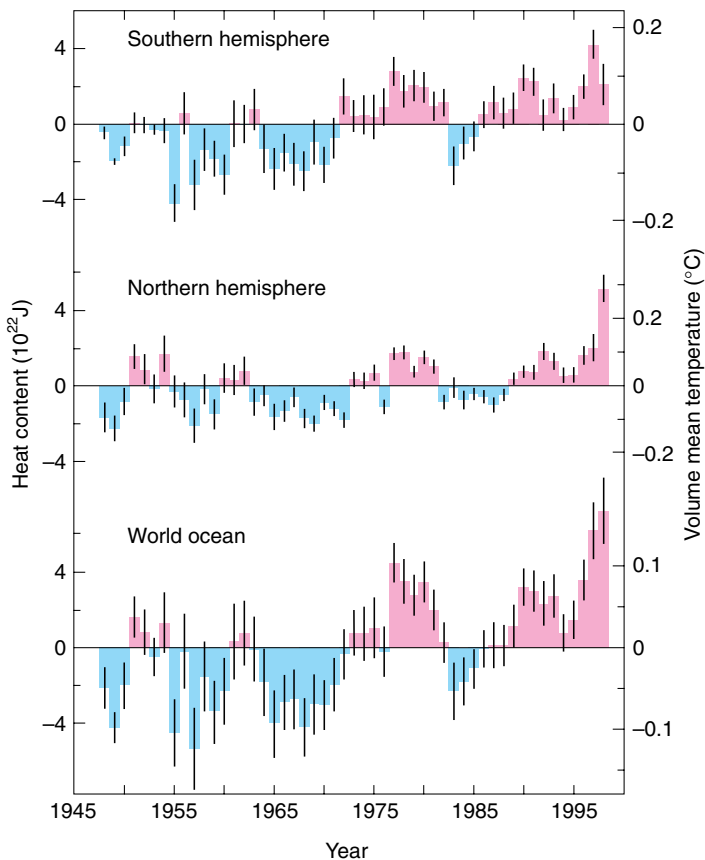


**Figure 2.11:** Time-series for 1948 to 1998 of ocean heat content anomalies in the upper 300 m for the two hemispheres and the global ocean. Note that  $1.5 \times 10^{22} \text{ J}$  equals 1 watt-year-m $^{-2}$  averaged over the entire surface of the earth. Vertical lines through each yearly estimate are  $\pm$  one standard error (Levitus *et al.*, 2000b).

1980s, as well as from ice-breaker data in the late 1980s and early 1990s. Warming is greatest in the Eurasian Basin. Annual surveys of the southern Canada Basin since 1979 (Melling, 1998), have shown a warming and deepening lower Atlantic layer, the lower halocline layer cooling by  $0.12^\circ\text{C}$  and the upper halocline layer warming by  $0.15^\circ\text{C}$ . Steele and Boyd (1998) compared winter temperature and salinity profiles obtained over the central and eastern Arctic Basins from submarine transects in 1995 and 1993 with Soviet data collected over the period 1950 to 1989 (Environmental Working Group, 1997). They showed that the cold halocline waters cover significantly less area in the newer data. This is consistent with a decreased supply of cold, fresh halocline waters from the Pacific Shelf areas.

#### Atlantic

The sub-arctic North Atlantic exhibits decadal variability in both temperature and salinity (Belkin *et al.*, 1998). Reverdin *et al.* (1997) found that the variability of salinity around the entire subarctic gyre for the period 1948 to 1990 was most prominent at periods of 10 years and longer, and extended from the surface to below the base of the winter mixed layer. This salinity signal was only coherent with elsewhere in the north-western Atlantic. A single spatial pattern explains 70% of the variance of the upper

ocean salt content of the subarctic gyre, corresponding to a signal propagating from the west to the north-east. Reverdin *et al.* also found that fluctuations in the outflow of fresh water from the Arctic are associated with periods of greater or fewer than usual northerly winds east of Greenland or off the Canadian Archipelago.

North Atlantic deep waters begin as intermediate waters in the Nordic seas. These waters have freshened over the 1980s and 1990s (Bönisch *et al.*, 1997). In addition, the absence of deep convection over the same period has caused Nordic Sea bottom waters to become warmer, saltier and less dense. The Faroes-Shetland Channel is the principal pathway between the north-east Atlantic and the Norwegian Sea and has been surveyed regularly since 1893 (Turrell *et al.*, 1999). Unfortunately, the quality of the salinity measurements was poor from 1930 through to 1960. Since the mid-1970s, the intermediate and bottom waters entering the North Atlantic through the channel have freshened at rates of 0.02/decade and 0.01/decade, respectively. The decreased salinities have resulted in decreased water densities and a decrease of between 1 and 7%/decade in the transport of deep water into the North Atlantic.

In the Labrador Sea, winter oceanic deep convection was intense during the earlier 1990s, extending to deeper than 2,400 m in 1992 to 1994. This produced a Labrador Sea water mass colder, denser and fresher than has been observed over at least the last five decades (Lazier, 1995; Dickson *et al.*, 1996).

Within the tropical and sub-tropical gyres of the North Atlantic, the deep and intermediate water masses are warming. Ocean station S (south-east of Bermuda, 32°17'N, 64°50'W) has been sampled bi-weekly since 1954. Joyce and Robins (1996) extended the hydrographic record from ocean station S back from 1954 to 1922 using nearby observations. They find an almost constant rate of warming over the 1,500 to 2,500 dbar layer of 0.05°C/decade over the 73-year period 1922 to 1995. This corresponds to a net downward heat flux of 0.7 Wm<sup>-2</sup>. Sections completed in 1958, 1985 and 1997 along 52°W and 66°W between 20°N to 35°N (Joyce *et al.*, 1999) show a rate of warming of 0.06°C/decade, similar to that seen at Bermuda but averaged over a larger 1,700 m depth interval. Trans-Atlantic sections along 24°N in 1957, 1981 and 1992 show a similar warming between 800 and 2,500 m (Parrilla *et al.*, 1994; Bryden *et al.*, 1996). The maximum warming at 1,100 m is occurring at a rate of 0.1°C/decade. At 8°N between 1957 and 1993, Arhan *et al.* (1998) showed warming from 1,150 and 2,800 m with the maximum warming of 0.15°C at 1,660 m.

The Antarctic bottom water in the Argentine Basin of the South Atlantic experienced a marked cooling (0.05°C) and freshening (0.008) during the 1980s (Coles *et al.*, 1996). The bottom waters of the Vema Channel at the northern end of the Argentine basin did not change significantly during the 1980s but warmed steadily during a 700-day set of current meter deployments from 1992 to 1994 (Zenk and Hogg, 1996).

#### *The Indian Ocean*

Bindoff and McDougall (2000) have examined changes between historical data collected mostly in the period 1959 to 1966 with WOCE data collected in 1987 in the southern Indian Ocean at

latitudes 30 to 35°S. They found warming throughout the upper 900 m of the water column (maximum average warming over this section of 0.5°C at 220 dbar).

### **2.2.3 Temperature of the Upper Air**

#### *Uncertainties in discerning changes*

Several measuring systems are available to estimate the temperature variations and trends of the air above the surface, though all contain significant time-varying biases as outlined below.

#### *Weather balloons*

The longest data sets of upper air temperature are derived from instruments carried aloft by balloons (radiosondes). Changes in balloon instrumentation and data processing over the years have been pervasive, however, resulting in discontinuities in these temperature records (Gaffen, 1994; Parker and Cox, 1995; Parker *et al.*, 1997). Gaffen *et al.* (2000b) attempted to identify these biases by using statistical tests to determine "change-points" – sudden temperature shifts not likely to be of natural origin (e.g., instrument changes). However, they found that alternative methods for identifying change points yield different trend estimates and that the analysis was hampered by the lack of complete documentation of instrument and data processing changes for many stations. This study, however, only analysed change points in the time-series of individual stations in isolation. Another technique, used successfully with surface data, relies on differences produced from comparisons among several stations in close proximity. In addition, Santer *et al.* (1999) noted that temperature trends estimated from radiosonde data sets are sensitive to how temperature shifts are dealt with, which stations are utilised, and the method used for areal averaging.

Worldwide temperatures from the Microwave Sounding Unit (MSU) data (Christy *et al.*, 2000) have been available from the beginning of 1979 for intercomparison studies. Parker *et al.* (1997) used the lower-stratospheric and lower-tropospheric MSU products to adjust monthly radiosonde reports for stations in Australia and New Zealand at times when instrumental or data-processing changes were documented. Some individual stratospheric corrections were as much as 3°C due to radiosonde instrument changes. The main disadvantage of the Parker *et al.* technique is that the raw MSU record has time-varying biases which must first be estimated and eliminated (Christy *et al.*, 2000).

Gaffen *et al.* (2000b) compared trends for 1959 to 1995, calculated using linear regression, for twenty-two stations with nearly complete data records at levels between 850 and 30 hPa. Each of these stations is included in two data sets created since the SAR: (a) monthly mean temperatures reported by the weather balloon station operators (Parker *et al.*, 1997; CLIMAT TEMP data) and (b) monthly mean temperatures calculated from archived daily weather balloon releases (Eskridge *et al.*, 1995; CARDS data). Decadal trends at individual sites differed randomly between the two data sets by typically 0.1°C/decade, with the largest differences at highest altitudes. In a few cases the differences were larger and statistically significant at the 1% level. The discrepancies were sometimes traceable to time-of-observation differences of the data used to calculate the averages.

The analysis of trends requires long station data records with minimal missing data. The records for 180 stations in the combined Global Climate Observing System Upper Air Network (GUAN) and the Angell (1988, 2000) network do not generally meet this standard, as only 74 of the GUAN stations, for instance, have at least 85% of tropospheric monthly means available for 1958 to 1998. In the lower stratosphere (up to 30 hPa), only twenty-two stations meet this requirement (Gaffen *et al.*, 2000b). These deficiencies present the dilemma of using either relatively small networks of stations with adequate data (the Southern Hemisphere, in particular, is poorly sampled) or larger networks with poorer quality data (adding uncertainty to the resulting trend estimates).

Characteristics, such as spatial coverage, of each data set derived from the weather balloon data are different. For example, Sterin (1999) used data from over 800 stations from the CARDS and telecommunicated data sets, with only gross spatial and temporal consistency checks. The data were objectively interpolated to all unobserved regions, introducing extra uncertainty. Parker *et al.* (1997) placed CLIMAT TEMP data into  $5^{\circ}$  latitude  $\times$   $10^{\circ}$  longitude grid boxes from about 400 sites, leaving unobserved boxes missing. Further data sets were created employing limited spatial interpolation and bias-adjustments, but uncertainties related to spatial under-sampling remain (Hurrell *et al.*, 2000). Angell (1988) placed observations from 63 stations into seven broad latitudinal bands, calculated the simple average for each band and produced global, hemispheric and zonal mean anomalies.

#### Satellites

Radiosondes measure temperatures at discrete levels, but satellite instruments observe the intensity of radiation from deep atmospheric layers. The advantage of satellites is the essentially uniform, global, coverage. The three temperature products that are commonly available from MSU are: the low to mid-troposphere (MSU 2LT, surface to about 8 km), mid-troposphere (MSU 2, surface to about 18 km, hence including some stratospheric emissions) and the lower stratosphere (MSU 4, 15 to 23 km, hence including some tropical tropospheric emissions) (Christy *et al.*, 2000). No other data, such as from radiosondes, are used to construct these MSU data sets. It is important to note that the troposphere and stratosphere are two distinct layers of the atmosphere with substantially different temperature variations and trends. The altitude of the troposphere/stratosphere boundary varies with latitude, being about 16 to 17 km in the tropics but only 8 to 10 km at high latitudes.

Since the SAR, several issues have emerged regarding MSU temperatures. Mo (1995) reported that for one of the longest-lived satellites (NOAA-12, 1991 to 1998) the non-linear calibration coefficients were erroneous, affecting MSU 2 and MSU 2LT. Wentz and Schabel (1998) discovered that satellite orbit decay introduces gradual, spurious cooling in MSU 2LT. Christy *et al.* (1998, 2000) found that instrument responses often differ between the laboratory assessments and on-orbit performance, requiring further corrections. Additional adjustments were also made by recalculating and removing spurious temperature trends due to diurnal effects induced by the east-west drift of the spacecraft (Christy *et al.*, 2000). The magnitude of the spurious trends (1979 to 1998) removed from version D compared to version C were:

orbit decay,  $-0.11$ ; instrument response,  $+0.04$  and diurnal drift,  $+0.03^{\circ}\text{C}/\text{decade}$ .

Version D of the MSU data is used in Figure 2.12. The SAR presented version B that for the low to mid-troposphere indicated a global trend about  $0.05^{\circ}\text{C}/\text{decade}$  more negative than version D (for 1979 to 1995). Quite separately, Prabhakara *et al.* (1998) generated a version of MSU 2 without corrections for satellite drift or instrument body effects, in many ways similar to MSU 2 version A of Spencer and Christy (1992a, 1992b).

The Stratospheric Sounding Unit (SSU) detects the intensity of thermal emissions and measures deep layer temperatures at altitudes above 20 km (Nash and Forrester, 1986). As with the MSU products, adjustments are required for radiometer biases, diurnal sampling and orbital drift (Chanin and Ramaswamy, 1999).

#### Rocketsondes and lidar

Data sets generated from rocketsondes have been updated (Golitsyn *et al.*, 1996; Lysenko *et al.*, 1997), providing temperature information to as high as 75 km. Important difficulties arise with these data due to different types of instrumentation, tidal cycles (amplitude  $2^{\circ}\text{C}$ ) and to assumed corrections for aerodynamic heating. The last set of adjustments has the most significant impact on trends. The approximately 11-year solar cycle forces a temperature perturbation of  $>1^{\circ}\text{C}$  in the mid- to upper stratosphere (30 to 50 km). Keckhut *et al.* (1999) and Dunkerton *et al.* (1998) created a quality-controlled data set of these measurements, which is used in Chanin and Ramaswamy (1999). The very limited number of launch sites leads to some uncertainty in deduced temperatures, and most launches were terminated in the mid-1990s.

Rayleigh lidar measurements began in 1979 at the Haute Provence Observatory in southern France and have spread to locations around the world. Lidar techniques generate the vertical profile of temperature from 30 to 90 km, providing absolute temperatures within  $2.5^{\circ}\text{C}$  accuracy. Chanin and Ramaswamy (1999) have combined MSU 4, SSU, radiosonde, lidar and rocketsonde data to estimate 5-km thick layer temperature variations for altitudes of 15 to 50 km, generally limited to the Northern Hemisphere mid-latitudes.

#### Reanalyses

The principle of reanalysis is to use observations in the data assimilation scheme of a fixed global weather forecasting model to create a dynamically consistent set of historical atmospheric analyses (Kalnay *et al.*, 1996). Within the assimilation scheme, potentially errant data are amended or excluded using comparisons with neighbours and/or calculated conditions. However, small, time-dependent biases in the observations, of magnitudes important for climate change, are virtually impossible to detect in the model, even in areas of adequate *in situ* data. Furthermore, in areas with few *in situ* data the reanalyses are often affected by inadequate model physics or satellite data for which time-varying biases have not been removed.

Though interannual variability is reproduced well, known discontinuities in reanalysed data sets indicate that further research is required to reduce time-dependent errors to a level suitable for climate change studies (Basist and Chelliah, 1997;

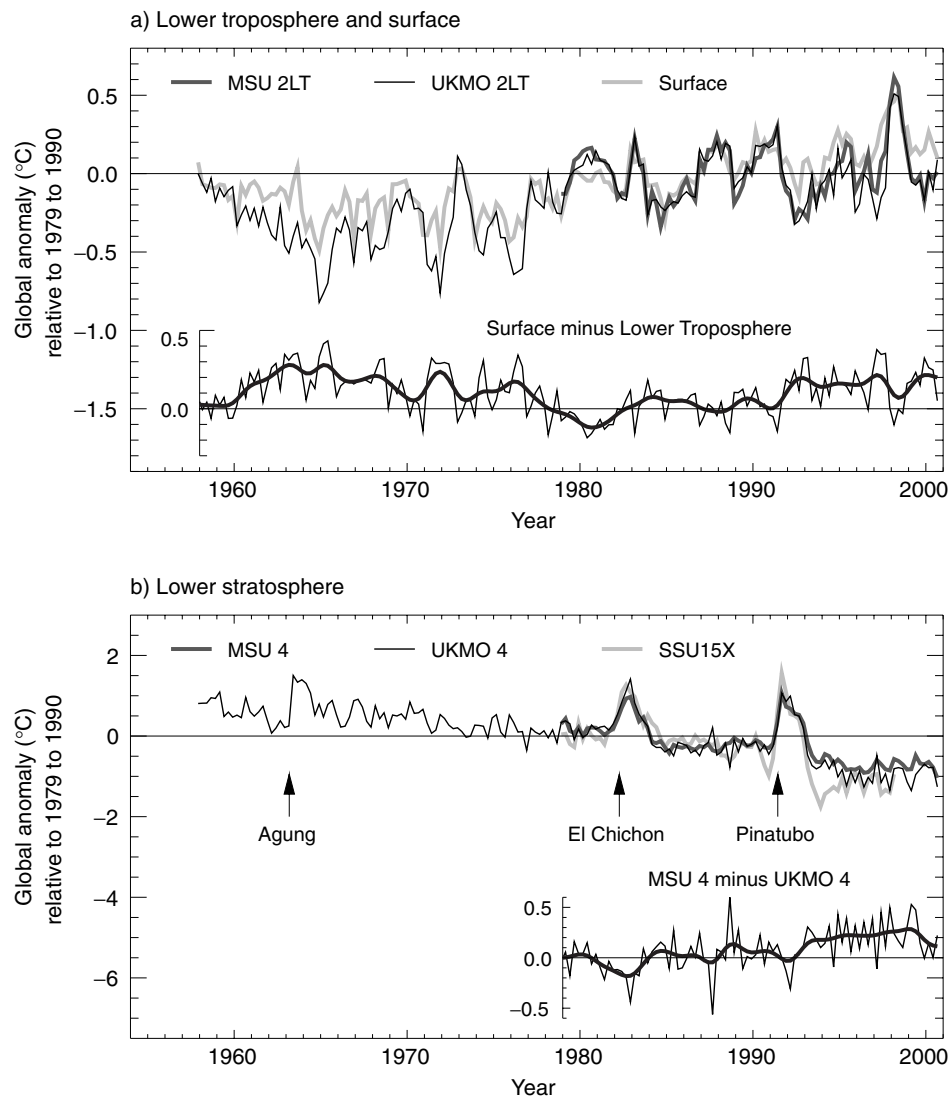


**Figure 2.12:** (a) Seasonal anomalies of global average temperature ( $^{\circ}\text{C}$ ), 1958 to 2000, relative to 1979 to 1990 for the lower troposphere, as observed from satellites (MSU 2LT) and balloons (UKMO 2LT), and for the surface (adapted from Jones *et al.*, 2001). Also shown (bottom graph) are the differences between the surface temperature anomalies and the averages of the satellite and balloon-based observations of the lower-tropospheric temperature anomalies. (b) As (a) but for the temperature of the lower stratosphere, as observed from satellites (MSU 4 and SSU 15X) and balloons (UKMO 4). The times of the major explosive eruptions of the Agung, El Chichon and Mt. Pinatubo volcanoes are marked. Also shown (bottom graph) are the differences between the MSU 4 and UKMO 4 based temperature anomalies.

Hurrell and Trenberth, 1998; Santer *et al.*, 1999, 2000; Stendel *et al.*, 2000). It is anticipated that future assessments of climate change will utilise reanalysis products to which substantial improvements will have been made. Data from the NCEP reanalysis are included below for comparison purposes, but longer-term stratospheric trends from NCEP are especially suspect due to a large shift in temperature when satellite data were incorporated for the first time in 1978 (Santer *et al.*, 1999).

#### 2.2.4 How do Surface and Upper Air Temperature Variations Compare?

In Figure 2.12 we display the surface, tropospheric and stratospheric temperature variations using representative data sets from those described above. Trend values ( $^{\circ}\text{C}/\text{decade}$ ) are shown in

Table 2.3 with 95% confidence intervals, which in part represent uncertainties due to temporal sampling, not those due to measurement error (see below). The effect of explosive volcanic events (Agung, 1963; El Chichon, 1982; and Mt. Pinatubo, 1991) is evident in Figure 2.12, as is a relative shift to warmer temperatures in the lower troposphere compared to the surface in the late 1970s, followed by large variations in both due to ENSO (particularly in 1998). After the shift in the late 1970s, the overall tropospheric temperature trend is near zero but the surface has warmed (see Figure 2.12a and Table 2.3).

Global variations and trends in the lower stratosphere are temporally more coherent than in the troposphere (Figure 2.12b), though the warming effects due to the volcanic eruptions are clearly evident. For the period 1958 to 2000, all stratospheric data sets except NCEP 4, which contains erroneous trends, show signif-

**Table 2.3:** As Table 2.1 but for annual average surface and upper air temperature anomalies from various data sets. The surface temperature trends are of combined land-surface air temperature (LSAT) and sea surface temperature (SST) or sea ice and sea surface temperature (ISST) anomalies. The upper air trends are of temperature anomalies corresponding to or approximately corresponding to temperature anomalies from MSU channels 2LT and 4. The tropical region is defined as the latitude band 20°S to 20°N for all the data sets except for the GISS LSAT + UKMO ISST data set where the region is defined as the latitude band 23.6°S to 23.6°N. The last line of the table shows trends in the differences between temperature anomalies for the surface, from the UKMO LSAT + UKMO SST data set, and for the lower troposphere, taken as the average of the UKMO 2LT and MSU 2LT anomalies for 1979 to 2000 and as the UKMO 2LT anomalies alone before 1979. None of the estimates of trends and errors account for uncertainties in the annual anomalies as these are not available. All calculations use data to the end of 2000 except for those for the NOAA data sets, which include data up to August 2000 only.

	1958 to 2000		1958 to 1978		1979 to 2000	
	Globe	Tropics	Globe	Tropics	Globe	Tropics
<b>Surface</b>						
UKMO LSAT + UKMO SST (Jones <i>et al.</i> , 2001)	<b>0.10</b> (0.05)	<b>0.08</b> (0.06)	-0.05 (0.07)	-0.09 (0.12)	<b>0.16</b> (0.06)	0.10 (0.10)
GISS LSAT + UKMO ISST (Hansen <i>et al.</i> , 1999; Rayner <i>et al.</i> , 2000)	<b>0.09</b> (0.04)	<b>0.09</b> (0.06)	-0.03 (0.07)	-0.09 (0.11)	<b>0.13</b> (0.07)	0.09 (0.10)
NCDC LSAT + NCEP SST (Quayle <i>et al.</i> , 1999; Reynolds and Smith, 1994)	<b>0.09</b> (0.05)	<b>0.09</b> (0.06)	-0.05 (0.06)	-0.08 (0.11)	<b>0.14</b> (0.06)	0.10 (0.11)
<b>Lower troposphere</b>						
UKMO 2LT (Parker <i>et al.</i> , 1997)	<b>0.11</b> (0.07)	<b>0.13</b> (0.08)	-0.03 (0.12)	0.07 (0.16)	0.03 (0.10)	-0.08 (0.12)
MSU 2LT (Christy <i>et al.</i> , 2000)					0.04 (0.11)	-0.06 (0.16)
NCEP 2LT (Stendel <i>et al.</i> , 2000)	<b>0.13</b> (0.07)	<b>0.08</b> (0.08)	0.02 (0.18)	-0.05 (0.17)	0.01 (0.11)	-0.07 (0.14)
NOAA 850–300hPa (Angell, 2000)	0.07 (0.08)	<b>0.07</b> (0.07)	-0.08 (0.15)	0.04 (0.20)	-0.03 (0.15)	-0.11 (0.19)
RIHMI 850–300hPa (Sterin, 1999)	<b>0.04</b> (0.04)	<b>0.07</b> (0.05)	-0.03 (0.06)	0.07 (0.08)	0.00 (0.07)	-0.06 (0.09)
<b>Lower stratosphere</b>						
UKMO 4 (Parker <i>et al.</i> , 1997)	<b>-0.39</b> (0.15)	<b>-0.31</b> (0.19)	<b>-0.37</b> (0.21)	-0.07 (0.51)	<b>-0.64</b> (0.47)	-0.50 (0.54)
MSU 4 (Christy <i>et al.</i> , 2000)					<b>-0.52</b> (0.48)	-0.29 (0.51)
NCEP 4 (Stendel <i>et al.</i> , 2000)	-0.25 (0.62)	-0.04 (0.32)	<b>-0.36</b> (0.33)	<b>-0.46</b> (0.29)	-0.61 (1.21)	-0.57 (0.77)
NOAA 100–50hPa (Angell, 2000)	<b>-0.64</b> (0.30)	<b>-0.58</b> (0.39)	-0.23 (0.22)	0.20 (0.43)	<b>-1.10</b> (0.58)	-0.68 (2.08)
RIHMI 100–50hPa (Sterin, 1999)	<b>-0.25</b> (0.12)	<b>-0.22</b> (0.12)	-0.20 (0.27)	-0.08 (0.10)	<b>-0.43</b> (0.24)	<b>-0.45</b> (0.28)
<b>Surface minus lower troposphere</b>						
	-0.01 (0.05)	-0.05 (0.07)	-0.03 (0.08)	<b>-0.16</b> (0.10)	<b>0.13</b> (0.06)	<b>0.17</b> (0.06)

icant negative trends (Table 2.3). Note that MSU 4, and simulations of MSU 4 (UKMO 4 and NCEP 4), include a portion of the upper troposphere below 100 hPa and so are expected to show less negative trends than those measuring at higher altitudes (e.g., the 100 to 50 hPa layers in Table 2.3 and the SSU in Figure 2.12b).

Blended information for 5 km thick levels in the stratosphere at 45°N compiled by Chanin and Ramaswamy (1999) show a negative trend in temperature increasing with height: -0.5°C/decade at 15 km, -0.8°C/decade at 20 to 35 km, and -2.5°C/decade at 50 km. These large, negative trends are consistent with models of the combined effects of ozone depletion and

increased concentrations of infrared radiating gases, mainly water vapour and carbon dioxide (Chapters 6 and 12).

The vertical profile of temperature trends based on surface data and radiosondes is consistent with the satellite temperatures. Global trends since 1979 are most positive at the surface, though less positive for night marine air temperatures in the Southern Hemisphere (see Section 2.2.2), near zero for levels between 850 to 300 hPa (1.5 to 8 km) and negative at 200 hPa (11 km) and above. Thus during the past two decades, the surface, most of the troposphere, and the stratosphere have responded differently to climate forcings because different physical processes have

dominated in each of these regions during that time (Trenberth *et al.*, 1992; Christy and McNider, 1994; NRC, 2000 and Chapter 12). On a longer time-scale, the tropospheric temperature trend since 1958, estimated from a sparser radiosonde network, is closer to that of the surface, about  $+0.10^{\circ}\text{C}/\text{decade}$  (Figure 2.12a and Table 2.3) (Angell, 1999, 2000; Brown *et al.*, 2000; Gaffen *et al.*, 2000a). Gaffen *et al.* (2000a) and Brown *et al.* (2000) noted a decreasing lower-tropospheric lapse rate from 1958 to 1980, and an increasing lower-tropospheric lapse rate after 1980 (Figure 2.12a). However, Folland *et al.* (1998) showed that global upper-tropospheric temperature has changed little since the late 1960s because the observed stratospheric cooling extended into the uppermost regions of the troposphere.

Between 1979 and 2000, the magnitude of trends between the surface and MSU 2LT is generally most similar in many parts of the Northern Hemisphere extra-tropics ( $20^{\circ}\text{N}$  to pole) where deep vertical mixing is often a characteristic of the troposphere. For example, the northern extra-tropical trends for the surface and MSU 2LT were  $0.28$  and  $0.21^{\circ}\text{C}/\text{decade}$ , respectively, and over the North American continent trends were  $0.27 \pm 0.24$  and  $0.28 \pm 0.23^{\circ}\text{C}/\text{decade}$ , respectively, with an annual correlation of 0.92. Over Europe the rates were  $0.38 \pm 0.36$  and  $0.38 \pm 0.30^{\circ}\text{C}/\text{decade}$ , respectively. Some additional warming of the surface relative to the lower troposphere would be expected in the winter half year over extra-tropical Asia (whole year warming rates of  $0.35 \pm 0.20$  and  $0.18 \pm 0.18^{\circ}\text{C}/\text{decade}$ , respectively), consistent with the vertical temperature structure of the increased positive phase of the Arctic Oscillation (Thompson *et al.*, 2000a, Figure 2.30). The vertical structure of the atmosphere in marine environments, however, generally reveals a relatively shallow inversion layer (surface up to 0.7 to 2 km) which is somewhat decoupled from the deep troposphere above (Trenberth *et al.*, 1992; Christy, 1995; Hurrell and Trenberth, 1996). Not only are local surface versus tropospheric correlations often near zero in these regions, but surface and tropospheric trends can be quite different (Chase *et al.*, 2000). This is seen in the different trends for the period 1979 to 2000 in the tropical band,  $0.10 \pm 0.10$  and  $-0.06 \pm 0.16^{\circ}\text{C}/\text{decade}$ , respectively (Table 2.3) and also in the southern extra-tropics where the trends are  $0.08 \pm 0.06$  and  $-0.05 \pm 0.08^{\circ}\text{C}/\text{decade}$ , respectively. Trends calculated for the differences between the surface and the troposphere for 1979 to 2000 are statistically significant globally at  $0.13 \pm 0.06^{\circ}\text{C}/\text{decade}$ , and even more so in the tropics at  $0.17 \pm 0.06^{\circ}\text{C}/\text{decade}$ . Statistical significance arises because large interannual variations in the parent time-series are strongly correlated and so largely disappear in the difference time-series (Santer *et al.*, 2000; Christy *et al.*, 2001). However, as implied above, they are not significant over many extra-tropical regions of the Northern Hemisphere such as North America and Europe and they are also insignificant in some Southern Hemisphere areas. The sequence of volcanic eruption, ENSO events, and the trends in the Arctic Oscillation have all been linked to some of this difference in warming rates (Michaels and Knappenburg, 2000; Santer *et al.*, 2000; Thompson *et al.*, 2000a; Wigley, 2000) and do explain a part of the difference in the rates of warming (see Chapter 12).

The linear trend is a simple measure of the overall tendency of a time-series and has several types of uncertainty; temporal

sampling uncertainty owing to short data sets, spatial sampling errors owing to incomplete spatial sampling, and various other forms of measurement error, such as instrument or calibration errors. Temporal sampling uncertainties are present even when the data are perfectly known because trends calculated for short periods are unrepresentative of other short periods, or of the longer term, due to large interannual to decadal variations. Thus confidence intervals for estimates of trend since 1979 due to temporal sampling uncertainty can be relatively large, as high as  $\pm 0.2^{\circ}\text{C}/\text{decade}$  below 300 hPa (Table 2.3, Santer *et al.*, 2000). Accordingly, the period from 1979 to 2000 provides limited information on long-term trends, or trends for other 22-year periods.

Uncertainties arising from measurement errors due to the factors discussed in Section 2.2.3, including incomplete spatial sampling, can be substantial. One estimate of this uncertainty can be made from comparisons between the various analyses in Table 2.3. For trends below 300 hPa, this uncertainty may be as large as  $\pm 0.10^{\circ}\text{C}/\text{decade}$  since 1979, though Christy *et al.* (2000) estimate the 95% confidence interval as  $\pm 0.06^{\circ}\text{C}$  for the MSU 2LT layer average. For example, Santer *et al.* (2000) find that when the satellite observations from MSU 2LT are masked to match the less than complete global coverage of the surface observations during the past few decades, the differences in the trends between the surface and the troposphere are reduced by about one third.

Summarising, it is very likely that the surface has warmed in the global average relative to the troposphere, and the troposphere has warmed relative to the stratosphere since 1979 (Figure 2.12a,b; Pielke *et al.*, 1998a,b; Angell, 1999, 2000; Brown *et al.*, 2000; Christy *et al.*, 2000; Gaffen *et al.*, 2000a; Hurrell *et al.*, 2000; NRC, 2000; Stendel *et al.*, 2000). However, the relative warming is spatially very variable and most significant in the tropics and sub-tropics. There is evidence that the troposphere warmed relative to the surface in the pre-satellite era (1958 to 1979, see Brown *et al.*, 2000; Gaffen *et al.*, 2000a), though confidence in this finding is lower. Uncertainties due to limited temporal sampling prevent confident extrapolation of these trends to other or longer time periods (Christy *et al.*, 2000; Hurrell *et al.*, 2000; NRC, 2000; Santer *et al.*, 2000). Some physical explanations for changes in the vertical profile of global temperature trends are discussed in Chapter 12 but a full explanation of the lower-tropospheric lapse rate changes since 1958 requires further research.

## 2.2.5 Changes in the Cryosphere

This chapter does not describe changes in the major ice sheets as this is dealt with in detail in Chapter 11.

### 2.2.5.1 Snow cover, including snowfall

Satellite records indicate that the Northern Hemisphere annual snow-cover extent (SCE) has decreased by about 10% since 1966 largely due to decreases in spring and summer since the mid-1980s over both the Eurasian and American continents (Figure 2.13a; Robinson, 1997, 1999). Winter and autumn SCE show no statistically significant change. Reduction in snow cover during the mid- to late 1980s was strongly related to temperature

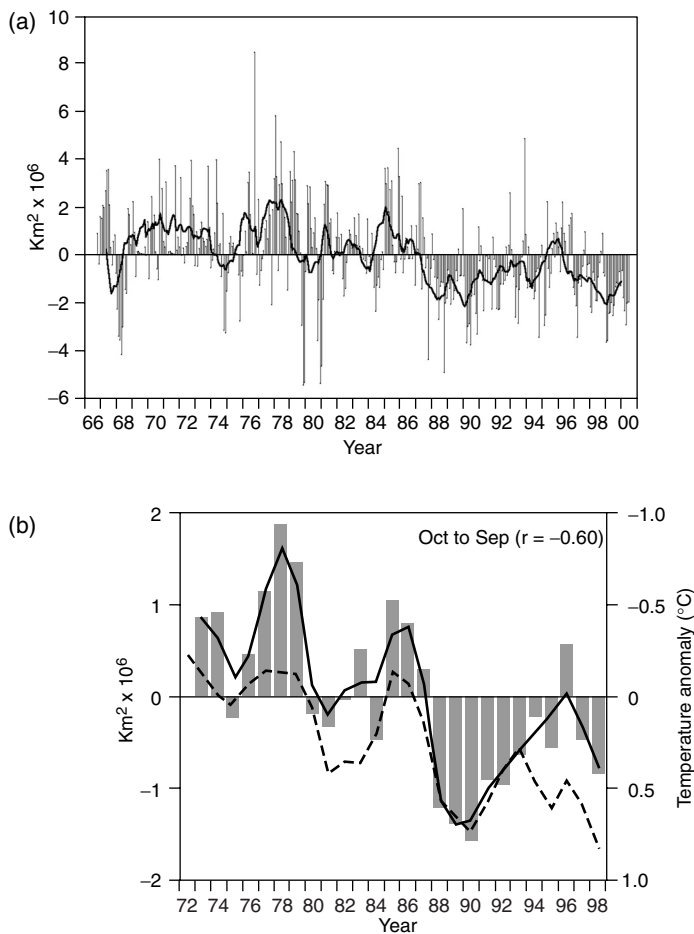


**Figure 2.13:** (a) Anomalies of monthly snow cover over the Northern Hemisphere lands (including Greenland) between November 1966 and May 2000. Also shown are twelve-month running anomalies of hemispheric snow extent, plotted on the seventh month of a given interval. Anomalies are calculated from NOAA/NESDIS snow maps. Mean hemispheric snow extent is 25.2 million  $\text{km}^2$  for the full period of record. The curve of running means is extrapolated by using period of record monthly means for 12 months in the late 1960s in order to create a continuous curve of running means. Missing months fell between May and October, and no winter months are missing. June 1999 to May 2000 values are based on preliminary analyses. (b) Seasonal snowcover anomalies (in million  $\text{km}^2$ ) versus temperature anomalies (in  $^\circ\text{C}$ ). Both snow and temperature anomalies are area averages over the region for which climatological values of seasonal snow-cover frequency (based on the 1973 to 1998 period) are between 10 and 90%. Season is indicated at the top of each panel. Axis for snow anomaly on the left-hand-side y axis, axis for temperature anomaly is on the right-hand-side y axis. Bar plot indicates time-series of snow cover anomalies. Continuous colour curve indicates nine-point weighted average of snow-cover anomaly. Dashed black curve indicates time-series of nine-point weighted average of area average temperature anomaly. Snow-cover calculations are based on the NOAA/NESDIS snow cover data for the period 1973 to 1998 (updated from Robinson *et al.*, 1993). Temperature calculations are based on the Jones data set, hence anomalies are with respect to the time period 1961 to 1990. Snow anomalies are with respect to the time period 1973 to 1998. Correlation coefficient ( $r$ ) between seasonal snow cover anomalies and temperature anomalies is indicated in parentheses. (Figure contributed by David A. Robinson and Anjuli Bamzai, Rutgers University.)

increases in snow covered areas (Figure 2.13b). There is a highly significant interannual (+0.6) and multi-decadal correlation between increases in the Northern Hemisphere spring land temperature and a reduction in the Northern Hemisphere spring snow cover since data have been available (1966). Snow cover extent has decreased about 10% since 1966. The improvements in the quantity and quality of the visible satellite imagery used to produce the operational snow-cover product cannot account for the observed changes in snow cover.

Longer regional time-series based on station records and reconstructions suggest that Northern Hemisphere spring and summer SCEs in the past decade have been at their lowest values in the past 100 years. In the other seasons, it is likely that extents in the latter portion of the 20th century exceeded those of earlier years (Brown, 2000).

Reconstructions for North America suggest that while there has been a general decrease in spring SCE since 1915, it is likely that winter SCE has increased (Brown and Goodison, 1996; Frei *et al.*, 1999; Hughes and Robinson, 1996; Hughes *et al.*, 1996). Similar to the results in North America, in Eurasia April SCE has significantly decreased; but lack of data has prevented an analysis of winter trends (Brown, 2000). Over Canada, there has been a general decrease in snow depth since 1946, especially during spring, in agreement with decreases in SCE (Brown and Braaten, 1998). Winter depths have declined over European Russia since 1900 (Meshcherskaya *et al.*, 1995), but have increased elsewhere over Russia in the past few decades (Fallot *et al.*, 1997). The common thread between studies that have examined seasonality is an overall reduction in spring snow cover in the latter half of the 20th century.

There have been relatively few studies of snowfall trends across the globe. Statistically significant increases in seasonal snowfall have been observed over the central USA in the 20th century (Hughes and Robinson, 1996). In recent decades, snowfall has also been heavier to the lee of the North American Great Lakes than earlier in the century (Leathers and Ellis, 1996). These findings are in line with observations from Canada and the former Soviet Union, reflecting a trend towards increased precipitation over the mid-latitude lands in the Northern Hemisphere (Groisman and Easterling, 1994; Brown and Goodison, 1996; Ye *et al.*, 1998).

### 2.2.5.2 Sea-ice extent and thickness

#### Sea-ice extent

Sea-ice extent is expected to become a sensitive indicator of a warming climate, although only recently have long records become available in the Arctic, and our knowledge of Antarctic sea-ice extent before the 1970s is very limited.

Sea-ice extent (the area within the ice-ocean margin) was observed from space from 1973 to 1976 using the ESMR (Electrically Scanning Microwave Radiometer) satellite-based instrument, and then continuously from 1978 using the SSMR (Scanning Multichannel Microwave Radiometer) (1978 to 1987) and SSM/I (Special Sensor Microwave/Imager) (1987 to present). By inter-calibrating data from different satellites, Bjørge *et al.* (1997) and subsequently Cavalieri *et al.* (1997) obtained uniform monthly estimates of sea-ice extent for both hemispheres from

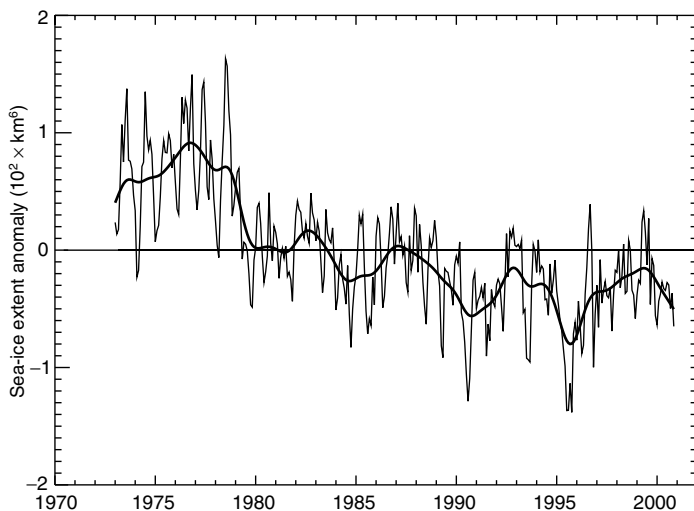


**Figure 2.14:** Monthly Arctic sea-ice extent anomalies, 1973 to 2000, relative to 1973 to 1996. The data are a blend of updated Walsh (Walsh, 1978), Goddard Space Flight Center satellite passive microwave (Scanning Multichannel Microwave Radiometer (SMMR) and Special Sensor Microwave/Imager (SSM/I)) derived data (Cavalieri *et al.*, 1997) and National Centers for Environmental Prediction satellite passive microwave derived data (Grumbine, 1996). Updated digitised ice data for the Great Lakes are also included (Assel, 1983).

November 1978 through to December 1996. Over this period, the sea-ice extent over the Northern Hemisphere showed a decrease of  $-2.8 \pm 0.3\%$ /decade (Parkinson *et al.*, 1999), consistent with Johannessen *et al.* (1995) (Figure 2.14). The Arctic decrease was strongest in the Eastern Hemisphere and most apparent in summer (Maslanik *et al.*, 1996; Parkinson *et al.*, 1999).

Hemispheric and regional data sets for the Arctic enable the satellite-derived trends in Figure 2.14 to be placed into a century scale context. Figure 2.15 shows annual time-series of the Northern Hemisphere ice extent by season from 1901 to 1999 using *in situ* data before the satellite era (Vinnikov *et al.*, 1999a). It should be emphasised that the spatial coverage of earlier data is not complete, with the largest data voids in the autumn and winter. Because few data were available, the variability of the autumn and wintertime series in Figure 2.15 is smaller during the early decades of the century. Essentially no data for summer and autumn are available for the World War II period. The summer decrease that is largely responsible for the overall downward trend during the satellite era is present during the entire second half of the 20th century (Figure 2.15). This decrease represents about 15% of the average summer extent in the first half of the 20th century. Spring values show a somewhat weaker negative trend over the same period with a total reduction of near 8%, but there is only a slight and uncertain downward trend in autumn and winter since about 1970.

The overall recent decrease of Arctic ice extent is, at first sight, consistent with the recent pattern of high latitude temperature change, which includes a warming over most of the sub-arctic land areas (Section 2.2.2.1). Some of this pattern of warming has been attributed to recent trends in the atmospheric circulation of the North Atlantic Oscillation and its Arctic-wide manifestation, the Arctic Oscillation (Section 2.6).

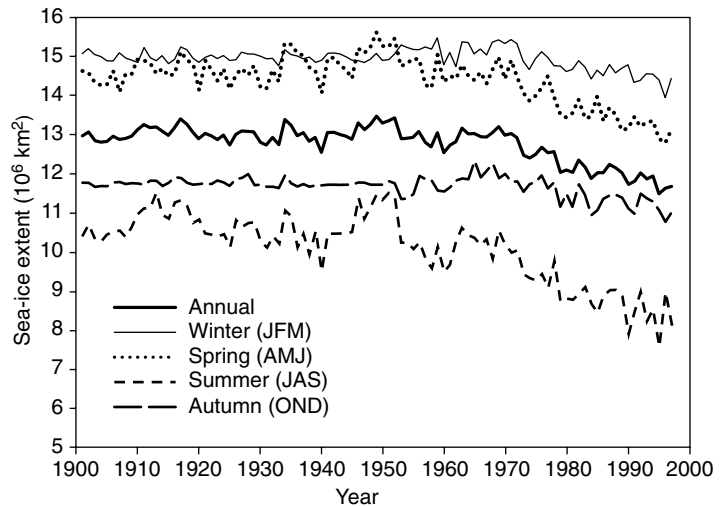


**Fig 2.15:** Time-series of annual and seasonal sea-ice extent in the Northern Hemisphere, 1901 to 1999, (Annual values from Vinnikov *et al.*, 1999b; seasonal values updated from Chapman and Walsh, 1993.)

Related to the decline in sea-ice extent is a decrease in the length of the sea-ice season (Parkinson, 2000) and an increase in the length of the Arctic summer melting season between 1979 and 1998, also derived from satellite data. The shortest season was 1979 (57 days) and the longest was in 1998 (81 days) with an increasing trend of 5 days per decade (Smith, 1998, updated). The 7% per decade reduction in the multi-year ice area during 1978 to 1998 is relatively large compared with an approximately 2%/decade decrease in the total ice area in winter (Johannessen *et al.*, 1999). This reflects greater summer melting, consistent with the results of Smith (1998).

Over the period 1979 to 1996, the Antarctic (Cavalieri *et al.*, 1997; Parkinson *et al.*, 1999) shows a weak increase of  $1.3 \pm 0.2\%$ /decade. Figure 2.16 (for 1973 to 1998) shows a new integrated data set of Antarctic sea-ice extent that was put together for the new European Centre for Medium-range Weather Forecasts (ECMWF) 40-year reanalysis that extends the record back to 1973. While showing the same weak increase after 1979, it also suggests greater ice extents in the mid-1970s. Although century scale time-series cannot be constructed for the Antarctic, de la Mare (1997) has used whaling ship logs to infer significantly greater ice extent in the Southern Ocean during the 1930s and 1940s than during recent decades. The indirect nature of the earlier evidence, however, introduces substantial uncertainty into this conclusion.

#### Antarctic Peninsula ice shelves

Although warming over Antarctica as a whole appears to have been perhaps half of a degree in the last half century (Jacka and Budd, 1998), the Antarctic Peninsula has warmed more rapidly, by more than  $2^\circ\text{C}$  since the 1940s (King, 1994). This regional

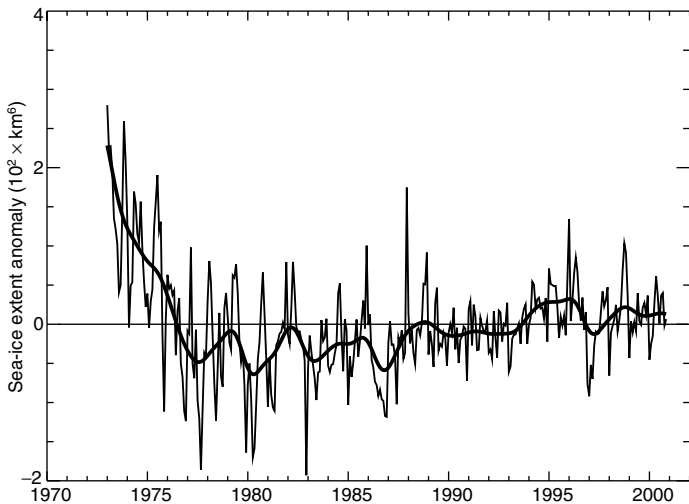


**Figure 2.16:** Monthly Antarctic sea-ice extent anomalies, 1973 to 2000, relative to 1973 to 1996. The data are a blend of National Ice Center (NIC) chart-derived data (Knight, 1984), Goddard Space Flight Center satellite passive-microwave (Scanning Multichannel Microwave Radiometer (SMMR) and Special Sensor Microwave/Imager (SSM/I)) derived data (Cavalieri *et al.*, 1997) and National Centers for Environmental Prediction satellite passive-microwave derived data (Grumbine, 1996). It is uncertain as to whether the decrease in interannual variability of sea ice after about 1988 is real or an observing bias.

warming, whose cause has yet to be fully discovered (but see Section 2.6.6), has led to a southerly migration of the climatic limit of ice shelves so that five ice shelves have retreated over the last century (Vaughan and Doake, 1996). The progressive retreat of ice shelves eventually resulted in the spectacular final-stage collapse of the Prince Gustav and parts of the Larsen ice shelves in 1995. Each left only a small residual shelf. After the collapse, James Ross Island, situated off the northern end of the Antarctic Peninsula, is now circumnavigable by ship for the first time since it was discovered in the early 19th century (Vaughan and Lachlan-Cope, 1995).

#### Sea-ice thickness

Our knowledge of sea-ice thickness in the Arctic comes largely from upward sonar profiling by USA and British submarines since 1958 and 1971, respectively. Rothrock *et al.* (1999) compared late summer September to October data from 1993, 1996 and 1997 from an USA civilian submarine research programme with data from six summer cruises from the period 1958 to 1976. Thickness was adjusted to mid-September values to account for seasonal variability. The significant decline in mean ice thickness was observed for all regions, increasing from the Canada Basin towards Europe (Figure 2.17). Overall, there was a mean reduction in thickness of 42% from 3.1 to 1.8 m the earlier period to the present.

Wadhams and Davis (2000) have compared ice thickness changes between October 1976 and September 1996 between  $81^{\circ}\text{N}$  and  $90^{\circ}\text{N}$  near the  $0^{\circ}$  meridian. The overall decline in mean sea-ice thickness between 1976 and 1996 was 43%. Over every one degree of latitude, both a significant decline in ice thickness

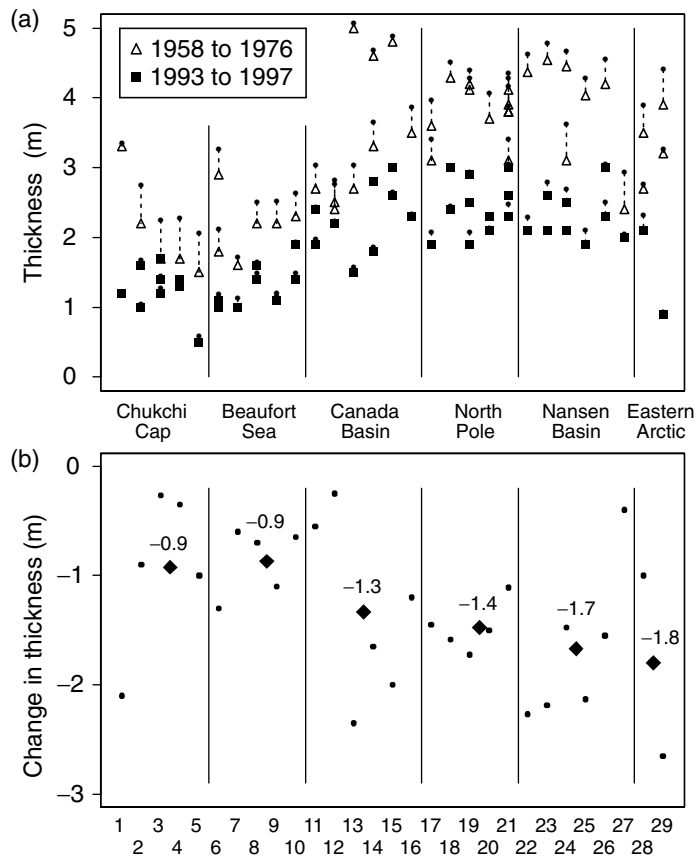


**Figure 2.17:** Mean ice thickness at places where early cruises were (nearly) collocated with cruises in the 1990s. Early data (1958 to 1976) are shown by open triangles, and those from the 1990s by solid squares, both seasonally adjusted to September 15. The small dots show the original data before the seasonal adjustment. The crossings are grouped into six regions separated by the solid lines. From Rothrock *et al.* (1999).

and some completely open water were observed. Despite these dramatic results, it is not known whether these changes reflect long-term change or a major mode of multi-decadal variability. Vinje *et al.* (1998) measured the thickness of ice exiting the Arctic Ocean through Fram Strait from 1990 to 1996 using moored upward looking sonars and reported a rather different result. The mean annual ice thickness in Fram Strait varied from 2.64 to 3.41 m. These observations were consistent with Arctic Ocean-wide ice thickness estimates made by drilling from Soviet Ice Stations from 1972 to 1981 and from submarine transects from 1960 to 1982, suggesting little change in ice thickness from the 1960s and 1970s to the 1990s.

Nagurnyi *et al.* (1994, 1999) used measurements of long surface gravity waves in the Arctic ice pack to estimate the mean ice thickness from wave attenuation. These measurements are available for the winters of 1978/79 to 1990/91. Johannessen *et al.* (1999) demonstrated a strong correlation between these ice thickness estimates and the area of multi-year (MY) ice in the Arctic Ocean as obtained from the SMMR and SSM/I. Both the area of MY ice and the ice thickness (winter) estimates show a decrease of 5 to 7%/decade, considerably less than the submarine

estimates (late summer). Even though the satellite measurements have continued for more than twenty years, they are inadequate to distinguish between changes due to long-term trends or interannual/inter-decadal variability (Johannessen *et al.*, 1999).

#### 2.2.5.3 Permafrost

About 25% of the land mass of the Northern Hemisphere is underlain by permafrost, including large regions of Canada, China, Russia and Alaska, with smaller permafrost areas in mountain chains of many other countries in both the Northern and Southern Hemisphere (Brown *et al.*, 1997; Zhang *et al.*, 1999). Permafrost in large part depends on climate. Over half of the world's permafrost is at temperatures a few degrees below 0°C. Temperature variations in near-surface permafrost (20 to 200 m depth) can be used as a sensitive indicator of the inter-annual and decade-to-century climatic variability and long-term changes in the surface energy balance (Lachenbruch and Marshall, 1986; Lachenbruch *et al.*, 1988; Clow *et al.*, 1991; Beltrami and Taylor, 1994; Majorowicz and Judge, 1994). Very small changes in surface climate can produce important changes in permafrost temperatures. Lachenbruch and Marshall (1986) used climate reconstructions from deep (>125 m depth) temperature measurements in permafrost to show that there has been a general warming of the permafrost in the Alaskan Arctic of 2 to 4°C over the last century.

Evidence of change in the southern extent of the discontinuous permafrost zone in the last century has also been recorded. In North America, the southern boundary of the discontinuous permafrost zone has migrated northward in response to warming after the Little Ice Age, and continues to do so today (Thie, 1974; Vitt *et al.*, 1994; Halsey *et al.*, 1995; Laberge and Payette, 1995; French and Egorov, 1998). In China both an increase in the lower altitudinal limit of mountain permafrost and a decrease in areal extent have been observed (Wang *et al.*, 2000).

Long-term monitoring of shallow permafrost began in earnest in the last few decades. Recent analyses indicate that permafrost in many regions of the earth is currently warming (Gravis *et al.*, 1988; Haeberli *et al.*, 1993; Osterkamp, 1994; Pavlov, 1994; Wang and French, 1994; Ding, 1998; Sharkhuu, 1998; Von der Mühll *et al.*, 1998; Weller and Anderson, 1998; Osterkamp and Romanovsky, 1999; Romanovsky and Osterkamp, 1999). However, the onset, magnitude (from a few tenths to a few degrees centigrade) and rate of warming varies regionally, and not all sites in a given region show the same trend (Osterkamp and Romanovsky, 1999). This variability, as well as short-term (decadal or less) trends superimposed on long-term (century) trends, is briefly discussed in Serreze *et al.* (2000). There has also been evidence of recent permafrost cooling into the mid-1990s in parts of north-eastern and north-western Canada (Allard *et al.*, 1995; Burn, 1998). However, there are regional data gaps, such as in the central and high Arctic in North America. A new international permafrost thermal monitoring network (Burgess *et al.*, 2000) is being developed to help address these gaps and document the spatial and temporal variability across the globe.

Properties of the surface and the active layer (that having seasonal freezing and thawing) affect surface heat exchanges in permafrost regions. Other conditions remaining constant, the

thickness of the active layer could be expected to increase in response to warming of the climate. A circumpolar network to monitor active-layer thickness at representative locations was developed in the 1990s to track long-term trends in active layer thickness (Nelson and Brown, 1997). Active layer thickness time-series are becoming available (Nelson *et al.*, 1998; Nixon and Taylor, 1998), and evidence of increasing thaw depths is starting to be reported (Pavlov, 1998; Wolfe *et al.*, 2000).

#### 2.2.5.4 Mountain glaciers

The recession of mountain glaciers was used in IPCC (1990) to provide qualitative support to the rise in global temperatures since the late 19th century. Work on glacier recession has considerable potential to support or qualify the instrumental record of temperature change and to cast further light on regional or worldwide temperature changes before the instrumental era. Two types of data from glaciers contain climatic information: (i) mass balance observations and (ii) data on the geometry of glaciers, notably glacier length. More comprehensive information is now becoming available and worldwide glacier inventories have been updated (e.g., IAHS (ICSI)/UNEP/UNESCO, 1999). Note that changes in the Greenland and Antarctic ice sheets are discussed in Chapter 11.

We first discuss mass balance observations. The specific mass balance is defined as the net annual gain or loss of mass at the glacier surface, per unit area of the surface. The mass balance averaged over an entire glacier is denoted by  $B_m$ . Systematic investigations of glacier mass balance started after 1945, so these records are shorter than the instrumental climate records normally available in the vicinity. In contrast to frequently made statements,  $B_m$  is not necessarily a more precise indicator of climate change than is glacier length. Time-series of  $B_m$  do contain year-to-year variability reflecting short-term fluctuations in meteorological quantities but of concern on longer time-scales is the effect of changing glacier geometry. A steadily retreating glacier will get thinner and the mass balance will become more negative because of a slowly increasing surface air temperature due to a lowering surface that is not reflected in a large-scale temperature signal. Climatic interpretation of long-term trends in of mass balance data requires the use of coupled mass balance-ice flow models to separate the climatic and geometric parts of the signal. Such studies have only just begun. However, mass balance observations are needed for estimating the contribution of glacier melt to sea level rise, so are discussed further in Chapter 11.

A wealth of information exists on the geometry of valley glaciers. Glacier records are very useful for studies of Holocene climate variability (e.g., Haeberli *et al.*, 1998; and Section 2.4). Written documents going back to the 16th century exist that describe catastrophic floods caused by the bursting of glacier-dammed lakes or arable land and farms destroyed by advancing glaciers, e.g., in 18th century Norway (Østrem *et al.*, 1977). A large amount of information is available from sketches, etchings, paintings and old photographs of glaciers, though many show the same glaciers (Holzhauser and Zumbühl, 1996). About fifty glaciers have two or more useful pictures from distinctly different times. In many cases geomorphologic evidence in the form of terminal moraines and trimlines can be used as reliable comple-

mentary information to construct the history of a glacier over the last few centuries. Systematic mapping of glaciers started only 100 years ago and has been limited to a few glaciers. The most comprehensive data are of length variations. Glacier length records complement the instrumental meteorological record because (i) some extend further back in time; (ii) some records are from remote regions where few meteorological observations exist; (iii) on average, glaciers exist at a significantly higher altitude than meteorological stations.

The last point is of particular interest in the light of the discrepancy between recent tropical glacier length reduction and lack of warming in the lower troposphere since 1979 indicated by satellites and radiosondes in the tropics (Section 2.2.3). Long-term monitoring of glacier extent provides abundant evidence that tropical glaciers are receding at an increasing rate in all tropical mountain areas. This applies to the tropical Andes (Brecher and Thompson, 1993; Hastenrath and Ames, 1995; Ames, 1998), Mount Kenya and Kilimanjaro (Hastenrath and Kruss, 1992; Hastenrath and Greischar, 1997) and to the glaciers in Irian Jaya (Peterson and Peterson, 1994).

Relating mass balance fluctuations to meteorological conditions is more complicated for tropical glaciers than for mid- and high latitude glaciers, and it has not been demonstrated that temperature is the most important factor. Nevertheless, the fast glacier recession in the tropics seems at first sight to be consistent with an increase in tropical freezing heights of 100 m over the period 1970 to 1986 as reported by Diaz and Graham (1996), corresponding to an increase of 0.5°C at tropical high mountain levels, which they also link to increases in tropical SST since the mid-1970s (Figure 2.10). However, although Gaffen *et al.* (2000) found a similar increase over 1960 to 1997, they found a lowering of freezing level over 1979 to 1997 which, at least superficially, is not consistent with glacier recession.

Figure 2.18 shows a representative selection of glacier length records from different parts of the world and updates the diagram in IPCC (1990). It is clear from Figure 2.18 that glacier retreat on the century time-scale is worldwide. The available data suggest that this retreat generally started later at high latitudes but in low and mid-latitudes the retreat generally started in the mid-19th century.

On the global scale, air temperature is considered by most glaciologists to be the most important factor reflecting glacier retreat. This is based on calculations with mass balance models (Greuell and Oerlemans, 1987; Oerlemans, 1992; Fleming *et al.*, 1997; Jóhannesson, 1997). For a typical mid-latitude glacier, a 30% decrease in cloudiness or a 25% decrease in precipitation would have the same effect as a 1°C temperature rise. Such changes in cloudiness or precipitation can occur locally or even regionally on a decadal time-scale associated with changes in circulation, but global trends of this size on a century time-scale are very unlikely. As mentioned in the SAR, Oerlemans (1994) concluded that a warming rate of  $0.66 \pm 0.20^\circ\text{C}$  per century at the mean glacier altitude could explain the linear part of the observed retreat of 48 widely distributed glaciers.

Glaciers are generally not in equilibrium with the prevailing climatic conditions and a more refined analysis should deal with the different response times of glaciers which involves modelling (Oerlemans *et al.*, 1998). It will take some time before a large

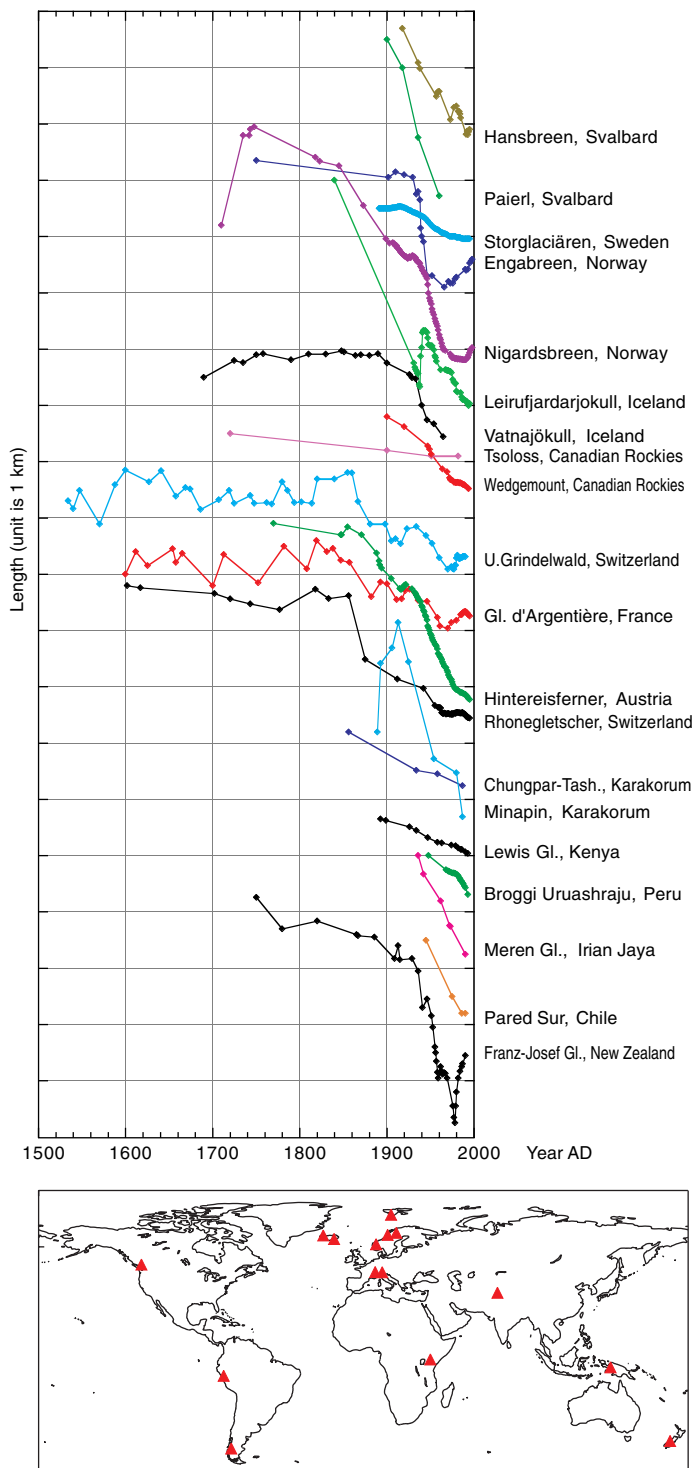


**Figure 2.18:** A collection of twenty glacier length records from different parts of the world. Curves have been translated along the vertical axis to make them fit in one frame. The geographical distribution of the data is also shown, though a single triangle may represent more than one glacier. Data are from the World Glacier Monitoring Service (<http://www.geo.unizh.ch/wgms/>) with some additions from various unpublished sources.

number of glaciers are modelled. Nevertheless, work done so far indicates that the response times of glacier lengths shown in Figure 2.18 are in the 10 to 70 year range. Therefore the timing of the onset of glacier retreat implies that a significant global warming is likely to have started not later than the mid-19th century. This conflicts with the Jones *et al.* (2001) global land instrumental temperature data (Figure 2.1), and the combined hemispheric and global land and marine data (Figure 2.7), where clear warming is not seen until the beginning of the 20th century. This conclusion also conflicts with some (but not all) of the palaeo-temperature reconstructions in Figure 2.21, Section 2.3, where clear warming, e.g., in the Mann *et al.* (1999) Northern Hemisphere series, starts at about the same time as in the Jones *et al.* (2001) data. These discrepancies are currently unexplained.

For the last two to three decades, far more records have been available than are shown in Figure 2.18. Many are documented at the World Glacier Monitoring Service in Zürich, Switzerland (e.g., IAHS (ICSI)/UNEP/UNESCO, 1998). The general picture is one of widespread retreat, notably in Alaska, Franz-Josef Land, Asia, the Alps, Indonesia and Africa, and tropical and subtropical regions of South America. In a few regions a considerable number of glaciers are currently advancing (e.g., Western Norway, New Zealand). In Norway this is very likely to be due to increases in precipitation owing to the positive phase of the North Atlantic Oscillation (Section 2.6), and in the Southern Alps of New Zealand and due to wetter conditions with little warming since about 1980. Finally, indications in the European Alps that current glacier recession is reaching levels not seen for perhaps a few thousand years comes from the exposure of radiocarbon-dated ancient remains in high glacial saddles. Here there is no significant ice flow and melting is assumed to have taken place *in situ* for the first time in millennia (e.g., the finding of the 5,000-year-old Oetzel “ice man”).

#### 2.2.5.5 Lake and river ice

Numerous studies suggest the importance of lake and river ice break-up as an index of climate variability and change, especially as related to temperature and snow cover (Palecki and Barry, 1986; Schindler *et al.*, 1990; Robertson *et al.*, 1992; Assel and Robertson, 1995; Anderson *et al.*, 1996; Wynne *et al.*, 1998; Magnuson *et al.*, 2000). Records of lake and river ice can be used to independently evaluate changes of temperature and, to some extent, snow cover. Like other proxy measurements they have limitations, and are subject to their own time-dependent biases such as changes in observers and protocols related to the identification of “ice on” and “ice off” conditions. Larger lakes often have the best records, but are often located near human settlements which can affect the homogeneity of the record, e.g., associated cooling water discharges and urban heat islands, so care is needed to select suitable lakes.

A recent analysis has been made of trends in 39 extensive Northern Hemisphere lake and river ice records over the 150-year period from 1846 to 1995. Ice break-up dates now occur on average about nine days earlier in the spring than at the beginning of the record, and autumn freeze-up occurs on average about ten days later (Magnuson *et al.*, 2000). Only one of the 39 records, in Japan, showed changes that indicate a slight cooling.

#### 2.2.6 Are the Retreat of Glaciers, Sea Ice, and Snow Cover Consistent with the Surface Temperature Trends?

A significant relationship has been found between interannual variations (correlation = -0.60) of the Northern Hemisphere snow-cover extent and land-surface air temperature in spring since the 1960s. However, the observed increase in temperature during the winter is not reflected in a reduced snow-cover extent. Reduced ice cover on the Northern Hemisphere lakes and rivers, primarily due to earlier onset in spring of ice-free conditions during the 20th century, is consistent with reduced snow cover extent in that season. Sea-ice retreat in the Arctic spring and summer is also consistent with an increase in spring, and to a lesser extent, summer temperatures in the high northern latitudes. Summer temperature increases have been less than in spring in nearby land areas, but Arctic sea-ice extent and especially thickness have markedly decreased. Nevertheless, there is only a small indication of reduced Arctic sea ice during winter when temperatures have also increased. Antarctic sea-ice extent has not decreased since the late 1970s, possibly related to recent indications of little change in Antarctic temperatures over much of the continent in that period. There is now ample evidence to support a major retreat of most mountain glaciers during the last 100 years in response to widespread increases in temperature. There has been especially fast glacial recession in the tropics in recent decades, although tropical temperatures in the free atmosphere near glacier levels have increased little since 1980 according to radiosonde and MSU data.

#### 2.2.7 Summary

Global surface temperatures have increased between 0.4 and 0.8°C since the late 19th century, but most of this increase has occurred in two distinct periods, 1910 to 1945 and since 1976. The rate of temperature increase since 1976 has been over 0.15°C/decade. Our confidence in the rate of warming has increased since the SAR due to new analyses including: model simulations using observed SSTs with and without corrections for time-dependent biases, new studies of the effect of urbanisation on global land temperature trends, new evidence for mass ablation of glaciers, continued reductions in snow-cover extent, and a significant reduction in Arctic sea-ice extent in spring and summer, and in thickness. However, there is some disagreement between warming rates in the various land and ocean-based data sets in the 1990s, though all agree on appreciable warming.

New analyses of mean daily maximum and minimum temperatures continue to support a reduction in the diurnal temperature range with minimum temperatures increasing at about twice the rate of maximum temperatures over the second half of the 20th century. Seasonally, the greatest warming since 1976 over land has occurred during the Northern Hemisphere winter and spring, but significant warming has also occurred in the Northern Hemisphere summer. Southern Hemisphere warming has also been strongest during the winter over land, but little difference between the seasons is apparent when both land and oceans are considered. The largest rates of warming continue to be found in the mid- and high latitude continental regions of the Northern Hemisphere.

Analyses of overall temperature trends in the low to mid-troposphere and near the surface since 1958 are in good agreement, with a warming of about 0.1°C per decade. Since the beginning of the satellite record (1979), however, low to mid-troposphere temperatures have warmed in both satellite and weather balloon records at a global rate of only 0.04 and 0.03°C/decade respectively. This is about 0.12°C/decade less than the rate of temperature increase near the surface since 1979. About half of this difference in warming rate is very likely to be due to the combination of differences in spatial coverage and the real physical affects of volcanoes and ENSO (Santer *et al.*, 2000), see also Chapter 12. The remaining difference remains unexplained, but is likely to be real. In the stratosphere, both satellites and weather balloons continue to show substantial cooling. The faster rate of recession of tropical mountain glaciers in the last twenty years than might have been expected from the MSU and radiosonde records remains unexplained, though some glaciers may still be responding to the warming indicated by radiosondes that occurred around 1976 to 1981.

## 2.3 Is the Recent Warming Unusual?

### 2.3.1 Background

To determine whether 20th century warming is unusual, it is essential to place it in the context of longer-term climate variability. Owing to the sparseness of instrumental climate records prior to the 20th century (especially prior to the mid-19th century), estimates of global climate variability during past centuries must often rely upon indirect “proxy” indicators – natural or human documentary archives that record past climate variations, but must be calibrated against instrumental data for a meaningful climate interpretation (Bradley, 1999, gives a review). Coarsely resolved climate trends over several centuries are evident in many regions e.g., from the recession of glaciers (Grove and Switsur, 1994; and Section 2.2.5.4) or the geothermal information provided by borehole measurements (Pollack *et al.*, 1998). Large-scale estimates of decadal, annual or seasonal climate variations in past centuries, however, must rely upon sources that resolve annual or seasonal climatic variations. Such proxy information includes width and density measurements from tree rings (e.g., Cook, 1995; see Fritts, 1991, for a review), layer thickness from laminated sediment cores (e.g., Hughen *et al.*, 1996; Lamoureux and Bradley, 1996), isotopes, chemistry, and accumulation from annually resolved ice cores (e.g., Claussen *et al.*, 1995; Fisher *et al.*, 1998), isotopes from corals (e.g., Tudhope *et al.*, 1995; Dunbar and Cole, 1999), and the sparse historical documentary evidence available over the globe during the past few centuries (see e.g., Bradley and Jones, 1995; Pfister *et al.*, 1998). Taken as a whole, such proxy climate data can provide global scale sampling of climate variations several centuries into the past, with the potential to resolve large-scale patterns of climate change prior to the instrumental period, albeit with important limitations and uncertainties.

The SAR examined evidence for climate change in the past, on time-scales of centuries to millennia. Based on information from a variety of proxy climate indicators, reconstructions of

mountain glacier mass and extent, and geothermal sub-surface information from boreholes, it was concluded that summer temperatures in the Northern Hemisphere during recent decades are the warmest in at least six centuries. While data prior to AD 1400 were considered too sparse for reliable inferences regarding hemispheric or global mean temperatures, regional inferences were nonetheless made about climate changes further back in time.

Since the SAR, a number of studies based on considerably expanded databases of palaeoclimate information have allowed more decisive conclusions about the spatial and temporal patterns of climate change in past centuries. A number of important advances have been in key areas such as ice core palaeoclimatology (e.g., White *et al.*, 1998a), dendroclimatology (e.g., Cook, 1995; Briffa *et al.*, 1998b), and geothermal palaeo-temperature estimation (e.g., Pollack *et al.*, 1998). Moreover, the latest studies based on global networks of “multi-proxy” data have proved particularly useful for describing global or hemispheric patterns of climate variability in past centuries (e.g., Bradley and Jones, 1993; Hughes and Diaz, 1994; Mann *et al.*, 1995; Fisher, 1997; Overpeck *et al.*, 1997; Mann *et al.*, 1998, 1999). Such estimates allow the observed trends of the 20th century to be put in a longer-term perspective. These have also allowed better comparisons with possible physical influences on climate forcings (Lean *et al.*, 1995; Crowley and Kim, 1996, 1999; Overpeck *et al.*, 1997; Mann *et al.*, 1998; Waple *et al.*, 2001), and for new evaluations of the low-frequency climate variability exhibited by numerical climate models (Barnett *et al.*, 1996; Jones *et al.*, 1998; Crowley and Kim, 1999; Delworth and Mann, 2000).

### 2.3.2 Temperature of the Past 1,000 Years

The past 1,000 years are a particularly important time-frame for assessing the background natural variability of the climate for climate change detection. Astronomical boundary conditions have strayed relatively little from their modern-day values over this interval (but see Section 2.3.4 for a possible caveat) and, with the latest evidence, the spatial extent of large-scale climate change during the past millennium can now be meaningfully characterised (Briffa *et al.*, 1998b; Jones *et al.*, 1998; Mann *et al.*, 1998; 1999; 2000a; 2000b). Moreover, estimates of volcanic and solar climate forcings are also possible over this period, allowing model-based estimates of their climate effects (Crowley and Kim, 1999; Free and Robock, 1999).

#### 2.3.2.1 Palaeoclimate proxy indicators

A “proxy” climate indicator is a local record that is interpreted using physical or biophysical principles to represent some combination of climate-related variations back in time. Palaeoclimate proxy indicators have the potential to provide evidence for large-scale climatic changes prior to the existence of widespread instrumental or historical documentary records. Typically, the interpretation of a proxy climate record is complicated by the presence of “noise” in which climate information is immersed, and a variety of possible distortions of the underlying climate information (e.g., Bradley, 1999; Ren, 1999a,b). Careful calibration and cross-validation procedures are necessary to establish a reliable relationship between a proxy indicator and the

climatic variable or variables it is assumed to represent, providing a “transfer” function through which past climatic conditions can be estimated. High-resolution proxy climate indicators, including tree rings, corals, ice cores, and laminated lake/ocean sediments, can be used to provide detailed information on annual or near-annual climate variations back in time. Certain coarser resolution proxy information (from e.g., boreholes, glacial moraines, and non-laminated ocean sediment records) can usefully supplement this high-resolution information. Important recent advances in the development and interpretation of proxy climate indicators are described below.

#### *Tree rings*

Tree-ring records of past climate are precisely dated, annually resolved, and can be well calibrated and verified (Fritts, 1976). They typically extend from the present to several centuries or more into the past, and so are useful for documenting climate change in terrestrial regions of the globe. Many recent studies have sought to reconstruct warm-season and annual temperatures several centuries or more ago from either the width or the density of annual growth rings (Briffa *et al.*, 1995; D'Arrigo *et al.*, 1996; Jacoby *et al.*, 1996; D'Arrigo *et al.*, 1998; Wiles *et al.*, 1998; Hughes *et al.*, 1999; Cook *et al.*, 2000). Recently, there has been a concerted effort to develop spatial reconstructions of past temperature variations (e.g., Briffa *et al.*, 1996) and estimates of hemispheric and global temperature change (e.g., Briffa *et al.*, 1998b; Briffa, 2000). Tree-ring networks are also now being used to reconstruct important indices of climate variability over several centuries such as the Southern Oscillation Index (Stahle *et al.*, 1998), the North Atlantic Oscillation (Cook *et al.*, 1998; Cullen *et al.*, 2001) and the Antarctic Oscillation Index (Villalba *et al.*, 1997) (see also Section 2.6), as well as patterns of pre-instrumental precipitation and drought (Section 2.5.2.2).

Several important caveats must be borne in mind when using tree-ring data for palaeoclimate reconstructions. Not least is the intrinsic sampling bias. Tree-ring information is available only in terrestrial regions, so is not available over substantial regions of the globe, and the climate signals contained in tree-ring density or width data reflect a complex biological response to climate forcing. Non-climatic growth trends must be removed from the tree-ring chronology, making it difficult to resolve time-scales longer than the lengths of the constituent chronologies (Briffa, 2000). Furthermore, the biological response to climate forcing may change over time. There is evidence, for example, that high latitude tree-ring density variations have changed in their response to temperature in recent decades, associated with possible non-climatic factors (Briffa *et al.*, 1998a). By contrast, Vaganov *et al.* (1999) have presented evidence that such changes may actually be climatic and result from the effects of increasing winter precipitation on the starting date of the growing season (see Section 2.7.2.2). Carbon dioxide fertilization may also have an influence, particularly on high-elevation drought-sensitive tree species, although attempts have been made to correct for this effect where appropriate (Mann *et al.*, 1999). Thus climate reconstructions based entirely on tree-ring data are susceptible to several sources of contamination or non-stationarity of response. For these reasons, investigators have increasingly found tree-ring data most

useful when supplemented by other types of proxy information in “multi-proxy” estimates of past temperature change (Overpeck *et al.*, 1997; Jones *et al.*, 1998; Mann *et al.*, 1998; 1999; 2000a; 2000b; Crowley and Lowery, 2000).

#### *Corals*

Palaeoclimate reconstructions from corals provide insights into the past variability of the tropical and sub-tropical oceans and atmosphere, prior to the instrumental period, at annual or seasonal resolutions, making them a key addition to terrestrial information. Because of their potential to sample climate variations in ENSO-sensitive regions, a modest network of high-quality coral site records can resolve key large-scale patterns of climate variability (Evans *et al.*, 1998). The corals used for palaeoclimate reconstruction grow throughout the tropics in relatively shallow waters, often living for several centuries. Accurate annual age estimates are possible for most sites using a combination of annual variations in skeletal density and geochemical parameters. Palaeoclimate reconstructions from corals generally rely on geochemical characteristics of the coral skeleton such as temporal variations in trace elements or stable isotopes or, less frequently, on density or variations in fluorescence. Dunbar and Cole (1999) review the use of coral records for palaeoclimatic reconstruction.

#### *Ice cores*

Ice cores from polar regions of northern Greenland, Canada and the islands of the North Atlantic and Arctic Oceans, Antarctica, and alpine, tropical and sub-tropical locations (e.g., Thompson, 1996) can provide several climate-related indicators. These indicators include stable isotopes (e.g.,  $^{18}\text{O}$ ), the fraction of melting ice, the rate of accumulation of precipitation, concentrations of various salts and acids, the implied atmospheric loading of dust pollen, and trace gases such as  $\text{CH}_4$  and  $\text{CO}_2$ .

Recently, there has been increased activity in creating high-resolution Antarctic ice core series e.g., for the past millennium (Peel *et al.*, 1996; Mayewski and Goodwin, 1997; Morgan and van Ommen, 1997). In certain regions, isotope information from ice cores shows the late 20th century temperatures as the warmest few decades in the last 1,000 years (Thompson *et al.*, 2000a). Key strengths of ice core information are their high resolution (annual or even seasonal where accumulations rates are particularly high – see van Ommen and Morgan, 1996, 1997), availability in polar and high-elevation regions where other types of proxy climate information like tree-ring data are not available, and their provision of multiple climate- and atmosphere-related variables from the same reasonably well dated physical location (e.g., the GISP2 core; White *et al.*, 1998a). A weakness of ice core data is regional sampling bias (high elevation or high latitude) and melt water and precipitation accumulation data are not easy to date accurately.

The best dated series are based on sub-annual sampling of cores and the counting of seasonal ice layers. Such series may have absolute dating errors as small as a few years in a millennium (Fisher *et al.*, 1996). Dating is sometimes performed using volcanic acid layers with assumed dates (e.g., Clausen *et al.*, 1995) but uncertainties in the volcanic dates can result in dating uncertainties throughout the core (Fisher *et al.*, 1998).

### Lake and ocean sediments

Annually laminated (varved) lake sediments offer considerable potential as high-resolution archives of palaeo-environmental conditions where other high-resolution proxy indicators are not available (e.g., arid terrestrial regions), and latitudes poleward of the treeline (Lamoureux and Bradley, 1996; Wohlfarth *et al.*, 1998; Hughen *et al.*, 2000). When annual deposition of the varves can be independently confirmed (e.g., through radiometric dating), they provide seasonal to interannual resolution over centuries to millennia. Varved sediments can be formed from biological processes or from the deposition of inorganic sediments, both of which are often influenced by climate variations. Three primary climate variables may influence lake varves: (a) summer temperature, serving as an index of the energy available to melt the seasonal snowpack, or snow and ice on glaciers; (b) winter snowfall, which governs the volume of discharge capable of mobilising sediments when melting; and (c) rainfall. Laminated lake sediments dominated by (a) can be used for inferences about past high latitude summer temperature changes (e.g., Overpeck *et al.*, 1997), while sediments dominated by the latter two influences can be used to estimate past drought and precipitation patterns (Section 2.5.2.2).

Ocean sediments may also be useful for high-resolution climate reconstructions. In rare examples, annually laminated sediments can be found (e.g., Hughen *et al.*, 1996; Black *et al.*, 1999) and it is possible to incorporate isotope and other information in climate reconstructions, much as varved lake sediments are used. Otherwise, sedimentation rates may sometimes still be sufficiently high that century-scale variability is resolvable (e.g., the Bermuda rise ocean sediment oxygen isotope record of Keigwin, 1996). Dating in such cases, however, must rely on radiometric methods with relatively poor age control.

### Borehole measurements

Borehole measurements attempt to relate profiles of temperature with depth to the history of temperature change at the ground surface. The present global database of more than 600 borehole temperature-depth profiles has the densest geographic coverage in North America and Europe, but sparser data are available in other regions (e.g., Australia, Asia, Africa and South America). The depths of the temperature profiles range from about 200 to greater than 1,000 m, allowing palaeo-temperature reconstructions back several hundred to a thousand years. Although large-scale temperature reconstructions have been made to more than a millennium ago (Huang *et al.*, 1997), they show substantial sensitivity to assumptions that are needed to convert the temperature profiles to ground surface temperature changes. Borehole data are probably most useful for climate reconstructions over the last five centuries (Pollack *et al.*, 1998).

Figure 2.19 shows a reconstructed global ground surface temperature history (Pollack *et al.*, 1998; see also Huang *et al.*, 2000) from an average of the 358 individual sites, most located in North America and Eurasia, but some located in Africa, South America and Australia (similar results are obtained by Huang *et al.*, 2000, using an updated network of 616 sites). Superimposed is an instrumental estimate of global surface air temperature (Jones and Briffa, 1992). The ensemble of reconstructions shows

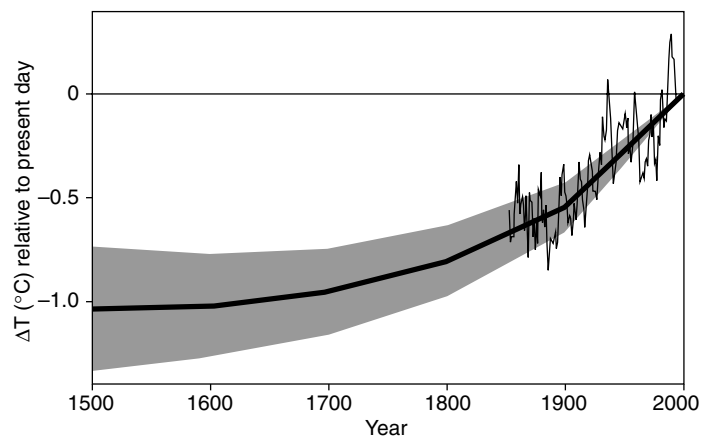


**Figure 2.19:** Reconstructed global ground temperature estimate from borehole data over the past five centuries, relative to present day. Shaded areas represent  $\pm$  two standard errors about the mean history (Pollack *et al.*, 1998). Superimposed is a smoothed (five-year running average) of the global surface air temperature instrumental record since 1860 (Jones and Briffa, 1992).

that the average ground temperature of the Earth has increased by about  $0.5^{\circ}\text{C}$  during the 20th century, and that this was the warmest of the past five centuries. About 80% of the sites experienced a net warming over this period. The estimated mean cumulative ground surface temperature change since 1500 is close to  $1.0 \pm 0.3^{\circ}\text{C}$ . Uncertainties due to spatial sampling (see Pollack *et al.*, 1998 and Huang *et al.*, 2000) are also shown. It should be noted that the temporal resolution of the borehole estimates decreases sharply back in time, making it perilous to compare the shape of the trend shown in Figure 2.19 with better-resolved trends determined from higher-resolution climate proxy data discussed below.

While borehole data provide a direct estimate of ground surface temperatures under certain simplifying assumptions about the geothermal properties of the earth near the borehole, a number of factors complicate their interpretation. Non-temperature-related factors such as land-use changes, natural land cover variations, long-term variations in winter snow cover and soil moisture change the sub-surface thermal properties and weaken the interpretation of the reconstructions as estimates of surface air temperature change. In central England, where seasonal snow cover is not significant, and major land-use changes occurred many centuries ago, borehole ground surface temperature trends do tend to be similar to those in long instrumental records (Jones, 1999). In contrast, Skinner and Majorowicz (1999) show that borehole estimates of ground surface temperature warming during the 20th century in north-western North America are 1 to  $2^{\circ}\text{C}$  greater than in corresponding instrumental estimates of surface air temperature. They suggest that this discrepancy may be due to land-use changes that can enhance warming of the ground surface relative to that of the overlying atmospheric boundary layer (see also Lewis, 1998). Such factors need to be better understood before borehole temperature measurements can be confidently interpreted.

### Documentary evidence

Historical documentary data are valuable sources of information about past climate (e.g., Brown and Issar, 1998; Bradley, 1999). However, their use requires great care, as such documents may be biased towards describing only the more extreme events, and are, in certain cases, prone to the use of inconsistent language between different writers and different epochs, and to errors in dating. As for all proxy information, historical documents require careful calibration and verification against modern instrumental data. Two areas particularly strong in historical documents describing climate are Europe and China. In Europe, attempts have been made to extend long climate series back in time using a combination of documentary evidence and fragmentary instrumental records (e.g., Pfister, 1995; Pfister *et al.*, 1998). Additional information about past climate change has also been obtained purely from documentary records in Europe (e.g., Martin-Vide and Barriendos, 1995; Brázdil, 1996; Pfister *et al.*, 1996, 1998, 1999; Pfister and Brázdil, 1999; Rodrigo *et al.*, 1999). In China, regional instrumental temperature series have been extended back over much of the past millennium using documentary data combined with inferences from ice cores and tree rings (Wang *et al.*, 1998a, 1998b; Wang and Gong, 2000).

### Mountain glacier moraines

The position of moraines or till left behind by receding glaciers can provide information on the advances (and, less accurately, the retreats) of mountain glaciers. Owing to the complex balance between local changes in melting and ice accumulation, and the effects of topography which influence mountain glaciers (see Section 2.2.5.4), it is difficult to reconstruct regional (as opposed to global) climate changes from the extent of mountain glaciers alone (Oerlemans, 1989). For example, both increased winter precipitation (through greater accumulation) and lower summer temperatures (through decreased melting or “ablation”) can lead to more positive glacial mass balances. The inertia of large glaciers dictates that they respond to climate change relatively slowly, with delays of decades or occasionally centuries. For smaller, fast moving glaciers in regions where precipitation and accumulation are moderate, temperature changes are usually the dominant factor influencing mountain glacier masses and lengths. Here glacier moraine evidence in combination with other lines of evidence can provide reliable information on past regional temperature changes (Salinger, 1995; Holzhauser and Zumbühl, 1996; Raper *et al.*, 1996; Salinger *et al.*, 1996).

#### 2.3.2.2 Multi-proxy synthesis of recent temperature change

Since the SAR there have been several attempts to combine various types of high-resolution proxy climate indicators to create large-scale palaeoclimate reconstructions that build on earlier work by e.g., Bradley and Jones (1993); Hughes and Diaz (1994) and Mann *et al.* (1995). Overpeck *et al.* (1997) and Fisher (1997) have sought to combine information from ice cores, varved lake sediment cores, and tree rings to reconstruct high latitude climate trends for past centuries. Jones *et al.* (1998) estimated extra-tropical Northern and Southern Hemisphere warm-season temperature changes during the past millennium using a sparse set of extra-tropical warm-season temperature proxy indicators (10 and

8 respectively). Mann *et al.* (1998) reconstructed global patterns of annual surface temperature several centuries back in time. They calibrated a combined terrestrial (tree ring, ice core and historical documentary indicator) and marine (coral) multi-proxy climate network against dominant patterns of 20th century global surface temperature. Averaging the reconstructed temperature patterns over the far more data-rich Northern Hemisphere half of the global domain, they estimated the Northern Hemisphere mean temperature back to AD 1400, a reconstruction which had significant skill in independent cross-validation tests. Self-consistent estimates were also made of the uncertainties. This work has now been extended back to AD 1000 (Figure 2.20, based on Mann *et al.*, 1999). The uncertainties (the shaded region in Figure 2.20) expand considerably in earlier centuries because of the sparse network of proxy data. Taking into account these substantial uncertainties, Mann *et al.* (1999) concluded that the 1990s were likely to have been the warmest decade, and 1998 the warmest year, of the past millennium for at least the Northern Hemisphere. Jones *et al.* (1998) came to a similar conclusion from largely independent data and an entirely independent methodology. Crowley and Lowery (2000) reached the similar conclusion that medieval temperatures were no warmer than mid-20th century temperatures. Borehole data (Pollack *et al.*, 1998) independently support this conclusion for the past 500 years although, as discussed earlier (Section 2.3.2.1), detailed interpretations comparison with long-term trends from such of such data are perilous owing to loss of temporal resolution back in time.

The largely independent multi-proxy Northern Hemisphere temperature reconstructions of Jones *et al.* (1998) and Mann *et al.* (1999) are compared in Figure 2.21, together with an independent (extra-tropical, warm-season) Northern Hemisphere temperature estimate by Briffa (2000) based on tree-ring density data. The estimated uncertainties shown are those for the smoothed Mann *et al.* series. Significant differences between the three reconstructions are evident during the 17th and early 19th centuries where either the Briffa *et al.* or Jones *et al.* series lie outside the estimated uncertainties in the Mann *et al.* series. Much of these differences appear to result from the different latitudinal and seasonal emphases of the temperature estimates. This conclusion is supported by the observation that the Mann *et al.* hemispheric temperature average, when restricted to just the extra-tropical (30 to 70°N band) region of the Northern Hemisphere, shows greater similarity in its trend over the past few centuries to the Jones *et al.* reconstruction. The differences between these reconstructions emphasise the importance of regional and seasonal variations in climate change. These are discussed in the next section.

#### 2.3.3 Was there a “Little Ice Age” and a “Medieval Warm Period”?

The terms “Little Ice Age” and “Medieval Warm Period” have been used to describe two past climate epochs in Europe and neighbouring regions during roughly the 17th to 19th and 11th to 14th centuries, respectively. The timing, however, of these cold and warm periods has recently been demonstrated to vary geographically over the globe in a considerable way (Bradley and

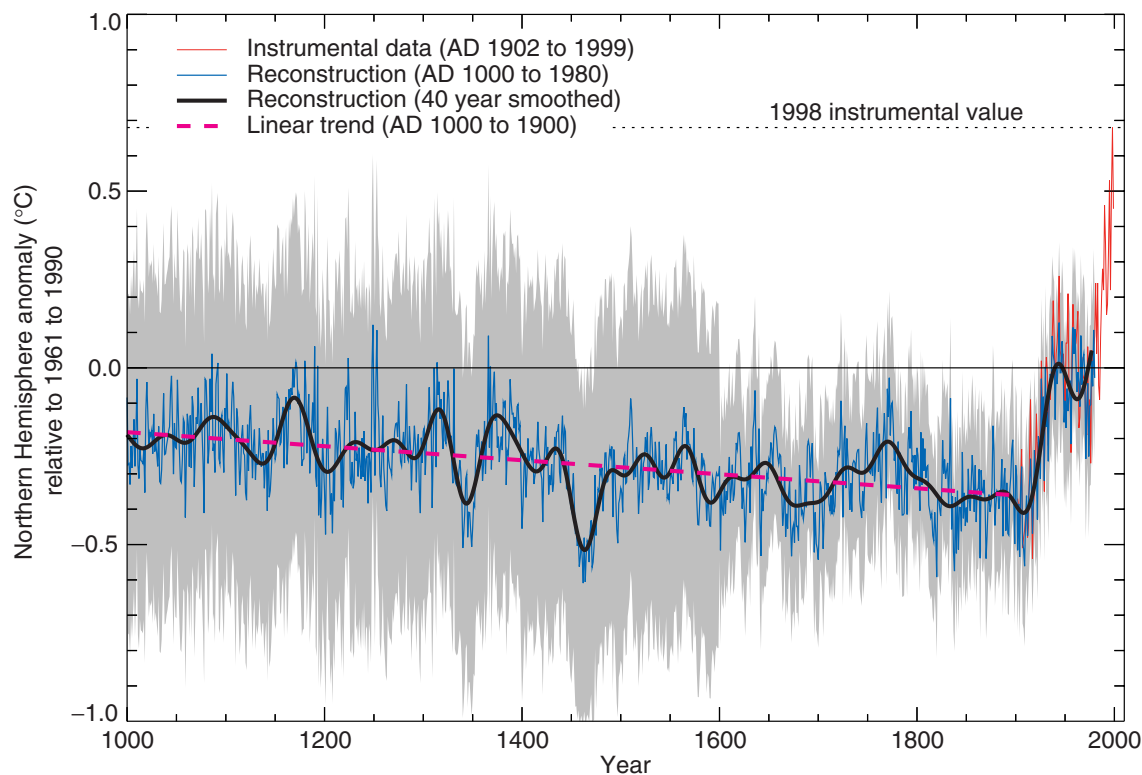


**Figure 2.20:** Millennial Northern Hemisphere (NH) temperature reconstruction (blue) and instrumental data (red) from AD 1000 to 1999, adapted from Mann *et al.* (1999). Smoother version of NH series (black), linear trend from AD 1000 to 1850 (purple-dashed) and two standard error limits (grey shaded) are shown.

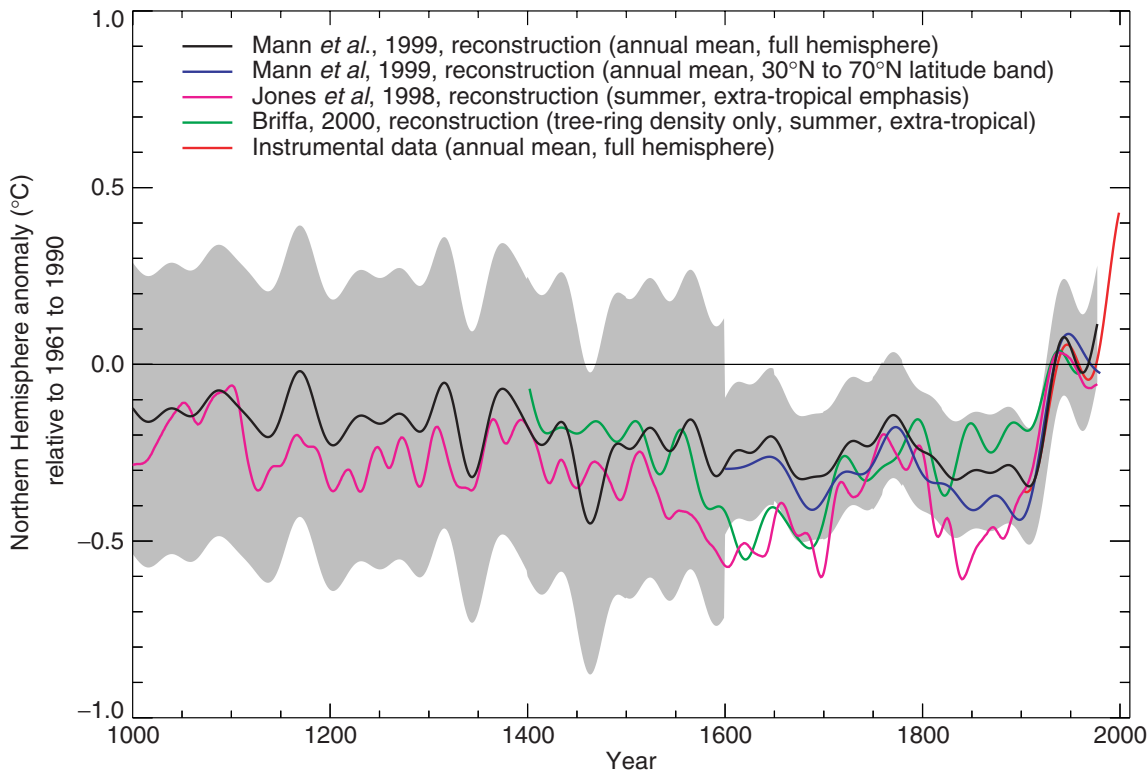


**Figure 2.21:** Comparison of warm-season (Jones *et al.*, 1998) and annual mean (Mann *et al.*, 1998, 1999) multi-proxy-based and warm season tree-ring-based (Briffa, 2000) millennial Northern Hemisphere temperature reconstructions. The recent instrumental annual mean Northern Hemisphere temperature record to 1999 is shown for comparison. Also shown is an extra-tropical sampling of the Mann *et al.* (1999) temperature pattern reconstructions more directly comparable in its latitudinal sampling to the Jones *et al.* series. The self-consistently estimated two standard error limits (shaded region) for the smoothed Mann *et al.* (1999) series are shown. The horizontal zero line denotes the 1961 to 1990 reference period mean temperature. All series were smoothed with a 40-year Hamming-weights lowpass filter, with boundary constraints imposed by padding the series with its mean values during the first and last 25 years.

Jones, 1993; Hughes and Diaz, 1994; Crowley and Lowery, 2000). Evidence from mountain glaciers does suggest increased glaciation in a number of widely spread regions outside Europe prior to the 20th century, including Alaska, New Zealand and Patagonia (Grove and Switsur, 1994). However, the timing of maximum glacial advances in these regions differs considerably, suggesting that they may represent largely independent regional climate changes, not a globally-synchronous increased glaciation (see Bradley, 1999). Thus current evidence does not support globally synchronous periods of anomalous cold or warmth over this timeframe, and the conventional terms of “Little Ice Age” and “Medieval Warm Period” appear to have limited utility in describing trends in hemispheric or global mean temperature changes in past centuries. With the more widespread proxy data and multi-proxy reconstructions of temperature change now available, the spatial and temporal character of these putative climate epochs can be reassessed.

Mann *et al.* (1998) and Jones *et al.* (1998) support the idea that the 15th to 19th centuries were the coldest of the millennium over the Northern Hemisphere overall. However, viewed hemispherically, the “Little Ice Age” can only be considered as a modest cooling of the Northern Hemisphere during this period of less than 1°C relative to late 20th century levels (Bradley and Jones, 1993; Jones *et al.*, 1998; Mann *et al.*, 1998; 1999; Crowley and Lowery, 2000). Cold conditions appear, however, to have been considerably more pronounced in particular regions. Such regional variability can be understood in part as reflecting accompanying changes in atmospheric circulation. The “Little Ice Age” appears to have been most clearly expressed in the North Atlantic region as altered patterns of atmospheric circulation (O’Brien *et al.*, 1995). Unusually cold, dry winters in central Europe (e.g., 1 to 2°C below normal during the late 17th century) were very likely to have been associated with more frequent flows of continental air from the north-east (Wanner *et al.*, 1995; Pfister, 1999). Such conditions are consistent (Luterbacher *et al.*, 1999) with the negative or enhanced easterly wind phase of the NAO (Sections 2.2.2.3 and 2.6.5), which implies both warm and cold anomalies over different regions in the North Atlantic sector. Such strong influences on European temperature demonstrate the difficulty in extrapolating the sparse early information about European climate change to the hemispheric, let alone global, scale. While past changes in the NAO have likely had an influence in eastern North America, changes in the El Niño phenomenon (see also Section 2.6), are likely to have had a particularly significant influence on regional temperature patterns over North America.

The hemispherically averaged coldness of the 17th century largely reflected cold conditions in Eurasia, while cold hemispheric conditions in the 19th century were more associated with cold conditions in North America (Jones *et al.*, 1998; Mann *et al.*, 2000b). So, while the coldest decades of the 19th century appear to have been approximately 0.6 to 0.7°C colder than the latter decades of the 20th century in the hemispheric mean (Mann *et al.*, 1998), the coldest decades for the North American continent were closer to 1.5°C colder (Mann *et al.*, 2000b). In addition, the timing of peak coldness was often specific to particular seasons. In Switzerland, for example, the first particularly cold winters appear to have been in the 1560s, with cold springs

beginning around 1568, and with 1573 the first unusually cold summer (Pfister, 1995).

The evidence for temperature changes in past centuries in the Southern Hemisphere is quite sparse. What evidence is available at the hemispheric scale for summer (Jones *et al.*, 1998) and annual mean conditions (Mann *et al.*, 2000b) suggests markedly different behaviour from the Northern Hemisphere. The only obvious similarity is the unprecedented warmth of the late 20th century. Speleothem evidence (isotopic evidence from calcite deposition in stalagmites and stalactites) from South Africa indicates anomalously cold conditions only prior to the 19th century, while speleothem (records derived from analysing stalagmites and stalactites) and glacier evidence from the Southern Alps of New Zealand suggests cold conditions during the mid-17th and mid-19th centuries (Salinger, 1995). Dendroclimatic evidence from nearby Tasmania (Cook *et al.*, 2000) shows no evidence of unusual coldness at these times. Differences in the seasons most represented by this proxy information prevent a more direct comparison.

As with the “Little Ice Age”, the posited “Medieval Warm Period” appears to have been less distinct, more moderate in amplitude, and somewhat different in timing at the hemispheric scale than is typically inferred for the conventionally-defined European epoch. The Northern Hemisphere mean temperature estimates of Jones *et al.* (1998), Mann *et al.* (1999), and Crowley and Lowery (2000) show temperatures from the 11th to 14th centuries to be about 0.2°C warmer than those from the 15th to 19th centuries, but rather below mid-20th century temperatures. The long-term hemispheric trend is best described as a modest and irregular cooling from AD 1000 to around 1850 to 1900, followed by an abrupt 20th century warming. Regional evidence is, however, quite variable. Crowley and Lowery (2000) show that western Greenland exhibited anomalous warmth locally only around AD 1000 (and to a lesser extent, around AD 1400), with quite cold conditions during the latter part of the 11th century, while Scandinavian summer temperatures appeared relatively warm only during the 11th and early 12th centuries. Crowley and Lowery (2000) find no evidence for warmth in the tropics. Regional evidence for medieval warmth elsewhere in the Northern Hemisphere is so variable that eastern, yet not western, China appears to have been warm by 20th century standards from the 9th to 13th centuries. The 12th and 14th centuries appear to have been mainly cold in China (Wang *et al.*, 1998a,b; Wang and Gong, 2000). The restricted evidence from the Southern Hemisphere, e.g., the Tasmanian tree-ring temperature reconstruction of Cook *et al.* (1999), shows no evidence for a distinct Medieval Warm Period.

Medieval warmth appears, in large part, to have been restricted to areas in and neighbouring the North Atlantic. This may implicate the role of ocean circulation-related climate variability. The Bermuda rise sediment record of Keigwin (1996) suggests warm medieval conditions and cold 17th to 19th century conditions in the Sargasso Sea of the tropical North Atlantic. A sediment record just south of Newfoundland (Keigwin and Pickart, 1999), in contrast, indicates cold medieval and warm 16th to 19th century upper ocean temperatures. Keigwin and Pickart (1999) suggest that these temperature contrasts were associated

with changes in ocean currents in the North Atlantic. They argue that the “Little Ice Age” and “Medieval Warm Period” in the Atlantic region may in large measure reflect century-scale changes in the North Atlantic Oscillation (see Section 2.6). Such regional changes in oceanic and atmospheric processes, which are also relevant to the natural variability of the climate on millennial and longer time-scales (see Section 2.4.2), are greatly diminished or absent in their influence on hemispheric or global mean temperatures.

### **2.3.4 Volcanic and Solar Effects in the Recent Record**

Recent studies comparing reconstructions of surface temperature and natural (solar and volcanic) radiative forcing (e.g., Lean *et al.*, 1995; Crowley and Kim, 1996, 1999; Overpeck *et al.*, 1997; Mann *et al.*, 1998; Damon and Peristykh, 1999; Free and Robock, 1999; Waple *et al.*, 2001) suggest that a combination of solar and volcanic influences have affected large-scale temperature in past centuries. The primary features of the Northern Hemisphere mean annual temperature histories of Mann *et al.* (1999a) and Crowley and Lowery (2000) from AD 1000 to 1900 have been largely reproduced based on experiments using an Energy Balance Model forced by estimates of these natural radiative forcings (Crowley, 2000; Mann, 2000) making the argument that the “Little Ice Age” and “Medieval Warm Period”, at the hemispheric mean scale, are consistent with estimates of naturally-forced climate variability. Several studies indicate that the combined effect of these influences has contributed a small component to the warming of the 20th century. Most of these studies isolate greenhouse radiative forcing as being dominant during late 20th century warming (see Crowley, 2000). This argues against a close empirical relationship between certain sun-climate parameters and large-scale temperature that has been claimed for the 20th century (Hoyt and Schatten, 1997). The reader is referred to Chapter 6 for a detailed discussion of these radiative forcings, and to Chapter 12 for comparisons of observed and model simulations of recent climate change.

### **2.3.5 Summary**

Since the SAR there have been considerable advances in our knowledge of temperature change over the last millennium. It is likely that temperatures were relatively warm in the Northern Hemisphere as a whole during the earlier centuries of the millennium, but it is much less likely that a globally-synchronous, well defined interval of “Medieval warmth” existed, comparable to the near global warmth of the late 20th century. Marked warmth seems to have been confined to Europe and regions neighbouring the North Atlantic. Relatively colder hemispheric or global-scale conditions did appear to set in after about AD 1400 and persist through the 19th century, but peak coldness is observed during substantially different epochs in different regions. By contrast, the warming of the 20th century has had a much more convincing global signature (see Figure 2.9). This is consistent with the palaeoclimate evidence that the rate and magnitude of global or hemispheric surface 20th century warming is likely to have been the largest of the millennium, with the 1990s and 1998 likely to

have been the warmest decade and year, respectively, in the Northern Hemisphere. Independent estimates of hemispheric and global ground temperature trends over the past five centuries from sub-surface information contained in borehole data confirm the conclusion that late 20th century warmth is anomalous in a long-term context. Decreasing temporal resolution back in time of these estimates and potential complications in inferring surface air temperature trends from sub-surface ground temperature measurements precludes, however, a meaningful direct comparison of the borehole estimates with high-resolution temperature estimates based on other proxy climate data. Because less data are available, less is known about annual averages prior to 1,000 years before the present and for conditions prevailing in most of the Southern Hemisphere prior to 1861.

## **2.4 How Rapidly did Climate Change in the Distant Past?**

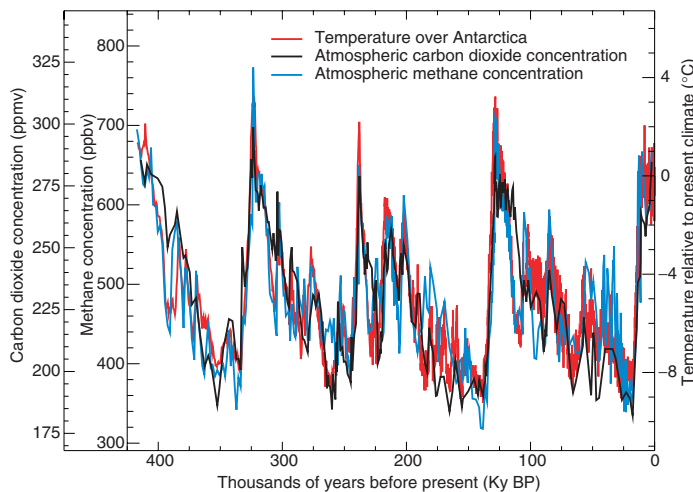
### **2.4.1 Background**

Only during the 1980s was the possibility of rapid climatic changes occurring at the time-scale of human life more or less fully recognised, largely due to the Greenland ice core drilled at Dye 3 in Southern Greenland (Dansgaard *et al.*, 1982, 1989). A possible link between such events and the mode of operation of the ocean was then subsequently suggested (Oeschger *et al.*, 1984; Broecker *et al.*, 1985; see Broecker, 1997, for a recent review). The SAR reviewed the evidence of such changes since the peak of the last inter-glacial period about 120 ky BP (thousands of years Before Present). It concluded that: (1) large and rapid climatic changes occurred during the last Ice Age and during the transition towards the present Holocene; (2) temperatures were far less variable during this latter period; and (3) suggestions that rapid changes may have also occurred during the last inter-glacial required confirmation.

These changes are now best documented from ice core, deep-sea sediment and continental records. Complementary and generally discontinuous information comes from coral and lake level data. The time-scale for the Pleistocene deep-sea core record is based on the orbitally tuned oxygen isotope record from marine sediments (Martinson *et al.*, 1987), constrained by two radiometrically dated horizons, the peak of the last inter-glacial (about 124 ky BP) and the Brunhes/Matuyama reversal of the Earth’s magnetic field at about 780 ky BP.  $^{14}\text{C}$ -dating is also used in the upper 50 ky BP; the result is a deep-sea core chronology believed to be accurate to within a few per cent for the last million years.  $^{14}\text{C}$ -dating is also used for dating continental records as well as the counting of annual layers in tree rings and varved lake records, whereas ice-core chronologies are obtained by combining layer counting, glaciological models and comparison with other dated records. The use of globally representative records, such as changes in continental ice volume recorded in the isotopic composition of deep-sea sediments, or changes in atmospheric composition recorded in air bubbles trapped in ice cores, now allow such local records to be put into a global perspective. Studies still largely focus on the more recent glacial-interglacial cycle (the last 120 to 130 ky). Table 2.4 is a guide to terminology.

**Table 2.4:** Guide to terminology used in palaeoclimate studies of the last 150,000 years.

“Event”, Stage	Estimated age (calendar years)
Holocene	~10 ky BP to present
Holocene maximum warming (also referred to as “climatic optimum”)	Variable?
Last deglaciation	~18 to 10 ky BP
Termination 1	~14 ky BP
Younger Dryas	~12.7 to 11.5 ky BP
Antarctic cold reversal	14 to 13 ky BP
Bölling-Allerød warm period	14.5 to 13 ky BP (Europe)
Last glacial	~74 to 14 ky BP
LGM (last glacial maximum)	~25 to 18 ky BP
Last interglacial peak	~124 ky BP
Termination 2	~130 ky BP
Eemian/MIS stage 5e	~128 to 118 ky BP
Heinrich events	Peaks of ice-rafted detritus in marine sediments, ~7 to 10 ky time-scale.
Dansgaard-Oeschger events	Warm-cold oscillations determined from ice cores with duration ~2 to 3 ky.
Bond cycles	A quasi-cycle during the last Ice Age whose period is equal to the time between successive Heinrich events.
Terminations	Periods of rapid deglaciation.

**Figure 2.22:** Variations of temperature, methane, and atmospheric carbon dioxide concentrations derived from air trapped within ice cores from Antarctica (adapted from Sowers and Bender, 1995; Blunier *et al.*, 1997; Fischer *et al.*, 1999; Petit *et al.*, 1999).

Before reviewing important recent information about rapid changes, we briefly mention progress made on two aspects of the palaeoclimate record of relevance for future climate. The first deals with the relationship between modern and past terrestrial data and SSTs around the time of the Last Glacial Maximum (about 20 ky BP); this is important because of the use of glacial data to validate climate models. New results obtained since the SAR both from marine and terrestrial sources (reviewed in Chapter 8), agree on a tropical cooling of about 3°C. The second concerns the greenhouse gas record ( $\text{CO}_2$  and  $\text{CH}_4$ ) which has now been considerably extended due to the recent completion of drilling of the Vostok ice

core in central East Antarctica. The strong relationship between  $\text{CO}_2$  and  $\text{CH}_4$  and Antarctic climate documented over the last climatic cycle has been remarkably confirmed over four climatic cycles, spanning about 420 ky (Figure 2.22). Present day levels of these two important greenhouse gases appear unprecedented during this entire interval (Petit *et al.*, 1999; and Figure 2.22). From a detailed study of the last three glacial terminations in the Vostok ice core, Fischer *et al.* (1999) conclude that  $\text{CO}_2$  increases started  $600 \pm 400$  years after the Antarctic warming. However, considering the large uncertainty in the ages of the  $\text{CO}_2$  and ice (1,000 years or more if we consider the ice accumulation rate uncertainty), Petit *et al.* (1999) felt it premature to ascertain the sign of the phase relationship between  $\text{CO}_2$  and Antarctic temperature at the initiation of the terminations. In any event,  $\text{CO}_2$  changes parallel Antarctic temperature changes during deglaciations (Sowers and Bender, 1995; Blunier *et al.*, 1997; Petit *et al.*, 1999). This is consistent with a significant contribution of these greenhouse gases to the glacial-interglacial changes by amplifying the initial orbital forcing (Petit *et al.*, 1999).

We also now have a better knowledge of climate variability over the last few climatic cycles as illustrated by selected palaeotemperature records back to about 400 ky (Figure 2.23). The amplitude of the glacial-interglacial temperature change was lower in tropical and equatorial regions (e.g., curve c) than in mid- and high latitudes (other curves). During glacial periods, the climate of the North Atlantic and adjacent regions (curves a and b) was more variable than in the Southern Hemisphere (curve d). Also (not shown), full glacial periods were characterised by very high fluxes of dust (seen in ice-core records and in continental and marine records). A combination of increased dust source area, stronger atmospheric transport and a weaker hydrological cycle (Yung *et al.*, 1996; Mahowald *et al.*, 1999; Petit *et al.*, 1999) probably generated these changes.

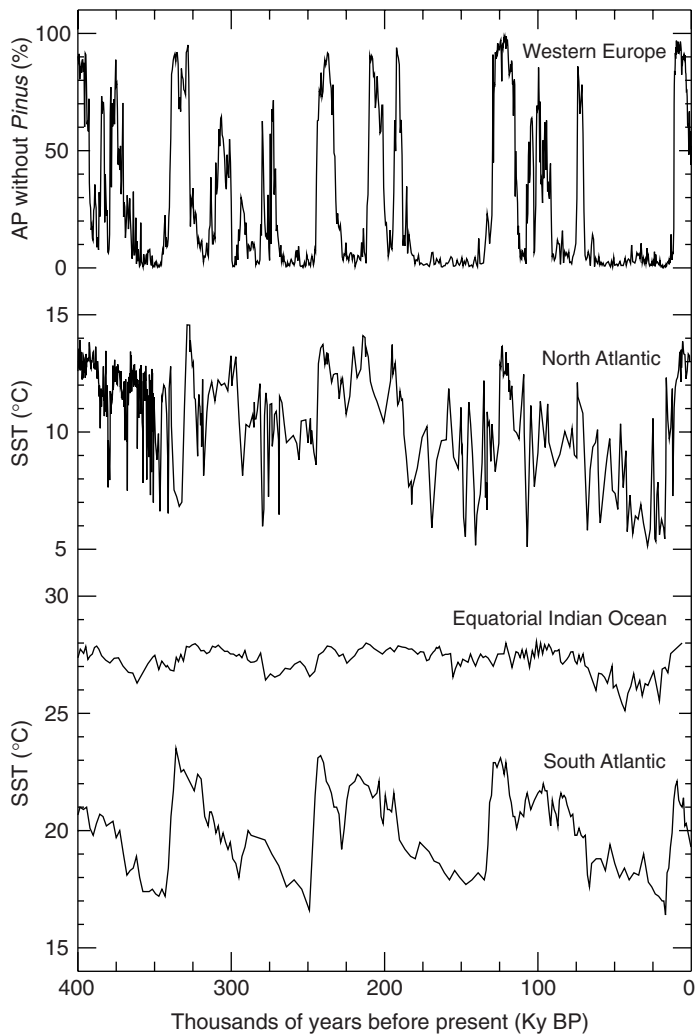


**Figure 2.23:** Time-series illustrating temperature variability over the last about 400 ky (updated from Rostek *et al.*, 1993; Schneider *et al.*, 1996; MacManus *et al.*, 1999; Reille *et al.*, 2000). The uppermost time-series describes the percentage of tree pollen that excludes pollen from pine tree species. The higher this percentage, the warmer was the climate.

#### 2.4.2 How Stable was the Holocene Climate?

Ice core, marine and terrestrial records show that the Holocene was marked by a millennial-scale mode of variability (Meese *et al.*, 1994; O'Brien *et al.*, 1995; Bond *et al.*, 1997; You *et al.*, 1997a,b). These variations affect both atmospheric (Mayewski *et al.*, 1997) and oceanic (Bianchi and McCave, 1999) indicators. The occurrence of very large floods in the south-western United States also reflects substantial low-frequency variability (Ely *et al.*, 1993). SSTs reconstructed from analyses of a sub-tropical, high sedimentation rate site off West Africa might indicate a remarkably high amplitude Holocene variability of 5 to 8°C on a time-scale about 1,500 years (deMenocal, 1998). During the later Holocene, New Zealand speleothems indicate a lowering of temperature after about 7 ky BP, with small advances of the mountain glaciers in the Southern Alps near about 4 and 2.5 ky BP (Salinger and McGlone, 1989). Speleothem records also

indicate a temperature decrease of about 1.5°C some 2 to 3 ky ago (Williams *et al.*, 1999). These indications are consistent with cooler periods at these times shown by South African speleothems (Partridge, 1997). By contrast, temperature peaks appeared in China at about 7 ky BP and at 5.5 to 6 ky BP (Wang and Gong, 2000).

Central Greenland ice cores and European lake isotopic records show correlated temperature variations within the Holocene, with a roughly 50% higher amplitude at Summit Greenland, compared to Europe (Figure 2.24). The most prominent event in both records occurred about 8,200 years BP (Alley *et al.*, 1997; von Grafenstein *et al.*, 1998; Barber *et al.*, 1999) when annual mean temperatures dropped by as much as 2°C in mid-Europe and the European alpine timberline fell by about 200 m (Wick and Tinner, 1999). The event may be related to a significant decrease of SST in the Norwegian Sea (Klitgaard-Kristensen *et al.*, 1998). Lake records from the southern border of the Sahara indicate extremely dry conditions during this time, and probably also during other cool but less dramatic events of this kind (Street-Perrot and Perrot, 1990; Gasse and Van Campo, 1994). The about 8,200 year cooling may also have been worldwide (Stager and Mayewski, 1997), although abrupt early Holocene climate changes recorded in a North American lake are thought to reflect a different event (Hu *et al.*, 1999). Thus cooling is indicated in the New Zealand Southern Alps, with small advances of the mountain glaciers at about 8,000 years BP (Salinger and McGlone, 1989).

Further abrupt climatic changes and reversals on millennial time-scales during the Holocene are documented from pollen and lake level records e.g., in Europe (Magny, 1995; Pazdur *et al.*, 1995; Combourieu-Nebout *et al.*, 1998), North Africa (Gasse *et al.*, 1990; Lamb *et al.*, 1995), North America (Jacobson *et al.*, 1987; Overpeck *et al.*, 1991) and Australia (Kershaw *et al.*, 1991). Holocene lake level changes in Europe have been shown to correlate (Magny, 1995; Yu and Harrisson, 1996) with millennial-scale changes in North Atlantic SST and salinity records (Duplessy *et al.*, 1992; Gasse and van Campo, 1994), suggesting a possible link between millennial thermohaline circulation variability and atmospheric circulation over Europe.

The early Holocene was generally warmer than the 20th century but the period of maximum warmth depends on the region considered. It is seen at the beginning of the Holocene (about 11 to 10 ky BP) in most ice cores from high latitude regions e.g., north-west Canada (Ritchie *et al.*, 1989), central Antarctica (Ciais *et al.*, 1992; Masson *et al.*, 2000) and in some tropical ice cores such as Huascaran in Peru (Thompson *et al.*, 1995). It is also seen during the early Holocene in the Guliya ice core in China (Thompson *et al.*, 1998) but not in two other Chinese cores (Dunde, Thompson *et al.*, 1989; and Dasuopu, to be published). North Africa experienced a greatly expanded monsoon in the early and mid-Holocene, starting at 11 ky BP (Petit-Maire and Guo, 1996), and declining thereafter. In New Zealand the warmest conditions occurred between about 10 to 8 ky BP, when there was a more complete forest cover than at any other time. Glacial activity was at a minimal level in the Southern Alps and speleothem analyses indicate temperatures were about 2°C warmer than present (Salinger and McGlone, 1989; Williams *et al.*, 1999).

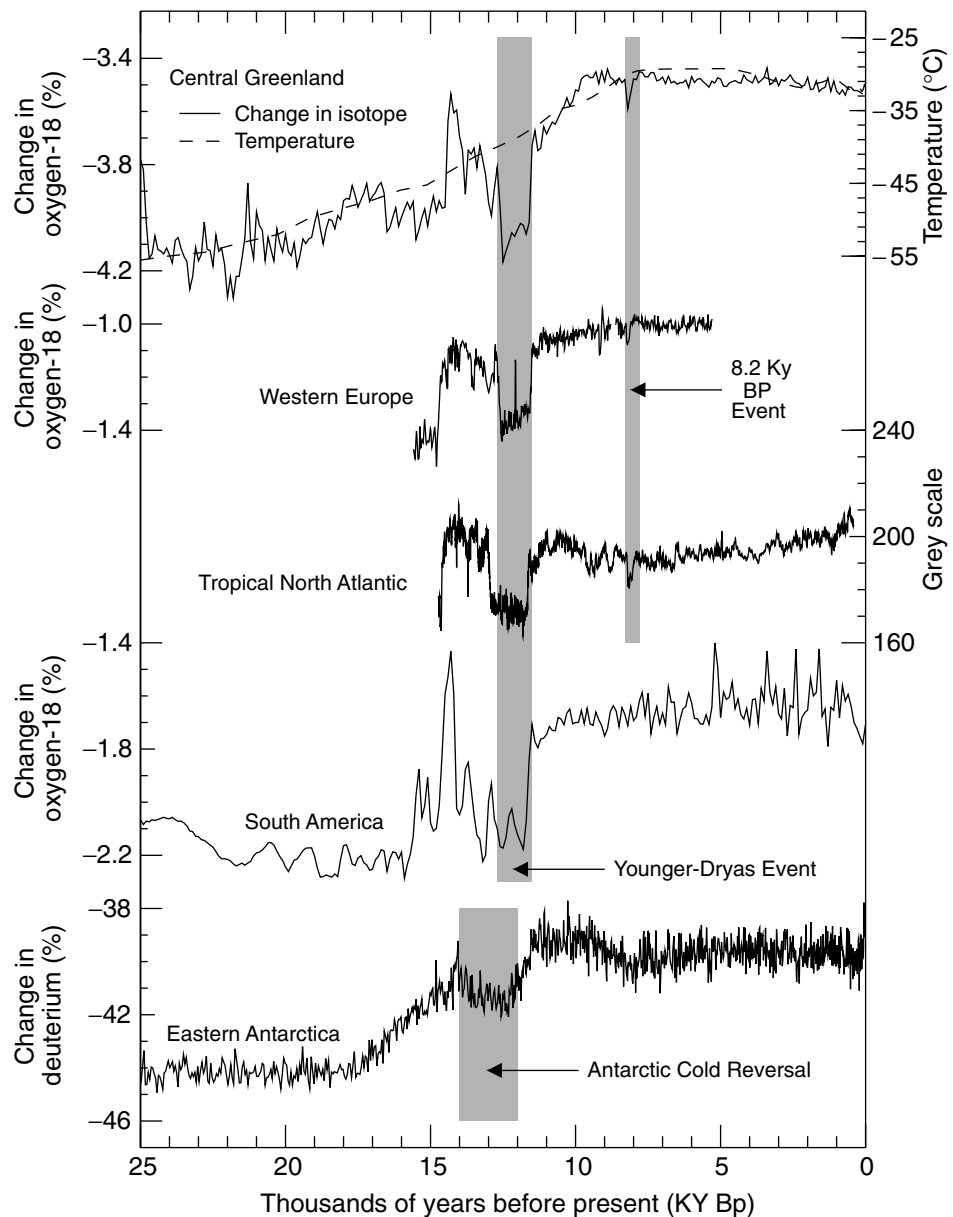


**Figure 2.24:** Records of climate variability during the Holocene and the last climatic transition, including the 8.2 ky BP event (adapted from Johnsen *et al.*, 1992; Hughen *et al.*, 1996; Thompson *et al.*, 1998; von Grafenstein *et al.*, 1999; Jouzel *et al.*, 2001). The shaded areas show the 8.2 ky BP event, the Younger Dryas event and the Antarctic Cold Reversal. The grey scale used in the Tropical North Atlantic record is a measure of sea surface temperature, deduced from the colour of plankton rich layers within an ocean sediment core.

By contrast, central Greenland (Dahl-Jensen *et al.*, 1998), and regions downstream of the Laurentide ice sheet, did not warm up until after 8 ky BP (including Europe: COHMAP Members, 1988; eastern North America: Webb *et al.*, 1993). The East Asian monsoon did not commence its expanded phase until after 8 ky BP (Sun and Chen, 1991; Harrison *et al.*, 1996; Yu and Qin, 1997; Ren and Zhang, 1998). A more detailed description of the climate at 6 ky BP as well as of the mechanisms involved is given in Chapter 8. Long-term climate changes during the Holocene are consistent with the effects of orbital forcing, modified by the persistence of the Laurentide ice sheet (which finally disappeared around 6 ky BP).

Seasonal to interannual climate variability may also have varied its character during the Holocene. This is a period for

which a variety of palaeo-proxies and archaeological investigations (e.g., Sandweiss *et al.*, 1996; Rodbell *et al.*, 1999) provide evidence for past variations in the strength and frequency of ENSO extremes. A 16-year long time-series of temperature and hydrological balance from a coral dated at 5,370 years BP from the Great Barrier Reef (Gagan *et al.*, 1998) implies that ENSO, or its teleconnections to Australia, were substantially different in the mid-Holocene than today. Mid-Holocene changes in the spectrum of ENSO variability have also been implicated by sedimentary palaeoclimatic records in Australasia (McGlone *et al.*, 1992; Shulmeister and Lees, 1995) and South America (Sandweiss *et al.*, 1996; Rodbell *et al.*, 1999).

To sum up, the Holocene shows both long-term trends (including changes in the nature of ENSO) and millennial time-

scale variability although the amplitude of the variability is small compared with that characteristic of Ice Ages. As more detailed information becomes available, the timing of the Holocene maximum warmth is seen to differ across the globe. There appears to be a south to north pattern, with southern latitudes displaying maximum warming a few millennia before the Northern Hemisphere regions. Interestingly, the Holocene appears by far the longest warm “stable” period (as far as seen from the Antarctic climate record) over the last 400 ky, with profound implications for the development of civilisation (Petit *et al.*, 1999).

#### **2.4.3 How Fast did Climate Change during the Glacial Period?**

The most extreme manifestation of climate change in the geological record is the transition from full glacial to full inter-glacial conditions. During the most recent glacial cycle, peak glacial conditions prevailed from about 25 to 18 ky BP. Temperatures close to those of today were restored by approximately 10 ky BP. However, warming was not continuous. The deglaciation was accomplished in two main stages, with a return to colder conditions (Younger Dryas/Antarctic Cold Reversal) or, at the least, a pause in the deglaciation.

The central Greenland ice core record (GRIP and GISP2) has a near annual resolution across the entire glacial to Holocene transition, and reveals episodes of very rapid change. The return to the cold conditions of the Younger Dryas from the incipient inter-glacial warming 13,000 years ago took place within a few decades or less (Alley *et al.*, 1993). The warming phase, that took place about 11,500 years ago, at the end of the Younger Dryas was also very abrupt and central Greenland temperatures increased by 7°C or more in a few decades (Johnsen *et al.*, 1992; Grootes *et al.*, 1993; Severinghaus *et al.*, 1998). Most of the changes in wind-blown materials and some other climate indicators were accomplished in a few years (Alley *et al.*, 1993; Taylor *et al.*, 1993; Hammer *et al.*, 1997). Broad regions of the Earth experienced almost synchronous changes over periods of 0 to 30 years (Severinghaus *et al.*, 1998), and changes were very abrupt in at least some regions (Bard *et al.*, 1987), e.g. requiring as little as 10 years off Venezuela (Hughen *et al.*, 1996). Fluctuations in ice conductivity indicate that atmospheric circulation was reorganised extremely rapidly (Taylor *et al.*, 1993). A similar, correlated sequence of abrupt deglacial events also occurred in the tropical and temperate North Atlantic (Bard *et al.*, 1987; Hughen *et al.*, 1996) and in Western Europe (von Grafenstein *et al.*, 1999).

A Younger-Dryas type event is also recorded in a Bolivian ice core (Thompson *et al.*, 1998; Sajama, South America in Figure 2.24) and in a major advance of a mountain glacier in the Southern Alps of New Zealand (Denton and Hendy, 1994). However there is recent evidence against a significant Younger Dryas cooling here (Singer *et al.*, 1998) and at other sites of the Southern Hemisphere (reviewed by Alley and Clarke, 1999). Instead, the Antarctic (and Southern Ocean) climate was characterised by a less pronounced cooling (the Antarctic Cold Reversal: Jouzel *et al.*, 1987) which preceded the Younger Dryas by more than 1 ky (Jouzel *et al.*, 1995; Sowers and Bender, 1995; Blunier *et al.*, 1997). Curiously, one coastal site in Antarctica,

Taylor Dome (Steig *et al.*, 1998) exhibited cooling in phase with the North Atlantic. Recent series obtained at Law Dome, another coastal site of East Antarctica, show instead a cold reversal preceding the Younger Dryas as in other Antarctic records. This suggests that the Taylor Dome record is of limited geographical significance but it also suggests that there is more to be discovered about this cooling event in the Southern Hemisphere.

The inception of deglacial warming about 14.5 ky BP was also very rapid, leading to the Bölling-Alleröd warm period in less than twenty years (Severinghaus and Brook, 1999). Almost synchronously, major vegetation changes occurred in Europe and North America with a rise in African lake levels (Gasse and van Campo, 1994). There was also a pronounced warming of the North Atlantic and North Pacific (Koç and Janssen, 1994; Sarnthein *et al.*, 1994; Kotilainen and Shackleton, 1995; Thunell and Mortyn, 1995; Wansaard, 1996; Watts *et al.*, 1996; Webb *et al.*, 1998).

The rate of temperature change during the recovery phase from the last glacial maximum provides a benchmark against which to assess warming rates in the late 20th century. Available data indicate an average warming rate of about 2°C/millennium between about 20 and 10 ky BP in Greenland, with lower rates for other regions. Speleothem data from New Zealand, and positions of mountain glacier moraine termini suggest warming rates of 2°C/millennium from 15 to 13 ky BP (Salinger and McGlone, 1989). Speleothem data for South Africa suggest a warming rate of 1.5°C/millennium (Partridge, 1997) over the same time period. On the other hand, very rapid warming at the start of the Bölling-Alleröd period, or at the end of the Younger Dryas may have occurred at rates as large as 10°C/50 years for a significant part of the Northern Hemisphere.

Oxygen isotope measurements in Greenland ice cores demonstrate that a series of rapid warm and cold oscillations called Dansgaard-Oeschger events punctuated the last glaciation (Figure 2.23, see North Atlantic SST panel, and Dansgaard *et al.*, 1993). Associated temperature changes may be as high as 16°C (Lang *et al.*, 1999). These oscillations are correlated with SST variations in several North Atlantic deep-sea cores (Bond *et al.*, 1993). There was clearly a close relation between these ice core temperature cycles and another prominent feature of North Atlantic deep-sea core records, the Heinrich events. Heinrich events occurred every 7,000 to 10,000 years during times of sea surface cooling in the form of brief, exceptionally large, discharges of icebergs from the Laurentide and European ice sheets which left conspicuous layers of detrital rocks in deep-sea sediments. Accompanying the Heinrich events were large decreases in the oxygen isotope ratio of planktonic foraminifera, providing evidence of lowered surface salinity probably caused by melting of drifting ice (Bond *et al.*, 1993). Heinrich events appear at the end of a series of saw-toothed shaped, near millennial temperature cycles. Each set of millennial cycles is known as a Bond cycle. Each cycle was characterised by a succession of progressively cooler relatively warm periods (interstadials) during the Ice Age period. Each cooling trend ended with a very rapid, high amplitude, warming and a massive discharge of icebergs. The impact of these Heinrich events on the climate system extended far beyond the northern North Atlantic. At the

time of major iceberg discharges, strong vegetation changes have been detected in Florida (Grimm *et al.*, 1993; Watts *et al.*, 1996), oceanic changes occurred in the Santa Barbara Basin off California (Behl and Kennet, 1996) and changes in loess grain-size, associated with atmospheric circulation changes, have been detected in China (Porter and An, 1995; Ding *et al.*, 1998).

Deep-sea cores also show the presence of ice rafting cycles in the intervals between Heinrich events (Bond and Lotti, 1995). Their duration varies between 2,000 and 3,000 years and they closely coincide with the Dansgaard-Oeschger events of the last glaciation. A study of the ice-rafted material suggests that, coincident with the Dansgaard-Oeschger cooling, ice within the Icelandic ice cap and within or near the Gulf of Saint Lawrence underwent nearly synchronous increases in rates of calving. The Heinrich events reflect a slower rhythm of iceberg discharges, probably from the Hudson Strait.

Air temperature, SST and salinity variations in the North Atlantic are associated with major changes in the thermohaline circulation. A core from the margin of the Faeroe-Shetland channel covering the last glacial period reveals numerous oscillations in benthic and planktonic foraminifera, oxygen isotopes and ice-rafterd detritus (Rasmussen *et al.*, 1996a). These oscillations correlate with the Dansgaard-Oeschger cycles, showing a close relationship between the deep ocean circulation and the abrupt climatic changes of the last glaciation. Warm episodes were associated with higher SST and the presence of oceanic convection in the Norwegian Greenland Sea. Cold episodes were associated with low SST and salinity and no convection in the Norwegian Greenland Sea (Rasmussen *et al.*, 1996b). Cores from the mid-latitudes of the North Atlantic show that the iceberg discharges in Heinrich events resulted in both low salinity and a reduced thermohaline circulation (Cortijo *et al.*, 1997; Vidal *et al.*, 1997).

These rapid climatic events of the last glacial period, best documented in Greenland and the North Atlantic, have smoothed counterparts in Antarctica (Bender *et al.*, 1994; Jouzel *et al.*, 1994). A peak in the concentration of the isotope beryllium-10 in ice cores (Yiou *et al.*, 1997a), changes in the concentration of atmospheric methane (Blunier *et al.*, 1998) and in the isotopic content of oxygen in ice cores (Bender *et al.*, 1999) indicate links between the Northern and Southern Hemisphere climates over this period. Large Greenland warming events around 36 and 45 ky BP lag their Antarctic counterparts by more than 1,000 years. This argues against coupling between northern and southern polar regions via the atmosphere but favours a connection via the ocean (Blunier *et al.*, 1998).

New evidence suggests that the North Atlantic has three modes of operation. These are: deep-water sinking in the GIN (Greenland-Iceland-Norwegian) Seas and the Labrador Sea, deep-water sinking in the North Atlantic or in the Labrador Sea but not the GIN Seas (Duplessy *et al.*, 1991; Labeyrie *et al.*, 1992) in the cold phase of Dansgaard-Oeschger events and at glacial maximum, and little deep-water sinking in the GIN or Labrador Seas (Heinrich events) (Sarnthein *et al.*, 1994; Vidal *et al.*, 1997, 1998; Alley and Clark, 1999; Stocker, 2000). The first type corresponds to modern, warm conditions. Shut-down of convection in the GIN Seas has a strong effect on the high

latitude Atlantic atmosphere and on areas that respond to it such as the monsoon regions of north Africa (Street-Perrott and Perrott, 1990). However, cross-equatorial Atlantic ocean surface transport that supplies the water for the formation of the Labrador Sea deep-water continues to remove heat from the South Atlantic under these conditions. The additional "Heinrich shut-down" of the North Atlantic and Labrador Sea deep-water formation allows this heat to remain in the South Atlantic (Crowley, 1992), and may increase deep-water formation either south of the area affected by melt-water injection (Vidal *et al.*, 1997, 1998) or in the Southern Ocean (Broecker, 1998). This reorganisation could cause warming of regions of the South Atlantic and downwind of it (Charles *et al.*, 1996; Blunier *et al.*, 1998) through a seesaw relationship with the North Atlantic. However, the behaviour of Taylor Dome in the Antarctic and several other southern sites (see above) which exhibit cooling in phase with the North Atlantic argue for an additional atmospheric link to some southern regions.

#### **2.4.4 How Stable was the Previous Inter-glacial?**

Assessment of present day climate variability benefits from comparison with conditions during inter-glacial periods that are broadly comparable with the Holocene. The most recent such inter-glacial began about 130 ky BP, lasting until about 71 ky BP when final deterioration into the last glacial began. However, only the Eemian interval, from about 130 to 120 ky BP corresponds to a climate as warm as, or warmer than, today e.g., Figure 2.22.

The study of atmospheric composition changes has revealed that rapid changes of properties observed for the lowest part of the Greenland cores (GRIP Project Members, 1993; Grootes *et al.*, 1993) do not correspond to climatic instabilities during the last inter-glacial (Chappellaz *et al.*, 1997). The extent to which climate was more or less stable during this last inter-glacial than during the Holocene is unclear. Early evidence from marine cores (CLIMAP, 1984; McManus *et al.*, 1994) and other ice cores (Jouzel *et al.*, 1993) indicated that the Eemian climate was rather stable. A high resolution North Atlantic record shows a lack of substantial fluctuations during the last inter-glacial but also indicates that the Eemian began and ended with abrupt changes in deep-water flow, with transitions occurring in less than 400 years (Adkins *et al.*, 1997). In New Zealand, there were at least three periods of milder climate than typical of the Holocene during the last inter-glacial (Salinger and McGlone, 1989). Study of an Indonesian fossil coral indicates that ENSO was robust during the last glacial period (Hughen *et al.*, 1999).

A rapid and significant cooling event within the Eemian period has been detected from European continental pollen records (Cheddadi *et al.*, 1998). High winter temperatures prevailed for 3.5 to 4 ky after the deglaciation, but then dropped by as much as 6 to 10°C in mid-Eemian times, accompanied by a decrease in precipitation. In Antarctica, the last inter-glacial is also marked by a short (about 5 ky) period of warm temperatures followed by a slightly cooler interval (Petit *et al.*, 1999). Further evidence for Eemian climate variability is found in marine records. An invasion of cold, low salinity water in the Norwegian

Sea (Cortijo *et al.*, 1994) was probably associated with a reduction in warm water transport by the North Atlantic Drift and the thermohaline circulation. Overall, the last inter-glacial appears, at least during its first part, warmer than present day climates by at least 2°C in many sites, i.e., comparable to anthropogenic warming expected by the year 2100. However, the geographical coverage of reliable and well-dated temperature time-series is too sparse to provide a global estimate.

#### 2.4.5 Summary

Current evidence indicates that very rapid and large temperature changes, generally associated with changes in oceanic and atmospheric circulation, occurred during the last glacial period and during the last deglaciation, particularly in higher latitudes of the Northern Hemisphere. During the warming phases, and the Younger Dryas pause, there is evidence of almost worldwide, nearly synchronous events. However, as with the Holocene maximum warming and the Last Glacial Maximum, these changes appear to have occurred asynchronously between the Northern Hemisphere and at least part of the Southern Hemisphere. During the Holocene smaller but locally quite large climate changes occurred sporadically; similar changes may have occurred in the last inter-glacial. Evidence is increasing, therefore, that a rapid reorganisation of atmospheric and ocean circulation (time-scales of several decades or more) can occur during inter-glacial periods without human interference.

### 2.5 How have Precipitation and Atmospheric Moisture Changed?

#### 2.5.1 Background

Increasing global surface temperatures are very likely to lead to changes in precipitation and atmospheric moisture, because of changes in atmospheric circulation, a more active hydrological cycle, and increases in the water holding capacity throughout the atmosphere. Atmospheric water vapour is also a climatically critical greenhouse gas, and an important chemical constituent in the troposphere and stratosphere.

Precipitation measurement and analysis are made more difficult by accompanying natural phenomena such as wind and the use of different instruments and techniques (Arkin and Ardanuy, 1989). Because of the substantial under-catch of precipitation gauges during solid precipitation, frequent light rainfall events, or windy conditions, the true precipitation in the Arctic is more than 50% higher than the measured values (Førland and Hanssen-Bauer, 2000). Gauge under-catch is substantially less in warmer, less windy climates with heavier rainfall. New, satellite-derived precipitation estimates offer the prospect of near-global climatologies covering at least one or two decades, but multi-decadal global changes cannot be estimated with high confidence.

For all these reasons it is useful to compare changes in many of the moisture-related variables, such as streamflow and soil moisture, with precipitation to help validate long-term precipitation trends.

#### 2.5.2 Changes in Precipitation and Related Variables

##### 2.5.2.1 Land

Overall, global land precipitation has increased by about 2% since the beginning of the 20th century (Jones and Hulme, 1996; Hulme *et al.*, 1998). The increase is statistically significant but has been neither spatially nor temporally uniform (Karl and Knight, 1998; Doherty *et al.*, 1999). Dai *et al.* (1997b) found a global secular increase in precipitation separate from ENSO and other modes of variability. Data from over 20,000 stations contributed to the changes since 1900 shown in Figure 2.25. The effects of changes in windshields on winter precipitation measurements were taken into account for most mid- and high latitude observations. Dai *et al.* (1997b) indicated that instrumental discontinuities are unlikely to significantly impact other observations.

##### Mid- and high latitudes

Over the 20th century, annual zonally averaged precipitation increased by between 7 to 12% for the zones 30°N to 85°N and by about 2% between 0°S to 55°S (Figure 2.25(ii)). The increase in the Northern Hemisphere is likely to be slightly biased because adjustments have not been made for the increasing fraction of precipitation falling in liquid as opposed to frozen form. The exact rate of precipitation increase depends on the method of calculating the changes, but the bias is expected to be small because the amount of annual precipitation affected by this trend is generally only about a few per cent. Nevertheless, this unsteady, but highly statistically significant trend toward more precipitation in many of these regions is continuing. For example, in 1998 the Northern Hemisphere high latitudes (55°N and higher) had their wettest year on record and the mid-latitudes have had precipitation totals exceeding the 1961 to 1990 mean every year since 1995.

Figure 2.25(i) shows mostly increasing precipitation in the Northern Hemisphere mid- and high latitudes, especially during the autumn and winter, but these increases vary both spatially and temporally. For example, precipitation over the United States has increased by between 5 to 10% since 1900 (Figure 2.25(ii)) but this increase has been interrupted by multi-year anomalies such as the drought years of the 1930s and early 1950s (Karl and Knight, 1998; Groisman *et al.*, 1999). The increase is most pronounced during the warm seasons. Using data selected to be relatively free of anthropogenic influences such as ground water pumpage or land use changes, several recent analyses (Lettenmaier *et al.*, 1999; Lins and Slack, 1999; Groisman *et al.*, 2001) have detected increases in streamflow across much of the contiguous United States, confirming the general tendency to increasing precipitation. However, Lins and Michaels (1994) found in some regions that increased streamflow did not relate well to an increase in rainfall. This has been further evaluated by Groisman *et al.* (2001) who show that changes in snow-cover extent also influence the timing and volume of streamflow.

Regionally, Mekis and Hogg (1999) showed that precipitation in Canada has increased by an average of more than 10% over the 20th century. Zhang *et al.* (2000) report an increase in Canadian heavy snowfall amounts north of 55°N and Akinremi *et al.* (1999) found rainfall significantly increasing in the Canadian

prairies from 1956 to 1995. Multi-decadal streamflow data in Canada are not extensive, but there are no apparent inconsistencies between observed changes in streamflow or precipitation (Zhang *et al.*, 2000).

Over the last 50 years there has been a slight decrease in annual precipitation over China (Zhai *et al.*, 1999a), which is supported by a significant (5% confidence level) decrease in the number of rainy days (3.9%/decade; Figure 2.25 (ii)). In contrast, the area affected by the upper 10% of heaviest precipitation has significantly increased. Zhai *et al.* (1999b) show a significant increase in precipitation over the middle and lower reaches of the Yangtze River and west China during the latter part of the 20th century, while also detecting a declining trend in precipitation over northern China.

There have been marked increases in precipitation in the latter part of the 20th century over northern Europe, with a general decrease southward to the Mediterranean (Schönwiese and Rapp, 1997; Figure 2.25(i)). Dry wintertime conditions over southern Europe and the Mediterranean (Piervitali *et al.*, 1998; Romero *et al.*, 1998) and wetter than normal conditions over many parts of northern Europe and Scandinavia (Hanssen-Bauer and Førland, 2000) are linked to strong positive values of the North Atlantic Oscillation, with more anticyclonic conditions over southern Europe and stronger westerlies over northern Europe (Section 2.6.5).

Based on recent research (Bogdanova and Mescherskaya, 1998; Groisman and Rankova, 2001), the precipitation trend for the last century over the former USSR as reported by the SAR was slightly overestimated. The new results indicate that precipitation has increased since 1891 by about 5% west of 90°E for both warm and cold seasons. Georgievsky *et al.* (1996) also noted increases in precipitation over the last several decades over western Russia, accompanied by increases in streamflow and a rise in the level of the Caspian Sea. In eastern Russia a negative precipitation trend since 1945 is embedded in the century-long positive precipitation trend (Figure 2.25(ii); Gruza *et al.*, 1999). Soil moisture data for large regions of Eurasia (Robock *et al.*, 2000) show large upward trends. The rate of increase is more than 1 cm/decade in the available soil moisture in the top 1 m of soil. These large positive trends occur simultaneously with positive trends in temperature that would normally reduce soil moisture. Increases in precipitation (and cloud cover, Section 2.5.5) are believed to have more than compensated for the increased losses due to evapotranspiration.

An analysis of rainfall data since 1910 by Haylock and Nicholls (2000) reveals a large decrease in total precipitation and related rain days in south-western Australia. Annual total rainfall has increased over much of Australia with significant increases of 15 to 20% in large areas. The increase in total rainfall has been accompanied by a significant 10% rise in the average number of rain days over Australia (Hennessy *et al.*, 1999). Elsewhere in the Southern Hemisphere, a long-term increase in precipitation in Argentina has been observed for the period 1900 to 1998 (Figure 2.25(i); Dai *et al.*, 1997b).

#### Tropics and sub-tropics

The increase in precipitation in the mid- and high latitudes contrasts with decreases in the northern sub-tropics (with

marginal statistical significance) which were largely responsible for the decade-long reduction in global land precipitation from the mid-1980s through the mid-1990s. Since the SAR, record low precipitation has been observed in equatorial regions, while the sub-tropics have recovered from their anomalously low values of the 1980s.

Regionally positive but non-significant trends have occurred in the rainy season rainfall in north-east Brazil and northern Amazonia (Marengo *et al.*, 1998). River data from northern Amazonia indicate wetter periods in the mid-1970s, and in 1990, as well as drier periods between 1980 to 1990, consistent with rainfall anomalies. Northern Amazonian rainfall appears to be modulated by multi-decadal climate variations.

There is little evidence for a long-term trend in Indian monsoonal rainfall but there are multi-decadal variations (Kumar *et al.*, 1999a,b). From 1906 to about 1960, monsoonal rainfall increased then decreased through 1974 and has increased since (see Section 2.6). In central America for much of the period from the early 1940s to present, western Mexico has experienced an increasingly erratic monsoonal rainfall (Douglas and Englehart, 1999).

Since 1976, increases in precipitation in the South Pacific have occurred to the north-east of the South Pacific Convergence Zone (SPCZ) while decreases have occurred to its south-west (Salinger *et al.*, 1996). Manton *et al.* (2001) found significant decreases in rain days since 1961 throughout Southeast Asia and western and central South Pacific, but increases in the north of French Polynesia and Fiji.

Streamflow data for major rivers in south-eastern South America for the period 1901 to 1995 show that streamflow has increased since the mid-1960s, and was accompanied by a significant decrease in the amplitude of the seasonal cycle of most of those rivers (Garcia and Vargas, 1998; Genta *et al.*, 1998). Figure 2.25(i) shows increases in precipitation since 1900 along the South American eastern coastal areas, with less extensive increases since 1976.

There has been a pattern of continued aridity since the late 1960s throughout North Africa south of the Sahara. This pattern is most persistent in the western region. The driest period was in the 1980s with some recovery occurring during the 1990s, particularly in the easternmost sectors where rainfall in some years was near or just above the long-term mean (Nicholson *et al.*, 2000). Southern Africa was relatively moist in the 1950s and 1970s (Nicholson *et al.*, 2000); but Hulme (1996) found significant decreases in precipitation being observed since the late 1970s. Early 2000, however, has seen flood-producing rains in the eastern part of southern Africa.

#### 2.5.2.2 Palaeo-drought

Palaeoclimate proxy evidence (tree rings, lake sediments and pollen evidence) has been used to estimate variability in drought and precipitation patterns in past centuries. Much of the recent research has emphasised the North American region (e.g., Cook *et al.*, 1999a), where a key conclusion is that the range of regional drought variability observed during the 20th century may not be representative of the larger range of

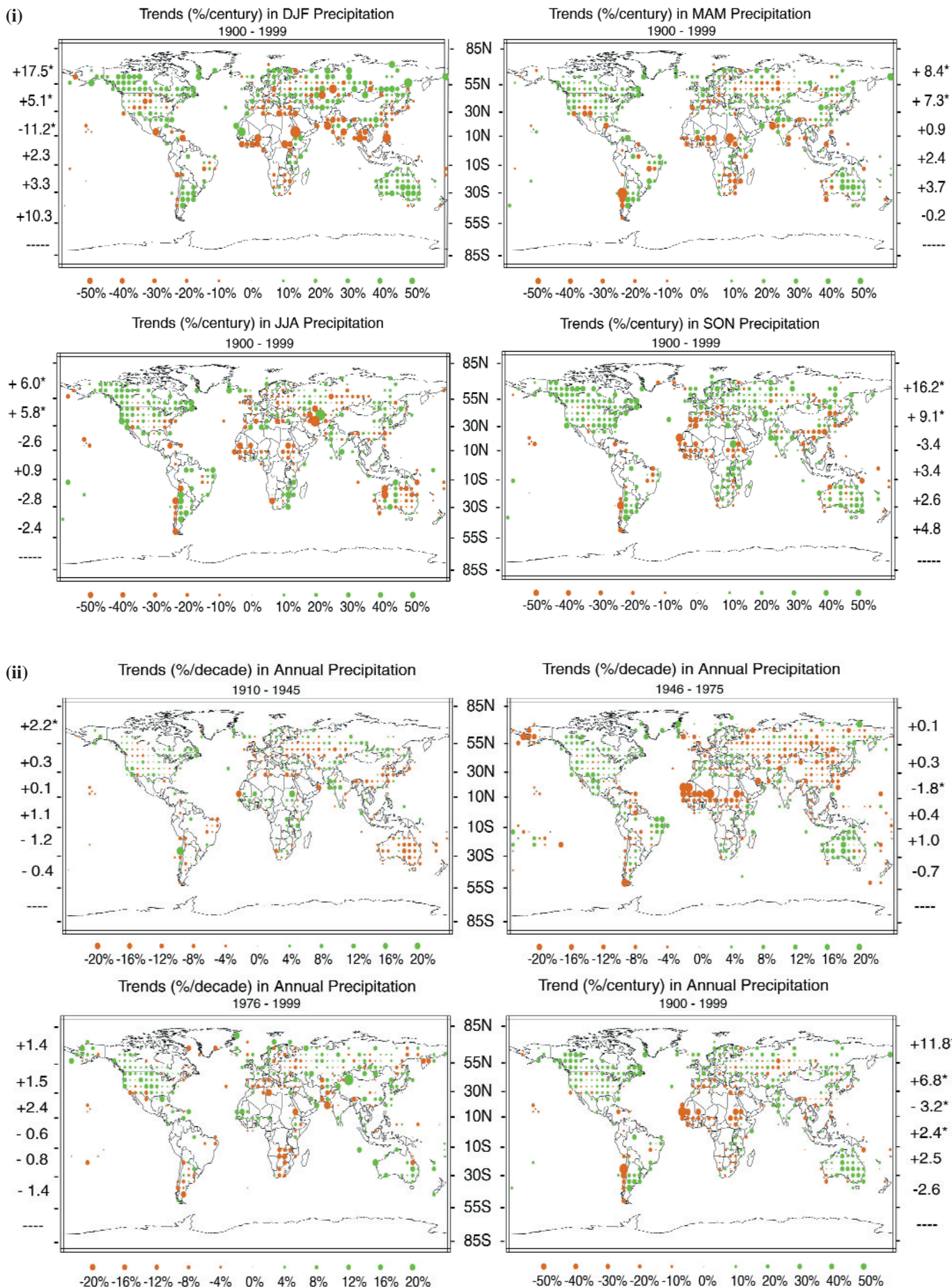


**Figure 2.25(i):** Trends for 1900 to 1999 for the four seasons.

Precipitation trends are represented by the area of the circle with green representing increases and brown representing decreases. Annual and seasonal trends were calculated using the following method.

Precipitation anomalies in physical units were calculated for each station based on 1961 to 1990 normals and averaged into  $5^\circ \times 5^\circ$  grid cells on a monthly basis. The 1961 to 1990 monthly mean precipitation for each grid cell was added to the monthly anomalies and the resulting grid cell values summed into annual and seasonal totals. This series was converted into percentages of normal precipitation, and trends calculated from the percentages. Average trends within six latitude bands ( $85^\circ\text{N}$  to  $55^\circ\text{N}$ ,  $55^\circ\text{N}$  to  $30^\circ\text{N}$ ,  $30^\circ\text{N}$  to  $10^\circ\text{N}$ ,  $10^\circ\text{N}$  to  $10^\circ\text{S}$ ,  $10^\circ\text{S}$  to  $30^\circ\text{S}$ ,  $30^\circ\text{S}$  to  $55^\circ\text{S}$ ) are shown in the legend of each map. The 1961 to 1990 monthly mean precipitation for the latitude band was added to the anomaly time-series and the resulting values totalled across all months within the season or year. The significance of each trend (based on a 5% level) was determined using a t-test and a non-parametric test statistic. Trends found to be significant under both tests are indicated with an asterisk.

**Figure 2.25(ii):** As in Figure 2.25(i) except annual trends for the three periods of changing rates of global temperature (shown in Figure 2.9) and the full period, 1900 to 1999. During the 100-year periods, calculation of grid cell trends required at least 66% of the years without missing data and at least three years of data within each decade except the first and last. During the shorter periods, calculation of grid cell trends required at least 75% of the years without missing data. Stations with more than one sixth of their data missing during the normal period and grid cells with more than one season or year without any measurable precipitation during the normal period were excluded from consideration. Due to the nature of trend estimation, it is not possible to cumulatively sum the trends for each of the three periods to obtain an overall trend.

drought evident in past centuries (Laird *et al.*, 1996; Woodhouse and Overpeck, 1998). Hughes and Graumlich (1996) and Hughes and Funkhouser (1999) provide evidence of multi-decadal mega-droughts in the western Great Basin of North America in the 10th to 14th centuries. Nonetheless, the 20th century dust bowl still stands out as the most extreme drought of the past several centuries, the period when North American continental scale reconstruction is possible. Swetnam and Betancourt (1998) argue that recent spring wetness in the American south-west is greater than that observed in at least the last thousand years. Evidence of significant changes in regional hydroclimatic patterns is not limited, however, to North America. Stine (1994) argues that enhanced drought conditions occurred synchronously in South America. Ice accumulation at Quelccaya in the Andes, and on the Dunde Ice Cap on the Tibetan Plateau (Thompson, 1996) was slower in the first half of the last millennium than the last 500 years, but 500-year averages are not easily related to the palaeo-temperature data (Figure 2.21). Pollen evidence indicates significant changes in summer rainfall patterns in China in the earlier centuries of the past millennium (Ren, 1998). The relationship between such past changes in regional drought and precipitation patterns, and large-scale atmospheric circulation patterns associated with ENSO, for example, is an area of active current research (e.g., Cole and Cook, 1998).

**2.5.2.3 Ocean**

The strong spatial variability inherent in precipitation requires the use of estimates based on satellite observations for many regions. Thus satellite data are essential to infer global changes in precipitation, as the oceans account for 70% of the global surface area. Since adequate observations were not made until the early 1970s, no satellite-based record is sufficiently long to permit estimates of century-long changes. The first satellite instrument specifically designed to make estimates of precipitation did not begin operation until 1987. At this time three data sets are available: (a) the Global Precipitation Climatology Project (GPCP) product, which spans the period from 1987 to the present (Huffman *et al.*, 1997); (b) the CPC Merged Analysis of Precipitation (CMAP) product, covering the period from 1979 to 1998 (Xie and Arkin, 1997); and (c) MSU-derived precipitation estimates since 1979 (Spencer, 1993). While the period from 1987 appears to be well observed, it is too short to draw conclusions regarding decadal-scale variations. The longer CMAP data set assumes that the various satellite-derived estimates have no trend over the period, and hence no longer time-scale conclusions are possible. Nonetheless, analyses of the CMAP product and associated data from the NCEP reanalysis project indicate that there have been substantial average increases in precipitation over the tropical oceans during the last twenty years, related to increased frequency and intensity of ENSO (Trenberth *et al.*, 2001). ENSO conditions are not related to positive precipitation anomalies everywhere over the tropical oceans (e.g., south-western Tropical Pacific).

### 2.5.3 Water Vapour

Although measurement problems hinder the analysis of long-term water vapour changes (Elliott, 1995; Rind, 1998), several recent studies tend to confirm and extend the findings of lower tropospheric water vapour increases reported in the SAR. Furthermore, new analyses indicate upward trends in near-surface humidity. Knowledge about changes in water vapour at upper tropospheric and lower stratospheric levels is of great importance because strong alterations in radiative forcing can result from small absolute changes in water vapour at these levels (Chapters 6 and 7). New data presented here from the SPARC WAVAS (Stratospheric Processes and their Role in Climate / Water Vapour Assessment) project (Kley *et al.*, 2000) are starting to cast light on changes at these levels. Note that water vapour pressure, and specific humidity (for a constant relative humidity) increase non-linearly with increasing temperature.

#### 2.5.3.1 Surface water vapour

Water vapour pressure, dew-point or relative humidity at the surface is conventionally measured using wet and dry bulb thermometers exposed in thermometer screens at climate stations. The quality of these data has been little studied. Wet bulb thermometers are not usually aspirated, so that the cooling of the wet bulb, and therefore the deduced specific or relative humidity, depends on the flow rate of air within the screen. This may often differ from the assumed airflow. Occasionally wet bulbs may dry out. Thus it is not possible to judge fully the accuracy of surface vapour pressure trends presented here.

Schönwiese *et al.* (1994) and Schönwiese and Rapp (1997) found small increases in surface vapour pressure over most of Europe from 1961 to 1990. The annual trends are weak. Statistically significant changes are confined to increases of about 0.5 to 1.5 hPa (relative to mean values of 12 to 15 hPa) in the southern and eastern Mediterranean region (with the largest increase in summer) and decreases of about 0.5 hPa over parts of Turkey (mainly in springtime).

Specific humidity trends over the United States were overwhelmingly positive for the period 1961 to 1995, with magnitudes of several per cent per decade, and with the largest and most statistically significant trends in spring and summer (Gaffen and Ross, 1999). Night-time specific humidity trends were generally stronger than daytime trends. Relative humidity showed smaller increases, especially in winter and spring. The specific humidity and derived dew point trends are broadly consistent, both spatially and in their day-night differences, with temperature trends. Schwartzman *et al.* (1998) found that the diurnal dewpoint cycle is changing over North America, with a relative decline in late afternoon and a small rise at midday.

Increases in water vapour over the former Soviet Union, Eastern China, the United States and tropical Western Pacific islands have been found in some seasons by Sun *et al.* (2000) in the second half of the 20th century, but with decreases in Canada in autumn. The selective character of the findings prevents any assessment of statistical significance. Wang and Gaffen (2001) found that specific humidity trends over China were overwhelmingly positive over 1951 to 1994, with the largest and most statistically significant trends in north-west China north of 35°N and

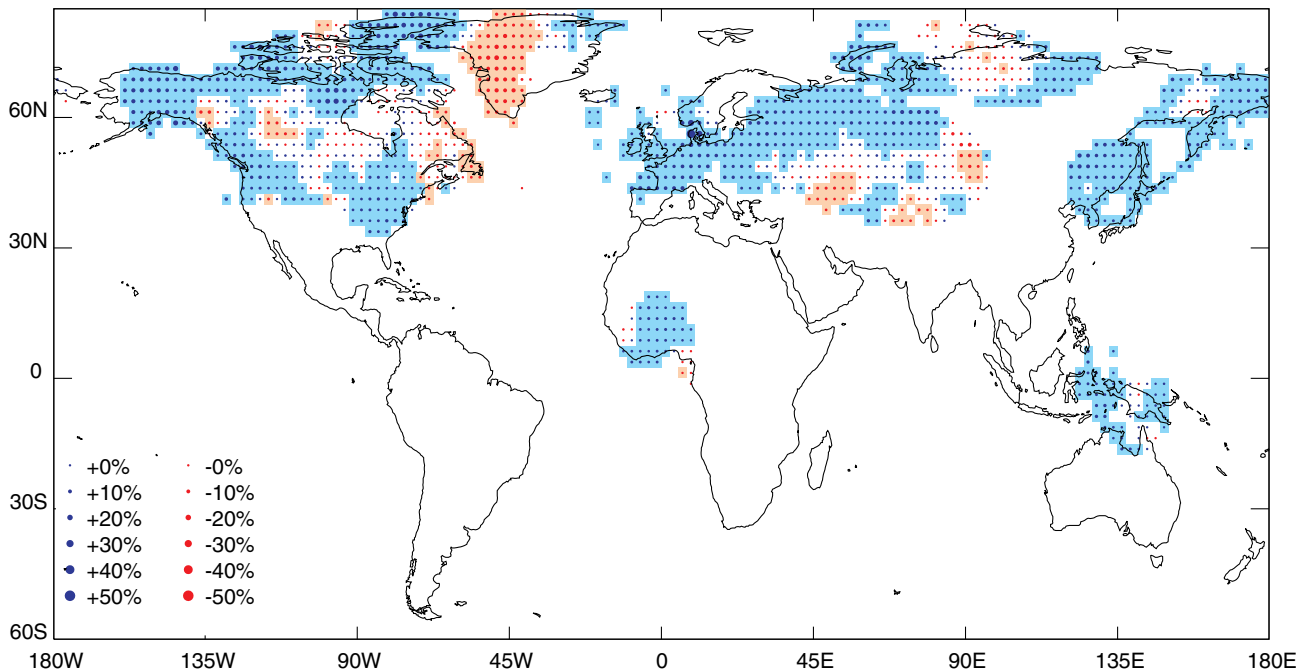


**Figure 2.26:** Trends in annual mean surface water vapour pressure, 1975 to 1995, expressed as a percentage of the 1975 to 1995 mean. Areas without dots have no data. Blue shaded areas have nominally significant increasing trends and brown shaded areas have significant decreasing trends, both at the 5% significance level. Biases in these data have been little studied so the level of significance may be overstated. From New *et al.* (2000).

west of 105°E. Trends were larger in summer and night-time trends were generally larger than daytime ones.

Recently New *et al.* (2000) have estimated linear trends for annual and seasonal values of surface vapour pressure over land using calculated monthly vapour pressure data from climate stations. Figure 2.26 shows trends for the 21 years from 1975 to 1995, corresponding to much of the recent period of global warming described in Section 2.2.2.3. Although the uncertain quality of the data prevents any definitive conclusions about statistical significance, nominal significance of trends at the 5% level was estimated after smoothing the annual data to reduce the influence of outliers at the beginning and end of this short series. Few Southern Hemisphere data have been analysed, but Figure 2.26 shows that there have been widespread nominally significant increases in annual mean water vapour in the Northern Hemisphere. These increases are reflected in the individual seasons, although nominally significant annual mean increases are more extensive. Regional decreases over eastern Canada are explained by colder conditions in the winter half year associated with the increasingly positive phase of the North Atlantic Oscillation (Section 2.6.5).

### 2.5.3.2 Lower-tropospheric water vapour

Radiosonde and satellite observations of water vapour above the surface have been analysed for evidence of long-term change. Both data sources have had serious data quality and temporal homogeneity problems (Elliott, 1995), although recent work to determine trends in water vapour from the surface to 500 hPa since 1973 has been based on radiosonde data judged to be largely unaffected by these problems (Ross and Elliott, 2001). Published satellite data are insufficiently homogeneous or too short in length to deduce reliable trends or low-frequency variations.

#### *Radiosonde observations*

Ross and Elliott (1996, 1998) analysed surface-to-500 hPa precipitable water over the Northern Hemisphere for 1973 to 1995 using quality-controlled data. Increases in precipitable water were found over North America except for north-east Canada. Over Eurasia,

only China and the Pacific islands show coherent regional increases. The remainder of Eurasia shows a mixture of positive and negative trends, with a tendency for negative trends over Eastern Europe and western Russia. Mid-tropospheric water vapour trends tend to be of the same sign as temperature trends over North America, China, and the Pacific, but elsewhere the temperature trends are more consistently positive than the water vapour trends. Figure 2.27 summarises the results. Lower-tropospheric dew-point data for the period 1961 to 1995 also show increases, though smaller than those for the 1973 to 1995 period, and few are statistically significant (Ross and Elliott, 2001).

Zhai and Eskridge (1997) found increases of about 1 to 3%/decade in surface-to-200 hPa precipitable water over China for 1970 to 1990. Increases were most significant in spring. Percentage trends were larger over the 700 to 400 hPa layer than the surface-700 hPa layer. Gutzler (1996) found that specific humidity data at 1,000, 700, and 300 hPa at four western tropical Pacific radiosonde stations from 1973 to 1993 gave increases of 3 to 9%/decade, with larger percentage increases at increasing height above the surface. In contrast, Peixoto and Oort (1996) found decreases in zonal mean relative humidity between 1974 and 1988. The decreases are more marked at 300 hPa, where they are more likely to be associated with instrument changes than at lower levels, and are more pronounced at higher latitudes than in the tropics.

### 2.5.3.3 Upper-tropospheric and lower-stratospheric water vapour

Recently assessed increases in lower stratospheric water vapour mixing ratio over the last few decades are likely to have caused a decrease in stratospheric temperatures by an amount comparable to that produced by ozone decreases (Forster and Shine, 1999; Smith *et al.*, 2001) (see lower-stratospheric temperature trends in Section 2.2.3). These changes also impact on ozone chemistry (Chapter 4) and on radiative forcing of the atmosphere (Chapters 6 and 7). Data from over twenty-five instruments that measure water vapour concentration and relative humidity in the upper troposphere and stratosphere were recently compared and

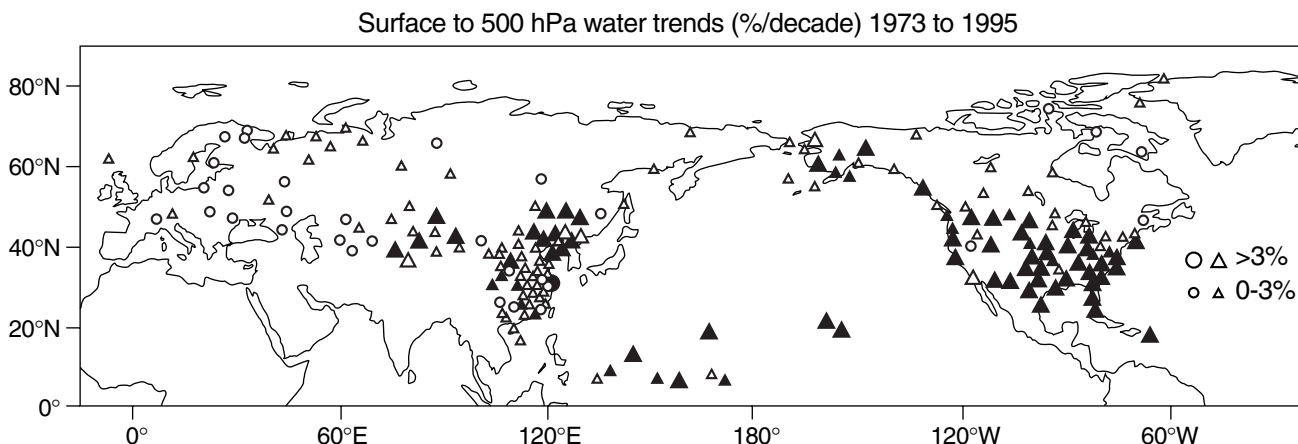


**Figure 2.27:** Annually averaged trends in surface to 500 hPa precipitable water at 0000UTC for the period 1973 to 1995. Positive trends are indicated by triangles and negative trends by circles. Filled symbols indicate the trends were statistically significant at the 5% level according to the Spearman test. The two sizes of symbols give an indication of the magnitude of the trend. From Ross and Elliott (2001).

assessed in the international SPARC study (Kley *et al.*, 2000). The purpose of the study, which included measurements made by both *in situ* and remote sensing techniques utilising balloons, aircraft and satellites, was to determine the data quality and to estimate the magnitude of any trends. The study showed that some stratospheric instruments have sampled over a long enough period that several overlapping time-series of intermediate length (8 to 15 years) can be used to help evaluate stratospheric changes. A reasonable degree of consistency was found among stratospheric measurements made from near the tropopause up to as high as 50 km (about 1 hPa). Most observations were within  $\pm 10\%$  of the grand mean of all measurements to which they were compared.

Accurate balloon observations of lower-stratospheric water vapour are available from 1964 to 1976 over Washington, D.C. and from 1980 to present over Boulder, Colorado, USA (e.g., Mastenbrook, 1968; Harries, 1976; Mastenbrook and Oltmans, 1983; Oltmans and Hofmann, 1995). The SPARC study shows that these point measurements are nevertheless representative of global stratospheric conditions above about 18 to 20 km, but not of the lowest stratosphere where there can be significant regional and seasonal changes. A positive lower stratosphere trend of about 1 to 1.5%/year in specific humidity (about 0.04 ppm/year) since the mid-1960s is indicated by the balloon data (Oltmans *et al.*, 2000). The increase was not monotonic but showed several rapid rises with plateaux in between. Even though the recent satellite record is relatively short, these measurements have revealed changes of the same character. The satellite results show a spatial pattern of trends in the lower stratosphere, and suggest a slowing in the positive trend after 1996 (Smith *et al.*, 2000). Although not definitive, these observations are consistent in suggesting that lower-stratospheric water vapour has increased globally on average at about 1%/year over at least the past forty years, but at a variable rate.

Although radiosondes have made observations of water vapour in the upper troposphere (i.e., above 500 hPa) since the 1950s, these observations have suffered from instrumental errors (Elliott and Gaffen, 1991). Peixoto and Oort (1996) have re-examined these observations for the period 1974 to 1988 and found large trends in upper-tropospheric humidity at the 300 hPa level. They concluded that these trends were unrealistically large and were likely to be due to instrument changes. Satellite observations of upper-tropospheric humidity (UTH) measurements made by TOVS (Television infrared observation satellite Operational Vertical Sounder) since 1979, and representative of a deep layer between 500 to 200 hPa, show very large interannual variability (Bates *et al.*, 1996). The SPARC assessment of these observations (Kley *et al.*, 2000) indicated that they were of sufficient quality for trend analyses. The SPARC study and an analysis by Bates and Jackson (2001) show large regional trends that are attributed to circulation changes associated with ENSO, decadal variability over equatorial Africa, and decadal variability of the Arctic Oscillation (see Section 2.6). Statistically significant positive trends of 0.1%/year are found for 10°N to 10°S, and a non-significant trend of 0.04%/year for 60°N to 60°S, but this includes a component negative trend of -0.1%/year for 30°S to 60°S. The trends in large zonal bands

tend to be residuals from cancellations in sign and magnitude of much larger regional trends. These UTH trends should be treated with caution especially in the deep tropics because of significant interannual variability and persistence, both of which hamper trend detection.

In summary, *in situ* and radiosonde measurements tend to show increasing water vapour in the lower troposphere and near the surface, though this is not seen everywhere, and data quality is still an issue. The longer, more reliable data sets suggest multi-decadal increases in atmospheric water vapour of several per cent per decade over regions of the Northern Hemisphere. New analyses of balloon and satellite records indicate that stratospheric water vapour above 18 km shows an increase of about 1%/year for the period 1981 to 2000 but with a slowing of the positive trend after 1996. Satellite observations of upper-tropospheric humidity from 1980 to 1997 show statistically significant positive trends of 0.1%/year for the zone 10°N to 10°S.

## 2.5.4 Evaporation

Only evaporation from the land surface is discussed, as nothing new since the SAR has emerged on oceanic evaporation changes.

### 2.5.4.1 Land

The SAR reported widespread decreases of pan evaporation over the USA and Russia during the 20th century. Pan evaporation measurements are an index of evaporation from a surface with an unlimited supply of water (potential evaporation). Interpretation of this result involving potential evaporation as a decrease in actual land surface evaporation is contradictory to the temperature and precipitation increase reported in these areas, and the general intensification of the hydrological cycle over northern extra-tropical land areas (Brutsaert and Parlange, 1998). Further analysis by Lawrimore and Peterson (2000) supports Brutsaert and Parlange's (1998) interpretation, as does Golubev *et al.* (2001). Using parallel observations of actual evaporation and pan evaporation at five Russian experimental sites, Golubev *et al.* (2001) developed a method to estimate actual land surface evaporation from the pan evaporation measurements. They showed that using this method, actual evaporation is shown to have increased during the second half of the 20th century over most dry regions of the United States and Russia. Similarly, over humid maritime regions of the eastern United States (and north-eastern Washington state) actual evaporation during the warm season was also found to increase. Only over the heavily forested regions of Russia and the northern United States did actual evaporation decrease. The increase in actual evaporation is related to the greater availability of moisture at the surface, due to increases in precipitation and the higher temperatures.

## 2.5.5 Clouds

Clouds are important in the Earth's climate system because of their effects on solar radiation, terrestrial radiation and precipitation. Different cloud types contribute to total cloud amount and are associated with a wide variety of thermal and dynamic processes in the climate system (see Chapter 7, Section 7.2.2).

Therefore knowing the variations in total cloud amount and different cloud types would significantly contribute to improving our understanding of the role of clouds in contemporary climate change. Several analyses of cloud amounts for regions of the world have been performed since the SAR. Problems with data homogeneity, particularly concerning biases with changing times of observation (Sun and Groisman, 2000; Sun *et al.*, 2001) have been addressed in several studies, but other issues continue to be a source of uncertainty.

#### 2.5.5.1 Land

Dai *et al.* (1997a, 1999) and Kaiser (1998) examined cloud cover changes over the former USSR and China during the last four to five decades, to add to earlier analyses for Europe, the United States, Canada, and Australia by Henderson-Sellers (1992) and Karl and Steurer (1990). These studies show 20th century increases in cloud cover over much of the United States (mostly confined to the first 80 years) and the former USSR, which are significantly negatively correlated with changes in the diurnal range of surface air temperature (DTR) (as shown earlier in Figure 2.3). Sun and Groisman (2000) showed that in the former USSR low-level cloud cover significantly decreased during the period 1936 to 1990. However, this was more than offset by a significant increase in cumulus and cirrus clouds during the past several decades. Over much of China, however, daytime and night-time total cloud cover exhibited significant decreasing trends of 1 to 2% sky cover/decade for both day and night observations between 1951 and 1994 (Kaiser, 1998, 2000), which the DTR failed to follow (Figure 2.3). This discrepancy may result from the increasing effect of industrial aerosols on the DTR since the late 1970s (Dai *et al.*, 1999). Tuomenvirta *et al.* (2000) show increasing trends in cloud cover during the period 1910 to 1995 for northern Europe, which are consistent with decreases in the DTR. A new analysis (Neff, 1999) reveals a dramatic increase (15 to 20%) of spring and summer cloud amount at the South Pole during the past four decades in this region. This appears to be related to the observed delay in the breakdown of the spring polar vortex and is believed to be related to decreases in stratospheric temperatures.

There are few analyses of the amounts of various cloud types or changes over the tropics and sub-tropics. Correlations with observed precipitation and clouds observed by satellites suggest that much of the increase in the total cloud amount is likely to have resulted from increases in thick, precipitating clouds (Dai *et al.*, 1997a). Hahn *et al.* (1996) show decreasing decadal scale trends in cloud cover over much of China, as well as over most of South America and Africa for the period 1971 to 1991. The latter two areas have little surface-based information.

#### 2.5.5.2 Ocean

The SAR presented analyses of inter-decadal changes in marine cloud coverage. The data have now been re-examined and doubt has been cast on some of the previous findings (Bajuk and Leovy, 1998a; Norris, 1999). Additional data have also reversed some of the previous trends. In the SAR a 3% increase in cumulonimbus clouds was reported for the period 1952 to 1981. An update of

this analysis showed a gradual rise in cumulonimbus cloud amount from the mid-1950s to the mid-1970s, with a gradual decline thereafter (Bajuk and Leovy, 1998a). Bajuk and Leovy (1998b) cast doubt on the homogeneity of the cloud amounts derived from ship data. They find that inter-decadal variations of the frequency of occurrence of cloud amount for a given cloud type are generally unrelated to similar time-scale variations in SST and large-scale divergence of the surface winds. Nonetheless, some regional changes and variations based on ship reports of low and middle clouds are likely to be rather robust. Variations in these categories of cloud are consistent with variations of other climate system variables. Examples include: (1) a long-term upward trend in altostratus and nimbostratus across the mid-latitude North Pacific and North Atlantic Oceans (Parungo *et al.*, 1994; Norris and Leovy, 1995); (2) ENSO related variations in the frequency of low cloud types across the Pacific and Indian Oceans (Bajuk and Leovy, 1998b); and (3) interannual variations in summer season stratiform clouds across the North Pacific (Norris *et al.*, 1998). Norris (1999) found an increase in total sky cover of approximately 2%, and an increase of approximately 4% in low cloud cover in his analyses of ship reports between 1952 and 1995. He finds no evidence for changes in observation practices that may have affected these trends. The trends are dominated by a globally consistent mode and are as large or larger in the tropics and Southern Hemisphere as in the Northern Hemisphere. This argues against attribution to increased anthropogenic aerosol amounts.

#### 2.5.5.3 Global

Although satellite estimates of changes and variations in cloud amount and type contain systematic biases, Rossow and Schiffer (1999) showed improved calibration and cloud detection sensitivities for the International Satellite Cloud Climatology Program (ISCCP) data set. Using data from 1983 to 1994, a globally increasing trend in monthly mean cloudiness reversed during the late 1980s and early 1990s. There now appears to be an overall trend toward reduced total cloud amounts over both land and ocean during this period. An estimate for aircraft-induced cirrus cover for the late 1990s ranges from 0 to 0.2% of the surface of the Earth (IPCC, 1999).

#### 2.5.6 Summary

Since the SAR, land surface precipitation has continued to increase in the Northern Hemisphere mid- and high latitudes; over the sub-tropics, the drying trend has been ameliorated somewhat. Where data are available, changes in annual streamflow relate well to changes in total precipitation. Over the Southern Hemisphere land areas no pronounced changes in total precipitation are evident since the SAR. The changes in precipitation in mid- and high latitudes over land have a strong correlation with long-term changes in total cloud amount. Little can be said about changes in ocean precipitation as satellite data sets have not yet been adequately tested for time-dependent biases. Changes in water vapour have been analysed most for selected Northern Hemisphere regions, and show an emerging pattern of surface and tropospheric water vapour increases over the past few

decades, although there are still untested or uncorrected biases in these data. Limited data from the stratosphere also suggest increases in water vapour but this result must be viewed with great caution. Over land, an increase in cloud cover of a few per cent since the turn of the century is observed, which is shown to closely relate to changes in the diurnal temperature range. Changes in ocean cloud amount and type show systematic increases of a few per cent since the 1950s, but these relate poorly to SST or surface wind divergence changes, casting some doubt on the integrity of the trends. No changes in observing practices can be identified, however, that might have led to time-dependent biases in the ocean cloud amount and frequency statistics.

## 2.6 Are the Atmospheric/Oceanic Circulations Changing?

### 2.6.1 Background

Changes or fluctuations in atmospheric and oceanic circulation are important elements of climate. Such circulation changes are the main cause of variations in climate elements on a regional scale, sometimes mediated by parallel changes in the land surface (IPCC, 1990, 1996). ENSO and NAO are such examples. On decadal time-scales, the Pacific Decadal Oscillation (PDO) and the related Inter-decadal Pacific Oscillation (IPO) may account for approximately half the global mean variation in surface temperatures. They are also prominently linked to regional variations in temperature and precipitation (Higgins *et al.*, 2000). This section documents regional changes and slow fluctuations in atmospheric circulation over past decades, and demonstrates that these are consistent with large-scale changes in other variables, especially temperature and precipitation. Note that there is much evidence that many of the atmospheric circulation changes we observe, particularly in the extra-tropics, are the net result of irregular fluctuations between preferred states of the atmosphere (Palmer, 1993, 1999) that last for much shorter times. Thus changes in circulation on decadal time-scales involve changes in the frequency of such states. Chapter 7 discusses this in more detail. The focus of this section is on long-term variation and change, rather than on shorter-term variability.

### 2.6.2 El Niño-Southern Oscillation and Tropical/Extra-tropical Interaction

ENSO is the primary global mode of climate variability in the 2 to 7 year time band. El Niño is defined by SST anomalies in the eastern tropical Pacific while the Southern Oscillation Index (SOI) is a measure of the atmospheric circulation response in the Pacific-Indian Ocean region. This sub-section assesses the variability of ENSO over the past few centuries.

Multiproxy-based reconstructions of the behaviour of ENSO have recently been attempted for the past few centuries, including a boreal winter season SOI reconstruction based on highly ENSO-sensitive tree-ring indicators (Stahle *et al.*, 1998). A multiproxy-based reconstruction of the boreal cold-season (Oct-Mar) NINO 3 (SST anomalies in the tropical Pacific from 5°N to 5°S, 150°W to 90°W) index (Mann *et al.*, 2000b) has also been made. Figure 2.28 compares the behaviour of these

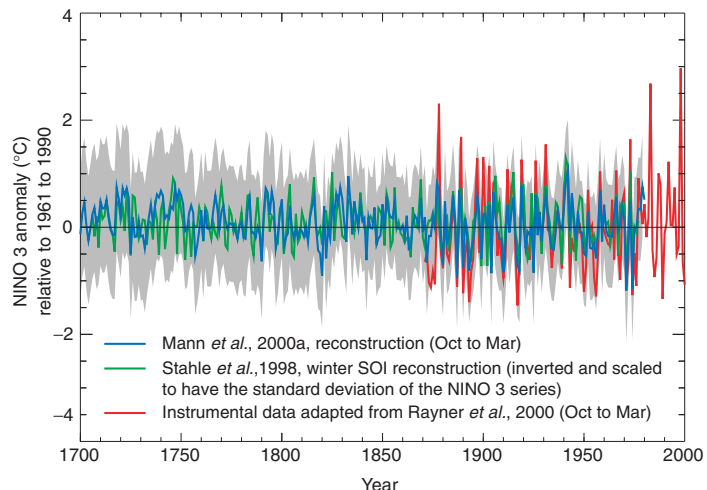


**Figure 2.28:** Reconstructions since 1700 of proxy-based ENSO indices. Shown are the Northern Hemisphere cold-season (Oct-Mar) mean NINO 3 index of Mann *et al.* (2000a) and the Northern Hemisphere winter SOI index of Stahle *et al.* (1998). The SOI series is scaled to have the same standard deviation as the NINO 3 index, and is reversed in sign to be positively correlated with the NINO 3 series. An instrumental NINO 3 index from 1871 to 2000 is shown for comparison (Rayner *et al.*, 2000; see also Figure 2.29), with two standard error limits (grey shaded) of the proxy NINO 3 reconstruction.

two series with recent ENSO behaviour. The SOI reconstruction has been rescaled to have the sign and variance of the NINO 3 reconstruction; the two reconstructions, based on independent methods and partially independent data, have a linear correlation ( $r=0.64$ ) during the pre-calibration interval. While the estimated uncertainties in these reconstructed series are substantial, they suggest that the very large 1982/83 and 1997/98 warm events might be outside the range of variability of the past few centuries. However, the reconstructions tend to underestimate the amplitude of ENSO events, as is clearly evident for the large 1877/78 event. Only a richer network of ENSO-sensitive proxy indicators can improve this situation, such as the new long tropical coral series becoming available (see Dunbar and Cole, 1999).

Instrumental records have been examined to search for possible changes in ENSO over the past 120 years. Three new reconstructions of SST in the eastern Equatorial Pacific (Figure 2.29) that use optimum interpolation methods exhibit strong similarities. The dominant 2 to 6 year time-scale in ENSO is apparent. Both the activity and periodicity of ENSO have varied considerably since 1871 with considerable irregularity in time. There was an apparent “shift” in the temperature of the tropical Pacific around 1976 to warmer conditions, discussed in the SAR, which appeared to continue until at least 1998. During this period ENSO events were more frequent, intense or persistent. It is unclear whether this warm state continues, with the persistence of the long La Niña from late 1998 until early 2001. ENSO has been related to variations of precipitation and temperature over much of the tropics and sub-tropics, and some mid-latitude areas.

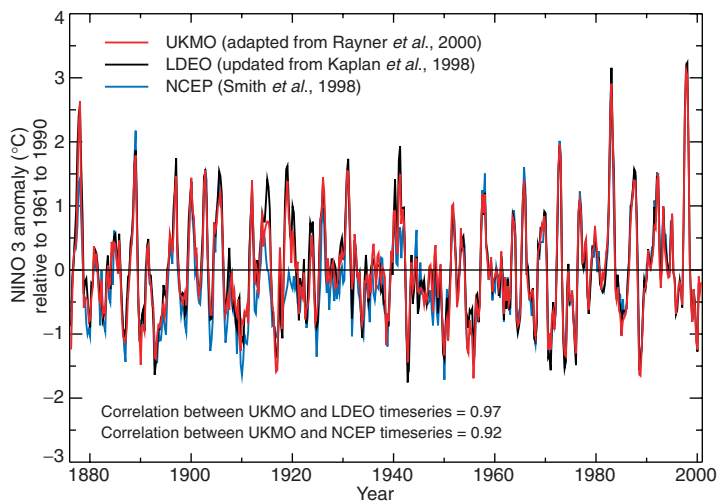


**Figure 2.29:** El Niño-La Niña variations from 1876 to 2000 measured by sea surface temperature in the region 5°N to 5°S, 150 to 90°W. Reconstructions using pattern analysis methods from (a) red: UK Met Office (UKMO) Hadley Centre sea ice and sea surface temperature data set version 1 (Rayner *et al.*, 2000); (b) black: from the Lamont-Doherty Earth Observatory (LDEO) (Kaplan *et al.*, 1998); (c) blue: the National Centers for Environmental Prediction (NCEP) analysis (Smith *et al.*, 1998). 1876 is close to the earliest date for which reasonably reliable reconstructions can be made.

A number of recent studies have found changes in the interannual variability of ENSO over the last century, related in part to an observed reduction in ENSO variability between about 1920 and 1960. Various studies (Wang and Wang, 1996; Torrence and Compo, 1998; Torrence and Webster, 1998; Kestin *et al.*, 1999) show more robust signals in the quasi-biennial and ‘classical’ 3 to 4 year ENSO bands (3.4 and 7 years) during the first and last 40 to 50 years of the instrumental record. A period of very weak signal strength (with a near 5-year periodicity) occurs in much of the intervening epoch.

The 1990s have received considerable attention, as the recent behaviour of ENSO seems unusual relative to that of previous decades. A protracted period of low SOI from 1990 to 1995, during which several weak to moderate El Niño events occurred with no intervening La Niña events (Goddard and Graham, 1997) was found by some studies (e.g., Trenberth and Hoar, 1996) to be statistically very rare. Whether global warming is influencing El Niño, especially given the remarkable El Niño of 1997/98, is a key question (Trenberth, 1998b), especially as El Niño affects global temperature itself (Section 2.2 and Chapter 7).

### 2.6.3 Decadal to Inter-decadal Pacific Oscillation, and the North Pacific Oscillation

Recently, ‘ENSO-like’ spatial patterns in the climate system, which operate on decadal to multi-decadal time-scales, have been identified. This lower-frequency SST variability is less equatorially confined in the central and eastern Pacific, and relatively more prominent over the extra-tropics, especially the north-west

Pacific, and has a similar counterpart in night marine air temperatures (Tanimoto *et al.*, 1993; Folland *et al.*, 1999a; Allan, 2000). The corresponding sea level pressure (SLP) signature is also strongest over the North Pacific, and its December–February counterpart in the mid-troposphere more closely resembles the Pacific-North America (PNA) pattern (Zhang *et al.*, 1997b; Livezey and Smith, 1999). There is ambiguity about whether inter-decadal Pacific-wide features are independent of global warming. In the longer Folland *et al.* (1999) analyses since 1911 they appear to be largely independent, but in the Livezey and Smith analysis of more recent SST data they are an integral part of a global warming signal. Using a different method of analysis of data since 1901, Moron *et al.* (1998) find a global warming signal whose pattern in the Pacific is intermediate between these two analyses.

The PDO of Mantua *et al.* (1997), with lower-frequency variations in the leading North Pacific SST pattern, may be related to the same Pacific-wide features, and parallels the dominant pattern of North Pacific SLP variability. The relationship is such that cooler than average SSTs occur during periods of lower than average SLP over the central North Pacific and *vice versa*. Recently, the IPO, a Pacific basin-wide feature, has been described, which includes low-frequency variations in climate over the North Pacific (Power *et al.*, 1998, 1999; Folland *et al.*, 1999a). The time-series of this feature is broadly similar to the inter-decadal part of the North Pacific PDO index of Mantua *et al.* (1997). The IPO may be a Pacific-wide manifestation of the PDO and seems to be part of a continuous spectrum of low-frequency modulation of ENSO, and so may be partly stochastic. When the IPO is in a positive phase, SST over a large area of the south-west Pacific is cold, as is SST over the extra-tropical north-west Pacific. SST over the central tropical Pacific is warm but less obviously warm over the equatorial far eastern Pacific unlike ENSO. Warmth also extends into the tropical west Pacific, unlike the situation on the ENSO time-scale.

The IPO shows three major phases this century: positive from 1922 to 1946 and from 1978 to at least 1998, with a negative phase between 1947 and 1976. Arguably, the structure of this pattern, nearly symmetrical about the equator and only subtly different from ENSO, is a strong indication of the importance of the tropical Pacific for many remote climates on all time-scales (Garreaud and Battisti, 1999). Power *et al.* (1999) showed that the two phases of the IPO appear to modulate year-to-year ENSO precipitation variability over Australia. Salinger and Mullan (1999) showed that prominent sub-bidecadal climate variations in New Zealand, identified in the temperature signal by Folland and Salinger (1995), are related to a SST pattern like the IPO. The IPO is a significant source of decadal climate variation throughout the South Pacific, and modulates ENSO climate variability in this region (Salinger *et al.*, 2001). Similarly, the PDO (and likely the IPO) may play a key role in modulating ENSO teleconnections across North America on inter-decadal time-scales (Gershunov and Barnett, 1998; Livezey and Smith, 1999).

A simple and robust index of climate variability over the North Pacific is the area-weighted mean SLP, averaged over most of the extra-tropical North Pacific Ocean, of Trenberth and Hurrell

(1994). A general reduction in SLP after about 1976 has been particularly evident during the winter half (November to March) of many of these years. This is characterised by a deeper-than-normal Aleutian low pressure system, accompanied by stronger-than-normal westerly winds across the central North Pacific and enhanced southerly to south-westerly flow along the west coast of North America, as reviewed in the SAR (Figure 3.17). Consequently, there have been increases in surface air temperature and SST over much of western North America and the eastern North Pacific, respectively, over the past two decades, especially in winter, but decreases in SST, or only modest warming, over parts of the central extra-tropical North Pacific (Figure 2.10). Numerous studies have suggested that the mid-1970s changes in the atmospheric and oceanic circulation may reflect one or more low-frequency variations over the North Pacific, one being the PDO (Kawamura, 1994; Latif and Barnett, 1994; Mann and Park, 1994, 1996; Deser and Blackmon 1995; Zhang *et al.*, 1997b; White and Cayan, 1998; Enfield and Mestas-Núñez, 1999).

#### 2.6.4 Monsoons

Variations in the behaviour of the North African summer monsoon were highlighted in IPCC (1990). Moron (1997) demonstrated that long-term variations of Sahel annual rainfall, particularly the wet 1950s and the dry 1970 to 1980s, are seen over the Guinea coast area, although trends are strongest in the Sahel. The significant decrease in Guinea coast rainfall (Ward, 1998) is present in both the first and second rainy seasons, but is strongest in the second. Janicot *et al.* (1996) and Moron (1997) demonstrated that the moderate influence of ENSO (towards drier conditions) has increased since 1960, with warm events associated more strongly with large-scale anomalous dry conditions over the Guinea and Sahel belts. Ward *et al.* (1999) show that the Sahel has become moderately wetter since 1987, despite the increased drying influence of ENSO events, a trend that continued to 1999 (Parker and Horton, 2000). This recent behaviour may be related to a quasi-hemispheric variation of SST (e.g., Enfield and Mestas-Núñez, 1999) shown to be related to Sahel rainfall by Folland *et al.* (1986), and which may be related to the recent strong increase in North Atlantic SST mentioned in Section 2.2.2.2. Many other parts of tropical Africa are influenced by ENSO towards either drier or wetter conditions than normal, sometimes modulated by regional SST anomalies near Africa (e.g., Nicholson and Kim, 1997; Nicholson, 1997; Indeje *et al.*, 2000), but few trends can be discerned.

Multi-decadal and decadal variations of the Indian monsoon have been widely noted (e.g., Pant and Kumar, 1997) but links with El Niño do not now seem straightforward (Slingo *et al.*, 1999). However, despite the recent strong El Niño episodes, the inverse relationship between the ENSO and the Indian summer monsoon (weak monsoon arising from an ENSO event) has broken down in the recent two decades (Kumar *et al.*, 1999a). This link operated on multi-decadal time-scales with NINO 3 SST until at least 1970. Kumar *et al.* suggest that persistently increased surface temperatures over Eurasia in winter and spring (Figure 2.10) have favoured an enhanced land-ocean thermal

gradient conducive to stronger monsoons; they also observe a shift away from India in the sinking node of the Walker circulation in El Niño. Changes have also occurred in relationships with Indian monsoon precursors (Kumar *et al.*, 1999b). One possibility is that warming over the Indian Ocean (Figures 2.9, 2.10) may have increased moisture and rainfall for a given state of the atmospheric circulation (Kitoh *et al.*, 1997). There may be a link to multi-decadal variations in Pacific SST, but this remains to be investigated, together with other monsoon indices (e.g., Goswami *et al.*, 1997).

It has been known for some time that the position of the western North Pacific sub-tropical high affects the East Asian monsoon. Gong and Wang (1999a) showed that summer (June to August) precipitation over central and eastern China near 30°N is positively correlated with the intensity of the high, with negative correlations to the north and south. A location of the sub-tropical high further south than normal is conducive to heavy summer rainfall in this region. Time-series of the sub-tropical high show an increase in areal extent in the 1920s, then another increase from the mid-1970s to 1998, giving frequent wet summers in this region in recent years. The north-east winter monsoon has also shown low-frequency variations. Thus the strength of the Siberian high increased to a peak around 1968, and then weakened to a minimum around 1990 (Gong and Wang, 1999b), in phase with the increased frequency of the positive phase of the NAO (Wallace, 2000 and next section). This is likely to have contributed to strong recent winter warming in China shown in Figure 2.10.

#### 2.6.5 The Northern Hemisphere excluding the North Pacific Ocean

The atmospheric circulation over the Northern Hemisphere has exhibited anomalous behaviour over the past several decades. In particular, the dominant patterns of atmospheric variability in the winter half-year have tended to be strongly biased to one phase. Thus SLP has been lower than average over the mid- and high latitudes of the North Atlantic Ocean, as well as over much of the Arctic, while it has been higher than average over the sub-tropical oceans, especially the Atlantic. Moreover, in the past thirty years, changes in these leading patterns of natural atmospheric variability appear to be unusual in the context of the observational record.

The dominant pattern of atmospheric circulation variability over the North Atlantic is known as the NAO, and its wintertime index is shown in Figure 2.30 (updated from Hurrell, 1995). As discussed in the SAR, positive values of the NAO give stronger than average westerlies over the mid-latitudes of the Atlantic with low SLP anomalies in the Icelandic region and over much of the Arctic and high SLP anomalies across the sub-tropical Atlantic and into southern Europe. The positive, enhanced westerly, phase of the NAO is associated with cold winters over the north-west Atlantic and warm winters over Europe, Siberia and eastern Asia (Thompson and Wallace, 2001) as well as wet conditions from Iceland to Scandinavia and dry winters over southern Europe. A sharp reversal is evident in the NAO index starting around 1970 from a negative towards a positive phase.

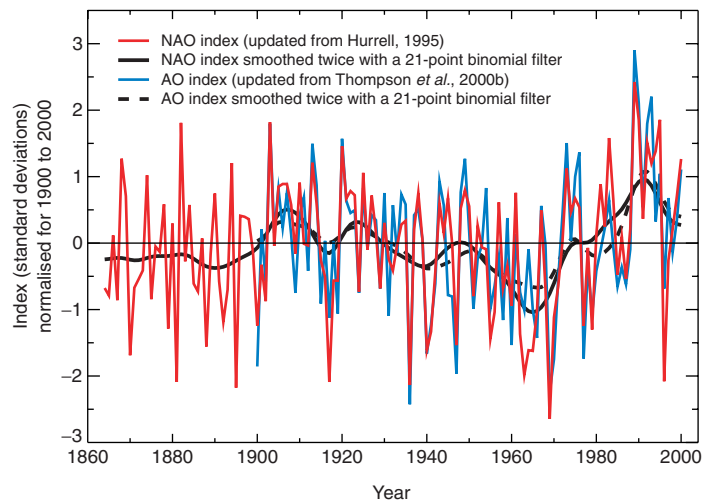


**Figure 2.30:** December to March North Atlantic Oscillation (NAO) indices, 1864 to 2000, and Arctic Oscillation (AO) indices, 1900 to 2000, updated from Hurrell (1995) and updated from Thompson and Wallace (2000) and Thompson *et al.* (2000b), respectively. The indices were normalised using the means and standard deviations from their common period, 1900 to 2000, smoothed twice using a 21-point binomial filter where indicated and then plotted according to the years of their Januaries.

Since about 1985, the NAO has tended to remain in a strong positive phase, though with substantial interannual variability. Hurrell (1996) and Thompson *et al.* (2000a) showed that the recent upward trend in the NAO accounts for much of the regional surface winter half-year warming over northern Europe and Asia north of about 40°N over the past thirty years, as well as the cooling over the north-west Atlantic (see Section 2.2.2.3). Moreover, when circulation changes over the North Pacific are also considered, much of the pattern of the Northern Hemisphere winter half-year surface temperature changes since the mid-1970s can be explained. This can be associated with changes in the NAO, and in the PNA atmospheric pattern related to ENSO or the PDO (Graf *et al.*, 1995; Wallace *et al.*, 1995; Shabbar *et al.*, 1997; Thompson and Wallace, 1998, 2000).

The changes in atmospheric circulation over the Atlantic are also connected with much of the observed pressure fall over the Arctic in recent years (Walsh *et al.*, 1996). Other features related to the circulation changes include the strengthening of sub-polar westerlies from the surface of the North Atlantic up, in winter as high as the lower stratosphere (Thompson *et al.*, 2000a) and pronounced regional changes in precipitation patterns (Hurrell, 1995; Dai *et al.*, 1997b; Hurrell and van Loon 1997; Section 2.5.2.1). Associated precipitation increases have resulted in the notable advance of some Scandinavian glaciers (Hagen *et al.*, 1995), while decreases to the south of about 50°N have contributed to the further retreat of Alpine glaciers (Frank, 1997; see also Section 2.2.5.3).

The NAO is regarded (largely) by some as the regional expression of a zonally symmetrical hemispheric mode of variability characterised by a seesaw of atmospheric mass between the polar cap and the mid-latitudes in both the Atlantic

and Pacific Ocean basins (Thompson and Wallace, 1998, 2001). This mode has been named the AO (Figure 2.30). The time-series of the NAO and AO are quite similar: the correlation of monthly anomalies of station data SLP series of NAO and AO is about 0.7 (depending on their exact definitions and epochs) while seasonal variations shown in Figure 2.30 have even higher correlations. The NAO and AO can be viewed as manifestations of the same basic phenomenon (Wallace, 2000).

Changes and decadal fluctuations in sea-ice cover in the Labrador and Greenland Seas, as well as over the Arctic, appear well correlated with the NAO (Chapman and Walsh, 1993; Maslanik *et al.*, 1996; McPhee *et al.*, 1998; Mysak and Venegas, 1998; Parkinson *et al.*, 1999; Deser *et al.*, 2000). The relationship between the SLP and ice anomaly fields is consistent with the idea that atmospheric circulation anomalies force the sea-ice variations (Prisenberg *et al.*, 1997). Feedbacks or other influences of winter ice anomalies on the atmosphere have been more difficult to detect, although Deser *et al.* (2000) suggest that a local response of the atmospheric circulation to the reduced sea-ice cover east of Greenland in recent years is also apparent (see also Section 2.2.5.2).

A number of studies have placed the recent positive values of the NAO into a longer-term perspective (Jones *et al.*, 1997a; Appenzeller *et al.*, 1998; Cook *et al.*, 1998; Luterbacher *et al.*, 1999; Osborn *et al.*, 1999) back to the 1700s. The recent strength of the positive phase of the NAO seems unusual from these reconstructions but, as in Figure 2.28, these proxy data reconstructions may underestimate variability. An extended positive phase occurred in the early 20th century (Figure 2.30), particularly pronounced in January (Parker and Folland, 1988), comparable in length to the recent positive phase. Higher-frequency variability of the NAO also appears to have varied. Hurrell and van Loon (1997) showed that quasi-decadal (6 to 10 year) variability has become more pronounced over the latter half of the 20th century, while quasi-biennial variability dominated in the early instrumental record.

## 2.6.6 The Southern Hemisphere

Since the SAR there has been more emphasis on analysis of decadal variability over the Southern Hemisphere. The Southern Hemisphere gridded SLP data for the period 1950 to 1994 show two dominant modes in annual average values, similar to those identified by Karoly *et al.* (1996) using station data. The first mode unambiguously represents the Southern Oscillation and reflects the tendency towards more frequent and intense negative phases over the past several decades. The second mode represents anomalies throughout the mid-latitude regions across the Indian Ocean and western Pacific, which contrast with anomalies elsewhere.

The Trans-Polar Index (TPI) is the only large-scale station pressure-based extra-tropical Southern Hemisphere circulation index in regular use. It is based on the normalised pressure difference between New Zealand and South America and has been recalculated and extended by Jones *et al.* (1999b). On decadal and longer time-scales the TPI reflects movement in the phase of wave number one around the Southern Hemisphere.

Troughing (low pressure) was more frequent in the New Zealand region in the 1920s, and at a maximum in the 1940s. Anticyclonicity was favoured from the late 1950s to 1976, with troughing in the South American sector. Troughing was again apparent in the New Zealand sector in the 1990s (Salinger *et al.*, 1996).

A leading mode of variability in the extra-tropical Southern Hemisphere circulation on interannual to multi-decadal time-scales is a zonally elongated north-south dipole structure over the Pacific, stretching from the sub-tropics to the Antarctic coast (Mo and Higgins, 1998; Kidson, 1999; Kiladis and Mo, 1999). It is strongly related to ENSO variability. The lower-frequency dipole structure contributes to variability in blocking frequency across the far south Pacific (Renwick, 1998; Renwick and Revell, 1999).

ENSO variability is also implicated in the modulation of a ‘High Latitude Mode’ (HLM) (Kidson, 1988; Karoly, 1990), especially over the austral summer. The HLM is now also called the ‘Antarctic Oscillation’ (AAO); they appear to be the same phenomenon with the same structure (Thompson and Wallace, 2000). The AAO is a zonal pressure fluctuation between mid- and high latitudes of the Southern Hemisphere, centred on 55 to 60°S. It has recently been further studied (Gong and Wang, 1999c; Kidson, 1999; Thompson and Wallace, 2001; Figure 2.31) and shown to extend into the lower stratosphere between the Antarctic and the sub-tropical latitudes of the Southern Hemisphere. The AAO appears to persist all year but may be most active from mid-October to mid-December when it extends into the stratosphere (Thompson and Wallace, 2001). In its high index phase, it consists of low pressure or heights above the Antarctic and the near Southern Ocean with high heights north of about 50°S. Although the data are sparse, there is evidence that, like the NAO, the AAO has tended to move more towards a positive index phase, despite lower pressures being observed over the New Zealand region during the 1990s. This change is also associated with increasing westerly winds in mid-latitudes. Thompson and Wallace (2001) show that most of Antarctica is rather cold in this phase, except for the Antarctic Peninsula which is warm due to additional advection of relatively warm air from seas to the west. This may explain some of the behaviour of Antarctic temperatures in the last two decades (Figure 2.10; Comiso, 2000).

Other work has identified the likely existence of an Antarctic Circumpolar Wave (ACW) (Jacobs and Mitchell, 1996; White and Peterson, 1996), a multi-annual climate signal in the Southern Ocean, with co-varying and perhaps coupled SST and SLP anomalies that move around the Southern Ocean. Its long-term variability is not yet known.

### 2.6.7 Summary

The interannual variability of ENSO has fluctuated substantially over the last century, with notably reduced variability during the period 1920 to 1960, compared with adjacent periods. It remains unclear whether global warming has influenced the shift towards less frequent La Niña episodes from 1976 to 1998, including the abnormally protracted ENSO

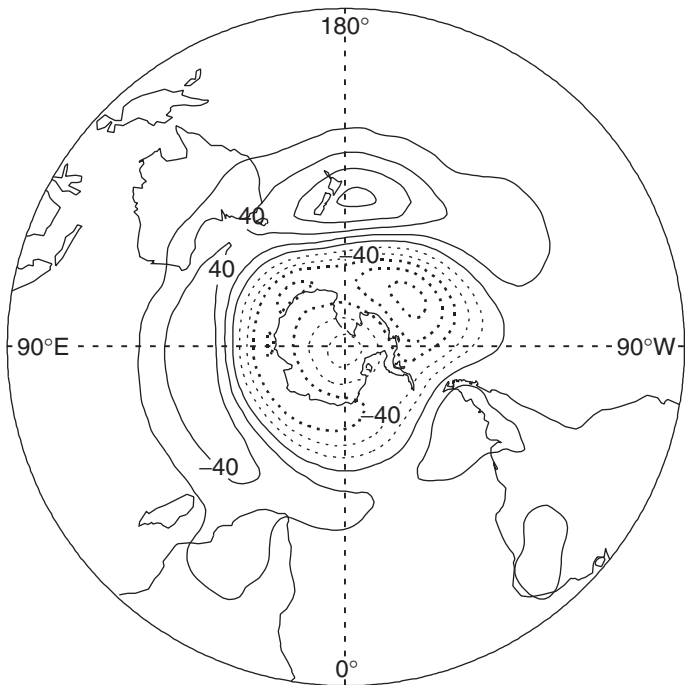


**Figure 2.31:** The High Latitude Mode (Kidson, 1988) or Antarctic Oscillation (AAO), defined as the first orthogonal pattern (covariance eigenvector of the Southern Hemisphere monthly surface pressure, January 1958 to December 1997) (Gong and Wang, 1999c; Kiladis and Mo, 1999). Data from NCAR/NCEP Reanalysis (Kalnay *et al.*, 1996). Note that Thompson and Wallace (2000) use 850 hPa height to define their AAO.

1990 to 1995 event and the exceptionally strong 1982/83 and 1997/98 events. Analysis of SST patterns indicates that a global warming pattern may have increased the background temperature in the region most affected by ENSO, but there is some ambiguity in the details of this pattern.

Since the SAR, ‘ENSO-like’ features operating on decadal to multi-decadal time-scales have been identified, such as the PDO and IPO. They appear to be part of a continuous spectrum of ENSO variability that has subtly changing SST patterns as time-scales increase and which may have distinctive effects on regional climate around the Pacific basin. For the period since 1900, El Niño (La Niña) events are more prevalent during positive (negative) phases of the IPO.

In the Northern Hemisphere, pronounced changes in winter atmospheric and oceanic circulations over the North Pacific in the 1970s (the North Pacific Oscillation) have been paralleled by wintertime circulation changes over the North Atlantic, recorded by the NAO. In the North Pacific, spatially coherent changes have occurred in surface temperature across the North Pacific and western North America, while the enhanced westerly phase of the NAO has caused considerable winter half-year temperature and precipitation changes over a vast area of extra-tropical Eurasia. In the Southern Hemisphere, a feature quite like the NAO, the HLM or the AAO, also appears to have moved into an enhanced westerly phase in middle latitudes.

## 2.7 Has Climate Variability, or have Climate Extremes, Changed?

### 2.7.1 Background

Changes in climate variability and extremes of weather and climate events have received increased attention in the last few years. Understanding changes in climate variability and climate extremes is made difficult by interactions between the changes in the mean and variability (Meehl *et al.*, 2000). Such interactions vary from variable to variable depending on their statistical distribution. For example, the distribution of temperatures often resembles a normal distribution where non-stationarity of the distribution implies changes in the mean or variance. In such a distribution, an increase in the

mean leads to new record high temperatures (Figure 2.32a), but a change in the mean does not imply any change in variability. For example, in Figure 2.32a, the range between the hottest and coldest temperatures does not change. An increase in variability without a change in the mean implies an increase in the probability of both hot and cold extremes as well as the absolute value of the extremes (Figure 2.32b). Increases in both the mean and the variability are also possible (Figure 2.32c), which affects (in this example) the probability of hot and cold extremes, with more frequent hot events with more extreme high temperatures and fewer cold events. Other combinations of changes in both mean and variability would lead to different results.

Consequently, even when changes in extremes can be documented, unless a specific analysis has been completed, it is often uncertain whether the changes are caused by a change in the mean, variance, or both. In addition, uncertainties in the rate of change of the mean confound interpretation of changes in variance since all variance statistics are dependent on a reference level, i.e., the mean.

For variables that are not well approximated by normal distributions, like precipitation, the situation is even more complex, especially for dry climates. For precipitation, for example, changes in the mean total precipitation can be accompanied by other changes like the frequency of precipitation or the shape of the distribution including its variability. All these changes can affect the various aspects of precipitation extremes including the intensity of precipitation (amount per unit time).

This section considers the changes in variability and extremes simultaneously for two variables, temperature and precipitation. We include new analyses and additional data compiled since the SAR which provide new insights. We also assess new information related to changes in extreme weather and climate phenomena, e.g., tropical cyclones, tornadoes, etc. In these analyses, the primary focus is on assessing the stationarity (e.g., the null hypothesis of no change) of these events, given numerous inhomogeneities in monitoring.

### 2.7.2 Is There Evidence for Changes in Variability or Extremes?

The issues involved in measuring and assessing changes in extremes have recently been comprehensively reviewed by Trenberth and Owen (1999), Nicholls and Murray (1999), and Folland *et al.* (1999b). Despite some progress described below, there remains a lack of accessible daily climate data sets which can be intercompared over large regions (Folland *et al.*, 2000). Extremes are a key aspect of climate change. Changes in the frequency of many extremes (increases or decreases) can be surprisingly large for seemingly modest mean changes in climate (Katz, 1999) and are often the most sensitive aspects of climate change for ecosystem and societal responses. Moreover, changes in extremes are often most sensitive to inhomogeneous climate monitoring practices, making assessment of change more difficult than assessing the change in the mean.

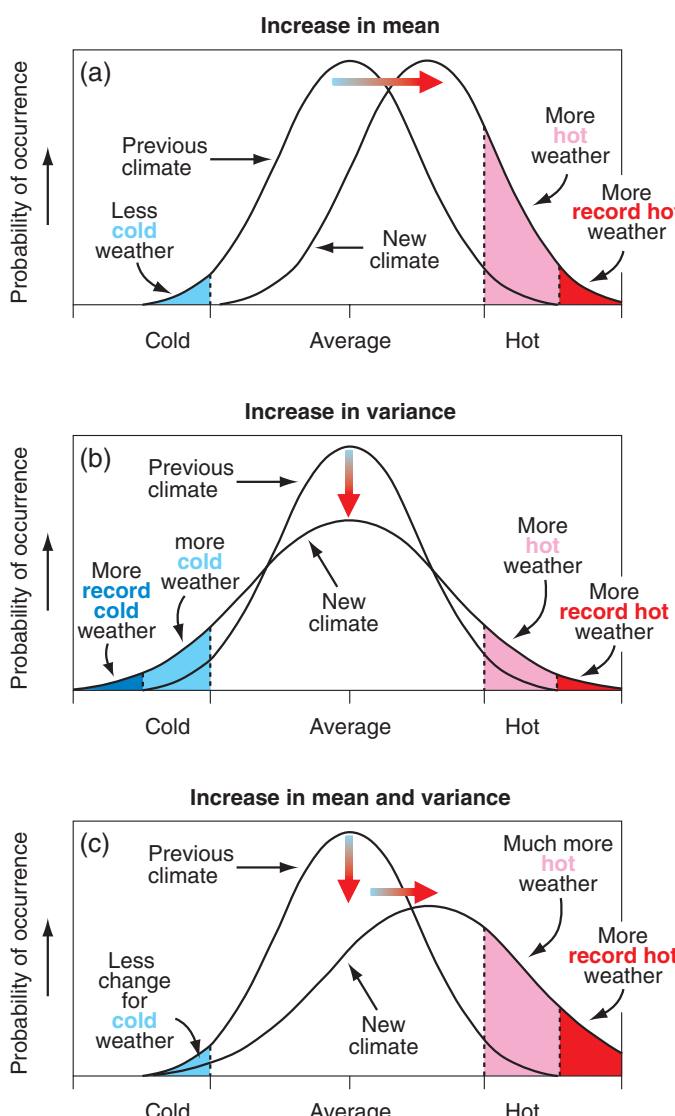


**Figure 2.32:** Schematic showing the effect on extreme temperatures when (a) the mean temperature increases, (b) the variance increases, and (c) when both the mean and variance increase for a normal distribution of temperature.

### 2.7.2.1 Temperature

Given the number of ways in which extreme climate events and variability about the mean can be defined, (e.g., extreme daily temperatures, large areas experiencing unusual temperatures, severity of heat waves, number of frosts or freezes, changes in interannual variability of large area temperatures, etc.) extreme care must be exercised in generalising results. Here we assess the evidence for changes in temperature extremes or variability, first based on global analyses and then on more detailed regional analyses.

Parker *et al.* (1994) compared the interannual variability of seasonal temperature anomalies from the 1954 to 1973 period to the 1974 to 1993 period for most of the globe. They found a small increase in variability overall with an especially large increase in central North America. By restricting the analyses to the latter half of the 20th century, Parker *et al.* (1994) minimised the potential biases due to an increasing number of observations in this period. Several other studies found a reduction in other aspects of variability over longer time periods. Jones (1999) also analysed global data and found no change in variability, but since 1951 the rise in global mean temperatures can be attributed to an increase (decrease) in areas with much above (below) normal temperatures. They also analysed the change in the aggregated total of much below and much above normal temperatures (upper and lower ten percentiles). They found little overall change, except for a reduced number of much above or below normal temperatures during the 1960s and 1970s. Michaels *et al.* (1998) examined  $5^\circ$  latitude  $\times$   $5^\circ$  longitude monthly temperature anomalies for many grid cells around the world and found an overall decrease in intra-annual variance over the past 50 to 100 years. They also examined the daily maximum and minimum temperatures from the United States, China, and the former Soviet Union and found a general decline in the intra-monthly temperature variability. As reported in the SAR, a related analysis by Karl *et al.* (1995b) found reduced day-to-day variability during the 20th century in the Northern Hemisphere, particularly in the United States and China. Recently, Collins *et al.* (2000) has identified similar trends in Australia. By analysing a long homogenised daily temperature index for four stations in Northern Europe, Moberg *et al.* (2000) also found a progressive reduction in all-seasons inter-daily variability of about 7% between 1880 and 1998. Balling (1998) found an overall decrease in the spatial variance of both satellite-based lower-tropospheric measurements from 1979 to 1996 and in near-surface air temperatures from 1897 to 1996.

Consequently, there is now little evidence to suggest that the interannual variability of global temperatures has increased over the past few decades, but there is some evidence to suggest that the variability of intra-annual temperatures has actually quite widely decreased. Several analyses find a decrease in spatial and temporal variability of temperatures on these shorter time-scales.

There have been a number of new regional studies related to changes in extreme temperature events during the 20th century. Gruza *et al.* (1999) found statistically significant increases in the number of days with extreme high temperatures across Russia using data back to 1961 and on a monthly basis back to 1900. Frich *et al.* (2001) analysed data spanning the last half of the 20th century across most of the Northern Hemisphere mid- and high

latitudes and found a statistically significant increase (5 to  $>15\%$ ) in the growing season length in many regions. Heino *et al.* (1999) also found that there has been a reduction in the number of days with frost (the number of days with minimum temperature  $\leq 0^\circ\text{C}$ ) in northern and central Europe. Thus, some stations now have as many as 50 fewer days of frost per year compared with earlier in the 20th century. Easterling *et al.* (2000) found there has been a significant decrease in the number of days below freezing over the central United States (about seven per year). For Canada, Bonsal *et al.* (2001) also found fewer days with extreme low temperatures during winter, spring and summer, and more days with extreme high temperatures during winter and spring. This has led to a significant increase in the frost-free period. Decreasing numbers of days with freezing temperatures have been found in Australia and New Zealand over recent decades (Plummer *et al.*, 1999; Collins *et al.*, 2000). In addition, while increases in the frequency of warm days have been observed, decreases in the number of cool nights have been stronger. Frich *et al.* (2001) show a reduced number of days with frost across much of the globe (Figure 2.33) while Michaels *et al.* (2000) find that much of the warming during the 20th century has been during the cold season in the mid- to high latitudes, consistent with the reduction of extremely low temperatures. Frich *et al.* (2001) have also found a statistically significant reduction in the difference between the annual extremes of daily maximum and minimum temperatures during the latter half of the 20th century. In China, strong increases in the absolute minimum temperature have been observed, with decreases in the 1-day seasonal extreme maximum temperature (Zhai *et al.*, 1999a) since the 1950s. Wang and Gaffen (2001), however, for a similar period, found an increase in ‘hot’ days in China. Hot days were defined as those days above the 85th percentile during July and August based on an ‘apparent temperature’ index related to human discomfort in China (Steadman, 1984). The number of extremely cold days has also been shown to be decreasing in China (Zhai *et al.*, 1999a). Manton *et al.* (2001) found significant increases in hot days and warm nights, and decreases in cool days and cold nights since 1961 across the Southeast Asia and South Pacific Region. Jones *et al.* (1999c) have analysed the 230-year-long daily central England data set that has been adjusted for observing inhomogeneities. They found that the increase in temperature observed in central England corresponds mainly to a reduction in the frequency of much below normal daily temperatures. An increase of the frequency of much above normal temperatures was less apparent.

Analyses of 20th century trends in the United States of short-duration episodes (a few days) of extreme hot or cold weather did not show any significant changes in frequency or intensity (Kunkel *et al.*, 1996, 1999; Karl and Knight, 1997). For Australia, Collins *et al.* (2000) found higher frequencies of multi-day warm nights and days, and decreases in the frequency of cool days and nights. In an extensive assessment of the change in frequency of heat waves during the latter half of the 20th century, Frich *et al.* (2001) find some evidence for an increase in heat-wave frequency, but several regions have opposite trends (Figure 2.33c). The extreme heat in the United States during several years in the 1930s dominates the time-series of heat waves in that region. On the other hand, trends in the frequency of extreme apparent tempera-

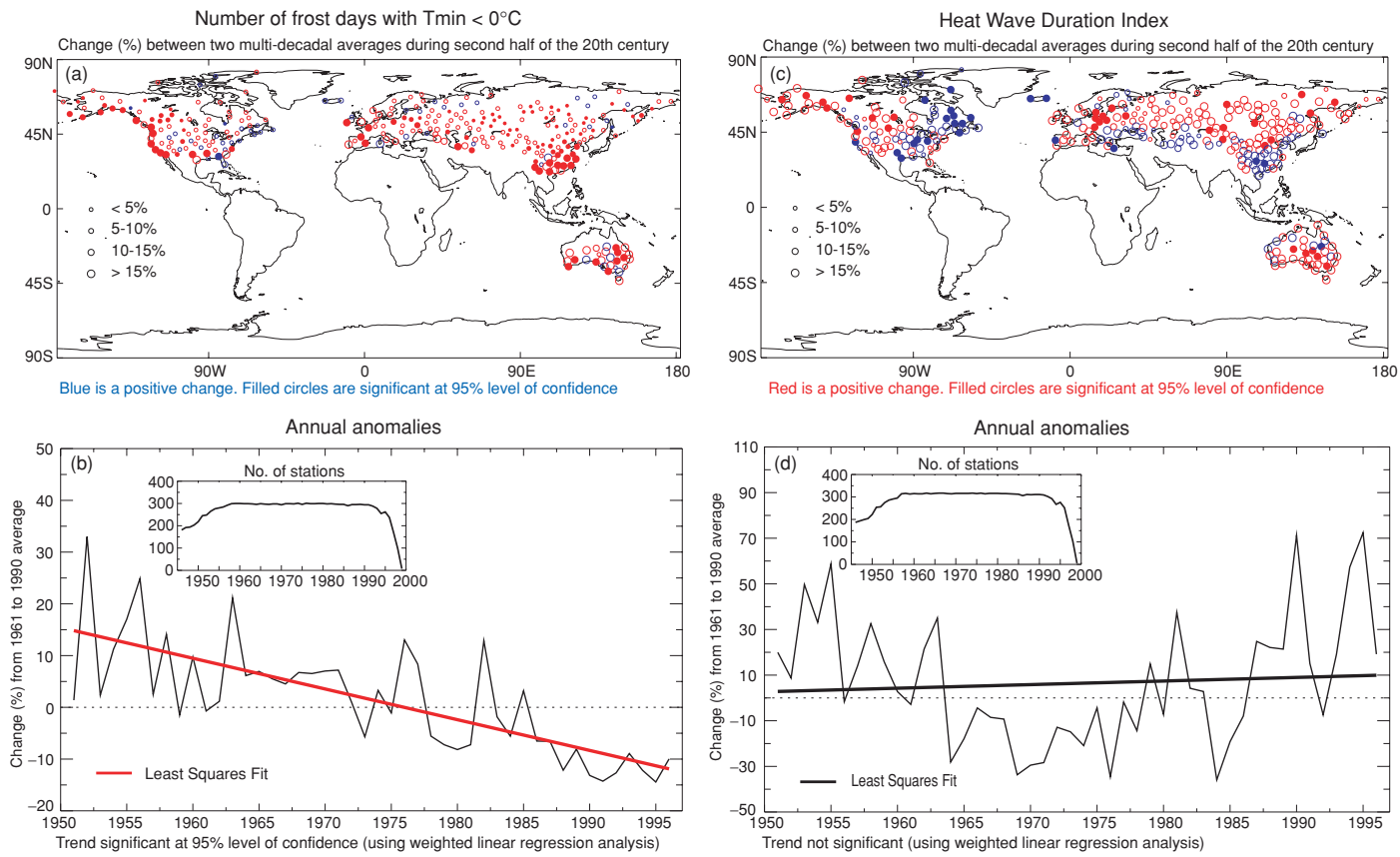


**Figure 2.33:** Changes in the number of frost days (a, b) and in heat-wave duration (c, d) from Frich *et al.* (2001). Panel (a) shows the percent changes in the total number of days with a minimum temperature of less than  $0^{\circ}\text{C}$  between the first and last half of the period, approximately 1946 to 1999. The red circles indicate negative changes and the blue circles indicate positive changes. Panel (c) shows percentage changes in the maximum number of consecutive days (for periods with  $>5$  such days) with maximum temperatures  $>5^{\circ}\text{C}$  above the 1961 to 1990 daily normal. The changes are for the first and second half of the period, approximately 1946 to 1999. The red circles indicate positive changes and the blue circles indicate negative changes. In both panels, the size of each circle reflects the size of the change and solid circles represent statistically significant changes. Panels (b) and (d) show the average annual values of these quantities expressed as percentage differences from their 1961 to 1990 average values. The trend shown in panel (b) is statistically significant at the 5% level.

tures are significantly larger for 1949 to 1995 during summer over most of the USA (Gaffen and Ross, 1998). Warm humid nights more than doubled in number over 1949 to 1995 at some locations. Trends in nocturnal apparent temperature in the USA, however, are likely to be associated, in part, with increased urbanisation. Nevertheless, using methods and data sets to minimise urban heat island effects and instrument changes, Easterling *et al.* (2000) arrived at conclusions similar to those of Gaffen and Ross (1998).

During the 1997/98 El Niño event, global temperature records were broken for sixteen consecutive months from May 1997 through to August 1998. Karl *et al.* (2000) describe this as an unusual event and such a monthly sequence is unprecedented in the observational record. More recently, Wigley (2000) argues that if it were not for the eruption of Mt. Pinatubo, an approximately equal number of record-breaking temperatures would have been set during the El Niño of 1990/91. As temperatures continue to warm, more events like these are likely, especially when enhanced by other factors, such as El Niño.

### 2.7.2.2 Precipitation

A better understanding of the relationship between changes in total precipitation and intense precipitation events has been achieved since the SAR. Although many areas of the globe have not been analysed, and considerable data remain inaccessible, enough data have been analysed to confirm some basic properties of the changes in extreme precipitation. Groisman *et al.* (1999) developed a simple statistical model of the frequency of daily precipitation based on the gamma distribution. They applied this model to a variety of regions around the world (40% of the global land area) during the season of greatest precipitation. Although Wilks (1999) shows that the gamma distribution under some circumstances can underestimate the probability of the highest rainfall amounts, Groisman *et al.* (1999) applied the distribution to the upper 5 and 10 percentiles of the distribution which are less subject to underestimation. Their analysis period varied from region to region, but within each region it generally spanned at least the last several decades, and for some regions much of the 20th century (Australia, United States, Norway, and South

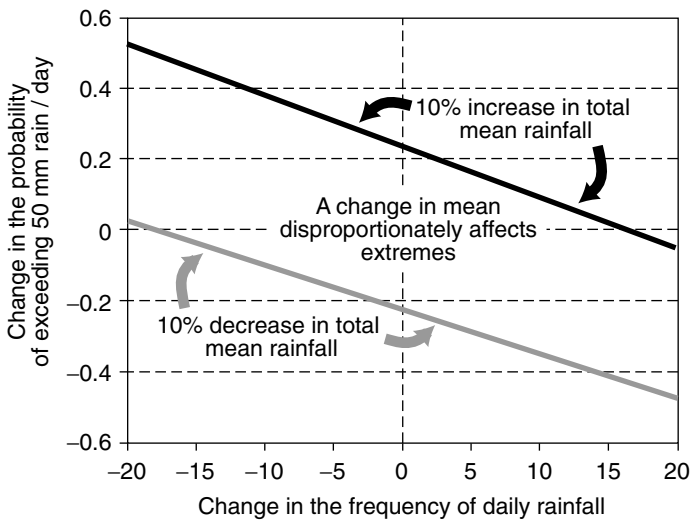


**Figure 2.34:** An example (from Groisman *et al.*, 1999) of the sensitivity of the frequency of heavy daily rainfall to a shift in the mean total rainfall, based on station data from Guangzhou, China. This example uses a threshold of 50 mm of precipitation per day. It shows the effects of a 10% increase and a 10% decrease in mean total summer rainfall, based on a gamma distribution of the rainfall with a constant shape parameter.

Africa). In the model used by Groisman *et al.* (1999), the mean total precipitation is also proportional to the shape and scale parameters of the gamma distribution as well as to the probability of precipitation on any given day. The shape parameter of the gamma distribution tends to be relatively stable across a wide range of precipitation regimes, in contrast to the scale parameter. Given the conservative nature of the shape parameter, it is possible to illustrate the relationships between changes in the mean total precipitation, the probability of precipitation (which is proportional to the number of days with precipitation), and changes in heavy precipitation (Figure 2.34). Given no change in the frequency (number of days) of precipitation, a 10% change in the mean total precipitation is amplified to a larger percentage change in heavy precipitation rates compared to the change in the mean. Using the statistical theory of extremes, Katz (1999) obtained results consistent with those of Groisman *et al.* (1999). For many regions of the world it appears that the changes in the frequency or probability of precipitation events are either small enough, or well enough expressed in the high rainfall rates (Karl and Knight, 1998; Gruza *et al.*, 1999; Haylock and Nicholls, 2000) that an increase in the mean total precipitation is disproportionately reflected in increased heavy precipitation rates (Figure 2.35).

Given the patterns of mean total precipitation changes (Section 2.5.2) during the 20th century, it could be anticipated that, in general, for those areas with increased mean total precipitation, the percentage increase in heavy precipitation rates should be significantly larger, and *vice versa* for total precipitation decreases. Regional analyses of annual precipitation in the United States (Karl and Knight, 1998; Trenberth, 1998a; Kunkel *et al.*, 1999); Canada (Stone *et al.*, 1999); Switzerland (Frei and Schär, 2001); Japan (Iwashima and Yamamoto, 1993; Yamamoto and Sakurai, 1999); wintertime precipitation in the UK (Osborn *et al.*, 2000); and rainy season precipitation in Norway, South

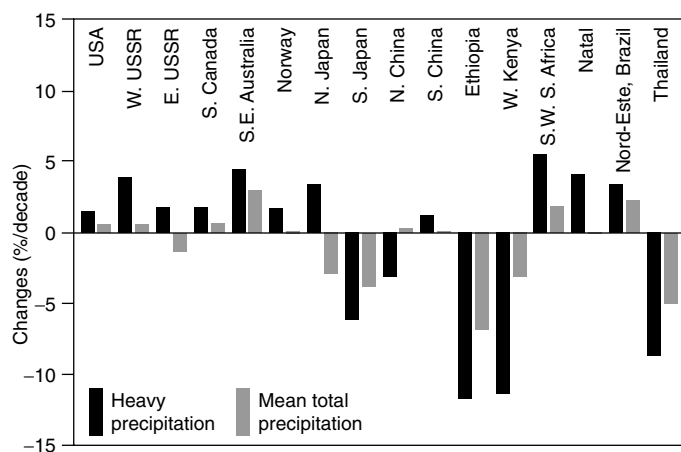


**Figure 2.35:** Linear trends (%/decade) of heavy precipitation (above the 90th percentile) and total precipitation during the rainy season over various regions of the globe. Seasons for each region usually span at least 50 years. Note that the magnitudes of the changes in heavy precipitation frequencies are always higher than changes in mean precipitation totals (Easterling *et al.*, 2000).

Africa, the Nord Este of Brazil, and the former USSR (Groisman *et al.*, 1999; Gruza *et al.*, 1999; Easterling *et al.*, 2000) confirm this characteristic of an amplified response for the heavy and extreme events.

Increases in heavy precipitation have also been documented even when mean total precipitation decreases (for example, see Northern Japan in Figure 2.35, or Manton *et al.*, 2001). This can occur when the probability of precipitation (the number of events) decreases, or if the shape of the precipitation distribution changes, but this latter situation is less likely (Buffoni *et al.*, 1999; Groisman *et al.*, 1999; Brunetti *et al.*, 2000a,b). For example, in Siberia for the summer season during the years 1936 to 1994 there was a statistically significant decrease in total precipitation of 1.3%/decade, but the number of days with precipitation also decreased. This resulted in an increase (1.9%/decade) in the frequency of heavy rainfall above 25 mm. The opposite can also occur when the number of rainfall events increases; thus Førland *et al.* (1998) found no trends in 1-day annual maximum precipitation in the Nordic countries, even when mean total precipitation increased.

There has also been a 10 to 45% increase in heavy rainfall, as defined by the 99th percentile of daily totals, over many regions of Australia from 1910 to 1995, but few individual trends were statistically significant (Hennessy *et al.*, 1999). In southwest Australia, however, a 15% decrease has been observed in winter rainfall on very wet days (Hennessy *et al.*, 1999; Haylock and Nicholls, 2000).

In Niger, a recent analysis of hourly rainfall data (Shinoda *et al.*, 1999) reveals that the droughts in the 1970s and 1980s were characterised primarily by a reduced frequency of heavy rainfall events (those exceeding 30 mm/day) rather than by a reduction in rainfall amount within heavy events. Such a result is still consistent with the model of Groisman *et al.* (1999), as a decrease in the

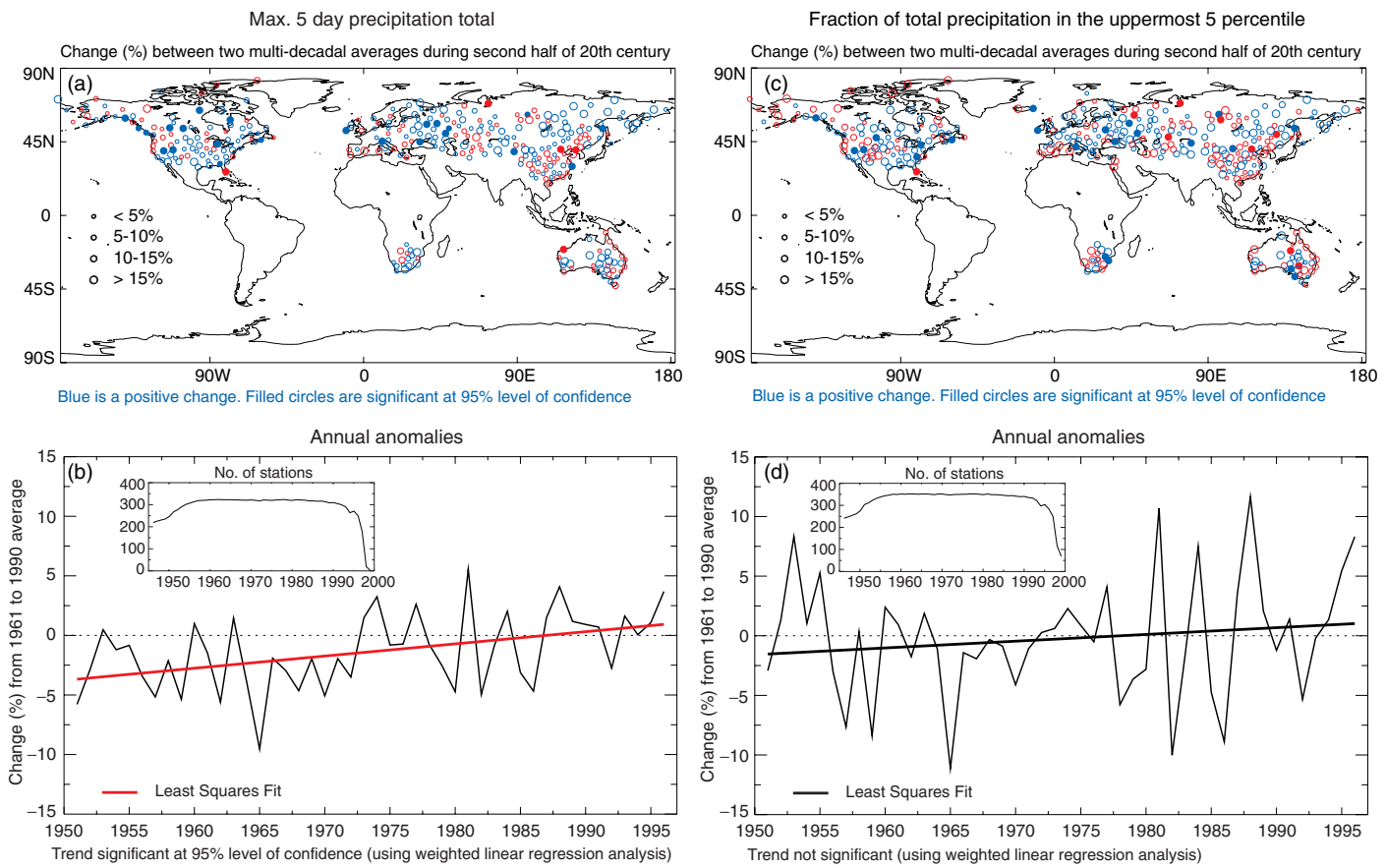


**Figure 2.36:** Changes in the maximum annual 5-day precipitation total (a, b) and in the proportion of annual precipitation occurring on days on which the 95th percentile of daily precipitation, defined over the period 1961 to 1990, was exceeded (c, d). The analysis shown is from Frich *et al.* (2001). Panels (a) and (c) show percentage changes in these quantities between the first and last half of the period, approximately 1946 to 1999. In both panels, the red circles indicate negative changes and the blue circles indicate positive changes. The size of each circle reflects the size of the change and solid circles represent statistically significant changes. Panels (b) and (d) show the average annual values of the quantities expressed as percentage differences from their 1961 to 1990 average values. The trend shown in panel (b) is statistically significant at the 5% level.

frequency of rainfall events has been responsible for the decrease in total rainfall. In the Sahel region of Nigeria, however, there has been a decrease in the heaviest daily precipitation amounts, coincident with an overall decrease in annual rainfall. This pattern is apparent throughout the Sudano-Sahel Zone, including the Ethiopian plateau (Nicholson, 1993; Tarhule and Woo, 1998; Easterling *et al.*, 2000). Again, it is apparent that there has been an amplified response of the heaviest precipitation rates relative to the percentage change in total precipitation.

Since large portions of the mid- and high latitude land areas have had increasing precipitation during the last half the 20th century, the question arises as to how much of this area is affected by increases in heavy and extreme precipitation rates. The Frich *et al.* (2001) analysis suggests an overall increase in the area affected by more intense daily rainfall. Figure 2.36 shows that widely distributed parts of the mid- and high latitudes have locally statistically significant increases in both the proportion of mean annual total precipitation falling into the upper five percentiles and in the annual maximum consecutive 5-day precipitation total. However, for the regions of the globe sampled taken as a whole, only the latter statistic shows a significant increase. Regional analyses in

Russia (Gruza *et al.*, 1999), the United States (Karl and Knight, 1998) and elsewhere (Groisman *et al.*, 1999; Easterling *et al.*, 2000) confirm this trend. Although the trends are by no means uniform, as would be anticipated with the relatively high spatial and interannual variability of precipitation, about 10% of the stations analysed show statistically significant increases at the 5% level. This equates to about a 4% increase in the annual maximum 5-day precipitation total (Figure 2.36b). The number of stations reflecting a locally significant increase in the proportion of total annual precipitation occurring in the upper five percentiles of daily precipitation totals outweighs the number of stations with significantly decreasing trends by more than 3 to 1 (Figure 2.36c). Although not statistically significant when averaging over all stations, there is about a 1% increase in the proportion of daily precipitation events occurring in the upper five percentiles (Figure 2.36d). Overall, it is likely that there has been a 2 to 4% increase in the number of heavy precipitation events when averaged across the mid- and high latitudes.

It has been noted that an increase (or decrease) in heavy precipitation events may not necessarily translate into annual peak (or low) river levels. For example, in the United States, Lins

and Slack (1999) could not detect an increase in the upper quantiles of streamflow, despite the documented increase in heavy and extreme precipitation events. It is possible that this null result is partly due to the method of analysis, but it is also attributable to the timing of the annual peak streamflow discharge, which in the United States is usually in late winter or early spring. A reduced snow cover extent in the mountainous West changes the peak river flow, as does timing of increases in heavy and extreme precipitation reported in the United States, which is best reflected during the warm season. Groisman *et al.* (2001) and Zhang *et al.* (2000) also show reduced peak streamflow in areas with reduced spring snow cover extent. Nonetheless, in much of the United States where spring snow melt does not dominate peak or normal flow, Groisman *et al.* (2001) show increasing high streamflow related to increasing heavy precipitation.

It is noteworthy that the influence of warmer temperatures and increased water vapour in the atmosphere (Section 2.5.3) are not independent events, and are likely to be jointly related to increases in heavy and extreme precipitation events.

### 2.7.3 Is There Evidence for Changes in Extreme Weather or Climate Events?

In this section we assess changes in the intensity and frequency of various weather phenomena. One aspect of change that is important, but which is beyond the analysis of present records, relates to changes in the tracks of storms. Severe storms are often rare, so the analysis of large areas and long lengths of homogeneous storm records are required to assess changes. So far this combination of data is not available.

#### 2.7.3.1 Tropical cyclones

This section updates the information provided in the SAR regarding changes in tropical cyclones across various ocean basins and those affecting the nearby continents. As reported in the SAR, a part of the multi-decadal trend of tropical cyclones occurring in the Australian region ( $105^{\circ}$  to  $160^{\circ}$ E) is likely to be artificial, as the forecasters in the region no longer classify some weak ( $>990$  hPa central pressure) systems as “cyclones” (Nicholls *et al.*, 1998). By considering only the moderate and intense tropical cyclones (central pressure  $\leq 990$  hPa), this artificial trend is eliminated. The remaining moderate and strong tropical cyclones reveal a numerical decline since the late 1980s, but the trend is not statistically significant. Similarly, the trend in intense tropical cyclones (minimum central pressure below 970 hPa) is not significantly different from zero. Nicholls *et al.* (1998) attributed the decrease in moderate cyclones to more frequent occurrences of El Niño during the 1980s and 1990s. However, a weak trend in the intense tropical cyclones implies that while ENSO modulates the total frequency of cyclones in the region, other factors must be more important in regulating their intensity. For example, new work by Higgins and Shi (2000) and Maloney and Hartmann (2001) show that 30 to 80 day Madden-Julian oscillations modulate tropical cyclone activity.

As reported in the SAR, the north-east sub-tropical Pacific has experienced a significant upward trend in tropical cyclone frequency in the short period examined, but additional data since

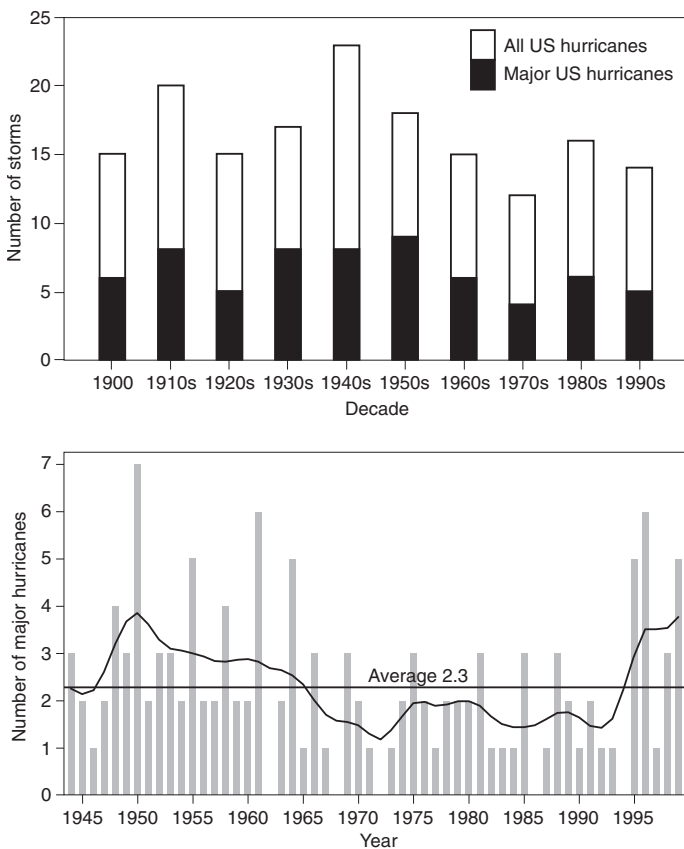


**Figure 2.37:** Top figure, decadal variations in hurricanes making landfall in the USA (updated from Karl *et al.*, 1995). Bottom figure, interannual variability in the number of major hurricanes (Saffir-Simpson categories 3, 4, and 5) and the long-term average across the North Atlantic (from Landsea *et al.*, 1999).

that time show no appreciable trend. There is no appreciable long-term variation of the total number of tropical storm strength cyclones observed in the north Indian, south-west Indian and south-west Pacific Oceans east of  $160^{\circ}$ E. (Neumann, 1993; Lander and Guard, 1998). For the north-west sub-tropical Pacific basin, Chan and Shi (1996) found that the frequency of typhoons and the total number of tropical storms and typhoons have been more variable since about 1980. There was an increase from 1981 to 1994, which was preceded by a nearly identical magnitude of decrease from about 1960 to 1980. No analysis has been done on the frequency of intense typhoons (having winds of at least 50 m/s) due to an overestimation of the intensity of such storms in the 1950s and 1960s (Black, 1993).

There has been an extensive analysis of the North Atlantic basin for the entire basin back to 1944, and also for the United States landfall tropical storms and hurricanes back to 1899. The all-basin data, however, have been affected by a bias in the measurement of strong hurricanes. This bias has been removed in an approximate way to provide estimates of the true occurrence of intense (or major) hurricanes since 1944 in the North Atlantic (Landsea, 1993). Earlier events lack reliable data on the strong inner core of the hurricanes. The United States record of landfall frequency and intensity of hurricanes is very reliable because of

the availability of central pressure measurements at landfall (Jarrell *et al.*, 1992). Both of these data sets continue to show considerable inter-decadal variability, but no significant long-term trends (Figure 2.37, from Landsea *et al.*, 1999). Active years occurred from the late 1940s to the mid-1960s, quiet years occurred from the 1970s to the early 1990s, and then there was a shift again to active conditions from 1995 to 1999. Concurrent with these frequency changes, there have been periods with a strong mean intensity of the North Atlantic tropical cyclones (mid-1940s to the 1960s and 1995 to 1999) and a weak intensity (1970s to early 1990s). There has been no significant change in the peak intensity reached by the strongest hurricane each year (Landsea *et al.*, 1996). As might be anticipated, there is a close correspondence between the intensity of hurricanes in the North Atlantic and those making landfall in the United States (Figure 2.37).

Using historical records, Fernandez-Partagas and Diaz (1996) estimated that overall Atlantic tropical storm and hurricane activity for the years 1851 to 1890 was 12% lower than the corresponding forty year period of 1951 to 1990, although little can be said regarding the intense hurricanes. They based this assessment upon a constant ratio of USA landfalling tropical cyclones to all-basin activity, which is likely to be valid for multi-decadal time-scales. However, this also assumes that Fernandez-Partagas and Diaz were able to uncover all USA landfalling tropical cyclones back to 1851, which may be more questionable.

### 2.7.3.2 Extra-tropical cyclones

Extra-tropical cyclones are baroclinic low pressure systems that occur throughout the mid-latitudes of both hemispheres. Their potential for causing property damage, particularly as winter storms, is well documented, where the main interest is in wind and wind-generated waves. In place of direct wind measurements, which suffer from lack of consistency of instrumentation, methodology and exposure, values based on SLP gradients have been derived which are more reliable for discerning long-term changes. Over the oceans, the additional measurements of wave heights and tide gauge measurements provide additional ways of indirectly evaluating changes in extra-tropical storm strength and frequency (see Chapter 11, Section 11.3.3). Global analyses of changes in extra-tropical storm frequency and intensity have not been attempted, but there have been several large-scale studies. Jones *et al.* (1999c) developed a gale index of geostrophic flow and vorticity over the UK for the period 1881 to 1997. This revealed an increase in the number of severe gale days over the UK since the 1960s, but no long-term increase when considering the century period. Serreze *et al.* (1997) found increases in cold season cyclones in the Arctic region for the period 1966 to 1993. Angel and Isard (1998) found significant increases in strong cyclones (<993 mb) in the Great Lakes region from 1900 to 1990 during the cold season. Graham and Diaz (2001) find evidence for increases in strong cyclones over the Pacific Ocean between 25 and 40°N since 1948 and link the increase to increasing sea surface temperatures in the western Tropical Pacific. Alexandersson *et al.* (1998, 2000) similarly studied extreme geostrophic wind events in the north-western European area based on homogenised observations during the period 1881 to 1998. These studies revealed an increase in the number of

extreme wind events around and to the north of the North Sea. The WASA group (1998) similarly investigated the storm related sea level variations at gauge stations in the south-eastern part of the North Sea. They found no long-term trend during the last 100 years, but a clear rise since a minimum of storminess in the 1960s, which is consistent with the rise in extreme geostrophic wind found by Jones *et al.* (1999c). This increase is also consistent with changes in the NAO (Figure 2.30). Some analyses have focused on hemispheric changes in cyclone activity. Lambert (1996) analysed gridded SLP over both the North Atlantic and North Pacific Oceans for the period 1891 to 1991. He found a significant increase in intense extra-tropical storms, especially over the last two decades of his analysis, but the data were not completely homogenised. Simmonds and Keay (2000) used data from 1958 to 1997 in the Southern Hemisphere and found an increase in cyclone activity through 1972 before decreasing through 1997 with strong decreases during the 1990s.

Hourly values of water levels provide a unique record of tropical and extra-tropical storms where stations exist. Zhang *et al.* (1997a) have analysed century-long records along the East Coast of the United States. They calculated several different measures of storm severity, but did not find any long-term trends. On the other hand, they did find that the effect of sea level rise over the last century has exacerbated the beach erosion and flooding from modern storms that would have been less damaging a century ago.

Another proxy for cyclone intensity is wave height (see Chapter 11, Section 11.3.3). Several studies report increased wave height over the past three decades in the North Atlantic (approximately 2.5 cm/yr) and in coastal areas, though no longer-term trends were evident (Carter and Draper, 1988; Bacon and Carter, 1991; Bouws *et al.*, 1996; Kushnir *et al.*, 1997; WASA Group, 1998).

It appears that recent work points towards increases over time in extra-tropical cyclone activity during the latter half of the 20th century in the Northern Hemisphere, and decreased activity in the Southern Hemisphere. However, the mechanisms involved are not clear, and it is not certain whether the trends are multi-decadal fluctuations, or rather part of a longer-term trend. Furthermore decreased cyclone activity in higher latitudes of the Southern Hemisphere is not obviously consistent with an increase in the positive phase of the Antarctic Oscillation in the last fifteen years or so (Section 2.6.6). A more fundamental question is whether we would expect more or fewer extra-tropical cyclones with increased warming. As pointed out by Simmonds and Keay (2000), the specific humidity increases as temperatures increase, and this increased moisture should enhance extra-tropical cyclones, but Zhang and Wang (1997) suggest that cyclones transport energy more efficiently in a more moist atmosphere, therefore requiring fewer extra-tropical cyclones (see Chapters 7 and 10 for more discussion).

### 2.7.3.3 Droughts and wet spells

In the SAR, an intensification of the hydrological cycle was projected to occur as the globe warms. One measure of such intensification is to examine whether the frequency of droughts and wet spells are increasing. Karl *et al.* (1995c) examined the

proportion of land areas having a severe drought and a severe moisture surplus over the United States. Dai *et al.* (1998) extended this analysis to global land areas using the water balance approach of the Palmer Drought Severity Index. Long-term global trends for 1900 to 1995 are relatively small for both severe drought and wet area statistics. However, during the last two to three decades, there have been some increases in the globally combined severe dry and wet areas, resulting from increases in either the dry area, e.g., over the Sahel, eastern Asia and southern Africa or the wet areas, e.g., over the United States and Europe. Most of the increases occurred after 1970. Except for the Sahel, however, the magnitude of dry and wet areas of the recent decades is not unprecedented during this century, but it should be noted that rainfall in the Sahel since the height of the drought has substantially increased. In related work, Frich *et al.* (2001) found that in much of the mid- and high latitudes, there has been a statistically significant increase in both the number of days with precipitation exceeding 10 mm per day and in the number of consecutive days with precipitation during the second half of the 20th century.

Recent changes in the areas experiencing severe drought or wet spells are closely related to the shift in ENSO towards more warm events since the late 1970s, and coincide with record high global mean temperatures. Dai *et al.* (1998) found that for a given value of ENSO intensity, the response in areas affected by drought or excessive wetness since the 1970s is more extreme than prior to the 1970s, also suggesting an intensification of the hydrological cycle.

#### 2.7.3.4 Tornadoes, hail and other severe local weather

Small-scale severe weather phenomena (SCSWP) are primarily characterised by quasi-random temporal and spatial events. These events, in turn, have local and regional impacts, often with significant damage and sometimes loss of life. Tornadoes and thunderstorms and related phenomena such as lightning, hail, wind, dust, water spouts, downpours and cloudbursts belong to this group. In the light of the very strong spatial variability of SCSWP, the density of surface meteorological observing stations is too coarse to measure all such events. Moreover, areally consistent values of SCSWP are inherently elusive. Statistics of relatively rare events are not stable at single stations, observational practices can be subjective and change over time, and the metadata outlining these practices are often not readily available to researchers. For these reasons, monitoring the occurrence of local maxima and minima in smoothed SCSWP series, as well as checking for trends of the same sign for different but related SCSWP (e.g., thunderstorms, hail, cloud bursts), are important for checking inconsistencies. Because of the inherent difficulty in working with these data, there have been relatively few large-scale analyses of changes and variations in these events. Nonetheless, a few new regional analyses have been completed since the SAR.

A regional analysis by Dessens (1995) and more recent global analysis by Reeve and Toumi (1999) show that there is a significant interannual correlation between hail and lightning and mean minimum temperature and wet bulb temperatures. Using a three-year data set, Reeve and Toumi (1999) found a statistically

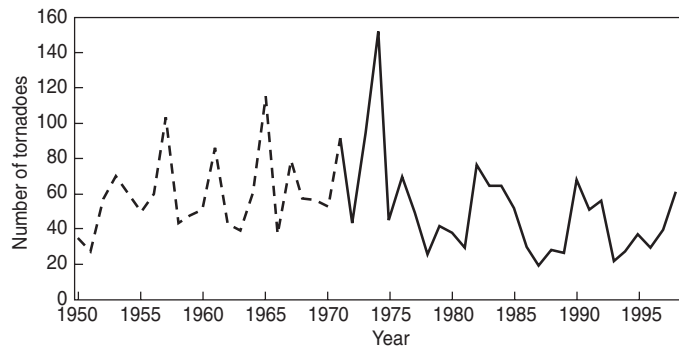


**Figure 2.38:** Annual total number of very strong through violent (F3–F5) tornadoes reported in the USA, which are defined as having estimated wind speeds from approximately 70 to 164 ms<sup>-1</sup>. The Fujita tornado classification scale was implemented in 1971. Prior to 1971, these data are based on storm damage reports (National Climatic Data Center, NOAA).

significant relationship between lightning frequency and wet bulb temperature. They show that with a 1°C increase in global wet-bulb temperature there is a 40% increase in lightning activity, with larger increases over the Northern Hemisphere land areas (56%). Unfortunately, there are few long-term data sets that have been analysed for lightning and related phenomena such as hail or thunderstorms, to calculate multi-decadal hemispheric or global trends.

A regional analysis assessed the temporal fluctuations and trends in hail-day and thunder-day occurrences during a 100-year period, from 1896 to 1995, derived from carefully screened records of 67 stations distributed across the United States. Upward hail day trends were found in the High Plains–Rockies and the south-east, contrasting with areas with no trend in the northern Midwest and along the East Coast, and with downward trends elsewhere (Changnon and Changnon, 2000). The major regions of decrease and increase in hail activity match regions of increased and decreased thunder activity for 1901 to 1980 well (Changnon, 1985; Gabriel and Changnon, 1990) and also crop-hail insurance losses (Changnon *et al.*, 1996; Changnon and Changnon, 1997). In general, hail frequency shows a general decrease for most of the United States over the last century, with increases over the High Plains, the region where most of the crop-hail damage occurs in the United States. So, despite an increase in minimum temperature of more than 1°C since 1900 and an increase in tropospheric water vapour over the United States since 1973 (when records are deemed reliable), no systematic increase in hail or thunder days was found.

In south Moravia, Czech Republic, a decreasing linear trend in the frequency of thunderstorms, hailstorms and heavy rain from 1946 to 1995 was related to a significant decrease in the occurrence of these phenomena during cyclonic situations, when 90% of these phenomena occur in that region (Brázdil and Vais, 1997). Temperatures have increased in this area since 1946.

Since 1920, the number of tornadoes reported annually in the United States has increased by an order of magnitude, but this increase reflects greater effectiveness in collecting tornado

reports (Doswell and Burgess, 1988; Grazulis, 1993; Grazulis *et al.*, 1998). On the other hand, severe tornadoes are not easily overlooked. Restricting the analysis to very strong and violent tornadoes results in a much different assessment (Figure 2.38) showing little long-term change, though some years like 1974 show a very large number of tornadoes. Furthermore, consideration of the number of days with tornadoes, rather than number of tornadoes, reduces the artificial changes that result from modern, more detailed damage surveys (e.g., Doswell and Burgess, 1988). The data set of “significant” tornado days developed by Grazulis (1993) shows a slow increase in number of days with significant tornadoes from the early 1920s through the 1960s, followed by a decrease since that time.

#### 2.7.4 Summary

Based on new analyses since the SAR, it is likely that there has been a widespread increase in heavy and extreme precipitation events in regions where total precipitation has increased, e.g., the mid- and high latitudes of the Northern Hemisphere. Increases in the mean have often been found to be amplified in the highest precipitation rates total. In some regions, increases in heavy rainfall have been identified where the total precipitation has decreased or remained constant, such as eastern Asia. This is attributed to a decrease in the frequency of precipitation. Fewer areas have been identified where decreases in total annual precipitation have been associated with decreases in the highest precipitation rates, but some have been found. Temperature variability has decreased on intra-seasonal and daily time-scales in limited regional studies. New record high night-time minimum temperatures are lengthening the freeze and frost season in many mid- and high latitude regions. The increase in global temperatures has resulted mainly from a significant reduction in the frequency of much below normal seasonal mean temperatures across much of the globe, with a corresponding smaller increase in the frequency of much above normal temperatures. There is little sign of long-term changes in tropical storm intensity and frequency, but inter-decadal variations are pronounced. Owing to incomplete data and relatively few analyses, we are uncertain as to whether there has been any large-scale, long-term increase in the Northern Hemisphere extra-tropical cyclone intensity and frequency though some, sometimes strong, multi-decadal variations and recent increases were identified in several regions. Limited evidence exists for a decrease in cyclone frequency in the Southern Hemisphere since the early 1970s, but there has been a paucity of analyses and data. Recent analyses of changes in severe local weather (tornadoes, thunder days, lightning and hail) in a few selected regions provide no compelling evidence for widespread systematic long-term changes.

#### 2.8 Are the Observed Trends Internally Consistent?

It is very important to compare trends in the various indicators to see if a physically consistent picture emerges, as this will critically affect the final assessment of our confidence in any such changes. A number of qualitative consistencies among the

various indicators of climate change have increased our confidence in our analyses of the historical climate record: Figure 2.39a and b summarises the changes in various temperature and hydrological indicators, respectively, and provides a measure of confidence about each change. Of particular relevance are the changes identified below:

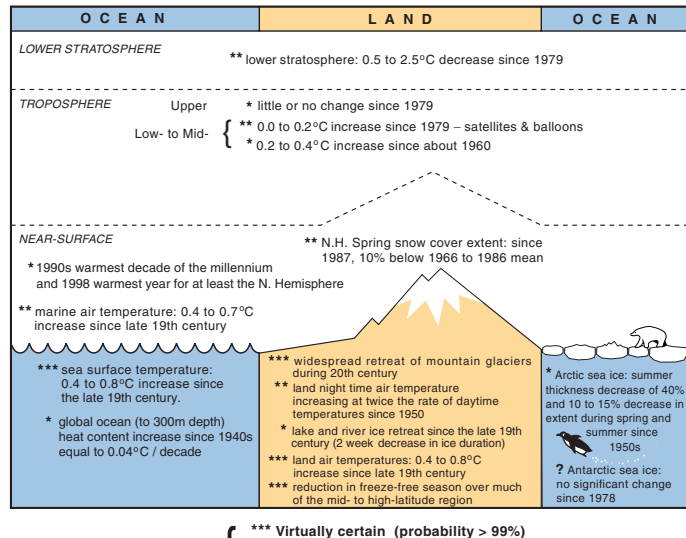
- Temperature over the global land and oceans, with two estimates for the latter, are measured and adjusted independently, yet all three show quite consistent increasing trends (0.52 to 0.61°C/century) over the 20th century.
- The nearly worldwide decrease in mountain glacier extent and mass is consistent with 20th century global temperature increases. A few recent exceptions in maritime areas have been affected by atmospheric circulation variations and related precipitation increases.
- Though less certain, substantial proxy evidence points to the exceptional warmth of the late 20th century relative to the last 1,000 years. The 1990s are likely to have been the warmest decade of the past 1,000 years over the Northern Hemisphere as a whole.
- Satellite and balloon measurements agree that lower-tropospheric temperatures have increased only slightly since 1979, though there has been a faster rate of global surface temperature increase. Balloon measurements indicate a larger lower-tropospheric temperature increase since 1958, similar to that shown by global surface temperature measurements over the same period. Balloon and satellite measurements agree that lower-stratospheric temperatures have declined significantly since 1979.
- Since 1979, trends in worldwide land-surface air temperature derived from weather stations in the Northern Hemisphere, in regions where urbanisation is likely to have been strong, agree closely with satellite derived temperature trends in the lower troposphere above the same regions. This suggests that urban heat island biases have not significantly affected surface temperature over the period.
- The decrease in the continental diurnal temperature range since around 1950 coincides with increases in cloud amount and, at least since the mid-1970s in the Northern Hemisphere, increases in water vapour.
- Decreases in spring snow cover extent since the 1960s, and in the duration of lake and river ice over at least the last century, relate well to increases in Northern Hemispheric surface air temperatures.
- The systematic decrease in spring and summer Arctic sea-ice extent in recent decades is broadly consistent with increases of temperature over most of the adjacent land and ocean. The large reduction in the thickness of summer and early autumn Arctic sea ice over the last thirty to forty years is consistent

with this decrease in spatial extent, but we are unsure to what extent poor temporal sampling and multi-decadal variability are affecting the conclusions.

- The increases in lower-tropospheric water vapour and temperature since the mid-1970s are qualitatively consistent with an enhanced hydrological cycle. This is in turn consistent with a greater fraction of precipitation being delivered from extreme and heavy precipitation events, primarily in areas with increasing precipitation, e.g., mid- and high latitudes of the Northern Hemisphere.
- Where data are available, changes in precipitation generally correspond with consistent changes in streamflow and soil moisture.

We conclude that the variations and trends of the examined indicators consistently and very strongly support an increasing global surface temperature over at least the last century, although substantial shorter-term global and regional deviations from this warming trend are very likely to have occurred.

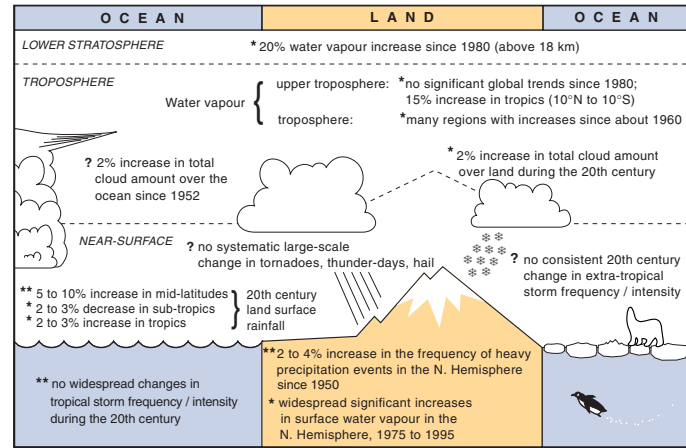
### Temperature Indicators



Likelihood: {  
 \*\*\* Virtually certain (probability > 99%)  
 \*\* Very likely (probability ≥ 90% but < 99%)  
 \* Likely (probability > 66% but < 90%)  
 ? Medium likelihood (probability > 33% but ≤ 66%)

**Figure 2.39a:** Schematic of observed variations of various temperature indicators.

### Hydrological and Storm-Related Indicators



Likelihood: {  
 \*\*\* Virtually certain (probability > 99%)  
 \*\* Very likely (probability ≥ 90% but < 99%)  
 \* Likely (probability > 66% but < 90%)  
 ? Medium likelihood (probability > 33% but ≤ 66%)

**Figure 2.39b:** Schematic of observed variations of various hydrological and storm-related indicators.

## References

- Adkins**, J.F., E.W. Boyle, L. Keigwin and E. Cortijo, 1997: Variability of the North Atlantic thermohaline circulation during the Last interglacial period. *Nature*, **390**, 154-156.
- Akinremi**, O.O., S.M. McGinn and H.W. Cutforth, 1999: Precipitation trends on the Canadian Prairies. *J. Climate*, **12**, 2996-3003.
- Alexandersson**, H., T. Schmith, K. Iden and H. Tuomenvirta, 1998: Long-term variations of the storm climate over NW Europe. *Global Atmosphere and Ocean Systems*, **6**, 97-120.
- Alexandersson**, H., T. Schmith, K. Iden and H. Tuomenvirta, 2000: Trends in storms in NW Europe derived from an updated pressure data set. *Clim. Res.*, **14**, 71-73.
- Allan**, R.J., 2000: ENSO and climatic variability in the last 150 years. In: *El Niño and the Southern Oscillation: Multiscale Variability, Global and Regional Impacts*, edited by Diaz, H.F. and V. Markgraf, Cambridge University Press, Cambridge, UK, pp. 3-56.
- Allard**, M., B. Wang and J.A. Pilon, 1995: Recent cooling along the southern shore of Hudson Strait Quebec, Canada, documented from permafrost temperature measurements. *Arctic and Alpine Research*, **27**, 157-166.
- Alley**, R.B. and P.U. Clark, 1999: The deglaciation of the Northern Hemisphere: a global perspective. *Ann. Rev. Earth Planet. Sci.*, **149**-182.
- Alley**, R.B., D.A. Meese, C.A. Shuman, A.J. Gow, K.C. Taylor, P.M. Grootes, J.W.C. White, M. Ram, E.D. Waddington, P.A. Mayewski and G.A. Zielinski, 1993: Abrupt increase in Greenland snow accumulation at the end of the Younger Dryas event. *Nature*, **362**, 527-529.
- Alley**, R.B., P.A. Mayewski, T. Sowers, M. Stuiver, K.C. Taylor and P.U. Clark, 1997: Holocene climatic instability: A prominent, widespread event 8200 years ago. *Geology*, **25**, 483-486.
- Ames**, A., 1998: A documentation of glacier tongue variations and lake development in the Cordillera Blanca, Peru. *Z. Gletscherkd. Glazialgeol.*, **34**(1), 1-36.
- Anderson**, W.L., D.M. Robertson and J.J. Magnuson, 1996: Evidence of recent warming and El Nino-related variations in ice breakup of Wisconsin Lakes. *Limnol. Oceanogr.*, **41**(5), 815-821.
- Angel**, J.R. and S.A. Isard, 1998: The frequency and intensity of Great Lake cyclones. *J. Climate*, **11**, 61-71.
- Angell**, J.K., 1988: Variations and trends in tropospheric and stratospheric global temperatures, 1958-87. *J. Climate*, **1**, 1296-1313.
- Angell**, J.K., 1999: Comparison of surface and tropospheric temperature trends estimated from a 63-station radiosonde network, 1958-1998. *Geophys. Res. Lett.*, **26**, 2761-2764.
- Angell**, J.K., 2000: Difference in radiosonde temperature trend for the period 1979-1998 of MSU data and the period 1959-1998 twice as long. *Geophys. Res. Lett.*, **27**, 2177-2180.
- Appenzeller**, C., T.F. Stocker and M. Anklin, 1998: North Atlantic oscillation dynamics recorded in Greenland ice cores. *Science*, **282**, 446-449.
- Arhan**, M., H. Mescier, B. Bourles and Y. Gouriou, 1998: Hydrographic sections across the Atlantic at 7°30'N and 4°30'S. *Deep Sea Res., Part I*, **45**, 829-872.
- Arkin**, P.A. and P.E. Ardanuy, 1989: Estimating climatic-scale precipitation from space: a review. *J. Climate*, **2**, 1229-1238.
- Assel**, R.A., 1983: Description and analysis of a 20-year (1960-79) digital ice-concentration database for the Great Lakes of North America. *Ann. Glaciol.*, **4**, 14-18.
- Assel**, R.A. and D.M. Robertson, 1995: Changes in winter air temperatures near Lake Michigan during 1851-1993 as determined from regional lake-ice records. *Limnol. Oceanogr.*, **40**, 165-176.
- Bacon**, S. and D.J.T. Carter, 1991: Wave Climate Changes in the North Atlantic and the North Sea. *Int. J. Climatol.*, **11**, 545-558.
- Bajuk**, L.J. and C.B. Leovy, 1998a: Are there real interdecadal variations in marine low clouds? *J. Climate*, **11**, 2910-2921.
- Bajuk**, L.J. and C.B. Leovy, 1998b: Seasonal and interannual variations in stratiform and convective clouds over the tropical Pacific and Indian Oceans from ship observations. *J. Climate*, **11**, 2922-2941.
- Balling**, R.C., Jr., 1998: Analysis of daily and monthly spatial variance components in historical temperature records. *Physical Geography*, **18**, 544-552.
- Barber**, D.C., A. Dyke, C. Hillaire-Marcel, A.E. Jennings, J.T. Andrews, M.W. Kerwin, G. Bilodeau, R. McNeely, J. Southon, M.D. Morehead and J.M. Gagnon, 1999: Forcing of the cold event of 8,200 years ago by catastrophic drainage of Laurentide lakes. *Nature*, **400**, 344-347.
- Bard**, E., M. Arnold, P. Maurice, J. Duprat, J. Moyes and J.C. Duplessy, 1987: Retreat velocity of the North Atlantic polar front during the last deglaciation determined by <sup>14</sup>C accelerator mass spectrometry. *Science*, **328**, 791-794.
- Barnett**, T.P., B. Santer, P.D. Jones and R.S. Bradley, 1996: Estimates of low frequency natural variability in near-surface air temperature. *The Holocene*, **6**, 255-263.
- Basist**, A.N. and M. Chelliah, 1997: Comparison of tropospheric temperatures derived from the NCEP/NCAR reanalysis, NCEP operational analysis and the Microwave Sounding Unit. *Bull. Am. Met. Soc.*, **78**, 1431-1447.
- Bates**, J.J. and D.L. Jackson, 2001: Trends in upper tropospheric humidity, *Geophys. Res. Lett.*, in press.
- Bates**, J., X. Wu and D. Jackson, 1996: Interannual variability of upper-tropospheric water vapor band brightness temperature. *J. Climate*, **9**, 427-438.
- Behl**, R.J. and J.P. Kennet, 1996: Brief interstadial events in the Santa Barbara basin, NE Pacific, during the past 60 kyr. *Nature*, **379**, 243-246.
- Belkin**, I.M., S. Levitus, J. Anotonov and S.-A. Malmberg, 1998: "Great Salinity Anomalies" in the North Atlantic. *Progress in Oceanography*, **41**, 1-68.
- Beltrami**, H. and A.E. Taylor, 1994: Records of climatic change in the Canadian Arctic: Combination of geothermal and oxygen isotope data yields high resolution ground temperature histories. *EOS, Transactions, American Geophysical Union*, **75**(44), 75.
- Bender**, M., T. Sowers, M.L. Dickson, J. Orchado, P. Grootes, P.A. Mayewski and D.A. Meese, 1994: Climate connection between Greenland and Antarctica during the last 100,000 years. *Nature*, **372**, 663-666.
- Bender**, M., B. Malaize, J. Orchado, T. Sowers and J. Jouzel, 1999: High precision correlations of Greenland and Antarctic ice core records over the last 100 kyr. *Geophysical Monograph*, **112**, Mechanisms of global climate change at millennial timescales, edited by P.U. Clark, R.S. Webb and L.D. Keigwin, 149-164.
- Bianchi**, G.G. and N.I. McCave, 1999: Holocene periodicity in North Atlantic climate and deep-ocean flow South of Iceland. *Nature*, **397**, 515-517.
- Bigg**, G.R. and M. Inonue, 1992: Rossby waves and El Nino 1935-1946. *Quart. J. R. Met. Soc.*, **118**, 125-152.
- Bindoff**, N.L. and T.J. McDougall, 2000: Decadal changes along an Indian Ocean section at 32°S. and their interpretation. *J. Phys. Oceanogr.*, **30**, 1207-1222.
- Bjørø**, E., O.M. Johannessen and M.W. Miles, 1997: Analysis of merged SMMR/SSMI time series of Arctic and Antarctic sea ice parameters, *Geophys. Res. Lett.*, **24**, 413-416.
- Black**, D.E., L.C. Peterson, J.T. Overpeck, A. Kaptan, M.N. Evans and M. Kashgarian, 1999: Eight centuries of North Atlantic Ocean Atmosphere Variability. *Science*, **286**, 1709-1713.
- Black**, P.G., 1993: Evolution of maximum wind estimates in typhoons. In: *Tropical Cyclone Disasters*, edited by J. Lighthill, Z. Zhemin, G. Holland and K. Emanuel, Peking University Press, Beijing, 104-115.
- Blunier**, T., J. Schwander, B. Stauffer, T. Stocker, A. Dällenbach, A. Indermühle, J. Tschumi, J. Chappellaz, D. Raynaud, J.M. Barnola,

- 1997: Timing of the Antarctic Cold Reversal and the atmospheric CO<sub>2</sub> increase with respect to the Younger Dryas event. *Geophys. Res. Lett.*, **24**(21), 2683-2686.
- Blunier**, T., J. Chappellaz, J. Schwander, A. Dällenbach, B. Stauffer, T. Stocker, D. Raynaud, J. Jouzel, H.B. Clausen, C.U. Hammer and S.J. Johnsen, 1998: Asynchrony of Antarctic and Greenland climate change during the last glacial period. *Nature*, **394**, 739-743.
- Bogdanova**, E.G. and A.V. Mestcherskaya, 1998: Influence of moistening losses on the homogeneity of annual precipitation time series. *Russian Meteorol. Hydrol.*, **11**, 88-99.
- Bond**, G. and R. Lotti, 1995: Iceberg discharges into the North Atlantic on millennial time scales during the last glaciation. *Science*, **267**, 1005-1010.
- Bond**, G., W.S. Broecker, S.J. Johnsen, J. McManus, L.D. Labeyrie, J. Jouzel and G. Bonani, 1993: Correlations between climate records from North Atlantic sediments and Greenland ice. *Nature*, **365**, 143-147.
- Bond**, G., Showers, W. Cheseby, M. Lotti, R. Almasi, P. deMenocal, P. Priore, P. Cullen, H.I. Hajdas and G. Bonani, 1997: A pervasive Millennial-scale cycle in North Atlantic Holocene and glacial climates. *Science*, **278**, 1257-1266.
- Bönisch**, G., J. Blindheim, J.L. Bullister, P. Schlosser and D.W.R. Wallace, 1997: Long-term trends of temperature, salinity, density, and transient tracers in the central Greenland Sea. *J. Geophys. Res.*, **102**(C8), 18553-18571.
- Bonsal**, B.R., X. Zhang, L.A. Vincent and W.D. Hogg, 2001: Characteristics of daily and extreme temperatures over Canada. *J. Climate*, in press.
- Bottomley**, M., C.K. Folland, J. Hsiung, R.E. Newell and D.E. Parker, 1990: Global Ocean Surface Temperature Atlas "GOSTA". HMSO, London, 20pp+iv, 313 plates.
- Bouws**, E., D.Jannink and G.J. Komen, 1996: The Increasing Wave Height in the North Atlantic Ocean. *Bull. Am. Met. Soc.*, **77**, 2275-2277.
- Bradley**, R.S., 1999: Paleoclimatology: reconstructing climates of the Quaternary Harcourt. Academic Press, San Diego, 610 pp.
- Bradley**, R.S. and P.D. Jones, 1993: 'Little Ice Age' summer temperature variations: their nature and relevance to recent global warming trends. *The Holocene*, **3**, 367-376.
- Bradley**, R.S. and P.D. Jones (eds.), 1995: Climate Since A.D. 1500. (Revised edition) Routledge, London, 706 pp.
- Brázdil**, R., 1996: Reconstructions of past climate from historical sources in the Czech Lands. In: *Climatic Variations and Forcing Mechanisms of the Last 2000 Years*, P.D. Jones, R.S. Bradley and J. Jouzel (eds.), NATO ASI Series, Springer Verlag, Berlin, Heidelberg, **41**, 409-431.
- Brázdil**, R. and T. Vais, 1997: Thunderstorms and related weather extremes in south Moravia, Czech Republic in 1946-1995: Data, results, impacts. *Preprints of the Workshop on Indices and Indicators for Climate Extremes, NOAA/NCDC, Asheville NC USA*, 3-6 June 1997, 4 pp.
- Brázdil**, R., M. Budykov, I. Auer, R. Böhm, T. Cegnar, P. Fasko, M. Lapin, M. Gajic-Capka, K. Zaninovic, E. Koleva, T. Niedzwiedz, S. Szalai, Z. Ustrnul and R.O. Weber, 1996: Trends of maximum and minimum daily temperatures in central and southeastern Europe. *Int. J. Climatol.*, **16**, 765-782.
- Brecher**, H.H. and L.G. Thompson, 1993: Measurement of the retreat of Qori Kalis glacier in the tropical Andes of Peru by terrestrial photogrammetry. *Photogrammetric Engineering and Remote Sensing*, **59**(6), 1017-1022.
- Briffa**, K.R., 2000: Annual climate variability in the Holocene: interpreting the message of ancient trees. *Quat. Sci. Rev.*, **19**, 87-105.
- Briffa**, K.R., P.D. Jones, F.H. Schweingruber, S.G. Shiyatov, and E.R. Cook, 1995: Unusual twentieth-century summer warmth in a 1,000-year temperature record from Siberia. *Nature*, **376**, 156-159.
- Briffa**, K.R., P.D. Jones, F.H. Schweingruber, S.G. Shiyatov and E.A. Vaganov, 1996: Development of a North Eurasian chronology network: Rationale and preliminary results of comparative ring-width and densitometric analyses in northern Russia. In: *Tree Rings, Environment, and Humanity. Radiocarbon 1996*, J.S. Dean, D.M. Meko and T.W. Swetnam (eds.), Department of Geosciences, The University of Arizona, Tucson, pp. 25-41.
- Briffa**, K.R., F.H. Schweingruber, P.D. Jones, T.J. Osborn, S.G. Shiyatov and E.A. Vaganov, 1998a: Reduced sensitivity of recent tree-growth to temperature at high northern latitudes. *Nature*, **391**, 678-682.
- Briffa**, K.R., P.D. Jones, F.H. Schweingruber and T.J. Osborn, 1998b: Influence of volcanic eruptions on Northern Hemisphere summer temperature over the past 600 years. *Nature*, **393**, 450-455.
- Broecker**, W.S., 1997: Thermohaline circulation, the Achilles heel of our climate system: Will man-made CO<sub>2</sub> upset the current balance? *Science*, **278**, 1582-1588.
- Broecker**, W.S., 1998: Paleocean circulation during the last deglaciation - A bipolar seasaw? *Paleoceanography*, **13**, 119-121.
- Broecker**, W.S., D.M. Peteet and D. Rind, 1985: Does the ocean-atmosphere system have more than one mode of operation? *Nature*, **315**, 21-26.
- Brown**, J., O.J. Ferrians, Jr., J.A. Heginbottom and E.S. Melnikov, 1997: Circum-Arctic map of permafrost and ground-ice conditions. *U.S. Geological Survey Circum-Pacific Map CP- 45*, 1:10,000,000, Reston, Virginia.
- Brown**, N. and A. Issar (eds.), 1998: Water, Environment and Society in Times of Climatic Change. Kluwer, pp. 241-271.
- Brown**, R.D., 2000: Northern Hemisphere snow cover variability and change, 1915-1997. *J. Climate*, **13**, 2339-2355.
- Brown**, R.D. and B.E. Goodison, 1996: Interannual variability in reconstructed Canadian snow cover, 1915-1992. *J. Climate*, **9**, 1299-1318.
- Brown**, R.D. and R.O. Braaten, 1998: Spatial and temporal variability of Canadian monthly snow depths, 1946-1995. *Atmosphere-Ocean*, **36**, 37-45.
- Brown**, S.J., D.E. Parker, C.K. Folland and I. Macadam, 2000: Decadal variability in the lower-tropospheric lapse rate. *Geophys. Res. Lett.*, **27**, 997-1000.
- Brunet-India**, M., E. Aguilar, O. Saladie, J. Sigro and D. Lopez, 1999a: Evolución térmica reciente de la región catalana a partir de la construcción de series climáticas regionales. In: Raso Nadal, J. M. and Martín-Vide, J.: *La Climatología española en los albores del siglo XXI*, Barcelona: Publicaciones de la A.E.C., Serie A, **1**, 91-101.
- Brunet-India**, M., E. Aguilar, O. Saladie, J. Sigro and D. Lopez, 1999b: Variaciones y tendencias contemporáneas de la temperatura máxima, mínima y amplitud térmica diaria en el NE de España, In: Raso Nadal, J. M. Martín-Vide, J.: *La Climatología española en los albores del siglo XXI*, Barcelona: Publicaciones de la A.E.C., Serie A, **1**, 103-112.
- Brunetti**, M., L. Buffoni, M. Maugeri and T. Nanni, 2000a: Trends of minimum and maximum daily temperatures in Italy from 1865 to 1996. *Theoretical and Applied Climatology*, **66**, 49-60.
- Brunetti**, M., S. Cecchini, M. Maugeri and T. Nanni, 2000b: Solar and terrestrial signals in precipitation and temperature in Italy from 1865 to 1996. *Advances in Geosciences*, W. Schroeder (Editor), IAGA, pp. 124-133.
- Brutsaert**, W. and M.B. Parlange, 1998: Hydrological cycle explains the evaporation paradox. *Nature*, **396**, 30.
- Bryden**, H.L., M.J. Griffiths, A.M. Lavin, R.C. Millard, G. Parrilla and W.M. Smethie, 1996: Decadal changes in water masses characteristics at 24°N in the subtropical Atlantic Ocean. *J. Climate*, **9**, 3162-3186.
- Buffoni**, L., M. Maugeri and T. Nanni, 1999: Precipitation in Italy from 1833 to 1996. *Theoretical and Applied Climatology*, **63**, 33-40.
- Burgess**, M.M., S.L. Smith, J. Brown, V. Romanovsky and K. Hinkel,

- 2000: The Global Terrestrial Network for Permafrost (GTNet-P): permafrost monitoring contributing to global climate observations. *Geological Survey of Canada, Current Research 2000E-14*, 8 pp. (online, <http://www.nrcan.gc.ca/gsc/bookstore>)
- Burn, C.R.**, 1998: Field investigations of permafrost and climatic change in northwest North America; *Proceedings of Seventh International Conference on Permafrost*, Yellowknife, Canada, June 1998, Université Laval, Quebec, Collection Nordicana No. 57, pp. 107-120
- Carmack, E.C.**, R.W. MacDonald, R.W. Perkin, F.A. McLaughlin and R.J. Pearson, 1995: Evidence for warming of Atlantic water in the southern Canadian Basin of the Arctic Ocean: Results from the Larsen-93 expedition. *Geophys. Res. Lett.*, **22**, 1061-1064.
- Carter, D.J.T.** and L. Draper, 1988: Has the Northeast Atlantic Become Rougher? *Nature*, **332**, 494.
- Cavalieri, D.J.**, P. Gloersen, C.L. Parkinson, J.C. Comiso and H.J. Zwally, 1997: Observed hemispheric asymmetry in global sea ice changes. *Science*, **278**, 1104-1106.
- Chan, J.C.L.** and J. Shi, 1996: Long-term trends and interannual variability in tropical cyclone activity over the western North Pacific. *Geophys. Res. Lett.*, **23**, 2765-2767.
- Changnon, D.** and S.A. Changnon, 1997: Surrogate data to estimate crop-hail loss. *J. Appl. Met.*, **36**, 1202-1210.
- Changnon, S.A.**, 1985: Secular variations in thunder-day frequencies in the twentieth century. *J. Geophys. Res.*, **90**, 6181-6194.
- Changnon, S.A.** and D. Changnon, 2000: Long-term fluctuations in hail incidences in the United States. *J. Climate*, **13**, 658-664.
- Changnon, S.A.**, D. Changnon, E.R. Fosse, D.C. Hoganson, R.J. Roth and J. Totsch, 1996: Impacts and Responses of the Weather Insurance Industry to Recent Weather Extremes. *Final Report to UCAR from Changnon Climatologist*, CRR-41, Mahomet, IL, 166 pp.
- Chanin, M.L.** and V. Ramaswamy, 1999: "Trends in Stratospheric Temperatures" in WMO (World Meteorological Organization), Scientific Assessment of Ozone Depletion: 1998, *Global Ozone Research and Monitoring Project - Report No. 44*, Geneva, pp. 5.1-5.59.
- Chao, Y.**, M. Ghil and J.C. McWilliams, 2000: Pacific Interdecadal variability in this century's sea surface temperatures. *Geophys. Res. Lett.*, **27**, 2261-2264.
- Chapman, W.L.** and J.E. Walsh, 1993: Recent variations of sea ice and air temperature in high latitudes. *Bull. Am. Met. Soc.*, **74**, 33-47.
- Chappellaz, J.**, E. Brook, T. Blunier and B. Malaizé, 1997: CH<sub>4</sub> and δ<sup>18</sup>O of O<sub>2</sub> records from Greenland ice: A clue for stratigraphic disturbance in the bottom part of the Greenland Ice Core Project and the Greenland Ice Sheet Project 2 ice-cores. *J. Geophys. Res.*, **102**, 26547-26557.
- Charles, C.D.**, J. Lynch-Stieglitz, U.S. Nienemann and R.G. Fairbanks, 1996: Climate connections between the two hemispheres revealed by deep sea sediment core/ice core correlations. *Earth Planet Sci. Lett.*, **142**, 19-27.
- Chase, T.N.**, R.A. Pielke Sr., J.A. Knaff, T.G.F. Kittel and J.L. Eastman, 2000: A comparison of regional trends in 1979-1997 depth-averaged tropospheric temperatures. *Int. J. Climatol.*, **20**, 503-518.
- Cheddadi, R.**, K. Mamakowa, J. Guiot, J.L. de Beaulieu, M. Reille, V. Andrieu, W. Grasnoszewski and O. Peyron, 1998: Was the climate of the Eemian stable ? A quantitative climate reconstruction from seven European climate records. *Paleogeography, Paleoclimatology, Paleoecology*, **143**, 73-85.
- Christy, J.R.**, 1995: Temperature above the surface. *Clim. Change*, **31**, 455-474.
- Christy, J.R.** and R. T. McNider, 1994: Satellite greenhouse warming. *Nature*, **367**, 325.
- Christy, J.R.**, R.W. Spencer and E. Lobl, 1998: Analysis of the merging procedure for the MSU daily temperature time series. *J. Climate*, **5**, 2016-2041.
- Christy, J.R.**, R.W. Spencer and W.D. Braswell, 2000: MSU tropospheric temperatures: Dataset construction and radiosonde comparisons. *J. Atmos. Oceanic Tech.*, **17**, 1153-1170.
- Christy, J.R.**, D.E. Parker, S.J. Brown, I. Macadam, M. Stendel and W.B. Norris, 2001: Differential trends in tropical sea surface and atmospheric temperatures. *Geophys. Res. Lett.*, **28**, 183-186.
- Ciaia, P.**, J.R. Petit, J. Jouzel, C. Lorius, N.I. Barkov, V. Lipenkov and V. Nicolaïev, 1992: Evidence for an Early Holocene climatic optimum in the Antarctic deep ice core record. *Clim. Dyn.*, **6**, 169-177.
- Clausen, H.B.**, C.U. Hammer, J. Christensen, C.S. Schott Hvidberg, D. Dahl-Jensen, M. Legrand and J.P. Steffensen, 1995: 1250 years of global volcanism as revealed by central Greenland ice cores. In: *Ice Core Studies of Global Biogeochemical Cycles*, Nato ASI, Series I, vol 30., edited by R.J. Delmas, Springer-Verlag, New York, pp. 517-532.
- CLIMAP Project Members**, 1984: The last interglacial ocean. *Quat. Res.*, **21**, 123-224.
- Clow, G.D.**, A.H. Lachenbruch and C.P. McKay, 1991: Investigation of borehole temperature data for recent climate changes: Examples from Alaskan Arctic and Antarctica. In: *Proceedings of the International Conference on the Role of Polar Regions in Global Change*, June 11-15, 1990, Geophysical Institute, University of Alaska, Fairbanks, vol. 2, 533.
- COHMAP Members**, 1988: Climatic changes of the last 18,000 years: observations and model simulations. *Science*, **241**, 1043-1052.
- Cole, J.E.** and E.R. Cook, 1998: The changing relationship between ENSO variability and moisture balance in the continental United States. *Geophys. Res. Lett.*, **25**, 4529-4532.
- Coles, V.J.**, M.S. McCartney, D.B. Olson and W.M. Smethie Jr., 1996: Changes in the Antarctic bottom water properties in the western South Atlantic in the late 1980's. *J. Geophys. Res.*, **101**(C4), 8957-8970.
- Collins, D.A.**, P.M. Della-Marta, N. Plummer and B.C. Trewin, 2000: Trends in annual frequencies of extreme temperature events in Australia. *Australian Meteorological Magazine*, **49**, 277-292.
- Combourieu-Nebout, N.**, M. Paterne and J.L. Turon, 1998: A high-resolution record of the last deglaciation in the Central Mediterranean Sea: Palaeovegetation and palaeohydrological evolution. *Quat. Sci. Rev.*, **17**, 303-317.
- Comiso, F.**, 2000: Variability and trends in Antarctic temperatures from in situ and satellite infrared measurements. *J. Climate*, **13**, 1674-1696.
- Cook, E.R.**, 1995: Temperature histories in tree rings and corals. *Clim. Dyn.*, **11**, 211-222.
- Cook, E.R.**, R.D. D'Arrigo and K.R. Briffa, 1998: A reconstruction of the North Atlantic Oscillation using tree-ring chronologies from North America and Europe. *The Holocene*, **8**, 9-17.
- Cook, E.R.**, D.M. Meko, D.W. Stahle and M.K. Cleaveland, 1999: Drought reconstructions for the continental United States. *J. Climate*, **12**, 1145-1162.
- Cook, E.R.**, B.M. Buckley and R.D. D'Arrigo, 2000: Warm-Season Temperatures since 1600 B.C. Reconstructed from Tasmanian Tree Rings and Their Relationship to Large-Scale Sea Surface Temperature Anomalies. *Clim. Dyn.*, **16**, 79-91.
- Cortijo, E.**, J. Duplessy, L. Labeyrie, H. Leclaire, J. Duprat and T. van Weering, 1994: Eemian cooling in the Norwegian Sea and North Atlantic ocean preceding ice-sheet growth. *Nature*, **372**, 446-449.
- Cortijo, E.**, L.D. Labeyrie, L. Vidal, M. Vautravers, M. Chapman, J.C. Duplessy, M. Elliot, M. Arnold and G. Auffret, 1997: Changes in the sea surface hydrology associated with Heinrich event 4 in the North Atlantic Ocean (40-60°N). *Earth Planet. Sci. Lett.*, **146**, 29-45.
- Crowley, T.J.**, 1992: North Atlantic Deep Water Cools The Southern Hemisphere. *Paleoceanography*, **7**, 489-497.
- Crowley, T.J.**, 2000: Causes of Climate Change Over the Past 1000 Years. *Science*, **289**, 270-277.
- Crowley, T.J.** and K.Y. Kim, 1996: Comparison of proxy records of

- climate change and solar forcing. *Geophys. Res. Lett.*, **23**, 359-362.
- Crowley**, T.J. and K.Y. Kim, 1999: Modeling the temperature response to forced climate change over the last six centuries. *Geophys. Res. Lett.*, **26**, 1901-1904.
- Crowley**, T.J. and T. Lowery, 2000: How warm was the Medieval warm period? *Ambio*, **29**, 51-54.
- Cullen**, H., R. D'Arrigo, E. Cook and M.E. Mann, 2001: Multiproxy-based reconstructions of the North Atlantic Oscillation over the past three centuries. *Paleoceanography*, **16**, 27-39.
- Dahl-Jensen**, D., K. Mosegaard, N. Gundestrup, G.D. Clow, S.J. Johnsen, A.W. Hansen and N. Balling, 1998: Past temperatures directly from the Greenland ice sheet. *Science*, **282**, 268-271.
- Dai**, A., A.D. DelGenio and I.Y. Fung, 1997a: Clouds, precipitation, and temperature range. *Nature*, **386**, 665-666.
- Dai**, A., I.Y. Fung and A.D. Del Genio, 1997b: Surface observed global land precipitation variations during 1900-88. *J. Climate*, **10**, 2943-2962.
- Dai**, A., K.E. Trenberth and T.R. Karl, 1998: Global variations in droughts and wet spells: 1900-1995. *Geophys. Res. Lett.*, **25**, 3367-3370.
- Dai**, A., K.E. Trenberth and T.R. Karl, 1999: Effects of clouds, soil moisture, precipitation and water vapor on diurnal temperature range. *J. Climate*, **12**, 2452-2473.
- Damon**, P.E. and A.N. Peristykh, 1999: Solar cycle length and 20th century Northern Hemisphere Warming. *Geophys. Res. Lett.*, **26**, 2469-2472.
- Dansgaard**, W., H.B. Clausen, N. Gundestrup, C.U. Hammer, S.J. Johnsen, P. Krinstindottir and N. Reeh, 1982: A new Greenland deep ice core. *Science*, **218**, 1273-1277.
- Dansgaard**, W., J.W. White and S.J. Johnsen, 1989: The abrupt termination of the Younger Dryas climate event. *Nature*, **339**, 532-534.
- Dansgaard**, W., S.J. Johnsen, H.B. Clausen, D. Dahl-Jensen, N.S. Gundestrup, C.U. Hammer, C.S. Hvidberg, J.P. Steffensen, A.E. Sveinbjörnsdóttir, J. Jouzel and G. Bond, 1993: Evidence for general instability of past climate from a 250 kyr ice core. *Nature*, **364**, 218-219.
- D'Arrigo**, R.D., E.R. Cook and G.C. Jacoby, 1996: Annual to decadal-scale variations in northwest Atlantic sector temperatures inferred from Labrador tree rings. *Canadian Journal of Forest Research*, **26**, 143-148.
- D'Arrigo**, R.D., E.R. Cook, M.J. Salinger, J. Palmer, P.J. Krusic, B.M. Buckley and R. Villalba, 1998: Tree-ring records from New Zealand: long-term context for recent warming trend. *Clim. Dyn.*, **14**, 191-199.
- De la Mare**, W.K., 1997: Abrupt mid-twentieth century decline in Antarctic sea-ice extent from whaling records. *Nature*, **389**, 57-60.
- Delworth**, T.L. and M.H. Mann, 2000: Observed and simulated multidecadal variability in the Northern Hemisphere. *Clim. Dyn.*, **16**, 661-676.
- de Menocal**, P., 1998: Subtropical signatures of millennial-scale Holocene climate variability. International Conference of Paleoceanography.
- Denton**, G. and C.H. Hendy, 1994: Younger Dryas age advance of the Franz Josef glacier in the Southern Alps of New Zealand. *Science*, **264**, 1434-1437.
- Deser**, C. and M.L. Blackmon, 1995: On the relationship between tropical and North Pacific sea surface temperature variations. *J. Climate*, **8**, 1677-1680.
- Deser**, C., J.E. Walsh and M.S. Timlin, 2000: Arctic sea ice variability in the context of recent wintertime atmospheric circulation trends. *J. Climate*, **13**, 617-633.
- Dessens**, J., 1995: Severe convective weather in the context of a nighttime global warming. *Geophys. Res. Lett.*, **22**, 1241-1244.
- Diaz**, H.F. and H.F. Graham, 1996: Recent changes in tropical freezing heights and the role of sea surface temperature. *Nature*, **383**, 152-155.
- Dickson**, R.R., J. Lazier, J. Meincke, P. Rhines and J. Swift, 1996: Long-term co-ordinated changes in the convective activity of the North Atlantic. *Prog. Oceanogr.*, **38**, 241-295.
- Diggle**, P.J., K.Y. Liang and S.L. Zeger, 1999: Analysis of longitudinal data. Clarendon Press, Oxford, 253 pp.
- Ding**, Y., 1998: Recent degradation of permafrost in China and the response to climatic warming. In: *Proceedings of the Seventh International Conference on Permafrost*, Yellowknife, Canada, June 1998, Université Laval, Quebec, Collection Nordicana No. 57, pp. 221-224.
- Ding**, Z.L., N.W. Rutter, T.S. Liu, J.M. Sun, J.Z. Ren, D. Rokosh and S.F. Xiong, 1998: Correlation of Dansgaard-Oeschger cycles between Greenland ice and Chinese loess. *Paleoclimates*, **2**, 281-291.
- Doherty**, R.M., M. Hulme and C.G. Jones, 1999: A gridded reconstruction of land and ocean precipitation for the extended Tropics from 1974-1994. *Int. J. Climatol.*, **19**, 119-142.
- Doswell**, C.A. III and D.W. Burgess, 1988: On some issues of United States tornado climatology. *Mon. Wea. Rev.*, **116**, 495-501.
- Douglas**, A.V. and P.J. Englehart, 1999: Inter-monthly variability of the Mexican summer monsoon. *Proceedings of the Twenty-Second Annual Climate Diagnostics and Prediction Workshop*, Berkeley, CA, October 6-10, 1997, Washington, D.C.: U.S. Department of Commerce, NOM, NTIS #PB97-159164, pp. 246-249.
- Dunbar**, R.B. and J.E. Cole, 1999: Annual Records of Tropical Systems, (ARTS): A PAGES Report 99-1/CLIVAR Initiative: Recommendations for Research. Summary of scientific priorities and implementation strategies: *ARTS Planning Workshop*, Kauai, Hawaii, PAGES Report 99-1.
- Dunkerton**, T., D. Delisi and M. Baldwin, 1998: Middle atmosphere cooling trend in historical rocketsonde data. *Geophys. Res. Lett.*, **25**, 3371-3374.
- Duplessy**, J.C., L. Labeyrie, A. Juillet-Leclerc, F. Maitre, J. Duprat and M. Sarnthein, 1991: Surface salinity reconstruction of the North Atlantic Ocean during the last glacial maximum. *Oceanologica Acta*, **14**, 311-324.
- Duplessy**, J.C., L. Labeyrie, M. Arnold, M. Paterné, J. Duprat and T.C.E. van Weering, 1992: Changes in surface salinity of the North Atlantic Ocean during the last deglaciation. *Nature*, **358**, 485-487.
- Easterling**, D.R., B. Horton, P.D. Jones, T.C. Peterson, T.R. Karl, D.E. Parker, M.J. Salinger, V. Razuvayev, N. Plummer, P. Jamason and C.K. Folland, 1997: Maximum and minimum temperature trends for the globe. *Science*, **277**, 364-367.
- Easterling**, D.R., J.L. Evans, P.Ya. Groisman, T.R. Karl, K.E. Kunkel and P. Ambenje, 2000: Observed variability and trends in extreme climate events. *Bull. Am. Met. Soc.*, **81**, 417-425.
- Elliott**, W.P., 1995: On detecting long-term changes in atmospheric moisture. *Clim. Change*, **31**, 349-367.
- Elliott**, W. and D. Gaffen, 1991: On the utility of radiosonde humidity archives for climate studies. *Bull. Am. Met. Soc.*, **72**, 1507-1520.
- Ely**, L.L., E. Yehouda, V.R. Baker and D.R. Cayan, 1993: A 5000-year record of extreme floods and climate change in the Southwestern United States. *Science*, **262**, 410-412.
- Enfield**, D.B. and A.M. Mestas-Nuñez, 1999: Multiscale variabilities in global sea surface temperatures and their relationships with tropospheric climate patterns. *J. Climate*, **12**, 2719-2733.
- Environmental Working Group (EWG)**, 1997: *Joint U.S.-Russian Atlas of the Arctic Ocean [CD-ROM]*, Natl. Snow and Ice Data Centre, Boulder, Colorado, USA.
- Eskridge**, R.E., O.A. Alduchov, I.V. Chernykh, Z. Panmao, A.C. Polansky and S.R. Doty, 1995: A Comprehensive aerological reference data set (CARDS): Rough and systematic errors. *Bull. Am. Met. Soc.*, **76**, 1759-1775.
- Evans**, J.S., R. Toumi, J.E. Harries, M.P. Chipperfield and J.R. Russell III, 1998: Trends in stratospheric humidity and the sensitivity of ozone to those trends. *J. Geophys. Res.*, **103**, 8715-8725.
- Fallot**, J.-M., R.G. Barry and D. Hoogstrate, 1997: Variations of mean cold season temperature, precipitation and snow depths during the

- last 100 years in the Former Soviet Union (FSU). *Hydrol. Sci. J.*, **42**, 301-327.
- Fernandez-Partagas**, J. and H.F. Diaz, 1996: Atlantic hurricanes in the second half of the 19th Century. *Bull. Am. Met. Soc.*, **77**, 2899-2906.
- Fischer**, H., M. Wahlen, J. Smith, D. Mastroiani and B. Deck, 1999: Ice core records of atmospheric CO<sub>2</sub> around the last three glacial terminations. *Science*, **283**, 1712-1714.
- Fisher**, D.A. 1997: High resolution reconstructed Northern Hemisphere temperatures for the last few centuries: using regional average tree ring, ice core and historical annual time series. Paper U32C-7 in *Supplement to EOS, Transactions*, American Geophysical Union Vol. 78 No. 46, abstract.
- Fisher**, D.A., R.M. Koerner, K. Kuivinen, H.B. Clausen, S.J. Johnsen, J.P. Steffensen, N. Gundestrup and C.U. Hammer, 1996: Inter-comparison of ice core (O-18) and precipitation records from sites in Canada and Greenland over the last 3500 years and over the last few centuries in detail using EOF techniques. In: *Climate Variations and Forcing Mechanisms of the Last 2000 Years*, edited by P.D. Jones, R.S. Bradley and J. Jouzel, NATO ASI Series I, Vol. 41, pp. 297-328.
- Fisher**, D.A., R.M. Koerner, J.C. Bourgeois, G. Zielinski, C. Wake, C.U. Hammer, H.B. Clausen, N. Gundestrup, S.J. Johnsen, K. Goto-Azuma, T. Hondoh, E. Blake and M. Gerasimoff, 1998: Penny Ice Cap, Baffin Island, Canada, and the Wisconsinan Foxe Dome Connection: two states of Hudson Bay ice cover. *Science*, **279**, 692-695.
- Fleming**, K.M., J.A. Dowdeswell and J. Oerlemans, 1997: Modelling the mass balance of northwest Spitsbergen glaciers and response to climate change. *Ann. Glaciol.*, **24**, 203-210.
- Folland**, C.K. and D.E. Parker, 1995: Correction of instrumental biases in historical sea surface temperature data. *Quart. J. R. Met. Soc.*, **121**, 319-367.
- Folland**, C.K. and M.J. Salinger, 1995: Surface temperature trends in New Zealand and the surrounding ocean, 1871-1993. *Int. J. Climatol.*, **15**, 1195-1218.
- Folland**, C.K., D.E. Parker and T.N. Palmer, 1986: Sahel rainfall and worldwide sea temperatures 1901-85. *Nature*, **320**, 602-607.
- Folland**, C.K., R.W. Reynolds, M. Gordon and D.E. Parker, 1993: A study of six operational sea surface temperature analyses. *J. Climate*, **6**, 96-113.
- Folland**, C.K., M.J. Salinger and N. Rayner, 1997: A comparison of annual South Pacific island and ocean surface temperatures. *Weather and Climate*, **17**, 23-42.
- Folland**, C.K., D.M.H. Sexton, D.J. Karoly, C.E. Johnson, D.P. Rowell and D.E. Parker, 1998: Influences of anthropogenic and oceanic forcing on recent climate change. *Geophys. Res. Lett.*, **25**, 353-356.
- Folland**, C.K., D.E. Parker, A.W. Colman and R. Washington, 1999a: Large scale modes of ocean surface temperature since the late nineteenth century. In: *Beyond El Niño: Decadal and Interdecadal Climate Variability*, A. Navarra (ed.), Springer-Verlag, Berlin, pp. 73-102.
- Folland**, C.K., C. Miller, D. Bader, M. Crowe, P. Jones, N. Plummer, D.E. Parker, J. Rogers and P. Scholefield, 1999b: Workshop on Indices and Indicators for climate extremes, Asheville, NC, USA, 3-6 June 1999: Breakout Group C: Temperature indices for Climate Extremes. *Clim. Change*, **42**, 31-43.
- Folland**, C.K., N. Rayner, P. Frich, T. Basnett, D. Parker and B. Horton, 2000: Uncertainties in climate data sets – a challenge for WMO. *WMO Bull.*, **49**, 59-68.
- Folland**, C.K., N.A. Rayner, S.J. Brown, T.M. Smith, S.S. Shen, D.E. Parker, I. Macadam, P.D. Jones, R.N. Jones, N. Nicholls and D.M.H. Sexton, 2001: Global temperature change and its uncertainties since 1861. *Geophys. Res. Lett.*, in press.
- Førland**, E.J. and I. Hassen-Bauer, 2000: Increased precipitation in the Norwegian Arctic: True or false? *Clim. Change*, **46**, 485-509.
- Førland**, E.J., H. Alexandersson, A. Drebs, I. Hassen-Bauer, H. Vedin and O.E. Tveito, 1998: Trends in maximum 1-day precipitation in the Nordic region, *DNMI-KLIMA* 14/98, pp. 55, Norwegian Meteorological Institute, N-0313 Oslo, Norway.
- Forster**, P.M. and K.P. Shine, 1999: Stratospheric water vapour changes as a possible contributor to observed stratospheric cooling. *Geophys. Res. Lett.*, **26**, 3309-3312.
- Frank**, P., 1997: Changes in the glacier area in the Austrian Alps between 1973 and 1992 derived from LANDSAT data. *MPI report* 242, 21 pp.
- Free**, M. and A. Robock, 1999: Global Warming in the Context of the Little Ice Age. *J. Geophys. Res.*, **104** (D16), 19057-19070.
- Freeland**, H., K. Denman, C.S. Wong, F. Whitney and R. Jacques, 1997: Evidence of change in the winter mixed layer in the Northeast Pacific Ocean. *Deep Sea Res., Part I*, **44**(12), 2117-2129.
- Frei**, A., D.A. Robinson and M.G. Hughes, 1999: North American snow extent: 1900-1994. *Int. J. Climatol.*, **19**, 1517-1534.
- Frei**, C. and C. Schär, 2001: Detection probability of trends in rare events: Theory and application to heavy precipitation in the Alpine Region. *J. Climate*, **14**, 1568-1584.
- French**, H.M. and I.E. Egorov, 1998: 20th century variations in the southern limit of permafrost near Thompson, northern Manitoba, Canada. In: *Proceedings of Seventh International Conference on Permafrost*, Yellowknife, Canada, June 1998, Université Laval, Quebec, Collection Nordicana No. 57, pp. 297-304.
- Frich**, P., L.V. Alexander, P. Della-Marta, B. Gleason, M. Haylock, A. Klein-Tank and T. Peterson, 2001: Observed coherent changes in climatic extremes during the second half of the 20th Century. *Clim. Res.*, in press.
- Fritts**, H.C., 1976: Tree Rings and Climate. Academic Press, London.
- Fritts**, H.C., 1991: Reconstructing large-scale climatic patterns from Tree Ring Data. The University of Arizona Press, Tucson.
- Gabriel**, K.R. and S.A. Changnon, 1990: Temporal features in thunder days in the United States. *Clim. Change*, **15**, 455-477.
- Gaffen**, D.J., 1994: Temporal inhomogeneities in radiosonde temperature records. *J. Geophys. Res.*, **99**, 3667-3676.
- Gaffen**, D.J. and R.J. Ross, 1998: Increased summertime heat stress in the U.S. *Nature*, **396**, 529-530.
- Gaffen**, D.J. and R.J. Ross, 1999: Climatology and trends of U.S. surface humidity and temperature. *J. Climate*, **13**, 811-828.
- Gaffen**, D.J., B.D. Santer, J.S. Boyle, J.R. Christy, N.E. Graham and R. J. Ross, 2000a: Multidecadal changes in the vertical structure of the tropical troposphere. *Science*, **287**, 1242-1245.
- Gaffen**, D.J., M.A. Sargent, R.E. Habermann and J.R. Lazante, 2000b: Sensitivity of tropospheric and stratospheric temperature trends to radiosonde data quality. *J. Climate*, **13**, 1776-1796.
- Gagan**, M.K., L.K. Ayliffe, D. Hopley, J.A. Cali, G.E. Mortimer, J. Chappell, M.T. McCulloch and M.J. 1998: Heat, temperature and surface-ocean water balance of the mid-Holocene tropical western Pacific. *Science*, **279**, 1014-1018.
- Gallo**, K.P., D.R. Easterling and T.C. Peterson, 1996: The influence of land use/land cover on climatological values of the diurnal temperature range. *J. Climate*, **9**, 2941-2944.
- Garcia**, N.O. and W.M. Vargas, 1998: The temporal climatic variability in the 'Rio de la Plata' Basin displayed by the river discharges. *Clim. Change*, **38**, 359-379.
- Garreaud**, R.D. and D.S. Battisti, 1999: Interannual (ENSO) and interdecadal variability in the Southern Hemisphere tropospheric circulation. *J. Climate*, **12**, 2113-2123.
- Gasse**, F. and E. Van Campo, 1994: Abrupt post-glacials events in West asia and north Africa. *Earth Planet Sci. Lett.*, **126**, 453-456.
- Gasse**, F., R. Tehet and A. Durand, 1990: The arid-humid transition in the Sahara and the Sahel during the last deglaciation. *Nature*, **346**, 141-146.
- Genta**, J.L., G. Perez-Iribarren and C.R. Mechoso, 1998: A recent increasing trend in the streamflow of rivers in southeastern South America. *J. Climate*, **11**, 2858-2862.

- Georgievsky**, V.Yu., A.V. Ezhov, A.L. Shalygin, I.A. Shiklomanov and A.I. Shiklomanov, 1996: Assessment of the effect of possible climate changes on hydrological regime and water resources of rivers in the former USSR. *Russian Meteorol. And Hydrol.*, **11**, 66-74.
- Gershunov**, A. and T.P. Barnett, 1998: Interdecadal modulation of ENSO teleconnections. *Bull. Am. Met. Soc.*, **79**, 2715-2725.
- Goddard**, L. and N.E. Graham, 1997: El Niño in the 1990s. *J. Geophys. Res.*, **102**, 10423-10436.
- Golitsyn**, G.S., A.I. Semenov, N.N. Shefov, L.M. Fishkova, E.V. Lysenko and S.P. Perov, 1996: Long-term temperature trends in the middle and upper atmosphere. *Geophys. Res. Lett.*, **23**, 1741-1744.
- Golubev**, V.S., J.H. Lawrimore, P.Ya. Groisman, N.A. Speranskaya, S.A. Zhuravin, M.J. Menne, T.C. Peterson and R.W. Malone, 2001: Evaporation changes over the contiguous United States and the Former USSR: The re-assessment. *Geophys. Res. Lett.*, in press.
- Gong**, D.Y. and S.W. Wang, 1999a: Experiments on the reconstruction of historical monthly mean northern hemispheric 500hPa heights from surface data. *Report on the Department of Geophysics, Peking University*.
- Gong**, D.Y. and S.W. Wang, 1999b: Variability of the Siberian High and the possible connection to global warming. *Acta Geographica Sinica*, **54** (2), 142-150 (in Chinese).
- Gong**, D.Y. and S.W. Wang, 1999c: Definition of Antarctic Oscillation index. *Geophys. Res. Lett.*, **26**, 459-462.
- Goswami**, B.N., V. Krishnamurthy and H. Annamalai, 1997: A broad scale circulation index for the interannual variability of the Indian summer monsoon. *Report No. 46, COLA*, 4041 Powder Mill Road, Suite 302, Calverton, MD, 20705, USA.
- Graf**, H.F., J. Perlitz, I. Kirchner and I. Schult, 1995: Recent northern winter climate trends, ozone changes and increased greenhouse gas forcing. *Contrib. Phys. Atmos.*, **68**, 233-248.
- Graham**, N.E. and H.F. Diaz, 2001: Evidence for intensification of North Pacific Winter Cyclones since 1948. *J. Climate*, in press.
- Gravis**, G.F., N.G. Moskalenko and A.V. Pavlov, 1988: Perennial changes in natural complexes of the cryolithozone. In: *Proceedings of the Fifth International Conference on Permafrost*, Trondheim, Norway, vol. 1, 165-169.
- Grazulis**, T.P., 1993: Significant Tornadoes, 1680-1991. *Environmental Films*, St. Johnsbury, VT, 1326 pp.
- Grazulis**, T.P., C.A. Doswell III, H.E. Brooks and M. Biddle, 1998: A new perspective of the societal impacts of North American tornadoes covering two centuries. Preprints, *19th Conference on Severe Local Storms*. American Meteorological Society, Minneapolis, MN, 196-199.
- Greuell**, J.W. and J. Oerlemans, 1987: Sensitivity studies with a mass balance model including temperature profile calculations inside the glacier. *Zeits. Gletscherk. Glaziageol.*, **22**, 101-124.
- Grimm**, E.C., G.L. Jacobson, W.A. Watts, B.C.S. Hansen and K.A. Maasch, 1993: A 50000-year record of climate oscillations from Florida and its temporal correlation with the Heinrich events. *Science*, **261**, 198-200.
- GRIP** project members, 1993: Climatic instability during the last interglacial period revealed in the Greenland summit ice-core. *Nature*, **364**, 203-207.
- Groisman**, P.Ya. and D. Easterling, 1994: Variability and trends of total precipitation and snowfall over the United States and Canada. *J. Climate*, **7**, 184-205.
- Groisman**, P.Ya. and E.Ya. Rankova, 2001: Precipitation trends over the Russian permafrost-free zone: Removing the artifacts of pre-processing. *Int. J. Climatol.*, in press.
- Groisman**, P.Ya., T.R. Karl, D.R. Easterling, R.W. Knight, P.B. Jamason, K.J. Hennessy, R. Suppiah, C.M. Page, J. Wibig, K. Fortuniak, V.N. Razuvayev, A. Douglas, E. Førland and P.M. Zhai, 1999: Changes in the probability of heavy precipitation: Important indicators of climatic change. *Clim. Change*, **42**, 243-283.
- Groisman**, P.Ya., R.W. Knight and T.R. Karl, 2001: Heavy precipitation and high streamflow in the United States: Trends in the 20th century. *Bull. Am. Met. Soc.*, **82**, 219-246.
- Grootes**, P.M., M. Stuiver, J.W.C. White, S.J. Johnsen and J. Jouzel, 1993: Comparison of the oxygen isotope records from the GISP2 and GRIP Greenland ice cores. *Nature*, **366**, 552-554.
- Grove**, J.M. and R. Switsur, 1994: Glacial geological evidence for the Medieval Warm Period. *Clim. Change*, **26**, 143-169.
- Grumbine**, R.W., 1996: Automated Passive Microwave Sea Ice Concentration Analysis at NCEP. US Department of Commerce, National Oceanic and Atmospheric Administration, National Weather Service, National Centers for Environmental Prediction, Technical Note, OMB contribution 120, March, 1996, 13 pp. Also: (<http://polar.wwb.noaa.gov/seacie/docs/ssmi.auto/ssmi120.html>)
- Gruza**, G., E. Rankova, V. Razuvayev and O. Bulygina, 1999: Indicators of climate change for the Russian Federation. *Clim. Change*, **42**, 219-242.
- Gutzler**, D., 1996: Low-frequency ocean-atmosphere variability across the tropical western Pacific. *J. Atmos. Sci.*, **53**, 2773-2785.
- Haeberli**, W., G. Cheng, A.P. Gorunov and S.A. Harris, 1993: Mountain permafrost and climatic change. *Permafrost and Periglacial Processes*, **4**, 165-174.
- Haeberli**, W., M. Hoelzle and S. Suter (eds.), 1998: Into the second century of worldwide glacier monitoring: prospects and strategies, A contribution to the International Hydrological Programme (IHP) and the Global Environment Monitoring System (GEMS). *UNESCO Studies and Reports in Hydrology*, 56, Paris.
- Hagen**, J.O., K. Melvold, T. Eiken, E. Isaksson and B. Lefauconnier, 1995: Recent trends in the mass balance of glaciers in Scandinavia and Svalbard. *Proceedings of the international symposium on environmental research in the Arctic*. Watanabe, Okitsugu (Eds.), Tokyo, Japan, 19-21 July, 1995, National Institute of Polar Research, 343-354.
- Hahn**, C.J., S.G. Warren and J. London, 1996: Edited synoptic cloud reports from ships and land stations over the globe, 1982-1991. Rep#NDP026B, 45 pp. [Available from Carbon Dioxide Information Analysis Center, Oak Ridge National Laboratory, P.O. Box 2008, Oak Ridge, TN 37831-6050.]
- Halsey**, L.A., D.H. Vitt and S.C. Zoltai, 1995: Disequilibrium response of permafrost in boreal continental western Canada to climate change. *Clim. Change*, **30**, 57-73.
- Hammer**, C.U., H.B. Clausen and C.C. Langway, 1997: 50,000 years of recorded global volcanism. *Clim. Change*, **35**, 1-15.
- Hanawa**, K., S. Yasunaka, T. Manabe and N. Iwasaka, 2000: Examination of correction to historical SST data using long-term coastal SST data taken around Japan. *J. Met. Soc. Japan*, **78**, 187-195.
- Hansen**, J. and S. Lebedeff, 1988: Global surface temperatures: update through 1987. *Geophys. Res. Lett.*, **15**, 323-326.
- Hansen**, J.E., M. Sato, A. Lacis, R. Ruedy, I. Tegen and E. Matthews, 1998: Climate forcings in the Industrial era. *Proc. Natl. Acad. Sci., USA*, **95**, 12753-12758.
- Hansen**, J., R. Ruedy, J. Glascoe and M. Sato, 1999: GISS analysis of surface temperature change. *J. Geophys. Res.*, **104**(D24), 30997-31022.
- Hanssen-Bauer**, I. and E.J. Førland, 2000: Temperature and precipitation variations in Norway 1900-1994 and their links to atmospheric circulation. *Int. J. Climatol.*, **20**, 1693-1708.
- Harries**, J.E., 1976: The distribution of water vapor in the stratosphere. *Rev. Geophys. Space Phys.*, **14**, 565-575.
- Harrison**, S.P., G. Yu and P.E. Tarasov, 1996: Late quaternary lake-level record from Northern Eurasia. *Quat. Res.*, **45**, 138-159.
- Hastenrath**, S. and P.D. Kruss, 1992: The dramatic retreat of Mount Kenya's glaciers between 1963 and 1987: greenhouse forcing. *Ann. Glaciol.*, **16**, 127-133.
- Hastenrath**, S. and A. Ames, 1995: Recession of Yanamarey glacier in

- Cordillera Blanca, Peru during the 20th century. *J. Glaciol.*, **41**(137), 191-196.
- Hastenrath**, S. and L. Greischar, 1997: Glacier recession on Kilimanjaro, East Africa, 1912-89. *J. Glaciol.*, **43**, 455-459.
- Haylock**, M. and N. Nicholls, 2000: Trends in extreme rainfall indices for an updated high quality data set for Australia, 1910-1998. *Int. J. Climatol.*, **20**, 1533-1541.
- Heino**, R., R. Brázdil, E. Forland, H. Tuomenvirta, H. Alexandersson, M. Beniston, C. Pfister, M. Rebetez, G. Rosenhagen, S. Rösner and J. Wibig, 1999: Progress in the study of climatic extremes in Northern and Central Europe. *Clim. Change*, **42**, 151-181.
- Helland-Hansen**, B. and F. Nansen, 1920: Temperature variations in the North Atlantic Ocean and in the atmosphere. Introductory studies on the cause of climatological variations. *Smithsonian Miscellaneous Collections*, 70(4), publication 2537, Washington, DC.
- Henderson-Sellers**, A., 1992: Continental cloudiness changes this century. *Geo Journal*, **27**, 255-262.
- Hennessy**, K.J., R. Suppiah and C.M. Page, 1999: Australian rainfall changes, 1910-1995. *Australian Meteorological Magazine*, **48**, 1-13.
- Higgins**, R.W. and W. Shi, 2000: Dominant factors responsible for interannual variability of the summer monsoon in the southwestern United States. *J. Climate*, **13**, 759-776.
- Higgins**, R.W., A. Leetmaa, Y. Xue and A. Barnston, 2000: Dominant factors influencing the seasonal predictability of US precipitation and surface air temperature. *J. Climate*, **13**, 3994-4017.
- Holzhauser**, H. and H.J. Zumbühl, 1996: To the history of the Lower Grindelwald Glacier during the last 2800 years - paleosols, fossil wood and historical pictorial records - new results. *Z. Geomorph. N. F.*, **104**, 95-127.
- Hoyt**, D.V. and K.H. Schatten, 1997: The role of the sun in climatic change. Oxford University Press, Oxford, 279 pp.
- Hu**, F.S., D. Slawinski, H.E.J. Wright, E. Ito, R.G. Johnson, K.R. Kelts, R.F. McEwan and A. Boedigheimer, 1999: Abrupt changes in North American climate during early Holocene times. *Nature*, **400**, 437-440.
- Huang**, S., H.N. Pollack and P.Y. Shen, 1997: Late quaternary temperature changes seen in world-wide continental heat flow measurements. *Geophys. Res. Lett.*, **24**, 1947-1950.
- Huang**, S., H.N. Pollack and P.Y. Shen, 2000: Temperature trends over the past five centuries reconstructed from borehole temperatures. *Nature*, **403**, 756-758.
- Huffman**, G., R.F. Adler, P.A. Arkin, J. Janowiak, P. Xie, R. Joyce, R. Ferraro, A. Chang, A. McNab, A. Gruber and B. Rudolf, 1997: The Global Precipitation Climatology Project (GPCP) merged precipitation data sets. *Bull. Am. Met. Soc.*, **78**, 5-20.
- Hughen**, K.A., J.T. Overpeck, L.C. Peterson and S. Trumbore, 1996: Rapid climate changes in the tropical Atlantic region during the last deglaciation. *Nature*, **380**, 51-54.
- Hughen**, K.H., D.P. Schrag, S.B. Jacobsen and W. Hantor, 1999: El Niño during the last interglacial period recorded by a fossil coral from Indonesia. *Geophys. Res. Lett.*, **26**, 3129-3132.
- Hughen**, K.A., J.T. Overpeck and R. Anderson, 2000: Recent warming in a 500-year paleoclimate record from Upper Soper Lake, Baffin Island, Canada. *The Holocene*, **10**, 9-19.
- Hughes**, M.G. and D.A. Robinson, 1996: Historical snow cover variability in the Great Plains region of the USA: 1910 through to 1993. *Int. J. Climatol.*, **16**, 1005-1018.
- Hughes**, M.G., A. Frei and D.A. Robinson, 1996: Historical analysis of North American snow cover extent: merging satellite and station derived snow cover observations. *Proc. 1996 Eastern Snow Conf.*, Williamsburg, VA, 21-32.
- Hughes**, M.K. and H.F. Diaz, 1994: Was there a "Medieval Warm Period" and if so, where and when? *Clim. Change*, **26**, 109-142.
- Hughes**, M.K. and L.J. Graumlich, 1996: Multimillennial dendroclimatic records from Western North America. In: *Climatic Variations and Forcing Mechanisms of the Last 2000 Years*, R.S. Bradley, P.D. Jones and J. Jouzel (eds.), Springer Verlag, Berlin, pp. 109-124.
- Hughes**, M.K. and G. Funkhouser, 1999: Extremes of moisture availability reconstructed from tree rings for recent millennia in the Great Basin of Western North America. In: *The Impacts of Climatic Variability on Forests*, Beinstone, M. and J. Innes (eds.), Springer-Verlag, Berlin, pp. 99-107.
- Hughes**, M.K., E.A. Vaganov, S. Shiyatov, R. Touchan and G. Funkhouser, 1999: Twentieth century summer warmth in northern Yakutia in a 600 year context. *The Holocene*, **9**, 603-308.
- Hulme**, M., 1996: Recent climatic change in the world's drylands. *Geophys. Res. Lett.*, **23**, 61-64.
- Hulme**, M., T.J. Osborn and T.C. Johns, 1998: Precipitation sensitivity to global warming: Comparison of observations with HadCM2 simulations. *Geophys. Res. Lett.*, **25**, 3379-3382.
- Hurrell**, J.W., 1995: Decadal trends in the North Atlantic Oscillation regional temperatures and precipitation. *Science*, **269**, 676-679.
- Hurrell**, J.W., 1996: Influence of variations in extratropical wintertime teleconnections on Northern Hemisphere temperatures. *Geophys. Res. Lett.*, **23**, 665-668.
- Hurrell**, J.W. and K.E. Trenberth, 1996: Satellite versus surface estimates of air temperature since 1979. *J. Climate*, **9**, 2222-2232.
- Hurrell**, J.W. and H. van Loon, 1997: Decadal variations in climate associated with the North Atlantic Oscillation. *Clim. Change*, **36**, 301-326.
- Hurrell**, J.W. and K.E. Trenberth, 1998: Difficulties in obtaining reliable temperature trends: reconciling the surface and satellite Microwave Sounding Unit records. *J. Climate*, **11**, 945-967.
- Hurrell**, J.W. and K.E. Trenberth, 1999: Global sea surface temperature analyses: multiple problems and their implications for climate analysis, modeling and reanalysis, *Bull. Am. Met. Soc.*, **80**, 2661-2678.
- Hurrell**, J.W., S.J. Brown, K.E. Trenberth and J.R. Christy, 2000: Comparison of tropospheric temperatures from radiosondes and satellites: 1979-1998. *Bull. Am. Met. Soc.*, **81**, 2165-2177.
- IAHS(ICS/UNEP/UNESCO**, 1998: Fluctuations of the Glaciers, 1990-95. W. Haeberli, M. Hoelzle, S. Suter and R. Frauenfelder (eds.), *World Glacier Monitoring Service*, University and ETH, Zurich.
- IAHS(ICS/UNEP/UNESCO**, 1999: Glacier mass balance bulletin no. 5, W. Haeberli, M. Hoelzle and R. Frauenfelder (eds.), *World Glacier Monitoring Service*, University and ETH, Zurich.
- Indeje**, M., H.M. Semazzi and L.J. Ogollo, 2000: ENSO signals in East African rainfall seasons. *Int. J. Climatol.*, **20**, 19-46.
- IPCC**, 1990: Climate Change, The IPCC Scientific Assessment. J.T. Houghton, G.J. Jenkins and J.J. Ephraums (eds.), Cambridge University Press, Cambridge, UK, 365 pp.
- IPCC**, 1992: Climate Change 1992: The Supplementary Report to the IPCC Scientific Assessment. J.T. Houghton, B.A. Callander and S.K. Varney (eds.), Cambridge University Press, Cambridge, UK, 198 pp.
- IPCC**, 1996: Climate Change 1995: The Science of Climate Change. Contribution of Working Group I to the Second Assessment Report of the Intergovernmental Panel on Climate Change [Houghton, J.T., L.G. Meira Filho, B.A. Callander, N. Harris, A. Kattenberg, and K. Maskell (eds.)]. Cambridge University Press, Cambridge, United Kingdom and New York, NY, USA, 572 pp.
- IPCC**, 1999: IPCC Special Report Aviation and the Global Atmosphere. Cambridge University Press, Cambridge, UK, 373 pp.
- Iwashima**, T. and R. Yamamoto, 1993: A statistical analysis of the extreme events: Long-term trend of heavy daily precipitation. *J. Met. Soc. Japan*, **71**, 637-640.
- Jacka**, T.H. and W.F. Budd, 1998: Detection of temperature and sea-ice-extent change in the Antarctic and Southern Ocean, 1949-96. *Ann. Glaciol.*, **27**, 553-559.
- Jacobs**, G.A. and J.L. Mitchell, 1996: Ocean circulation variations

- associated with the Antarctic Circumpolar Wave. *Geophys. Res. Lett.*, **23**, 2947-2950.
- Jacobson**, G.L., T. Webb III and E.C. Grimm, 1987: Patterns and rates of vegetation change during deglaciation of eastern North America. In: *North American and Adjacent Oceans during the Last Deglaciation* (eds. W.F. Ruddiman and H.E. Wright), Decade of North American Geology, G.S.A., Boulder, CO, pp. 277-288.
- Jacoby**, G.C., R.D. D'Arrigo and T. Davaajamts, 1996: Mongolian tree rings and 20th century warming. *Science*, **273**, 771-773.
- Janicot**, S., V. Moron and B. Fontaine, 1996: Sahel droughts and ENSO dynamics. *Geophys. Res. Lett.*, **23**, 551-554.
- Jarrell**, J.D., P.J. Hebert and M. Mayfield, 1992: Hurricane experience levels of coastal county populations from Texas to Maine. *NOAA Tech. Memo*, NWS NHC 46, Coral Gables, Florida, USA, 152 pp.
- Johannessen**, O.M., M.W. Miles and E. Bjørø, 1995: The Arctic's shrinking sea ice. *Nature*, **376**, 126-127.
- Johannessen**, O.M., E.V. Shalina and M.W. Miles, 1999: Satellite evidence for an Arctic Sea Ice Cover in Transformation. *Science*, **286**, 1937-1939.
- Jóhannesson**, T., 1997: The response of two Icelandic glaciers to climate warming computed with a degree-day glacier mass balance model coupled to a dynamic glacier model. *J. Glaciol.*, **43**, 321-327.
- Johnsen**, S.J., H.B. Clausen, W. Dansgaard, K. Fuhrer, N. Gundestrup, C.U. Hammer, P. Iversen, J. Jouzel, B. Stauffer and J.P. Steffensen, 1992: Irregular glacial interstadials recorded in a new Greenland ice core. *Nature*, **359**, 311-313.
- Johnson**, G.C. and A.H. Orsi, 1997: Southwest Pacific Ocean water-mass changes between 1968/69 and 1990/91. *J. Climate*, **10**, 306-316.
- Jones**, E.P., K. Aagaard, E.C. Carmack, R.W. MacDonald, F.A. McLaughlin, R.G. Perkin and J.H. Swift, 1996: Recent Changes in Arctic Ocean Thermohaline Structure: Results from the Canada/US 1994 Arctic Ocean Section. *Mem. Natl. Inst. Polar Res. Special Issue*, **51**, 307-315.
- Jones**, P.D., 1994: Hemispheric surface air temperature variations: a reanalysis and an update to 1993. *J. Climate*, **7**, 1794-1802.
- Jones**, P.D., 1999: Classics in physical geography revisited – Manley's CET series. *Progress in Physical Geography*, **23**, 425-428.
- Jones**, P.D. and K.R. Briffa, 1992: Global surface air temperature variations during the twentieth century: Part 1, spatial temporal and seasonal details. *The Holocene*, **2**, 165-179.
- Jones**, P.D. and M. Hulme, 1996: Calculating regional climatic time series for temperature and precipitation: methods and illustrations. *Int. J. Climatol.*, **16**, 361-377.
- Jones**, P.D., P.Ya. Groisman, M. Coughlan, N. Plummer, W.C Wang, and T.R. Karl, 1990: Assessment of urbanization effects in time series of surface air temperature over land. *Nature*, **347**, 169-172.
- Jones**, P.D., T. Jónsson and D. Wheeler, 1997a: Extension of the North Atlantic Oscillation using early instrumental pressure observations from Gibraltar and south-west Iceland. *Int. J. Climatol.*, **17**, 1433-1450.
- Jones**, P.D., T.J. Osborn and K.R. Briffa, 1997b: Estimating sampling errors in large-scale temperature averages. *J. Climate*, **10**, 2548-2568.
- Jones**, P.D., K.R. Briffa, T.P., Barnett and S.F.B. Tett, 1998: High-resolution palaeoclimatic records for the last millennium: interpretation, integration and comparison with General Circulation Model control run temperatures. *The Holocene*, **8**, 455-471.
- Jones**, P.D., M. New, D.E. Parker, S. Martin and I.G. Rigor, 1999a: Surface air temperature and its changes over the past 150 years. *Rev. Geophys.*, **37**, 173-199.
- Jones**, P.D., M.J. Salinger and A.B. Mullan, 1999b: Extratropical circulation indices in the Southern Hemisphere. *Int. J. Climatol.*, **19**, 1301-1317.
- Jones**, P.D., E.B. Horton, C.K. Folland, M. Hulme, D.E. Parker and T.A. Basnett, 1999c: The use of indices to identify changes in climatic extremes. *Clim. Change*, **42**, 131-149.
- Jones**, P.D., T.J. Osborn, K.R. Briffa, C.K. Folland, E.B. Horton, L.V. Alexander, D.E. Parker and N.A. Rayner, 2001: Adjusting for sampling density in grid box land and ocean surface temperature time series. *J. Geophys. Res.*, **106**, 3371-3380.
- Jouzel**, J., C. Lorius, J.R. Petit, C. Genthon, N.I. Barkov, V.M. Kotlyakov and V.M. Petrov, 1987: Vostok ice core: a continuous isotope temperature record over the last climatic cycle (160,000 years). *Nature*, **329**, 402-408.
- Jouzel**, J., C. Lorius, J.M. Barnola, M. Bender, J. Bender, J. Chappelaz, C. Genthon, V.M. Kotlyakov, V. Lipenkov, C. Lorius, J.R. Petit, D. Raynaud, G. Raisbeck, C. Ritz, T. Sowers, M. Stievenard, F. Yiou and P. Yiou, 1993: Extending the Vostok ice core record of paleoclimate to the penultimate glacial period. *Nature*, **364**, 407-412.
- Jouzel**, J., C. Lorius, S.J. Johnsen and P. Grootes, 1994: Climate instabilities: Greenland and Antarctic records. *C.R. Acad. Sci. Paris*, t 319, série II, pp. 65-77.
- Jouzel**, J., R. Vaikmae, J.R. Petit, M. Martin, Y. Duclos, M. Stievenard, C. Lorius, M. Toots, M.A. Mélières, L.H. Burckle, N.I. Barkov and V.M. Kotlyakov, 1995: The two-step shape and timing of the last deglaciation in Antarctica. *Clim. Dyn.*, **11**, 151-161.
- Jouzel**, J., V. Masson, O. Cattani, S. Falourd, M. Stievenard, B. Stenni, A. Longinelli, S.J. Johnson, J.P. Steffensen, J.R. Petit, J. Schwander and R. Souchez, 2001: A new 27 kyr high resolution East Antarctic climate record. *Geophys. Res. Lett.*, in press.
- Joyce**, T.M. and P. Robbins, 1996: The long-term hydrographic record at Bermuda. *J. Climate*, **9**, 3121-3131.
- Joyce**, T.M., R.S. Pickart and R.C. Millard, 1999: Long-term hydrographic changes at 52° and 66°W in the North Atlantic Subtropical Gyre and Caribbean. *Deep-Sea Res., Part II*, **46**, 245-278.
- Kagan**, R.L., 1997: Averaging of Meteorological Fields. *Translation by UK Ministry of Defence Linguistic Services of original Russian 1979 text*. Eds: L.S. Gandon and T.M. Smith, Kluwer, London, 279 pp.
- Kaiser**, D.P., 1998: Analysis of total cloud amount over China, 1951-1994. *Geophys. Res. Lett.*, **25**, 3599-3602.
- Kaiser**, D.P., 2000: Decreasing cloudiness over China! An updated analysis examining additional variables. *Geophys. Res. Lett.*, **27**, 2193-2196.
- Kalnay**, E., M. Kanamitsu, R. Kistler, W. Collins, D. Deaven, I. Gandin, M. Iredell, S. Saha, G. White, J. Woollen, Y. Zhu, M. Chelliah, W. Ebisuzaki, W. Higgins, J. Janowiak, K.C. Mo, C. Ropelewski, J. Wang, A. Leetmaa, R. Reynolds, R. Jenne and D. Joseph, 1996: The NCEP/NCAR 40-year Reanalysis Project. *Bull. Am. Met. Soc.*, **77**, 437-471.
- Kaplan**, A., Y. Kushnir, M.A. Cane and M. Benno Blumenthal, 1997: Reduced space optimal analysis for historical data sets: 136 years of Atlantic sea surface temperatures. *J. Geophys. Res.*, **102**(C13), 27835-27860.
- Kaplan**, A., M.A. Cane, Y.A. Kushnir and A.C. Clement, 1998: Analyses of global sea surface temperature, 1856-1991. *J. Geophys. Res.*, **103**(C9), 18567-18589.
- Karl**, T.R. and P.M. Steurer, 1990: Increased cloudiness in the United States during the first half of the twentieth century: fact or fiction? *Geophys. Res. Lett.*, **17**, 1925-1928.
- Karl**, T.R. and R.W. Knight, 1997: The 1995 Chicago heat wave: How likely is a recurrence? *Bull. Am. Met. Soc.*, **78**, 1107-1119.
- Karl**, T.R. and R.W. Knight, 1998: Secular trends of precipitation amount, frequency, and intensity in the USA. *Bull. Am. Met. Soc.*, **79**, 231-241.
- Karl**, T.R., V.E. Derr, D.R. Easterling, C.K. Folland, D.J. Hofmann, S. Levitus, N. Nicholls, D.E. Parker and G.W. Withee, 1995a: Critical issues for long-term climate monitoring. *Clim. Change*, **31**, 185-221, 1995a and In: *Long-term climate Monitoring by the Global Climate Observing System*, T. Karl (ed.), Kluwer, Dordrecht, pp. 55-91.
- Karl**, T.R., R.W. Knight and N. Plummer, 1995b: Trends in high-

- frequency climate variability in the twentieth century. *Nature*, **377**, 217-220.
- Karl**, T.R., R.W. Knight, D.R. Easterling and R.G. Quayle, 1995c: Trends in U.S. climate during the Twentieth Century. *Consequences*, **1**, 3-12.
- Karl**, T.R., R.W. Knight, and B. Baker, 2000: The record breaking global temperatures of 1997 and 1998: evidence for an increase in the rate of global warming? *Geophys. Res. Lett.*, **27**, 719-722.
- Karoly**, D.J., 1990: The role of transient eddies in low-frequency zonal variations of the Southern Hemisphere circulation. *Tellus*, **42A**, 41-50.
- Karoly**, D.J., P. Hope and P.D. Jones, 1996: Decadal variations of the Southern Hemisphere circulation. *Int. J. Climatol.*, **16**, 723-738.
- Katz**, R.W., 1999: Extreme value theory for precipitation: Sensitivity analysis for climate change. *Advances in Water Resources*, **23**, 133-139.
- Kawamura**, R., 1994: A rotated EOF analysis of global sea surface temperature variability with interannual and interdecadal scales. *J. Phys. Oceanogr.*, **24**, 707-715.
- Keckhut**, P., F.J. Schmidlin, A. Hauchecorne and M.-L. Chanin, 1999: Stratospheric and mesospheric cooling trend estimates from US rocketsondes at low latitude stations ( $8^{\circ}\text{S}$ - $34^{\circ}\text{N}$ ), taking into account instrumental changes and natural variability. *J. Atmos. And Solar-Terr. Phys.*, **61**, 447-459.
- Keigwin**, L., 1996: The Little Ice Age and Medieval Warm Period in the Sargasso Sea. *Science*, **274**, 1504-1508.
- Keigwin**, L.D. and R.S. Pickart, 1999: Slope water current over the Laurentian Fan on Interannual to Millennial Time Scales. *Science*, **286**, 520-523.
- Kershaw**, A.P., D.M. D'Costa, J.R.C.M. Mason and B.E. Wagstaff, 1991: Palynological evidence for Quaternary vegetation and environments of Mainland Southeastern Australia. *Quat. Sci. Rev.*, **10**, 391-404.
- Kestin**, T.S., D.J. Karoly, J.I. Jano and N.A. Rayner, 1999: Time-frequency variability of ENSO and stochastic simulations. *J. Climate*, **11**, 2258-2272.
- Kidson**, J.W., 1988: Interannual variations in the Southern Hemisphere circulation. *J. Climate*, **1**, 1177-1198.
- Kidson**, J.W., 1999: Principal modes of Southern Hemisphere low frequency variability obtained from NCEP/NCAR reanalyses. *J. Climate*, **12**, 2808-2830.
- Kiladis**, G.N. and K.C. Mo, 1999: Interannual and intraseasonal variability in the Southern Hemisphere, Chapter 8. In: *Meteorology of the Southern Hemisphere*, American Meteorological Society, Boston.
- King**, J.C., 1994: Recent climate variability in the vicinity of the Antarctic Peninsula. *J. Climate*, **14**, 357-361.
- Kley**, D., J.M. Russell and C. Phillips (eds.), 2000: SPARC Assessment of upper tropospheric and stratospheric water vapour. WCRP-No. 113, WMO/TD-No. 1043, SPARC Report No.2, 325 pp.
- Klitgaard-Kristensen**, D., H.P. Sejrup, H. Haflidason, S. Johnsen and M. Spurk, 1998: The short cold period 8,200 years ago documented in oxygen isotope records of precipitation in Europe and Greenland. *J. Quaternary Sciences*, **13**, 165-169.
- Knight**, R.W., 1984: Introduction to a new sea-ice database. *Ann. Glaciol.*, **5**, 81-84.
- Koç**, N. and E. Jansen, 1994: Response of the high-latitude Northern-Hemisphere to orbital climate forcing-evidence from the Nordic seas. *Geology*, **22**, 523-526.
- Kotilainin**, A.T. and N.J. Shackleton, 1995: Rapid climate variability in the North Pacific Ocean during the past 95,000 years. *Nature*, **377**, 323-326.
- Kumar**, K., K. Rupa, K.K. Kumar and G.B. Pant, 1994: Diurnal asymmetry of surface temperature trends over India. *Geophys. Res. Lett.*, **21**, 677-680.
- Kumar**, K.K., R. Kleeman, M.A. Crane and B. Rajaopalan, 1999a: Epochal changes in Indian monsoon-ENSO precursors. *Geophys. Res. Lett.*, **26**, 75-78.
- Kumar**, K.K., B. Rajaopalan and M.A. Crane, 1999b: On the weakening relationship between the Indian monsoon and ENSO. *Science*, **284**, 2156-2159.
- Kunkel**, K.E., S.A. Changnon, B.C. Reinke and R.W. Arritt, 1996: The July 1995 heat wave in the Midwest: A climatic perspective and critical weather factors. *Bull. Am. Met. Soc.*, **77**, 1507-1518.
- Kunkel**, K.E., K. Andsager and D.R. Easterling, 1999: Long-term trends in extreme precipitation events over the conterminous United States and Canada. *J. Climate*, **12**, 2515-2527.
- Kushnir**, Y., V.J. Cardon, J.G. Greenwood and M.A. Cane, 1997: The recent increase in North Atlantic wave heights. *J. Climate*, **10**, 2107-2113.
- Laberge**, M.J. and S. Payette, 1995: Long-term monitoring of permafrost change in a palsa peatland in northern Quebec, Canada: 1983-1993. *Arctic and Alpine Research*, **27**, 167-171.
- Labeyrie**, L., J.C. Duplessy, J. Duprat, A. Juillet-Leclerc, J. Moyes, E. Michel, N. Kallel and N.J. Shackleton, 1992: Changes in vertical structure of the North Atlantic Ocean between glacial and modern times. *Quat. Sci. Rev.*, **11**, 401-413.
- Lachenbruch**, A.H. and B.V. Marshall, 1986: Changing climate: geothermal evidence from permafrost in the Alaskan Arctic. *Science*, **234**, 689-696.
- Lachenbruch**, A.H., T.T Cladouhos and R.W. Saltus, 1988: Permafrost temperature and the changing climate. In: *Proceedings of the Fifth International Conference on Permafrost*, Trondheim, Norway, 3, 9-17.
- Laird**, K.R., S.C. Fritz, K.A. Maasch and B.F. Cumming, 1996: Greater Drought Intensity and frequency before AD 1200 in the Northern Great Plains. *Nature*, **384**, 552-554.
- Lamb**, H.F., F. Gasse, A. Bekaddour, N. El Hamouti, S. van der Kaars, W.T. Perkins, N.J. Pearce and C.N. Roberts, 1995: Relation between century-scale Holocene arid intervals in temperate and tropical zones. *Nature*, **373**, 134-137.
- Lambert**, S.J., 1996: Intense extratropical Northern Hemisphere winter cyclone events: 1189-1991. *J. Geophys. Res.*, **101**, 21319-21325.
- Lamoureux**, S.F. and R.S. Bradley, 1996: A 3300 year varved sediment record of environmental change from northern Ellesmere Island, Canada. *J. Paleolimnology*, **16**, 239-255.
- Lander**, M.A. and C.P. Guard, 1998: A look at global tropical cyclone activity during 1995: Contrasting high Atlantic activity with low activity in other basins. *Mon. Wea. Rev.*, **126**, 1163-1173.
- Landsea**, C.W., 1993: A climatology of intense (or major) Atlantic hurricanes. *Mon. Wea. Rev.*, **121**, 1703-1713.
- Landsea**, C.W., N. Nicholls, W.M. Gray and L.A. Avila, 1996: Downward trends in the frequency of intense Atlantic hurricanes during the past five decades. *Geophys. Res. Lett.*, **23**, 1697-1700.
- Landsea**, C.W., R.A. Pielke, Jr., A.M. Mestas-Nunez and J.A. Knaff, 1999: Atlantic basin hurricanes: Indices of climatic changes. *Clim. Change*, **42**, 89-129.
- Lang**, C., M. Leuenberger, J. Schwander and J. Johnsen, 1999:  $16^{\circ}\text{C}$  rapid temperature variation in central Greenland 70000 years ago. *Science*, **286**, 934-937.
- Latif**, M. and T.P. Barnett, 1994: Causes of decadal climate variability over the North Pacific and North America. *Science*, **266**, 634-637.
- Lawrimore**, J.H. and T.C. Peterson, 2000: Pan evaporation trends in dry and humid regions of the United States. *J. Hydrometeorol.*, **1**, 543-546.
- Lazier**, J.R.N., 1995: The salinity decrease in the Labrador Sea over the past thirty years. In: *Natural Climate Variability on Decade-to-Century Time Scales*, D.G. Martinson, K. Bryan, M. Ghil, M.M. Hall, T. Karl, E.S. Sarachik, S. Sorooshian, and L.D. Talley (eds.), National Academy Press, Washington, D.C., pp. 295-305.
- Lean**, J., J. Beer and R.S. Bradley, 1995: Reconstruction of solar irradiance since 1610: Implications for climatic change. *Geophys. Res. Lett.*, **22**, 3195-3198.
- Leathers**, D.J. and A.W. Ellis, 1996: Synoptic mechanisms associated

- with snowfall increases to the lee of Lakes Erie and Ontario. *Int. J. Climatol.*, **16**, 1117-1135.
- Lettenmaier**, D.P., A.W. Wood, R.N. Palmer, E.F. Wood and E.Z. Stakhiv, 1999: Water resources implications of global warming: A U.S. regional perspective. *Clim. Change*, **43**, 537-579.
- Levitus**, S. and J. Antonov, 1997: Variability of heat storage of and the rate of heat storage of the world ocean. NOAA NESDIS Atlas 16, US Government Printing Office, Washington, D.C., 6 pp., 186 figures.
- Levitus**, S., R. Gelfeld, T. Boyer and D. Johnson, 1994: Results of the NODC and IOC Data Archaeology and Rescue projects In: *Key to Oceanographic Records Documentation No. 19*, National Oceanographic Data Center, Washington, D.C., 67 pp.
- Levitus**, S., R. Gelfeld, M. E. Conkright, T. Boyer, D. Johnson, T. O'Brien, C. Stephens, C. Forgy, O. Baranova, I. Smolyar, G. Trammell and R. Moffatt, 2000a: Results of the NODC and IOC Data Archaeology and Rescue projects. In: *Key to Oceanographic Records Documentation No. 19*, National Oceanographic Data Center, Washington, D.C., 19 pp.
- Levitus**, S., J. Antonov, T.P. Boyer and C. Stephens, 2000b: Warming of the World Ocean. *Science*, **287**, 2225-2229.
- Lewis**, T., 1998: The effect of deforestation on ground surface temperatures. *Global and Planetary Change*, **18**, 1-13.
- Lins**, H.F. and P.J. Michaels, 1994: Increasing U.S. streamflow linked to greenhouse forcing. *Eos Trans. AGU*, **75**, 281, 284-285.
- Lins**, H F. and J.R. Slack, 1999: Streamflow trends in the United States. *Geophys. Res. Lett.*, **26**, 227-230.
- Livezey**, R.E. and T.M. Smith, 1999: Covariability of aspects of North American climate with global sea surface temperatures on interannual to interdecadal timescales. *J. Climate*, **12**, 289-302.
- Luterbacher**, J., C. Schmutz, D. Gyalistras, E. Xoplaki and H. Wanner, 1999: Reconstruction of monthly NAO and EU indices back to A.D. 1675. *Geophys. Res. Lett.*, **26**, 759-762.
- Lysenko**, E.V., G. Nelidova and A. Prostova, 1997: Changes in the stratospheric and mesospheric thermal conditions during the last 3 decades: 1. The evolution of a temperature trend. *Izvestia, Atmos. and Oceanic Physics*, **33**(2), 218-225.
- MacManus**, J., D.W. Oppo and J.L. Cullen, 1999: A 0.5 Million-Year Record of Millenial scale climate variability in the North Atlantic. *Science*, **283**, 971-975.
- Magnuson**, J.J., D.M. Robertson, B.J. Benson, R.H. Wynne, D.M. Livingston, T. Arai, R.A. Assel, R.G. Barry, V. Card, E. Kuusisto, N.G. Granin, T.D. Prowse, K.M. Stewart and V.S. Vuglinski, 2000: Historical trends in lake and river ice cover in the Northern Hemisphere. *Science*, **289**, 1743-1746.
- Magy**, M., 1995: Successive oceanic and solar forcing indicated by Younger Dryas and early Holocene climatic oscillations in the Jura. *Quat. Res.*, **43**, 279-285.
- Mahowald**, N., K.E. Kohfeld, M. Hansson, Y. Balkanski, S.P. Harrison, I.C. Prentice, M. Schulz and H. Rodhe, 1999: Dust sources and deposition during the last glacial maximum and current climate: a comparison of model results with paleodata from ice cores and marine sediments. *J. Geophys. Res.*, **104**, 15895-15916.
- Majorowicz**, J.A. and A. Judge, 1994: Climate induced ground warming at the southern margins of permafrost. *EOS, Transactions, American Geophysical Union*, **75**(44), 84.
- Maloney**, E.D. and D.L. Hartmann, 2001: The Madden-Julian Oscillation, Barotropic Dynamics, and North Pacific Tropical Cyclone Formation, Part I: Observations. *J. Atmos. Sci.*, in press.
- Mann**, M.E., 2000: Lessons for a New Millennium. *Science*, **289**(14), 253-254.
- Mann**, M.E. and J. Park, 1994: Global-scale modes of surface temperature variability on interannual to century timescales. *J. Geophys. Res.*, **99**, 25819-25833.
- Mann**, M.E. and J. Park, 1996: Joint spatiotemporal modes of surface temperature and sea level pressure variability in the Northern Hemisphere during the last century. *J. Climate*, **9**, 2137-2162.
- Mann**, M.E., J. Park and R.S. Bradley, 1995: Global interdecadal and century-scale oscillations during the past five centuries. *Nature*, **378**, 266-270.
- Mann**, M.E., R.S. Bradley and M.K. Hughes, 1998: Global-scale temperature patterns and climate forcing over the past six centuries. *Nature*, **392**, 779-787.
- Mann**, M.E., R.S. Bradley, and M.K. Hughes, 1999: Northern Hemisphere Temperatures During the Past Millennium: Inferences, Uncertainties, and Limitations. *Geophys. Res. Lett.*, **26**, 759-762.
- Mann**, M.E., R.S. Bradley and M.K. Hughes, 2000a: Long-term variability in the El Niño Southern Oscillation and associated teleconnections. In: *El Niño and the Southern Oscillation: Multiscale Variability and its Impacts on Natural Ecosystems and Society*, H.F. Diaz and V. Markgraf (eds.), Cambridge University Press, Cambridge, UK, 357-412.
- Mann**, M.E., E. Gille, R.S. Bradley, M.K. Hughes, J.T. Overpeck, F.T. Keimig and W. Gross, 2000b: Global temperature patterns in past centuries: An interactive presentation. *Earth Interactions*, **4**/4, 1-29.
- Manton**, M.J., P.M. Della-Marta, M.R. Haylock, K.J. Hennessy, N. Nicholls, L.E. Chambers, D.A. Collins, G. Daw, A. Finet, D. Gunawan, K. Inape, H. Isobe, T.S. Kestin, P. Lafale, C.H. Leyu, T. Lwin, L. Maitrepierre, N. Ouprasitwong, C.M. Page, J. Pahalad, N. Plummer, M.J. Salinger, R. Suppiah, V.L. Tran, B. Trewhin, I. Tibig and D. Yee, 2001: Trends in extreme daily rainfall and temperature in Southeast Asia and the South Pacific: 1961-1998. *Int. J. Climatol.*, **21**, 269-284.
- Mantua**, N.J., S.R. Hare, Y. Zhang, J.M. Wallace and R.C. Francis, 1997: A Pacific interdecadal climate oscillation with impacts on salmon production. *Bull. Am. Met. Soc.*, **78**, 1069-1079.
- Marengo**, J.A., J. Tomasella and C.R. Uvo, 1998: Trends in streamflow and rainfall in tropical South America: Amazonia, Eastern Brazil and Northwestern Peru. *J. Geophys. Res.*, **103**, 1775-1783.
- Martinson**, D.G., N.G. Pisias, J.D. Hays, J. Imbrie, T.C. Moore and N.J. Shackleton, 1987: Age Dating and the Orbital Theory of the Ice Ages: Development of a High-Resolution 0-300,000 Years Chronostratigraphy. *Quat. Res.*, **27**, 1-30.
- Martin-Vide**, J. and M. Barriendos, 1995: The use of rogation ceremony records in climatic reconstruction: A case study from Catalonia (Spain). *Clim. Change*, **30**, 201-221.
- Maslanik**, J.A., M.C. Serreze and R.G. Barry, 1996: Recent decreases in Arctic summer ice cover and linkages to atmospheric circulation anomalies. *Geophys. Res. Lett.*, **23**, 1677-1680.
- Masson**, V., F. Vimeux, J. Jouzel, V. Morgan, M. Delmotte, C. Hammer, S.J. Johnsen, V. Lipenkov, J.R. Petit, E. Steig, M. Stivenard and R. Sousmis Vaikmae, 2000: Holocene climate variability in Antarctica based on 11 ice-core isotopic records. *Quat. Res.*, **54**, 348-358.
- Mastenbrook**, H.J., 1968: Water vapor distribution in the stratosphere and high troposphere. *J. Atmos. Sci.*, **25**, 299-311.
- Mastenbrook**, H.J. and S. Oltmans, 1983: Stratospheric water vapor variability for Washington D.C./Boulder, CO.: 1964-1982. *J. Atmos. Sci.*, **40**, 2157-2165.
- Mayewski**, P.A. and I.D. Goodwin, 1997: International Trans-Antarctic Scientific Expedition (ITASE). *PAGES/SCAR Workshop Report Series*, 97-1.Bern Switzerland, 48 pp.
- Mayewski**, P.A., L.D. Meeker, M.S. Twickler, S. Whitlow, Y. Qinzhao, W.B. Lyons and M. Prentice, 1997: Major features and forcing of high-latitude northern hemisphere atmospheric circulation using a 110,000-year-long glaciochemical series. *J. Geophys. Res.*, **102**, 26345-26366.
- McGlone**, M.S., A.P. Kershaw and V. Markgraf, 1992: El Niño/Southern Oscillation and climatic variability in Australasian and South American paleoenvironmental records. In: *El Niño: Historical and paleoclimatic aspects of the Southern Oscillation*, H.F. Diaz and V. Markgraf (eds.), Cambridge, Cambridge University Press, pp. 435-

- 462.
- McManus**, J.F., G.C. Bond, W.S. Broecker, S. Johnsen, L. Labeyrie and S. Higgins, 1994: High-resolution climate records from the North Atlantic during the last interglacial. *Nature*, **317**, 326-329.
- McPhee**, M.G., T.P. Stanton, J.H. Morison and D.G. Martinson, 1998: Freshening of the upper ocean in the Arctic: Is perennial sea ice disappearing? *Geophys. Res. Lett.*, **25**, 1729-1732.
- Meehl**, G.A., J. Arblaster and W. Strand, 1998: Global decadal scale climate variability. *Geophys. Res. Lett.*, **25**, 3983-3986.
- Meehl**, G.A., T. Karl, D.R. Easterling, S. Changnon, R. Pielke, Jr., D. Changnon, J. Evans, P.Ya. Groisman, T.R. Knutson, K.E. Kunkel, L.O. Mearns, C. Parmesan, R. Pulwarty, T. Root, R.T. Sylves, P. Whetton and F. Zwiers, 2000: An introduction to trends in extreme weather and climate events: Observations, socioeconomic impacts, terrestrial ecological impacts, and model projections. *Bull. Am. Met. Soc.*, **81**, 413-416.
- Meese**, D.A. and 13 others, 1994: The accumulation record from the GISP2 core as an indicator of climate change throughout the Holocene. *Science*, **266**, 1680-1682.
- Mekis**, E. and W.D. Hogg, 1999: Rehabilitation and analysis of Canadian daily precipitation time series. *Atmosphere-Ocean*, **37**(1), 53-85.
- Melling**, H., 1998: Hydrographic changes in the Canada Basin of the Arctic Ocean, 1979-1996. *J. Geophys. Res.*, **103**(C4), 7637-7645.
- Meshcherskaya**, A.V., I.G. Belyankina and M.P. Golod, 1995: Monitoring tolshching cnozhnogo pokprova v osnovioi zerno proizvodyashchei zone Byvshego SSSR za period instrumental'nykh nablyudenii. *Izvestiya Akad. Nauk SSR, Sser. Geograf.*, pp. 101-110.
- Michaels**, P.J. and P.C. Knappenberger, 2000: Natural signals in the MSU lower tropospheric temperature record. *Geophys. Res. Lett.*, **27**, 2905-2908.
- Michaels**, P.J., R.C. Balling, Jr., R.S. Vose and P.C. Knappenberger, 1998: Analysis of trends in the variability of daily and monthly historical temperature measurements. *Clim. Res.*, **10**, 27-33.
- Michaels**, P.J., P.C. Knappenberger, R.C. Balling Jr. and R.E. Davis, 2000: Observed warming in cold anticyclones. *Clim. Res.*, **14**, 1-6.
- Minobe**, S., 1997: A 50-70 year climatic oscillation over the North Pacific and North America. *Geophys. Res. Lett.*, **24**, 683-686.
- Mo**, K.C. and R.W. Higgins, 1998: The Pacific South American modes and tropical convection during the Southern Hemisphere winter. *Mon. Wea. Rev.*, **126**, 1581-1596.
- Mo**, T., 1995: A study of the Microwave Sounding Unit on the NOAA-12 satellite. *IEEE Trans. Geoscience and Remote Sensing*, **33**, 1141-1152.
- Moberg**, A., P.D. Jones, M. Barriendos, H. BergstrØm, D. Camuffo, C. Cocheo, T.D. Davies, G. Demar'e, J. Martin-Vide, M. Maugeri, R. Rodriguez and T. Verhoeve, 2000: Day-to-day temperature variability trends in 160-275-year long European instrumental records. *J. Geophys. Res.*, **105**(D18), 22849-22868.
- Morgan**, V.I. and T.D. van Ommen, 1997: Seasonality in late-Holocene climate from ice core records. *The Holocene*, **7**, 351-354.
- Moron**, V., 1997: Trend, decadal and interannual variability in annual rainfall in subequatorial and tropical North Africa (1900-1994). *Int. J. Climatol.*, **17**, 785-806.
- Moron**, V., R. Vautard and M. Ghil, 1998: Trends, Interdecadal and interannual oscillations in global sea-surface temepratures. *Clim. Dyn.*, **14**, 545-569.
- Mysak**, L.A. and S.A. Venegas, 1998: Decadal climate oscillations in the Arctic: a new feedback loop for atmospheric-ice-ocean interactions. *Geophys. Res. Lett.*, **25**, 3607-3610.
- Nagurnyi**, A.P., V.G. Korostelev and P.A. Abaza, 1994: Wave method for evaluating the effective thickness of sea ice in climate monitoring. *Bulletin of the Russian Academy of Sciences, Physics Supplement, Physics of Vibrations*, pp. 168-241.
- Nagurnyi**, A.P., V.G. Korostelev and V.V. Ivanov, 1999: Multiyear variability of sea ice thickness in the Arctic Basin measured by elastic-gravity oscillation of the ice cover. *Meteorologiya i gidrologiya*, **3**, 72-78.
- Nash**, J. and G.F. Forrester, 1986: Long-term monitoring of stratospheric temperature trends using radiance measurements obtained by the TIROS-N series of NOAA spacecraft. *Adv. Space Res.*, **6**, 37-44.
- National Climatic Data Center (NCDC)**, 1997: Products and Services Guide, Asheville, NC: US Department of Commerce, NOAA, 60 pp.
- Neff**, W.D., 1999: Decadal time scale trends and variability in the tropospheric circulation over the South Pole. *J. Geophys. Res.*, **104**(D22), 27217-27251.
- Nelson**, F.E. and J. Brown, 1997: Global change and permafrost. *Frozen Ground*, **21**, 21-24.
- Nelson**, F.E., K.M. Hinkel, N.I. Shiklomanov, G.R. Mueller, L.L. Miller and D.A. Walker, 1998: Active-layer thickness in north-central Alaska: systematic sampling, scale, and spatial autocorrelation. *J. Geophys. Res.*, **103**, 28963-28973.
- Neumann**, C.J., 1993: Global Overview, Global Guide to Tropical Cyclone Forecasting. WMO/TC-No. 560, Report No. TCP-31, World Meteorological Organization, Geneva, pp. 1.1-1.43.
- New**, M., M. Hulme and P.D. Jones, 2000: Representing twentieth century space-time climate variability, II: Development of 1901-1996 monthly grids of terrestrial surface climate. *J. Climate*, **13**, 2217-2238.
- Nicholls**, N. and W. Murray, 1999: Workshop on Indices and Indicators for climate extremes, Asheville, NC, USA, 3-6 June 1999. Breakout Group B: Precipitation. *Clim. Change*, **42**, 23-29.
- Nicholls**, N., C.W. Landsea and J. Gill, 1998: Recent trends in Australian region tropical cyclone activity. *Met. Atmos. Phys.*, **65**, 197-205.
- Nicholson**, S.E., 1993: An overview of African rainfall fluctuations of the last decade. *J. Climate*, **6**, 1463-1466.
- Nicholson**, S.E., 1997: An analysis of the ENSO signal in the tropical Atlantic and western Indian oceans. *Int. J. Climatol.*, **17**, 345-375.
- Nicholson**, S.E. and J. Kim, 1997: The relationship of the El Niño-Southern Oscillation to African rainfall. *Int. J. Climatol.*, **17**, 117-135.
- Nicholson**, S.E., B. Some and B. Kane, 2000: An analysis of recent rainfall conditions in west Africa, including the rainy seasons of the 1997 El Niño and the 1998 La Niña years. *J. Climate*, **13**, 2628-2640.
- Nixon**, F.M. and A.E. Taylor, 1998: Regional active layer monitoring across the sporadic, discontinuous and continuous permafrost zones, Mackenzie Valley, northwestern Canada. In: *Proceedings of the Seventh International Conference on Permafrost* (Lewcowicz, A.G. and M. Allard (eds.)) Centre d'Etudes Nordiques, Université Laval, Québec, pp. 815-820.
- Norris**, J.R., 1999: On trends and possible artifacts in global ocean cloud cover between 1952 and 1995. *J. Climate*, **12**, 1864-1870.
- Norris**, J.R. and C.B. Leovy, 1995: Comments on "Trends in global marine cloudiness and anthropogenic sulphur". *J. Climate*, **8**, 2109-2110.
- Norris**, J.R., Y. Zhang and J.M. Wallace, 1998: Role of low clouds in summertime atmosphere-ocean interactions over the North Pacific. *J. Climate*, **11**, 2482-2490.
- NRC (National Research Council)**, 2000: Reconciling Observations of Global Temperature Change. National Academy Press, Washington D.C., 85 pp.
- O'Brien**, S., P.A. Mayewski, L.D. Meeker, D.A. Meese, M.S. Twickler and S.I. Whitlow, 1995: Complexity of Holocene climate as reconstructed from a Greenland ice core. *Science*, **270**, 1962-1964.
- Oerlemans**, J., 1989: On the response of valley glaciers to climatic change. In: *Glacier fluctuations and climatic change*, J. Oerlemans, (ed.), Dordrecht, Kluwer Academic, pp. 353-372.
- Oerlemans**, J., 1992: Climate sensitivity of glaciers in southern Norway: application of an energy-balance model to Nigardsbreen, Hellstugubreen and Alfotbreen. *J. Glaciol.*, **38**, 223-232.
- Oerlemans**, J., 1994: Quantifying global warming from the retreat of

- glaciers. *Science*, **264**, 243-245.
- Oerlemans**, J., B. Anderson, A. Hubbard, P. Huybrechts, T. Jóhannesson, W.H. Knap, M. Schmeits, A.P. Stroeven, R.S.W. van de Wal, J. Wallinga and Z. Zuo, 1998: Modelling the response of glaciers to climate warming. *Clim. Dyn.*, **14**, 267-274.
- Oeschger**, H., J. Beer, U. Siegenthaler, B. Stauffer, W. Dansgaard and C.C. Langway, 1984: Late glacial climate history from ice cores. In: *Climate processes and climate sensitivity*, J.E. Hansen and T. Takahashi (eds.), American Geophysical Union, Washington.
- Oltmans**, S.J. and D.J. Hofmann, 1995: Increase in lower-stratospheric water vapour at a mid-latitude Northern Hemisphere site from 1981-1994. *Nature*, **374**, 146-149.
- Oltmans**, S.J., S.H. Voemel, D. Hofmann, K. Rosenlof and D. Kley, 2000: The increase in stratospheric water vapor from balloon-borne, frostpoint hygrometer measurements at Washington, DC and Boulder, Colorado. *Geophys. Res. Lett.*, **27**, 3453-3456.
- Osborn**, T.J., K.R. Briffa, S.F.B. Tett and P.D. Jones, 1999: Evaluation of the North Atlantic Oscillation as simulated by a coupled climate model. *Clim. Dyn.*, **15**, 685-702.
- Osborn**, T.J., M. Hulme, P.D. Jones and T.A. Basnett, 2000: Observed trends in the daily intensity of United Kingdom precipitation. *Int. J. Climatol.*, **20**, 347-364.
- Osterkamp**, T.E., 1994: Evidence for warming and thawing of discontinuous permafrost in Alaska. *EOS, Transactions*, American Geophysical Union, **75**, 85.
- Osterkamp**, T.E. and V.E. Romanovsky, 1999: Evidence for warming and thawing of discontinuous permafrost in Alaska. *Permafrost and Periglacial Processes*, **10**(1), 17-37.
- Østrem**, G., O. Liestøl and B. Wold, 1977: Glaciological investigations at Nigardsbreen, Norway. *Norsk Geogr. Tidsskr.*, **30**, 187-209.
- Overpeck**, J.T., P.J. Bartlein and T. Webb III, 1991: Potential magnitude of future vegetation change in eastern North America: Comparisons with the past. *Science*, **252**, 692-695.
- Overpeck**, J., K. Hughen, D. Hardy, R. Bradley, R. Case, M. Douglas, B. Finney, K. Gajewski, G. Jacoby, A. Jennings, S. Lamoureux, A. Lasca, G. MacDonald, J. Moore, M. Retelle, S. Smith, A. Wolfe and G. Zielinski, 1997: Arctic environmental change of the last four centuries. *Science*, **278**, 1251-1256.
- Palecki**, M.A. and R.G. Barry, 1986: Freeze-up and break-up of lakes as an index of temperature changes during the transition seasons: A case study for Finland. *J. Clim. Appl. Met.*, **25**, 893-902.
- Palmer**, T.N., 1993: A nonlinear dynamical perspective on climate change. *Weather*, **48**, 313-326.
- Palmer**, T.N., 1999: A nonlinear dynamical perspective on climate prediction. *J. Climate*, **12**, 575-591.
- Pant**, G.B. and K.R. Kumar, 1997: Climates of South Asia, John Wiley, Chichester, 320pp.
- Parker**, D.E., 1994: Effects of changing exposures of thermometers at land stations. *Int. J. Climatol.*, **14**, 102-113.
- Parker**, D.E. and C.K. Folland, 1988: The nature of climatic variability. *Met. Mag.*, **117**, 201-210.
- Parker**, D.E. and D.I. Cox, 1995: Towards a consistent global climatological rawinsonde data-base. *Int. J. Climatol.*, **15**, 473-496.
- Parker**, D.E. and E.B. Horton, 1999: Global and regional climate in 1998. *Weather*, **54**, 173-184.
- Parker**, D.E. and E.B. Horton, 2000: Global and regional climate in 1999. *Weather*, **55**, 188-199.
- Parker**, D.E., P.D. Jones, C.K. Folland and A. Bevan, 1994: Interdecadal changes of surface temperature since the late nineteenth century. *J. Geophys. Res.*, **99**, 14373-14399.
- Parker**, D.E., C.K. Folland and M. Jackson, 1995: Marine surface temperature: observed variations and data requirements. *Clim. Change*, **31**, 559-600.
- Parker**, D.E., H. Wilson, P.D. Jones, J. Christy and C.K. Folland, 1996: The impact of Mount Pinatubo on climate. *Int. J. Climatol.*, **16**, 487-497.
- Parker**, D.E., M. Gordon, D.P.N. Cullum, D.M.H. Sexton, C.K. Folland and N. Rayner, 1997: A new global gridded radiosonde temperature data base and recent temperature trends. *Geophys. Res. Lett.*, **24**, 1499-1502.
- Parkinson**, C.L., 2000: Variability of Arctic sea ice. The view from space, an 18-year record. *Arctic*, **53**, 341-358.
- Parkinson**, C.L., D.J. Cavalieri, P. Gloersen, H.J. Zwally and J.C. Comiso, 1999: Arctic sea ice extents, areas, and trends, 1978-1996. *J. Geophys. Res.*, **104**(C9), 20837-20856.
- Parrilla**, G., A. Lavín, H.L. Bryden, M.J. García and R. Millard, 1994: Rising temperatures in the subtropical North Atlantic Ocean over the past 35 years. *Nature*, **369**, 48-51.
- Partridge**, T.C., 1997: Cainozoic environmental change in southern Africa, with special emphasis on the last 200,000 years. *Progress in Physical Geography*, **21**, 3-22.
- Parungo**, F., J.F. Boatman, H. Sievering, S.W. Wilkison and B.B. Hicks, 1994: Trends in global marine cloudiness and anthropogenic sulphur. *J. Climate*, **7**, 434-440.
- Pavlov**, A.V., 1994: Current changes of climate and permafrost in the Arctic and Sub-Arctic of Russia. *Permafrost and Periglacial Processes*, **5**, 101-110.
- Pavlov**, A.V., 1998: Active layer monitoring in Northern West Siberia. *Proceedings of the Seventh International Conference on Permafrost*, Yellowknife, Canada, June 1998, Université Laval, Quebec, Collection Nordicana No. 57, pp. 875-881.
- Pazdur**, A., M.R. Fontugne and T. Goslar, 1995: Late glacial and Holocene water-level changes of the Gosciaz Lake, central Poland, derived from carbon-isotope studies of laminated sediment. *Quat. Sci. Rev.*, **14**, 125-135.
- Peel**, D.A., R. Mulvaney, E.C. Pasteur and C. Chenery, 1996: Climate changes in the Atlantic Sector of Antarctica over the past 500 years from ice-core and other evidence. In: *Climate Variations and Forcing Mechanisms of the Last 2000 Years*. NATO ASI Series I vol 41, P.D. Jones, R.S. Bradley and J. Jouzel (eds.), pp. 243-262.
- Peixoto**, J.P. and A.H. Oort, 1996: The climatology of relative humidity in the atmosphere. *J. Climate*, **9**, 3443-3463.
- Peterson**, J.A. and L.F. Peterson, 1994: Ice retreat from the neoglacial maxima in the Puncak Jayakesuma area, Republic of Indonesia. *Z. Gletscherkd. Glazialgeol.*, **30**, 1-9.
- Peterson**, T.C. and R.S. Vose, 1997: An overview of the global historical climatology network temperature data base. *Bull. Am. Met. Soc.*, **78**, 2837-2849.
- Peterson**, T.C., H. Daan, and P.D. Jones, 1997: Initial selection of a GCOS surface network. *Bull. Am. Met. Soc.*, **78**, 2145-2152.
- Peterson**, T.C., T.R. Karl, P.F. Jamason, R. Knight and D.R. Easterling, 1998a: The first difference method: maximizing station density for the calculation of long-term temperature change. *J. Geophys. Res. - Atmos.*, **103**, 25967-25974.
- Peterson**, T.C., D.R. Easterling, T.R. Karl, P. Groisman, N. Nicholls, N. Plummer, S. Torok, I. Auer, R. Boehm, D. Gullett, L. Vincent, R. Heino, H. Tuomenvirta, O. Mestre, T. Szentimrey, J. Salinger, E.J. Førland, I. Hanssen-Bauer, H. Alexandersson, P. Jones and D. Parker, 1998b: Homogeneity adjustments of in situ atmospheric climate data: a review. *Int. J. Climatol.*, **18**, 1495-1517.
- Peterson**, T.C., K.P. Gallo, J. Livermore, T.W. Owen, A. Huang and D.A. McKittrick, 1999: Global rural temperature trends. *Geophys. Res. Lett.*, **26**, 329-332.
- Petit**, J.R., J. Jouzel, D. Raynaud, N.I. Barkov, J.M. Barnola, I. Basile, M. Bender, J. Chappellaz, J. Davis, G. Delaygue, M. Delmotte, V.M. Kotlyakov, M. Legrand, V.Y. Lipenkov, C. Lorius, L. Pepin, C. Ritz, E. Saltzman and M. Stievenard, 1999: Climate and Atmospheric History of the Past 420,000 years from the Vostok Ice Core, Antarctica. *Nature*, **399**, 429-436.
- Petit-Maire** and Z.T. Guo, 1996: Mise en évidence de variations

- cimatiques, holocenes rapides, en phase dans les deserts actuels de Chine du nor et due Nord de l'Afrique, *C.R. Acad. Sci.*, Paris, 322, Serie Iia, pp. 847-851.
- Pfister**, C., 1995: Monthly temperature and precipitation in central Europe from 1525-1979: quantifying documentary evidence on weather and its effects. In: *Climate since A.D. 1500*, R.S. Bradley and P.D.Jones (eds.), Routledge, London, pp. 118-142.
- Pfister**, C., 1999: Wetternachhersage: 500 Jahre Klimavariationen und Naturkatastrophen 1496-1995. Paul Haupt, Bern, 304 pp.
- Pfister**, C. and R. Brázil, 1999: Climatic Variability in Sixteenth-Century Europe and its Social Dimension: A Synthesis. In: *Climatic Variability in Sixteenth-Century Europe and its Social Dimension*, C. Pfister, R. Brázil and R. Glaser (eds.), *Special Issue of Clim. Change*, **43**, 5-54.
- Pfister**, C., G. Kleinlogel, G. Schwarz-Zanetti and M. Wegmann, 1996: Winters in Europe: The fourteenth century. *Clim. Change*, **34**, 91-108.
- Pfister**, C., J. Luterbacher, G. Schwarz-Zanetti and M. Wegmann, 1998: Winter air temperature variations in Central Europe during the Early and High Middle Ages (A.D. 750-1300). *Holocene*, **8**, 547-564.
- Pfister**, C., R. Brázil, R. Glaser, M. Barriendos Vallvé, D. Camuffo, M. Deutsch, P. Dobrovoln?, S. Enzi, E. Guidoboni, O. Kotyza, S. Militzer, L. Rácz, and F.S. Rodrigo, 1999: Documentary Evidence on Climate in Sixteenth-Century Europe. In: *Climatic Variability in Sixteenth-Century Europe and its Social Dimension*, C. Pfister, R. Brázil and R. Glaser (eds.), Kluwer, Dordrecht, *Special Issue of Clim. Change*, **43**, 55-110.
- Pielke**, Sr. , R.A., J. Eastman, T.N. Chase, J. Knaff and T.G.F. Kittel, 1998a: Errata to 1973-1996 Trends in depth-averaged tropospheric temperature. *J. Geophys. Res.*, **103**(D14), 16927-16933.
- Pielke**, Sr. , R.A., J. Eastman, T.N. Chase, J. Knaff and T.G.F. Kittel, 1998b: 1973-1996 Trends in depth-averaged tropospheric temperature. *J. Geophys. Res.*, **103**(D22), 28909-28912.
- Piervitali**, E., M. Colacino and M. Conte, 1998: Rainfall over the Central-Western Mediterranean basin in the period 1951-1995. Part I: Precipitation trends. *Geophysics and Space Physics*, **21C**(3), 331-344.
- Plummer**, N., M.J. Salinger, N. Nicholls, R. Suppiah, K.J. Hennessy, R.M. Leighton, B.C. Trewhin, C.M. Page and J.M. Lough, 1999: Changes in climate extremes over the Australian region and New Zealand during the twentieth century. *Clim. Change*, **42**, 183-202.
- Pollack**, H., S. Huang and P.Y. Shen, 1998: Climate change revealed by subsurface temperatures: A global perspective. *Science* , **282**, 279-281.
- Polovina**, J.J., G.T. Mitchum and G.T. Evans, 1995: Decadal and basin-scale variation in mixed layer depth and the impact on biological production in the Central and North Pacific, 1960-88. *Deep Sea Res., Part I*, **42**(10), 1701-1716.
- Porter**, S.C. and Z. An, 1995: Correlation between climate events in the North Atlantic and China during the last glaciation. *Nature*, **375**, 305-308.
- Power**, S., F. Tseitkin, S. Torok, B. Lavery, R. Dahni and B. McAvaney, 1998: Australian temperature, Australian rainfall and the Southern Oscillation, 1910-1992: coherent variability and recent changes. *Australian Met. Mag.*, **47**, 85-101.
- Power**, S., T. Casey, C.K. Folland, A. Colman and V. Mehta, 1999: Inter-decadal modulation of the impact of ENSO on Australia. *Clim. Dyn.*, **15**, 319-323.
- Prabhakara**, C., R. Iacobassi Jr. and J.-M. Yoo, 1998: Global warming deduced from MSU. *Geophys. Res. Lett.*, **25**, 1927-1930.
- Prisenberg**, S.J., I.K. Peterson, S. Narayanan and J.U. Umoh, 1997: Interaction between atmosphere, ice cover, and ocean off Labrador and Newfoundland from 1962-1992. *Can. J. Aquat. Sci.*, **54**, 30-39.
- Quadfasel**, D., A. Sy and B. Rudels, 1993: A ship of opportunity section to the North Pole: Upper ocean temperature observations. *Deep Sea Res.,* **40**, 777-789.
- Quayle**, R.G., T.C. Peterson, A.N. Basist and C.S. Godfrey, 1999: An operational near-real-time global temperature index. *Geophys. Res. Lett.*, **26**, 333-335.
- Quintana-Gomez**, R.A., 1999: Trends of maximum and minimum temperatures in northern South America. *J. Climate*, **12**, 2104-2112.
- Raper**, S.C.B., K.R. Briffa and T.M.L. Wigley, 1996: Glacier change in northern Sweden from AD 500: a simple geometric model of Storglaciären. *J. Glaciol.*, **42**, 341-351.
- Rasmussen**, T.L., E. Thomsen, L.D. Labeyrie and T.C.E. van Weering, 1996a: Circulation changes in the Faeroe-Shetland Channel correlating with cold events during the last glacial period (58-10 ka). *Geology*, **24**, 937-940.
- Rasmussen**, T.L., T.C.E. van Weering and L.D. Labeyrie, 1996b: Climatic instability, ice sheets and ocean dynamics at high northern latitudes during the last glacial period (58-10 ka). *Quaternary Science Reviews*, **15**, 1-10.
- Rayner**, N.A., E.B. Horton, D.E. Parker, C.K. Folland and R.B. Hackett, 1996: Version 2.2 of the global sea-ice and sea surface temperature data set, 1903-1994. *Climate Research Technical Note* 74, 43pp. (Available from National Meteorological Library, London Road, Bracknell, UK, RG12 2SZ).
- Rayner**, N.A., D.E. Parker, P. Frich, E.B. Horton, C.K. Folland and L.V. Alexander, 2000: SST and sea-ice fields for ERA40. In *Proc. Second Int. WCRP Conf. On Reanalyses*, Wokefield Park, Reading, UK, 23-27 August 1999. WCRP-109, WMO/TD-NO. 985.
- Reeve**, N. and R. Toumi, 1999: Lightning activity as an indicator of climate change. *Quart. J. R. Met. Soc.*, **125**, 893-903.
- Reille**, M., J.L. de Beaulieu, H. Svobodova, V. Andrieu-Ponel and C. Goeyry, 2000: Pollen biostratigraphy of the last five climatic cycles from a long continental sequence from the Velay region (Massif Central, France). *J. Quat. Sci.*, **15**, 665-685.
- Ren**, G., 1998: Pollen evidence for increased summer rainfall in the Medieval warm period at Maili, Northeast China. *Geophys. Res. Lett.*, **25**, 1931-1934.
- Ren**, G., 1999a: Some palaeoclimatological problems associated with the present global warming. *J. Appl. Met.*, **7**(3), 361-370 (in Chinese with English abstract).
- Ren**, G., 1999b: Some progresses and problems in Paleoceanography. *Scientia Geographic Sinica*, **19**, 368-378.
- Ren**, G. and L. Zhang, 1998: A preliminary mapped summary of Holocene pollen data for Northeast China. *Quat. Sci. Rev.*, **17**, 669-688.
- Renwick**, J.A., 1998: ENSO-related variability in the frequency of South Pacific blocking. *Mon. Wea. Rev.*, **126**, 3117-3123.
- Renwick**, J.A. and M.J. Revell, 1999: Blocking over the South Pacific and Rossby Wave Propagation. *Mon. Wea. Rev.*, **127**, 2233-2247.
- Reverdin**, G., D.R. Cayan and Y. Kushnir, 1997: Decadal variability of hydrography in the upper northern North Atlantic in 1948-1990. *J. Geophys. Res.*, **102**(C4), 8505-8531.
- Reynolds**, R.W., 1993: Impact of Mount Pinatubo aerosols on satellite-derived sea surface temperatures. *J. Climate*, **6**, 768-774.
- Reynolds**, R.W. and T.M. Smith, 1994: Improved global sea surface temperature analyses using optimum interpolation. *J. Climate*, **7**, 929-948.
- Rind**, D., 1998: Just add water vapor. *Science*, **281**, 1152-1153.
- Ritchie**, J.C., L.C. Cwynar and R.W. Spear, 1983: Evidence from Northwest Canada for an early Holocene Milankovitch thermal maximum. *Nature*, **305**, 126-128.
- Robertson**, D.M., R.R. Ragotzkie and J.J. Magnuson, 1992: Lake ice records used to detect historical and future climatic changes. *Clim. Change*, **21**, 407-427.
- Robinson**, D.A., 1997: Hemispheric snow cover and surface albedo for model validation. *Ann. Glaciol.*, **25**, 241-245.
- Robinson**, D.A., 1999: Northern Hemisphere snow cover during the

- satellite era. *Proc. 5th Conf. Polar Met. and Ocean.*, Dallas, TX, American Meteorological Society, Boston, MA, pp. 255-260.
- Robinson**, D.A., K.F. Dewey and R.R. Heim, 1993: Global snow cover monitoring: An update. *Bull. Am. Met. Soc.*, **74**, 1689-1696.
- Robock**, A., Y.V. Konstantin, G. Srinivasan, J.K. Entin, S.E. Hollinger, N.A. Speranskaya, S. Liu and A. Namkhai, 2000: The global soil moisture data bank. *Bull. Am. Met. Soc.*, **81**, 1281-1299.
- Rodbell**, D., G.O. Seltzer, D.M. Anderson, D.B. Enfield, M.B. Abbott and J.H. Newman, 1999: A high-resolution 15000 year record of El Nino driven alluviation in southwestern Ecuador. *Science*, **283**, 516-520.
- Rodrigo**, F.S., M.J. Esteban-Parra, D. Pozo-Vazquez and Y. Castro-Diez, 1999: A 500-year precipitation record in Southern Spain. *Int. J. Climatol.*, **19**, 1233-1253.
- Romanovsky**, V.E. and T.E. Osterkamp, 1999: Permafrost Temperature Dynamics in Alaska and East Siberia During the Last 50 years. 11th Arctic Forum, ARCUS, Washington, DC, March 22-23.
- Romero**, R., J.A. Guijarro, C. Ramis and S. Alonso, 1998: A 30-year (1964-1993) daily rainfall data base for the Spanish Mediterranean regions: First exploratory study. *Int. J. Climatol.*, **18**, 541-560.
- Ross**, R.J. and W.P. Elliott, 1996: Tropospheric water vapor climatology and trends over North America: 1973-93. *J. Climate*, **9**, 3561-3574.
- Ross**, R.J. and W.P. Elliott, 1998: Northern hemisphere water vapor trends. Ninth Symposium on Global Change Studies, Amer. Meteor. Soc., Preprints, pp. 39-41.
- Ross**, R.J. and W.P. Elliott, 2001: Radiosonde-based Northern Hemisphere tropospheric water vapour trends. *J. Climate*, **14**, 1602-1612.
- Rossow**, W.B. and R.A. Schiffer, 1999: Advances in understanding clouds from ISCCP. *Bull. Am. Met. Soc.*, **80**, 2261-2287.
- Rostek**, F., G. Ruhland, F. Bassinot, P.J. Müller, L. Labeyrie, Y. Lancelot and E. Bard, 1993: Reconstructing sea surface temperature and salinity using  $\delta^{18}\text{O}$  and alkenone records. *Nature*, **364**, 319-321.
- Rothrock**, D.A., Y. Yu and G.A. Maykut, 1999: Thinning of the Arctic Sea-Ice Cover. *Geophys. Res. Lett.*, **26**, 3469-3472.
- Salinger**, M.J., 1995: Southwest Pacific temperature: trends in maximum and minimum temperatures. *Atmos. Res.*, **37**, 87-100.
- Salinger**, M.J. and M.S. McGlone, 1989: New Zealand Climate – The past two million years. The New Zealand Climate report 1990, Royal Society of New Zealand, Wellington, 13-17.
- Salinger**, M.J. and A.B. Mullan, 1999: New Zealand climate: temperature and precipitation variations and their links with atmospheric circulation. *Int. J. Climatol.*, **19**, 1049-1071.
- Salinger**, M.J., R.J. Allan, N. Bindoff, J. Hannah, B. Lavery, Z. Lin, J. Lindesay, N. Nicholls, N. Plummer and S. Torok, 1996: Observed variability and change in climate and sea level in Australia, New Zealand and the South Pacific. In: *Greenhouse: Coping with Climate Change*, W.J. Bouma, G.I. Pearman and M.R. Manning (eds.), CSIRO, Melbourne, Australia, pp. 100-126.
- Salinger**, M.J., J.A. Renwick and A.B. Mullan, 2001: Interdecadal Pacific Oscillation and South Pacific climate. *Int. J. Climatol.*, accepted.
- Sandweiss**, D.H., J.B. Richardson III, E.J. Reitz, H.B.R. Rollins and K.A. Maasch, 1996: Geoarcheological evidence from Paru for a 5000 years B.P. onset of El Nino. *Science*, **273**, 1531-1533.
- Santer**, B.D., J.J. Hnilo, T.M.L. Wrigley, J.S. Boyle, C. Doutriaux, M. Fiorino, D.E. Parker and K.E. Taylor, 1999: Uncertainties in observational based estimates of temperature change in the free atmosphere. *J. Geophys. Res.*, **104**, 6305-6333.
- Santer**, B.D., T.M.L. Wigley, J.S. Boyle, D.J. Gaffen, J.J. Hnilo, D. Nychka, D.E. Parker and K.E. Taylor, 2000: Statistical significance of trend differences in layer-average temperature time series. *J. Geophys. Res.*, **105**, 7337-7356.
- SAR**, see IPCC, 1996.
- Sarnthein**, M., K. Winn, S.J.A. Jung, J.C. Duplessy, L. Labeyrie, H. Erlenkeuser and G. Ganssen, 1994: Changes in east Atlantic deep water circulation over the last 30,000 years. *Paleoceanography*, **9**, 209-267.
- Schindler**, D.W., K.G. Beaty, E.J. Fee, D.R. Cruikshank, E.R. Devruyn, D.L. Findlay, G.A. Linsey, J.A. Shearer, M.P. Stainton and M.A. Turner, 1990: Effects of climatic warming on lakes of the central boreal forest. *Science*, **250**, 967-970.
- Schneider**, R.R., P.J. Müller, G. Ruhland, G. Meinecke, H. Schmidt and G. Wefer, 1996: Late Quaternary surface temperatures and productivity in east-equatorial South Atlantic: Response to changes in trade/monsoon wind forcing and surface water advection, 1996. In: *The South Atlantic: Present and Past Circulation*, G. Wefer, W.H. Berger, G. Siedler and D. Webb (eds.), Springer-Verlag, Berlin , pp. 527-551.
- Schönwiese**, C.D. and J. Rapp, 1997: Climate Trend Atlas of Europe Based on Observations 1891-1990. Kluwer Academic Publishers, Dordrecht, 228 pp.
- Schönwiese**, C.D., J. Rapp, T. Fuchs, and M. Denhard, 1994: Observed climate trends in Europe 1891-1990. *Meteorol. Zeitschrift*, **3**, 22-28.
- Schwartzman**, P.D., P.J. Michaels and P.C. Knappenberger, 1998: Observed changes in the diurnal dewpoint cycles across North America. *Geophys. Res. Lett.*, **25**, 2265-2268.
- Serreze**, M.C., F. Carse and R.G. Barry, 1997: Icelandic low cyclone activity climatological features, linkages with the NAO, and relationships with recent changes in the Northern Hemisphere circulation. *J. Climate*, **10**, 453-464.
- Serreze**, M.C., J.E. Walsh, F.S. Chapin III, T. Osterkamp, M. Dyurgerov, V. Romanovsky, W.C. Oechel, J. Morison, T. Zhang and R.G. Barry, 2000: Observational evidence of recent change in the northern high-latitude environment. *Clim. Change*, **46**, 159-207.
- Severinghaus**, J.P. and E. Brook, 1999: Abrupt climate change at the End of the last glacial period inferred from trapped air in polar ice. *Science*, **286**, 930-934.
- Severinghaus**, J.P., T. Sowers, E. Brook, R.B. Alley and M.L. Bender, 1998: Timing of abrupt climate change at the end of the Younger Dryas interval from thermally fractionated gases in polar ice. *Nature*, **391**, 141-146.
- Shabbar**, A., K. Higuchi, W. Skinner and J.L. Knox, 1997: The association between the BWA index and winter surface temperature variability over eastern Canada and west Greenland. *Int. J. Climatol.*, **17**, 1195-1210.
- Sharkhuu**, N., 1998: Trends of permafrost development in the Selenge River Basin, Mongolia. *Proceedings of the Seventh International Conference on Permafrost*, Yellowknife, Canada, June 1998, Université Laval, Quebec, Collection Nordicana No. 57, pp. 979-986.
- Shen**, S.S., M. Thomas, C.F. Ropelewski and R.E. Livezey, 1998: An optimal regional averaging method with error estimates and a test using tropical Pacific SST data. *J. Climate*, **11**, 2340-2350.
- Shinoda**, M., T. Okatani and M. Saloum, 1999: Diurnal variations of rainfall over Niger in the West African Sahel: A comparison between wet and drought years. *Int. J. Climatol.*, **19**, 81-94.
- Shulmeister**, J. and B.G. Lees, 1995: Pollen evidence form tropical Australia for the onset of an ENSO-dominated climate at c. 4000 BP. *The Holocene*, **5**, 10-18.
- Simmonds**, I. and K. Keay, 2000: Variability of Southern Hemisphere extratropical cyclone behavior, 1958-97. *J. Climate*, **13**(3), 550-561.
- Singer**, C., J. Shulmeister and B. McLea, 1998: Evidence against a significant Younger Dryas cooling event in New Zealand. *Science*, **281**, 812-814.
- Skinner**, W.R. and J.A. Majorowicz, 1999: Regional climatic warming and associated twentieth century land-cover changes in north-western North America. *Clim. Res.*, **12**, 39-52.
- Slingo**, J.M., D.P. Rowell, K.R. Sperber, and F. Nortley, 1999: On the predictability of the interannual behaviour of the Madden-Julian Oscillation and its relationship with El Nino. *Quart. J. R. Met. Soc.*,

- 125**, 583-609.
- Smith**, C.A., R. Toumi and J.D. Haigh, 2000: Seasonal trends in stratospheric water vapor. *Geophys. Res. Lett.*, **27**, 1687-1690.
- Smith**, C.A., J.D. Haigh and R. Toumi, 2001: Radiative forcing due to trends in stratospheric water vapor. *Geophys. Res. Lett.*, **28**, 179-182.
- Smith**, D.M., 1998: Recent increase in the length of the melt season of perennial Arctic sea ice. *Geophys. Res. Lett.*, **25**, 655-658.
- Smith**, T.M., R.W. Reynolds, R.E. Livezey and D.C. Stokes, 1996: Reconstruction of historical sea surface temperatures using empirical orthogonal functions. *J. Climate*, **9**, 1403-1420.
- Smith**, T.M., R.E. Livezey and S.S. Shen, 1998: An improved method for analyzing sparse and irregularly distributed SST data on a regular grid: The tropical Pacific Ocean. *J. Climate*, **11**, 1717-1729.
- Sowers**, T. and M. Bender, 1995: Climate records covering the last deglaciation. *Science*, **269**, 210-214.
- Spencer**, R.W., 1993: Global oceanic precipitation from the MSU during 1979-92 and comparisons to other climatologies. *J. Climate*, **6**, 1301-1326.
- Spencer**, R.W. and J.R. Christy, 1992a: Precision and radiosonde validation of satellite gridpoint temperature anomalies, Part I: MSU channel 2. *J. Climate*, **5**, 847-857.
- Spencer**, R.W. and J.R. Christy, 1992b: Precision and radiosonde validation of satellite gridpoint temperature anomalies, Part II: A tropospheric retrieval and trends 1979-90. *J. Climate*, **5**, 858-866.
- Stager**, J.C. and P.A. Mayewski, 1997: Abrupt Early to Mid-Holocene Climatic transition registered at the Equator and the Poles. *Science*, **276**, 1834-1836.
- Stahle**, D.W., M.K. Cleaveland, M.D. Therrell, D.A. Gay, R.D. D'Arrigo, P.J. Krusic, E.R. Cook, R.J. Allan, J.E. Cole, R.B. Dunbar, M.D. Moore, M.A. Stokes, B.T. Burns, J. Villanueva-Diaz and L.G. Thompson, 1998: Experimental Dendroclimatic Reconstruction of the Southern Oscillation. *Bull. Am. Met. Soc.*, **79**, 2137-2152.
- Steadman**, R.G., 1984: A universal scale of apparent temperature. *J. Clim. Appl. Met.*, **23**, 1674-1687.
- Steele**, M. and T. Boyd, 1998: Retreat of the cold halocline layer in the Arctic Ocean. *J. Geophys. Res.*, **103**(C5), 10419-10435.
- Steig**, E., E.J. Brook, J.W.C. White, C.M. Sucher, M.L. Bender, S.J. Lehman, D.L. Morse, E.D. Waddington and G.D. Clow, 1998: Synchronous climate changes in Antarctica and the North Atlantic. *Science*, **282**, 92-95.
- Stendel**, M., J.R. Christy and L. Bengtsson, 2000: Assessing levels of uncertainty in recent temperature time series. *Clim. Dyn.*, **16**(8), 587-601.
- Sterin**, A.M., 1999: An analysis of linear trends in the free atmosphere temperature series for 1958-1997. *Meteorologai Gidrologia*, **5**, 52-68.
- Stine**, S., 1994: Extreme and persistent drought in California and Patagonia during medieval time. *Nature*, **369**, 546-549.
- Stocker**, T.F., 2000: Past and further reorganization in the climate system. *Quat. Sci. Rev.*, **19**, 301-319.
- Stone**, D.A., A.J. Weaver and F.W. Zwiers, 1999: Trends in Canadian precipitation intensity. *Atmos. Ocean*, **2**, 321-347.
- Street-Perrott**, F.A. and R.A. Perrott, 1990: Abrupt climate fluctuations in the tropics: the influence of Atlantic ocean circulation. *Nature*, **343**, 607-612.
- Sun**, B. and P.Ya. Groisman, 2000: Cloudiness variations over the former Soviet Union. *Int. J. Climatol.*, **20**, 1097-1111.
- Sun**, B., P.Ya. Groisman, R.S. Bradley, and F.T. Keimig, 2000: Temporal changes in the observed relationship between cloud cover and surface air temperature. *J. Climate*, **13**, 4341-4357.
- Sun**, B., P.Ya. Groisman and I.I. Mokhov, 2001: Recent changes in cloud type frequency and inferred increases in convection over the United States and the Former USSR. *J. Climate*, **14**, 1864-1880.
- Sun**, X.J. and Y.S. Chen, 1991: Palynological records of the last 11,000 years in China. *Quat. Sci. Rev.*, **10**, 537-544.
- Swetnam**, T.W. and J. L. Betancourt, 1998: Mesoscale disturbance and ecological response to decadal climate variability in the American Southwest. *J. Climate*, **11**, 3128-3147.
- Tanimoto**, Y., N. Iwasaka, K. Hanawa and Y. Toba, 1993: Characteristic variations of sea surface temperature with multiple time scales in the North Pacific. *J. Climate*, **6**, 1153-1160.
- Tarhule**, A. and M. Woo, 1998: Changes in rainfall characteristics in northern Nigeria. *Int. J. Climatol.*, **18**, 1261-1271.
- Taylor**, K.C., G.W. Lamorey, G.A. Doyle, R.B. Alley, P.M. Grootes, P.A. Mayewski, J.W.C. White and L.K. Barlow, 1993: The "flickering switch" of late Pleistocene climate change. *Nature*, **361**, 432-436.
- Thie**, J., 1974: Distribution and thawing of permafrost in the southern part of the discontinuous permafrost zone in Manitoba. *Arctic*, **27**, 189-200.
- Thompson**, D.W.J. and J.M. Wallace, 1998: The Arctic oscillation signature in the wintertime geopotential height and temperature fields. *Geophys. Res. Lett.*, **25**, 1297-1300.
- Thompson**, D.W.J. and J.M. Wallace, 2000: Annual modes in the extratropical circulation Part I: month-to-month variability. *J. Climate*, **13**, 1000-1016.
- Thompson**, D.W.J. and J.M. Wallace, 2001: Regional climate impacts of the Northern Hemisphere annular mode and associated climate trends. *Nature*, in press.
- Thompson**, D.W.J., J.M. Wallace and G.C. Hegerl, 2000b: Annual modes in the extratropical circulation Part II: trends. *J. Climate*, **13**, 1018-1036.
- Thompson**, L.G., 1996: Climate changes for the last 2000 years inferred from ice core evidence in tropical ice cores. In: *Climate Variations and Forcing Mechanisms of the Last 2000 Years, NATO ASI Series I*, P.D. Jones, R.S. Bradley and J. Jouzel (eds.), **41**, 281-297.
- Thompson**, L.G. and 13 others, 1989: Pleistocene climate record from Qinghai-Tibetan Plateau ice cores. *Science*, **246**, 474-477.
- Thompson**, L.G., E. Mosley-Thompson, M.E. Davis, P.N. Lin, K.A. Henderson, J. Cole-Dai, J.F. Bolzan and K.B. Liu, 1995: Late Glacial Stage and Holocene Tropical Ice Core Records from Huascarán, Peru. *Science*, **269**, 46-50.
- Thompson**, L.G., M.E. Davis, E. Mosley-Thompson, T.A. Sowers, K.A. Henderson, V.S. Zagorodnov, P.N. Lin, V.N. Mikhalenko, R.K. Campen, J.F. Bolzan, J. Cole-Dai and B. Francou, 1998: A 25,000-year tropical climate history from Bolivian ice cores. *Science*, **282**, 1858-1864.
- Thompson**, L.G., T. Yao, E. Mosley-Thompson, M.E. Davis, K.A. Henderson and P.N. Lin, 2000a: A high resolution millennial record of the South Asian Monsoon from Himalayan ice cores. *Science*, **289**, 1916-1919.
- Thunell**, R.C. and P.G. Mortyn, 1995: Glacial climate instability in the northeast Pacific Ocean. *Nature*, **376**, 504-506.
- Torrence**, C. and G.P. Compo, 1998: A practical guide to wavelet analysis. *Bull. Am. Met. Soc.*, **79**, 61-78.
- Torrence**, C. and P.J. Webster, 1998: The annual cycle of persistence in the El Niño/Southern Oscillation. *Quart. J. R. Met. Soc.*, **124**, 1985-2004.
- Torrence**, C. and P.J. Webster, 1999: Interdecadal changes in the ENSO-monsoon system. *J. Climate*, **12**, 2679-2690.
- Trenberth**, K.E., 1998a: Atmospheric moisture residence times and cycling: Implications for rainfall rates with climate change. *Clim. Change*, **39**, 667-694.
- Trenberth**, K.E., 1998b: El Niño and global warming. *J. Marine Education*, **15**, 12-18.
- Trenberth**, K.E. and J.W. Hurrell, 1994: Decadal atmosphere-ocean variations in the Pacific. *Clim. Dyn.*, **9**, 303-319.
- Trenberth**, K.E. and T.J. Hoar, 1996: The 1990-1995 El Niño-Southern Oscillation event: longest on record. *Geophys. Res. Lett.*, **23**, 57-60.
- Trenberth**, K.E. and T.W. Owen, 1999: Workshop on Indices and Indicators for climate extremes, Asheville, NC, USA, 3-6 June 1999:

- Breakout Group A: Storms. *Clim. Change*, **42**, 9-21.
- Trenberth**, K.E., J.R. Christy and J.W. Hurrell, 1992: Monitoring global monthly mean surface temperatures. *J. Climate*, **5**, 1405-1423.
- Trenberth**, K.E., J.M. Caron and D.P. Stepaniak, 2001: The Atmospheric Energy Budget and Implications for Surface Fluxes and Ocean Heat Transports. *Clim. Dyn.*, **17**, 259-276.
- Tudhope**, A.W., G.B. Shimmield, C.P. Chilcott, M. Jebb, A.E. Fallick and A.N. Dagleish, 1995: Recent changes in climate in the far western equatorial Pacific and their relationship to the Southern Oscillation: oxygen isotope records from massive corals, Papua, New Guinea. *Earth and Planetary Science Letters*, **136**, 575-590.
- Tuomenvirta**, H., H. Alexandersson, A. Drebs, P. Frich and P.O. Nordli, 2000: Trends in Nordic and Arctic temperature extremes and ranges. *J. Climate*, **13**, 977-990.
- Turrell**, W.R., G. Slesser, R.D. Adams, R. Payne and P.A. Gillibrand, 1999: Decadal variability in the composition of Faroe Shetland Channel bottom water. *Deep Sea Res. Part I*, **46**, 1-25.
- Vaganov**, E.A., M.K. Hughes, A.V. Kirdyanov, F.H. Schweingruber and P.P. Silkin, 1999: Influence of snowfall and melt timing on tree growth in subarctic Eurasia. *Nature*, **400**, 149-151.
- Van Ommen**, T.D. and V. Morgan, 1996: Peroxide concentrations in the DSS ice core, Law Dome, Antarctica. *J. Geophys. Res.*, **101**(D10), 15147-15152.
- Van Ommen**, T.D. and V. Morgan, 1997: Calibrating the ice core paleothermometer using seasonality. *J. Geophys. Res.*, **102**(D8), 9351-9357.
- Vaughan**, D.G. and T. Lachlan-Cope, 1995: Recent retreat of ice shelves on the Antarctic Peninsula. *Weather*, **50**, 374-376.
- Vaughan**, D.G. and C.S.M. Doake, 1996: Recent atmospheric warming and retreat of ice shelves on the Antarctic Peninsula. *Nature*, **379**, 328-331.
- Vidal**, L., L.D. Labeyrie, E. Cortijo, M. Arnold, J.C. Duplessy, E. Michel, S. Becque and T.C.E. van Weering, 1997: Evidence for changes in the North Atlantic Deep Water linked to meltwater surges during the Heinrich events. *Earth Planet. Sci. Lett.*, **146**, 13-27.
- Vidal**, L., L.D. Labeyrie and T.C.E. van Weering, 1998: Benthic  $\delta^{18}\text{O}$  records in the North Atlantic over the last glacial period (60-10 kyr): Evidence for brine formation. *Paleoceanography*, **13**, 245-251.
- Villalba**, R., E.R. Cook, R. D'Arrigo, G.C. Jacoby, P.D. Jones, J.M. Salinger and J. Palmer, 1997: Sea-level pressure variability around Antarctica since A.D. 1750 inferred from subantarctic tree-ring records. *Clim. Dyn.*, **13**, 375-390.
- Vincent**, L.A., 1998: A technique for the identification of inhomogeneities in Canadian temperature series. *J. Climate*, **11**, 1094-1104.
- Vincent**, L.A. and D.W. Gullett, 1999: Canadian historical and homogeneous temperature datasets for climate change analysis. *Int. J. Climatol.*, **19**, 1375-1388.
- Vinje**, T., N. Nordlund and Å. Kvambekk, 1998: Monitoring ice thickness in Fram Strait. *J. Geophys. Res.*, **103**(C5), 10437-10449.
- Vinnikov**, K.Ya., P.Ya. Groisman and K.M. Lugina, 1990: Empirical data on contemporary global climate changes (temperature and precipitation). *J. Climate*, **3**, 662-677.
- Vinnikov**, K.Y., A. Robock, S. Qiu and J.K. Entin, 1999a: Optimal design of surface networks for observation of soil moisture. *J. Geophys. Res.*, **104**, 19743-19749.
- Vinnikov**, K.Y., A. Robock, R.J. Stouffer, J.E. Walsh, C.L. Parkinson, D.J. Cavalieri, J.F.B. Mitchell, D. Garrett and V.F. Zakharov, 1999b: Global warming and Northern Hemisphere sea ice extent. *Science*, **286**, 1934-1937.
- Vitt**, D.H., L.A. Halsey and S.C. Zoltai, 1994: The bog landforms of continental western Canada in relation to climate and permafrost patterns. *Arctic and Alpine Res.*, **26**, 1-13.
- Vonder Mühl**, D., T. Stucki and W. Haeberly, 1998: Borehole temperatures in Alpine permafrost: a ten years series. *Proceedings of the Seventh International Conference on Permafrost*, Yellowknife, Canada, June 1998, Université Laval, Quebec, Collection Nordicana No. 57, pp. 1089-1096.
- von Grafenstein**, U., H. Erlenkeuser, J. Muller, J. Jouzel and S.J. Johnsen, 1998: The cold event 8,200 years ago documented in oxygen isotope records of precipitation in Europe and Greenland. *Clim. Dyn.*, **14**, 73-81.
- von Grafenstein**, U., H. Erlenkeuser, A. Brauer, J. Jouzel and S.J. Johnsen, 1999: A mid-European decadal isotope-climate record from 15,500 to 5,000 years B.P. *Science*, **284**, 1654-1657.
- Wadhams**, P. and N.R. Davis, 2000: Further evidence of sea ice thinning in the Arctic Ocean. *Geophys. Res. Lett.*, **27**, 3973-3976.
- Wallace**, J.M., 2000: North Atlantic Oscillation / Northern Hemisphere annular mode: Two paradigms - One phenomenon. *Quart. J. R. Met. Soc.*, **126**, 791-805.
- Wallace**, J.M., Y. Zhang and J.A. Renwick, 1995: Dynamic contribution to hemispheric mean temperature trends. *Science*, **270**, 780-783.
- Wallis**, T.W.R., 1998: A subset of core stations from the Comprehensive Aerological Data Set (CARDs). *J. Climate*, **12**, 272-282.
- Walsh**, J.E., 1978: Data set on Northern Hemisphere sea-ice extent. *Glaciological Data, Report GD-2*, World Data Center-A for Glaciology (Snow and Ice), part 1, pp. 49-51.
- Walsh**, J.M., W.L. Chapman and T.L. Shy, 1996: Recent decrease of sea level pressure in the central Arctic. *J. Climate*, **9**, 480-486.
- Wang**, B. and H.M. French, 1994: Climate controls and high-altitude permafrost, Qinghai-Xizang (Tibet) Plateau, China. *Permafrost and Periglacial Processes*, **5**, 87-100.
- Wang**, B. and Y. Wang, 1996: Temporal structure of the Southern Oscillation as revealed by waveform and wavelet analysis. *J. Climate*, **9**, 1586-1598.
- Wang**, S.L., H.J. Jin, S. Li and L. Zhao, 2000: Permafrost Degradation on the Qinghai-Tibet Plateau and its Environmental Impacts. *Permafrost and Periglacial Processes*, **11**, 43-53.
- Wang**, S.W. and D.Y. Gong, 2000: Climate in China during the four special periods in Holocene. *Progress in Nature Science*, **10**(5), 379-386.
- Wang**, S.W., J. Ye, D. Gong and J. Zhu, 1998a: Construction of mean annual temperature series for the last one hundred years in China. *Quart. J. Appl. Met.*, **9**(4), 392-401 (in Chinese).
- Wang**, S.W., J. Ye and D. Gong, 1998b: Climate in China during the Little Ice Age. *Quaternary Sciences*, **1**, 54-64 (in Chinese).
- Wang**, X.L. and D.J. Gaffen, 2001: Late twentieth century climatology and trends of surface humidity and temperature in China. *J. Climate*, in press.
- Wanner**, H., C. Pfister, R. Bräzdil, P. Frich, K. Fruydendahl, T. Jonsson, J. Kington, H.H. Lamb, S. Rosenorn and E. Wishman, 1995: Wintertime European circulation patterns during the Late Maunder Minimum Cooling Period (1675-1704). *Theor. Appl. Climatol.*, **51**, 167-175.
- Wansard**, G., 1996: Quantification of paleotemperature changes during isotopic stage 2 in the La Draga continental sequence (NE Spain) based on the Mg/Ca ratio of freshwater ostracods. *Quaternary Science Review*, **15**, 237-245.
- Waple**, A., M.E. Mann and R.S. Bradley, 2001: Long-term Patterns of Solar Irradiance Forcing in Model Experiments and Proxy-based Surface Temperature Reconstructions. *Clim. Dyn.*, in press.
- Ward**, M.N., 1998: Diagnosis and short-lead time prediction of summer rainfall in tropical North Africa and interannual and multi-decadal timescales. *J. Climate*, **11**, 3167-3191.
- Ward**, M.N., P.J. Lamb, D.H. Portis, M. El Hamly, and R. Sebbari, 1999: Climate Variability in Northern Africa: Understanding Droughts in the Sahel and the Mahgreb. In: *Beyond El Niño: Decadal and Interdecadal Climate Variability*, A. Navarra (ed.), Springer, Berlin, pp. 119-140.
- WASA Group** (von Storch et al.), 1998: Changing waves and storms in the Northeast Atlantic? *Bull. Am. Met. Soc.*, **79**, 741-760.

- Watts**, W.A., J.R.M. Allen and B. Huntley, 1996: Vegetation history and palaeoclimate of the last glacial period at Lago Grande Di Monticchio, Southern Italy. *Quat. Sci. Rev.*, **15**, 133-151.
- Webb**, I., Thompson and J.E. Kutzbach, 1998: An introduction to Late Quaternary Climates: Data Syntheses and Model Experiments. *Quat. Sci. Rev.*, **17**, 465-471.
- Weber**, R.O., P. Talkner and G. Stefanicki, 1994: Asymmetric diurnal temperature change in the Alpine region. *Geophys. Res. Lett.*, **21**, 673-676.
- Weller**, G. and P.A. Anderson (eds.), 1998: Implications of Global Change in Alaska and the Bering Sea Region. *Proceedings of a Workshop, June 1997, Centre for Global Change and Arctic System Research*, University of Alaska Fairbanks, Fairbanks, Alaska, 157 pp.
- Wentz**, F.J. and M. Schabel, 1998: Effects of orbital decay on satellite-derived lower-tropospheric temperature trends. *Nature*, **394**, 661-664.
- White**, J.W.C., L.K. Barlow, D.A. Fisher, P. Grootes, J. Jouzel, S. Johnsen, and P.A. Mayewski, 1998a: The climate signal in the stable isotopes of snow from Summit Greenland: results of comparisons with modern climate observations. *Special Issue J. Geophys. Res.*, American Geophysical Union, 26425-26440.
- White**, W.B. and R. Peterson, 1996: An Antarctic circumpolar wave in surface pressure, wind, temperature, and sea ice extent. *Nature*, **380**, 699-702.
- White**, W.B. and D.R. Cayan, 1998: Quasi-periodicity and global symmetries in interdecadal upper ocean temperature variability. *J. Geophys. Res.*, **103**(C10), 21335-21354.
- White**, W.B., J. Lean, D.R. Cayan and M.D. Dettinger, 1997: A response of global upper ocean temperature to changing solar irradiance. *J. Geophys. Res.*, **102**, 3255-3266.
- White**, W.B., D.R. Cayan and J. Lean, 1998b: Global upper ocean heat storage response to radiative forcing from changing solar irradiance and increasing greenhouse gas/aerosol concentrations. *J. Geophys. Res.*, **103**, 21355-21366.
- Wick**, L. and W. Tinner, 1999: Vegetation changes and timberline fluctuations in the Central Alps as indicators of Holocene climate oscillations. *Arctic and Alpine Research*, **29**, 445-458.
- Wigley**, T.M.L., 2000: ENSO, volcanoes and record-breaking temperatures. *Geophys. Res. Lett.*, **27**, 4101-4104.
- Wiles**, G.C., R.D. D'Arrigo and G.C. Jacoby, 1998: Gulf of Alaska atmosphere-ocean variability over recent centuries inferred from coastal tree-ring records. *Clim. Change*, **38**, 289-306.
- Wilks**, D.S., 1999: Interannual variability and extreme-value characteristics of several stochastic daily precipitation models. *Agric. For. Meteorol.*, **93**, 153-169.
- Williams**, P.W., A. Marshall, D.C. Ford and A.V. Jenkinson, 1999: Palaeoclimatic interpretation of stable isotope data from Holocene speleotherms of the Waitomo district, North Island, New Zealand. *Holocene*, **9**, 649-657.
- Wohlfarth**, B., H. Linderson, B. Holmquist and I. Cato, 1998: The climatic significance of clastic varves in the Angermanalven Estuary, northern Sweden, AD 1860-1950. *The Holocene*, **8**, 525-534.
- Wolfe**, S.A., E. Kotler and F.M. Nixon, 2000: Recent warming impacts in the Mackenzie Delta, Northwest Territories, and northern Yukon Territory coastal areas. *Geological Survey of Canada, Current Research 2000-B1*, 9 pp.
- Wong**, A.P.S., N.L. Bindoff and J.A. Church, 1999: Large-scale freshening of intermediate waters in the Pacific and Indian Oceans. *Nature*, **400**, 440-443.
- Woodhouse**, C.A. and J.T. Overpeck, 1998: 2000 years of drought variability in the central United States. *Bull. Am. Met. Soc.*, **79**, 2693-2714.
- Wynne**, R.H., T.M. Lilles, M.K. Clayton and J.J. Magnuson, 1998: The predominant spatial trends of mean ice breakup dates can be attributed to latitude and snowfall. *Photogrammetric Engineering and Remote Sensing*, ISSN: 0099-1112 (Falls Church, VA), **64**, 607-618.
- Xie**, P. and P.A. Arkin, 1997: Global precipitation: A 17-year monthly analysis based on gauge observations, satellite estimates and numerical model outputs. *Bull. Am. Met. Soc.*, **78**, 2539-2558.
- Yamamoto**, R. and Y. Sakurai, 1999: Long-term intensification of extremely heavy rainfall intensity in recent 100 years. *World Resource Rev.*, **11**, 271-281.
- Ye**, H., H.R. Cho and P.E. Gustafson, 1998: The changes in Russian winter snow accumulation during 1936-83 and its spatial patterns. *J. Climate*, **11**, 856-863.
- Yiou**, F., G.M. Raisbeck., S. Baumgartner, J. Beer, C. Hammer, S. Johnsen, J. Jouzel, P.W. Kubik, J. Lestringuez, M. Stievenard, M. Suter and P. Yiou, 1997a: Beryllium 10 in the Greenland Ice Core Project ice core at Summit Greenland. *J. Geophys. Res.*, **102**, 26783-26794.
- Yiou**, P., K. Fuhrer, L.D. Meeker, J. Jouzel, S.J. Johnsen and P.A. Mayewski, 1997b: Paleoclimatic variability inferred from the spectral analysis of Greenland and Antarctic ice core data. *J. Geophys. Res.*, **102**, 26441-26454.
- Yu**, G. and S.P. Harrison, 1996: An evaluation of the simulated water balance of Eurasia and northern Africa at 6000 y BP using lake status data. *Clim. Dyn.*, **12**, 723-735.
- Yu**, G. and B. Qin, 1997: Holocene temperature and precipitation reconstructions and monsoonal climates in eastern China using pollen data. *Paleoclimates*, **2**, 1-32.
- Yung**, Y.L., T. Lee, C.H. Wang and Y.T. Shieh, 1996: Dust: A diagnostic of the hydrologic cycle during the Last Glacial Maximum. *Science*, **271**, 962-963.
- Zenk**, W. and N. Hogg, 1996: Warming trend in Antarctic Bottom Water flowing into the Brazil Basin. *Deep Sea Res., Part I*, **43**, 1461-1473.
- Zhai**, P.M. and R.E. Eskridge, 1997: Atmospheric water vapor over China. *J. Climate*, **10**, 2643-2652.
- Zhai**, P.M. and F.M. Ren, 1999: Changes of China's maximum and minimum temperatures in 1951-1990. *Acta Meteor. Sinica*, **13**, 278-290.
- Zhai**, P.M., A. Sun, F. Ren, X. Liu, B. Gao and Q. Zhang, 1999a: Changes of climate extremes in China. *Clim. Change*, **42**, 203-218.
- Zhai**, P.M., F.M. Ren and Q. Zhang, 1999b: Detection of trends in China's precipitation extremes. *Acta Meteorologica Sinica*, **57**, 208-216.
- Zhang**, K., B.C. Douglas and S.P. Leatherman, 1997a: East Coast storm surges provide unique climate record. *EOS Trans. American Geophysical Union*, **78**(37).
- Zhang**, T., R.G. Barry, K. Knowles, J.A. Heginbottom and J. Brown, 1999: Statistics and characteristics of permafrost and ground-ice distribution in the Northern Hemisphere. *Polar Geography*, **2**, 132-154.
- Zhang**, X., L.A. Vincent, W.D. Hogg and A. Niitsoo, 2000: Temperature and precipitation trends in Canada during the 20th Century. *Atmosphere-Ocean*, **38**, 395-429.
- Zhang**, Y. and W.C. Wang, 1997: Model-simulated northern winter cyclone and anticyclone activity under a greenhouse warming scenario. *J. Climate*, **10**, 1616-1634.
- Zhang**, Y., J.M. Wallace and D.S. Battisti, 1997b: ENSO-like interdecadal variability: 1900-93. *J. Climate*, **10**, 1004-1020.



# 3

---

## The Carbon Cycle and Atmospheric Carbon Dioxide

---

### **Co-ordinating Lead Author**

I.C. Prentice

### **Lead Authors**

G.D. Farquhar, M.J.R. Fasham, M.L. Goulden, M. Heimann, V.J. Jaramillo, H.S. Kheshgi, C. Le Quéré,  
R.J. Scholes, D.W.R. Wallace

### **Contributing Authors**

D. Archer, M.R. Ashmore, O. Aumont, D. Baker, M. Battle, M. Bender, L.P. Bopp, P. Bousquet, K. Caldeira,  
P. Ciais, P.M. Cox, W. Cramer, F. Dentener, I.G. Enting, C.B. Field, P. Friedlingstein, E.A. Holland,  
R.A. Houghton, J.I. House, A. Ishida, A.K. Jain, I.A. Janssens, F. Joos, T. Kaminski, C.D. Keeling,  
R.F. Keeling, D.W. Kicklighter, K.E. Kohfeld, W. Knorr, R. Law, T. Lenton, K. Lindsay, E. Maier-Reimer,  
A.C. Manning, R.J. Matear, A.D. McGuire, J.M. Melillo, R. Meyer, M. Mund, J.C. Orr, S. Piper, K. Plattner,  
P.J. Rayner, S. Sitch, R. Slater, S. Taguchi, P.P. Tans, H.Q. Tian, M.F. Weirig, T. Whorf, A. Yool

### **Review Editors**

L. Pitelka, A. Ramirez Rojas

# Contents

---

<b>Executive Summary</b>	185		
<b>3.1 Introduction</b>	187	3.5.2 Interannual Variability in the Rate of Atmospheric CO <sub>2</sub> Increase	208
<b>3.2 Terrestrial and Ocean Biogeochemistry: Update on Processes</b>	191	3.5.3 Inverse Modelling of Carbon Sources and Sinks	210
3.2.1 Overview of the Carbon Cycle	191	3.5.4 Terrestrial Biomass Inventories	212
3.2.2 Terrestrial Carbon Processes	191		
3.2.2.1 Background	191	<b>3.6 Carbon Cycle Model Evaluation</b>	213
3.2.2.2 Effects of changes in land use and land management	193	3.6.1 Terrestrial and Ocean Biogeochemistry Models	213
3.2.2.3 Effects of climate	194	3.6.2 Evaluation of Terrestrial Models	214
3.2.2.4 Effects of increasing atmospheric CO <sub>2</sub>	195	3.6.2.1 Natural carbon cycling on land	214
3.2.2.5 Effects of anthropogenic nitrogen deposition	196	3.6.2.2 Uptake and release of anthropogenic CO <sub>2</sub> by the land	215
3.2.2.6 Additional impacts of changing atmospheric chemistry	197	3.6.3 Evaluation of Ocean Models	216
3.2.2.7 Additional constraints on terrestrial CO <sub>2</sub> uptake	197	3.6.3.1 Natural carbon cycling in the ocean	216
3.2.3 Ocean Carbon Processes	197	3.6.3.2 Uptake of anthropogenic CO <sub>2</sub> by the ocean	216
3.2.3.1 Background	197		
3.2.3.2 Uptake of anthropogenic CO <sub>2</sub>	199	<b>3.7 Projections of CO<sub>2</sub> Concentration and their Implications</b>	219
3.2.3.3 Future changes in ocean CO <sub>2</sub> uptake	199	3.7.1 Terrestrial Carbon Model Responses to Scenarios of Change in CO <sub>2</sub> and Climate	219
<b>3.3 Palaeo CO<sub>2</sub> and Natural Changes in the Carbon Cycle</b>	201	3.7.2 Ocean Carbon Model Responses to Scenarios of Change in CO <sub>2</sub> and Climate	219
3.3.1 Geological History of Atmospheric CO <sub>2</sub>	201	3.7.3 Coupled Model Responses and Implications for Future CO <sub>2</sub> Concentrations	221
3.3.2 Variations in Atmospheric CO <sub>2</sub> during Glacial/inter-glacial Cycles	202	3.7.3.1 Methods for assessing the response of atmospheric CO <sub>2</sub> to different emissions pathways and model sensitivities	221
3.3.3 Variations in Atmospheric CO <sub>2</sub> during the Past 11,000 Years	203	3.7.3.2 Concentration projections based on IS92a, for comparison with previous studies	222
3.3.4 Implications	203	3.7.3.3 SRES scenarios and their implications for future CO <sub>2</sub> concentration	223
<b>3.4 Anthropogenic Sources of CO<sub>2</sub></b>	204	3.7.3.4 Stabilisation scenarios and their implications for future CO <sub>2</sub> emissions	224
3.4.1 Emissions from Fossil Fuel Burning and Cement Production	204	3.7.4 Conclusions	224
3.4.2 Consequences of Land-use Change	204		
<b>3.5 Observations, Trends and Budgets</b>	205	<b>References</b>	225
3.5.1 Atmospheric Measurements and Global CO <sub>2</sub> Budgets	205		

## Executive Summary

### ***CO<sub>2</sub> concentration trends and budgets***

Before the Industrial Era, circa 1750, atmospheric carbon dioxide (CO<sub>2</sub>) concentration was  $280 \pm 10$  ppm for several thousand years. It has risen continuously since then, reaching 367 ppm in 1999.

The present atmospheric CO<sub>2</sub> concentration has not been exceeded during the past 420,000 years, and likely not during the past 20 million years. The rate of increase over the past century is unprecedented, at least during the past 20,000 years.

The present atmospheric CO<sub>2</sub> increase is caused by anthropogenic emissions of CO<sub>2</sub>. About three-quarters of these emissions are due to fossil fuel burning. Fossil fuel burning (plus a small contribution from cement production) released on average  $5.4 \pm 0.3$  PgC/yr during 1980 to 1989, and  $6.3 \pm 0.4$  PgC/yr during 1990 to 1999. Land use change is responsible for the rest of the emissions.

The rate of increase of atmospheric CO<sub>2</sub> content was  $3.3 \pm 0.1$  PgC/yr during 1980 to 1989 and  $3.2 \pm 0.1$  PgC/yr during 1990 to 1999. These rates are less than the emissions, because some of the emitted CO<sub>2</sub> dissolves in the oceans, and some is taken up by terrestrial ecosystems. Individual years show different rates of increase. For example, 1992 was low (1.9 PgC/yr), and 1998 was the highest (6.0 PgC/yr) since direct measurements began in 1957. This variability is mainly caused by variations in land and ocean uptake.

Statistically, high rates of increase in atmospheric CO<sub>2</sub> have occurred in most El Niño years, although low rates occurred during the extended El Niño of 1991 to 1994. Surface water CO<sub>2</sub> measurements from the equatorial Pacific show that the natural source of CO<sub>2</sub> from this region is reduced by between 0.2 and 1.0 PgC/yr during El Niño events, counter to the atmospheric increase. It is likely that the high rates of CO<sub>2</sub> increase during most El Niño events are explained by reductions in land uptake, caused in part by the effects of high temperatures, drought and fire on terrestrial ecosystems in the tropics.

Land and ocean uptake of CO<sub>2</sub> can now be separated using atmospheric measurements (CO<sub>2</sub>, oxygen (O<sub>2</sub>) and <sup>13</sup>CO<sub>2</sub>). For 1980 to 1989, the ocean-atmosphere flux is estimated as  $-1.9 \pm 0.6$  PgC/yr and the land-atmosphere flux as  $-0.2 \pm 0.7$  PgC/yr based on CO<sub>2</sub> and O<sub>2</sub> measurements (negative signs denote net uptake). For 1990 to 1999, the ocean-atmosphere flux is estimated as  $-1.7 \pm 0.5$  PgC/yr and the land-atmosphere flux as  $-1.4 \pm 0.7$  PgC/yr. These figures are consistent with alternative budgets based on CO<sub>2</sub> and <sup>13</sup>CO<sub>2</sub> measurements, and with independent estimates based on measurements of CO<sub>2</sub> and <sup>13</sup>CO<sub>2</sub> in sea water. The new 1980s estimates are also consistent with the ocean-model based carbon budget of the IPCC WGI Second Assessment Report (IPCC, 1996a) (hereafter SAR). The new 1990s estimates update the budget derived using SAR methodologies for the IPCC Special Report on Land Use, Land Use Change and Forestry (IPCC, 2000a).

The net CO<sub>2</sub> release due to land-use change during the 1980s has been estimated as 0.6 to 2.5 PgC/yr (central estimate 1.7 PgC/yr). This net CO<sub>2</sub> release is mainly due to deforestation in the tropics. Uncertainties about land-use changes limit the

accuracy of these estimates. Comparable data for the 1990s are not yet available.

The land-atmosphere flux estimated from atmospheric observations comprises the *balance* of net CO<sub>2</sub> release due to land-use changes and CO<sub>2</sub> uptake by terrestrial systems (the “residual terrestrial sink”). The residual terrestrial sink is estimated as  $-1.9$  PgC/yr (range  $-3.8$  to  $+0.3$  PgC/yr) during the 1980s. It has several likely causes, including changes in land management practices and fertilisation effects of increased atmospheric CO<sub>2</sub> and nitrogen (N) deposition, leading to increased vegetation and soil carbon.

Modelling based on atmospheric observations (inverse modelling) enables the land-atmosphere and ocean-atmosphere fluxes to be partitioned between broad latitudinal bands. The sites of anthropogenic CO<sub>2</sub> uptake in the ocean are not resolved by inverse modelling because of the large, natural background air-sea fluxes (outgassing in the tropics and uptake in high latitudes). Estimates of the land-atmosphere flux north of 30°N during 1980 to 1989 range from  $-2.3$  to  $-0.6$  PgC/yr; for the tropics,  $-1.0$  to  $+1.5$  PgC/yr. These results imply substantial terrestrial sinks for anthropogenic CO<sub>2</sub> in the northern extra-tropics, and in the tropics (to balance deforestation). The pattern for the 1980s persisted into the 1990s.

Terrestrial carbon inventory data indicate carbon sinks in northern and tropical forests, consistent with the results of inverse modelling.

East-west gradients of atmospheric CO<sub>2</sub> concentration are an order of magnitude smaller than north-south gradients. Estimates of continental-scale CO<sub>2</sub> balance are possible in principle but are poorly constrained because there are too few well-calibrated CO<sub>2</sub> monitoring sites, especially in the interior of continents, and insufficient data on air-sea fluxes and vertical transport in the atmosphere.

### ***The global carbon cycle and anthropogenic CO<sub>2</sub>***

The global carbon cycle operates through a variety of response and feedback mechanisms. The most relevant for decade to century time-scales are listed here.

#### *Responses of the carbon cycle to changing CO<sub>2</sub> concentrations*

- Uptake of anthropogenic CO<sub>2</sub> by the ocean is primarily governed by ocean circulation and carbonate chemistry. So long as atmospheric CO<sub>2</sub> concentration is increasing there is net uptake of carbon by the ocean, driven by the atmosphere-ocean difference in partial pressure of CO<sub>2</sub>. The fraction of anthropogenic CO<sub>2</sub> that is taken up by the ocean declines with increasing CO<sub>2</sub> concentration, due to reduced buffer capacity of the carbonate system. The fraction taken up by the ocean also declines with the rate of increase of atmospheric CO<sub>2</sub>, because the rate of mixing between deep water and surface water limits CO<sub>2</sub> uptake.
- Increasing atmospheric CO<sub>2</sub> has no significant fertilisation effect on marine biological productivity, but it decreases pH. Over a century, changes in marine biology brought about by changes in calcification at low pH could increase the ocean uptake of CO<sub>2</sub> by a few percentage points.

- Terrestrial uptake of CO<sub>2</sub> is governed by net biome production (NBP), which is the balance of net primary production (NPP) and carbon losses due to heterotrophic respiration (decomposition and herbivory) and fire, including the fate of harvested biomass. NPP increases when atmospheric CO<sub>2</sub> concentration is increased above present levels (the “fertilisation” effect occurs directly through enhanced photosynthesis, and indirectly through effects such as increased water use efficiency). At high CO<sub>2</sub> concentration (800 to 1,000 ppm) any further direct CO<sub>2</sub> fertilisation effect is likely to be small. The effectiveness of terrestrial uptake as a carbon sink depends on the transfer of carbon to forms with long residence times (wood or modified soil organic matter). Management practices can enhance the carbon sink because of the inertia of these “slow” carbon pools.

#### *Feedbacks in the carbon cycle due to climate change*

- Warming reduces the solubility of CO<sub>2</sub> and therefore reduces uptake of CO<sub>2</sub> by the ocean.
- Increased vertical stratification in the ocean is likely to accompany increasing global temperature. The likely consequences include reduced outgassing of upwelled CO<sub>2</sub>, reduced transport of excess carbon to the deep ocean, and changes in biological productivity.
- On short time-scales, warming increases the rate of heterotrophic respiration on land, but the extent to which this effect can alter land-atmosphere fluxes over longer time-scales is not yet clear. Warming, and regional changes in precipitation patterns and cloudiness, are also likely to bring about changes in terrestrial ecosystem structure, geographic distribution and primary production. The net effect of climate on NBP depends on regional patterns of climate change.

#### *Other impacts on the carbon cycle*

- Changes in management practices are very likely to have significant effects on the terrestrial carbon cycle. In addition to deforestation and afforestation/reforestation, more subtle management effects can be important. For example, fire suppression (e.g., in savannas) reduces CO<sub>2</sub> emissions from burning, and encourages woody plant biomass to increase. On agricultural lands, some of the soil carbon lost when land was cleared and tilled can be regained through adoption of low-tillage agriculture.
- Anthropogenic N deposition is increasing terrestrial NPP in some regions; excess tropospheric ozone (O<sub>3</sub>) is likely to be reducing NPP.
- Anthropogenic inputs of nutrients to the oceans by rivers and atmospheric dust may influence marine biological productivity, although such effects are poorly quantified.

#### *Modelling and projection of CO<sub>2</sub> concentration*

Process-based models of oceanic and terrestrial carbon cycling have been developed, compared and tested against *in situ* measurements and atmospheric measurements. The following are consistent results based on several models.

- Modelled ocean-atmosphere flux during 1980 to 1989 was in

the range -1.5 to -2.2 PgC/yr for the 1980s, consistent with earlier model estimates and consistent with the atmospheric budget.

- Modelled land-atmosphere flux during 1980 to 1989 was in the range -0.3 to -1.5 PgC/yr, consistent with or slightly more negative than the land-atmosphere flux as indicated by the atmospheric budget. CO<sub>2</sub> fertilisation and anthropogenic N deposition effects contributed significantly: their combined effect was estimated as -1.5 to -3.1 PgC/yr. Effects of climate change during the 1980s were small, and of uncertain sign.
- In future projections with ocean models, driven by CO<sub>2</sub> concentrations derived from the IS92a scenario (for illustration and comparison with earlier work), ocean uptake becomes progressively larger towards the end of the century, but represents a smaller fraction of emissions than today. When climate change feedbacks are included, ocean uptake becomes less in all models, when compared with the situation without climate feedbacks.
- In analogous projections with terrestrial models, the rate of uptake by the land due to CO<sub>2</sub> fertilisation increases until mid-century, but the models project smaller increases, or no increase, after that time. When climate change feedbacks are included, land uptake becomes less in all models, when compared with the situation without climate feedbacks. Some models have shown a rapid decline in carbon uptake after the mid-century.

Two simplified, fast models (ISAM and Bern-CC) were used to project future CO<sub>2</sub> concentrations under IS92a and six SRES scenarios, and to project future emissions under five CO<sub>2</sub> stabilisation scenarios. Both models represent ocean and terrestrial climate feedbacks, in a way consistent with process-based models, and allow for uncertainties in climate sensitivity and in ocean and terrestrial responses to CO<sub>2</sub> and climate.

- The reference case projections (which include climate feedbacks) of both models under IS92a are, by coincidence, close to those made in the SAR (which neglected feedbacks).
- The SRES scenarios lead to divergent CO<sub>2</sub> concentration trajectories. Among the six emissions scenarios considered, the projected range of CO<sub>2</sub> concentrations at the end of the century is 550 to 970 ppm (ISAM model) or 540 to 960 ppm (Bern-CC model).
- Variations in climate sensitivity and ocean and terrestrial model responses add at least -10 to +30% uncertainty to these values, and to the emissions implied by the stabilisation scenarios.
- The net effect of land and ocean climate feedbacks is always to increase projected atmospheric CO<sub>2</sub> concentrations. This is equivalent to reducing the allowable emissions for stabilisation at any one CO<sub>2</sub> concentration.
- New studies with general circulation models including interactive land and ocean carbon cycle components also indicate that climate feedbacks have the potential to increase atmospheric CO<sub>2</sub> but with large uncertainty about the magnitude of the terrestrial biosphere feedback.

### **Implications**

CO<sub>2</sub> emissions from fossil fuel burning are virtually certain to be the dominant factor determining CO<sub>2</sub> concentrations during the 21st century. There is scope for land-use changes to increase or decrease CO<sub>2</sub> concentrations on this time-scale. If all of the carbon so far released by land-use changes could be restored to the terrestrial biosphere, CO<sub>2</sub> at the end of the century would be 40 to 70 ppm less than it would be if no such intervention had occurred. By comparison, global deforestation would add two to four times more CO<sub>2</sub> to the atmosphere than reforestation of all cleared areas would subtract.

There is sufficient uptake capacity in the ocean to incorporate 70 to 80% of foreseeable anthropogenic CO<sub>2</sub> emissions to the atmosphere, this process takes centuries due to the rate of ocean mixing. As a result, even several centuries after emissions occurred, about a quarter of the increase in concentration caused by these emissions is still present in the atmosphere.

CO<sub>2</sub> stabilisation at 450, 650 or 1,000 ppm would require global anthropogenic CO<sub>2</sub> emissions to drop below 1990 levels, within a few decades, about a century, or about two centuries respectively, and continue to steadily decrease thereafter. Stabilisation requires that net anthropogenic CO<sub>2</sub> emissions ultimately decline to the level of persistent natural land and ocean sinks, which are expected to be small (<0.2 PgC/yr).

### **3.1 Introduction**

The concentration of CO<sub>2</sub> in the atmosphere has risen from close to 280 parts per million (ppm) in 1800, at first slowly and then progressively faster to a value of 367 ppm in 1999, echoing the increasing pace of global agricultural and industrial development. This is known from numerous, well-replicated measurements of the composition of air bubbles trapped in Antarctic ice. Atmospheric CO<sub>2</sub> concentrations have been measured directly with high precision since 1957; these measurements agree with ice-core measurements, and show a continuation of the increasing trend up to the present.

Several additional lines of evidence confirm that the recent and continuing increase of atmospheric CO<sub>2</sub> content is caused by anthropogenic CO<sub>2</sub> emissions – most importantly fossil fuel burning. First, atmospheric O<sub>2</sub> is declining at a rate comparable with fossil fuel emissions of CO<sub>2</sub> (combustion consumes O<sub>2</sub>). Second, the characteristic isotopic signatures of fossil fuel (its lack of <sup>14</sup>C, and depleted content of <sup>13</sup>C) leave their mark in the atmosphere. Third, the increase in observed CO<sub>2</sub> concentration has been faster in the northern hemisphere, where most fossil fuel burning occurs.

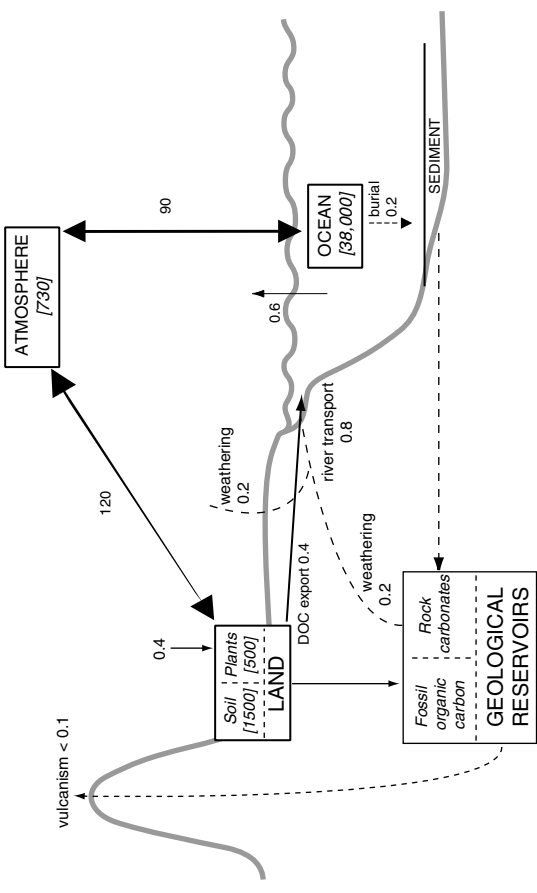
Atmospheric CO<sub>2</sub> is, however, increasing only at about half the rate of fossil fuel emissions; the rest of the CO<sub>2</sub> emitted either dissolves in sea water and mixes into the deep ocean, or is taken up by terrestrial ecosystems. Uptake by terrestrial ecosystems is due to an excess of primary production (photosynthesis) over respiration and other oxidative processes (decomposition or combustion of organic material). Terrestrial systems are also an

anthropogenic source of CO<sub>2</sub> when land-use changes (particularly deforestation) lead to loss of carbon from plants and soils. Nonetheless, the global balance in terrestrial systems is currently a net uptake of CO<sub>2</sub>.

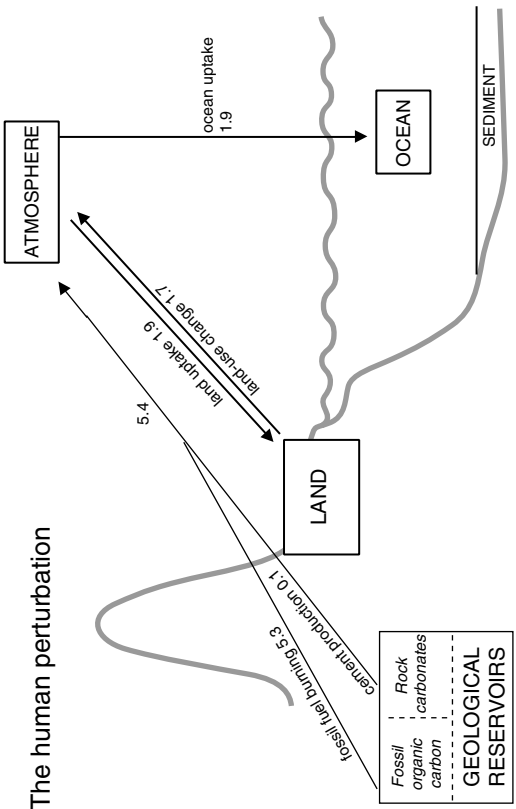
The part of fossil fuel CO<sub>2</sub> that is taken up by the ocean and the part that is taken up by the land can be calculated from the changes in atmospheric CO<sub>2</sub> and O<sub>2</sub> content because terrestrial processes of CO<sub>2</sub> exchange involve exchange of oxygen whereas dissolution in the ocean does not. Global carbon budgets based on CO<sub>2</sub> and O<sub>2</sub> measurements for the 1980s and 1990s are shown in Table 3.1. The human influence on the fluxes of carbon among the three “reservoirs” (atmosphere, ocean, and terrestrial biosphere) represent a small but significant perturbation of a huge global cycle (Figure 3.1).

This chapter summarises current knowledge of the global carbon cycle, with special reference to the fate of fossil fuel CO<sub>2</sub> and the factors that influence the uptake or release of CO<sub>2</sub> by the oceans and land. These factors include atmospheric CO<sub>2</sub> concentration itself, the naturally variable climate, likely climate changes caused by increasing CO<sub>2</sub> and other greenhouse gases, changes in ocean circulation and biology, fertilising effects of atmospheric CO<sub>2</sub> and nitrogen deposition, and direct human actions such as land conversion (from native vegetation to agriculture and vice versa), fire suppression and land management for carbon storage as provided for by the Kyoto Protocol (IPCC, 2000a). Any changes in the function of either the terrestrial biosphere or the ocean – whether intended or not – could potentially have significant effects, manifested within years to decades, on the fraction of fossil fuel CO<sub>2</sub> that stays in the atmosphere. This perspective has

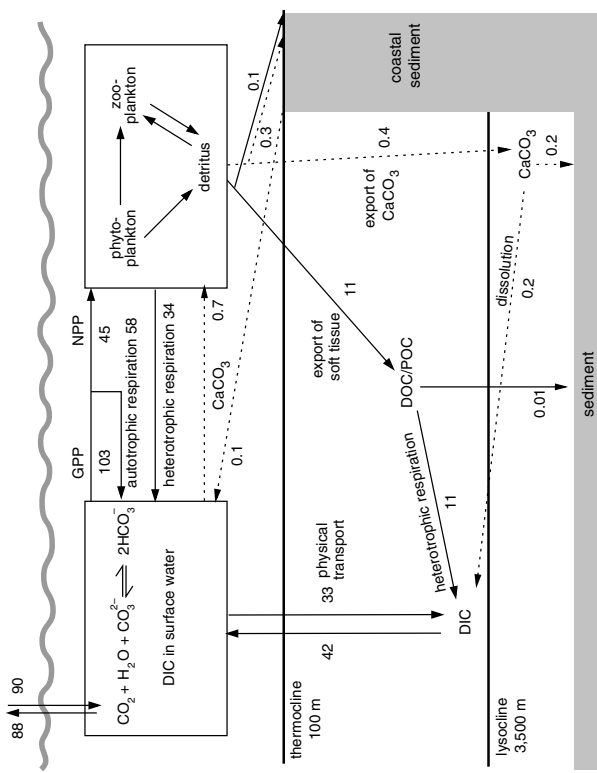
a) Main components of the natural carbon cycle



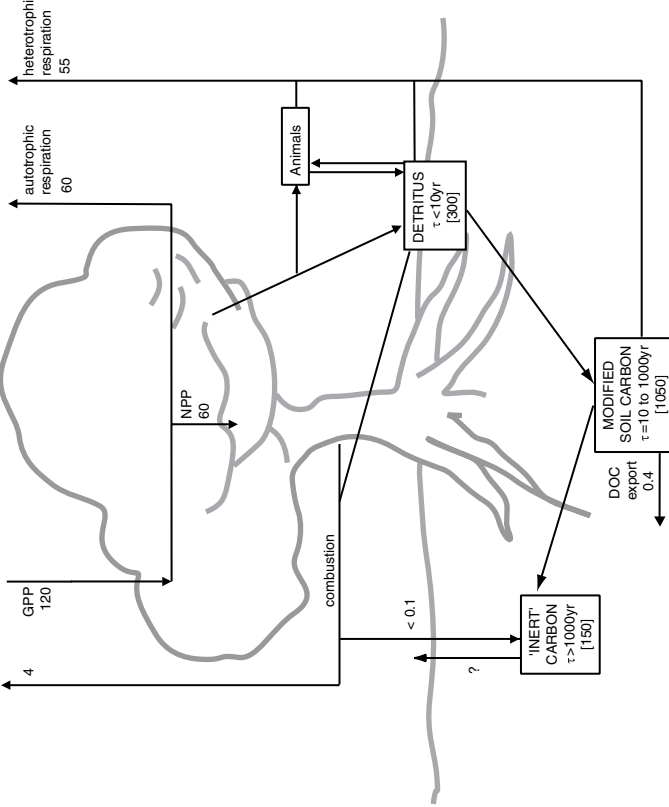
b) The human perturbation



c) Carbon cycling in the ocean



d) Carbon cycling on land



driven a great deal of research during the years since the IPCC WGI Second Assessment report (IPCC, 1996) (hereafter SAR) (Schimel *et al.*, 1996; Melillo *et al.*, 1996; Denman *et al.*, 1996). Some major areas where advances have been made since the SAR are as follows:

- Observational research (atmospheric, marine and terrestrial) aimed at a better quantification of carbon fluxes on local, regional and global scales. For example, improved precision and repeatability in atmospheric CO<sub>2</sub> and stable isotope measurements; the development of highly precise methods to measure changes in atmospheric O<sub>2</sub> concentrations; local terrestrial CO<sub>2</sub> flux measurements from towers, which are now being performed continuously in many terrestrial ecosystems; satellite observations of global land cover and change; and enhanced monitoring of geographical, seasonal and interannual variations of biogeochemical parameters in the sea, including measurements of the partial pressure of CO<sub>2</sub> (*p*CO<sub>2</sub>) in surface waters.
- Experimental manipulations, for example: laboratory and greenhouse experiments with raised and lowered CO<sub>2</sub> concentrations; field experiments on ecosystems using free-air carbon dioxide enrichment (FACE) and open-top chamber studies of raised CO<sub>2</sub> effects, studies of soil warming and nutrient enrichment effects; and *in situ* fertilisation experiments on marine ecosystems and associated *p*CO<sub>2</sub> measurements.

- Theory and modelling, especially applications of atmospheric transport models to link atmospheric observations to surface fluxes (inverse modelling); the development of process-based models of terrestrial and marine carbon cycling and programmes to compare and test these models against observations; and the use of such models to project climate feedbacks on the uptake of CO<sub>2</sub> by the oceans and land.

As a result of this research, there is now a more firmly based knowledge of several central features of the carbon cycle. For example:

- Time series of atmospheric CO<sub>2</sub>, O<sub>2</sub> and <sup>13</sup>CO<sub>2</sub> measurements have made it possible to observationally constrain the partitioning of CO<sub>2</sub> between terrestrial and oceanic uptake and to confirm earlier budgets, which were partly based on model results.
- *In situ* experiments have explored the nature and extent of CO<sub>2</sub> responses in a variety of terrestrial ecosystems (including forests), and have confirmed the existence of iron limitations on marine productivity.
- Process-based models of terrestrial and marine biogeochemical processes have been used to represent a complex array of feedbacks in the carbon cycle, allowing the net effects of these processes to be estimated for the recent past and for future scenarios.

**Figure 3.1:** The global carbon cycle: storages (PgC) and fluxes (PgC/yr) estimated for the 1980s. (a) *Main components of the natural cycle*. The thick arrows denote the most important fluxes from the point of view of the contemporary CO<sub>2</sub> balance of the atmosphere: gross primary production and respiration by the land biosphere, and physical air-sea exchange. These fluxes are approximately balanced each year, but imbalances can affect atmospheric CO<sub>2</sub> concentration significantly over years to centuries. The thin arrows denote additional natural fluxes (dashed lines for fluxes of carbon as CaCO<sub>3</sub>), which are important on longer time-scales. The flux of 0.4 PgC/yr from atmospheric CO<sub>2</sub> via plants to inert soil carbon is approximately balanced on a time-scale of several millenia by export of dissolved organic carbon (DOC) in rivers (Schlesinger, 1990). A further 0.4 PgC/yr flux of dissolved inorganic carbon (DIC) is derived from the weathering of CaCO<sub>3</sub>, which takes up CO<sub>2</sub> from the atmosphere in a 1:1 ratio. These fluxes of DOC and DIC together comprise the river transport of 0.8 PgC/yr. In the ocean, the DOC from rivers is respired and released to the atmosphere, while CaCO<sub>3</sub> production by marine organisms results in half of the DIC from rivers being returned to the atmosphere and half being buried in deep-sea sediments – which are the precursor of carbonate rocks. Also shown are processes with even longer time-scales: burial of organic matter as fossil organic carbon (including fossil fuels), and outgassing of CO<sub>2</sub> through tectonic processes (vulcanism). Emissions due to vulcanism are estimated as 0.02 to 0.05 PgC/yr (Williams *et al.*, 1992; Bickle, 1994). (b) *The human perturbation* (data from Table 3.1). Fossil fuel burning and land-use change are the main anthropogenic processes that release CO<sub>2</sub> to the atmosphere. Only a part of this CO<sub>2</sub> stays in the atmosphere; the rest is taken up by the land (plants and soil) or by the ocean. These uptake components represent imbalances in the large natural two-way fluxes between atmosphere and ocean and between atmosphere and land. (c) *Carbon cycling in the ocean*. CO<sub>2</sub> that dissolves in the ocean is found in three main forms (CO<sub>2</sub>, CO<sub>3</sub><sup>2-</sup>, HCO<sub>3</sub><sup>-</sup>, the sum of which is DIC). DIC is transported in the ocean by physical and biological processes. Gross primary production (GPP) is the total amount of organic carbon produced by photosynthesis (estimate from Bender *et al.*, 1994); net primary production (NPP) is what remains after autotrophic respiration, i.e., respiration by photosynthetic organisms (estimate from Falkowski *et al.*, 1998). Sinking of DOC and particulate organic matter (POC) of biological origin results in a downward flux known as export production (estimate from Schlitzer, 2000). This organic matter is transported and respired by non-photosynthetic organisms (heterotrophic respiration) and ultimately upwelled and returned to the atmosphere. Only a tiny fraction is buried in deep-sea sediments. Export of CaCO<sub>3</sub> to the deep ocean is a smaller flux than total export production (0.4 PgC/yr) but about half of this carbon is buried as CaCO<sub>3</sub> in sediments; the other half is dissolved at depth, and joins the pool of DIC (Milliman, 1993). Also shown are approximate fluxes for the shorter-term burial of organic carbon and CaCO<sub>3</sub> in coastal sediments and the re-dissolution of a part of the buried CaCO<sub>3</sub> from these sediments. (d) *Carbon cycling on land*. By contrast with the ocean, most carbon cycling through the land takes place locally within ecosystems. About half of GPP is respired by plants. The remainder (NPP) is approximately balanced by heterotrophic respiration with a smaller component of direct oxidation in fires (combustion). Through senescence of plant tissues, most of NPP joins the detritus pool; some detritus decomposes (i.e., is respired and returned to the atmosphere as CO<sub>2</sub>) quickly while some is converted to modified soil carbon, which decomposes more slowly. The small fraction of modified soil carbon that is further converted to compounds resistant to decomposition, and the small amount of black carbon produced in fires, constitute the “inert” carbon pool. It is likely that biological processes also consume much of the “inert” carbon as well but little is currently known about these processes. Estimates for soil carbon amounts are from Batjes (1996) and partitioning from Schimel *et al.* (1994) and Falloon *et al.* (1998). The estimate for the combustion flux is from Scholes and Andreae (2000). ‘τ’ denotes the turnover time for different components of soil organic matter.

**Box 3.1:** Measuring terrestrial carbon stocks and fluxes.

Estimating the carbon stocks in terrestrial ecosystems and accounting for changes in these stocks requires adequate information on land cover, carbon density in vegetation and soils, and the fate of carbon (burning, removals, decomposition). Accounting for changes in all carbon stocks in all areas would yield the net carbon exchange between terrestrial ecosystems and the atmosphere (NBP).

Global land cover maps show poor agreement due to different definitions of cover types and inconsistent sources of data (de Fries and Townshend, 1994). Land cover changes are difficult to document, uncertainties are large, and historical data are sparse. Satellite imagery is a valuable tool for estimating land cover, despite problems with cloud cover, changes at fine spatial scales, and interpretation (for example, difficulties in distinguishing primary and secondary forest). Aerial photography and ground measurements can be used to validate satellite-based observations.

The carbon density of vegetation and soils has been measured in numerous ecological field studies that have been aggregated to a global scale to assess carbon stocks and NPP (e.g., Atjay *et al.*, 1979; Olson *et al.*, 1983; Saugier and Roy, 2001; Table 3.2), although high spatial and temporal heterogeneity and methodological differences introduce large uncertainties. Land inventory studies tend to measure the carbon stocks in vegetation and soils over larger areas and/or longer time periods. For example, the United Nations Food and Agricultural Organisation (FAO) has been compiling forest inventories since 1946 providing detailed data on carbon stocks, often based on commercial wood production data. Inventory studies include managed forests with mixed age stands, thus average carbon stock values are often lower than those based on ecological site studies, which have generally been carried out in relatively undisturbed, mature ecosystems. Fluxes of carbon can be estimated from changes in inventoried carbon stocks (e.g., UN-ECE/FAO, 2000), or from combining data on land-use change with methods to calculate changes in carbon stock (e.g., Houghton, 1999). The greatest uncertainty in both methods is in estimating the fate of the carbon: the fraction which is burned, rates of decomposition, the effect of burning and harvesting on soil carbon, and subsequent land management.

Ecosystem-atmosphere CO<sub>2</sub> exchange on short time-scales can be measured using micrometeorological techniques such as eddy covariance, which relies on rapidly responding sensors mounted on towers to resolve the net flux of CO<sub>2</sub> between a patch of land and the atmosphere (Baldocchi *et al.*, 1988). The annual integral of the measured CO<sub>2</sub> exchange is approximately equivalent to NEP (Wofsy *et al.*, 1993; Goulden *et al.*, 1996; Aubinet *et al.*, 2000). This innovation has led to the establishment of a rapidly expanding network of long-term monitoring sites (FLUXNET) with many sites now operating for several years, improving the understanding of the physiological and ecological processes that control NEP (e.g., Valentini *et al.*, 2000). The distribution of sites is currently biased toward regrowing forests in the Northern Hemisphere, and there are still technical problems and uncertainties, although these are being tackled. Current flux measurement techniques typically integrate processes at a scale less than 1 km<sup>2</sup>.

**Table 3.1:** Global CO<sub>2</sub> budgets (in PgC/yr) based on intra-decadal trends in atmospheric CO<sub>2</sub> and O<sub>2</sub>. Positive values are fluxes to the atmosphere; negative values represent uptake from the atmosphere. The fossil fuel emissions term for the 1980s (Marland *et al.*, 2000) has been slightly revised downward since the SAR. Error bars denote uncertainty ( $\pm 1\sigma$ ), not interannual variability, which is substantially greater.

	1980s	1990s
Atmospheric increase	3.3 ± 0.1	3.2 ± 0.1
Emissions (fossil fuel, cement)	5.4 ± 0.3	6.3 ± 0.4
Ocean-atmosphere flux	-1.9 ± 0.6	-1.7 ± 0.5
Land-atmosphere flux*	-0.2 ± 0.7	-1.4 ± 0.7
<i>*partitioned as follows</i>		
Land-use change	1.7 (0.6 to 2.5)	NA
Residual terrestrial sink	-1.9 (-3.8 to 0.3)	NA

\* The land-atmosphere flux represents the balance of a positive term due to land-use change and a residual terrestrial sink. The two terms cannot be separated on the basis of current atmospheric measurements. Using independent analyses to estimate the land-use change component for the 1980s based on Houghton (1999), Houghton and Hackler (1999), Houghton *et al.* (2000), and the CCMLP (McGuire *et al.*, 2001) the residual terrestrial sink can be inferred for the 1980s. Comparable global data on land-use changes through the 1990s are not yet available.

### 3.2 Terrestrial and Ocean Biogeochemistry: Update on Processes

#### 3.2.1 Overview of the Carbon Cycle

The first panel of Figure 3.1 shows the major components of the carbon cycle, estimates of the current storage in the active compartments, and estimates of the gross fluxes between compartments. The second panel shows best estimates of the additional flux (release to the atmosphere – positive; uptake – negative) associated with the human perturbation of the carbon cycle during the 1980s. Note that the gross amounts of carbon annually exchanged between the ocean and atmosphere, and between the land and atmosphere, represent a sizeable fraction of the atmospheric CO<sub>2</sub> content – and are many times larger than the total anthropogenic CO<sub>2</sub> input. In consequence, an imbalance in these exchanges could easily lead to an anomaly of comparable magnitude to the direct anthropogenic perturbation. This implies that it is important to consider how these fluxes may be changing in response to human activities.

To understand how the changing global environment may alter the carbon cycle, it is necessary to further analyse the fluxes and examine the physicochemical and biological processes that determine them. The remaining two panels of Figure 3.1 indicate the main constituent fluxes in the terrestrial and marine systems, with current estimates of their magnitude. The following sections explain the controls on these fluxes, with special reference to processes by which anthropogenic changes may influence the overall carbon balance of the land and oceans on time-scales from years to centuries.

#### 3.2.2 Terrestrial Carbon Processes

##### 3.2.2.1 Background

Higher plants acquire CO<sub>2</sub> by diffusion through tiny pores (stomata) into leaves and thus to the sites of photosynthesis. The total amount of CO<sub>2</sub> that dissolves in leaf water amounts to about 270 PgC/yr, i.e., more than one-third of all the CO<sub>2</sub> in the atmosphere (Farquhar *et al.*, 1993; Ciais *et al.*, 1997). This quantity is measurable because this CO<sub>2</sub> has time to exchange oxygen atoms with the leaf water and is imprinted with the corresponding <sup>18</sup>O “signature” (Francey and Tans, 1987; Farquhar *et al.*, 1993). Most of this CO<sub>2</sub> diffuses out again without participating in photosynthesis. The amount that is “fixed” from the atmosphere, i.e., converted from CO<sub>2</sub> to carbohydrate during photosynthesis, is known as gross primary production (GPP). Terrestrial GPP has been estimated as about 120 PgC/yr based on <sup>18</sup>O measurements of atmospheric CO<sub>2</sub> (Ciais *et al.*, 1997). This is also the approximate value necessary to support observed plant growth, assuming that about half of GPP is incorporated into new plant tissues such as leaves, roots and wood, and the other half is converted back to atmospheric CO<sub>2</sub> by autotrophic respiration (respiration by plant tissues) (Lloyd and Farquhar, 1996; Waring *et al.*, 1998).

Annual plant growth is the difference between photosynthesis and autotrophic respiration, and is referred to as net primary production (NPP). NPP has been measured in all major

ecosystem types by sequential harvesting or by measuring plant biomass (Hall *et al.*, 1993). Global terrestrial NPP has been estimated at about 60 PgC/yr through integration of field measurements (Table 3.2) (Atjay *et al.*, 1979; Saugier and Roy, 2001). Estimates from remote sensing and atmospheric CO<sub>2</sub> data (Ruimy *et al.*, 1994; Knorr and Heimann, 1995) concur with this value, although there are large uncertainties in all methods. Eventually, virtually all of the carbon fixed in NPP is returned to the atmospheric CO<sub>2</sub> pool through two processes: heterotrophic respiration (Rh) by decomposers (bacteria and fungi feeding on dead tissue and exudates) and herbivores; and combustion in natural or human-set fires (Figure 3.1d).

Most dead biomass enters the detritus and soil organic matter pools where it is respired at a rate that depends on the chemical composition of the dead tissues and on environmental conditions (for example, low temperatures, dry conditions and flooding slow down decomposition). Conceptually, several soil carbon pools are distinguished. Detritus and microbial biomass have a short turnover time (<10 yr). Modified soil organic carbon has decadal to centennial turnover time. Inert (stable or recalcitrant) soil organic carbon is composed of molecules more or less resistant to further decomposition. A very small fraction of soil organic matter, and a small fraction of burnt biomass, are converted into inert forms (Schlesinger, 1990; Kuhlbusch *et al.*, 1996). Natural processes and management regimes may reduce or increase the amount of carbon stored in pools with turnover times on the order of tens to hundreds of years (living wood, wood products and modified soil organic matter) and thus influence the time evolution of atmospheric CO<sub>2</sub> over the century.

The difference between NPP and Rh determines how much carbon is lost or gained by the ecosystem in the absence of disturbances that remove carbon from the ecosystem (such as harvest or fire). This carbon balance, or net ecosystem production (NEP), can be estimated from changes in carbon stocks, or by measuring the fluxes of CO<sub>2</sub> between patches of land and the atmosphere (see Box 3.1). Annual NEP flux measurements are in the range 0.7 to 5.9 MgC/ha/yr for tropical forests and 0.8 to 7.0 MgC/ha/yr for temperate forests; boreal forests can reach up to 2.5 MgC/ha/yr although they have been shown to be carbon-neutral or to release carbon in warm and/or cloudy years (Valentini *et al.*, 2000). Integration of these and other results leads to an estimated global NEP of about 10 PgC/yr, although this is likely to be an overestimate because of the current biased distribution of flux measuring sites (Bolin *et al.*, 2000).

When other losses of carbon are accounted for, including fires, harvesting/removals (eventually combusted or decomposed), erosion and export of dissolved or suspended organic carbon (DOC) by rivers to the oceans (Schlesinger and Melack, 1981; Sarmiento and Sundquist, 1992), what remains is the net biome production (NBP), i.e., the carbon accumulated by the terrestrial biosphere (Schulze and Heimann, 1998). This is what the atmosphere ultimately “sees” as the net land uptake on a global scale over periods of a year or more. NBP is estimated in this chapter to have averaged  $-0.2 \pm 0.7$  PgC/yr during the 1980s and  $-1.4 \pm 0.7$  PgC/yr during the 1990s, based on atmospheric measurements of CO<sub>2</sub> and O<sub>2</sub> (Section 3.5.1 and Table 3.1).

**Box 3.2:** Maximum impacts of reforestation and deforestation on atmospheric CO<sub>2</sub>.

Rough upper bounds for the impact of reforestation on atmospheric CO<sub>2</sub> concentration over a century time-scale can be calculated as follows. Cumulative carbon losses to the atmosphere due to land-use change during the past 1 to 2 centuries are estimated as 180 to 200 PgC (de Fries *et al.*, 1999) and cumulative fossil fuel emissions to year 2000 as 280 PgC (Marland *et al.*, 2000), giving cumulative anthropogenic emissions of 480 to 500 PgC. Atmospheric CO<sub>2</sub> content has increased by 90 ppm (190 PgC). Approximately 40% of anthropogenic CO<sub>2</sub> emissions has thus remained in the atmosphere; the rest has been taken up by the land and oceans in roughly equal proportions (see main text). Conversely, if land-use change were completely reversed over the 21st century, a CO<sub>2</sub> reduction of  $0.40 \times 200 = 80$  PgC (about 40 ppm) might be expected. This calculation assumes that future ecosystems will not store more carbon than pre-industrial ecosystems, and that ocean uptake will be less because of lower CO<sub>2</sub> concentration in the atmosphere (see Section 3.2.3.1).

A higher bound can be obtained by assuming that the carbon taken up by the land during the past 1 to 2 centuries, i.e. about half of the carbon taken up by the land and ocean combined, will be retained there. This calculation yields a CO<sub>2</sub> reduction of  $0.70 \times 200 = 140$  PgC (about 70 ppm). These calculations are not greatly influenced by the choice of reference period. Both calculations require the extreme assumption that a large proportion of today's agricultural land is returned to forest.

The maximum impact of total deforestation can be calculated in a similar way. Depending on different assumptions about vegetation and soil carbon density in different ecosystem types (Table 3.2) and the proportion of soil carbon lost during deforestation (20 to 50%; IPCC, 1997), complete conversion of forests to climatically equivalent grasslands would add 400 to 800 PgC to the atmosphere. Thus, global deforestation could theoretically add two to four times more CO<sub>2</sub> to the atmosphere than could be subtracted by reforestation of cleared areas.

**Table 3.2:** Estimates of terrestrial carbon stocks and NPP (global aggregated values by biome).

Biome	Area ( $10^9$ ha)		Global Carbon Stocks (PgC) <sup>f</sup>						Carbon density (MgC/ha)			NPP (PgC/yr)		
	WBGU <sup>a</sup>	MRS <sup>b</sup>	WBGU <sup>a</sup>			MRS <sup>b</sup>	IGBP <sup>c</sup>		WBGU <sup>a</sup>	MRS <sup>b</sup>	IGBP <sup>c</sup>	Atjay <sup>a</sup>	MRS <sup>b</sup>	
			Plants	Soil	Total									
Tropical forests	1.76	1.75	212	216	428	340	213	553	120	123	194	122	13.7	21.9
Temperate forests	1.04	1.04	59	100	159	139 <sup>e</sup>	153	292	57	96	134	147	6.5	8.1
Boreal forests	1.37	1.37	88 <sup>d</sup>	471	559	57	338	395	64	344	42	247	3.2	2.6
Tropical savannas & grasslands	2.25	2.76	66	264	330	79	247	326	29	117	29	90	17.7	14.9
Temperate grasslands & shrublands	1.25	1.78	9	295	304	23	176	199	7	236	13	99	5.3	7.0
Deserts and semi deserts	4.55 <sup>h</sup>	2.77	8	191	199	10	159	169	2	42	4	57	1.4	3.5
Tundra	0.95	0.56	6	121	127	2	115	117	6	127	4	206	1.0	0.5
Croplands	1.60	1.35	3	128	131	4	165	169	2	80	3	122	6.8	4.1
Wetlands <sup>g</sup>	0.35	–	15	225	240	–	–	–	43	643	–	–	4.3	–
Total	15.12	14.93 <sup>h</sup>	466	2011	2477	654	1567	2221					59.9	62.6

<sup>a</sup> WBGU (1988); forest data from Dixon *et al.* (1994); other data from Atjay *et al.* (1979).

<sup>b</sup> MRS: Mooney, Roy and Saugier (MRS) (2001). Temperate grassland and Mediterranean shrubland categories combined.

<sup>c</sup> IGBP-DIS (International Geosphere-Biosphere Programme – Data Information Service) soil carbon layer (Carter and Scholes, 2000) overlaid with De Fries *et al.* (1999) current vegetation map to give average ecosystem soil carbon.

<sup>d</sup> WBGU boreal forest vegetation estimate is likely to be too high, due to high Russian forest density estimates including standing dead biomass.

<sup>e</sup> MRS temperate forest estimate is likely to be too high, being based on mature stand density.

<sup>f</sup> Soil carbon values are for the top 1 m, although stores are also high below this depth in peatlands and tropical forests.

<sup>g</sup> Variations in classification of ecosystems can lead to inconsistencies. In particular, wetlands are not recognised in the MRS classification.

<sup>h</sup> Total land area of  $14.93 \times 10^9$  ha in MRS includes  $1.55 \times 10^9$  ha ice cover not listed in this table. In WBGU, ice is included in deserts and semi-deserts category.

By definition, for an ecosystem in steady state, Rh and other carbon losses would just balance NPP, and NBP would be zero. In reality, human activities, natural disturbances and climate variability alter NPP and Rh, causing transient changes in the terrestrial carbon pool and thus non-zero NBP. If the rate of carbon input (NPP) changes, the rate of carbon output (Rh) also changes, in proportion to the altered carbon content; but there is a time lag between changes in NPP and changes in the slower responding carbon pools. For a *step* increase in NPP, NBP is expected to increase at first but to relax towards zero over a period of years to decades as the respiring pool “catches up”. The globally averaged lag required for Rh to catch up with a change in NPP has been estimated to be of the order of 10 to 30 years (Raich and Schlesinger, 1992). A *continuous* increase in NPP is expected to produce a sustained positive NBP, so long as NPP is still increasing, so that the increased terrestrial carbon has not been processed through the respiring carbon pools (Taylor and Lloyd, 1992; Friedlingstein *et al.*, 1995a; Thompson *et al.*, 1996; Kicklighter *et al.*, 1999), and provided that the increase is not outweighed by compensating increases in mortality or disturbance.

The terrestrial system is currently acting as a global sink for carbon (Table 3.1) despite large releases of carbon due to deforestation in some regions. Likely mechanisms for the sink are known, but their relative contribution is uncertain. Natural climate variability and disturbance regimes (including fire and herbivory) affect NBP through their impacts on NPP, allocation to long- versus short-lived tissues, chemical and physical properties of litter, stocks of living biomass, stocks of detritus and soil carbon, environmental controls on decomposition and rates of biomass removal. Human impacts occur through changes in land use and land management, and through indirect mechanisms including climate change, and fertilisation due to elevated CO<sub>2</sub> and deposition of nutrients (most importantly, reactive nitrogen). These mechanisms are discussed individually in the following sections.

### 3.2.2.2 Effects of changes in land use and land management

Changes in land use and management affect the amount of carbon in plant biomass and soils. Historical cumulative carbon losses due to changes in land use have been estimated to be 180 to 200 PgC by comparing maps of “natural” vegetation in the absence of human disturbance (derived from ground-based information (Matthews, 1983) or from modelled potential vegetation based on climate (Leemans, 1990)) to a map of current vegetation derived from 1987 satellite data (de Fries *et al.*, 1999). Houghton (1999, 2000) estimated emissions of 121 PgC (approximately 60% in tropical areas and 40% in temperate areas) for the period 1850 to 1990 from statistics on land-use change, and a simple model tracking rates of decomposition from different pools and rates of regrowth on abandoned or reforested land. There was substantial deforestation in temperate areas prior to 1850, and this may be partially reflected in the difference between these two analyses. The estimated land-use emissions during 1850 to 1990 of 121 PgC (Houghton, 1999, 2000) can be compared to estimated net terrestrial flux of 39 PgC to the atmosphere over the same period inferred from an atmospheric

increase of 144 PgC (Etheridge *et al.*, 1996; Keeling and Whorf, 2000), a release of 212 PgC due to fossil fuel burning (Marland *et al.*, 2000), and a modelled ocean-atmosphere flux of about -107 PgC (Gruber, 1998; Sabine *et al.*, 1999; Feely *et al.*, 1999a). The difference between the net terrestrial flux and estimated land-use change emissions implies a residual land-atmosphere flux of -82 PgC (i.e., a terrestrial sink) over the same period. Box 3.2 indicates the theoretical upper bounds for additional carbon storage due to land-use change, similar bounds for carbon loss by continuing deforestation, and the implications of these calculations for atmospheric CO<sub>2</sub>.

Land use responds to social and economic pressures to provide food, fuel and wood products, for subsistence use or for export. Land clearing can lead to soil degradation, erosion and leaching of nutrients, and may therefore reduce the subsequent ability of the ecosystem to act as a carbon sink (Taylor and Lloyd, 1992). Ecosystem conservation and management practices can restore, maintain and enlarge carbon stocks (IPCC, 2000a). Fire is important in the carbon budget of some ecosystems (e.g., boreal forests, grasslands, tropical savannas and woodlands) and is affected directly by management and indirectly by land-use change (Apps *et al.*, 1993). Fire is a major short-term source of carbon, but adds to a small longer-term sink (<0.1 PgC/yr) through production of slowly decomposing and inert black carbon.

### Forests

Deforestation has been responsible for almost 90% of the estimated emissions due to land-use change since 1850, with a 20% decrease of the global forest area (Houghton, 1999). Deforestation appears to be slowing slightly in tropical countries (FAO, 1997; Houghton, 2000), and some deforested areas in Europe and North America have been reforested in recent decades (FAO, 1997). Managed or regenerated forests generally store less carbon than natural forests, even at maturity. New trees take up carbon rapidly, but this slows down towards maturity when forests can be slight sources or sinks (Buchmann and Schulze, 1999). To use land continuously in order to take up carbon, the wood must be harvested and turned into long-lived products and trees must be re-planted. The trees may also be used for biomass energy to avoid future fossil fuel emissions (Hall *et al.*, 2000). Analysis of scenarios for future development show that expanded use of biomass energy could reduce the rate of atmospheric CO<sub>2</sub> increase (IPCC 1996b; Leemans *et al.*, 1996; Edmonds *et al.*, 1996; Ishitani *et al.*, 1996; IPCC, 2000a). IPCC (1996b) estimated that slowing deforestation and promoting natural forest regeneration and afforestation could increase carbon stocks by about 60 to 87 PgC over the period 1995 to 2050, mostly in the tropics (Brown *et al.*, 1996).

### Savannas and grasslands – fire and grazing

Grasslands and mixed tree-grass systems are vulnerable to subtle environmental and management changes that can lead to shifts in vegetation state (Scholes and Archer, 1997; House and Hall, 2001). Livestock grazing on these lands is the land use with the largest global areal extent (FAO, 1993a). Extensive clearing of trees (for agricultural expansion) has occurred in some areas. In

other areas, fire suppression, eradication of indigenous browsers and the introduction of intensive grazing and exotic trees and shrubs have caused an increase in woody plant density known as woody encroachment or tree thickening (Archer *et al.*, 2001). This process has been estimated to result in a CO<sub>2</sub> sink of up to 0.17 PgC/yr in the USA during the 1980s (Houghton *et al.*, 1999) and at least 0.03 PgC/yr in Australia (Burrows, 1998). Grassland ecosystems have high root production and store most of their carbon in soils where turnover is relatively slow, allowing the possibility of enhancement through management (e.g., Fisher *et al.*, 1994).

#### *Peatlands/wetlands*

Peatlands/wetlands are large reserves of carbon, because anaerobic soil conditions and (in northern peatlands) low temperatures reduce decomposition and promote accumulation of organic matter. Total carbon stored in northern peatlands has been estimated as about 455 PgC (Gorham, 1991) with a current uptake rate in extant northern peatlands of 0.07 PgC/yr (Clymo *et al.*, 1998). Anaerobic decomposition releases methane (CH<sub>4</sub>) which has a global warming potential (GWP) about 23 times that of CO<sub>2</sub> (Chapter 6). The balance between CH<sub>4</sub> release and CO<sub>2</sub> uptake and release is highly variable and poorly understood. Draining peatlands for agriculture increases total carbon released by decomposition, although less is in the form of CH<sub>4</sub>. Forests grown on drained peatlands may be sources or sinks of CO<sub>2</sub> depending on the balance of decomposition and tree growth (Minkkinen and Laine, 1998).

#### *Agricultural land*

Conversion of natural vegetation to agriculture is a major source of CO<sub>2</sub>, not only due to losses of plant biomass but also, increased decomposition of soil organic matter caused by disturbance and energy costs of various agricultural practices (e.g., fertilisation and irrigation; Schlesinger, 2000). Conversely, the use of high-yielding plant varieties, fertilisers, irrigation, residue management and reduced tillage can reduce losses and enhance uptake within managed areas (Cole *et al.*, 1996; Blume *et al.*, 1998). These processes have led to an estimated increase of soil carbon in agricultural soils in the USA of 0.14 PgC/yr during the 1980s (Houghton *et al.*, 1999). IPCC (1996b) estimated that appropriate management practices could increase carbon sinks by 0.4 to 0.9 PgC/yr, or a cumulative carbon storage of 24 to 43 PgC over 50 years; energy efficiency improvements and production of energy from dedicated crops and residues would result in a further mitigation potential of 0.3 to 1.4 PgC/yr, or a cumulative carbon storage of 16 to 68 PgC over 50 years (Cole *et al.*, 1996).

#### *Scenarios*

The IPCC Special Report on Land Use, Land-Use Change and Forestry (IPCC, 2000a) (hereafter SRLULUCF) derived scenarios of land-use emissions for the period 2008 to 2012. It was estimated that a deforestation flux of 1.79 PgC/yr is likely to be offset by reforestation and afforestation flux of -0.20 to -0.58 PgC/yr, yielding a net release of 1.59 to 1.20 PgC/yr (Schlamadinger *et al.*, 2000). The potential for net carbon storage from several "additional activities" such as improved land

management and other land-use changes was estimated to amount to a global land-atmosphere flux in the region of -1.3 PgC/yr in 2010 and -2.5 PgC/yr in 2040, not including wood products and bioenergy (Sampson *et al.*, 2000).

#### *3.2.2.3 Effects of climate*

Solar radiation, temperature and available water affect photosynthesis, plant respiration and decomposition, thus climate change can lead to changes in NEP. A substantial part of the interannual variability in the rate of increase of CO<sub>2</sub> is likely to reflect terrestrial biosphere responses to climate variability (Section 3.5.3). Warming may increase NPP in temperate and arctic ecosystems where it can increase the length of the seasonal and daily growing cycles, but it may decrease NPP in water-stressed ecosystems as it increases water loss. Respiratory processes are sensitive to temperature; soil and root respiration have generally been shown to increase with warming in the short term (Lloyd and Taylor, 1994; Boone *et al.*, 1998) although evidence on longer-term impacts is conflicting (Trumbore, 2000; Giardina and Ryan, 2000; Jarvis and Linder, 2000). Changes in rainfall pattern affect plant water availability and the length of the growing season, particularly in arid and semi-arid regions. Cloud cover can be beneficial to NPP in dry areas with high solar radiation, but detrimental in areas with low solar radiation. Changing climate can also affect the distribution of plants and the incidence of disturbances such as fire (which could increase or decrease depending on warming and precipitation patterns, possibly resulting under some circumstances in rapid losses of carbon), wind, and insect and pathogen attacks, leading to changes in NBP. The global balance of these positive and negative effects of climate on NBP depends strongly on regional aspects of climate change.

The climatic sensitivity of high northern latitude ecosystems (tundra and taiga) has received particular attention as a consequence of their expanse, high carbon density, and observations of disproportionate warming in these regions (Chapman and Walsh, 1993; Overpeck *et al.*, 1997). High-latitude ecosystems contain about 25% of the total world soil carbon pool in the permafrost and the seasonally-thawed soil layer. This carbon storage may be affected by changes in temperature and water table depth. High latitude ecosystems have low NPP, in part due to short growing seasons, and slow nutrient cycling because of low rates of decomposition in waterlogged and cold soils. Remotely sensed data (Myneni *et al.*, 1997) and phenological observations (Menzel and Fabian, 1999) independently indicate a recent trend to longer growing seasons in the boreal zone and temperate Europe. Such a trend might be expected to have increased annual NPP. A shift towards earlier and stronger spring depletion of atmospheric CO<sub>2</sub> has also been observed at northern stations, consistent with earlier onset of growth at mid- to high northern latitudes (Manning, 1992; Keeling *et al.*, 1996a; Randerson, 1999). However, recent flux measurements at individual high-latitude sites have generally failed to find appreciable NEP (Oechel *et al.*, 1993; Goulden *et al.*, 1998; Schulze *et al.*, 1999; Oechel *et al.*, 2000). These studies suggest that, at least in the short term, any direct effect of warming on NPP may be more than offset by an increased respiration of soil

carbon caused by the effects of increased depth of soil thaw. Increased decomposition, may, however also increase nutrient mineralisation and thereby indirectly stimulate NPP (Melillo *et al.*, 1993; Jarvis and Linder, 2000; Oechel *et al.*, 2000).

Large areas of the tropics are arid and semi-arid, and plant production is limited by water availability. There is evidence that even evergreen tropical moist forests show reduced GPP during the dry season (Malhi *et al.*, 1998) and may become a carbon source under the hot, dry conditions of typical El Niño years. With a warmer ocean surface, and consequently generally increased precipitation, the global trend in the tropics might be expected to be towards increased NPP, but changing precipitation patterns could lead to drought, reducing NPP and increasing fire frequency in the affected regions.

#### 3.2.2.4 Effects of increasing atmospheric CO<sub>2</sub>

CO<sub>2</sub> and O<sub>2</sub> compete for the reaction sites on the photosynthetic carbon-fixing enzyme, Rubisco. Increasing the concentration of CO<sub>2</sub> in the atmosphere has two effects on the Rubisco reactions: increasing the rate of reaction with CO<sub>2</sub> (carboxylation) and decreasing the rate of oxygenation. Both effects increase the rate of photosynthesis, since oxygenation is followed by photorespiration which releases CO<sub>2</sub> (Farquhar *et al.*, 1980). With increased photosynthesis, plants can develop faster, attaining the same final size in less time, or can increase their final mass. In the first case, the overall rate of litter production increases and so the soil carbon stock increases; in the second case, both the below-ground and above-ground carbon stocks increase. Both types of growth response to elevated CO<sub>2</sub> have been observed (Masle, 2000).

The strength of the response of photosynthesis to an increase in CO<sub>2</sub> concentration depends on the photosynthetic pathway used by the plant. Plants with a photosynthetic pathway known as C<sub>3</sub> (all trees, nearly all plants of cold climates, and most agricultural crops including wheat and rice) generally show an increased rate of photosynthesis in response to increases in CO<sub>2</sub> concentration above the present level (Koch and Mooney, 1996; Curtis, 1996; Mooney *et al.*, 1999). Plants with the C<sub>4</sub> photosynthetic pathway (tropical and many temperate grasses, some desert shrubs, and some crops including maize and sugar cane) already have a mechanism to concentrate CO<sub>2</sub> and therefore show either no direct photosynthetic response, or less response than C<sub>3</sub> plants (Wand *et al.*, 1999). Increased CO<sub>2</sub> has also been reported to reduce plant respiration under some conditions (Drake *et al.*, 1999), although this effect has been questioned.

Increased CO<sub>2</sub> concentration allows the partial closure of stomata, restricting water loss during transpiration and producing an increase in the ratio of carbon gain to water loss ("water-use efficiency", WUE) (Field *et al.*, 1995a; Drake *et al.*, 1997; Farquhar, 1997; Körner, 2000). This effect can lengthen the duration of the growing season in seasonally dry ecosystems and can increase NPP in both C<sub>3</sub> and C<sub>4</sub> plants.

Nitrogen-use efficiency also generally improves as carbon input increases, because plants can vary the ratio between carbon and nitrogen in tissues and require lower concentrations of photosynthetic enzymes in order to carry out photosynthesis

at a given rate; for this reason, low nitrogen availability does not consistently limit plant responses to increased atmospheric CO<sub>2</sub> (McGuire *et al.*, 1995; Lloyd and Farquhar, 1996; Curtis and Wang, 1998; Norby *et al.*, 1999; Körner, 2000). Increased CO<sub>2</sub> concentration may also stimulate nitrogen fixation (Hungate *et al.*, 1999; Vitousek and Field, 1999). Changes in tissue nutrient concentration may affect herbivory and decomposition, although long-term decomposition studies have shown that the effect of elevated CO<sub>2</sub> in this respect is likely to be small (Norby and Cortufo, 1998) because changes in the C:N ratio of leaves are not consistently reflected in the C:N ratio of leaf litter due to nitrogen retranslocation (Norby *et al.*, 1999).

The process of CO<sub>2</sub> "fertilisation" thus involves direct effects on carbon assimilation and indirect effects such as those via water saving and interactions between the carbon and nitrogen cycles. Increasing CO<sub>2</sub> can therefore lead to structural and physiological changes in plants (Pritchard *et al.*, 1999) and can further affect plant competition and distribution patterns due to responses of different species. Field studies show that the relative stimulation of NPP tends to be greater in low-productivity years, suggesting that improvements in water- and nutrient-use efficiency can be more important than direct NPP stimulation (Luo *et al.*, 1999).

Although NPP stimulation is not automatically reflected in increased plant biomass, additional carbon is expected to enter the soil, via accelerated ontogeny, which reduces lifespan and results in more rapid shoot death, or by enhanced root turnover or exudation (Koch and Mooney, 1996; Allen *et al.*, 2000). Because the soil microbial community is generally limited by the availability of organic substrates, enhanced addition of labile carbon to the soil tends to increase heterotrophic respiration unless inhibited by other factors such as low temperature (Hungate *et al.*, 1997; Schlesinger and Andrews, 2000). Field studies have indicated increases in soil organic matter, and increases in soil respiration of about 30%, under elevated CO<sub>2</sub> (Schlesinger and Andrews, 2000). The potential role of the soil as a carbon sink under elevated CO<sub>2</sub> is crucial to understanding NEP and long-term carbon dynamics, but remains insufficiently well understood (Trumbore, 2000).

C<sub>3</sub> crops show an average increase in NPP of around 33% for a doubling of atmospheric CO<sub>2</sub> (Koch and Mooney, 1996). Grassland and crop studies combined show an average biomass increase of 14%, with a wide range of responses among individual studies (Mooney *et al.*, 1999). In cold climates, low temperatures restrict the photosynthetic response to elevated CO<sub>2</sub>. In tropical grasslands and savannas, C<sub>4</sub> grasses are dominant, so it has been assumed that trees and C<sub>3</sub> grasses would gain a competitive advantage at high CO<sub>2</sub> (Gifford, 1992; Collatz *et al.*, 1998). This is supported by carbon isotope evidence from the last glacial maximum, which suggests that low CO<sub>2</sub> favours C<sub>4</sub> plants (Street-Perrott *et al.*, 1998). However, field experiments suggest a more complex picture with C<sub>4</sub> plants sometimes doing better than C<sub>3</sub> under elevated CO<sub>2</sub> due to improved WUE at the ecosystem level (Owensby *et al.*, 1993; Polley *et al.*, 1996). Highly productive forest ecosystems have the greatest potential for *absolute* increases in productivity due to CO<sub>2</sub> effects. Long-term field studies on young trees have

typically shown a stimulation of photosynthesis of about 60% for a doubling of CO<sub>2</sub> (Saxe *et al.*, 1998; Norby *et al.*, 1999). A FACE experiment in a fast growing young pine forest showed an increase of 25% in NPP for an increase in atmospheric CO<sub>2</sub> to 560 ppm (DeLucia *et al.*, 1999). Some of this additional NPP is allocated to root metabolism and associated microbes; soil CO<sub>2</sub> efflux increases, returning a part (but not all) of the extra NPP to the atmosphere (Allen *et al.*, 2000). The response of mature forests to increases in atmospheric CO<sub>2</sub> concentration has not been shown experimentally; it may be different from that of young forests for various reasons, including changes in leaf C:N ratios and stomatal responses to water vapour deficits as trees mature (Curtis and Wang, 1998; Norby *et al.*, 1999).

At high CO<sub>2</sub> concentrations there can be no further increase in photosynthesis with increasing CO<sub>2</sub> (Farquhar *et al.*, 1980), except through further stomatal closure, which may produce continued increases in WUE in water-limited environments. The shape of the response curve of global NPP at higher CO<sub>2</sub> concentrations than present is uncertain because the response at the level of gas exchange is modified by incompletely understood plant- and ecosystem-level processes (Luo *et al.*, 1999). Based on photosynthetic physiology, it is likely that the additional carbon that could be taken up globally by enhanced photosynthesis as a direct consequence of rising atmospheric CO<sub>2</sub> concentration is small at atmospheric concentrations above 800 to 1,000 ppm. Experimental studies indicate that some ecosystems show greatly reduced CO<sub>2</sub> fertilisation at lower concentrations than this (Körner, 2000).

### 3.2.2.5 Effects of anthropogenic nitrogen deposition

Nitrogen availability is an important constraint on NPP (Vitousek *et al.*, 1997), although phosphorus and calcium may be more important limiting nutrients in many tropical and subtropical regions (Matson, 1999). Reactive nitrogen is released into the atmosphere in the form of nitrogen oxides (NO<sub>x</sub>) during fossil fuel and biomass combustion and ammonia emitted by industrial regions, animal husbandry and fertiliser use (Chapter 4). This nitrogen is then deposited fairly near to the source, and can act as a fertiliser for terrestrial plants. There has been a rapid increase in reactive nitrogen deposition over the last 150 years (Vitousek *et al.*, 1997; Holland *et al.*, 1999). Much field evidence on nitrogen fertilisation effects on plants (e.g., Chapin, 1980; Vitousek and Howarth, 1991; Bergh *et al.*, 1999) supports the hypothesis that additional nitrogen deposition will result in increased NPP, including the growth of trees in Europe (Specker *et al.*, 1996). There is also evidence (Fog, 1988; Bryant *et al.*, 1998) that N fertilisation enhances the formation of modified soil organic matter and thus increases the residence time of carbon in soils.

Tracer experiments with addition of the stable isotope <sup>15</sup>N provide insight into the short-term fate of deposited reactive nitrogen (Gundersen *et al.*, 1998). It is clear from these experiments that most of the added N added to the soil surface is retained in the ecosystem rather than being leached out via water transport or returned to the atmosphere in gaseous form (as N<sub>2</sub>, NO, N<sub>2</sub>O or NH<sub>3</sub>). Studies have also shown that the tracer is found initially in the soil

(Nadelhoffer *et al.*, 1999), but that it enters the vegetation after a few years (Clark 1977; Schimel and Chapin, 1996; Delgado *et al.*, 1996; Schulze, 2000).

There is an upper limit to the amount of added N that can fertilise plant growth. This limit is thought to have been reached in highly polluted regions of Europe. With nitrogen saturation, ecosystems are no longer able to process the incoming nitrogen deposition, and may also suffer from deleterious effects of associated pollutants such as ozone (O<sub>3</sub>), nutrient imbalance, and aluminium toxicity (Schulze *et al.*, 1989; Aber *et al.*, 1998).

### 3.2.2.6 Additional impacts of changing atmospheric chemistry

Current tropospheric O<sub>3</sub> concentrations in Europe and North America cause visible leaf injury on a range of crop and tree species and have been shown to reduce the growth and yield of crops and young trees in experimental studies. The longer-term effects of O<sub>3</sub> on forest productivity are less certain, although significant negative associations between ozone exposure and forest growth have been reported in North America (McLaughlin and Percy, 2000) and in central Europe (Braun *et al.*, 2000). O<sub>3</sub> is taken up through stomata, so decreased stomatal conductance at elevated CO<sub>2</sub> may reduce the effects of O<sub>3</sub> (Semenov *et al.*, 1998, 1999). There is also evidence of significant interactions between O<sub>3</sub> and soil water availability in effects on stem growth or NPP from field studies (e.g., McLaughlin and Downing, 1995) and from modelling studies (e.g., Ollinger *et al.*, 1997). The regional impacts of O<sub>3</sub> on NPP elsewhere in the world are uncertain, although significant impacts on forests have been reported close to major cities. Fowler *et al.* (2000) estimate that the proportion of global forests exposed to potentially damaging ozone concentrations will increase from about 25% in 1990 to about 50% in 2100.

Other possible negative effects of industrially generated pollution on plant growth include effects of soil acidification due to deposition of NO<sub>3</sub><sup>-</sup> and SO<sub>4</sub><sup>2-</sup>. Severe forest decline has been observed in regions with high sulphate deposition, for instance in parts of eastern Europe and southern China. The wider effects are less certain and depend on soil sensitivity. Fowler *et al.* (2000) estimate that 8% of global forest cover received an annual sulphate deposition above an estimated threshold for effects on acid sensitive soils, and that this will increase to 17% in 2050. The most significant long-term effect of continued acid deposition for forest productivity may be through depletion of base cations, with evidence of both increased leaching rates and decreased foliar concentrations (McLaughlin and Percy, 2000), although the link between these changes in nutrient cycles and NPP needs to be quantified.

### 3.2.2.7 Additional constraints on terrestrial CO<sub>2</sub> uptake

It is very likely that there are upper limits to carbon storage in ecosystems due to mechanical and resource constraints on the amount of above ground biomass and physical limits to the amount of organic carbon that can be held in soils (Scholes *et al.*, 1999). It is also generally expected that increased above-ground NPP (production of leaves and stem) will to some extent be counterbalanced by an increased rate of turnover of the biomass as upper limits are approached.

### 3.2.3 Ocean Carbon Processes

#### 3.2.3.1 Background

The total amount of carbon in the ocean is about 50 times greater than the amount in the atmosphere, and is exchanged with the atmosphere on a time-scale of several hundred years. Dissolution in the oceans provides a large sink for anthropogenic CO<sub>2</sub>, due in part to its high solubility, but above all because of its dissociation into ions and interactions with sea water constituents (see Box 3.3).

The annual two-way gross exchange of CO<sub>2</sub> between the atmosphere and surface ocean is about 90 PgC/yr, mediated by molecular diffusion across the air-sea interface. Net CO<sub>2</sub> transfer can occur whenever there is a partial pressure difference of CO<sub>2</sub> across this interface. The flux can be estimated as the product of a gas transfer coefficient, the solubility of CO<sub>2</sub>, and the partial pressure difference of CO<sub>2</sub> between air and water. The gas transfer coefficient incorporates effects of many physical factors but is usually expressed as a non-linear function of wind speed alone. There is considerable uncertainty about this function (Liss and Merlivat, 1986; Wanninkhof, 1992; Watson *et al.*, 1995). Improvements in the ability to measure CO<sub>2</sub> transfer directly (e.g., Wanninkhof and McGillis, 1999) may lead to a better knowledge of gas transfer coefficients.

Despite extensive global measurements conducted during the 1990s, measurements of surface water pCO<sub>2</sub> remain sparse, and extensive spatial and temporal interpolation is required in order to produce global fields. Takahashi *et al.* (1999) interpolated data collected over three decades in order to derive monthly values of surface water pCO<sub>2</sub> over the globe for a single “virtual” calendar year (1995). A wind speed dependent

gas transfer coefficient was used to calculate monthly net CO<sub>2</sub> fluxes. The resulting estimates, although subject to large uncertainty, revealed clear regional and seasonal patterns in net fluxes.

Regional net CO<sub>2</sub> transfers estimated from contemporary surface water pCO<sub>2</sub> data should not be confused with the uptake of anthropogenic CO<sub>2</sub>. The uptake of anthropogenic CO<sub>2</sub> is the *increase* in net transfer over the pre-industrial net transfer, and is therefore superimposed on a globally varying pattern of relatively large natural transfers. The natural transfers result from heating and cooling, and biological production and respiration. Carbon is transferred within the ocean from natural sink regions to natural source regions via ocean circulation and the sinking of carbon rich particles. This spatial separation of natural sources and sinks dominates the regional distribution of net annual air-sea fluxes.

CO<sub>2</sub> solubility is temperature dependent, hence air-sea heat transfer contributes to seasonal and regional patterns of air-sea CO<sub>2</sub> transfer (Watson *et al.*, 1995). Net cooling of surface waters tends to drive CO<sub>2</sub> uptake; net warming drives outgassing. Regions of cooling and heating are linked via circulation, producing vertical gradients and north-south transports of carbon within the ocean (e.g., of the order 0.5 to 1 PgC/yr southward transport in the Atlantic Basin; Broecker and Peng, 1992; Keeling and Peng, 1995; Watson *et al.*, 1995; Holfort *et al.*, 1998).

Biological processes also drive seasonal and regional distributions of CO<sub>2</sub> fluxes (Figure 1c). The gross primary production by ocean phytoplankton has been estimated by Bender *et al.* (1994) to be 103 PgC/yr. Part of this is returned to DIC through autotrophic respiration, with the remainder being net primary production, estimated on the basis of global remote sensing data

#### Box 3.3: The varying CO<sub>2</sub> uptake capacity of the ocean.

Because of its solubility and chemical reactivity, CO<sub>2</sub> is taken up by the ocean much more effectively than other anthropogenic gases (e.g., chlorofluorocarbons (CFCs) and CH<sub>4</sub>). CO<sub>2</sub> that dissolves in seawater is found in three main forms. The sum of these forms constitutes dissolved inorganic carbon (DIC). The three forms are: (1) dissolved CO<sub>2</sub> (non-ionic, about 1% of the total) which can be exchanged with the atmosphere until the partial pressure in surface water and air are equal, (2) bicarbonate ion (HCO<sub>3</sub><sup>-</sup>, about 91%); and (3) carbonate ion (CO<sub>3</sub><sup>2-</sup>, about 8%). As atmospheric CO<sub>2</sub> increases, the dissolved CO<sub>2</sub> content of surface seawater increases at a similar rate, but most of the added CO<sub>2</sub> ends up as HCO<sub>3</sub><sup>-</sup>. Meanwhile, the CO<sub>3</sub><sup>2-</sup> content decreases, since the net effect of adding CO<sub>2</sub> is a reaction with CO<sub>3</sub><sup>2-</sup> to form HCO<sub>3</sub><sup>-</sup> (Figure 3.1). There is therefore less available CO<sub>3</sub><sup>2-</sup> to react with further CO<sub>2</sub> additions, causing an increasing proportion of the added CO<sub>2</sub> to remain in its dissolved form. This restricts further uptake, so that the overall ability of surface sea water to take up CO<sub>2</sub> decreases at higher atmospheric CO<sub>2</sub> levels. The effect is large. For a 100 ppm increase in atmospheric CO<sub>2</sub> above today's level (i.e., from 370 to 470 ppm) the DIC concentration increase of surface sea water is already about 40% smaller than would have been caused by a similar 100 ppm increase relative to pre-industrial levels (i.e., from 280 to 380 ppm). The contemporary DIC increase is about 60% greater than would result if atmospheric CO<sub>2</sub> were to increase from 750 to 850 ppm.

The uptake capacity for CO<sub>2</sub> also varies significantly due to additional factors, most importantly seawater temperature, salinity and alkalinity (the latter being a measurable quantity approximately equal to [HCO<sub>3</sub><sup>-</sup>] + 2 × [CO<sub>3</sub><sup>2-</sup>]). Alkalinity is influenced primarily by the cycle of CaCO<sub>3</sub> formation (in shells and corals) and dissolution (see Figure 3.1c).

to be about 45 PgC/yr (Longhurst *et al.*, 1995; Antoine *et al.*, 1996; Falkowski *et al.*, 1998; Field *et al.*, 1998; Balkanski *et al.*, 1999). About 14 to 30% of the total NPP occurs in coastal areas (Gattuso *et al.*, 1998). The resulting organic carbon is consumed by zooplankton (a quantitatively more important process than herbivory on land) or becomes detritus. Some organic carbon is released in dissolved form (DOC) and oxidised by bacteria (Ducklow, 1999) with a fraction entering the ocean reservoir as net DOC production (Hansell and Carlson, 1998). Sinking of particulate organic carbon (POC) composed of dead organisms and detritus together with vertical transfer of DOC create a downward flux of organic carbon from the upper ocean known as "export production". Recent estimates for global export production range from roughly 10 to 20 PgC/yr (Falkowski *et al.*, 1998; Laws *et al.*, 2000). An alternative estimate for global export production of 11 PgC/yr has been derived using an inverse model of physical and chemical data from the world's oceans (Schlitzer, 2000). Only a small fraction (about 0.1 PgC) of the export production sinks in sediments, mostly in the coastal ocean (Gattuso *et al.*, 1998). Heterotrophic respiration at depth converts the remaining organic carbon back to DIC. Eventually, and usually at another location, this DIC is upwelled into the ocean's surface layer again and may re-equilibrate with the atmospheric CO<sub>2</sub>. These mechanisms, often referred to as the biological pump, maintain higher DIC concentrations at depth and cause atmospheric CO<sub>2</sub> concentrations to be about 200 ppm lower than would be the case in the absence of such mechanisms (Sarmiento and Toggweiler, 1984; Maier-Reimer *et al.*, 1996).

Marine organisms also form shells of solid calcium carbonate (CaCO<sub>3</sub>) that sink vertically or accumulate in sediments, coral reefs and sands. This process depletes surface CO<sub>3</sub><sup>2-</sup>, reduces alkalinity, and tends to increase pCO<sub>2</sub> and drive more outgassing of CO<sub>2</sub> (see Box 3.3 and Figure 3.1). The effect of CaCO<sub>3</sub> formation on surface water pCO<sub>2</sub> and air-sea fluxes is therefore counter to the effect of organic carbon production. For the surface ocean globally, the ratio between the export of organic carbon and the export of calcium carbonate (the "rain ratio") is a critical factor controlling the overall effect of biological activity on surface ocean pCO<sub>2</sub> (Figure 3.1; Archer and Maier-Reimer, 1994). Milliman (1993) estimated a global production of CaCO<sub>3</sub> of 0.7 PgC/yr, with roughly equivalent amounts produced in shallow water and surface waters of the deep ocean. Of this total, approximately 60% accumulates in sediments. The rest re-dissolves either in the water column or within the sediment. An estimate of CaCO<sub>3</sub> flux analogous to the export production of organic carbon, however, should include sinking out of the upper layers of the open ocean, net accumulation in shallow sediments and reefs, and export of material from shallow systems into deep sea environments. Based on Milliman's (1993) budget, this quantity is about 0.6 PgC/yr ( $\pm$  25 to 50 % at least). The global average rain ratio has been variously estimated from models of varying complexity to be 4 (Broecker and Peng, 1982), 3.5 to 7.5 (Shaffer, 1993), and 11 (Yamanaka and Tajika, 1996). (It should be noted that rain ratios are highly depth dependent due to rapid oxidation of organic carbon at shallow depth compared to the

depths at which sinking CaCO<sub>3</sub> starts to dissolve.) If one accepts an organic carbon export production value of 11 PgC/yr (Schlitzer, 2000), then only Yamanaka and Tajika's (1996) value for the rain ratio approaches consistency with the observation-based estimates of the export of CaCO<sub>3</sub> and organic carbon from the ocean surface layer.

The overall productivity of the ocean is determined largely by nutrient supply from deep water. There are multiple potentially limiting nutrients: in practice nitrate and/or phosphate are commonly limiting (Falkowski *et al.*, 1998; Tyrell, 1999). Silicate plays a role in limiting specific types of phytoplankton and hence in determining the qualitative nature of primary production, and potentially the depth to which organic carbon sinks. A role for iron in limiting primary productivity in regions with detectable phosphate and nitrate but low productivity (HNLC or "high nutrient, low chlorophyll regions") has been experimentally demonstrated in the equatorial Pacific (Coale *et al.*, 1996) and the Southern Ocean (Boyd *et al.*, 2000). In both regions artificial addition of iron stimulated phytoplankton growth, resulting in decreased surface-water pCO<sub>2</sub>. In HNLC regions, the supply of iron from deep water, while an important source, is generally insufficient to meet the requirements of phytoplankton. An important additional supply of iron to surface waters far removed from sediment and riverine sources is aeolian transport and deposition (Duce and Tindale, 1991; Fung *et al.*, 2000; Martin, 1990). This aeolian supply of iron may limit primary production in HNLC regions, although the effect is ultimately constrained by the availability of nitrate and phosphate. Iron has been hypothesised to play an indirect role over longer time-scales (e.g., glacial-interglacial) through limitation of oceanic nitrogen fixation and, consequently, the oceanic content of nitrate (Falkowski *et al.*, 1998; Broecker and Henderson, 1998; Box 3.4). The regional variability of oceanic nitrogen fixation (Gruber and Sarmiento, 1997) and its temporal variability and potential climate-sensitivity have recently become apparent based on results from long time-series and global surveys (Karl *et al.*, 1997; Hansell and Feely, 2000).

Carbon (organic and inorganic) derived from land also enters the ocean via rivers as well as to some extent via groundwater. This transport comprises a natural carbon transport together with a significant anthropogenic perturbation. The global natural transport from rivers to the ocean is about 0.8 PgC/yr, half of which is organic and half inorganic (Meybeck 1982, 1993; Sarmiento and Sundquist 1992; Figure 3.1). Additional fluxes due to human activity have been estimated (Meybeck, 1993) to be about 0.1 PgC/yr (mainly organic carbon). Much of the organic carbon is deposited and/or respired and outgassed close to land, mostly within estuaries (Smith and Hollibaugh, 1993). The outgassing of anthropogenic carbon from estuaries can be a significant term in comparison with regional CO<sub>2</sub> emissions estimates (e.g., 5 to 10% for Western Europe; Frankignoulle *et al.*, 1998). The natural DIC transport via rivers, however, is part of a large-scale cycling of carbon between the open ocean and land associated with dissolution and precipitation of carbonate minerals. This natural cycle drives net outgassing from the ocean of the order 0.6 PgC/yr globally,

which should be included in any assessment of net air-sea and atmosphere-terrestrial biosphere transfers (Sarmiento and Sundquist, 1992) and ocean transports (e.g., Holfort *et al.*, 1998).

### 3.2.3.2 Uptake of anthropogenic CO<sub>2</sub>

Despite the importance of biological processes for the ocean's natural carbon cycle, current thinking maintains that the oceanic uptake of anthropogenic CO<sub>2</sub> is primarily a physically and chemically controlled process superimposed on a biologically driven carbon cycle that is close to steady state. This differs from the situation on land because of the different factors which control marine and terrestrial primary productivity. On land, experiments have repeatedly shown that current CO<sub>2</sub> concentrations are limiting to plant growth (Section 3.2.2.4). In the ocean, experimental evidence is against control of productivity by CO<sub>2</sub> concentrations, except for certain species at lower than contemporary CO<sub>2</sub> concentrations (Riebesell *et al.*, 1993; Falkowski, 1994). Further, deep ocean concentrations of major nutrients and DIC are tightly correlated, with the existing ratios closely (but not exactly, see Section 3.2.3.3) matching the nutritional requirements of marine organisms (the "Redfield ratios": Redfield *et al.*, 1963). This implies that as long as nutrients that are mixed into the ocean surface layer are largely removed by organic carbon production and export, then there is little potential to drive a net air-sea carbon transfer simply through alteration of the global rate of production. Terrestrial ecosystems show greater variability in this respect because land plants have multiple ways to acquire nutrients, and have greater plasticity in their chemical composition (Melillo and Gosz, 1983). There are, however, extensive regions of the ocean surface where major nutrients are not fully depleted, and changes in these regions may play a significant role in altering atmosphere-ocean carbon partitioning (see Section 3.2.3.3).

The increase of atmospheric *p*CO<sub>2</sub> over pre-industrial levels has tended to increase uptake into natural CO<sub>2</sub> sink regions and decreased release from natural outgassing regions. Contemporary net air-sea fluxes comprise spatially-varying mixtures of natural and anthropogenic CO<sub>2</sub> flux components and cannot be equated with anthropogenic CO<sub>2</sub> uptake, except on a global scale. Uptake of anthropogenic CO<sub>2</sub> is strongest in regions where "old" waters, which have spent many years in the ocean interior since their last contact with the atmosphere, are re-exposed at the sea surface to a contemporary atmosphere which now contains anthropogenic CO<sub>2</sub> (e.g., Sarmiento *et al.*, 1992; Doney, 1999). In an upwelling region, for example, the natural component of the air-sea flux may be to outgas CO<sub>2</sub> to the atmosphere. The higher atmospheric *p*CO<sub>2</sub> of the contemporary atmosphere acts to reduce this outgassing relative to the natural state, implying that more carbon remains in the ocean. This represents uptake of anthropogenic CO<sub>2</sub> by a region which is a source of CO<sub>2</sub> to the atmosphere. The additional carbon in the ocean resulting from such uptake is then transported by the surface ocean circulation, and eventually stored as surface waters sink, or are mixed, into the deep ocean interior. Whereas upwelling into the surface layer is quantitatively balanced on a global scale by sinking, the locations where deep waters rise and sink can be separated by large horizontal distances.

Air-sea gas transfer allows older waters to approach a new

steady state with higher atmospheric CO<sub>2</sub> levels after about a year at the sea surface. This is fast relative to the rate of ocean mixing, implying that anthropogenic CO<sub>2</sub> uptake is limited by the rate at which "older" waters are mixed towards the air-sea interface. The rate of exposure of older, deeper waters is therefore a critical factor limiting the uptake of anthropogenic CO<sub>2</sub>. In principle, there is sufficient uptake capacity (see Box 3.3) in the ocean to incorporate 70 to 80% of anthropogenic CO<sub>2</sub> emissions to the atmosphere, even when total emissions of up to 4,500 PgC are considered (Archer *et al.*, 1997). The finite rate of ocean mixing, however, means that it takes several hundred years to access this capacity (Maier-Reimer and Hasselmann, 1987; Enting *et al.*, 1994; Archer *et al.*, 1997). Chemical neutralisation of added CO<sub>2</sub> through reaction with CaCO<sub>3</sub> contained in deep ocean sediments could potentially absorb a further 9 to 15% of the total emitted amount, reducing the airborne fraction of cumulative emissions by about a factor of 2; however the response time of deep ocean sediments is in the order of 5,000 years (Archer *et al.*, 1997).

Using time-series and global survey data, the increasing oceanic carbon content has been directly observed, although the signal is small compared to natural variability and requires extremely accurate measurements (Sabine *et al.*, 1997). A long-term increase of surface water CO<sub>2</sub> levels tracking the mean atmospheric CO<sub>2</sub> increase has been observed in the ocean's subtropical gyres (Bates *et al.*, 1996; Winn *et al.*, 1998) and the equatorial Pacific (Feely *et al.*, 1999b). However, very few such time-series exist and the response of other important oceanic regions to the atmospheric *p*CO<sub>2</sub> increase cannot yet be assessed. Inter-decadal increases in DIC concentrations at depth have been resolved from direct measurements (Wallace, 1995; Peng *et al.*, 1998; Ono *et al.*, 1998; Sabine *et al.*, 1999). The total amounts of anthropogenic CO<sub>2</sub> accumulated in the ocean since the pre-industrial era can also be estimated from measurements using recent refinements (Gruber *et al.*, 1996) of long-standing methods for separating the natural and anthropogenic components of oceanic DIC. A comparison of such analyses with ocean model results is presented in Section 3.6.3.

### 3.2.3.3 Future changes in ocean CO<sub>2</sub> uptake

This section lists processes that may be important for the future uptake of anthropogenic CO<sub>2</sub>. These changes can represent changes in anthropogenic CO<sub>2</sub> uptake itself (mainly physical and chemical processes), or changes in the natural biologically-linked cycling of carbon between the atmosphere and ocean.

#### *Physical and chemical processes*

**Buffering changes.** The capacity of surface waters to take up anthropogenic CO<sub>2</sub> is decreasing as CO<sub>2</sub> levels increase (see Box 3.3). The magnitude of this effect is substantial. This decrease in uptake capacity of the ocean makes atmospheric CO<sub>2</sub> more sensitive to anthropogenic emissions and other changes in the natural cycling of carbon.

**Emissions rate.** Even assuming no other changes to the carbon cycle, the proportion of emitted CO<sub>2</sub> that can be taken up by the ocean decreases as the rate of emission increases. This is due to the finite rate of exposure of 'older', deeper waters to the anthropogenic CO<sub>2</sub> contained in the atmosphere.

**Warming.** CO<sub>2</sub> is less soluble in warmer water, and the equilibrium *p*CO<sub>2</sub> in seawater increases by about 10 to 20 ppm per °C temperature increase. Warming of surface water would therefore tend to increase surface water *p*CO<sub>2</sub>, driving CO<sub>2</sub> from the surface ocean to the atmosphere. The expected effect of such warming on atmospheric CO<sub>2</sub> may be smaller, depending on the rate of exchange between ocean surface waters and the deep ocean at high latitudes (e.g., Bacastow, 1993).

**Vertical mixing and stratification.** Several coupled atmosphere-ocean models have shown global warming to be accompanied by an increase in vertical stratification (see Chapter 7). Such a change would reduce the rate of mixing between surface and deep waters, and therefore reduce the effective volume of the ocean that is exposed to high atmospheric CO<sub>2</sub>. On its own, this effect would tend to reduce the ocean CO<sub>2</sub> uptake. However, changes in stratification may also drive changes in the natural carbon cycle. The magnitude and even the sign of changes in the natural cycle are much more difficult to predict because of the complexity of ocean biological processes (Sarmiento *et al.*, 1998; Matear and Hirst, 1999).

#### *Biologically-linked processes*

Qualitative and quantitative changes in carbon uptake arising from changes in marine ecosystems are more speculative (Denman *et al.*, 1996; Falkowski *et al.*, 1998; Watson and Liss, 1998), but are likely to have occurred over glacial-interglacial time-scales (Section 3.3). Falkowski *et al.* (1998) listed three major classes of biologically linked factors that can in principle alter the air-sea partitioning of CO<sub>2</sub>: (1) changes in surface nutrient utilisation (e.g., in HNLC areas); (2) changes in total ocean content of major nutrients; (3) changes in the elemental composition of biogenic material (including the rain ratio). Our incomplete understanding of present day nutrient controls on productivity limits our ability to predict future changes in ocean biology and their effect on CO<sub>2</sub> levels. For example, the possible identification of changes in deep ocean C:N:P ratios (Pahlow and Riebesell, 2000) leaves open the question of the extent to which ocean biological carbon cycling is in steady state, or is likely to remain so in the future.

**Changes in surface nutrient utilisation.** Changes in the utilisation of surface nutrients in HNLC regions have the potential to alter export production and carbon storage in the ocean interior. Most attention focuses on the role of inadvertent or deliberate changes in the external supply of iron to such regions. The sign of possible future responses of ocean biota due to iron supply changes is difficult to assess. Future iron supply may increase due to erosion (enhanced by agriculture and urbanisation) which tends to increase dust export and aeolian iron deposition (Tegen and Fung, 1995). Conversely, a globally enhanced hydrological cycle and increased water-use efficiency of terrestrial plants may tend to reduce future dust export (Harrison *et al.*, 2001). The delivery of dust to the HNLC regions will be sensitive to regional changes in erosion and the hydrological cycle, affecting the important regions of dust export, rather than to global scale changes (Dai *et al.*, 1998).

Surface nutrient supply could be reduced if ocean stratification reduces the supply of major nutrients carried to the surface waters from the deep ocean (Sarmiento *et al.*, 1998). The impact of strati-

fication on marine productivity depends on the limiting factor. In regions limited by deep ocean nutrients, stratification would reduce marine productivity and the strength of the export of carbon by biological processes. Conversely, stratification also increases the light exposure of marine organisms, which would increase productivity in regions where light is limiting.

**Changes in total ocean content of major nutrients.** Changes in the delivery of the major biologically limiting nutrients (N, P, Fe, Si) from riverine, atmospheric or sedimentary sources, or changes in removal rates (e.g., denitrification), could alter oceanic nutrient inventories and hence export production and ocean carbon storage. On the global scale, the upward fluxes of major nutrients are slightly depleted in N relative to P with respect to the nutrient requirements of phytoplankton (Fanning, 1992). This relative supply of N versus P may be sensitive to climate and circulation related changes in the rate of fixed-nitrogen removal by denitrification (Ganeshram *et al.*, 1995) or via changes in the rate of nitrogen fixation. Changes in river flow and composition are also affecting the supply of nutrients (Frankignoulle *et al.*, 1998). The hypothesised link between nitrogen fixation in certain ocean regions and the external iron supply (Falkowski, 1997; Wu *et al.*, 2000) could play a role in future nutrient and carbon budgets. Nitrogen fixation rates may also be affected by changes in stratification and mixing. For example, Karl *et al.* (1997) have identified interannual variability in nitrogen fixation rates in the subtropical Pacific which are apparently linked to ENSO variability in upper ocean dynamics.

**Changes in the elemental composition of biogenic material.** The structure and biogeochemistry of marine ecosystems can be affected by numerous climate-related factors including temperature, cloudiness, nutrient availability, mixed-layer physics and sea-ice extent. In turn the structure of marine ecosystems, and particularly the species composition of phytoplankton, exert a control on the partitioning of carbon between the ocean and the atmosphere. For example, a change in distribution of calcareous versus siliceous planktonic organisms could affect CO<sub>2</sub> uptake in the future, as it may have done in the past (Archer and Maier-Reimer, 1994). Precipitation of CaCO<sub>3</sub> by marine organisms (calcification) removes dissolved CO<sub>3</sub><sup>2-</sup>, thus decreasing surface water alkalinity and reducing the capacity of sea water to dissolve atmospheric CO<sub>2</sub> (see Box 3.3). Recent experimental evidence suggests that as a direct result of increasing atmospheric and surface water *p*CO<sub>2</sub> levels, oceanic calcification will decrease significantly over the next 100 years. Model-based calculations suggest that decreases in coral reef calcification rates of the order 17 to 35% relative to pre-industrial rates are possible (Kleypas *et al.*, 1999). Experimental studies with corals have confirmed such effects (Langdon *et al.*, 2000). Field and laboratory studies have shown that planktonic calcification is also highly sensitive to *p*CO<sub>2</sub> levels. The calcification rate of coccolithophorids decreases by 16 to 83% at *p*CO<sub>2</sub> levels of 750 ppm (Riebesell *et al.*, 2000). Such an effect would tend to favour CO<sub>2</sub> storage in the upper ocean and act as a negative feedback on atmospheric growth rates of CO<sub>2</sub>. However, long-term predictions of such biological responses are hampered by a lack of understanding concerning physiological acclimation and genetic adaptations of species to increasing *p*CO<sub>2</sub>.

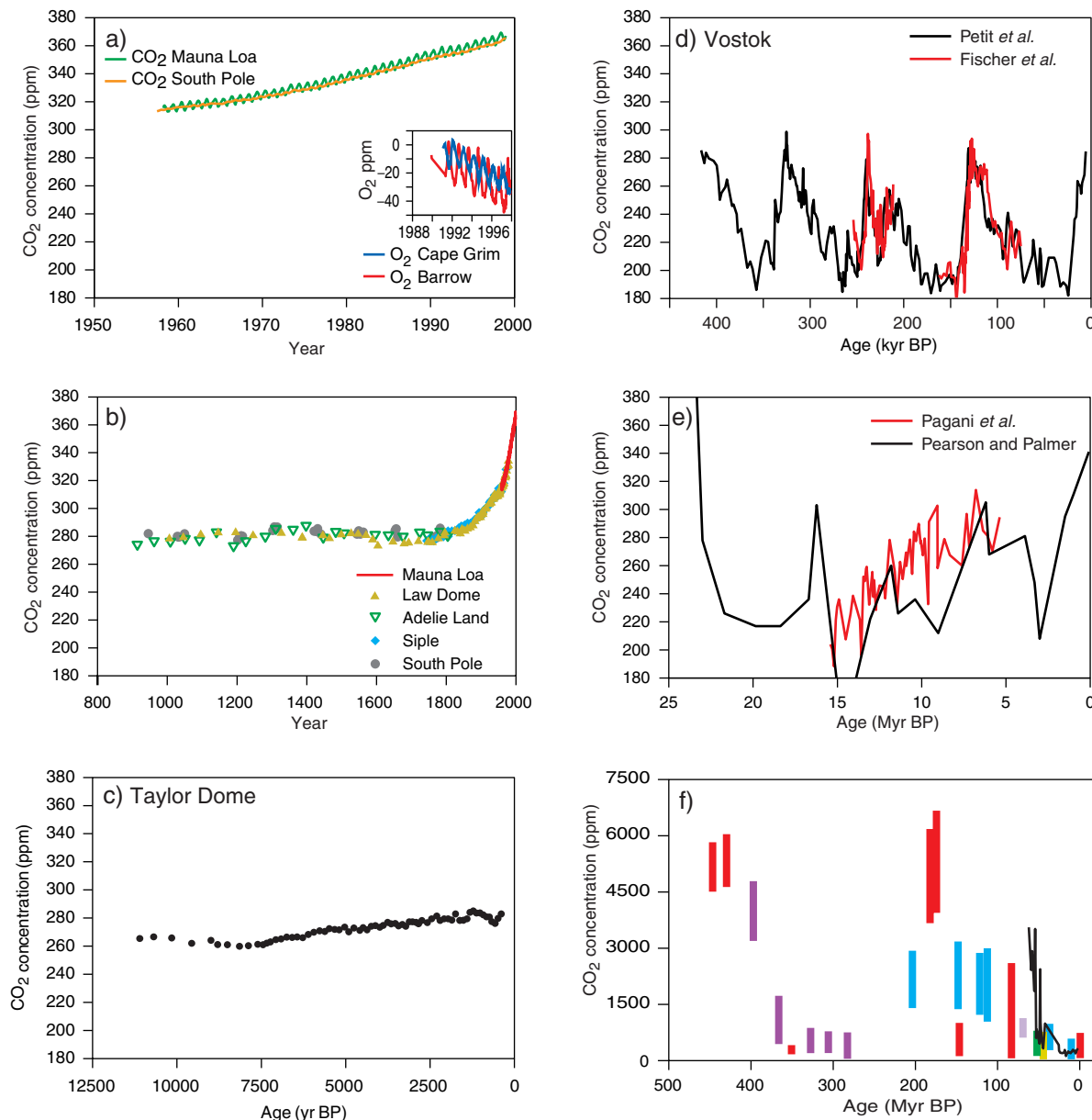


**Figure 3.2:** Variations in atmospheric CO<sub>2</sub> concentration on different time-scales. (a) Direct measurements of atmospheric CO<sub>2</sub> concentration (Keeling and Whorf, 2000), and O<sub>2</sub> from 1990 onwards (Battle *et al.*, 2000). O<sub>2</sub> concentration is expressed as the change from an arbitrary standard. (b) CO<sub>2</sub> concentration in Antarctic ice cores for the past millennium (Siegenthaler *et al.*, 1988; Neftel *et al.*, 1994; Barnola *et al.*, 1995; Etheridge *et al.*, 1996). Recent atmospheric measurements at Mauna Loa (Keeling and Whorf, 2000) are shown for comparison. (c) CO<sub>2</sub> concentration in the Taylor Dome Antarctic ice core (Indermühle *et al.*, 1999). (d) CO<sub>2</sub> concentration in the Vostok Antarctic ice core (Petit *et al.*, 1999; Fischer *et al.*, 1999). (e) Geochemically inferred CO<sub>2</sub> concentrations, from Pagani *et al.* (1999a) and Pearson and Palmer (2000). (f) Geochemically inferred CO<sub>2</sub> concentrations: coloured bars represent different published studies cited by Berner (1997). The data from Pearson and Palmer (2000) are shown by a black line. (BP = before present.)

### 3.3 Palaeo CO<sub>2</sub> and Natural Changes in the Carbon Cycle

#### 3.3.1 Geological History of Atmospheric CO<sub>2</sub>

Atmospheric CO<sub>2</sub> concentration has varied on all time-scales during the Earth's history (Figure 3.2). There is evidence for very high CO<sub>2</sub> concentrations (>3,000 ppm) between 600 and 400 Myr BP and between 200 and 150 Myr BP (Figure 3.2f). On long time-scales, atmospheric CO<sub>2</sub> content is determined by the

balance among geochemical processes including organic carbon burial in sediments, silicate rock weathering, and vulcanism (Berner, 1993, 1997). In particular, terrestrial vegetation has enhanced the rate of silicate weathering, which consumes CO<sub>2</sub> while releasing base cations that end up in the ocean. Subsequent deep-sea burial of Ca and Mg (as carbonates, for example CaCO<sub>3</sub>) in the shells of marine organisms removes CO<sub>2</sub>. The net effect of slight imbalances in the carbon cycle over tens to hundreds of millions of years has been to reduce

**Box 3.4:** Causes of glacial/inter-glacial changes in atmospheric CO<sub>2</sub>.

One family of hypotheses to explain glacial/inter-glacial variations of atmospheric CO<sub>2</sub> relies on physical mechanisms that could change the dissolution and outgassing of CO<sub>2</sub> in the ocean. The solubility of CO<sub>2</sub> is increased at low temperature, but reduced at high salinity. These effects nearly cancel out over the glacial/inter-glacial cycle, so simple solubility changes are not the answer. Stephens and Keeling (2000) have proposed that extended winter sea ice prevented outgassing of upwelled, CO<sub>2</sub>-rich water around the Antarctic continent during glacial times. A melt-water “cap” may have further restricted outgassing of CO<sub>2</sub> during summer (François *et al.*, 1997). These mechanisms could explain the parallel increases of Antarctic temperature and CO<sub>2</sub> during deglaciation. However, they require less vertical mixing to occur at low latitudes than is normally assumed. The relative importance of high and low latitudes for the transport of CO<sub>2</sub> by physical processes is not well known, and may be poorly represented in most ocean carbon models (Toggweiler, 1999; Broecker *et al.*, 1999).

Several authors have hypothesised increased utilisation of surface nutrients by marine ecosystems in high latitudes, leading to stronger vertical gradients of DIC and thus reduced atmospheric CO<sub>2</sub> during glacial times (Sarmiento and Toggweiler, 1984; Siegenthaler and Wenk, 1984; Knox and McElroy, 1984). Other hypotheses call for an increased external supply of nutrients to the ocean (McElroy, 1983; Martin *et al.*, 1990; Broecker and Henderson, 1998). The supply of iron-rich dust to the Southern Ocean is increased during glacial periods, due to expanded deserts in the Patagonian source region (Andersen *et al.*, 1998; Mahowald *et al.*, 1999; Petit *et al.*, 1999); dust-borne iron concentration in Antarctic ice is also increased (Edwards *et al.*, 1998). Fertilisation of marine productivity by iron from this source could have influenced atmospheric CO<sub>2</sub>. Most of these mechanisms, however, can only account for about 30 ppm, or less, of the change (Lefèvre and Watson, 1999; Archer and Johnson, 2000). Palaeo-nutrient proxies have also been used to argue against large changes in total high latitude productivity (Boyle, 1988; Rickaby and Elderfield, 1999; Elderfield and Rickaby, 2000), even if the region of high productivity in the Southern Ocean may have been shifted to the north (Kumar *et al.*, 1995; François *et al.*, 1997). Increased productivity over larger regions might have been caused by decreased denitrification (Altabet *et al.*, 1995; Ganeshram *et al.*, 1995) or iron stimulated N<sub>2</sub> fixation (Broecker and Henderson, 1998) leading to an increase in the total ocean content of reactive nitrogen.

Another family of hypotheses invokes ocean alkalinity changes by a variety of mechanisms (Opdyke and Walker, 1992; Archer and Maier-Reimer, 1994; Kleypas, 1997), including increased silica supply through dust, promoting export production by siliceous rather than calcareous phytoplankton (Harrison, 2000). Although there is geochemical evidence for higher ocean pH during glacial times (Sanyal *et al.*, 1995), a large increase in alkalinity would result in a much deeper lysocline, implying an increase in CaCO<sub>3</sub> preservation that is not observed in deep-sea sediments (Catubig *et al.*, 1998; Sigman *et al.*, 1998; Archer *et al.*, 2000).

Given the complex timing of changes between climate changes and atmospheric CO<sub>2</sub> on glacial-interglacial time-scales, it is plausible that more than one mechanism has been in operation; and indeed most or all of the hypotheses encounter difficulties if called upon individually to explain the full magnitude of the change.

atmospheric CO<sub>2</sub>. The rates of these processes are extremely slow, hence they are of limited relevance to the atmospheric CO<sub>2</sub> response to emissions over the next hundred years.

It is pertinent, however, that photosynthesis evolved at a time when O<sub>2</sub> concentrations were far less than at present. O<sub>2</sub> has accumulated in the atmosphere over geological time because photosynthesis results in the burial of reduced chemical species: pyrite (FeS<sub>2</sub>) derived from sulphur-reducing bacteria, and organic carbon. This accumulation has consequences for terrestrial and marine ecosystems today. Primary production is carbon limited in terrestrial ecosystems in part because of (geologically speaking) low CO<sub>2</sub> concentrations, and in part because Rubisco (the enzyme that fixes CO<sub>2</sub> in all plants) also has an affinity for O<sub>2</sub> that reduces its efficiency in photosynthesis (see Section 3.2.2.4). Primary production is iron limited in some marine ecosystems mainly because of the extreme insolubility of Fe(III), the predominant form of iron in the present, O<sub>2</sub>-rich environment. These difficulties faced by contemporary organisms represent a legacy of earlier evolution under very different biogeochemical conditions.

In more recent times, atmospheric CO<sub>2</sub> concentration continued to fall after about 60 Myr BP and there is geochemical evidence that concentrations were <300 ppm by about 20 Myr BP

(Pagani *et al.*, 1999a; Pearson and Palmer, 1999, 2000; Figure 3.2e). Low CO<sub>2</sub> concentrations may have been the stimulus that favoured the evolution of C<sub>4</sub> plants, which increased greatly in abundance between 7 and 5 Myr BP (Cerling *et al.*, 1993, 1997; Pagani *et al.*, 1999b). Although contemporary CO<sub>2</sub> concentrations were exceeded during earlier geological epochs, they are likely higher now than at any time during the past 20 million years.

### 3.3.2 Variations in Atmospheric CO<sub>2</sub> during Glacial/inter-glacial Cycles

The purity of Antarctic ice allows the CO<sub>2</sub> concentration in trapped air bubbles to be accurately measured (Tschumi and Stauffer, 2000). The CO<sub>2</sub> record from the Vostok ice core is the best available for the glacial/inter-glacial time-scale and covers the past four glacial/inter-glacial cycles (420 kyr) with a resolution of 1 to 2 kyr (Petit *et al.*, 1999; Fischer *et al.*, 1999). The general pattern is clear (Figure 3.2d): atmospheric CO<sub>2</sub> has been low (but  $\geq 180$  ppm) during glacial periods, and higher (but  $\leq 300$  ppm) during interglacials. Natural processes during the glacial-interglacial cycles have maintained CO<sub>2</sub> concentrations within

these bounds, despite considerable variability on multi-millennial time-scales. The present CO<sub>2</sub> concentration is higher than at any time during the 420 kyr period covered by the Vostok record.

The terrestrial biosphere stores 300 to 700 Pg *more* carbon during interglacial periods than during glacial periods, based on a widely accepted interpretation of the δ<sup>13</sup>C record in deep-sea sediments (Shackleton, 1977; Bird *et al.*, 1994; Crowley, 1995). Terrestrial modelling studies (e.g., Friedlingstein *et al.*, 1995b; Peng *et al.*, 1998) have reached the same conclusion. Thus, the terrestrial biosphere does not cause the difference in atmospheric CO<sub>2</sub> between glacial and interglacial periods. The cause must lie in the ocean, and indeed the amount of atmospheric change to be accounted for must be augmented to account for a fraction of the carbon transferred between the land and ocean. The mechanism remains controversial (see Box 3.4). In part this is because a variety of processes that could be effective in altering CO<sub>2</sub> levels on a century time-scale can be largely cancelled on multi-millennial time-scales by changes in CaCO<sub>3</sub> sedimentation or dissolution, as discussed in Section 3.2.3.1.

Orbital variations (Berger, 1978) are the pacemaker of climate change on multi-millennial time-scales (Hays *et al.*, 1976). Atmospheric CO<sub>2</sub> is one of many Earth system variables that show the characteristic ‘Milankovitch’ periodicities, and has been implicated as a key factor in locking natural climate changes to the 100 kyr eccentricity cycle (Shackleton, 2000). Whatever the mechanisms involved, lags of up to 2,000 to 4,000 years in the drawdown of CO<sub>2</sub> at the start of glacial periods suggests that the low CO<sub>2</sub> concentrations during glacial periods amplify the climate change but do not initiate glaciations (Lorius and Oeschger, 1994; Fischer *et al.*, 1999). Once established, the low CO<sub>2</sub> concentration is likely to have enhanced global cooling (Hewitt and Mitchell, 1997). During the last deglaciation, rising CO<sub>2</sub> paralleled Southern Hemisphere warming and was ahead of Northern Hemisphere warming (Chapter 2).

During glacial periods, the atmospheric CO<sub>2</sub> concentration does not track the ‘fast’ changes in climate (e.g., decade to century scale warming events) associated with Dansgaard-Oeschger events, although there are CO<sub>2</sub> fluctuations of up to 20 ppm associated with the longer-lived events (Stauffer *et al.*, 1998; Indermühle *et al.*, 2000) (see Chapter 2 for explanations of these terms). During the last deglaciation, atmospheric CO<sub>2</sub> concentration continued to increase, by about 12 ppm, through the Younger Dryas cold reversal (12.7 to 11.6 kyr BP) seen in Northern Hemisphere palaeoclimate records (Fischer *et al.*, 1999; Smith *et al.*, 1999). Palaeo-oceanographic evidence shows that the Younger Dryas event was marked by a prolonged shut-down of the thermohaline circulation, which is likely to have been triggered by the release of melt water into the North Atlantic. Similar behaviour, with a slight rise in CO<sub>2</sub> accompanying a major Northern Hemisphere cooling and shutdown of North Atlantic Deep Water production, has been produced in a coupled atmosphere-ocean model (Marchal *et al.*, 1998). The observed CO<sub>2</sub> rise during the Younger Dryas period was modest, suggesting that atmospheric CO<sub>2</sub> has, under natural conditions, been well buffered against abrupt changes in climate, including thermohaline collapse. This buffering is a direct consequence of the large reservoir of DIC in the ocean.

### 3.3.3 Variations in Atmospheric CO<sub>2</sub> during the Past 11,000 Years

Natural variations in CO<sub>2</sub> during the past 11,000 years (Figure 3.2c) have been small (about 20 ppm) according to the best available measurements, which are from the Taylor Dome ice core (Smith *et al.*, 1999; Indermühle *et al.*, 1999). These measurements show a short-lived maximum around 11 kyr BP, followed by a slight fall, which may have been caused by increasing carbon storage in the terrestrial biosphere. Atmospheric CO<sub>2</sub> concentration was about 260 ppm at its Holocene minimum around 8 kyr BP and increased towards about 280 ppm in the pre-industrial period. The same pattern and the same CO<sub>2</sub> concentration levels over the past 8 kyr have also been shown in another ice core, BH7 near Vostok (Peybernès *et al.*, 2000). The causes of these changes are not known. Preliminary δ<sup>13</sup>C measurements (see Box 3.6) suggest that this increase may have been due to a gradual reduction in terrestrial carbon storage (Indermühle *et al.*, 1999; Smith *et al.*, 1999) but others have considered an oceanic explanation more likely.

Atmospheric CO<sub>2</sub> concentrations have also been reconstructed indirectly, from stomatal index measurements on sub-fossil leaves (Van de Water *et al.*, 1994; Beerling *et al.*, 1995; Rundgren and Beerling, 1999; Wagner *et al.*, 1999). Stomatal density and stomatal index of many species respond to atmospheric CO<sub>2</sub> (Woodward, 1987; Woodward and Bazzaz, 1988) but are influenced by other environmental variables as well (Poole *et al.*, 1996). One recent stomatal index record, interpreted as implying high (up to 350 ppm) and rapidly fluctuating CO<sub>2</sub> concentrations in the early Holocene (Wagner *et al.*, 1999), is clearly incompatible with the ice core record of Indermühle *et al.* (1999), whereas a continuous stomatal index record from 9 kyr BP onwards (Rundgren and Beerling, 1999) has shown concentration trends consistent with the ice-core records.

Figure 3.2b shows the excellent agreement among different high-resolution Antarctic ice cores covering the past 1,000 years. Atmospheric CO<sub>2</sub> concentration fell by about 8 to 10 ppm during the Little Ice Age (from 1280 to 1860, see Chapter 2) (Figure 3.2b, c; Barnola *et al.*, 1995; Etheridge *et al.*, 1996; Indermühle *et al.*, 1999; Rundgren and Beerling, 1999). A slight contemporaneous increase in δ<sup>13</sup>C of atmospheric CO<sub>2</sub> has led to the suggestion that this effect was caused by enhanced carbon storage on land (Francey *et al.*, 1999b; Trudinger *et al.*, 1999).

### 3.3.4 Implications

The Vostok record of atmospheric CO<sub>2</sub> and Antarctic climate is consistent with a view of the climate system in which CO<sub>2</sub> concentration changes amplify orbitally-induced climate changes on glacial/inter-glacial time-scales (Shackleton, 2000). Changes during the present inter-glacial (until the start of the anthropogenic CO<sub>2</sub> rise) have been small by comparison. Although complete explanations for these changes in the past are lacking, high-resolution ice core records establish that the human-induced increase of atmospheric CO<sub>2</sub> over the past century is at least an order of magnitude faster than has occurred during the preceding 20,000 years.

### 3.4 Anthropogenic Sources of CO<sub>2</sub>

#### 3.4.1 Emissions from Fossil Fuel Burning and Cement Production

Current anthropogenic emissions of CO<sub>2</sub> are primarily the result of the consumption of energy from fossil fuels. Estimates of annual global emissions from fossil fuel burning and cement production have been made for the period from 1751 through 1999. Figure 3.3 summarises emissions over the period from 1959 to 1999 (Keeling and Whorf, 2000).

Estimates of annual global emissions from fossil fuel burning and cement production by Marland *et al.* (2000) span the period from 1751 through to 1997, reaching a maximum in 1997 of 6.6 PgC/yr (0.2 PgC/yr of this was from cement production). The primary data for these estimates are annual energy statistics compiled by the United Nations (2000). Emissions for 1998 and 1999 have been estimated based on energy statistics compiled by British Petroleum (2000). Emission factors (IPCC, 1997) were applied to consumption statistics (British Petroleum, 2000) to calculate emissions over the period 1990 to 1999. Emissions were then scaled to match the estimates for emissions from fossil fuel burning and cement production from Marland *et al.* (2000) over the overlap period from 1990 to 1997. The scaled emission estimates, therefore, implicitly include emissions from cement production.

The average value of emissions for the 1980s given by Marland *et al.* (2000) is  $5.44 \pm 0.3$  PgC/yr, revised from the earlier estimate (Marland *et al.* 1994; Andres *et al.* 2000) of  $5.46 \pm 0.3$  PgC/yr used in the SAR and in the Special Report on Radiative Forcing (IPCC, 1994) (hereafter SRRF). Estimated emissions rose from 6.1 PgC/yr in 1990 to 6.5 PgC/yr in 1999. The average value of emissions in the 1990s was  $6.3 \pm 0.4$  PgC/yr.

#### 3.4.2 Consequences of Land-use Change

About 10 to 30% of the current total anthropogenic emissions of CO<sub>2</sub> are estimated to be caused by land-use conversion. Such estimates rely on land cover data sets which are highly variable, and estimates of average carbon density of vegetation types, which are also highly variable with stand age and local conditions (see Box 3.1). Hence they cannot be specified as accurately as is possible for fossil fuel emissions. Historical emissions are treated in Section 3.2.2.2; this section focuses on the contemporary situation.

Net land-use flux, comprising the balance of positive terms due to deforestation and negative terms due to regrowth on abandoned agricultural land, has been estimated based on land-use statistics and simple models of rates of decomposition and regrowth, excluding possible climate, CO<sub>2</sub> and N fertilisation effects (Houghton, 1999). Not all land-use emissions are included, for example mining of peatlands. The analysis of Houghton (1999) indicated that the net flux due to land-use change was  $2.0 \pm 0.8$  PgC/yr during the 1980s, almost entirely due to deforestation of tropical regions. Temperate forests were found to show an approximate balance between carbon uptake in regrowing forests and carbon lost in oxidation of wood

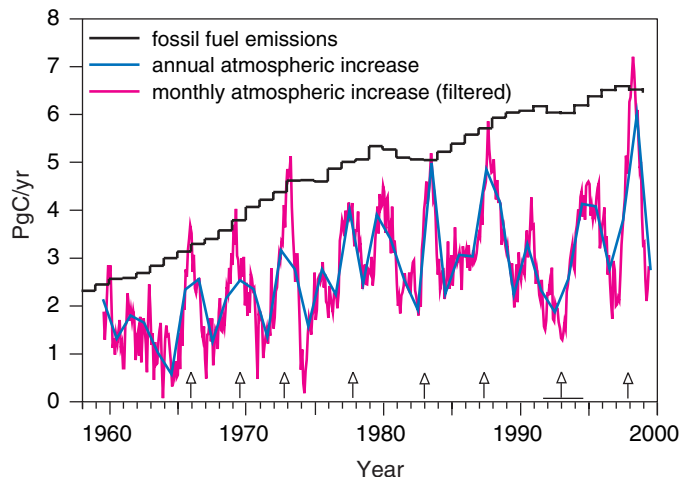


**Figure 3.3:** Fossil fuel emissions and the rate of increase of CO<sub>2</sub> concentration in the atmosphere. The annual atmospheric increase is the measured increase during a calendar year. The monthly atmospheric increases have been filtered to remove the seasonal cycle. Vertical arrows denote El Niño events. A horizontal line defines the extended El Niño of 1991 to 1994. Atmospheric data are from Keeling and Whorf (2000), fossil fuel emissions data are from Marland *et al.* (2000) and British Petroleum (2000), see explanations in text.

products, except in Europe, which showed a small net accumulation. The estimate of 2.0 PgC/yr is somewhat higher than Houghton and Hackler's (1995) earlier estimate of 1.6 PgC/yr for the same period, which was used in the SAR, because of a reanalysis of data from tropical Asia (Houghton and Hackler, 1999). However, other recent analyses by the same authors reduce the estimated emissions from the Brazilian Amazon by half (Houghton *et al.*, 2000), and point to other previously unaccounted for sinks of carbon in the USA such as fire suppression and woody encroachment, and changes in the management of agricultural soils (Houghton *et al.*, 1999). Consideration of these additional studies brings the overall total back down to  $1.7 \pm 0.8$  PgC/yr (Houghton, 2000), as given in the SRLULUCF.

An independent analysis (see Section 3.6.2.2) by the Carbon Cycle Model Linkage Project (CCMLP) also calculated the marginal effects of land-use changes on the global terrestrial carbon budget (McGuire *et al.*, 2001). Land-use change data (conversions between native vegetation and crops) were derived from Ramankutty and Foley (2000). The estimates obtained for net land-use flux during the 1980s were between 0.6 and 1.0 PgC/yr, i.e., substantially smaller than the fluxes calculated by Houghton (1999). The reasons for this discrepancy are unclear. The CCMLP estimates may be too low because they neglected conversions to pasture. However, data presented in Houghton (1999) indicate that the main changes during recent decades were due to land conversion for crops. A more important difference may lie in the timing of deforestation in different regions in the tropics, where Ramankutty and Foley (2000) show higher overall rates in the 1970s and lower rates in the 1980s than Houghton does (1999).

**Box 3.5:** The use of O<sub>2</sub> measurements to assess the fate of fossil fuel CO<sub>2</sub>.

The amount of CO<sub>2</sub> that remains in the atmosphere each year has been consistently less than the amount emitted by fossil fuel burning. This is because some CO<sub>2</sub> dissolves and mixes in the ocean, and some is taken up by the land. These two modes of uptake have different effects on the concentration of O<sub>2</sub> in the atmosphere. Fossil fuel burning consumes O<sub>2</sub> and causes a decline in atmospheric O<sub>2</sub> concentration (Figure 3.4). Dissolution of CO<sub>2</sub> in the ocean has no effect on atmospheric O<sub>2</sub>. Terrestrial uptake of CO<sub>2</sub>, by contrast, implies that photosynthesis (which releases O<sub>2</sub>) is exceeding respiration and other oxidation processes, including fire (which consume O<sub>2</sub>). Thus, net terrestrial uptake of CO<sub>2</sub> implies a net release of O<sub>2</sub>, in a known stoichiometric ratio. This difference can be used to partition the total CO<sub>2</sub> uptake into land and ocean components, as shown graphically in Figure 3.4. Strictly speaking, the atmospheric O<sub>2</sub> – CO<sub>2</sub> budget method can only distinguish between net non-biological ocean uptake and net biospheric uptake, which in principle includes both the terrestrial and the marine biosphere. However, since biological oxygen uptake is not expected to have changed significantly during recent decades because of nutrient limitations in most parts of the ocean (see Section 3.2.3.2), this inferred biospheric uptake is attributed to the land.

Measurement of changes in O<sub>2</sub> presents a technical challenge because changes of a few ppm caused by fossil fuel burning have to be determined against a background concentration of 209,000 ppm (about 21%). For technical reasons, O<sub>2</sub> is measured relative to N<sub>2</sub>, the main constituent of the atmosphere, as a reference gas. For simplicity this chapter refers to O<sub>2</sub> concentrations, although strictly it is O<sub>2</sub> : N<sub>2</sub> ratios that are measured. The impact of nitrification-denitrification changes on atmospheric N<sub>2</sub> content are assumed not to be problematic because they are small and the inventory of N<sub>2</sub> is very large. Increases in ocean temperatures (Levitus *et al.*, 2000), because of their effect on the temperature dependent solubility, induce small outgassing fluxes of O<sub>2</sub> and N<sub>2</sub> (Keeling *et al.*, 1993) that have to be taken into account (see Figure 3.4) although their magnitude is only approximately known. Impacts on atmospheric O<sub>2</sub> caused by changes in the ventilation of deeper, oxygen depleted waters have been observed on interannual time-scales (Keeling *et al.*, 1993; Bender *et al.*, 1996). They could also occur on longer time-scales, e.g., through increased ocean stratification induced by ocean warming.

Another analysis calculated a substantially higher net source due to land-use change in the tropics of  $2.4 \pm 1.0 \text{ PgC/yr}$  during the 1980s (Fearnside, 2000). This analysis did not deal with temperate regions, and is not used in the global budget estimates.

No complete global assessment of deforestation effects covering the 1990s is available. Rates of deforestation appear to be declining. The FAO (1997) tropical forest assessment reported annual losses of  $15.5 \times 10^6 \text{ ha}$  in the 1980s, and  $13.7 \times 10^6 \text{ ha}$  in 1990 to 1995. Independent studies show a significant decline in deforestation rates in the Amazon region (Skole and Tucker, 1993; Fearnside, 2000). The annual flux of carbon from land-use change for the period from 1990 to 1995 has been estimated to be  $1.6 \text{ PgC/yr}$  from 1990 to 1995, consisting of a source of  $1.7 \text{ PgC/yr}$  in the tropics and a small sink in temperate and boreal areas (Houghton, 2000).

### 3.5 Observations, Trends and Budgets

#### 3.5.1 Atmospheric Measurements and Global CO<sub>2</sub> Budgets

Continuous time-series of highly precise measurements of the atmospheric composition are of central importance to current understanding of the contemporary carbon cycle. CO<sub>2</sub> has been measured at the Mauna Loa and South Pole stations since 1957 (Keeling *et al.*, 1995; Figure 3.2a), and through a global surface sampling network developed in the 1970s that is becoming progressively more extensive and better inter-calibrated (Conway *et al.*, 1994; Keeling *et al.*, 1995). Associated measurements of δ<sup>13</sup>C in atmospheric CO<sub>2</sub> began in 1977 (Francey *et al.*, 1995; Keeling *et al.*, 1995; Tropier *et al.*, 1996). More recently, comple-

mentary information has been available from O<sub>2</sub> concentrations (measured as ratios of O<sub>2</sub>:N<sub>2</sub>, see Box 3.5), which have been regularly measured since the early 1990s (Keeling and Shertz, 1992; Keeling *et al.*, 1993; Bender *et al.*, 1996; Keeling *et al.*, 1996b; Battle *et al.*, 2000; Manning, 2001; Figure 3.2a). O<sub>2</sub> concentration data for the 1980s have been gleaned by two methods: sampling of archived air flasks that were collected during the 1980s (Langenfelds *et al.*, 1999), and measuring the air trapped in Antarctic firn (Battle *et al.*, 1996).

In addition to fossil fuel CO<sub>2</sub> emissions, Figure 3.3 shows the observed seasonally corrected growth rate of the atmospheric CO<sub>2</sub> concentrations, based on the two longest running atmospheric CO<sub>2</sub> recording stations (Keeling and Whorf, 2000). It is evident from this comparison that a part of the anthropogenic CO<sub>2</sub> has not remained in the atmosphere; in other words, CO<sub>2</sub> has been taken up by the land or the ocean or both. This comparison also shows that there is considerable interannual variability in the total rate of uptake.

O<sub>2</sub> and CO<sub>2</sub> measurements are used here to provide observationally-based budgets of atmospheric CO<sub>2</sub> (Table 3.1). CO<sub>2</sub> budgets are presented here (Table 3.1) for the 1980s (for comparison with previous work; Table 3.3), and for the 1990s. The reported error ranges are based on uncertainties of global fossil fuel emissions, determination of the decadal average changes in the atmospheric CO<sub>2</sub> concentration, and O<sub>2</sub>:N<sub>2</sub> ratio; and uncertainties in the assumed O<sub>2</sub>:CO<sub>2</sub> stoichiometric ratios in the combustion of fossil fuels and in photosynthesis and respiration. The error ranges reflect *uncertainties* of the decadal mean averaged values; they do not reflect interannual variability in annual values, which far exceeds uncertainty in

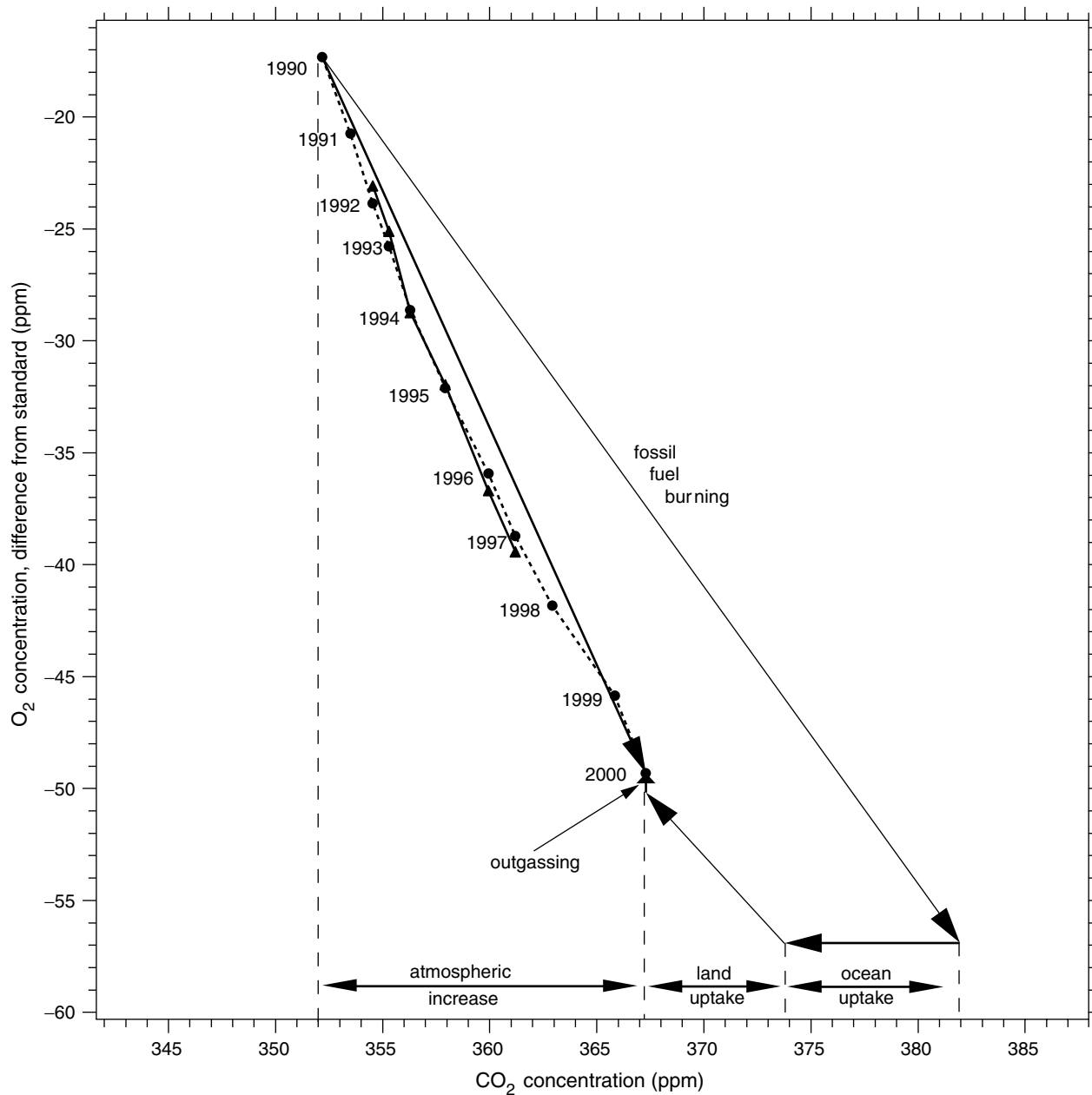


**Figure 3.4:** Partitioning of fossil fuel CO<sub>2</sub> uptake using O<sub>2</sub> measurements (Keeling and Shertz, 1992; Keeling *et al.*, 1993; Battle *et al.*, 1996, 2000; Bender *et al.*, 1996; Keeling *et al.*, 1996b; Manning, 2001). The graph shows the relationship between changes in CO<sub>2</sub> (horizontal axis) and O<sub>2</sub> (vertical axis). Observations of annual mean concentrations of O<sub>2</sub>, centred on January 1, are shown from the average of the Alert and La Jolla monitoring stations (Keeling *et al.*, 1996b; Manning, 2001; solid circles) and from the average of the Cape Grim and Point Barrow monitoring stations (Battle *et al.*, 2000; solid triangles). The records from the two laboratories, which use different reference standards, have been shifted to optimally match during the mutually overlapping period. The CO<sub>2</sub> observations represent global averages compiled from the stations of the NOAA network (Conway *et al.*, 1994) with the methods of Tans *et al.* (1989). The arrow labelled “fossil fuel burning” denotes the effect of the combustion of fossil fuels (Marland *et al.*, 2000; British Petroleum, 2000) based on the relatively well known O<sub>2</sub>:CO<sub>2</sub> stoichiometric relation of the different fuel types (Keeling, 1988). Uptake by land and ocean is constrained by the known O<sub>2</sub>:CO<sub>2</sub> stoichiometric ratio of these processes, defining the slopes of the respective arrows. A small correction is made for differential outgassing of O<sub>2</sub> and N<sub>2</sub> with the increased temperature of the ocean as estimated by Levitus *et al.* (2000).

**Box 3.6:** Stable carbon isotopes in atmospheric CO<sub>2</sub>.

$\delta^{13}\text{C}$ , a measure of the relative abundance of the two stable carbon isotopes,  $^{13}\text{C}$  and  $^{12}\text{C}$ , in atmospheric CO<sub>2</sub> gives in principle similar possibilities to O<sub>2</sub> for the partitioning of atmospheric CO<sub>2</sub> uptake (Keeling *et al.*, 1979, 1980; Mook *et al.*, 1983; Keeling *et al.*, 1989; Francey *et al.*, 1995; Keeling *et al.*, 1995). The principle of using  $\delta^{13}\text{C}$  to separate land and ocean components of the carbon budget relies on the fractionation during photosynthesis by C<sub>3</sub> plants, which discriminates against  $^{13}\text{C}$ . This fractionation leads to biospheric carbon being depleted in  $^{13}\text{C}$  by about 18‰ relative to the atmosphere. In contrast, exchanges with the ocean involve relatively small fractionation effects. Changes in the  $^{13}\text{C}/^{12}\text{C}$  ratio of atmospheric CO<sub>2</sub> thus indicate the extent to which concurrent CO<sub>2</sub> variations can be ascribed to variations in biospheric uptake. The calculation also requires specification of the turnover times of carbon in the ocean and on land, because fossil fuel burning implies a continuous release of isotopically light carbon to the atmosphere. This leads to a lowering of the atmospheric  $^{13}\text{C}/^{12}\text{C}$  isotope ratio, which takes years to centuries to work its way through the carbon cycle (Keeling *et al.*, 1980; Tans *et al.*, 1993; Ciais *et al.*, 1995a,b).

There are some complications. C<sub>3</sub> plants discriminate against  $^{13}\text{C}$  more strongly than C<sub>4</sub> plants (Lloyd and Farquhar, 1994), thus the distributions of C<sub>3</sub> and C<sub>4</sub> photosynthesis need to be known. The oceanic disequilibrium can in principle be estimated observationally (Tans *et al.*, 1993; Heimann and Maier-Reimer, 1996; Bacastow *et al.*, 1996; Gruber *et al.*, 1999), while the terrestrial disequilibrium has to be estimated by means of models (e.g., Ciais *et al.*, 1999). Langenfelds *et al.* (1999) and Battle *et al.* (2000) have shown that recently estimated values for the disequilibrium terms lead to consistency between the partitioning of CO<sub>2</sub> uptake into land and ocean uptake based on O<sub>2</sub> and on  $\delta^{13}\text{C}$  measurements.

the decadal mean rate of increase, as is further discussed in Section 3.5.2. The salient facts are as follows:

- During the 1980s, fossil fuel emissions were on average  $5.4 \pm 0.3$  PgC/yr and atmospheric CO<sub>2</sub> content increased on average by  $3.3 \pm 0.1$  PgC/yr. Partitioning of CO<sub>2</sub> uptake was estimated based on archived flask O<sub>2</sub> measurements (Langenfelds *et al.*, 1999) for the 1979 to 1997 period, taking the O<sub>2</sub> trend during 1991 to 1997 (Battle *et al.*, 2000) into account. The resulting estimate of the ocean-atmosphere flux was  $-1.9 \pm 0.6$  PgC/yr and of the land-atmosphere flux  $-0.2 \pm 0.7$  PgC/yr. This partitioning is adopted here in Table 3.1. It is corroborated by independent O<sub>2</sub> measurements in Antarctic firn (Battle *et al.*, 1996). Restricting the analysis to the Battle *et al.* (1996) data for the 1980 to 1989 period, an ocean-atmosphere flux of  $-1.8 \pm 1.0$  PgC/yr and a land-atmosphere flux of  $-0.4 \pm 1.0$  PgC/yr were obtained, i.e., results indistinguishable from the values in Table 3.1.
- Despite a greater emission rate of  $6.3 \pm 0.4$  PgC/yr (see Section 3.4.1), the average atmospheric increase during the 1990s was  $3.2 \pm 0.1$  PgC/yr, i.e., about the same as during the 1980s. An exceptionally low rate of increase during the early 1990s was balanced by a high rate during the late 1990s. Based on the longest existing O<sub>2</sub> records from La Jolla (California, USA) and Alert (northern Canada) (Keeling *et al.*, 1996b; Manning, 2001; see Figure 3.4), the ocean-atmosphere flux during the 1990s was  $-1.7 \pm 0.5$  PgC/yr and the land-atmosphere flux was  $-1.4 \pm 0.7$  PgC/yr.

Ocean uptake in the 1980s as estimated from O<sub>2</sub> and CO<sub>2</sub> measurements thus agrees with the estimates in the SRRF (Schimel *et al.*, 1995) and the SAR (Schimel *et al.*, 1996) (although these were model-based estimates; this section presents only observationally-based estimates (Table 3.3)). Considering the uncertainties, the ocean sink in the 1990s was not significantly different from that in

the 1980s. The land-atmosphere flux was close to zero in the 1980s, as also implied by the SAR budget. The land appears to have taken up more carbon during the 1990s than during the 1980s. The causes cannot yet be reliably quantified, but possible mechanisms include a slow down in deforestation (Section 3.4.2), and climate variability that resulted in temporarily increased land and/or ocean uptake in the early 1990s (Section 3.5.2). These budgets are consistent with information from atmospheric  $\delta^{13}\text{C}$  measurements (see Box 3.6 and Table 3.4) and with budgets presented in the SRLULUCF (Bolin *et al.*, 2000) except that estimated ocean uptake is smaller, and land uptake accordingly larger, than given in the SRLULUCF (see Table 3.3, footnote *i*).

Several alternative approaches to estimating the ocean-atmosphere and land-atmosphere fluxes of CO<sub>2</sub> are summarised in Table 3.4. Alternative methods for estimating the global ocean-atmosphere flux, based on surface-water  $p\text{CO}_2$  measurements and ocean  $\delta^{13}\text{C}$  changes (Quay *et al.*, 1992; Tans *et al.*, 1993, Heimann and Maier-Reimer, 1996; Sonnerup *et al.*, 1999), respectively, have yielded a range of  $-1.5$  to  $-2.8$  PgC/yr (for various recent periods). The total anthropogenic CO<sub>2</sub> added to the ocean since pre-industrial times can also be estimated indirectly using oceanic observations (Gruber *et al.*, 1996). A global value of  $107 \pm 27$  PgC by 1990 can be estimated from the basin-scale values of  $40 \pm 9$  PgC for the Atlantic in the 1980s (Gruber, 1998),  $20 \pm 3$  PgC for the Indian Ocean in 1995 (Sabine *et al.*, 1999), and the preliminary value of 45 PgC for the Pacific Ocean in 1990 to 1996 (Feely *et al.*, 1999a) with a large uncertainty of the order of  $\pm 15$  PgC. Assuming that accumulation of CO<sub>2</sub> in the ocean follows a curve similar to the (better known) accumulation in the atmosphere, the value for the ocean-atmosphere flux for 1980 to 1989 would be between  $-1.6$  and  $-2.7$  PgC/yr. Although each individual method has large uncertainty, all of these ocean-based measurements give results comparable with the fluxes presented in Table 3.1. Consideration of model-based estimates of ocean uptake in Table 3.4 is deferred to Section 3.6.2.2.

**Table 3.3:** Comparison of the global CO<sub>2</sub> budgets from Table 3.1 with previous IPCC estimates<sup>a,b,c</sup> (units are PgC/yr).

	1980s				1990s	1989 to 1998
	This chapter	SRLULUCF <sup>d</sup>	SAR <sup>e</sup>	SRRF <sup>f</sup>	This chapter	SRLULUCF <sup>d</sup>
Atmospheric increase	3.3 ± 0.1	3.3 ± 0.1	3.3 ± 0.1	3.2 ± 0.1	3.2 ± 0.1	3.3 ± 0.1
Emissions (fossil fuel, cement)	5.4 ± 0.3	5.5 ± 0.3	5.5 ± 0.3	5.5 ± 0.3	6.4 ± 0.4	6.3 ± 0.4
Ocean-atmosphere flux	-1.9 ± 0.6	-2.0 ± 0.5 <sup>i</sup>	-2.0 ± 0.5	-2.0 ± 0.5	-1.7 ± 0.5	-2.3 ± 0.5 <sup>i</sup>
Land-atmosphere flux*	-0.2 ± 0.7 <sup>g</sup>	-0.2 ± 0.6	-0.2 ± 0.6	-0.3 ± 0.6	-1.4 ± 0.7	-0.7 ± 0.6
*partitioned as follows						
Land-use change	1.7 (0.6 to 2.5) <sup>g</sup>	1.7 ± 0.8	1.6 ± 1.0	1.6 ± 1.0	insufficient data	1.6 ± 0.8 <sup>j</sup>
Residual terrestrial sink	-1.9 (-3.8 to 0.3)	-1.9 ± 1.3	-1.8 ± 1.6 <sup>h</sup>	-1.9 ± 1.6		-2.3 ± 1.3

<sup>a</sup> Positive values are fluxes to the atmosphere; negative values represent uptake from the atmosphere.

<sup>b</sup> Previous IPCC carbon budgets calculated ocean uptake and land-use change from models. The residual terrestrial sink was inferred. Here the implied land-atmosphere flux (with its error) is derived from these previous budgets as required for comparison with Table 3.1.

<sup>c</sup> Error ranges are expressed in this book as 67% confidence intervals ( $\pm 1\sigma$ ). Previous IPCC estimates have used 90% confidence intervals ( $\pm 1.6\sigma$ ). These error ranges have been scaled down as required for comparison with Table 3.1. Uncertainty ranges for land-use change emissions have not been altered in this way.

<sup>d</sup> IPCC Special Report on Land Use, Land-use Change and Forestry (SRLULUCF) (IPCC, 2000a; Bolin *et al.*, 2000).

<sup>e</sup> IPCC Second Assessment Report (SAR) (IPCC, 1996a; Schimel *et al.*, 1996).

<sup>f</sup> IPCC Special Report on Radiative Forcing (SRRF) (Schimel *et al.*, 1995).

<sup>g</sup> Ranges based on Houghton (1999, 2000), Houghton and Hackler (1999), and CCMLP model results (McGuire *et al.*, 2001).

<sup>h</sup> The sink of  $0.5 \pm 0.5$  PgC/yr in “northern forest regrowth” cited in the SAR budget is assigned here to be part of the residual terrestrial sink, following Bolin *et al.* (2000).

<sup>i</sup> Based on an ocean carbon cycle model (Jain *et al.*, 1995) used in the IPCC SAR (IPCC, 1996; Harvey *et al.*, 1997), tuned to yield an ocean-atmosphere flux of 2.0 PgC/yr in the 1980s for consistency with the SAR. After re-calibration to match the mean behaviour of OCMIP models and taking account of the effect of observed changes in temperature aon CO<sub>2</sub> and solubility, the same model yields an ocean-atmosphere flux of -1.7 PgC/yr for the 1980s and -1.9 PgC/yr for 1989 to 1998.

<sup>j</sup> Based on annual average estimated emissions for 1989 to 1995 (Houghton, 2000).

The land-atmosphere flux based on atmospheric measurements represents the *balance* of a net land-use flux (currently a positive flux, or carbon source, dominated by tropical deforestation) and a residual component which is, by inference, a negative flux or carbon sink. Using the land-atmosphere flux estimates from Table 3.1, assuming that land-use change contributed +1.7 PgC/yr to the atmosphere during the 1980s (Section 3.4.2), then a residual terrestrial flux of -1.9 PgC/yr (i.e., a residual sink of similar magnitude to the total ocean uptake) is required for mass balance. This is the term popularly (and misleadingly) known as the “missing sink”. The central estimate of its magnitude agrees with previous analyses, e.g., in the SAR (if “northern forest regrowth” is combined with “residual terrestrial sink” terms in the SAR budget; Schimel *et al.*, 1996) and the SRLULUCF (Bolin *et al.*, 2000) (Table 3.3). The uncertainty around this number is rather large, however, because it compounds the uncertainty in the atmospheric budget with a major uncertainty about changes in land use. Using an error range corresponding to 90% confidence intervals around the atmospheric estimate of -0.2 PgC/yr (i.e.,  $1.6\sigma$ , giving confidence intervals of  $\pm 1.1$  PgC/yr), and taking the range of estimates for CO<sub>2</sub> released due to land-use change during the 1980s from Section 3.4.2, the residual terrestrial sink is estimated to range from -3.8 to +0.3 PgC/yr for the 1980s. Model-based analysis of the components of the residual terrestrial sink (Table 3.4) is discussed in Section 3.6.2.2.

### 3.5.2 Interannual Variability in the Rate of Atmospheric CO<sub>2</sub> Increase

The rate of increase in the globally averaged atmospheric concentration of CO<sub>2</sub> varies greatly from year to year. “Fast” and “slow” years have differed by 3 to 4 PgC/yr within a decade (Figure 3.3). This variability cannot be accounted for by fossil fuel emissions, which do not show short-term variability of this magnitude. The explanation must lie in variability of the land-atmosphere flux or the ocean-atmosphere flux or both. Variability in both systems could be induced by climate variability.

An association between CO<sub>2</sub> variability and El Niño in particular has been reported for over twenty years and has been confirmed by recent statistical analyses (Bacastow, 1976; Keeling and Revelle, 1985; Thompson *et al.*, 1986; Siegenthaler, 1990; Elliott *et al.*, 1991; Braswell *et al.*, 1997; Feely *et al.*, 1997; Dettinger and Ghil, 1998; Rayner *et al.*, 1999b). During most of the observational record, El Niño events have been marked by high rates of increase in atmospheric CO<sub>2</sub> concentration compared with surrounding years, in the order of  $> 1$  PgC/yr higher during most El Niño events (Figure 3.3). Direct measurements of oceanic CO<sub>2</sub> in the equatorial Pacific over the last 20 years have shown that the natural efflux of CO<sub>2</sub> from this region is reduced by between 0.2 to 1.0 PgC/yr during El Niño (Keeling and Revelle, 1985; Smethie *et al.*, 1985; Takahashi *et al.*, 1986; Inoue and Sugimura, 1992; Wong *et al.*, 1993; Feely *et al.*, 1997;

**Table 3.4:** Alternative estimates of ocean-atmosphere and land-atmosphere fluxes.

	<b>Ocean-atmosphere flux</b>	<b>Land-atmosphere flux</b>
<b>Oceanic observations</b>		
<b>1970 to 1990</b>		
Ocean $^{13}\text{C}$ inventory	$-2.1 \pm 0.8^{\text{a}}$ $-2.1 \pm 0.9^{\text{b}}$	
<b>1985 to 1995</b>		
Ocean $^{13}\text{C}$ inventory	$-1.5 \pm 0.9^{\text{c}}$	
<b>1995</b>		
Surface-water $p\text{CO}_2$	$-2.8 \pm 1.5^{\text{d}}$	
<b>1990</b>		
Inventory of anthropogenic $\text{CO}_2$	$-1.6$ to $-2.7^{\text{e}}$	
<b>Atmospheric observations</b>		
<b>1980 to 1989</b>		
$\text{O}_2$ in Antarctic firn	$-1.8^{\text{f}}$	$-0.4^{\text{f}}$
<b>1990 to 1999</b>		
Atmospheric $\text{CO}_2$ and $\delta^{13}\text{C}$	$-1.8^{\text{g}}$ $-2.4^{\text{h}}$	$-1.4^{\text{g}}$ $-0.8^{\text{h}}$
<b>Models</b>		
<b>1980 to 1989</b>		
OCMIP	$-1.5$ to $-2.2^{\text{i}}$	$-0.3$ to $-1.5^{\text{j}*}$
CCMLP *		<i>*partitioned as follows:</i>
<i>*partitioned as follows:</i>		
Land-use change		$0.6$ to $1.0$
$\text{CO}_2$ and N fertilisation		$-1.5$ to $-3.1$
Climate variability		$-0.2$ to $+0.9$

Sources of data:

<sup>a</sup> Quay *et al.* (1992).

<sup>b</sup> Heimann and Maier-Reimer (1996).

<sup>c</sup> Gruber and Keeling (2001).

<sup>d</sup> Takahashi *et al.* (1999) with  $-0.6$  PgC/yr correction for land-ocean river flux.

<sup>e</sup> Gruber (1998), Sabine *et al.* (1999); Feely *et al.* (1999a), assuming that the ocean and atmospheric  $\text{CO}_2$  increase follow a similar curve.

<sup>f</sup> This chapter, from data of Battle *et al.* (1996).

<sup>g</sup> Updated calculation of Ciais *et al.* (1995b); Tans *et al.* (1989); Trolier *et al.* (1996) (no error bars given).

<sup>h</sup> Keeling and Piper (2000) (no error bars given).

<sup>i</sup> Orr *et al.* (2000), Orr and Dutay (1999).

<sup>j</sup> McGuire *et al.* (2001).

1999b), mainly due to the reduced upwelling of  $\text{CO}_2$ -rich waters (Archer *et al.*, 1996). The ocean response to El Niño in the most active region thus tends to increase global  $\text{CO}_2$  uptake, counter to the increasing atmospheric concentration. Although it cannot be ruled out that other ocean basins may play a significant role for global interannual variability in ocean-atmosphere flux, the existing oceanic measurements suggest (by default) that the response of the terrestrial biosphere is the cause of the typically high rates of  $\text{CO}_2$  increase during El Niño.

Associated variations in the north-south gradient of  $\text{CO}_2$  indicate that the El Niño  $\text{CO}_2$  anomalies originate in the tropics (Conway *et al.*, 1994; Keeling and Piper, 2000). Typical El Niño events are characterised by changed atmospheric circula-

tion and precipitation patterns (Zeng, 1999) that give rise to high tropical land temperatures (which would be expected to increase Rh and reduce NPP); concurrent droughts which reduce NPP, especially in the most productive regions such as the Amazon rain forest; and increased incidence of fires in tropical regions. Increased cloudiness associated with enhanced south-east Asian monsoons during the late phase of El Niño has also been suggested as a factor reducing global NPP (Yang and Wang, 2000). Typically, although not invariably, the rate of atmospheric  $\text{CO}_2$  increase declines around the start of an El Niño, then rapidly rises during the late stages (Elliott *et al.*, 1991; Conway *et al.*, 1994). It has been suggested that this pattern represents early onset of enhanced ocean  $\text{CO}_2$  uptake,

followed by reduced terrestrial CO<sub>2</sub> uptake or terrestrial CO<sub>2</sub> release (Feely *et al.*, 1987, 1999b; Rayner *et al.*, 1999b; Yang and Wang, 2000).

Atmospheric δ<sup>13</sup>C and, more recently, O<sub>2</sub> measurements have been used to partition the interannual variability of the atmospheric CO<sub>2</sub> increase into oceanic and terrestrial components. Analyses based on δ<sup>13</sup>C by Keeling *et al.* (1995) and Francey *et al.* (1995) reached contradictory conclusions, but the discrepancies are now thought to be due at least in part to δ<sup>13</sup>C measurement calibration problems during the 1980s, which have largely been resolved during the 1990s (Francey *et al.*, 1999a). For the 1990s, a range of analyses using different atmospheric observations and/or data analysis techniques estimate that the amplitude of annual peak to peak variation associated with the ocean is about 2 to 3 PgC/yr and the amplitude associated with the terrestrial biosphere is about 4 to 5 PgC/yr (Rayner *et al.*, 1999a; Joos *et al.*, 1999a; Battle *et al.*, 2000 (O<sub>2</sub>-based analysis); Keeling and Piper, 2000; Manning, 2001). A similar partitioning was estimated by Bousquet *et al.* (2000) based on the spatial pattern of CO<sub>2</sub> measurements using the approach described in the next section (3.5.3). However, the various reconstructed time sequences of terrestrial and ocean uptake differ in many details and do not provide conclusive evidence of the mechanisms involved.

The early 1990s were unusual in that the growth rate in atmospheric CO<sub>2</sub> was low (1.9 PgC/yr in 1992), especially in the Northern Hemisphere (Conway *et al.*, 1994), while an extended El Niño event occurred in the equatorial Pacific. Various mechanisms have been suggested, but none fully explain this unusual behavior of the carbon cycle. The slow down in the CO<sub>2</sub> increase has been linked to the predominantly mid- to high latitude cooling caused by the Pinatubo eruption (Conway *et al.*, 1994; Ciais *et al.*, 1995a,b; Schimel *et al.*, 1996), but there is no proof of any connection between these events. Other partial explanations could come from a temporary slow down of tropical deforestation (Houghton *et al.*, 2000), or natural decadal variability in the ocean-atmosphere or land-atmosphere fluxes (Keeling *et al.*, 1995). In any case, the slowdown proved to be temporary, and the El Niño of 1998 was marked by the highest rate of CO<sub>2</sub> increase on record, 6.0 PgC/yr.

### 3.5.3 Inverse Modelling of Carbon Sources and Sinks

Inverse modelling attempts to resolve regional patterns of CO<sub>2</sub> uptake and release from observed spatial and temporal patterns in atmospheric CO<sub>2</sub> concentrations, sometimes also taking into consideration O<sub>2</sub> and/or δ<sup>13</sup>C measurements. The most robust results are for the latitudinal partitioning of sources and sinks between northern and southern mid- to high latitudes and the tropics. The observed annual mean latitudinal gradient of atmospheric CO<sub>2</sub> concentration during the last 20 years is relatively large (about 3 to 4 ppm) compared with current measurement accuracy. It is however not as large as would be predicted from the geographical distribution of fossil fuel burning – a fact that suggests the existence of a northern sink for CO<sub>2</sub>, as already recognised a decade ago (Keeling *et al.*, 1989; Tans *et al.*, 1990; Enting and Mansbridge, 1991).

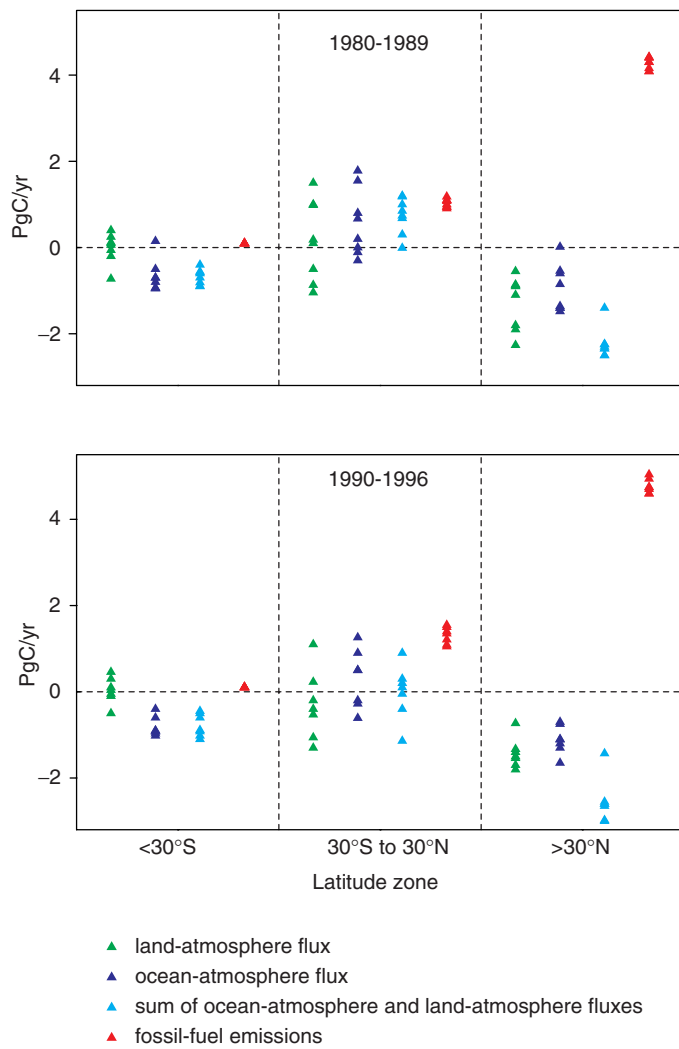


**Figure 3.5:** Inverse model estimates of fossil fuel CO<sub>2</sub> uptake by latitude bands according to eight models using different techniques and sets of atmospheric observations (results summarised by Heimann, 2001). Positive numbers denote fluxes to the atmosphere; negative numbers denote uptake from the atmosphere. The ocean-atmosphere fluxes represent mainly the natural carbon cycle; the land-atmosphere fluxes may be considered as estimates of the uptake of anthropogenic CO<sub>2</sub> by the land (with some caveats as discussed in the text). The sum of land-atmosphere and ocean-atmosphere fluxes is shown because it is somewhat better constrained by observations than the separate fluxes, especially for the 1980s when the measurement network was less extensive than it is today. The 1990s are represented by the period 1990 to 1996 only, because when this exercise was carried out the modelling groups did not have access to all of the necessary data for more recent years.

The nature of this sink, however, cannot be determined from atmospheric CO<sub>2</sub> concentration measurements alone. It might reflect, at least in part, a natural source-sink pattern of oceanic CO<sub>2</sub> fluxes (Keeling *et al.*, 1989; Broecker and Peng, 1992). This view is supported by the early atmospheric CO<sub>2</sub> data from the 1960s (Bolin and Keeling, 1963) which do not show a clear latitudinal gradient, despite the fact that at that time the fossil

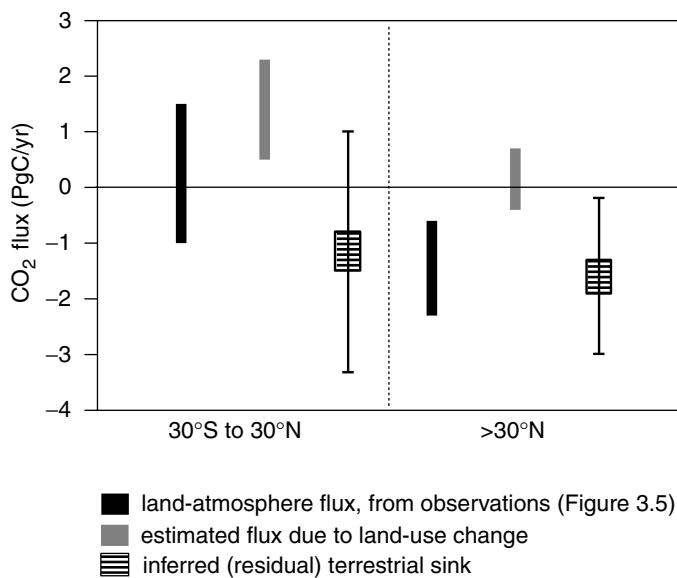


**Figure 3.6:** Partitioning the 1980s land-atmosphere flux for the tropics and the northern extratropics. The residual terrestrial sink in different latitude bands can be inferred by subtracting the land-use change flux for the 1980s (estimated by modelling studies: Houghton, 1999; Houghton and Hackler, 1999; Houghton *et al.*, 2000; McGuire *et al.*, 2001) from the net land-atmosphere flux as obtained from atmospheric observations by inverse modelling for the same period (Heimann, 2001; results from Figure 3.5). Positive numbers denote fluxes to the atmosphere; negative numbers denote uptake from the atmosphere. This calculation is analogous to the global budget calculation in Table 3.1, but now the model results are broken down geographically and the land-atmosphere fluxes are obtained by inverse modelling. The upper and lower bounds on the residual sink are obtained by pairing opposite extremes of the ranges of values accepted for the two terms in this calculation (for example, by subtracting the bottom of the range of values for land-use change with the top of the range for the land-atmosphere flux). The mid-ranges are obtained by combining similar extremes (for example, subtracting the bottom of the range for land-use change emissions from the bottom of the range land-atmosphere flux).

emissions were already at least half as large as in the 1990s. Quantitative analysis shows that the Northern Hemisphere sink has not changed much in magnitude since the 1960s (Keeling *et al.*, 1989; Fan *et al.*, 1999). On the other hand, the existing air-sea flux measurements do not support the idea of a large oceanic uptake of CO<sub>2</sub> in the Northern Hemisphere (Tans *et al.*, 1990; Takahashi, 1999). An alternative view, therefore, locates a significant fraction of this Northern Hemisphere sink on land. This view is corroborated, at least for the 1990s, by analyses of the concurrent latitudinal gradients of δ<sup>13</sup>C (Ciais *et al.*, 1995a,b) and O<sub>2</sub> (Keeling *et al.*, 1996b).

Results of analyses for the 1980s and 1990 to 1996, carried out by eight modelling groups using different atmospheric transport models, observational data, constraints and mathematical procedures, are summarised in Figure 3.5. Only the most robust findings, i.e., estimates of the mean carbon balance for three latitude bands averaged over the two time periods, are

shown. The latitude bands are: “southern extratropics” (>30°S), “tropics” (30°S to 30°N) and “northern extratropics” (>30°N). The carbon balance estimates are broken down into land and ocean compartments within each latitude band (Heimann, 2001).

Although the ranges of the estimates in Figure 3.5 limit the precision of any inference from these analyses, some clear features emerge. The inferred ocean uptake pattern shows the sum of two components: the natural carbon cycle in which CO<sub>2</sub> is outgassed in the tropics and taken up in the extratropics, and the perturbation uptake of anthropogenic CO<sub>2</sub>. Separation of these two components cannot be achieved from atmospheric measurements alone.

The estimates for the land, on the other hand, in principle indicate the locations of terrestrial anthropogenic CO<sub>2</sub> uptake (albeit with caveats listed below). For 1980 to 1989, the inverse-model estimates of the land-atmosphere flux are –2.3 to –0.6 PgC/yr in the northern extratropics and –1.0 to +1.5 PgC/yr in the tropics. These estimates imply that anthropogenic CO<sub>2</sub> was taken up *both* in the northern extratropics and in the tropics (balancing deforestation), as illustrated in Figure 3.6. The estimated land-atmosphere flux in the southern extratropics is estimated as close to zero, which is expected given the small land area involved. Estimates of CO<sub>2</sub> fluxes for the period 1990 to 1996 show a general resemblance to those for the 1980s. For 1990 to 1996, the inverse-model estimates of the land-atmosphere flux are –1.8 to –0.7 PgC/yr in the northern extratropics and –1.3 to +1.1 PgC/yr in the tropics. These results suggest a tendency towards a reduced land-atmosphere flux in the tropics, compared to the 1980s. Such a trend could be produced by reduced deforestation, increased CO<sub>2</sub> uptake or a combination of these.

Inverse modelling studies usually attempt greater spatial resolution of sources and sinks than is presented in this section. However, there are large unresolved differences in longitudinal patterns obtained by inverse modelling, especially in the northern hemisphere and in the tropics (Enting *et al.*, 1995; Law *et al.*, 1996; Fan *et al.*, 1998; Rayner *et al.*, 1999a; Bousquet *et al.*, 1999; Kaminski *et al.*, 1999). These differences may be traced to different approaches and several difficulties in inverse modelling of atmospheric CO<sub>2</sub> (Heimann and Kaminski, 1999):

- The longitudinal variations in CO<sub>2</sub> concentration reflecting net surface sources and sinks are on annual average typically <1 ppm. Resolution of such a small signal (against a background of seasonal variations up to 15 ppm in the Northern Hemisphere) requires high quality atmospheric measurements, measurement protocols and calibration procedures within and between monitoring networks (Keeling *et al.*, 1989; Conway *et al.*, 1994).
- Inverse modelling results depend on the properties of the atmospheric transport models used. The north-south transport of the models can be checked by comparing simulations of the relatively well-known inert anthropogenic tracer SF<sub>6</sub> with measured atmospheric concentrations of this tracer, as recently investigated in the TRANSCOM intercomparison project (Denning *et al.*, 1999). Unfortunately there is no currently

measured tracer that can be used to evaluate the models' representation of longitudinal transport. Furthermore, the strong seasonality of the terrestrial CO<sub>2</sub> flux in the Northern Hemisphere together with covarying seasonal variations in atmospheric transport may induce significant mean annual gradients in concentration which do not reflect net annual sources and sinks, but which nevertheless have to be modelled correctly if inverse model calculations are to be reliable (Bolin and Keeling, 1963; Heimann *et al.*, 1986; Keeling *et al.*, 1989; Denning *et al.*, 1995; Law *et al.*, 1996). Even the sign of this so-called "rectifier effect" is uncertain. Some scientists believe that it may be responsible for a part of the apparent Northern Hemisphere uptake of CO<sub>2</sub> implied by inverse modelling results (Taylor, 1989; Taylor and Orr, 2000).

- The spatial partitioning of CO<sub>2</sub> uptake could also be distorted by a few tenths of 1 PgC/yr because the atmospheric concentration gradients also reflect the natural fluxes induced by weathering, transport of carbon by rivers and subsequent outgassing from the ocean (see Figure 3.1) (Sarmiento and Sundquist, 1992; Aumont *et al.*, 2001b). Furthermore, the effects of atmospheric transport of carbon released as CO and CH<sub>4</sub> (especially from incomplete fossil fuel burning, tropical biomass burning, and CH<sub>4</sub> from tropical wetlands) with subsequent oxidation to CO<sub>2</sub> is generally neglected. Their inclusion in the inversion leads to corrections of the latitudinal partitioning of up to 0.1 PgC/yr (Enting and Mansbridge, 1991).
- The distribution of atmospheric CO<sub>2</sub> measurement stations (Figure 3.7) is uneven, and severely underrepresents the continents. This underrepresentation is due in part to the problem of finding continental locations where measurements will not be overwhelmed by local sources and sinks.
- Because of the finite number of monitoring stations, the mathematical inversion problem is highly underdetermined. In principle a multitude of different surface source/sink configurations are compatible with the atmospheric data, within their measurement accuracy. Therefore, in order to extract a meaningful solution, additional information on the sources and sinks has to be introduced into the calculation. Examples of this additional information include maps of air-sea fluxes from observations or ocean models, patterns of terrestrial CO<sub>2</sub> exchanges inferred by terrestrial models, and remote sensing data. Thus, many methodological choices about the use of auxiliary data can influence the outcome of the analysis.

Interannual variability of climate is likely to strongly influence the spatial distribution of CO<sub>2</sub> sources and sinks, so that analyses based on a few years of data are insufficient to establish a long-term trend.

In conclusion, the present atmospheric measurement network, current information on air-sea fluxes and current understanding of vertical atmospheric transport are not sufficient to allow full use of the potential of inverse modelling techniques to infer geographically detailed source-sink distributions of anthropogenic CO<sub>2</sub>.

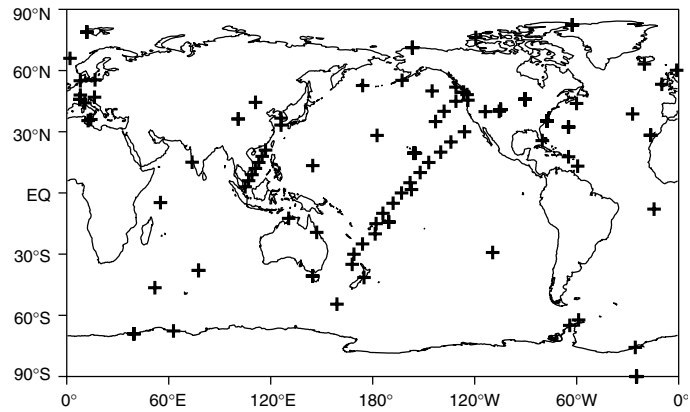


**Figure 3.7:** The atmospheric CO<sub>2</sub> measuring station network as represented by GLOBAL VIEW-CO<sub>2</sub> (Comparative Atmosphere Data Integration Project – Carbon Dioxide, NOAA/CMDL, <http://www.cmdl.noaa.gov/ccg/co2>).

### 3.5.4 Terrestrial Biomass Inventories

Inventory studies measure changes in carbon stocks over large areas, and can thus provide spatially aggregated estimates of large-scale fluxes of CO<sub>2</sub> over multi-annual time-scales (Box 3.1). Mid- and high latitude forests are covered by extensive national inventories based on repeated measurements of many thousands of plots. Inventories in the tropics are by comparison generally inadequate, particularly in view of the high rates of land-use change and extremely heterogeneous carbon density in many tropical ecosystems. There are still therefore large uncertainties in attempting to balance the terrestrial carbon budget on a global scale using inventory data.

The FAO Temperate and Boreal Forest Resource Assessment (TBFRA-2000) is a recent synthesis of inventories of forests and other wooded lands in Annex I (developed) countries for the early 1990s (UN-ECE/FAO, 2000). Many countries reported substantial increases in forest areas in recent years, as well as increasing carbon density in existing forests. According to TBFRA-2000, the land-atmosphere flux was -0.9 PgC/yr for all Annex I countries combined (the net annual increment of trees accounted for -1.5 PgC/yr, while losses due to fellings were 0.6 PgC/yr). Of this flux, -0.8 PgC/yr was due to uptake in "northern" forests (Europe, CIS, Japan and North America). An earlier review of individual regional and national studies by Dixon *et al.* (1994), highlighted in the IPCC WGII Second Assessment Report (IPCC, 1996b; Brown *et al.*, 1996), gave a range of -0.6 to -0.9 PgC/yr for the land atmosphere flux in northern forests. While TBFRA-2000 estimated biomass of woody vegetation only, the analyses reviewed in Dixon *et al.* (1994) included other vegetation, soils, litter and wood products. Under the United Nations Framework Convention for Climate Change (UNFCCC) signatory countries are required to report greenhouse gas emissions, including those from land-use change and forestry. Compilation of these data implies a land-atmosphere flux of -0.6 PgC/yr for all Annex I countries, and -0.6 PgC/yr for Annex I countries in the northern latitudes only (UNFCCC, 2000). While the TBFRA synthesised

country statistics and adjusted data to fit FAO definitions and methodologies for calculating carbon stocks, the UNFCCC report summarises emissions data reported by each country according to IPCC guidelines; interpretation of guidelines is variable, and not all countries had reported data on land use. The implications of definitions and methodologies in calculating carbon fluxes, particularly in relation to implementation of the Kyoto Protocol, is discussed in detail in the SRLULUCF (IPCC, 2000a).

A recent compilation of data from 478 permanent plots in mature tropical moist forests throughout the tropics over at least two decades found these were taking up carbon due to increasing rates of tree growth. Extrapolation from these plots led to an estimated land-atmosphere flux of  $(0.6 \pm 0.3)$  PgC/yr in Latin America; growth trends in African and Asian forests were not significantly different from zero (Phillips *et al.*, 1998). This net uptake is offset by emissions due to deforestation. Dixon *et al.* (1994) estimated tropical forests overall to be a net source of carbon with a land-atmosphere flux  $1.7 \pm 0.4$ , based mostly on FAO (1993b) inventory data and simple models of the effect of land-use change (Houghton, 1995). It will not be possible to assess trends and fluxes for the 1990s in the tropics from inventory data until a full data set is available from the FAO Global Forest Resources Assessment 2000. Among those countries that have reported land-use emissions data to the UNFCCC, there are significant discrepancies between the primary data used in emissions inventories and the data available in international surveys; for example, rates of deforestation differ from rates reported by FAO (1993b) by as much as a factor of six (Houghton and Ramakrishna, 1999).

The results of globally aggregated forest inventories show a greater uptake of carbon in forest growth than model-based calculations of the marginal effects of land-use change (e.g., Houghton, 2000). Thus, inventory studies provide independent evidence for the existence of a residual terrestrial sink; and they show that a substantial part of this sink, at least, is located in northern extratropical and tropical forests. Additional evidence from individual inventory studies in mature forests that have not undergone land-use changes shows that carbon stocks in such forests are increasing (e.g., Lugo and Brown, 1993; Phillips *et al.*, 1998; Schulze *et al.*, 1999). The difference between the northern extra-tropical land-atmosphere flux of around  $-0.8$  PgC/yr calculated by inventories (TBFRA-2000) and that of  $-0.1$  PgC/yr from land-use statistics (Houghton, 2000), both for the early 1990s, implies a residual terrestrial sink on the order of  $-0.7$  PgC/yr in northern mid- and high latitudes. Combining this with the estimated sink of  $-0.6$  PgC/yr in mature tropical moist forests (Phillips *et al.*, 1998) makes it plausible that at least a significant fraction of the current global terrestrial sink (Table 3.1) could be explained by an increase of carbon stocks in extant forests. The inventory-based estimate of land-atmosphere flux in northern forests ( $-0.8$  PgC/yr) is at the positive end of the range calculated by inverse modelling studies for the  $>30^\circ\text{N}$  latitude band from 1990 to 1996 ( $-1.8$  to  $-0.7$  PgC/yr, Section 3.5.3), either because of biases in inverse modelling that might tend to increase apparent uptake in the north (Section 3.5.3), or because possible sinks in other ecosys-

tems (e.g., temperate grassland soils) have not been considered in the inventories. In the tropics, the difference between the uptake of carbon estimated by inventory studies in mature forests of Latin America ( $-0.6$  PgC/yr) (Phillips *et al.*, 1998) and the estimated emissions due to deforestation in the tropics of  $1.7$  PgC/yr (Houghton, 2000) yields an estimated land-atmosphere flux of  $1.1$  PgC/yr, which is at the positive end of the range calculated by inverse modelling studies for  $30^\circ\text{S}$  to  $30^\circ\text{N}$  ( $-1.3$  to  $+1.1$  PgC/yr, Section 3.5.3). Again, it should be noted that possible additional sinks (e.g., in savannas) are neglected by the land-use and inventory-based calculations.

### 3.6 Carbon Cycle Model Evaluation

#### 3.6.1 Terrestrial and Ocean Biogeochemistry Models

The interactions of complex processes as discussed in Section 3.2 can be analysed with models that incorporate current knowledge at the process level, including syntheses of experimental results. Process-based models make it possible to explore the potential consequences of climate variability for the global carbon cycle, and to project possible future changes in carbon cycling associated with changes in atmospheric and ocean circulation. Models can be run with prescribed inputs such as observations of surface climate and CO<sub>2</sub> or the output of climate models. They can also be coupled to atmospheric general circulation models (Cox *et al.*, 2000; Friedlingstein *et al.*, 2000), to allow simulation of a wider range of interactions between climate and the carbon cycle.

Process-based terrestrial models used in carbon cycle studies are (a) terrestrial biogeochemical models (TBMs), which simulate fluxes of carbon, water and nitrogen coupled within terrestrial ecosystems, and (b) dynamic global vegetation models (DGVMs), which further couple these processes interactively with changes in ecosystem structure and composition (competition among different plant functional types; Prentice *et al.*, 2000). The treatment of carbon-nutrient interaction varies widely; for example, some models treat nitrogen supply explicitly as a constraint on NPP, while others do not. There are currently about 30 TBMs and <10 DGVMs. Cramer and Field (1999) and Cramer *et al.* (2001) reported results from intercomparisons of TBMs and DGVMs respectively. A current international project, Ecosystem Model/Data Intercomparison (EMDI), aims to test models of both types against a large set of terrestrial measurements, in order to better constrain the modelled responses of terrestrial carbon cycling to changes in CO<sub>2</sub> and climate.

Process-based ocean models used in carbon cycle studies include surface exchange of CO<sub>2</sub> with the atmosphere, carbon chemistry, transport by physical processes in the ocean, and transport by marine biology. The parametrization of marine biology can be classified as (a) nutrient-based models where the export of carbon below the surface ocean (approximately the top 50 m) is a function of surface nutrient concentration, (b) nutrient-restoring models in which biological carbon fluxes are set to the rates required for maintaining observed nutrient concentration gradients against dissipation by ocean mixing, and (c) models that explicitly represent the food chain involving nutrients, phytoplankton, zooplankton and detritus (NPZD models). In

current models, the uptake of anthropogenic CO<sub>2</sub> is controlled mainly by physical transport and surface carbon chemistry, whereas the natural carbon cycle is controlled by physical, chemical and biological processes. The Ocean Carbon Cycle Model Intercomparison Project (OCMIP) compared the performance of four ocean models with respect to natural and anthropogenic tracers (Sarmiento *et al.*, 2000; Orr *et al.*, 2001), and is currently undergoing a similar comparison with 13 models and an extended data set (Orr and Dutay, 1999).

### 3.6.2 Evaluation of Terrestrial Models

Evaluation of terrestrial carbon cycle models requires different types of data to test processes operating on a range of time-scales from hours to centuries (see Section 3.2.2), including short-term environmental responses of CO<sub>2</sub> and water fluxes between vegetation canopies and the atmosphere (e.g., Cienciala *et al.*, 1998), responses of ecosystem carbon balance to interannual climate variability (e.g. Kindermann *et al.*, 1996; Heimann *et al.*, 1997; Gérard *et al.*, 1999; Knorr, 2000; Prentice *et al.*, 2000), and longer-term consequences of historical land-use change (McGuire *et al.*, 2001). Differences and uncertainties in model behaviour have been evaluated through model intercomparison (Cramer *et al.*, 1999, 2001) and sensitivity analyses (Knorr, 2000; Knorr and Heimann, 2001a).

#### 3.6.2.1 Natural carbon cycling on land

Terrestrial model evaluation has traditionally been carried out as comparisons with *in situ* field observations of ecosystem variables (e.g., Raich *et al.*, 1991; Foley, 1994; Haxeltine and Prentice, 1996). The largest data sets of relevant field measurements are for NPP and soil carbon content. Other “target” variables include soil moisture, nitrogen mineralisation rate, and the amounts of carbon and nitrogen in different compartments of the ecosystem. Such comparisons have generally shown reasonable agreement between observed and modelled geographic patterns of these variables, but they do not test the time-dependent response of models to environmental variability.

Time-dependent data sets for *in situ* comparisons are now becoming available, thanks to eddy-covariance measurements of CO<sub>2</sub> fluxes (Section 3.2.2.1; Box 3.1). Daily and seasonal cycles of CO<sub>2</sub> and water fluxes provide a test of the coupling between the carbon and hydrological cycles as simulated by terrestrial models (Cienciala *et al.*, 1998). Flux measurements are now being carried out on a multi-annual basis at an increasing number of stations, although global coverage remains uneven, with the greatest concentration in Europe and North America and few measurements from the tropics (see Box 3.1). Field campaigns have started to retrieve flux data from more remote regions (e.g., Schulze *et al.*, 1999). The Large-scale Biosphere Atmosphere Experiment in Amazonia, LBA, will yield more comprehensive data on the carbon, water and energy exchanges of tropical terrestrial ecosystems and will allow a more rigorous evaluation of the performance of models in the tropics than has been possible up until now (e.g., Tian *et al.*, 1998). As current models show conflicting

responses of global NPP to climate (Cramer *et al.*, 1999), systematic comparisons with seasonal and interannual flux measurements are a priority to reduce uncertainties in terrestrial carbon modelling.

Terrestrial models have also been evaluated at a global scale by comparing simulated ecosystem water balance with river runoff (e.g., Neilson and Marks, 1994; Foley *et al.*, 1996; Kucharik *et al.*, 2000), and simulated seasonal leaf area with satellite observations of “greenness”, often based on the normalised difference vegetation index (NDVI) (Field *et al.*, 1995b; de Fries *et al.*, 1995). NDVI data can be translated into estimates of the plant-absorbed fraction of incoming photosynthetically active radiation (FPAR) (Asrar *et al.*, 1992), which is related to leaf area index (LAI). The first terrestrial model intercomparison showed differences among model simulations of LAI and its seasonality (Bondeau *et al.*, 1999). More recently, it has been shown that constraining a terrestrial model with remotely sensed spatial patterns of FPAR can lead to a reduction of uncertainty in NPP simulations by about one third (Knorr and Heimann, 2001b). Agreement with patterns of remotely sensed FPAR has thus become a standard benchmark for terrestrial models (Haxeltine and Prentice, 1996; Kucharik *et al.*, 2000) and attention has been focused on improving the simulation of LAI and its seasonal variations.

A more direct test of the simulated net exchange of CO<sub>2</sub> between the terrestrial biosphere and the atmosphere is provided by comparison with atmospheric CO<sub>2</sub> measurements at remote monitoring sites. The comparison requires the use of an atmospheric transport model to simulate CO<sub>2</sub> as a passive tracer (Kaminski *et al.*, 1996). The seasonal cycle of atmospheric CO<sub>2</sub> shows a strong latitudinal pattern in amplitude and phase, and is dominated by the terrestrial biosphere (Heimann *et al.*, 1998). The ability to simulate this seasonal cycle thus constitutes a benchmark for terrestrial models’ response to climate (Denning *et al.*, 1996; Hunt *et al.*, 1996; Heimann *et al.*, 1998; Nemry *et al.*, 1999). Generally, the observed seasonal cycles of CO<sub>2</sub> in northern and tropical latitudes can be well simulated, with terrestrial models using NDVI data as input (Knorr and Heimann, 1995), or by fully prognostic models, including DGVMs (Prentice *et al.*, 2000).

Major features of interannual variability of the CO<sub>2</sub> increase are also simulated by terrestrial models (Kindermann *et al.*, 1996; Heimann *et al.*, 1997; Gérard *et al.*, 1999; Ito and Oikawa, 2000; Knorr, 2000; Prentice *et al.*, 2000). This finding supports the hypothesis (Section 3.5.2) that terrestrial effects are important in determining the interannual variability of CO<sub>2</sub> uptake. During typical El Niño events, terrestrial model results consistently show strongly reduced CO<sub>2</sub> uptake or CO<sub>2</sub> release by the land. This result has been obtained with a range of models, even when the models differ substantially in the relative sensitivities of NPP and heterotrophic respiration to temperature (Heimann *et al.*, 1997; Knorr, 2000). The low CO<sub>2</sub> growth rate during the early 1990s has been simulated by some terrestrial models (Prentice *et al.*, 2000; Knorr, 2000).

At the longest time-scales of interest, spanning the industrial period, models of the natural terrestrial carbon cycle show a pronounced response to rising atmospheric CO<sub>2</sub> levels

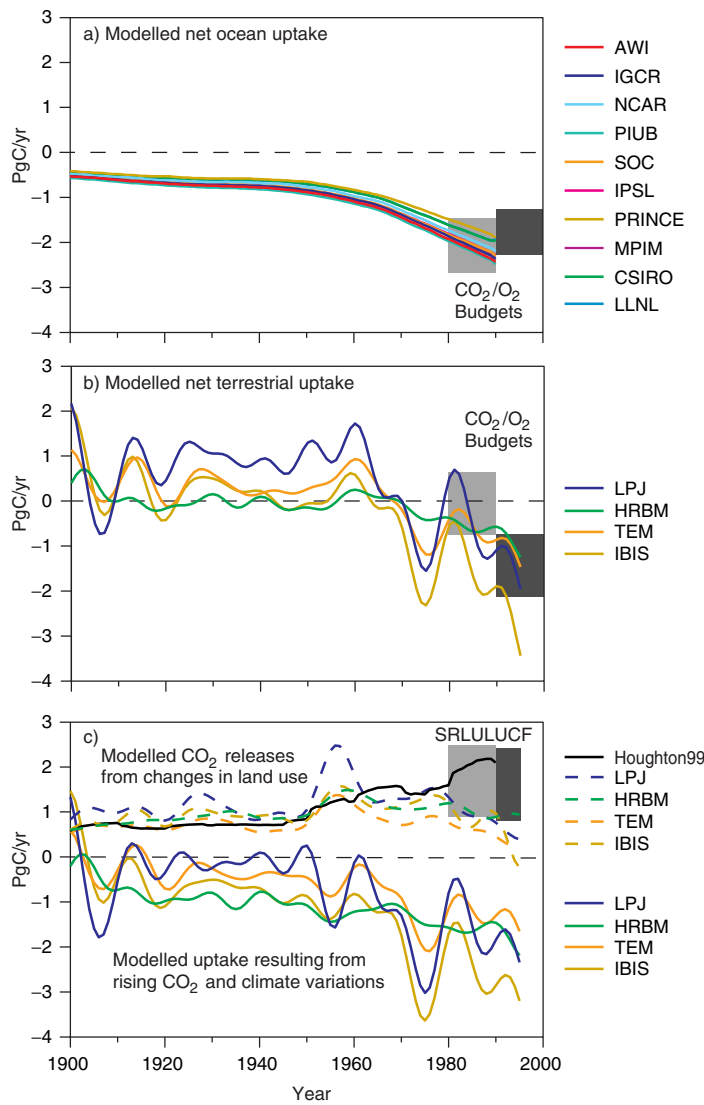


**Figure 3.8:** Modelled fluxes of anthropogenic CO<sub>2</sub> over the past century. (a) Ocean model results from OCMIP (Orr and Dutay, 1999; Orr *et al.*, 2000); (b), (c) terrestrial model results from CCMLP (McGuire *et al.*, 2001). Positive numbers denote fluxes to the atmosphere; negative numbers denote uptake from the atmosphere. The ocean model results appear smooth because they contain no interannual variability, being forced only by historical changes in atmospheric CO<sub>2</sub>. The results are truncated at 1990 because subsequent years were simulated using a CO<sub>2</sub> concentration scenario rather than actual measurements, leading to a likely overestimate of uptake for the 1990s. The terrestrial model results include effects of historical CO<sub>2</sub> concentrations, climate variations, and land-use changes based on Ramankutty and Foley (2000). The results were smoothed using a 10-year running mean to remove short-term variability. For comparison, grey boxes denote observational estimates of CO<sub>2</sub> uptake by the ocean in panel (a) and by the land in panel (b) (from Table 3.1). Land-use change flux estimates from Houghton *et al.* (1999) are shown by the black line in panel (c). The grey boxes in panel (c) indicate the range of decadal average values for the land-use change flux accepted by the SRLULUCF (Bolin *et al.*, 2000) for the 1980s and for 1990 to 1995.

as a result of CO<sub>2</sub> fertilisation, generally larger than the NPP response to the climate change over this period (Kicklighter *et al.*, 1999). According to CCMLP results, the CO<sub>2</sub> increase maintains a lead of NPP over Rh and an increase of the amplitude of the seasonal CO<sub>2</sub> cycle (McGuire *et al.*, 2001), consistent with long-term observations (Keeling *et al.*, 1996a), which indicate an increase in amplitude of about 20% since accurate atmospheric measurements began. However, the magnitude of this effect was greatly over- or under estimated by some models, reflecting unresolved differences in the parameterization of the CO<sub>2</sub> fertilisation response.

### 3.6.2.2 Uptake and release of anthropogenic CO<sub>2</sub> by the land

The most comprehensive model-based estimates of the terrestrial components of the anthropogenic CO<sub>2</sub> budget are those that have been produced by the CCMLP. McGuire *et al.* (2001) used two TBMs and two DGVMs driven by changes in atmospheric CO<sub>2</sub>, then changes in CO<sub>2</sub> with historical changes in climate (from observations), and finally changes in CO<sub>2</sub> and climate with land-use change from Ramankutty and Foley (2000) (Figure 3.8; Table 3.4). In these simulations, CO<sub>2</sub> fertilisation accounted for a land-atmosphere flux of -0.9 to -3.1 PgC/yr, land-use change a positive flux of 0.6 to 1.0 PgC/yr, and climate variability a small additional effect of uncertain sign, -0.2 to 0.9 PgC/yr during the 1980s. The total land-atmosphere flux simulated for the 1980s amounted to -0.3 to -1.5 PgC/yr, which is consistent with or slightly more negative than the observationally-based estimate of  $-0.2 \pm 0.7$  PgC/yr (Table 3.1). Net uptake by all models reported in McGuire *et al.* (2001) is shown to be occurring mainly in tropical, temperate and boreal forests – consistent with forest inventory data (Section 3.5.4) – while some regions (notably semi-arid tropical and sub-tropical regions) show net carbon loss. The model estimates of the CO<sub>2</sub> source due to land-use change are substantially smaller than the estimate of Houghton (1999) (Section 3.4.2). This divergence primarily reflects disagreements between the Houghton (1999) and Ramankutty and Foley (2000) data sets as to the timing of tropical deforestation in different regions (see Section 3.4.2).

There is no general agreement on how to model the linkage between reactive nitrogen deposition and vegetation productivity, and recent model estimates of the additional effect of anthropogenic nitrogen fertilisation on the global carbon cycle vary widely. The anthropogenic nitrogen input itself (Holland *et al.*, 1999), the fate of anthropogenic nitrogen in the ecosystem (Nadelhoffer *et al.*, 1999; Jenkinson *et al.*, 1999), and changes in ecosystem nitrogen fixation (Vitousek and Field, 1999) represent major sources of uncertainty. Estimates of the anthropogenic nitrogen effect range from -0.2 PgC/yr (Nadelhoffer *et al.*, 1999) to -1.1 or -1.4 PgC/yr (Holland *et al.*, 1997). The model with the smallest CO<sub>2</sub> fertilisation effect (-0.9 PgC/yr) in the McGuire *et al.* (2001) study has been shown to respond strongly to anthropogenic nitrogen input, yielding a combined (CO<sub>2</sub> and nitrogen) fertilisation effect of -1.5 PgC/yr. A modelling study by Lloyd (1999) suggests that CO<sub>2</sub> and nitrogen fertilisation effects may be synergistic. Evaluation of model results on carbon-nitrogen coupling against experimental results is a current research focus.

### 3.6.3 Evaluation of Ocean Models

Natural and anthropogenic tracers have been extensively measured, most recently as part of the Joint Global Ocean Flux Study (JGOFS) and World Ocean Circulation Experiment (WOCE). Because of these measurement campaigns, such tracers provide important opportunities to evaluate representations of ocean physics and biogeochemistry in models.

#### 3.6.3.1 Natural carbon cycling in the ocean

Most global ocean models of the carbon cycle are successful in reproducing the main vertical and horizontal features of ocean carbon content (Maier-Reimer, 1993; Aumont, 1998; Murnane *et al.*, 1999). The observed features reasonably reproduced by all ocean models are the mean vertical gradient in DIC, with enriched deep ocean concentrations (Goyet and Davies, 1997), and the spatial patterns of surface  $p\text{CO}_2$  with outgassing in the tropics and uptake at higher latitudes (Takahashi *et al.*, 1999). Furthermore, models which incorporate marine biology (including DOC and plankton dynamics) roughly reproduce the seasonal cycle of surface ocean  $p\text{CO}_2$ , atmospheric  $\text{O}_2$  after it has been corrected for seasonal land variability, and surface chlorophyll (Six and Maier-Reimer, 1996; Stephens *et al.*, 1998; Aumont *et al.*, 2001a). Ocean carbon models can also roughly reproduce the phase and amplitude of interannual variability of ocean  $p\text{CO}_2$  in the equatorial Pacific (Winguth *et al.*, 1994; Le Quéré *et al.*, 2000) in agreement with available observations (Feely *et al.*, 1997; 1999b; Boutin *et al.*, 1999).

Although many first-order features can be reproduced by global models, there are still important aspects of the ocean carbon cycle that are not well simulated, because either marine biology or ocean physics are imperfectly reproduced. Ocean carbon models have difficulties in reproducing the spatial structure of the deep ocean  $^{14}\text{C}$  (Orr *et al.*, 2001), which suggests problems in simulating the physical exchange of carbon between surface and the deep ocean. Models display their largest disagreements where fewest observations exist, in particular in the important region of the Southern Ocean where the mixing of tracers is subject to large uncertainties (Caldeira and Duffy, 2000; Sarmiento *et al.*, 2000; Orr *et al.*, 2001). In spite of these differences, all ocean carbon models estimate zero interhemispheric transport of carbon (Sarmiento *et al.*, 2000) whereas a transport as large as 1 PgC/yr has been inferred from atmospheric  $\text{CO}_2$  measurements (Keeling *et al.*, 1989). Consideration of the global transport of carbon by rivers reduces the discrepancy but does not remove it (Sarmiento and Sundquist, 1992; Aumont *et al.*, 2001b). Atmospheric  $\text{CO}_2$  and  $\text{O}_2$  measurements suggest that interhemispheric transport may be incorrectly simulated by ocean models (Stephens *et al.*, 1998), and could hint at difficulties in modelling heat transport (Murnane *et al.*, 1999). Recent data from the Southern Ocean, however, seem closer to model results (Stephens, 1999) and the question about interhemispheric transport thus remains open. These problems could partly be resolved by a better representation of the physical transport of carbon in the ocean, especially isopycnal diffusion, sub-grid eddy mixing, and sea-ice formation (Stephens *et al.*, 1999).

Three common problems related to marine biology in global ocean models are discussed here. First, most models poorly represent the formation and dissolution of  $\text{CaCO}_3$ , which controls alkalinity. This process is often parameterized as a function of direct or indirect observations (salinity, temperature, nutrients). Although correct for the present day ocean, this parametrization may not hold for past or future conditions with different ocean circulation and surface water fluxes. The alkalinity cycle is difficult to represent because the rate of  $\text{CaCO}_3$  formation derived from observations is consistently larger than the one required by models for reproducing observed deep ocean alkalinity (Maier-Reimer, 1993; Yamanaka and Tajika, 1996). Second, marine productivity tends to be underestimated by models in sub-tropical regions and overestimated in the equatorial oceans and at high latitudes in the North Pacific and Southern Oceans. The overestimation may be caused by limitation in plankton growth by iron (Coale *et al.*, 1996; Boyd *et al.*, 2000; Archer and Johnson, 2000), while underestimation in the sub-tropics partly stems from neglecting mesoscale variability (McGillicuddy and Robinson, 1997; Oschlies and Garçon, 1998). The remaining discrepancies might be attributed in part to more complex processes involving nitrogen fixation (Karl *et al.*, 1997). Finally, the tight coupling between carbon and either nitrogen or phosphate, which is generally implicit in ocean carbon models, precludes the simulation of past or future marine biological feedback mechanisms that involve a partial decoupling between carbon and nutrients (see Section 3.2.3).

#### 3.6.3.2 Uptake of anthropogenic $\text{CO}_2$ by the ocean

Ocean uptake is constrained to some degree by observations of anthropogenic tracers. Three transient tracers are commonly used. First, anthropogenic  $\text{CO}_2$  itself gives a direct benchmark for model estimates of the quantity and distribution of anthropogenic  $\text{CO}_2$  that has penetrated the ocean since the pre-industrial era. Anthropogenic  $\text{CO}_2$  can be inventoried by an indirect method whereby carbon concentration is compared to what would be expected from water exposed to pre-industrial air (Gruber *et al.*, 1996). The  $^{14}\text{CO}_2$  released in the early 1960s by atmospheric nuclear testing (commonly called bomb  $^{14}\text{C}$ ) provides a second tracer; the content of bomb  $^{14}\text{C}$  in the ocean is used to constrain global air-sea  $\text{CO}_2$  exchange (Wanninkhof *et al.*, 1992), and ocean model results can be compared with its penetration depth as a benchmark for vertical transport (Broecker *et al.*, 1995). Bomb  $^{14}\text{C}$  is computed by subtracting the observed  $^{14}\text{C}$  concentration from an estimate of its pre-industrial value (Broecker *et al.*, 1995). Finally, CFCs also constrain the downward transport of tracers in ocean models. No natural background needs to be subtracted from CFCs. None of these three tracers provide a perfect indicator of anthropogenic  $\text{CO}_2$  uptake:  $\text{CO}_2$  equilibrates with the atmosphere ten times faster than  $^{14}\text{C}$  and ten times slower than CFCs; anthropogenic  $\text{CO}_2$  and  $^{14}\text{C}$  are indirectly estimated. As part of the Ocean Carbon-Cycle Model Intercomparison Project (OCMIP), a comparison of carbon models with respect to all three anthropogenic tracers is in progress (Orr and Dutay, 1999; Orr *et al.*, 2001).

Although regional estimates show discrepancies, modelled estimates of anthropogenic tracers agree reasonably well with observations when integrated globally. The mean value of the penetration depth of bomb  $^{14}\text{C}$  for all observational sites during

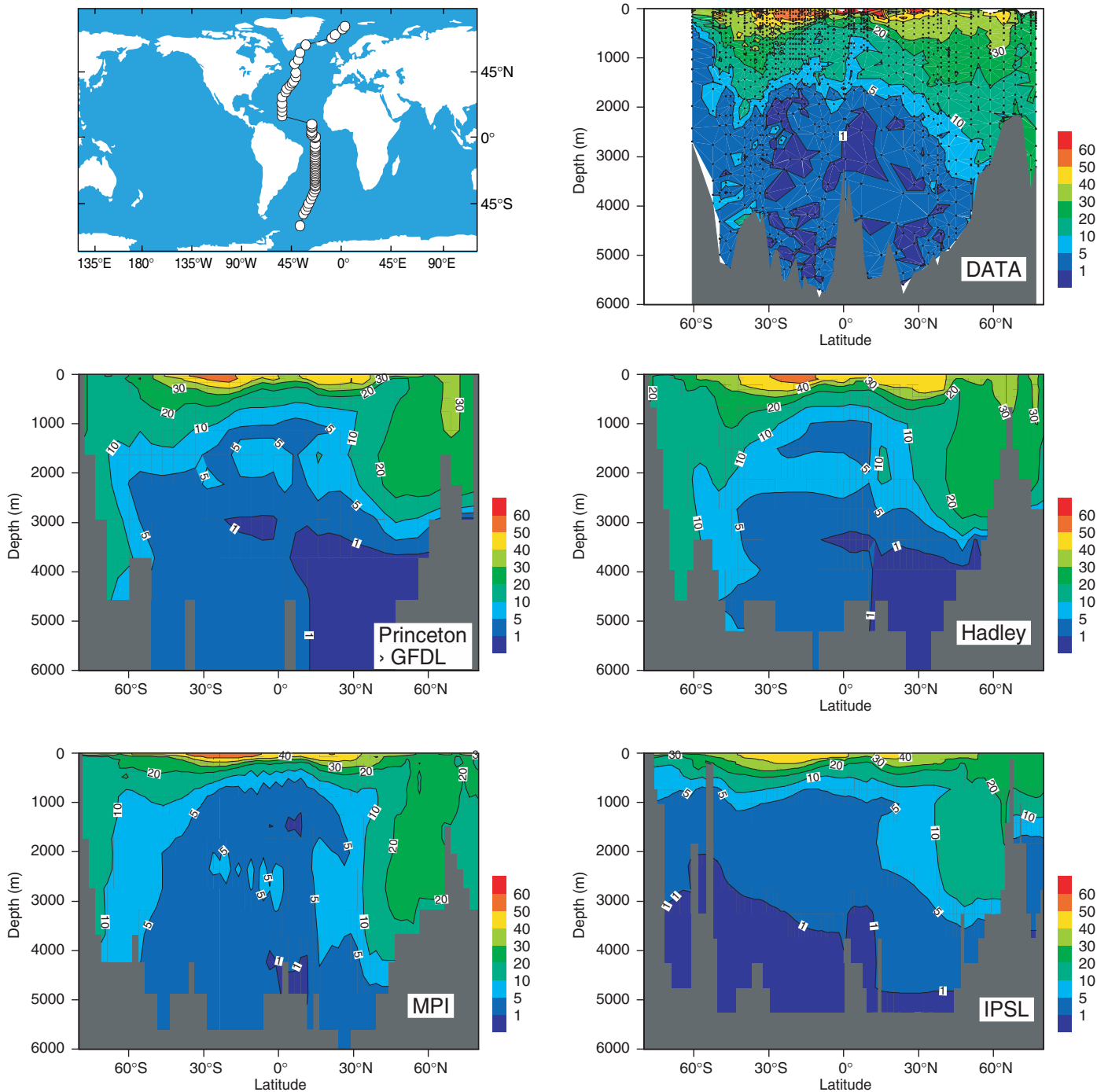


**Figure 3.9:** Anthropogenic CO<sub>2</sub> in the Atlantic Ocean (μmol/kg): comparison of data and models. The top left panel shows the sampling transect; the top right panel shows estimates of anthropogenic CO<sub>2</sub> content along this transect using observations from several cruises between 1981 and 1989 (Gruber, 1998). Anthropogenic CO<sub>2</sub> is not measured directly but is separated from the large background of oceanic carbon by an indirect method based on observations (Gruber *et al.*, 1996). The remaining panels show simulations of anthropogenic CO<sub>2</sub> content made with four ocean carbon models forced by the same atmospheric CO<sub>2</sub> concentration history (Orr *et al.*, 2000).

the late 1970s is  $390 \pm 39$  m (Broecker *et al.*, 1995). For the same years and stations, modelled estimates range between 283 and 376 m (Orr *et al.*, 2001). Modelled and observed CFC concentrations have been compared locally but not yet globally (England 1995; Robitaille and Weaver, 1995; Orr and Dutay, 1999). Modelled anthropogenic CO<sub>2</sub> inventory since 1800 is

comparable to the estimate of  $40 \pm 9$  PgC for the Atlantic Ocean (Gruber, 1998) and  $20 \pm 3$  PgC for the Indian Ocean (Sabine *et al.*, 1999; Orr *et al.*, 2001). Latitude-depth profiles of anthropogenic CO<sub>2</sub> in the Atlantic, extracted from data and from models, are shown in Figure 3.9. Modelled CO<sub>2</sub> uptake for the global ocean between 1800 and 1990 ranges between 100 and

133 PgC (Figure 3.8), comparable to the preliminary data-based estimate of  $107 \pm 27$  PgC for the global ocean, which includes the Pacific value of  $45 \pm 15$  PgC (Feely *et al.*, 1999a). Although in reasonable agreement with basin and global estimates of anthropogenic CO<sub>2</sub>, modelled inventories exhibit large differences at the regional scale: models tend to underestimate the inventory of anthropogenic CO<sub>2</sub> between 50°S and 50°N in the Atlantic and Indian Oceans, and to overestimate it at high latitudes (Sabine *et al.*, 1999; Orr *et al.*, 2001). In the Southern Ocean the uptake of anthropogenic CO<sub>2</sub> varies by a factor of two among models (Orr *et al.*, 2001). The difficulty for models in reproducing the spatial structure of anthropogenic tracers may be indicative of problems in ocean physics mentioned earlier, and may be responsible for the increasing range of model estimates when future CO<sub>2</sub> uptake is projected by the same models (Figure 3.10c).

The most recent model estimates of the ocean-atmosphere flux obtained with process-based models are  $-1.5$  to  $-2.2$  for 1980 to 1989 (Table 3.4), in agreement with earlier model estimates for the same period (Enting *et al.*, 1994; Orr *et al.*, 2001). These estimates are fully consistent with the budget based on atmospheric observations alone (Table 3.1), with estimates based on  $p\text{CO}_2$  and  $\delta^{13}\text{C}$  observations (Table 3.4), and with the SAR estimate of  $-2.0 \pm 0.8$  PgC/yr. Figure 3.8 shows modelled ocean CO<sub>2</sub> uptake for 1900 to 2000. (These results do not include natural variability and therefore appear smoother than in reality.) The oceanic regions absorbing the largest quantities of anthropogenic CO<sub>2</sub> according to models are those where older waters come in contact with the atmosphere, such as high latitudes and upwelling regions of the equator. In contrast, modelled sub-tropical regions rapidly saturate at atmospheric CO<sub>2</sub> level and do not absorb large quantities of anthropogenic CO<sub>2</sub> (Sarmiento *et al.*, 1992; Orr *et al.*, 2001).

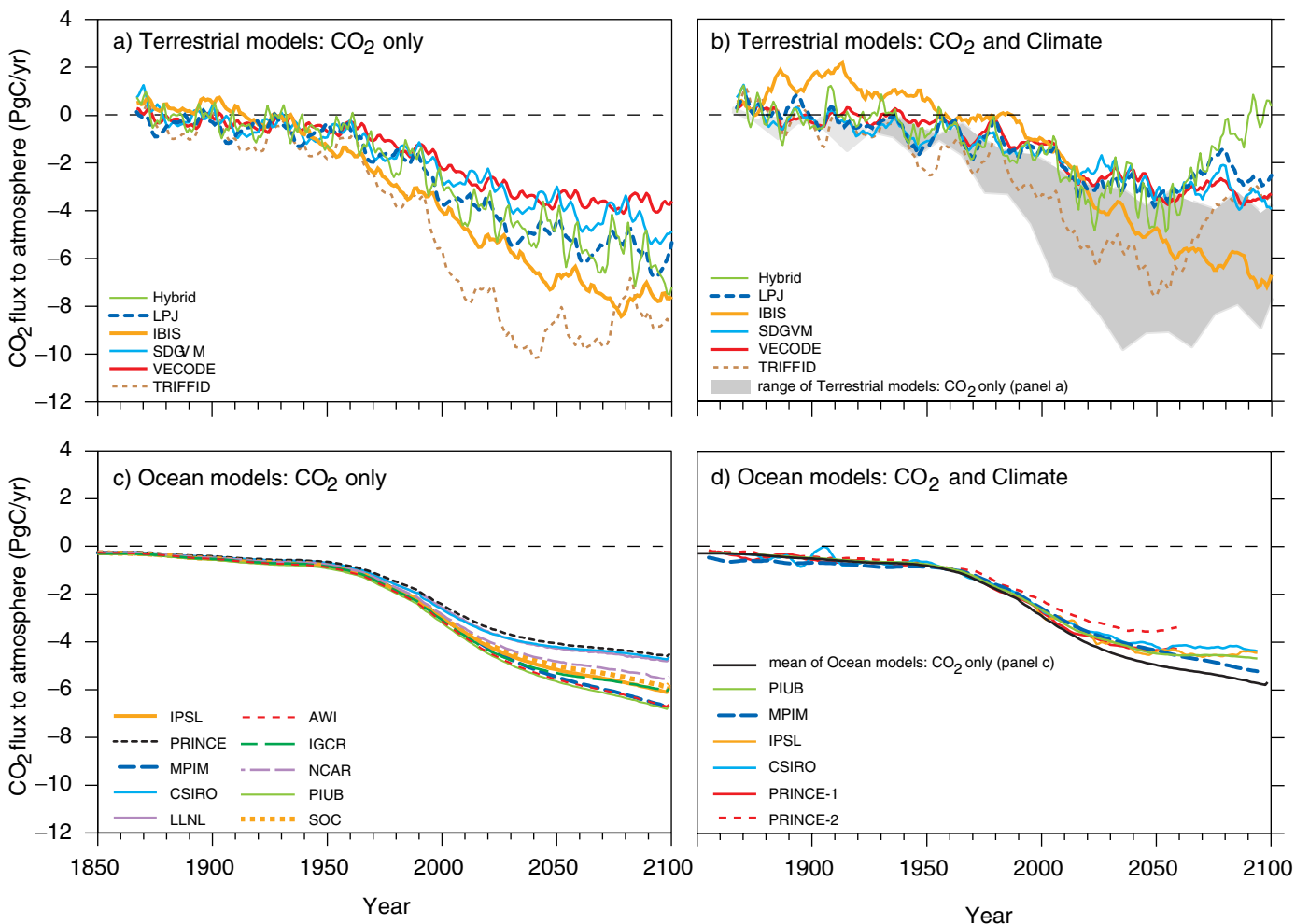


**Figure 3.10:** Projections of anthropogenic CO<sub>2</sub> uptake by process-based models. Six dynamic global vegetation models were run with IS92a CO<sub>2</sub> concentrations as given in the SAR: (a) CO<sub>2</sub> only, and (b) with these CO<sub>2</sub> concentrations plus simulated climate changes obtained from the Hadley Centre climate model with CO<sub>2</sub> and sulphate aerosol forcing from IS92a (Cramer *et al.*, 2000). Panel (b) also shows the envelope of the results from panel (a) (in grey). (c) Ten process-based ocean carbon models were run with the same CO<sub>2</sub> concentrations, assuming a constant climate (Orr and Dutay, 1999; Orr *et al.*, 2000). A further six models were used to estimate the climate change impact on ocean CO<sub>2</sub> uptake as a proportional change from the CO<sub>2</sub>-only case. The resulting changes were imposed on the mean trajectory of the simulations shown in panel (c), shown by the black line in panel (d), yielding the remaining trajectories in panel (d). The range of model results in panel (d) thus represents only the climate change impact on CO<sub>2</sub> uptake; the range does not include the range of representations of ocean physical transport, which is depicted in panel (c).

### 3.7 Projections of CO<sub>2</sub> Concentration and their Implications

#### 3.7.1 Terrestrial Carbon Model Responses to Scenarios of Change in CO<sub>2</sub> and Climate

Possible feedbacks from terrestrial carbon cycling to atmospheric CO<sub>2</sub> were assessed using multiple models by Cramer *et al.* (2001). Six DGVMs (Figure 3.10a) (Foley *et al.*, 1996; Brovkin *et al.*, 1997; Friend *et al.*, 1997; Woodward *et al.*, 1998; Huntingford *et al.*, 2000; Sitch, 2000) were driven first by CO<sub>2</sub> concentrations derived from the IS92a emissions scenario as in the SAR, and then with CO<sub>2</sub> changes plus climate changes derived from the HadCM2 coupled ocean-atmosphere general circulation model simulation including sulphate aerosol effects as described by Mitchell *et al.* (1995). Except for one empirical model (VECODE; Brovkin *et al.*, 1997), the models included explicit representation of all the following processes: the CO<sub>2</sub> fertilisation effect on NPP (modelled explicitly in terms of photosynthesis, respiration, and feedbacks associated with carbon allocation); responses of NPP to climate specific to each plant functional type (PFT); competition among PFTs for light and water; dynamic shifts in vegetation structure due to climate and CO<sub>2</sub> effects; competitive limits to above-ground biomass; natural disturbance regimes and their interaction with PFT composition; soil temperature and moisture effects on heterotrophic respiration. Two models include an interactive N cycle. Land use and anthropogenic N deposition were not considered.

Driven by increases in CO<sub>2</sub> beyond the present day, the modelled sink due to CO<sub>2</sub> fertilisation continued to increase. By the middle of the 21st century the simulated land-atmosphere flux due to CO<sub>2</sub> was in the range -8.7 to -3.6 PgC/yr. Beyond mid-century the rate of increase became less, due to the declining photosynthetic response to CO<sub>2</sub>. When the climate change scenario was included as well as the CO<sub>2</sub> increase, modelled uptake was reduced compared with the CO<sub>2</sub>-only analysis. At mid-century, climate change reduced the uptake by 21 to 43%. A marked decline in terrestrial uptake after the mid-century was seen in two models, and one model had zero terrestrial uptake by 2100. By 2100 the range of model estimates of the land-atmosphere flux had widened to -6.7 to +0.4 PgC/yr. Increasing heterotrophic respiration in response to warming (Cao and Woodward, 1998a,b; Cramer *et al.*, 2001) was a common factor (but not the only one) leading to reduced land uptake. The differences among the modelled climate responses were largely due to unresolved discrepancies in the response of global NPP to temperature. The balance of positive versus negative regional effects of climate change on NPP was estimated differently by these models, to the extent that the sign of the global response of NPP to climate change alone was not consistent. In addition, one model simulated a partial replacement of the Amazon rainforest by C<sub>4</sub> grassland. This response was not shown, or occurred on a much smaller scale, in the other models. The details of this modelling exercise are presumably dependent on sensitivity of the particular climate model, and regional aspects of the simulated climate change (Cramer *et al.*, 2001).

#### 3.7.2 Ocean Carbon Model Responses to Scenarios of Change in CO<sub>2</sub> and Climate

Analogous simulations have been performed with several ocean carbon models (Figure 3.10c,d). To compute the impact of increasing CO<sub>2</sub> alone (no climate change), OCMIP models were forced to follow the atmospheric CO<sub>2</sub> concentration derived from the IS92a scenario as in the DGVM experiment (Figure 3.10a,b) (Orr and Dutay, 1999). All models agreed in projecting that the annual ocean-atmosphere flux of CO<sub>2</sub> continues to become larger, reaching -6.7 to -4.5 PgC/yr by 2100 (Figure 3.10c). Since surface conditions (temperature, wind speed, alkalinity) were prescribed, the range in model estimates stems only from different representations of physical transport processes.

Several atmosphere-ocean models were used to project the effect of climate change (Maier-Reimer *et al.*, 1996; Sarmiento *et al.*, 1998; Matear and Hirst, 1999; Joos *et al.*, 1999b; Bopp *et al.*, 2001). These models include most processes previously discussed, including all processes associated with carbonate chemistry and gas exchange, physical and biological transport of CO<sub>2</sub>, and changes in temperature, salinity, wind speed, and ice cover. They account for simple changes in biological productivity, but not for changes in external nutrient supply, species composition, pH, or Redfield ratios, all of which could be involved in more complex biological feedbacks. Coupled models estimate the impact of climate change as a departure, reported in per cent, from a "control" experiment modelling the effect of increasing atmospheric CO<sub>2</sub> alone.

In climate change simulations, warming of surface waters and increased stratification of the upper ocean produced an overall positive feedback that reduced the accumulated ocean uptake of CO<sub>2</sub> by 6 to 25% between 1990 and the middle of the 21st century, as compared with the CO<sub>2</sub>-only case. In the first part of the simulation, the climate-mediated feedback is mainly due to the temperature effect on CO<sub>2</sub> solubility (Sarmiento and Le Quéré, 1996; Matear and Hirst, 1999). Towards the mid-century, the impact of circulation changes becomes significant in most models, with the net effect of further reducing ocean CO<sub>2</sub> uptake. To investigate the effect of climate change on the IS92a scenario, the average of the OCMIP CO<sub>2</sub>-only projections (mean of results in Figure 3.10c) was used as a baseline and the reduction in atmosphere-ocean CO<sub>2</sub> flux caused by climate change (in per cent since the beginning of the simulation) was applied to this curve (Figure 3.10d). The range in model results (Figure 3.10d) must be attributed to uncertainties related to climate change feedback, and not to uncertainties in the modelling of physical transport as shown in Figure 3.10c.

The range of model estimates of the climate change impact is dependent on the choice of scenario for atmospheric CO<sub>2</sub> and on assumptions concerning marine biology (Joos *et al.*, 1999b). At high CO<sub>2</sub> concentrations, marine biology can have a greater impact on atmospheric CO<sub>2</sub> than at low concentrations because the buffering capacity of the ocean is reduced (see Box 3.3) (Sarmiento and Le Quéré, 1996). Although the impact of changes in marine biology is highly uncertain and many key processes discussed in Section 3.2.3.1 are not included in current models, sensitivity studies can provide approximate upper and lower

bounds for the potential impact of marine biology on future ocean CO<sub>2</sub> uptake. A sensitivity study of two extreme scenarios for nutrient supply to marine biology gave a range of 8 to 25% for the reduction of CO<sub>2</sub> uptake by mid-century (Sarmiento *et al.*, 1998). This range is comparable to other uncertainties, including those stemming from physical transport (Figure 3.10c).

### 3.7.3 Coupled Model Responses and Implications for Future CO<sub>2</sub> Concentrations

Carbon cycle models have indicated the potential for climate change to influence the rate of CO<sub>2</sub> uptake by both land (Section 3.7.1) and oceans (Section 3.7.2) and thereby influence the time course of atmospheric CO<sub>2</sub> concentration for any given emissions scenario. Coupled models are required to quantify these effects.

Two general circulation model simulations have included interactive land and ocean carbon cycle components (Cox *et al.*, 2000; Friedlingstein *et al.*, 2001). The Cox *et al.* (2000) model was driven by CO<sub>2</sub> emissions from the IS92a scenario (Leggett *et al.*, 1992) and the Friedlingstein *et al.* (2001) model was driven by CO<sub>2</sub> emissions from the SRES A2 scenario (IPCC, 2000b). Both simulations indicate a positive feedback, i.e., both CO<sub>2</sub> concentrations and climate change at the end of the 21st century are increased due to the coupling. The simulated magnitudes of the effect differ (+70 ppm, Friedlingstein *et al.*, 2001; +270 ppm, Cox *et al.*, 2000). In the Cox *et al.* (2000) simulation, which included a DGVM, the increased atmospheric CO<sub>2</sub> is caused mainly by loss of soil carbon and in part by tropical forest die back. The magnitude of the climate-carbon cycle feedback still has large uncertainties associated with the response of the terrestrial biosphere to climate change, especially the response of heterotrophic respiration and tropical forest NPP to temperature (Cox *et al.*, 2000; see Sections 3.2.2.3 and 3.7.1). In the following section, simplified models are used to assess these uncertainties.

#### 3.7.3.1 Methods for assessing the response of atmospheric CO<sub>2</sub> to different emissions pathways and model sensitivities

This section follows the approach of previous IPCC reports in using simplified, fast models (sometimes known as reduced-form models) to assess the relationship between CO<sub>2</sub> emissions and concentrations, under various assumptions about their future time course. Results are shown from two models, whose salient features are summarised in Box 3.7. The models lend themselves to somewhat different approaches to estimating uncertainties. In the ISAM model, “high-CO<sub>2</sub>” and “low-CO<sub>2</sub>” alternatives are calculated for every emissions scenario, based on tuning the model to match the range of responses included in the model

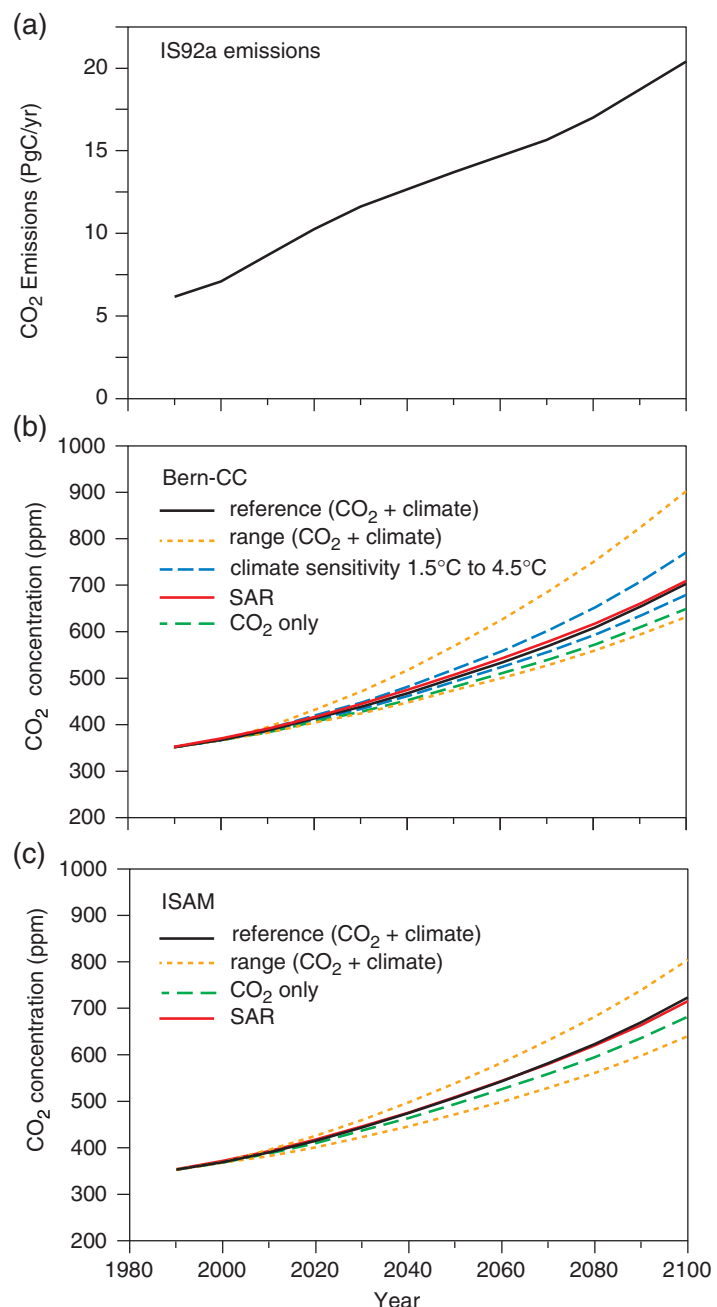


**Figure 3.11:** Projected CO<sub>2</sub> concentrations resulting from the IS92a emissions scenario. For a strict comparison with previous work, IS92a-based projections were made with two fast carbon cycle models, Bern-CC and ISAM (see Box 3.7), based on CO<sub>2</sub> changes only, and on CO<sub>2</sub> changes plus land and ocean climate feedbacks. Panel (a) shows the CO<sub>2</sub> emissions prescribed by IS92a; the panels (b) and (c) show projected CO<sub>2</sub> concentrations for the Bern-CC and ISAM models, respectively. Results obtained for the SAR, using earlier versions of the same models, are also shown. The model ranges for ISAM were obtained by tuning the model to approximate the range of responses to CO<sub>2</sub> and climate shown by the models in Figure 3.10, combined with a range of climate sensitivities from 1.5 to 4.5°C rise for a doubling of CO<sub>2</sub>. This approach yields a lower bound on uncertainties in the carbon cycle and climate. The model ranges for Bern-CC were obtained by combining different bounding assumptions about the behaviour of the CO<sub>2</sub> fertilisation effect, the response of heterotrophic respiration to temperature and the turnover time of the ocean, thus approaching an upper bound on uncertainties in the carbon cycle. The effect of varying climate sensitivity from 1.5 to 4.5°C is shown separately for Bern-CC. Both models adopted a “reference case” with mid-range behaviour of the carbon cycle and climate sensitivity of 2.5°C.

**Box 3.7:** Fast, simplified models used in this assessment.

The **Bern-CC** model comprises:

- A box-diffusion type ocean carbon model, (HILDA version K(z); Siegenthaler and Joos, 1992; Joos *et al.*, 1996), already used in the SAR. In addition to the SAR version, the effect of sea surface warming on carbonate chemistry is included (Joos *et al.*, 1999b).
- An impulse-response climate model (Hooss *et al.*, 1999), which converts radiative forcing into spatial patterns of changes in temperature, precipitation and cloud cover on a global grid. The patterns of the climate anomalies are derived from the first principal component of the climate response shown by the full three-dimensional atmosphere-ocean GCM, ECHAM-3/LSG (Voss and Mikolajewicz, 1999). Their magnitude is scaled according to the prescribed climate sensitivity.
- The terrestrial carbon model LPJ, as described in Sitch *et al.* (2000) and Cramer *et al.* (2001). LPJ is a process-based DGVM that falls in the mid-range of CO<sub>2</sub> and climate responses as shown in Cramer *et al.* (2001). It is used here at 3.75° × 2.5° resolution, as in Cramer *et al.* (2001).
- A radiative forcing module. The radiative forcing of CO<sub>2</sub>, the concentration increase of non-CO<sub>2</sub> greenhouse gases and their radiative forcing, direct forcing due to sulphate, black carbon and organic aerosols, and indirect forcing due to sulphate aerosols are projected using a variant of SAR models (Harvey *et al.*, 1997; Fuglestvedt and Berntsen, 1999) updated with information summarised in Chapters 4, 5 and 6. The concentrations of non-CO<sub>2</sub> greenhouse gases, aerosol loadings, and radiative forcings are consistent with those given in Appendix II.

Sensitivities of projected CO<sub>2</sub> concentrations to model assumptions were assessed as follows. Rh was assumed either to be independent of global warming (Giardina and Ryan, 2000; Jarvis and Linder 2000), or to increase with temperature according to Lloyd and Taylor (1994). CO<sub>2</sub> fertilisation was either capped after year 2000 by keeping CO<sub>2</sub> at the year 2000 value in the photosynthesis module, or increased asymptotically following Haxeltine and Prentice (1996). (Although apparently unrealistic, capping the CO<sub>2</sub> fertilisation in the model is designed to mimic the possibility that other, transient factors such as land management changes might be largely responsible for current terrestrial carbon uptake.) Transport parameters of the ocean model (including gas exchange) were scaled by a factor of 1.5 and 0.5. Average ocean uptake for the 1980s is 2.0 PgC/yr in the reference case, 1.46 PgC/yr for the “slow ocean” and 2.54 PgC/yr for the “fast ocean”, roughly in accord with the range of observational estimates (Table 3.1, Section 3.2.3.2). A “low-CO<sub>2</sub>” parametrization was obtained by combining the fast ocean and no response of Rh to temperature. A “high-CO<sub>2</sub>” parametrization was obtained by combining the slow ocean and capping CO<sub>2</sub> fertilisation. Climate sensitivity was set at 2.5 °C for a doubling of CO<sub>2</sub>. Effects of varying climate sensitivity from 1.5°C to 4.5°C are also shown for one case.

The **ISAM** model was described by Jain *et al.* (1994) and used in the SAR for CO<sub>2</sub>-only analyses, with a different set of model parameters from those used here (Jain, 2000). The full configuration of ISAM comprises:

- A globally aggregated upwelling-diffusion ocean model including the effects of temperature on CO<sub>2</sub> solubility and carbonate chemistry (Jain *et al.*, 1995).
- An energy balance climate model of the type used in the IPCC 1990 assessment (Hoffert *et al.*, 1980; Bretherton *et al.*, 1990). In this model, heat is transported as a tracer in the ocean and shares the same transport parameters as DIC.
- A six-box globally aggregated terrestrial carbon model including empirical parametrizations of CO<sub>2</sub> fertilisation and temperature effects on productivity and respiration (Harvey, 1989; Kheshgi *et al.*, 1996).
- The radiative forcing of CO<sub>2</sub> projected using a SAR model (Harvey *et al.*, 1997) modified with information summarised in Chapter 6. Radiative forcing from agents other than CO<sub>2</sub> are identical to that used in the Bern-CC model.

In addition to varying the climate sensitivity (1.5 to 4.5°C), parameters of the terrestrial and ocean components (strength of CO<sub>2</sub> fertilisation, temperature response of NPP and heterotrophic respiration; ocean heat and DIC transport) were adjusted to mimic the ranges of CO<sub>2</sub> and climate responses as shown by existing process-based models (Figure 3.10). A reference case was defined with climate sensitivity 2.5°C, ocean uptake corresponding to the mean of the ocean model results in Figure 3.10, and terrestrial uptake corresponding to the mean of the responses of the mid-range models LPJ, IBIS and SDGVM (Figure 3.10). A “low CO<sub>2</sub>” parametrization was chosen with climate sensitivity 1.5°C, and maximal CO<sub>2</sub> uptake by oceans and land; and a “high-CO<sub>2</sub>” parametrization with climate sensitivity 4.5°C, and minimal CO<sub>2</sub> uptake by oceans and land.

intercomparisons shown in Figure 3.10. Uncertainties cited from the ISAM model can be regarded as providing a lower bound on uncertainty since they do not admit possible behaviours outside the range considered in recent modelling studies. In the Bern-CC model, “high-CO<sub>2</sub>” and “low-CO<sub>2</sub>” alternatives are calculated by making bounding assumptions about carbon cycle processes (for example, in the high-CO<sub>2</sub> parametrization CO<sub>2</sub> fertilisation is capped at year 2000; in the low-CO<sub>2</sub> parametrization Rh does not increase with warming). This approach yields generally larger ranges of projected CO<sub>2</sub> concentrations than the ISAM approach. The ranges cited from the Bern-CC model can be regarded as approaching an upper bound on uncertainty, since the true system response is likely to be less extreme than the bounding assumptions, and because the combination of “best” and “worst” case assumptions for every process is intrinsically unlikely.

### 3.7.3.2 Concentration projections based on IS92a, for comparison with previous studies

Illustrative model runs (Figure 3.11) based on the IS92a scenario (Leggett *et al.*, 1992) are shown first so as to allow comparison with earlier model results presented in the SAR and the SRRF (Schimel *et al.*, 1995). In the SRRF comparison of eighteen global carbon cycle models (Enting *et al.*, 1994; Schimel *et al.*, 1995) the CO<sub>2</sub> fertilisation response of the land was calibrated to match the central estimate of the global carbon budget for the 1980s, assuming a land-use source of 1.6 PgC/yr in the 1980s and attributing the residual terrestrial sink to CO<sub>2</sub> fertilisation. This intercomparison yielded CO<sub>2</sub> concentrations in 2100 of 668 to 734 ppm; results presented in Schimel *et al.* (1996) (from the Bern model) gave 688 ppm. After recalibrating to match a presumed land-use source of 1.1 PgC/yr, implying a weaker CO<sub>2</sub> response, the 2100 CO<sub>2</sub> concentration was given as 712 ppm in the SAR (Schimel *et al.*, 1996). An IPCC Technical Paper (Wigley *et al.*, 1997) evaluated the sensitivity of IS92a results to this calibration procedure. Wigley *et al.*, (1997) found that a range of assumed values from 0.4 to 1.8 PgC/yr for the land-use source during the 1980s gave rise to a range of 2100 CO<sub>2</sub> concentrations from 667 to 766 ppm.

In contrast with the SAR, the results presented here are based on approximating the behaviour of spatially resolved process-based models in which CO<sub>2</sub> and climate responses are not constrained by prior assumptions about the global carbon budget. The CO<sub>2</sub>-only response of both models’ reference cases (Figure 3.11) leads to a 2100 CO<sub>2</sub> concentration of 682 ppm (ISAM) or 651 ppm (Bern-CC). These values are slightly lower than projected in the SAR – 715 ppm (ISAM; SAR version) and 712 ppm (Bern Model; SAR version) – because current process-based terrestrial models typically yield a stronger CO<sub>2</sub> response than was assumed in the SAR. With climate feedbacks included, the 2100 CO<sub>2</sub> concentration in the reference case becomes, by coincidence, effectively indistinguishable from that given in the SAR: 723 ppm (ISAM) and 706 ppm (Bern-CC). The ranges of 164 ppm or –12% / +11% (about the reference case) (ISAM) and 273 ppm or –10% / +28% (Bern-CC) in the 2100 CO<sub>2</sub> concentration indicate that there is significant uncertainty about the future CO<sub>2</sub> concentrations due to any one pathway of changes in emissions. Separate calculations with the Bern-CC model (Figure 3.11) show that the effect of changing climate sensitivity alone is less important than

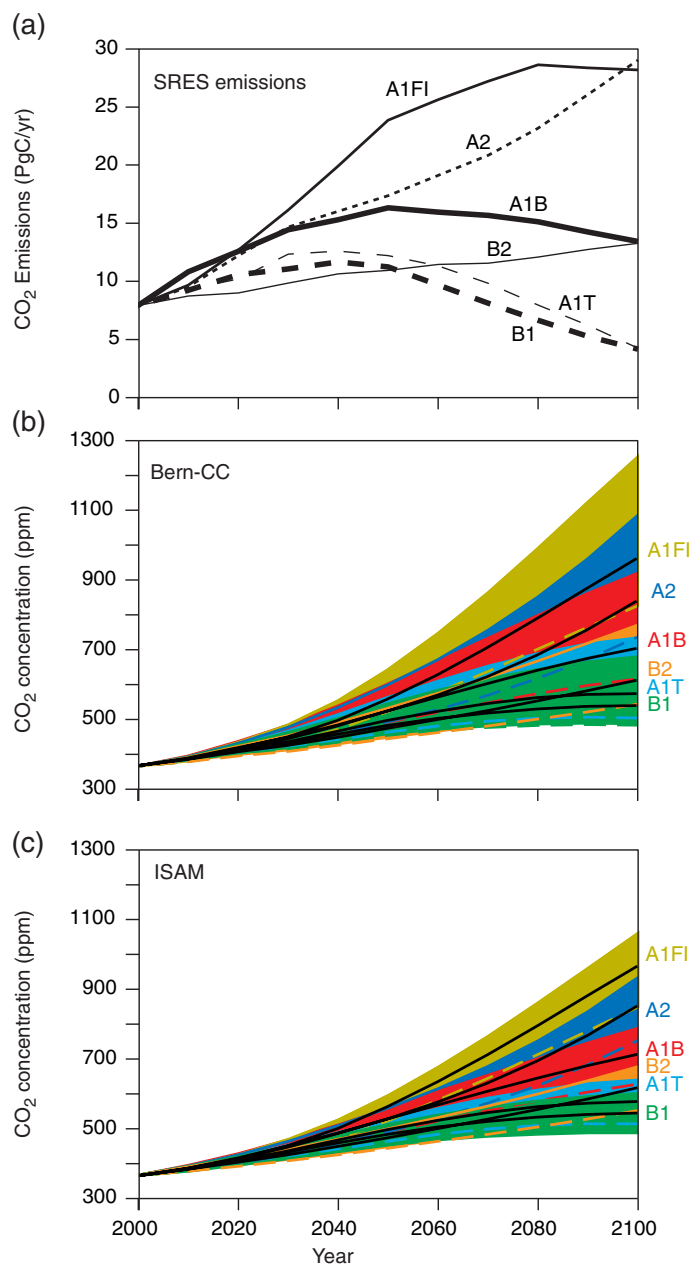


**Figure 3.12:** Projected CO<sub>2</sub> concentrations resulting from six SRES scenarios. The SRES scenarios represent the outcome of different assumptions about the future course of economic development, demography and technological change (see Appendix II). Panel (a) shows CO<sub>2</sub> emissions for the selected scenarios and panels (b) and (c) show resulting CO<sub>2</sub> concentrations as projected by two fast carbon cycle models, Bern-CC and ISAM (see Box 3.7 and Figure 3.11). The ranges represent effects of different model parametrizations and assumptions as indicated in the text and in the caption to Figure 3.11. For each model, and each scenario the reference case is shown by a black line, the upper bound (high-CO<sub>2</sub> parametrization) is indicated by the top of the coloured area, and the lower bound (low-CO<sub>2</sub> parametrization) by the bottom of the coloured area or (where hidden) by a dashed coloured line.

the effect of varying assumptions in the carbon cycle model's components. The effect of increasing climate sensitivity to 4.5 °C (increasing the climate feedback) is much larger than the effect of reducing climate sensitivity to 1.5 °C. The "low-CO<sub>2</sub>" parametrization of Bern-CC yields CO<sub>2</sub> concentrations closer to the reference case than the "high-CO<sub>2</sub>" parametrization, in which the terrestrial sink is forced to approach zero during the first few decades of the century due to the capping of the CO<sub>2</sub> fertilisation effect.

The reference simulations with ISAM yielded an implied average land-use source during the 1980s of 0.9 PgC/yr. The range was 0.2 to 2.0 PgC/yr. Corresponding values for Bern-CC were 0.6 PgC/yr and a range of 0.0 to 1.5 PgC/yr. These ranges broadly overlap the range estimates of the 1980s land-use source given in Table 3.1. Present knowledge of the carbon budget is therefore not precise enough to allow much narrowing of the uncertainty associated with future land and ocean uptake as expressed in these projections. However, the lowest implied land-use source values fall below the range given in Table 3.1.

### 3.7.3.3 SRES scenarios and their implications for future CO<sub>2</sub> concentration

The Special Report on Emissions Scenarios (SRES) (IPCC, 2000b) produced a series of scenarios, of which six are used here, representing outcomes of distinct narratives of economic development and demographic and technological change. In ISAM model runs with these scenarios, past fossil emissions (see Section 3.4.1), CO<sub>2</sub> concentrations (Enting *et al.*, 1994; Keeling and Whorf, 2000) and mean global temperatures (Jones *et al.*, 2000) were specified up to and including 1999; scenario-based analyses started in 2000. In the Bern-CC model runs, observed CO<sub>2</sub> (Etheridge, *et al.*, 1996, Keeling and Whorf, 2000) and past fossil emissions (Marland *et al.*, 1999) were prescribed, and historical temperature changes were modelled, based on radiative forcing from greenhouse gases and aerosols; again, scenario-based analyses started in 2000. Past emissions from changing land use were calculated in order to balance the carbon budget.

The six scenarios lead to substantial differences in projected CO<sub>2</sub> concentration trajectories (Figure 3.12). Significant uncertainties are introduced by the range of model parametrizations considered, so that the trajectories calculated for "adjacent" scenarios overlap, especially during the first half-century. The reference cases of the six scenarios account for a range of 2100 CO<sub>2</sub> concentrations from 541 to 963 ppm in the Bern-CC model and 549 to 970 ppm in the ISAM model. The uncertainties around the 2100 values due to model parametrizations are -12 to +10 % (ISAM) and -14 to +31 % (Bern-CC).

These uncertainties reflect incomplete understanding of climate sensitivity and the carbon cycle. They substantially limit our current ability to make quantitative predictions about the future consequences of a given emissions trajectory. Nevertheless, the results show that higher emissions are always expected to lead to higher projected atmospheric concentrations. They also show that the range of emissions scenarios currently accepted as plausible leads to a range of CO<sub>2</sub> concentrations that exceeds the likely upper bound of uncertainties due to differences among model parameterizations and assumptions.

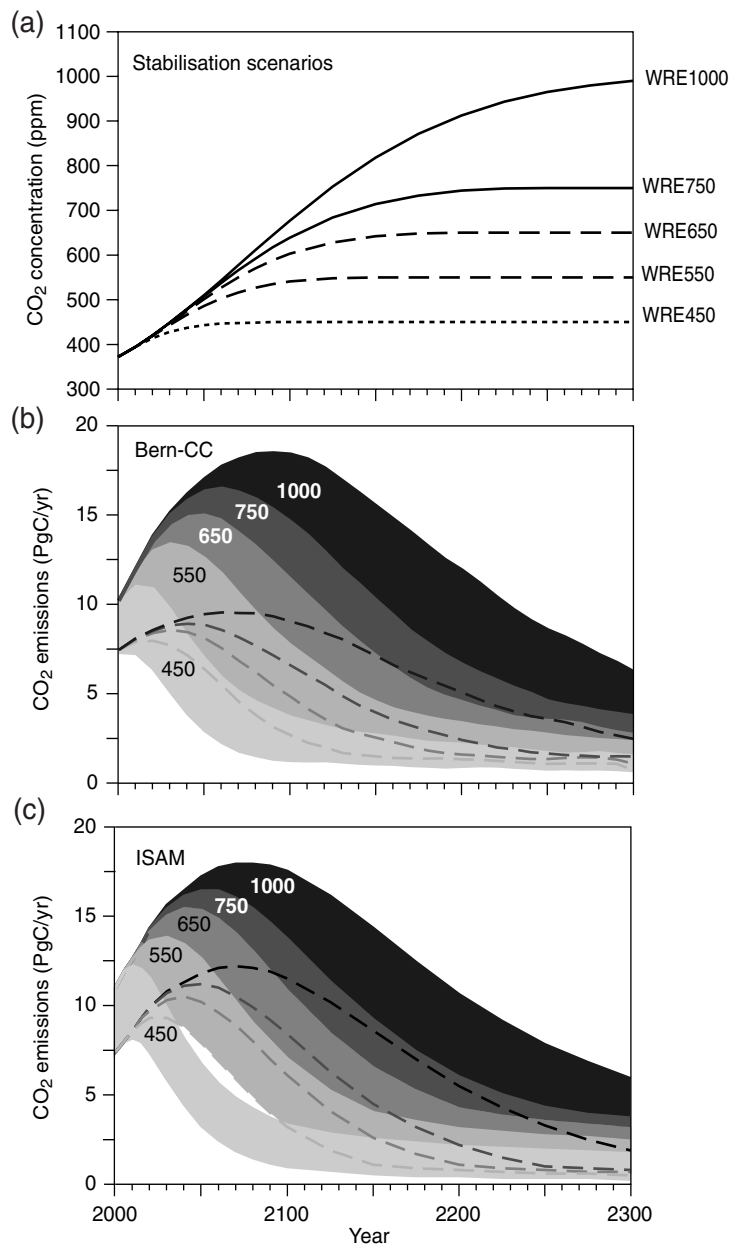


**Fig 3.13:** Projected CO<sub>2</sub> emissions leading to stabilisation of atmospheric CO<sub>2</sub> concentrations at different final values. Panel (a) shows the assumed trajectories of CO<sub>2</sub> concentration (WRE scenarios; Wigley *et al.*, 1996) and panels (b) and (c) show the implied CO<sub>2</sub> emissions, as projected with two fast carbon cycle models, Bern-CC and ISAM (see Box 3.7 and Figure 3.11). The ranges represent effects of different model parametrizations and assumptions as indicated in the text and in the caption to Figure 3.11. For each model, the upper and lower bounds (corresponding to low- and high-CO<sub>2</sub> parametrizations, respectively) are indicated by the top and bottom of the shaded area. Alternatively, the lower bound (where hidden) is indicated by a dashed line.

### 3.7.3.4 Stabilisation scenarios and their implications for future CO<sub>2</sub> emissions

Stabilisation scenarios illustrate implied rates of CO<sub>2</sub> emission that would arrive at various stable CO<sub>2</sub> concentration levels. These have been projected using a similar methodology to that applied in the analysis of emissions scenarios. The WRE trajectories follow CO<sub>2</sub> concentrations consistent with the IS92a scenario beginning in 1990 and branch off to reach constant CO<sub>2</sub> concentrations of 450, 550, 650, 750 and 1,000 ppm (Wigley *et al.*, 1996). The rationale for various alternative time trajectories and stabilisation levels is discussed in Chapter 2 of the IPCC WGIII Third Assessment Report (Morita *et al.*, 2001). Differences in emissions pathways for different time trajectories leading to a certain stabilisation target (e.g., S versus WRE profiles) are discussed in Schimel *et al.*, (1997). Here, we have calculated emissions for one set of emission profiles to illustrate differences in implied emissions that arise from updating models since the SAR.

As in Section 3.7.3.2, the models were initialised up to present. Then anthropogenic emissions for the prescribed CO<sub>2</sub> stabilization profiles were calculated; deduced emissions equal the change in modeled ocean and terrestrial carbon inventories plus the prescribed change in atmospheric CO<sub>2</sub> content. To estimate the strength of carbon cycle-climate feedbacks, global temperature (ISAM) and changes in the fields of temperature, precipitation and cloud cover (Bern-CC) were projected from CO<sub>2</sub> radiative forcing only, neglecting effects of other greenhouse gases and aerosols which are not specified in the WRE profiles. The results for the reference cases are not substantially different from those presented in the SAR (Figure 3.13). However, the range based on alternative model parametrizations is larger than presented in the SAR, mainly due to the range of simulated terrestrial CO<sub>2</sub> uptake. CO<sub>2</sub> stabilisation at 450, 650 or 1,000 ppm would require global anthropogenic CO<sub>2</sub> emissions to drop below 1990 levels, within a few decades, about a century, or about two centuries, respectively.

In all cases, once CO<sub>2</sub> concentration becomes constant, the implied anthropogenic emission declines steadily. This result was expected. It highlights the fact that to maintain a constant future CO<sub>2</sub> concentration, anthropogenic CO<sub>2</sub> emissions would ultimately have to be reduced to the level of persistent natural sinks. Persistent terrestrial sinks are not well quantified; peatlands may be a candidate, but the gradual rise in atmospheric CO<sub>2</sub> concentration during the present interglacial (Figure 3.2) argues against any such sink. Estimates of current uptake by peatlands are <0.1 PgC/yr (Clymo *et al.*, 1998). Mixing of ocean DIC between surface and deep waters should continue to produce ocean uptake for several centuries after an input of anthropogenic atmospheric CO<sub>2</sub> (Siegenthaler and Oeschger, 1978; Maier-Reimer and Hasselmann, 1987; Sarmiento *et al.*, 1992). This mixing is the main reason for continued uptake (and therefore positive calculated emissions) after stabilisation. However, the main, known natural sink expected to persist longer than a few centuries is that due to dissolution of CaCO<sub>3</sub> in ocean sediments, which increases ocean alkalinity and thereby allows additional CO<sub>2</sub> to dissolve in the ocean. For CO<sub>2</sub> concentrations about 1,000 ppm, this sink is estimated to be smaller than about -0.1 PgC/yr (Archer *et al.*, 1998). Thus, for any significant CO<sub>2</sub> emissions to

persist over centuries without continuing to increase atmospheric CO<sub>2</sub> would require some method of producing an artificial carbon sink.

### 3.7.4 Conclusions

The differences among the CO<sub>2</sub> concentrations projected with the various SRES scenarios considered are larger than the differences caused by inclusion or omission of climate-mediated feedbacks. The range of uptake rates projected by process-based models for any one scenario is, however, considerable, due to uncertainties about (especially) terrestrial ecosystem responses to high CO<sub>2</sub> concentrations, which have not yet been resolved experimentally, and uncertainties about the response of global NPP to changes in climate (Cramer *et al.*, 1999). A smaller feedback would be implied if, as some models indicate, global NPP increases with warming throughout the relevant range of climates and no forest die back occurs. Larger positive feedbacks would be implied if regional drying caused partial die back of tropical forests, as some of the DGVMs in Cramer *et al.* (2001), and one coupled climate-carbon model study of Cox *et al.* (2000), suggest; however, another coupled climate-carbon model study (Friedlingstein *et al.*, 2001) suggests a smaller feedback. Uncertainty also arises due to differences in the climate responses of ocean models, especially as regards the extent and effects (biological as well as physical) of increased stratification in a warmer climate (Joos *et al.*, 1999b).

In conclusion, *anthropogenic CO<sub>2</sub> emissions are virtually certain to be the dominant factor determining CO<sub>2</sub> concentrations throughout the 21st century*. The importance of anthropogenic emissions is underlined by the expectation that the proportion of emissions taken up by both ocean and land will decline at high atmospheric CO<sub>2</sub> concentrations (even if absolute uptake by the ocean continues to rise). There is considerable uncertainty in projections of future CO<sub>2</sub> concentration, because of uncertainty about the effects of climate change on the processes determining ocean and land uptake of CO<sub>2</sub>. These uncertainties do not negate the main finding that anthropogenic emissions will be the main control.

Large-scale manipulations of terrestrial ecosystems have been proposed as a means of slowing the increase of atmospheric CO<sub>2</sub> during the 21st century in support of the aims of the Kyoto Protocol (Tans and Wallace, 1999; IPCC, 2000a). Based on current understanding of land use in the carbon cycle, the impacts of future land use on terrestrial biosphere-atmosphere exchanges have the potential to modify atmospheric CO<sub>2</sub> concentrations on this time-scale. Direct effects of land-use changes are thought to represent about 10 to 30% of total anthropogenic CO<sub>2</sub> emissions (Table 3.1), so there is scope for either intended or unintended changes in land use to reduce or increase total anthropogenic emissions. But the possibilities for enhancing natural sinks have to be placed in perspective: a rough upper bound for the reduction in CO<sub>2</sub> concentration that could be achieved by enhancing terrestrial carbon uptake through land-use change over the coming century is 40 to 70 ppm (Section 3.2.2.2), to be considered against a two to four times larger potential for increasing CO<sub>2</sub> concentration by deforestation, and a >400 ppm range among the SRES scenarios (Figure 3.12).

## References

- Aber**, J., W. McDowell, K. Nadelhoffer, A. Magill, G. Bernstson, M. Kamakea, S. McNulty, W. Currie, L. Rustad, I. Fernandez, 1998: Nitrogen saturation in temperate forest ecosystems. *BioScience*, **48**, 921-934.
- Allen**, A.S., J.A. Andrews, A.C. Finzi, R. Matamala, D.D. Richter and W.H. Schlesinger, 2000: Effects of free-air CO<sub>2</sub> enrichment (FACE) on belowground processes in a *Pinus taeda* forest. *Ecological Applications*, **10**, 437-448.
- Altabet**, M.A., R. Francois, D.W. Murray, and W.L. Prell, 1995: Climate-Related Variations in Denitrification in the Arabian Sea From Sediment <sup>15</sup>N/<sup>14</sup>N Ratios. *Nature*, **373**, 506-509.
- Andersen**, K. K., A. Armengaud, and C. Genton, 1998: Atmospheric dust under glacial and interglacial conditions. *Geophysical Research Letters*, **25**, 2281-2284, 1998.
- Andres**, R. J., Marland, G., Boden, T., and Bischof, S., 2000: Carbon dioxide emissions from fossil fuel consumption and cement manufacture, 1751-1991, and an estimate of their isotopic composition and latitudinal distribution. In: *The Carbon Cycle*, [Wigley, T.M.L. and D.S. Schimel (eds.)]. Cambridge University Press, New York, pp. 53-62.
- Antoine**, D., J.M. Andre, and A. Morel, 1996: Oceanic primary production. 2. Estimation at global scale from satellite (coastal zone color scanner) chlorophyll. *Global Biogeochemical Cycles*, **10**, 57-69.
- Apps**, M.J., W.A. Kurz, R.J. Luxmoore, L.O. Nilsson, R.A. Sedjo, R. Schmidt, L.G. Simpson, and T.S. Vinson, 1993: Boreal Forests and Tundra. *Water Air Soil Pollution*, **70**, 39-53.
- Archer**, D.E. and E. Maier-Reimer, 1994: Effect of deep-sea sedimentary calcite preservation on atmospheric CO<sub>2</sub> concentration. *Nature*, **367**, 260-263.
- Archer**, D.E., and K. Johnson, 2000: A Model of the iron cycle in the ocean. *Global Biogeochemical Cycles*, **14**, 269-279.
- Archer**, D.E., T. Takahashi, S. Sutherland, J. Goddard, D. Chipman, K. Rodgers, and H. Ogura, 1996: Daily, seasonal and interannual variability of sea-surface carbon and nutrient concentration in the equatorial Pacific Ocean. *Deep-Sea Research Part II-Topical Studies in Oceanography*, **43**, 779-808.
- Archer**, D.E., H. Kheshgi, and E. Maier-Reimer, 1997: Multiple timescales for neutralization of fossil fuel CO<sub>2</sub>. *Geophysical Research Letters*, **24**, 405-408.
- Archer**, D.E., H. Kheshgi, and E. Maier-Reimer, 1998: Dynamics of fossil fuel CO<sub>2</sub> neutralization by marine CaCO<sub>3</sub>. *Global Biogeochemical Cycles*, **12**, 259-276.
- Archer**, D.E., A. Winguth, D. Lea, and N. Mahowald, 2000: What caused the glacial/interglacial atmospheric pCO<sub>2</sub> cycles? *Reviews of Geophysics*, **38**, 159-189.
- Archer**, S., T.W. Boutton, and K.A. Hibbard, 2001: Trees in grasslands: biogeochemical consequences of woody plant expansion. In: *Global Biogeochemical Cycles and their Interrelationship with Climate* [Schulze, E.-A., S.P. Harrison, M. Heimann, E.A. Holland, J. Lloyd, I.C. Prentice, and D.S. Schimel (eds.)], Academic Press.
- Asrar**, G., Myneni R.B., and Choudhury, B.J., 1992: Spatial heterogeneity in vegetation canopies and remote sensing of absorbed photosynthetically active radiation: a modeling study. *Remote Sensing Environment*, **41**, 85-103.
- Atjay**, G.L., P. Ketner, and P. Duvigneaud, 1979: Terrestrial primary production and phytomass. In: *The Global Carbon Cycle* [Bolin, B., E.T. Degens, S. Kempe, and P. Ketner (eds.)], John Wiley & Sons, Chichester, pp. 129-181.
- Aubinet**, M., A. Grelle, A. Ibrom, U. Rannik, J. Moncrieff, T. Foken, A.S. Kowalski, P.H. Martin, P. Berbigier, C. Bernhofer, R. Clement, J. Elbers, A. Granier, T. Grunwald, K. Morgenstern, K. Pilegaard, C. Rebmann, W. Snijders, R. Valentini and T. Vesala, 2000: Estimates of the annual net carbon and water exchange of forests: The EUROFLUX methodology. *Advances in Ecological Research*, **30**, 113-175.
- Aumont**, O., 1998: Étude du cycle naturel du carbone dans un modèle 3D de l'océan mondial. Ph.D. thesis, Université Pierre et Marie Curie, 4 place Jussieu, Paris 95005.
- Aumont**, O., S. Belviso and P. Monfray, 2001a: Dimethylsulfoniopropionate (DMSP) and dimethylsulfide (DMS) sea surface distributions simulated from a global 3-D ocean carbon cycle model. *Journal of Geophysical Research*, (in press)
- Aumont**, O., J.C. Orr, P. Monfray, W. Ludwig, P. Amiotte-Suchet and J.L. Probst, 2001b: Riverine-driven interhemispheric transport of carbon. *Global Biogeochemical Cycles*, (in press)
- Bacastow**, R.B., 1976: Modulation of atmospheric carbon dioxide by the southern oscillation. *Nature*, **261**, 116-118.
- Bacastow**, R.B., 1993: The effect of temperature change of the warm surface waters of the oceans on atmospheric CO<sub>2</sub>. *Global Biogeochemical Cycles*, **10**, 319-333.
- Bacastow**, R.B., C.D. Keeling, T.J. Lueker, M. Wahlen, and W.G. Mook, 1996: The <sup>13</sup>C Suess effect in the world surface oceans and its implications for oceanic uptake of CO<sub>2</sub> – Analysis of observations at Bermuda. *Global Biogeochemical Cycles*, **10**, 335-346.
- Baldocchi**, D.D., B.B. Hicks, T.P. Meyers, 1988: Measuring biosphere-atmosphere exchanges of biologically related gases with micrometeorological methods. *Ecology*, **69**, 1331-1340.
- Balkanski**, Y., P. Monfray, M. Battle, and M. Heimann, 1999: Ocean primary production derived from satellite data: An evaluation with atmospheric oxygen measurements. *Global Biogeochemical Cycles*, **13**, 257-271.
- Barnola**, J.M., M. Anklin, J. Porcheron, D. Raynaud, J. Schwander, and B. Stauffer, 1995: CO<sub>2</sub> evolution during the last millennium as recorded by Antarctic and Greenland ice. *Tellus Series B-Chemical and Physical Meteorology*, **47**, 264-272.
- Bates**, N.R., A.F. Michaels, and A.H. Knap, 1996: Seasonal and interannual variability of oceanic carbon dioxide species at the US JGOFS Bermuda Atlantic Time-series Study (BATS) site. *Deep-Sea Research Part II-Topical Studies in Oceanography*, **43**, 347-383.
- Batjes**, N.H., 1996: Total carbon and nitrogen in the soils of the world. *European Journal of Soil Science*, **47**: 151-163.
- Battle**, M., M. Bender, T. Sowers, P.P. Tans, J.H. Butler, J.W. Elkins, J.T. Ellis, T. Conway, N. Zhang, P. Lang, and A.D. Clarke, 1996: Atmospheric gas concentrations over the past century measured in air from firn at the South Pole. *Nature*, **383**, 231-235.
- Battle**, M., M. Bender, P.P. Tans, J.W.C. White, J.T. Ellis, T. Conway, and R.J. Francey, 2000: Global carbon sinks and their variability, inferred from atmospheric O<sub>2</sub> and δ<sup>13</sup>C. *Science*, **287**, 2467-2470.
- Beerling**, D.J., H.H. Birks, and F.I. Woodward, 1995: Rapid late-glacial atmospheric CO<sub>2</sub> changes reconstructed from the stomatal density record of fossil leaves. *Journal of Quaternary Science*, **10**, 379-384.
- Bender**, M., T. Sowers, and L. Labeyrie, 1994: The Dole effect and its variations during the last 130,000 years as measured in the VOSTOK ice core. *Global Biogeochemical Cycles*, **8**, 363-376.
- Bender**, M., T. Ellis, P. Tans, R. Francey, and D. Lowe, 1996: Variability in the O<sub>2</sub>/N<sub>2</sub> ratio of southern hemisphere air, 1991-1994 - Implications for the carbon cycle. *Global Biogeochemical Cycles*, **10**, 9-21.
- Berger**, A.L., 1978: Long-term variations of caloric insolation resulting from the Earth's orbital elements. *Quaternary Research*, **9**, 139-167.
- Bergh**, J., S. Linder, T. Lundmark, B. Elfving, 1999: The effect of water and nutrient availability on the productivity of Norway spruce in northern and southern Sweden. *Forest Ecology and Management*, **119**, 51-62.
- Berner**, R.A., 1993: Weathering and its effect on atmospheric CO<sub>2</sub> over phanerozoic time. *Chemical Geology*, **107**, 373-374.
- Berner**, R.A., 1997: The rise of plants and their effect on weathering and atmospheric CO<sub>2</sub>. *Science*, **276**, 544-546.

- Bickle, M.J.**, 1994: The role of metamorphic decarbonation reactions in returning strontium to the silicate sediment mass. *Nature*, **367**, 699-704.
- Bird, M.I.**, J. Lloyd, and G.D. Farquhar, 1994: Terrestrial carbon storage at the LGM. *Nature*, **371**, 585.
- Blume, H.P.**, H. Eger, E. Fleischhauer, A. Hebel, C. Reij, and K.G. Steiner, 1998: Towards sustainable land use. *Advances in Geoeocology*, **31**, 1625pp.
- Bolin, B.** and Keeling C.D., 1963: Large-scale atmospheric mixing as deduced from the seasonal and meridional variations of carbon dioxide. *Journal of Geophysical Research*, **68**, 3899-3920.
- Bolin, B.**, Sukumar, R., P. Ciais, W. Cramer, P. Jarvis, H. Kheshgi, C. Nobre, S. Semenov, W. Steffen, 2000: Global Perspective. In: *IPCC, Land Use, Land-Use Change, and Forestry. A Special Report of the IPCC* [Watson, R.T., I.R. Noble, B. Bolin, N.H. Ravindranath, D.J. Verardo and D.J. Dokken (eds.)]. Cambridge University Press, Cambridge, UK, pp. 23-51.
- Bondeau, A.**, D.W. Kicklighter, and J. Kaduk, 1999: Comparing global models of terrestrial net primary productivity (NPP): importance of vegetation structure on seasonal NPP estimates. *Global Change Biology*, **5**, 35-45.
- Boone, R.D.**, K.J. Nadelhoffer, J.D. Canary, and J.P. Kaye, 1998: Roots exert a strong influence on the temperature sensitivity of soil respiration. *Nature*, **396**, 570-572.
- Bopp, L.**, P. Monfray, O. Aumont, J.-L. Dufresne, H. LeTreut, G. Madec, L. Terray, and J. Orr, 2001: Potential impact of climate change on marine export production. *Global Biogeochemical Cycles* **15**(1), 81-100.
- Bousquet, P.**, P. Ciais, P. Peylin, M. Ramonet, and P. Monfray, 1999: Inverse modeling of annual atmospheric CO<sub>2</sub> sources and sinks 1. Method and control inversion. *Journal of Geophysical Research-Atmospheres*, **104**, 26161-26178.
- Bousquet, P.**, P. Peylin, P. Ciais, C. Le Quéré, P. Friedlingstein and P. P. Tans, 2000: Regional changes of CO<sub>2</sub> fluxes over land and oceans since 1980. *Science*, **290**, 1342-1346.
- Boutin, J.**, J. Etcheto, Y. Dandonneau, D.C.E. Bakker, R.A. Feely, H.Y. Inoue, M. Ishii, R.D. Ling, P.D. Nightingale, N. Metzl, and R. Wanninkhof, 1999: Satellite sea surface temperature: a powerful tool for interpreting in situ pCO<sub>2</sub> measurements in the equatorial Pacific Ocean. *Tellus Series B-Chemical and Physical Meteorology*, **51**, 490-508.
- Boyd, P.W.**, A. Watson, C.S. Law, E. Abraham, T. Trull, R. Murdoch, D.C.E. Bakker, A.R. Bowie, K. Buesseler, H. Chang, M. Charette, P. Croot, K. Downing, R. Frew, M. Gall, M. Hadfield, J. Hall, M. Harvey, G. Jameson, J. La Roche, M. Liddicoat, R. Ling, M. Maldonado, R.M. McKay, S. Nodder, S. Pickmere, R. Pridmore, S. Rintoul, K. Safi, P. Sutton, R. Strzepek, K. Tanneberger, S. Turner, A. Waite, and J. Zeldis, 2000: A mesoscale phytoplankton bloom in the polar Southern Ocean stimulated by iron fertilization. *Nature*, **407**, 695-702.
- Boyle, E.A.**, 1988: The role of vertical chemical fractionation in controlling late Quaternary atmospheric carbon dioxide. *Journal of Geophysical Research*, **93**, 15701-15714.
- Braun, S.**, Rihm, B., Schindler, C., and Fluckiger, W., 2000: Growth of mature beech in relation to ozone and nitrogen deposition: an epidemiological approach. *Water Air and Soil Pollution*, **116**, 357-364.
- Braswell, B.H.**, D.S. Schimel, E. Linder, and B. Moore, 1997: The response of global terrestrial ecosystems to interannual temperature variability. *Science*, **278**, 870-872.
- Bretherton, F.P.**, K. Bryan, and J.D. Woods, 1990: Time-dependent greenhouse-gas-induced climate change. In: *Climate Change, The IPCC Scientific Assessment* [Houghton, J.T., G.J. Jenkins and J.J. Ephraums (eds.)]. Cambridge University Press, Cambridge, pp. 173-194.
- British Petroleum Company**, 2000: BP Statistical Review of World Energy 1999. British Petroleum Company, London, UK.
- Broecker, W.S.**, and T.H. Peng, 1982: Tracers in the sea, Eldigio, Palisades, pp. 691.
- Broecker, W.S.** and T.H. Peng, 1992: Interhemispheric transport of carbon dioxide by ocean circulation. *Nature*, **356**, 587-589.
- Broecker, W.S.**, and G.M. Henderson, 1998: The sequence of events surrounding Termination II and their implications for the cause of glacial-interglacial CO<sub>2</sub> changes. *Paleoceanography*, **13**, 352-364.
- Broecker, W.S.**, S. Sutherland, W. Smethie, T.H. Peng, and G. Ostlund, 1995: Oceanic radiocarbon: separation of the natural and bomb components. *Global Biogeochemical Cycles*, **9**, 263-288.
- Broecker, W.**, J. Lynch-Stieglitz, D. Archer, M. Hofmann, E. Maier-Reimer, O. Marchal, T. Stocker, and N. Gruber, 1999: How strong is the Harvard-Bear constraint? *Global Biogeochemical Cycles*, **13**, 817-820.
- Brovkin, V.**, A. Ganopolski, and Y. Svirzhev, 1997: A continuous climate-vegetation classification for use in climate-biosphere studies. *Ecological Modelling*, **101**, 251-261.
- Brown, S.**, J. Sathaye, M. Cannell, P. Kauppi, P. Burschel, A. Grainger, J. Heuveldop, R. Leemans, P. Moura Costa, M. Pinard, S. Nilsson, W. Schopfhauser, R. Sedjo, N. Singh, M. Trexler, J. van Minnen, S. Weyers, 1996: Management of forests for mitigation of greenhouse gas emissions. In: *IPCC Climate Change 1995 - Impacts, Adaptations and Mitigation of Climate Change: Scientific-Technical Analyses, Contribution of Working Group II to the Second Assessment Report of the Intergovernmental Panel on Climate Change* [Watson, R.T., M.C. Zinyowera, R.H. Moss and D.J. Dokken (eds.)], Cambridge University Press, Cambridge, pp. 773-797.
- Bryant, D.M.**, E.A. Holland, T.R. Seastedt and M.D. Walker, 1998: Analysis of litter decomposition in an alpine tundra. *Canadian Journal of Botany-Revue Canadienne De Botanique*, **76**, 1295-1304.
- Buchmann, N.**, and E.D. Schulze, 1999: Net CO<sub>2</sub> and H<sub>2</sub>O fluxes of terrestrial ecosystems. *Global Biogeochemical Cycles*, **13**, 751-760.
- Burrows, W.H.**, J.F. Compton, and M.B. Hoffmann, 1998: Vegetation thickening and carbon sinks in the grazed woodlands of north-east Australia. In: *Proceedings Australian Forest Growers Conference*, Lismore, NSW, pp. 305-316.
- Caldeira, K.**, and P.B. Duffy, 2000: The role of the Southern Ocean in uptake and storage of anthropogenic carbon dioxide. *Science*, **287**, 620-622.
- Cao, M.**, and F.I. Woodward, 1998a: Dynamic responses of terrestrial ecosystem carbon cycling to global climate change. *Nature*, **393**, 249-252.
- Cao, M.K.**, and F.I. Woodward, 1998b: Net primary and ecosystem production and carbon stocks of terrestrial ecosystems and their responses to climate change. *Global Change Biology*, **4**, 185-198.
- Carter, A.J.** and R.J. Scholes, 2000: Spatial Global Database of Soil Properties. IGBP Global Soil Data Task CD-ROM. International Geosphere-Biosphere Programme (IGBP) Data Information Systems. Toulouse, France.
- Catubig, N.R.**, D.E. Archer, R. Francois, P. deMenocal, W. Howard and E.-F. Yu, 1998: Global deep-sea burial rate of calcium carbonate during the last glacial maximum. *Paleoceanography*, **13**, 298-310.
- Cerling, T.E.**, Y. Wang, and J. Quade, 1993: Expansion of C<sub>4</sub> ecosystems as an indicator of global ecological change in the late miocene. *Nature*, **361**, 344-345.
- Cerling, T.E.**, J.M. Harris, B.J. MacFadden, M.G. Leakey, J. Quade, V. Eisenmann, 1997: Global vegetation change through the Miocene-Pliocene boundary. *Nature*, **389**, 153-158.
- Chapin, F.S.**, 1980: The mineral-nutrition of wild plants. *Annual Review of Ecology and Systematics*, **11**, 233-260.
- Chapman, W.L.**, and J.E. Walsh, 1993: Recent variations of sea ice and air-temperature in high-latitudes. *Bulletin of the American Meteorological Society*, **74**, 33-47.
- Ciais, P.**, P.P. Tans, and M. Trolier, 1995a: A large northern-hemisphere

- terrestrial CO<sub>2</sub> sink indicated by the <sup>13</sup>C/<sup>12</sup>C ratio of atmospheric CO<sub>2</sub>. *Science*, **269**, 1098-1102.
- Ciais**, P., P.P. Tans, J.W.C. White, M. Trolier, R.J. Francey, J.A. Berry, D.R. Randall, P.J. Sellers, J.G. Collatz, and D.S. Schimel, 1995b: Partitioning of ocean and land uptake of CO<sub>2</sub> as inferred by  $\delta^{13}\text{C}$  measurements from the NOAA Climate Monitoring and Diagnostics Laboratory Global Air Sampling Network. *Journal of Geophysical Research-Atmospheres*, **100**, 5051-5070.
- Ciais**, P., A.S. Denning, P.P. Tans, J.A. Berry, D.A. Randall, G.J. Collatz, P.J. Sellers, J.W.C. White, M. Trolier, H.A.J. Meijer, R.J. Francey, P. Monfray, and M. Heimann, 1997: A three-dimensional synthesis study of  $\delta^{18}\text{O}$  in atmospheric CO<sub>2</sub>. 1. Surface Fluxes. *Journal of Geophysical Research - Atmosphere*, **102**, 5857-5872.
- Ciais**, P., P. Friedlingstein, D.S. Schimel, and P.P. Tans, 1999: A global calculation of the delta <sup>13</sup>C of soil respired carbon: Implications for the biospheric uptake of anthropogenic CO<sub>2</sub>. *Global Biogeochemical Cycles*, **13**, 519-530.
- Cienciala**, E., S. W. Running, A. Lindroth, A. Grelle, and M.G. Ryan, 1998: Analysis of carbon and water fluxes from the NOPEX boreal forest: comparison of measurements with Forest-BGC simulations. *Journal of Hydrology*, **212-213**, 62-78.
- Clark**, F.E., 1977: Internal cycling of <sup>15</sup>N in shortgrass prairie. *Ecology*, **58**, 1322-1333.
- Clymo**, R.S., J. Turunen, and K. Tolonen, 1998: Carbon accumulation in peatland. *Oikos*, **81**, 368-388.
- Coale**, K.H., K.S. Johnson, S.E. Fitzwater, R.M. Gordon, S. Tanner, F.P. Chavez, L. Ferioli, C. Sakamoto, P. Rogers, F. Millero, P. Steinberg, P. Nightingale, D. Cooper, W.P. Cochlan, M.R. Landry, J. Constantinou, G. Rollwagen, A. Trasvina, and R. Kudela, 1996: A massive phytoplankton bloom induced by an ecosystem-scale iron fertilization experiment in the equatorial Pacific Ocean. *Nature*, **383**, 495-501.
- Cole**, C.V., C. Cerri, K. Minami, A. Mosier, N. Rosenberg, D. Sauerbeck, J. Dumanski, J. Duxbury, J. Freney, R. Gupta, O. Heinemeyer, T. Kolchugina, J. Lee, K. Paustian, D. Powlson, N. Sampson, H. Tiessen, M. Van Noordwijk, Q. Zhao, I.P. Abrol, T. Barnwell, C.A. Campbell, R.L. Desjardin, C. Feller, P. Garin, M.J. Glendining, E.G. Gregorich, D. Johnson, J. Kimble, R. Lal, C. Montreal, D.S. Ojima, M. Padgett, W. Post, W. Sombroek, C. Tarnocai, T. Vinson, S. Vogel, and G. Ward, 1996: Agricultural options for mitigation of greenhouse gas emissions. In: *Climate Change 1995 – Impacts, Adaptations and Mitigation of Climate Change: Scientific–Technical Analyses* [Watson, R.T., M.C. Zinyowera and R.H. Moss (eds.)], Cambridge University Press, Cambridge, pp. 745-771.
- Collatz**, G.J., J.A. Berry, and J.S. Clark, 1998: Effects of climate and atmospheric CO<sub>2</sub> partial pressure on the global distribution of C<sub>4</sub> grasses: present, past, and future. *Oecologia*, **114**, 441-454.
- Conway**, T.J., P.P. Tans, L.S. Waterman, K.W. Thoning, D.R. Kitzis, K.A. Masarie, and N. Zhang, 1994: Evidence for interannual variability of the carbon cycle from the National Oceanic and Atmospheric Administration/Climate Monitoring and Diagnostics Laboratory global air sampling network. *Journal of Geophysical Research*, **99**, 22831-22855.
- Cox**, P.M., R.A. Betts, C.D. Jones, S.A. Spall, and I.J. Totterdell, 2000: Acceleration of global warming due to carbon-cycle feedbacks in a coupled model. *Nature*, **408**, 184-187.
- Cramer**, W. and C.B. Field, 1999: Comparing global models of terrestrial net primary productivity (NPP): introduction. *Global Change Biology*, **5**, III-IV.
- Cramer**, W., D.W. Kicklighter, A. Bondeau, B. Moore III, G. Churkina, B. Nemry, A. Ruimy, A.L. Schloss and the participants of the Potsdam NPP Model Intercomparison, 1999: Comparing global models of terrestrial net primary productivity (NPP) overview and key results. *Global Change Biology*, **5**, 1-16.
- Cramer**, W., A. Bondeau, F.I. Woodward, I.C. Prentice, R.A. Betts, V. Brovkin, P.M. Cox, V. Fisher, J.A. Foley, A.D. Friend, C. Kucharik, M.R. Lomas, N. Ramankutty, S. Sitch, B. Smith, A. White, and C. Young-Molling, 2001: Global response of terrestrial ecosystem structure and function to CO<sub>2</sub> and climate change: results from six dynamic global vegetation models. *Global Change Biology* (in press).
- Crowley**, T.J., 1995: Ice-age terrestrial carbon changes revisited. *Global Biogeochemical Cycles*, **9**, 377-389.
- Curtis**, P.S., 1996: A meta-analysis of leaf gas exchange and nitrogen in trees grown under elevated carbon dioxide. *Plant Cell and Environment*, **19**, 127-137.
- Curtis**, P.S., and X.Z. Wang, 1998: A meta-analysis of elevated CO<sub>2</sub> effects on woody plant mass, form, and physiology. *Oecologia*, **113**, 299-313.
- Dai**, A., and I.Y. Fung, 1993: Can climate variability contribute to the "missing" CO<sub>2</sub> sink? *Global Biogeochemical Cycles*, **7**, 599-609.
- Dai**, A., K.E. Trenberth and T.R. Karl, 1998: Global variations in droughts and wet spells: 1900-1995. *Geophysical Research Letters*, **25**, 3367-3370.
- De Fries**, R.S. and J.R.G. Townshend, 1994: NDVI-derived land-cover classifications at a global-scale. *International Journal of Remote Sensing*, **15**, 3567-3586.
- De Fries**, R.S., C.B. Field, I. Fung, C.O. Justice, S. Los, P.A. Matson, E. Matthews, H.A. Mooney, C.S. Potter, K. Prentice, P.J. Sellers, J.R.G. Townshend, C.J. Tucker, S.L. Ustin and P.M. Vitousek, 1995: Mapping the land-surface for global atmosphere-biosphere models - toward continuous distributions of vegetation functional- properties. *Journal of Geophysical Research-Atmospheres*, **100**, 20867-20882.
- De Fries**, R.S., C.B. Field, I. Fung, G.J. Collatz, and L. Bounoua, 1999: Combining satellite data and biogeochemical models to estimate global effects of human-induced land cover change on carbon emissions and primary productivity. *Global Biogeochemical Cycles*, **13**, 803-815.
- Delgado**, J.A., A.R. Mosier, D.W. Valentine, D.S. Schimel, and W.J. Parton, 1996: Long term <sup>15</sup>N studies in a catena of the shortgrass steppe. *Biogeochemistry*, **32**, 41-52.
- DeLucia**, E.H., J.G. Hamilton, S.L. Naidu, R.B. Thomas, J.A. Andrews, A. Finzi, M. Lavine, R. Matamala, J.E. Mohan, G.R. Hendrey, and W.H. Schlesinger, 1999: Net primary production of a forest ecosystem with experimental CO<sub>2</sub> enrichment. *Science*, **284**, 1177-1179.
- Denman**, K., E. Hofmann, and H. Marchant, 1996: Marine biotic responses to environmental change and feedbacks to climate, In: *Climate Change 1995. The Science of Climate Change*. [Houghton, J.T., L.G.M. Filho, B.A. Callander, N. Harris, A. Kattenberg, and K. Maskell (eds.)]. University Press, Cambridge, pp. 449-481.
- Denning**, A.S., I.Y. Fung, and D. Randall, 1995: Latitudinal gradient of atmospheric CO<sub>2</sub> due to seasonal exchange with land biota. *Nature*, **376**, 240-243.
- Denning**, A.S., D.A. Randall, G.J. Collatz, and P.J. Sellers, 1996: Simulations of terrestrial carbon metabolism and atmospheric CO<sub>2</sub> in a general circulation model. Part 2: Spatial and temporal variations of atmospheric CO<sub>2</sub>. *Tellus*, **48B**, 543-567.
- Denning**, A. S., M. Holzer, K. R. Gurney, M. Heimann, R. M. Law, P. J. Rayner, I. Y. Fung, S.-M. Fan, S. Taguchi, P. Friedlingstein, Y. Balkanski, J. Taylor, M. Maiss, and I. Levin, 1999: Three-dimensional transport and concentration of SF<sub>6</sub>: A model intercomparison study (TransCom 2). *Tellus*, **51B**, 266-297.
- Dettinger**, M.D. and M. Ghil, 1998: Seasonal and interannual variations of atmospheric CO<sub>2</sub> and climate. *Tellus Series B-Chemical and Physical Meteorology*, **50**, 1-24.
- Dixon**, R.K., S. Brown, R.A. Houghton, A.M. Solomon, M.C. Trexler and J. Wisniewski, 1994: Carbon Pools and Flux of Global Forest Ecosystems. *Science*, **263**, 185-190.
- Doney**, S.C., 1999: Major challenges confronting marine biogeochemical

- modeling. *Global Biogeochemical Cycles*, **13**, 705-714.
- Drake**, B.G., M.A. Gonzalez-Meler, and S.P. Long, 1997: More efficient plants: a consequence of rising atmospheric CO<sub>2</sub>? *Annual Review of Plant Physiology and Plant Molecular Biology*, **48**, 609-639.
- Drake**, B.G., J. Azcon-Bieto, J. Berry, J. Bunce, P. Dijkstra, J. Farrar, R.M. Gifford, M.A. Gonzalez-Meler, G. Koch, H. Lambers, J. Siedow and S. Wullschleger, 1999: Does elevated atmospheric CO<sub>2</sub> concentration inhibit mitochondrial respiration in green plants? *Plant Cell and Environment*, **22**, 649-657.
- Duce**, R.A., and N.W. Tindale, 1991: Atmospheric transport of iron and its deposition in the ocean. *Limnology and Oceanography*, **36**, 1715-1726.
- Ducklow**, H.W., 1999: The bacterial content of the oceanic euphotic zone. *FEMS Microbiology-Ecology*, **30**, 1-10.
- Edmonds**, J.A., M.A. Wise, R.D. Sands, R.A. Brown, and H.S. Kheshgi, 1996: Agriculture, Land Use, and Commercial Biomass Energy: A Preliminary Integrated Analysis of the Potential Role of Biomass Energy for Reducing Future Greenhouse Related Emissions. PNNL-111555. *Pacific Northwest National Laboratory, Washington, DC, USA*.
- Edwards**, R., P.N. Sedwick, V. Morgan, C.F. Boutron and S. Hong, 1998: Iron in ice cores from Law Dome, East Antarctica: implications for past deposition of aerosol iron. *Annals of Glaciology*, **27**, 365-370.
- Elderfield**, H. and R.E.M. Rickaby, 2000: Oceanic Cd/P ratio and nutrient utilization in the glacial Southern Ocean. *Nature*, **405**, 305-310.
- Elliott**, W.P., J.K. Angell and K.W. Thoning, 1991: Relation of atmospheric CO<sub>2</sub> to tropical sea and air temperatures and precipitation. *Tellus Series B-Chemical and Physical Meteorology*, **43**, 144-155.
- England**, M.H., 1995: Using chlorofluorocarbons to assess ocean climate models. *Geophysical Research Letters*, **22**, 3051-3054.
- Enting**, I.G. and J.V. Mansbridge, 1991: Latitudinal distribution of sources and sinks of CO<sub>2</sub> - results of an inversion study. *Tellus Series B-Chemical and Physical Meteorology*, **43**, 156-170.
- Enting**, I.G., T.M.L. Wigley, and M. Heimann, 1994: Future emissions and concentrations of carbon dioxide: Key ocean/atmosphere/land analyses. Division of Atmospheric Research, Commonw. Science and Ind. Research Organisation, Melbourne, Victoria.
- Enting**, I.G., C.M. Trudinger, and R.J. Francey, 1995: A Synthesis Inversion of the Concentration and  $\delta^{13}\text{C}$  of Atmospheric CO<sub>2</sub>. *Tellus Series B-Chemical and Physical Meteorology*, **47**, 35-52.
- Eppley**, R.W., and B.J. Peterson, 1979: Particulate organic-matter flux and planktonic new production in the deep ocean. *Nature*, **282**, 677-680.
- Etheridge**, D.M., L.P. Steele, R.L. Langenfelds, R.J. Francey, J.M. Barnola, and V.I. Morgan, 1996: Natural and anthropogenic changes in atmospheric CO<sub>2</sub> over the last 1000 years from air in Antarctic ice and firn. *Journal of Geophysical Research - Atmosphere*, **101**, 4115-4128.
- Falkowski**, P.G., 1994: The role of phytoplankton photosynthesis in global biogeochemical cycles. *Photosynthesis Research*, **39**, 235-258.
- Falkowski**, P.G., 1997: Evolution of the nitrogen cycle and its influence on the biological CO<sub>2</sub> pump in the ocean. *Nature*, **387**, 272-275.
- Falkowski**, P.G., R.T. Barber, and V. Smetacek, 1998: Biogeochemical controls and feedbacks on ocean primary production. *Science*, **281**, 200-206.
- Falloon**, P., Smith, P., Coleman, K. and Marshall, S. 1998: Estimating the size of the inert organic matter pool from total soil organic carbon content for use in the Rothamsted Carbon Model. *Soil Biology and Biochemistry*, **30**, 1207-1211.
- Fan**, S., M. Gloor, and J. Mahlman, S. Pacala, J. Sarmiento, T. Takahashi and P. Tans, 1998: A large terrestrial carbon sink in North America implied by atmospheric and oceanic carbon dioxide data and models. *Science*, **282**, 442-446.
- Fan**, S.M., Blaine T.L., and Sarmiento J.L., 1999: Terrestrial carbon sink in the Northern Hemisphere estimated from the atmospheric CO<sub>2</sub> difference between Mauna Loa and the South Pole since 1959. *Tellus Series B-Chemical and Physical Meteorology*, **51**, 863-870.
- Fanning**, K.A., 1992: Nutrient provinces in the sea: concentration ratios, reaction rate ratios, and ideal covariation. *Journal of Geophysical Research*, **97**, 5693-5712.
- FAO**, 1993a: 1992 Production Yearbook. FAO, Rome, Italy
- FAO**, 1993b: Forest Resources Assessment 1990. *Tropical Countries. FAO Forestry Pap. No. 112*. UN Food Agric. Org., Rome, Italy.
- FAO**, 1997: State of the world's forests. FAO, Rome, Italy.
- Farquhar**, G.D., 1997: Carbon dioxide and vegetation. *Science*, **278**, 1411.
- Farquhar**, G.D., S.V. von Caemmerer, and J.A. Berry, 1980: A biochemical-model of photosynthetic CO<sub>2</sub> assimilation in leaves of C<sub>3</sub> plants. *Planta*, **149**, 78-90.
- Farquhar**, G.D., J. Lloyd, J.A. Taylor, L.B. Flanagan, J.P. Syvertsen, K.T. Hubick, S.C. Wong, and J.R. Ehleringer, 1993: Vegetation effects on the isotope composition of oxygen in atmospheric CO<sub>2</sub>. *Nature*, **363**, 439-443.
- Fearnside**, P.M., 2000: Global warming and tropical land-use change: greenhouse gas emissions from biomass burning, decomposition and soils in forest conversion, shifting cultivation and secondary vegetation. *Climatic Change*, **46**, 115-158.
- Feely**, R.A., R.H. Gammon, B.A. Taft, P.E. Pullen, L.S. Waterman, T.J. Conway, J.F. Gendron and D.P. Wisegarver, 1987: Distribution of chemical tracers in the eastern equatorial Pacific during and after the 1982-1983 El Niño/Southern Oscillation event. *Journal of Geophysical Research*, **92**, 6545-6558.
- Feely**, R.A., R. Wanninkhof, C. Goyet, D.E. Archer, and T. Takahashi, 1997: Variability of CO<sub>2</sub> distributions and sea-air fluxes in the central and eastern equatorial Pacific during the 1991-1994 El Niño. *Deep-Sea Research Part II-Topical Studies in Oceanography*, **44**, 1851-1867.
- Feely**, R.A., C.L. Sabine, R.M. Key, and T.H. Peng, 1999a: CO<sub>2</sub> synthesis results: estimating the anthropogenic carbon dioxide sink in the Pacific ocean. *US JGOFS News*, **9**, 1-5.
- Feely**, R.A., R. Wanninkhof, T. Takahashi, and P. Tans, 1999b: Influence of El Niño on the equatorial Pacific contribution to atmospheric CO<sub>2</sub> accumulation. *Nature*, **398**, 597-601.
- Fearnside**, P.M., 2000: Global warming and tropical land-use change: Greenhouse gas emissions from biomass burning, decomposition and soils in forest conversion, shifting cultivation and secondary vegetation. *Climatic Change*, **46**, 115-158.
- Field**, C.B., R.B. Jackson, and H.A. Mooney, 1995a: Stomatal responses to increased CO<sub>2</sub>: implications from the plant to the global scale. *Plant Cell and Environment*, **18**, 1214-1225.
- Field**, C.B., J.T. Randerson, and C.M. Malmstrom, 1995b: Global net primary production - combining ecology and remote-sensing. *Remote Sensing of Environment*, **51**, 74-88.
- Field**, C.B., M.J. Behrenfeld, J.T. Randerson, and P. Falkowski, 1998: Primary production of the biosphere: Integrating terrestrial and oceanic components. *Science*, **281**, 237-240.
- Fischer**, H., M. Whalen, J. Smith, D. Mastrianni, and B. Deck, 1999: Ice core records of atmospheric CO<sub>2</sub> around the last three glacial terminations. *Science*, **283**, 1712-1714.
- Fisher**, M.J., I.M. Rao, M.A. Ayarza, C.E. Lascano, J.I. Sanz, R.J. Thomas, and R.R. Vera, 1994: Carbon storage by introduced deep-rooted grasses in the South-American Savannas. *Nature*, **371**, 236-238.
- Fog**, K., 1988: The effect of added nitrogen on the rate of decomposition of organic -matter. *Biological Reviews of the Cambridge Philosophical Society*, **63**, 433-462.
- Foley**, J.A., 1994: The sensitivity of the terrestrial biosphere to climatic

- change: A simulation of the middle Holocene. *Global Biogeochemical Cycles*, **8**, 505-525.
- Foley**, J.A., I.C. Prentice, N. Ramankutty, S. Levis, D. Pollard, S. Sitch, and A. Haxeltine, 1996: An integrated biosphere model of land surface processes, terrestrial carbon balance, and vegetation dynamics. *Global Biogeochemical Cycles*, **10**, 603-628.
- Foley**, N.A., S. Levis, and I.C. Prentice, 1998: Coupling dynamic models of climate and vegetation. *Global Change Biology*, **4**, 561-579.
- Fowler**, D., J.N. Cape, M. Coyle, C. Flechard, J. Kuylenstierna, K. Hicks, D. Derwent, C. Johnson, and D. Stevenson, 2000: The global exposure of forests to air pollutants. *Water Air and Soil Pollution*, **116**, 5-32.
- François**, R., M.A. Altabet, E.F. Yu, D.M. Sigman, M.P. Bacon, M. Frank, G. Bohrmann, G. Bareille and L.D. Labeyrie, 1997: Contribution of Southern Ocean surface-water stratification to low atmospheric CO<sub>2</sub> concentrations during the last glacial period. *Nature*, **389**, 929-935.
- Francey**, R.J., and P.P. Tans, 1987: Latitudinal variation in O<sup>18</sup> of atmospheric CO<sub>2</sub>. *Nature*, **327**, 495-497.
- Francey**, R.J., P.P. Tans, and C.E. Allison, 1995: Changes in oceanic and terrestrial carbon uptake since 1982. *Nature*, **373**, 326-330.
- Francey**, R., P. Rayner, R. Langenfelds, and C. Trudinger, 1999a: The inversion of atmospheric CO<sub>2</sub> mixing ratios and isotopic composition to constrain large-scale air-sea fluxes. In: *2nd international symposium CO<sub>2</sub> in the oceans*, Center for Global Environmental Research, National Institute for Environmental Study, Tsukuba, Japan, 237-243.
- Francey**, R.J., C.E. Allison, D.M. Etheridge, C.M. Trudinger, I.G. Enting, M. Leuenberger, R.L. Langenfelds, E. Michel, and L.P. Steele, 1999b: A 1000-year high precision record of delta <sup>13</sup>C in atmospheric CO<sub>2</sub>. *Tellus Series B-Chemical and Physical Meteorology*, **51**, 170-193.
- Frankignoulle**, M., G. Abril, A. Borges, I. Bourge, C. Canon, B. Delille, E. Libert, and J.-M. Théate, 1998: Carbon dioxide emission from European estuaries. *Science*, **282**, 434-436.
- Friedlingstein**, P., I. Fung, E. Holland, J. John, G. Brasseur, D. Erickson and D. Schimel, 1995a: On the contribution of CO<sub>2</sub> fertilization to the missing biospheric sink. *Global Biogeochemical Cycles*, **9**, 541-556.
- Friedlingstein**, P., K.C. Prentice, I.Y. Fung, J.G. John, and G.P. Brasseur, 1995b: Carbon-biosphere-climate interactions in the last glacial maximum climate. *Journal of Geophysical Research - Atmosphere*, **100**, 7203-7221.
- Friedlingstein**, P., L. Bopp, P. Caias, J.-L. Dufresne, L. Fairhead, H. LeTreut, P. Monfray, and J. Orr, 2001: Positive feedback between future climate change and the carbon cycle. Note du Pole de Modelisation, *Geophys. Res. Lett.*, **28**, 1543-1546.
- Friend**, A.D., A.K. Stevens, R.G. Knox, and M.G.R. Cannell, 1997: A process-based, terrestrial biosphere model of ecosystem dynamics (Hybrid v3.0). *Ecological Modelling*, **95**, 249-287.
- Fuglestvedt**, J.S., and T. Berntsen, 1999: A simple model for scenario studies of changes in global climate. *Technical Report # 1999:2*, Center for International Climate and Environmental Research, Oslo.
- Fung**, I.Y., S.K. Meyn, I. Tegen, S.C. Doney, J. John, and J.K.B. Bishop, 2000: Iron supply and demand in the upper ocean. *Global Biogeochemical Cycles*, **14**, 281-295.
- Gattuso**, J.-P., M. Frankignoulle and R. Wollast, 1998: Carbon and carbonate metabolism in coastal aquatic ecosystems. *Annual Review of Ecology and Systematics*, **29**, 405-434.
- Ganeshram**, R.S., T.F. Pedersen, S.E. Calvert, and J.W. Murray, 1995: Large changes in oceanic nutrient inventories from glacial to interglacial periods. *Nature*, **376**, 755-758.
- Gérard**, J.C., B. Nemry, L.M. Francois and P. Warnant, 1999: The interannual change of atmospheric CO<sub>2</sub>: contribution of subtropical ecosystems? *Geophys. Res. Lett.*, **26**, 243-246.
- Giardina**, C.P. and M.G. Ryan, 2000: Evidence that decomposition rates of organic carbon in mineral soil do not vary with temperature. *Nature*, **404**, 858-861.
- Gifford**, R.M., 1992: Implications of the globally increasing atmospheric CO<sub>2</sub> concentration and temperature for the Australian terrestrial carbon budget - integration using a simple-model. *Australian Journal of Botany*, **40**, 527-543.
- Gorham**, E., 1991: Northern peatlands - role in the carbon-cycle and probable responses to climatic warming. *Ecological Applications*, **1**, 182-195.
- Goulden**, M.L., J.W. Munger, S.M. Fan, B.C. Daube, and S.C. Wofsy, 1996: Exchange of carbon dioxide by a deciduous forest: Response to interannual climate variability. *Science*, **271**, 1576-1578.
- Goulden**, M.L., S.C. Wofsy, J.W. Harden, S.E. Trumbore, P.M. Crill, S.T. Gower, T. Fries, B.C. Daube, S.M. Fan, D.J. Sutton, A. Bazzaz, and J.W. Munger, 1998: Sensitivity of boreal forest carbon balance to soil thaw. *Science*, **279**, 214-217.
- Goyet**, C., and D. Davis, 1997: Estimation of total CO<sub>2</sub> concentration throughout the water column. *Deep-Sea Research Part I-Oceanographic Research Papers*, **44**, 859-877.
- Gruber**, N., 1998: Anthropogenic CO<sub>2</sub> in the Atlantic Ocean. *Global Biogeochemical Cycles*, **12**, 165-191.
- Gruber**, N., and J. L. Sarmiento, 1997: Global patterns of marine nitrogen fixation and denitrification. *Global Biogeochemical Cycles*, **11**, 235-266.
- Gruber**, N. and C. D. Keeling, 2001: An improved estimate of the isotopic air-sea disequilibrium of CO<sub>2</sub>: Implications for the oceanic uptake of anthropogenic CO<sub>2</sub>. *GRL*, vol. 28, pg 555-558.
- Gruber**, N., J.L. Sarmiento, and T.F. Stocker, 1996: An improved method for detecting anthropogenic CO<sub>2</sub> in the oceans. *Global Biogeochemical Cycles*, **10**, 809-837.
- Gruber**, N., C.D. Keeling, R.B. Bacastow, P.R. Guenther, T.J. Lueker, M. Wahlen, H.A.J. Meijer, W.G. Mook, and T.F. Stocker, 1999: Spatiotemporal patterns of carbon-13 in the global surface oceans and the oceanic Suess effect. *Global Biogeochemical Cycles*, **13**, 307-335.
- Gunderson**, P., B.A. Emmett, O.J. Kjønaas, C.J. Koopmans, A. Tietema, 1998: Impact of nitrogen deposition on nitrogen cycling in forests: a synthesis of NITREX data. *Forest Ecology and Management*, **101**, 37-55
- Hall**, D.O., J.M.O. Scurlock, H.R. Bolhar-Nordenkampf, P.C. Leegood, and S.P. Long, 1993: Photosynthesis and Production in a Changing Environment: A Field and Laboratory Manual, (eds.).] Chapman & Hall, London, 464pp.
- Hall**, D.O., J. House, and I. Scrase, 2000: An overview of biomass energy. In: *Industrial Uses of Biomass Energy: the Example of Brazil* [Rosillo-Calle, F., H. Rothman and S.V. Bajay (eds.)]. Taylor & Francis, London.
- Hansell**, D.A., and C.A. Carlson, 1998: Deep-ocean gradients in the concentration of dissolved organic carbon. *Nature*, **395**, 263-266.
- Hansell**, D.A., and R.A. Feely, 2000: Atmospheric intertropical convergence impacts surface ocean carbon and nitrogen biogeochemistry in the western tropical Pacific. *Geophys. Res. Lett.*, **27**, 1013-1016.
- Harrison**, K.G., 2000: Role of increased marine silica input on paleo-pCO<sub>2</sub> levels. *Paleoceanography*, **15**, 292-298.
- Harrison**, S.P., K.E. Kohfeld, C. Roelandt, and T. Claquin, 2001: The role of dust in climate changes today, at the last glacial maximum and in the future. *Earth Science Reviews* (in press).
- Harvey**, L.D.D., 1989: Effect of model structure on the response of terrestrial biosphere models to CO<sub>2</sub> and temperature increases. *Global Biogeochemical Cycles*, **3**, 137-153.
- Harvey**, L. D. D., Gregory, J., Hoffert, M., Jain, A., Lal, M., Leemans, R., Raper, S. C. B., Wigley, T. M. L., and de Wolde, J. R., 1997: *An introduction to simple climate models used in the IPCC Second Assessment Report. IPCC Technical Paper II*, [Houghton, J.T., L.G.

- Meira Filho, D.J. Griggs and K. Maskell (eds)]. IPCC, Geneva, Switzerland. 50 pp.
- Haxeltine**, A., and I.C. Prentice, 1996: BIOME3: An equilibrium terrestrial biosphere model based on ecophysiological constraints, resource availability, and competition among plant functional types. *Global Biogeochemical Cycles*, **10**, 693 - 709.
- Hays**, J.D., J. Imbrie, and N.J. Shackleton, 1976: Variations in Earths Orbit - Pacemaker of Ice Ages. *Science*, **194**, 1121-1132.
- Heimann**, M., 2001: Atmospheric Inversion Calculations Performed for IPCC Third Assesment Report Chapter 3 (The Carbon Cycle and Atmospheric CO<sub>2</sub>), Technical Reports - Max-Planck-Institute für Biogeochemie No. 2.
- Heimann**, M. and Maier-Reimer, E., 1996: On the relations between the oceanic uptake of CO<sub>2</sub> and its carbon isotopes. *Global Biogeochemical Cycles*, **10**, 89-110.
- Heimann**, M., and T. Kaminski, 1999: Inverse modelling approaches to infer surface trace gas fluxes from observed atmospheric mixing ratios. In: *Approaches to scaling a trace gas fluxes in ecosystems* [Bowman A.F. (ed.)]. Elsevier Science, pp. 277-295.
- Heimann**, M., C.D. Keeling, and I.Y. Fung, 1986: Simulating the atmospheric carbon dioxide distribution with a three dimensional tracer model. In: *The Changing Carbon Cycle: A Global Analysis* [J.R. Trabalka and D. E. Reichle (eds.)]. Springer-Verlag, New York.
- Heimann**, M., G. Esser, J. Kaduk, D. Kicklighter, G. Kohlmaier, D. McGuire, B. Morre III, C. Prentice, W. Sauf, A. Schloss, U. Wittenberg, and G. Würth, 1997: Interannual variability of CO<sub>2</sub> exchange fluxes as simulated by four terrestrial biogeochemical models. In: *Fifth International Carbon Dioxide Conference*, Cairns, Queensland, Australia.
- Heimann**, M., G. Esser, A. Haxeltine, J. Kaduk, D.W. Kicklighter, W. Knorr, G.H. Kohlmaier, A.D. McGuire, J. Melillo, B. Moore, R.D. Otto, I.C. Prentice, W. Sauf, A. Schloss, S. Sitch, U. Wittenberg, and G. Würth, 1998: Evaluation of Terrestrial Carbon Cycle Models Through Simulations of the Seasonal Cycle of Atmospheric CO<sub>2</sub> - First Results of a Model Intercomparison Study. *Global Biogeochemical Cycles*, **12**, 1-24.
- Hewitt**, C.D., and J.F.B. Mitchell, 1997: Radiative forcing and response of a GCM to ice age boundary conditions: cloud feedback and climate sensitivity. *Climate Dynamics*, **13**, 821-834.
- Hoffert**, M.I., A.J. Callegari, and C.T. Hsieh, 1980: The role of deep-sea heat-storage in the secular response to climatic forcing. *Journal of Geophysical Research-Oceans and Atmospheres*, **85**, 6667-6679.
- Holfort**, J., K.M. Johnson, B. Schneider, G. Siedler, and D.W.R. Wallace, 1998: Meridional transport of dissolved inorganic carbon in the South Atlantic Ocean. *Global Biogeochemical Cycles*, **12**, 479-499.
- Holland**, E.A., B.H. Braswell, J.F. Lamarque, A. Townsend, J. Sulzman, J.F. Muller, F. Dentener, G. Brasseur, H. Levy, J.E. Penner, and G.J. Roelofs, 1997: Variations in the predicted spatial distribution of atmospheric nitrogen deposition and their impact on carbon uptake by terrestrial ecosystems. *Journal of Geophysical Research - Atmosphere*, **102**, 15849-15866.
- Holland**, E.A., F.J. Dentener, B.H. Braswell, and J.M. Sulzman, 1999: Contemporary and pre-industrial global reactive nitrogen budgets. *Biogeochemistry*, **46**, 7-43.
- Hooss**, G., R. Voss, K. Hasselmann, E. Meier-Reimer, and F. Joss, 1999: A nonlinear impulse response model of the coupled carbon cycle-ocean-atmosphere climate system. Max-Planck-Institut für Meteorologie, Hamburg.
- Houghton**, R.A., 1995: Effects of land-use change, surface temperature, and CO<sub>2</sub> concentration on terrestrial stores of carbon. In: *Biotic Feedbacks in teh Global Climate System* [Woodwell, G.M. (ed.)]. Oxford University Press, London, pp. 333-350.
- Houghton**, R.A., 1999: The annual net flux of carbon to the atmosphere from cahgnes in land use 1850-1990. *Tellus*, **51B**, 298-313.
- Houghton**, R.A., 2000: A new estimate of global sources and sinks of carbon from land-use change. *EOS*, **81**, supplement s281.
- Houghton**, R.A., and J.L. Hackler, 1995: Continental scale estimates of the biotic carbon flux from land cover change: 1850-1980. ORNL/CDIAC-79, NDP-050. Oak Ridge National Laboratory, Oak Ridge, Tennessee, pp. 144.
- Houghton**, R.A., and J.L. Hackler, 1999: Emissions of carbon from forestry and land-use change in tropical Asia. *Global Change Biology*, **5**, 481-492.
- Houghton**, R.A., and K. Ramakrishna, 1999: A review of national emissions inventories from select non-annex I countries: Implications for counting sources and sinks of carbon. *Annual Review of Energy Environment*, **24**, 571-605.
- Houghton**, R.A., J.L. Hackler, and K.T. Lawrence, 1999: The US carbon budget: Contributions from land-use change. *Science*, **285**, 574-578.
- Houghton**, R.A., D.L. Skole, C.A. Nobre, J.L. Hackler, K.T. Lawerence and W.H. Chomentowski, 2000: Annual fluxes of carbon from deforestation and regrowth in the Brazilian Amazon. *Nature*, **403**, 301-304.
- House**, J.I., and D.O. Hall, 2001: Net primary production of savannas and tropical grasslands, In: *Terrestrial Global Productivity: Past, Present and Future* [Mooney, H., J. Roy and B. Saugier (eds.)], Academic Press, San Diego (in press).
- Hungate**, B.A., E.A. Holland, R.B. Jackson, F.S. Chapin, H.A. Mooney, and C.B. Field, 1997: The fate of carbon in grasslands under carbon dioxide enrichment. *Nature*, **388**, 576-579.
- Hungate**, B.A., P. Dijkstra, D.W. Johnson, C.R. Hinkle and B.G. Drake, 1999: Elevated CO<sub>2</sub> increases nitrogen fixation and decreases soil nitrogen mineralization in Florida scrub oak. *Global Change Biology*, **5**, 781-789.
- Hunt**, E.R., S.C. Piper, R. Nemani, C.D. Keeling, R.D. Otto, and S.W. Running, 1996: Global net carbon exchange and intra-annual atmospheric CO<sub>2</sub> concentrations predicted by an ecosystem process model and three dimensional atmospheric transport model. *Global Biogeochemical Cycles*, **10**, 431-456.
- Huntingford**, C., P.M. Cox, and T.M. Lenton, 2000. Contrasting responses of a simple terrestrial ecosystem model to global change. *Ecological Modelling*, **134**(1), 41-58.
- Indermühle**, A., T.F. Stocker, F. Joss, H. Fischer, H.J. Smith, M. Wahnen, B. Deck, D. Mastroianni, J. Tschumi, T. Blunier, R. Meyer, and B. Stauffer, 1999: Holocene carbon-cycle dynamics based on CO<sub>2</sub> trapped in ice at Taylor Dome, Antarctica. *Nature*, **398**, 121-126.
- Indermühle**, A., E. Monnin B Stauffer, T. Stocker, and M. Wahnen, 2000. Atmospheric CO<sub>2</sub> concentration from 60 to 20 kyr BP from Taylor Dome ice core, Antarctica, *Geophys. Res. Lett.* **29**, 753-758.
- Inoue**, H.Y., and Y. Sugimura, 1992: Variations and distributions of CO<sub>2</sub> in and over the equatorial pacific during the period from the 1986/88 El-Niño event to the 1988/89 La-Niña event. *Tellus Series B*, **44**, 1-22.
- Ishitani**, H., T.B. Johansson, and S. Al-Khouli, 1996: Energy Supply Mitigation Options. In: *Climate Change 1995. Impacts, Adaptations and Mitigation of Climate Change: Scientific-Technical Analyses. Contribution of Working Group II to the Second Assessment Report of the Intergovernmental Panel on Climate Change*. [Watson, R.T., M.C. Zinyowera and R.H. Moss (eds.)]. Cambridge University Press, Cambridge, pp. 587-648.
- IPCC**, 1994: Radiative Forcing of Climate Change and An Evaluation of the IPCC IS92 Emissions Scenarios [Houghton, J.T., L.G. Meira Filho, J. Bruce, Hoesung Lee, B.A. Callander, E. Haines, N. Harris and K. Maskell (eds.)]. Cambridge University Press, Cambridge, pp. 339.
- IPCC**, 1996a: Climate Change 1995. The Science of Climate Change. Contribution of Working Group I to the Second Assessment Report of the Intergovernmental Panel on Climate Change. [Houghton, J.T., L.G. Meira Filho, B.A. Callander, N. Harris, A. Kattenberg and K. Maskell (eds.)]. Cambridge University Press, Cambridge, UK.

- IPCC**, 1996b: Climate Change 1995. Impacts, Adaptations and Mitigation of Climate Change: Scientific-Technical Analyses. Contribution of Working Group II to the Second Assessment Report of the Intergovernmental Panel on Climate Change. [Watson, R.T., M.C. Zinyowera, R.H. Moss and D.J. Dokken (eds.)]. Cambridge University Press, Cambridge, UK.
- IPCC**, 1997: Revised 1996 IPCC Guidelines for National Greenhouse Gas Inventories. Reference Manual, Intergovernmental Panel on Climate Change. [Houghton, J.T., L.G. Meira Filho, B. Lim, K. Treanton, I. Matsumoto, Y. Bonduki, D.J. Griggs and B.A. Callender (eds.)]. Cambridge University Press, Cambridge, UK.
- IPCC**, 2000a: Land Use, Land-Use Change, and Forestry. A Special Report of the IPCC. [Watson, R.T., I.R. Noble, B. Bolin, N.H. Ravindranath, D.J. Verardo and D.J. Dokken (eds.)]. Cambridge University Press, Cambridge, UK.
- IPCC**, 2000b: Special Report on Emissions Scenarios. A Special Report of Working Group III of the intergovernmental Panel on Climate Change. [Nakićenović, N., J. Alcamo, G. Davis, B. de Vries, J. Fenhann, S. Gaffin, K. Gregory, A. Grübler, T. Yong Jung, T. Kram, E.L. La Rovere, L. Michaelis, S. Mori, T. Morita, W. Pepper, H. Pitcher, L. Price, K. Riahi, A. Roehrl, H.-H. Rogner, A. Sankovski, M. Schlesinger, P. Shukla, S. Smith, R. Swart, S. van Rooijen, N. Victor and Z. Dadi (eds.)]. Cambridge University Press, Cambridge, UK.
- Ito** A. and T. Oikawa, 2000: The large carbon emission from terrestrial ecosystem in 1998: A model simulation, *Journal of the Meterological Society of Japan*, **78**, 103-110
- Jain** A.K., 2000: The Web Interface of Integrated Science Assessment Model (ISAM). <http://frodo.atmos.uiuc.edu/isam>.
- Jain**, A.K., H.S. Kheshgi, and D.J. Wuebbles, 1994: Integrated Science Model for Assessment of Climate Change. Lawrence Livermore National Laboratory, UCRL-JC-116526.
- Jain**, A.K., H.S. Kheshgi, M.I. Hoffert, and D.J. Wuebbles, 1995: Distribution of radiocarbon as a test of global carbon-cycle models. *Global Biogeochemical Cycles*, **9**, 153-166.
- Jarvis**, P. and S. Linder, 2000: Botany - Constraints to growth of boreal forests. *Nature*, **405**, 904-905.
- Jenkinson**, D.S., K. Goulding, and D.S. Powlson, 1999: Nitrogen deposition and carbon sequestration. *Nature*, **400**, 629-629.
- Joos**, F., M. Bruno, R. Fink, U. Siegenthaler, T.F. Stocker, and C. Le Quéré, 1996: An efficient and accurate representation of complex oceanic and biospheric models of anthropogenic carbon uptake. *Tellus Series B*, **48**, 397-417.
- Joos**, F., R. Meyer, M. Bruno, and M. Leuenberger, 1999a: The variability in the carbon sinks as reconstructed for the last 1000 years. *Geophys. Res. Lett.*, **26**, 1437-1441.
- Joos**, F., G.-K. Plattner, T.F. Stocker, O. Marchal, and A. Schmittner, 1999b: Global warming and marine carbon cycle feedbacks on future atmospheric CO<sub>2</sub>. *Science*, **284**, 464-467.
- Jones**, P.D., Parker, D.E., Osborn, T.J., and Briffa, K.R., 2000: Global and hemispheric temperature anomalies - land and marine instrumental records. In: *Trends: A Compendium of Data on Global Change*, Oak Ridge National Laboratory, Oak Ridge, Tenn., U.S.A.
- Kaminski**, T., R. Giering, and M. Heimann, 1996: Sensitivity of the seasonal cycle of CO<sub>2</sub> at remote monitoring stations with respect to seasonal surface exchange fluxes determined with the adjoint of an atmospheric transport model. *Physics and Chemistry of the Earth*, **21**, 457-462.
- Kaminski**, T., M. Heimann, and R. Giering, 1999: A coarse grid three-dimensional global inverse model of the atmospheric transport - 1. Adjoint model and Jacobian matrix. *Journal of Geophysical Research-Atmospheres*, **104**, 18535-18553.
- Karl**, D., R. Letelier, L. Tupas, J. Dore, J. Christian, and D. Hebel, 1997: The role of nitrogen fixation in biogeochemical cycling in the subtropical North Pacific Ocean. *Nature*, **388**, 533-538.
- Keeling**, C.D., and R. Revelle, 1985: Effects of El-Niño southern oscillation on the atmospheric content of carbon-dioxide. *Meteoritics*, **20**, 437-450.
- Keeling**, C.D., and T.P. Whorf, 2000: Atmospheric CO<sub>2</sub> records from sites in the SIO air sampling network. In: *Trends: A compendium of data on global change*. Carbon Dioxide Information Analysis Center, Oak Ridge National Laboratory, Oak Ridge, Tenn., USA.
- Keeling**, C.D., and Piper S.C., 2000: Interannual variations of exchanges of atmospheric CO<sub>2</sub> and <sup>13</sup>CO<sub>2</sub> with the terrestrial biosphere and oceans from 1978 to 2000: III. Simulated sources and sinks. Scripps Institution of Oceanography Reference No. 00-14, University of California, San Diego, 68 pp.
- Keeling**, C.D., W.G. Mook, and P.P. Tans, 1979: Recent trends in the <sup>13</sup>C-<sup>12</sup>C ratio of atmospheric carbon-dioxide. *Nature*, **277**, 121-123.
- Keeling**, C.D., R.B. Bacastow, and P.P. Tans, 1980: Predicted shift in the <sup>13</sup>C-<sup>12</sup>C ratio of atmospheric carbon-dioxide. *Geophys. Res. Lett.*, **7**, 505-508.
- Keeling**, C.D., R.B. Bacastow, A.L. Carter, S.C. Piper, T.P. Whorf, M. Heimann, W.G. Mook, and H. Roeloffzen, 1989: A three dimensional model of atmospheric CO<sub>2</sub> transport based on observed winds: 1. Analysis of observational data. In: *Aspects of Climate Variability in the Pacific and the Western Americas* [Peterson D.H. (ed.)]. American Geophysical Union, Washington, DC, pp. 165-236.
- Keeling**, C.D., T.P. Whorf, M. Wahlen, and J. Vanderplicht, 1995: Interannual extremes in the rate of rise of atmospheric carbon dioxide since 1980. *Nature*, **375**, 666-670.
- Keeling**, C.D., J.F.S. Chin, and T.P. Whorf, 1996a: Increased activity of northern vegetation inferred from atmospheric CO<sub>2</sub> measurements. *Nature*, **382**, 146-149.
- Keeling**, R.F., 1988: Measuring correlations between atmospheric oxygen and carbon-dioxide mole fractions - a preliminary-study in urban air. *Journal Of Atmospheric Chemistry*, **7**, 153-176.
- Keeling**, R.F., and S.R. Shertz, 1992: Seasonal and interannual variations in atmospheric oxygen and implications for the global carbon cycle. *Nature*, **358**, 723-727.
- Keeling**, R.F., and T.H. Peng, 1995: Transport of Heat, CO<sub>2</sub> and O<sub>2</sub> by the Atlantic thermohaline circulation. *Philosophical Transactions of the Royal Society of London Series B*, **348**, 133-142.
- Keeling**, R.F., R.P. Najjar, and M.L. Bender, 1993: What atmospheric oxygen measurements can tell us about the global carbon-cycle. *Global Biogeochemical Cycles*, **7**, 37-67.
- Keeling**, R.F., S.C. Piper, and M. Heimann, 1996b: Global and hemispheric CO<sub>2</sub> sinks deduced from changes in atmospheric O<sub>2</sub> concentration. *Nature*, **381**, 218-221.
- Kheshgi**, H.S., A.K. Jain, and D.J. Wuebbles, 1996: Accounting for the missing carbon sink with the CO<sub>2</sub> fertilization effect. *Climatic Change*, **33**, 31-62.
- Kicklighter**, D.W., M. Bruno, S. Dönges, G. Esser, M. Heimann, J. Helfrich, F. Ift, F. Joos, J. Kadku, G.H. Kohlmaier, A.D. McGuire, J.M. Melillo, R. Meyer, B. Moore III, A. Nadler, I.C. Prentice, W. Sauf, A.L. Schloss, S. Sitch, U. Wittenberg, and G. Würth, 1999: A first order analysis of the potential of CO<sub>2</sub> fertilization to affect the global carbon budget: A comparison of four terrestrial biosphere models. *Tellus*, **51B**, 343-366.
- Kindermann**, J., G. Wurth, G.H. Kohlmaier, and F.W. Badeck, 1996: Interannual variation of carbon exchange fluxes in terrestrial ecosystems. *Global Biogeochemical Cycles*, **10**, 737-755.
- Klepper**, O., and B.J. De Haan, 1995: A sensitivity study of the effect of global change on ocean carbon uptake. *Tellus Series B*, **47**, 490-500.
- Kleypas**, J.A., 1997: Modeled estimates of global reef habitat and carbonate production since the last glacial maximum. *Paleoceanography*, **12**, 533-545.
- Kleypas**, J.A., R.W. Buddemeier, D. Archer, J.P. Gattuso, C. Langdon, and B.N. Opdyke, 1999: Geochemical consequences of increased atmospheric carbon dioxide on coral reefs. *Science*, **284**, 118-120.

- Knorr**, W., 2000: Annual and interannual CO<sub>2</sub> exchanges of the terrestrial biosphere: process-based simulations and uncertainties. *Global Ecology and Biogeography*, **9**, 225-252.
- Knorr**, W., and M. Heimann, 1995: Impact of drought stress and other factors on seasonal land biosphere CO<sub>2</sub> exchange studied through an atmospheric tracer transport model. *Tellus*, **47B**, 471-489.
- Knorr**, W. and M. Heimann, 2001a: Uncertainties in global terrestrial biosphere modeling, Part I: a comprehensive sensitivity analysis with a new photosynthesis and energy balance scheme. *Global Biogeochemical Cycles*, **15**(1), 207-225.
- Knorr**, W., and M. Heimann, 2001b: Uncertainties in global terrestrial biosphere modeling, Part II: global constraints for a process-based vegetation model. *Global Biogeochemical Cycles*, **15**(1), 227-246.
- Knox**, F. and M.B. McElroy, 1984: Changes in atmospheric CO<sub>2</sub>: influence of the marine biota at high latitude. *Journal of Geophysical Research*, **89**, 4629-4637.
- Koch**, G.W., and H.A. Mooney, 1996: Response of terrestrial ecosystems to elevated CO<sub>2</sub>: a synthesis and summary. In: *Carbon Dioxide and Terrestrial Ecosystems* [Koch, G.W. and H.A. Mooney (eds.)]. Academic Press, San Diego, pp. 415-429.
- Körner**, C., 2000: Biosphere responses to CO<sub>2</sub>-enrichment. *Ecological Applications*, **10**, 1590-1619.
- Kucharik**, C.J., J.A. Foley, C. Delire, V.A. Fisher, M.T. Coe, J.D. Leters, C. Young-Molling, N. Ramankutty, J.M. Norman and S.T. Gower, 2000: Testing the performance of a Dynamic Global Ecosystem Model: Water balance, carbon balance, and vegetation structure. *Global Biogeochemical Cycles*, **14**, 795-825.
- Kuhlbusch**, T.A.J., M.O. Andeae, H. Cahier, J.G. Goldammer, J.P. Lacaux, R. Shea, and P.J. Crutzen, 1996: Black carbon formation by savanna fires: Measurements and implications for the global carbon cycle. *Journal of Geophysical Research*, **101**, 23651-23665.
- Kumar**, N., R.F. Anderson, R.A. Mortlock, P.N. Froelich, P. Kubik, B. Dittrich-Hannen, and M. Suter, 1995: Increased biological productivity and export production in the glacial Southern Ocean. *Nature*, **378**, 675-680.
- Langenfelds**, R.L., R.J. Francey, and L.P. Steele, 1999: Partitioning of the global fossil CO<sub>2</sub> sink using a 19-year trend in atmospheric O<sub>2</sub>. *Geophys. Res. Lett.*, **26**, 1897-1900.
- Langdon**, C., T. Takahashi, C. Sweeney, D. Chipman, J. Goddard, F. Marubini, H. Aceves, H. Barnett and M. Atkinson, 2000: Effect of calcium carbonate saturation state on the calcification rate of an experimental coral reef. *Global Biogeochemical Cycles*, **14**, 639-654.
- Law**, R.M., P.J. Rayner, A.S. Denning, D. Erickson, I.Y. Fung, M. Heimann, S.C. Piper, M. Ramonet, S. Taguchi, J.A. Taylor, C.M. Trudinger, and I.G. Watterson, 1996: Variations in modeled atmospheric transport of carbon dioxide and the consequences for CO<sub>2</sub> inversions. *Global Biogeochemical Cycles*, **10**, 783-796.
- Laws**, E.A., P.G. Falkowski, W.O. Smith Jr., H. Ducklow, and J.J. McCarthy, 2000: Temperature effects on export production in the open ocean. *Global Biogeochemical Cycles*, **14**(4), 1231-1246.
- Le Quéré**, C., J. C. Orr, P. Monfray, O. Aumont, and G. Madec, 2000: Interannual variability of the oceanic sink of CO<sub>2</sub> from 1979 through 1997. *Global Biogeochemical Cycles*, **14**(4), 1247-1265.
- Leemans**, R., 1990: Global data sets collected and compiled by the Biosphere Project, Working Paper, International Institute for Applied Analysis (IIASA), Laxenburg, Austria.
- Leemans**, R., A. vanAmstel, C. Battjes, E. Kreileman, and S. Toet, 1996: The land cover and carbon cycle consequences of large-scale utilizations of biomass as an energy source. *Global Environmental Change-Human and Policy Dimensions*, **6**, 335-357.
- Lefèvre**, N., and A.J. Watson, 1999: Modeling the geochemical cycle of iron in the oceans and its impact on atmospheric CO<sub>2</sub> concentrations. *Global Biogeochemical Cycles*, **13**, 727-736.
- Leggett**, J.A., W.J. Pepper, and R.J. Swart, 1992: Emissions scenarios for the IPCC: an update. In: *Climate Change 1992. The Supplementary Report to the IPCC Scientific assessment*. [Houghton, J.T., B.A. Callander and S.K. Varney (eds.)]. Cambridge University Press, Cambridge, pp. 69-95.
- Levitus**, S., J.I. Antonov, T.P. Boyer, and C. Stephens, 2000: Warming of the world ocean. *Science*, **287**, 2225-2229.
- Liss**, P.S., and L. Merlivat, 1986: Air-sea gas exchange: Introduction and synthesis. In: *The Role of Air-Sea Exchange in Geochemical Cycling* [Buat-Ménard, P. (ed.)]. D. Reidel, Hingham, Massachusetts, 113-127.
- Lloyd**, J., 1999: The CO<sub>2</sub> dependence of photosynthesis, plant growth responses to elevated CO<sub>2</sub> concentrations and their interaction with soil nutrient status, II. Temperate and boreal forest productivity and the combined effects of increasing CO<sub>2</sub> concentrations and increased nitrogen deposition at a global scale. *Functional Ecology*, **13**, 439-459.
- Lloyd**, J., and G.D. Farquhar, 1994: <sup>13</sup>C discrimination during CO<sub>2</sub> assimilation by the terrestrial biosphere. *Oecologia*, **99**, 201-215.
- Lloyd**, J., and J.A. Taylor, 1994: On the temperature-dependence of soil respiration. *Functional Ecology*, **8**, 315-323.
- Lloyd**, J., and G.D. Farquhar, 1996: The CO<sub>2</sub> dependence of photosynthesis, plant growth responses to elevated atmospheric CO<sub>2</sub> concentrations, and their interaction with soil nutrient status. I. General principles and forest ecosystems. *Functional Ecology*, **10**, 4-32.
- Longhurst**, A., S. Sathyendranath, T. Platt, and C. Caverhill, 1995: An Estimate of global primary production in the ocean from satellite radiometer data. *Journal of Plankton Research*, **17**, 1245-1271.
- Lorius**, C., and H. Oeschger, 1994: Palaeo-perspectives - reducing uncertainties in global change. *Ambio*, **23**, 30-36.
- Lugo**, A.E. and S. Brown, 1993: Management of tropical soils as sinks or sources of atmospheric carbon. *Plant and Soil*, **149**, 27-41.
- Luo**, Y.Q., J. Reynolds, and Y.P. Wang, 1999: A search for predictive understanding of plant responses to elevated [CO<sub>2</sub>]. *Global Change Biology*, **5**, 143-156.
- Mahowald**, N., K.E. Kohfeld, M. Hansson, Y. Balkanski, S.P. Harrison, I.C. Prentice, H. Rodhe, and M. Schulz, 1999: Dust sources and deposition during the Last Glacial Maximum and current climate: a comparison of model results with paleodata from ice cores and marine sediments. *Journal of Geophysical Research*, **104**, 15,895-16,436.
- Maier-Reimer**, E., 1993: Geochemical cycles in an ocean general-circulation model - preindustrial tracer distributions. *Global Biogeochemical Cycles*, **7**, 645-677.
- Maier-Reimer**, E., and K. Hasselmann, 1987: Transport and storage of CO<sub>2</sub> in the ocean - An inorganic ocean-circulation carbon cycle model. *Climate Dynamics*, **2**, 63-90.
- Maier-Reimer**, E., U. Mikolajewicz, and A. Winguth, 1996: Future ocean uptake of CO<sub>2</sub> - Interaction between ocean circulation and biology. *Climate Dynamics*, **12**, 711-721.
- Malhi**, Y., A.D. Nobre, J. Grace, B. Kruijt, M.G.P. Pereira, A. Culf, S. Scott, 1998: Carbon dioxide transfer over a Central Amazonian rain forest. *Journal of Geophysical Research-Atmospheres*, **103**, 31593-31612.
- Manning**, A.C., 2001. *Temporal variability of atmospheric oxygen from both continuous measurements and a flask sampling network: Tools for studying the global carbon cycle*. Ph. D. thesis, University of California, San Diego, La Jolla, California, U.S.A., 190 pp.
- Manning**, M.R., 1992: Seasonal cycles in atmospheric CO<sub>2</sub> concentrations. In: *The Global Carbon Cycle: Proceedings of the NATO*. [M. Heimann, (ed.)]. Advanced Study Institute I15, Il Ciocco, September 8-20, 1991, Springer Verlag, Berlin.
- Marchal**, O., T.F. Stocker, and F. Joos, 1998: A latitude-depth, circulation biogeochemical ocean model for paleoclimate studies - development and sensitivities. *Tellus*, **50B**, 290-316.
- Marland**, G., R.J. Andres, and T.A. Boden, 1994: Global, regional, and national CO<sub>2</sub> emissions. In: *Trends 93: A Compendium of Data on*

- Global Change* [T. A. Boden, D. P. Kaiser, R. J. Sepanski, and F. W. Stoss (eds.)], Oak Ridge National Laboratory, ORNL/CDIAC-65, Oak Ridge, Tenn., USA, 505-584.
- Marland**, G., R.J. Andres, T.A. Boden, C. Hohnston, and A. Brenkert, 1999: Global, Regional, and National CO<sub>2</sub> Emission Estimates from Fossil Fuel Burning, Cement Production, and Gas Flaring: 1751-1996. Carbon Dioxide Information Analysis Center, Oak Ridge National Laboratory, Oak Ridge, Tenn., USA.
- Marland**, G., T.A. Boden, and R.J. Andres, 2000: Global, regional, and national CO<sub>2</sub> emissions. In: *Trends: A Compendium of Data on Global Change*. Carbon Dioxide Information Analysis Center, Oak Ridge National Laboratory, U. S. Department of Energy, Oak Ridge, Tenn., USA.
- Martin**, J., 1990: Glacial-interglacial CO<sub>2</sub> change: the iron hypothesis. *Paleoceanography*, **5**, 1-13.
- Martin**, J.H., S.E. Fitzwater, and R.M. Gordon, 1990: Iron deficiency limits phytoplankton growth in Antarctic waters. *Global Biogeochemical Cycles*, **4**, 5-12.
- Masle**, J. 2000: The effects of elevated CO<sub>2</sub> concentrations on cell division rates, growth patterns, and blade anatomy in young wheat plants are modulated by factors related to leaf position, vernalization, and genotype. *Plant Physiology*, **122**, 1399-1415.
- Matear**, R.J., and A.C. Hirst, 1999: Climate change feedback on the future oceanic CO<sub>2</sub> uptake. *Tellus Series B*, **51**, 722-733.
- Matson**, P.A., W.H. McDowell, A.R. Townsend and P.M. Vitousek, 1999: The globalization of N deposition: ecosystem consequences in tropical environments. *Biogeochemistry*, **46**, 67-83.
- Matthews**, E., 1983: Global vegetation and land-use - new high-resolution data-bases for climate studies. *Journal of Climate and Applied Meteorology*, **22**, 474-487.
- McElroy**, M.B., 1983: Marine biological-controls on atmospheric CO<sub>2</sub> and climate. *Nature*, **302**, 328-329.
- McGillicuddy**, D.J., and A.R. Robinson, 1997: Eddy-induced nutrient supply and new production in the Sargasso Sea. *Deep-Sea Research Part I-Oceanographic Research Papers*, **44**, 1427-1450.
- McGuire**, A.D., J.M. Melillo, and L.A. Joyce, 1995: The role of nitrogen in the response of forest net primary production to elevated atmospheric carbon-dioxide. *Annual Review of Ecology and Systematics*, **26**, 473-503.
- McGuire**, A.D., S. Sitch, J.S. Clein, R. Dargaville, G. Esser, J. Foley, M. Heimann, F. Joos, J. Kaplan, D.W. Kicklighter, R.A. Meier, J.M. Melillo, B. Moore III, I.C. Prentice, N. Ramankutty, T. Reichenau, A. Schloss, H. Tian, L.J. Williams, U. Wittenberg, 2001 Carbon balance of the terrestrial biosphere in the twentieth century: Analyses of CO<sub>2</sub>, climate and land-use effects with four process-based ecosystem models. *Global Biogeochemical Cycles*, **15**(1), 183-206.
- McLaughlin**, S., and Downing, D.J., 1995: Interactive effects of ambient ozone and climate measured on growth of mature forest trees. *Nature*, **374**, 252-254.
- McLaughlin**, S., and Percy, K., 2000: Forest health in North America: some perspectives on actual and potential roles of climate and air pollution. *Water Air and Soil Pollution*, **116**, 151-197.
- Melillo**, J.M., and J.R. Gosz, 1983: Interactions of biogeochemical cycles in forest ecosystems. In: *The major biogeochemical cycles and their interactions* [Bolin, B. and R.B. Cook (eds.)]. John Wiley and Sons, New York, pp. 177-222.
- Melillo**, J.M., A.D. McGuire, D.W. Kicklighter, B.M. III, C.J. Vörösmarty and A.L. Schloss, 1993: Global climate change and terrestrial net primary production. *Nature*, **363**, 234-240.
- Melillo**, J.M., I.C. Prentice, G.D. Farquhar, E.-D. Schulze, and O.E. Sala, 1996: Terrestrial biotic response to environmental change and feedbacks to climate, In: *Climate Change 1995. The Science of Climate Change*, [J.T. Houghton, L.G.M. Filho, B.A. Callander, N. Harris, A. Kattenberg and K. Maskell (eds.)]. University Press, Cambridge, pp. 449-481.
- Menzel**, A., and P. Fabian, 1999: Growing season extended in Europe. *Nature*, **397**, 659.
- Meybeck**, M., 1982: Carbon, nitrogen, and phosphorus transport by world rivers. *American Journal of Science*, **282**, 401-450.
- Meybeck**, M., 1993: Riverine transport of atmospheric carbon – sources, global typology and budget. *Water, Air and Soil Pollution*, **70**, 443-463
- Milliman**, J.D., 1993: Production and accumulation of calcium-carbonate in the ocean - budget of a nonsteady state. *Global Biogeochemical Cycles*, **7**, 927-957.
- Minkkinen**, K., and J. Laine, 1998: Long-term effect of forest drainage on the peat carbon stores of pine mires in Finland. *Canadian Journal of Forest Research-Revue Canadienne De Recherche Forestiere*, **28**, 1267-1275.
- Mitchell**, J.F.B., T.C. Johns, J.M. Gregory, and S.F.B. Tett, 1995: Climate response to increasing levels of greenhouse gases and sulphate aerosols. *Nature*, **376**, 501-504.
- Mook**, W.G., M. Koopmans, A.F. Carter, and C.D. Keeling, 1983: Seasonal, latitudinal, and secular variations in the abundance and isotopic-ratios of atmospheric carbon-dioxide. 1. Results from land stations. *Journal of Geophysical Research-Oceans and Atmospheres*, **88**, 915-933.
- Mooney**, H.A., J. Canadell, F.S. Chapin III, J.R. Ehleringer, Ch. Körner, R.E. McMurtrie, W.J. Parton, L.F. Pitelka, and E.D. Schulze, 1999: Ecosystem physiology responses to global change. In: *Implications of Global Change for Natural and Managed Ecosystems. A Synthesis of GCTE and Related Research. IGBP Book Series No. 4*, [Walker, B.H., W.L. Steffen, J. Canadell and J.S.I. Ingram (eds.)]. Cambridge University Press, Cambridge, pp. 141-189.
- Mooney**, H., J. Roy and B. Saugier (eds.) 2001. *Terrestrial Global Productivity: Past, Present and Future*, Academic Press, San Diego (in press).
- Morita**, T., J. Robinson, A. Adegbulugbe, J. Alcamo, E. Lebre La Rovere, N. Nakićenović, H. Pitcher, P. Raskin, V. Sokolov, B. de Vries, D. Zhou, 2001. Greenhouse gas emission mitigation scenarios and implications. In: *Climate Change: Mitigation. Contribution of Working Group III to the Third Assessment Report of the Intergovernmental Panel on Climate Change* [O. Davidson, B. Metz and R. Swart (eds.)]. Cambridge University Press, Cambridge, United Kingdom and New York, NY, USA, in press.
- Murnane**, R.J., J.L. Sarmiento, and C. Le Quéré, 1999: Spatial distribution of air-sea CO<sub>2</sub> fluxes and the interhemispheric transport of carbon by the oceans. *Global Biogeochemical Cycles*, **13**, 287-305.
- Myneni**, R.B., C.D. Keeling, C.J. Tucker, G. Asrar, and R.R. Nemani, 1997: Increased plant growth in the northern high latitudes from 1981 to 1991. *Nature*, **386**, 698-702.
- Nadelhoffer**, K.J., B.A. Emmett, and P. Gundersen, 1999: Nitrogen deposition makes a minor contribution to carbon sequestration in temperate forests. *Nature*, **398**, 145-148.
- Neftel**, A., H. Friedli, E. Moor, H. Lötscher, H. Oeschger, U. Siegenthaler, and B. Stauffer, 1994: Historical CO<sub>2</sub> record from the Siple station ice core. In: *Trends '93: A Compendium of Data on Global Change*. [T.A. Boden, D.P. Kaiser, R.J. Sepanski, and F.W. Stoss (eds.)], Carbon Dioxide Inf. Anal. Cent., Oak Ridge., pp. 11-14.
- Neilson**, R.P., and D. Marks, 1994: A global perspective of regional vegetation and hydrologic sensitivities from climatic change. *Journal of Vegetation Science*, **5**, 715-730.
- Nemry**, B., L. Francois, J.C. Gerard, A. Bondeau, and M. Heimann, 1999: Comparing global models of terrestrial net primary productivity (NPP): analysis of the seasonal atmospheric CO<sub>2</sub> signal. *Global Change Biology*, **5**, 65-76.
- Norby**, R.J. and M.F. Cotrufo, 1988: Global change - A question of litter quality. *Nature*, **396**, 17-18.
- Norby**, R.J., S.D. Wullschleger, C.A. Gunderson, D.W. Johnson, and R. Ceulemans, 1999: Tree responses to rising CO<sub>2</sub> in field experiments:

- implications for the future forest. *Plant Cell and Environment*, **22**, 683-714.
- Oechel**, W.C., S.J. Hastings, G. Vourlitis, M. Jenkins, G. Riechers, and N. Grulke, 1993: Recent change of arctic tundra ecosystems from a net carbon-dioxide sink to a source. *Nature*, **361**, 520-523.
- Oechel**, W.C., G.L. Vourlitis, S.J. Hastings, R.C. Zulueta, L. Hinzman, and D. Kane, 2000: Acclimation of ecosystem CO<sub>2</sub> exchange in the Alaskan Arctic in response to decadal climate warming. *Nature*, **406**, 978-981.
- Ollinger**, S.V., J.S. Aber, and P.B. Reich, 1997: Simulating ozone effects on forest productivity: interactions among leaf-, canopy-, and stand-level processes. *Ecological Applications*, **7**, 1237-1251.
- Olson**, J.S., J.A. Watts, and L.J. Allison, 1983: Carbon in Live Vegetation of Major World Ecosystems. Oak Ridge, Tennessee:Oak Ridge National Laboratory. ORNL-5862.
- Ono**, T., S. Watanabe, K. Okuda, and M. Fukasawa, 1998: Distribution of total carbonate and related properties in the North Pacific along 30 degrees N. *Journal of Geophysical Research-Oceans*, **103**, 30873-30883.
- Opdyke**, B.N., and J.C.G. Walker, 1992: Return of the coral-reef hypothesis - basin to shelf partitioning of CaCO<sub>3</sub> and Its Effect On Atmospheric CO<sub>2</sub>. *Geology*, **20**, 733-736.
- Orr**, J.C., and J.-C. Dutay, 1999: OCMIP mid-project workshop. *Research GAIM Newsletter*, **3**, 4-5.
- Orr**, J., E. Maier-Reimer, U. Mikolajewicz, P. Monfray, J. L. Sarmiento, J. R. Toggweiler, N. K. Taylor, J. Palmer, N. Gruber, C. L. Sabine, C. Le Quéré, R. M. Key, and J. Boutin, 2001: Estimates of anthropogenic carbon uptake from four 3-D global ocean models. *Global Biogeochemical Cycles*, **15**, 43-60.
- Oschlies**, A., and V. Garçon, 1998: Eddy-induced enhancement of primary production in a model of the north Atlantic Ocean. *Nature*, **394**, 266-269.
- Overpeck**, J., K. Hughen, D. Hardy, R. Bradley, R. Case, M. Douglas, B. Finney, K. Gajewski, G. Jacoby, A. Jennings, S. Lamoureux, A. Lasca, G. MacDonald, J. Moore, M. Retelle, S. Smith, A. Wolfe, and G. Zielinski, 1997: Arctic environmental change of the last four centuries. *Science*, **278**, 1251-1256.
- Owensby**, C.E., P.I. Coyne, and J.M. Ham, 1993: Biomass production in a tallgrass prairie ecosystem exposed to ambient and elevated CO<sub>2</sub>. *Ecological Applications*, **3**, 644-653.
- Pagani**, M., M.A. Arthur and K.H. Freeman, 1999a: Miocene evolution of atmospheric carbon dioxide. *Paleoceanography*, **14**, 273-292.
- Pagani**, M., K. Freeman, and M.A. Arthur, 1999b: Late Miocene atmospheric CO<sub>2</sub> concentrations and the expansion of C<sub>4</sub> grasses. *Science*, **285**, 876-879.
- Pahlow**, M., and U. Riebesell, 2000: Temporal trends in deep ocean Redfield ratios. *Science*, **287**, 831-833.
- Pearson**, P.N. and M.R. Palmer, 1999: Middle eocene seawater pH and atmospheric carbon dioxide concentrations. *Science*, **284**, 1824-1826.
- Pearson**, P.N. and M.R. Palmer, 2000: Atmospheric carbon dioxide concentrations over the past 60 million years. *Nature*, **406**, 695-699.
- Peng**, C.H., J. Guiot, and E.V. Campo, 1998: Past and future carbon balance of European ecosystems from pollen data and climatic models simulations. *Global Planetary Change*, **18**, 189-200.
- Petit**, J.R., J. Jouzel, D. Raynaud, N.I. Barkov, J.M. Barnola, I. Basile, M. Bender, J. Chappellaz, M. Davis, G. Delaygue, M. Delmotte, V.M. Kotlyakov, M. Legrand, V.Y. Lipenkov, C. Lorius, L. Pepin, C. Ritz, E. Saltzman, and M. Stievenard, 1999: Climate and atmospheric history of the past 420,000 years from the Vostok ice core, Antarctica. *Nature*, **399**, 429-436.
- Peybernès**, N., E. Michel, J.-M. Barnola, M. Delmotte, J. Chappellaz, and D. Raynaud, 2000: Information on carbon cycle during the last 8,000 years deduced from CO<sub>2</sub>, δ<sup>13</sup>CO<sub>2</sub> and CH<sub>4</sub> profiles obtained on a Vostok Ice core. Presented at: *EGS, Nice, France*, 25-26 April 2000.
- Phillips**, O.L., Y. Malhi, N. Higuchi, W.F. Laurance, P.V. Nunez, R.M. Vasquez, S.G. Laurance, L.V. Ferreira, M. Stern, S. Brown and J. Grace, 1998: Changes in the carbon balance of tropical forests: Evidence from long-term plots. *Science*, **282**, 439-442.
- Polley**, H.W., H.B. Johnson, H.S. Mayeux, and C.R. Tischler, 1996: Are some of the recent changes in grassland communities a response to rising CO<sub>2</sub> concentrations? In: *Carbon Dioxide, Populations, and Communities* [Körner, C. and F.A. Bazzaz (eds.)]. Academic Press, San Diego, pp. 177-195.
- Prentice**, I.C., M. Heimann, and S. Sitch, 2000: The carbon balance of the terrestrial biosphere: Ecosystem models and atmospheric observations. *Ecological Applications*, **10**, 1553-1573.
- Pritchard**, S.G., H.H. Rogers, S.A. Prior, and C.M. Peterson, 1999: Elevated CO<sub>2</sub> and plant structure: a review. *Global Change Biology*, **5**, 807-837.
- Pool**e, I., J.D.B. Weyers, T. Lawson and J.A. Raven, 1996: Variations in stomatal density and index: Implications for palaeoclimatic reconstructions. *Plant Cell and Environment*, **19**, 705-712.
- Quay**, P.D., B. Tilbrook, C.S. Won, 1992: Oceanic uptake of fossil fuel CO<sub>2</sub>: Carbon-13 evidence. *Science*, **256**, 74-79.
- Raich**, J.W., E.B. Rastetter, J.M. Melillo, D.W. Kicklighter, P.A. Steudler, B.J. Peterson, A.L. Grace, B. Moore and C.J. Vorosmarty, 1991: Potential net primary productivity in South-America - application of a global-model. *Ecological Applications*, **1**, 399-429.
- Raich**, J.W., and W.H. Schlesinger, 1992: The global carbon-dioxide flux in soil respiration and its relationship to vegetation and climate. *Tellus Series B-Chemical and Physical Meteorology*, **44**, 81-99.
- Ramankutty**, N., and J.A. Foley, 2000: Estimating historical changes in global land cover: Croplands from 1700 to 1992. *Global Biogeochemical Cycles*, **13**, 997-1027.
- Randerson**, J.T., C.B. Field, I.Y. Fung, and P.P. Tans, 1999: Increases in early season ecosystem uptake explain recent changes in the seasonal cycle of atmospheric CO<sub>2</sub> at high northern latitudes. *Geophys. Res. Lett.*, **26**, 2765-2768.
- Rayner**, P.J., I.G. Enting, R.J. Francey, and R. Langenfelds, 1999a: Reconstructing the recent carbon cycle from atmospheric CO<sub>2</sub>, δ<sup>13</sup>C and O<sub>2</sub>/N<sub>2</sub> observations. *Tellus*, **51B**, 213-232.
- Rayner**, P.J., R.M. Law, and R. Dargaville, 1999b: The relationship between tropical CO<sub>2</sub> fluxes and the El Niño - Southern Oscillation. *Geophys. Res. Lett.*, **26**, 493-496.
- Redfield**, A.C., B.H. Ketchum, and F.A. Richards, 1963: The influence of organisms on the composition of seawater. In: *The Sea* [Hill, M.N. (ed.)]. Wiley, New York, NY, pp. 26-77.
- Rickaby**, R.E.M., and H. Elderfield, 1999: Planktonic foraminiferal Cd/Ca: Paleonutrients or paleotemperature? *Paleoceanography*, **14**, 293-303.
- Riebesell**, U., D.A. Wolf-Gladrow, and V. Smetacek, 1993: Carbon-dioxide limitation of marine-phytoplankton growth-rates. *Nature*, **361**, 249-251.
- Riebesell**, U., I. Zondervan, B. Rost, P.D. Tortell, R.E. Zeebe, and F.M. Morel, 2000: Reduced calcification of marine phytoplankton in response to increased atmospheric CO<sub>2</sub>. *Nature*, **407**, 364-367.
- Robitaille**, D.Y., and A.J. Weaver, 1995: Validation of sub-grid-scale mixing schemes using CFCs in a global ocean model. *Geophys. Res. Lett.*, **22**, 2917-2920.
- Ruimy**, A., B. Saugier, and G. Dedieu, 1994: Methodology for the estimation of terrestrial net primary production from remotely sensed data. *Journal of Geophysical Research-Atmosphere*, **99**, 5263-5283.
- Rundgren**, M., and D. Beerling, 1999: A Holocene CO<sub>2</sub> record from the stomatal index of subfossil Salix herbacea L. leaves from northern Sweden. *Holocene*, **9**, 509-513.
- Sabine**, C.L., D.W.R. Wallace, and F.J. Millero, 1997: Survey of CO<sub>2</sub> in the Oceans reveals clues about global carbon cycle. *EOS, Transaction of the American Geophysical Union*, **78**, 54-55.
- Sabine**, C.L., R.M. Key, K.M. Johnson, F.J. Millero, A. Poisson, J.L.

- Sarmiento, D.W.R. Wallace, and C.D. Winn, 1999: Anthropogenic CO<sub>2</sub> inventory of the Indian Ocean. *Global Biogeochemical Cycles*, **13**, 179-198.
- Sampson**, R.N. and R.J. Scholes, 2000: Additional Human-Induced Activities-Article 3.4. In: *Land Use, Land-Use Change, and Forestry* [Watson, R.T., I.R. Noble, B. Bolin, N.H. Ravindranath, D.J. Verardo and D.J. Dokken (eds.)]. Cambridge University Press, Cambridge, UK, pp. 181-282.
- Sanyal**, A., N.G. Hemming, G.N. Hanson, and W.S. Broecker, 1995: Evidence for a higher pH in the glacial ocean from boron isotopes in foraminifera. *Nature*, **373**, 234-236.
- Sarmiento**, J.L., and J.R. Toggweiler, 1984: A new model for the role of the oceans in determining atmospheric pCO<sub>2</sub>. *Nature*, **308**, 621-624.
- SAR**, see IPCC (1996a).
- Sarmiento**, J.L., J.C. Orr, and U. Siegenthaler, 1992: A perturbation simulation of CO<sub>2</sub> uptake in an ocean general- circulation model. *Journal of Geophysical Research-Oceans*, **97**, 3621-3645.
- Sarmiento**, J.L., and E.T. Sundquist, 1992: Revised budget for the oceanic uptake of anthropogenic carbon- dioxide. *Nature*, **356**, 589-593.
- Sarmiento**, J.L., and C. Le Quéré, 1996: Oceanic carbon dioxide uptake in a model of century-scale global warming. *Science*, **274**, 1346-1350.
- Sarmiento**, J.L., T.M.C. Hughes, R.J. Stouffer, and S. Manabe, 1998: Simulated response of the ocean carbon cycle to anthropogenic climate warming. *Nature*, **393**, 245-249.
- Sarmiento**, J.L., P. Monfray, E. Maier-Reimer, O. Aumont, R. Murnane, and J. C. Orr, 2000: Sea-air CO<sub>2</sub> fluxes and carbon transport: a comparison of three ocean general circulation models. *Global Biogeochemical Cycles*, **14**(4), 1267-1281.
- Saugier**, B., and J. Roy, 2001: Estimations of global terrestrial productivity: converging towards a single number? In: *Global terrestrial productivity: past, present and future* [Roy, J., B. Saugier and H.A. Mooney (eds.)]. Academic Press, (in press).
- Saxe**, H., D.S. Ellsworth, and J. Heath, 1998: Tree and forest functioning in an enriched CO<sub>2</sub> atmosphere. *New Phytologist*, **139**, 395-436.
- Schimel**, J.P., and F.S. Chapin, 1996: Tundra plant uptake of amino acid and NH4<sup>+</sup> nitrogen in situ: Plants compete well for amino acid N. *Ecology*, **77**, 2142-2147.
- Schimel**, D.S., B.H. Braswell, E.A. Holland, R. McKeown, D.S. Ojima, T.H. Painter, W.J. Parton, and A.R. Townsend, 1994: Climatic, edaphic and biotic controls over carbon and turnover of carbon in soils. *Global Biogeochemical Cycles*, **8**, 279-293.
- Schimel**, D., I.G. Enting, M. Heimann, T.M.L. Wigley, D. Raynaud, D. Alves, and U. Siegenthaler, 1995: CO<sub>2</sub> and the carbon cycle. In: *Climate Change 1994: Radiative Forcing of Climate Change and an Evaluation of the IPCC IS92 Emission Scenarios* [Houghton, J.T., L.G. Meira Filho, J. Bruce, Hoesung Lee, B.A. Callander, E. Haites, E. Harris, K. Maskell (eds.)]. Cambridge University Press, Cambridge, pp. 35-71.
- Schimel**, D., D. Alves, I. Enting, M. Heimann, F. Joos, D. Raynaud, and T. Wigley, 1996: CO<sub>2</sub> and the carbon cycle. In: *Climate Change 1995: The Science of Climate Change: Contribution of WGI to the Second Assessment Report of the IPCC* [Houghton, J.T., L.G. Meira Filho, B.A. Callander, N. Harris, A. Kattenberg and K. Maskell (eds.)]. Cambridge University Press, Cambridge, pp. 65-86.
- Schimel**, D., M. Grubb, F. Joos, R. Kaufmann, R. Moss, W. Ogana, R. Richels, and T.M.L. Wigley, 1997: *Stabilization of Atmospheric Greenhouse Gases: Physical, Biological and Socio-economic Implications — IPCC Technical Paper 3* [Houghton, J.T., L.G. Meira Filho, D.J. Griggs and K. Maskell (eds.)]. Intergovernmental Panel on Climate Change, Bracknell, UK , 53 pp.
- Schlundadinger**, B. and T. Karjalainen, 2000: Afforestation, Reforestation, and Deforestation (ARD) Activites. In: *Land Use, Land-Use Change, and Forestry* [Watson, R.T., I.R. Noble, B. Bolin, N.H. Ravindranath, D.J. Verardo and D.J. Dokken (eds.)]. Cambridge University Press, Cambridge, UK, pp. 127-181.
- Schlesinger**, W.H., 1990: Evidence from chronosequence studies for a low carbon-storage potential of soils. *Nature*, **348**, 233-234.
- Schlesinger**, W.H., 2000: Carbon sequestration in soils. *Science*, **284**, 2095.
- Schlesinger**, W.H. and J.M. Melack, 1981: Transport of organic-carbon in the worlds rivers. *Tellus*, **33**, 172-187
- Schlesinger**, W.H., and J.A. Andrews, 2000: Soil respiration and the global carbon cycle. *Biogeochemistry*, **48**, 7-20.
- Schlitzer**, R. 2000: Applying the adjoint method for biogeochemical modeling: export of particulate organic matter in the world ocean. In: *Inverse methods in global biogeochemical cycles* [Kasibhatla, P., M. Heimann, P. Rayner, N. Mahowald, R.G. Prinn, and D.E. Hartley (eds.)], Geophysical Monograph Series, **114**, 107-124.
- Scholes**, R.J., and S.R. Archer, 1997: Tree-grass interactions in savannas. *Annual Review of Ecology and Systematics*, **28**, 517-544.
- Scholes**, M., and M.O. Andreae, 2000: Biogenic and pyrogenic emissions from Africa and their impact on the global atmosphere. *Ambio*, **29**, 23-29.
- Scholes**, R.J., E.D. Schulze, L.F. Pitelka, and D.O. Hall, 1999: Biogeochemistry of terrestrial ecosystems. In: *The terrestrial biosphere and global change* [Walker B., Steffen W., Canadell J. and Ingram J. (eds.)]. Cambridge University Press., Cambridge, pp. 271-303.
- Schulze**, E.D., 2000: Carbon and Nitrogen Cycling in European Forest Ecosystems. *Ecological Studies Vol. 142.*, Springer Verlag.
- Schulze**, E.D., and M. Heimann, 1998: Carbon and water exchange of terrestrial ecosystems. In: *Asian change in the context of global change* [Galloway, J.N. and J. Melillo (eds.)]. Cambridge University Press, Cambridge.
- Schulze**, E.D., W. Devries, and M. Hauhs, 1989: Critical loads for nitrogen deposition on forest ecosystems. *Water Air and Soil Pollution*, **48**, 451-456.
- Schulze**, E.D., J. Lloyd, F.M. Kelliher, C. Wirth, C. Rebmann, B. Luhker, M. Mund, A. Knohl, I.M. Milyukova, W. Schulze, W. Ziegler, A.B. Varlagin, A.F. Sogachev, R. Valentini, S. Dore, S. Grigoriev, O. Kolle, M.I. Panfyorov, N. Tchebakova, and N.N. Vygodskaya, 1999: Productivity of forests in the Eurosiberian boreal region and their potential to act as a carbon sink - a synthesis. *Global Change Biology*, **5**, 703-722.
- Semenov**, S.M., I.M. Kounina, and B.A. Koukhta, 1998: An ecological analysis of anthropogenic changes in ground-level concentrations of O<sub>3</sub>, SO<sub>2</sub>, and CO<sub>2</sub> in Europe. *Doklady Biological Sciences*, **361**, 344-347.
- Semenov**, S.M., I.M. Kounina, and B.A. Koukhta, 1999: Tropospheric ozone and plant growth in Europe., Publishing Centre, 'Meteorology and Hydrology', Moscow, 208 pp.
- Shackleton**, N.J., 1977: Carbon-13 in Uvigerina: Tropical rainforest history and the equatorial Pacific carbonate dissolution cycles. In: *The Fate of Fossil Fuel CO<sub>2</sub> in the Oceans* [Anderson, N.R. and A. Malahoff (eds.)], 401-427.
- Shackleton**, N.J., 2000: The 100,000-year ice-age cycle identified and found to lag temperatrue, carb on dioxide, and orbital eccentricity. *Science*, **289**, 1897-1902.
- Shaffer**, G., 1993: Effects of the marine carbon biota on global carbon cycling. In: *The Global Carbon Cycle* [Heimann, M. (ed.)]. **I 15**, Springer Verlag, Berlin, pp. 431-455.
- Siegenthaler**, U., 1990: Biogeochemical Cycles - El-Niño and Atmospheric CO<sub>2</sub>. *Nature*, **345**, 295-296.
- Siegenthaler**, U. and H. Oeschger, 1978: Predicting future atmospheric carbon-dioxide levels. *Science*, **199**, 388-395
- Siegenthaler**, U., and T. Wenz, 1984: Rapid atmospheric CO<sub>2</sub> variations and ocean circulation. *Nature*, **308**, 624-627.
- Siegenthaler**, U. and F. Joos, 1992: Use of a simple-model for studying oceanic tracer distributions and the global carbon-cycle. *Tellus Series*

- B-Chemical and Physical Meteorology*, **44**, 186-207.
- Siegenthaler**, U., H. Friedli, H. Loetscher, E. Moor, A. Neftel, H. Oeschger and B. Stauffer, 1988: Stable-isotope ratios and concentration of CO<sub>2</sub> in air from polar ice cores. *Annals of Glaciology*, **10**, 1-6.
- Sigman**, D.M., D.C. McCorkle, and W.R. Martin, 1998: The calcite lysocline as a constraint on glacial/interglacial low-latitude production changes. *Global Biogeochemical Cycles*, **12**, 409-427.
- Sitch**, S., 2000: *The role of vegetation dynamics in the control of atmospheric CO<sub>2</sub> content*. PhD thesis, University of Lund, Sweden, 213 pp.
- Six**, K.D., and E. Maier-Reimer, 1996: Effects of plankton dynamics on seasonal carbon fluxes in an ocean general circulation model. *Global Biogeochemical Cycles*, **10**, 559-583.
- Skole**, D. and C. Tucker, 1993: Tropical deforestation and habitat fragmentation in the Amazon - satellite data from 1978 to 1988. *Science*, **260**, 1905-1910.
- Smethie**, W.M., T. Takahashi, and D.W. Chipman, 1985: Gas-exchange and CO<sub>2</sub> flux in the tropical atlantic-ocean determined from <sup>222</sup>Rn and pCO<sub>2</sub> measurements. *Journal of Geophysical Research-Oceans*, **90**, 7005-7022.
- Smith**, H.J., H. Fischer, M. Wahnen, D. Mastroianni, and B. Deck, 1999: Dual modes of the carbon cycle since the Last Glacial Maximum. *Nature*, **400**, 248-250.
- Smith**, S.V., and J.T. Hollibaugh, 1993: Coastal metabolism and the oceanic organic-carbon balance. *Reviews of Geophysics*, **31**, 75-89.
- Sonnerup**, R. E., Quay P. D., McNichol A. P., Bullister J. L., Westby T. A., and Anderson H. L., 1999: Reconstructing the oceanic C-13 Suess effect. *Global Biogeochemical Cycles*, **13**, 857-872
- Spiecker**, H., K. Mielikäinen, M. Köhl, J.P. Skovsgaard, 1996: Growth trends in European forests. *European Forest Institute Research Report No. 5*, Springer Verlag, Berlin-Heidelberg.
- Stauffer**, B., T. Blunier, A. Dällenbach, A. Indermühle, J. Schwander, T.F. Stocker, J. Tschumi, J. Chappellaz, D. Raynaud, C.U. Hammer and H.B. Clausen, 1998: Atmospheric CO<sub>2</sub> concentration and millennial-scale climate change during the last glacial period. *Nature*, **392**, 59-62.
- Stephens**, B.B., 1999: *Field-based atmospheric oxygen measurements and the ocean carbon cycle*. Unpublished Ph.D. thesis, Univ. of California, USA.
- Stephens**, B.B., and R.F. Keeling, 2000: The influence of Antarctic sea ice on glacial-interglacial CO<sub>2</sub> variations. *Nature*, **404**, 171-174.
- Stephens**, B.B., R.F. Keeling, and M. Heimann, 1998: Testing global ocean carbon cycle models using measurements of atmospheric O<sub>2</sub> and CO<sub>2</sub> concentration. *Global Biogeochemical Cycles*, **12**, 213-230.
- Street-Perrott**, F.A., Y. Huang, R.A. Perrott, and G. Eglinton, 1998: Carbon isotopes in lake sediments and peats of last glacial age: implications for the global carbon cycle, In: *Stable Isotopes* [Griffiths H. (ed.)]. BIOS Scientific Publishers Ltd, pp. 381-396.
- Takahashi**, T., J. Goddard, S. Sutherland, D.W. Chipman, and C. C. Breeze, 1986: Seasonal and geographic variability of carbon dioxide sink/source in the ocean areas, Lamont Doherty Geol. Obs., Palisades, New York, 66 pp.
- Takahashi**, T., R. H. Wanninkhof, R. A. Feely, R. F. Weiss, D. W. Chipman, N. Bates, J. Olafson, C. Sabine, and S.C. Sutherland, 1999: Net sea-air CO<sub>2</sub> flux over the global oceans: An improved estimate based on the sea-air pCO<sub>2</sub> difference. In: *Proceedings of the 2nd International Symposium CO<sub>2</sub> in the Oceans*, Center for Global Environmental Research, National Institute for Environmental Studies, Tsukuba, Japan, 9-15.
- Tans**, P.P., and D.W.R. Wallace, 1999: Carbon cycle research after Kyoto. *Tellus*, **51B**, 562-571.
- Tans**, P.P., T.J. Conway, and T. Nakazawa, 1989: Latitudinal distribution of the sources and sinks of atmospheric carbon dioxide derived from surface observations and atmospheric transport model. *Journal of Geophysical Research*, **94**, 5151-5172.
- Tans**, P.P., I.Y. Fung, and T. Takahashi, 1990: Observational constraints on the global atmospheric CO<sub>2</sub> budget. *Science*, **247**, 1431-1438.
- Tans**, P.P., J.A. Berry, and R.F. Keeling, 1993: Oceanic <sup>13</sup>C/<sup>12</sup>C observations - a new window on ocean CO<sub>2</sub> uptake. *Global Biogeochemical Cycles*, **7**, 353-368.
- Taylor**, J. A., 1989. "A stochastic Lagrangian atmospheric transport model to determine global CO<sub>2</sub> sources and sinks: a preliminary discussion." *Tellus B*, **41**(3), 272-285.
- Taylor**, J.A., and J. Lloyd, 1992: Sources and sinks of atmospheric CO<sub>2</sub>. *Australian Journal of Botany*, **40**, 407-418.
- Taylor**, J.A., and J.C. Orr, 2000: The natural latitudinal distribution of atmospheric CO<sub>2</sub>. *Global and Planetary Change*, **26**, 375-386.
- Tegen**, I., and I. Fung, 1995: Contribution to the atmospheric mineral aerosol load from land surface modification. *Journal of Geophysical Research*, **100**, 18707-18726.
- Thompson**, M.L., I.G. Enting, G.I. Pearman, and P. Hyson, 1986. Interannual variation of atmospheric CO<sub>2</sub> concentration. *Journal of Atmospheric Chemistry*, **4**, 125-155.
- Thompson**, M.V., J.T. Randerson, C.M. Malmstrom, and C.B. Field, 1996: Change in net primary production and heterotrophic respiration: How much is necessary to sustain the terrestrial carbon sink? *Global Biogeochemical Cycles*, **10**, 711-726.
- Tian**, H.Q., J.M. Melillo, and D.W. Kicklighter, 1998: Effect of interannual climate variability on carbon storage in Amazonian ecosystems. *Nature*, **396**, 664-667.
- Toggweiler**, J.R., 1999: Variation of atmospheric CO<sub>2</sub> by ventilation of the ocean's deepest water. *Paleoceanography*, **14**, 571-588.
- Trolier**, M., J.W.C. White, P.P. Tans, K.A. Masarie, and P.A. Gemery, 1996: Monitoring the isotopic composition of atmospheric CO<sub>2</sub> - measurements from the NOAA Global Air Sampling Network. *Journal of Geophysical Research - Atmosphere*, **101**, 25897-25916.
- Trudinger**, C.M., I.G. Enting, R.J. Francey, D.M. Etheridge, and P.J. Rayner, 1999: Long-term variability in the global carbon cycle inferred from a high-precision CO<sub>2</sub> and delta <sup>13</sup>C ice-core record. *Tellus*, **51B**, 233-248.
- Trumbore**, S., 2000: Age of soil organic matter and soil respiration: radiocarbon constraints on belowground C dynamics. *Ecological Applications*, **10**, 399-411.
- Tschumi**, J., and B. Stauffer, 2000. Reconstructing past atmospheric CO<sub>2</sub> concentrations based on ice-core analyses: open questions due to in situ production of CO<sub>2</sub> in ice. *Journal of Glaciology*, **46**, 45-53.
- Tyrell**, T., 1999: The relative influences of nitrogen and phosphorus on oceanic primary production. *Nature*, **400**, 525-531.
- UNFCCC** (United Nations Framework Convention on Climate Change), 2000: Methodological Issue. Land-use, land-use change and forestry. Synthesis report on national greenhouse gas information reported by Annex I Parties for the land-use change and forestry sector and agricultural soils category. Note by the Secretariat. Subsidiary Body for Scientific and Technological Advice. FCCC/SBSTA/2000/3. Bonn, Germany. 48pp.
- United Nations**, 2000: The United Nations Energy Statistics Database, United Nations Statistical Division, New York.
- UN-ECE/FAO** (United Nations Economics Commision for Europe/Food and Agriculture Organization of the United Nations), 2000: Forest Resources of Europe, CIS, North America, Australia, Japan and New Zealand (industrialized temperate/boreal countries) UN-ECE/FAO Contribution to the Global Forest Resources Assessment 2000. In: *Geneva Timber and Forest Study Papers*, No. 17, United Nations, New York, Geneva, pp. 445.
- Valentini**, R., G. Matteucci, A.J. Dolman, E.D. Schulze, C. Rebmann, E.J. Moors, A. Granier, P. Gross, N.O. Jensen, K. Pilegaard, A. Lindroth, A. Grelle, C. Bernhofer, T. Grunwald, M. Aubinet, R. Ceulemans, A.S. Kowalski, T. Vesala, U. Rannik, P. Berbigier, D. Loustau, J. Guomundsson, H. Thorgeirsson, A. Ibrom, K. Morgenstern, R. Clement, J. Moncrieff, L. Montagnani, S. Minerbi and P.G. Jarvis,

- 2000: Respiration as the main determinant of carbon balance in European forests. *Nature*, **404**, 861-865.
- Van de Water**, P.K., S.W. Leavitt and J.L. Betancourt, 1994: Trends in stomatal density and  $^{13}\text{C}/^{12}\text{C}$  ratios of pinus- flexilis needles during last glacial-interglacial cycle. *Science*, **264**, 239-243.
- Vitousek**, P.M. and R.W. Howarth, 1991: Nitrogen limitation on land and in the sea - how can it occur. *Biogeochemistry*, **13**, 87-115.
- Vitousek**, P.M. and C.B. Field, 1999: Ecosystem constraints to symbiotic nitrogen fixers: a simple model and its implications. *Biogeochemistry*, **46**, 179-202.
- Vitousek**, P.M., J.D. Aber, R.W. Howarth, G.E. Likens, P.A. Matson, D.W. Schindler, W.H. Schlesinger, D.G. Tilman, 1997: Human alteration of the global nitrogen cycle: sources and consequences. *Ecological Applications*, **7**, 737-750.
- Voss**, R., and U. Mikolajewicz, 1999: Long-term climate changes due to increased  $\text{CO}_2$  concentration in the coupled atmosphere-ocean general circulation model ECHAM3/LSG. *Technical Report # 298*, Max-Planck-Institut für Meteorologie, Hamburg.
- Wagner**, F., S.J.P. Bohncke, D.L. Dilcher, W.M. Kurschner, B. van Geel, and H. Visscher, 1999: Century-scale shifts in early Holocene atmospheric  $\text{CO}_2$  concentration. *Science*, **284**, 1971-1973.
- Wallace**, D.W.R., 1995: Monitoring global ocean carbon inventories. Ocean observing system development panel background., Texas A&M University, College Station, TX, 54pp.
- Wand**, S.J.E., G.F. Midgley, M.H. Jones, and P.S. Curtis, 1999: Responses of wild  $\text{C}_4$  and  $\text{C}_3$  grass (Poaceae) species to elevated atmospheric  $\text{CO}_2$  concentration: a meta-analytic test of current theories and perceptions. *Global Change Biology*, **5**, 723-741.
- Wanninkhof**, R., 1992: Relationship between wind-speed and gas-exchange over the ocean. *Journal of Geophysical Research-Oceans*, **97**, 7373-7382.
- Wanninkhof**, R., and W.R. McGillis, 1999: A cubic relationship between air-sea  $\text{CO}_2$  exchange and wind speed. *Geophys. Res. Lett.*, **26**, 1889-1892.
- Waring**, R.H., J.J. Landsberg, and M. Williams, 1998: Net primary production of forests: a constant fraction of gross primary production? *Tree Physiology*, **18**, 129-134.
- Watson**, A.J., and P.S. Liss, 1998: Marine biological controls on climate via the carbon and sulphur geochemical cycles. *Philosophical Transactions of the Royal Society of London Series B-Biological Sciences*, **353**, 41-51.
- Watson**, A.J., P.D. Nightingale, and D.J. Cooper, 1995: Modeling atmosphere ocean  $\text{CO}_2$  transfer. *Philosophical Transactions of the Royal Society of London Series B-Biological Sciences*, **348**, 125-132.
- WBGU**, (Wissenschaftlicher Beirat der Bundesregierung Globale Umweltveränderungen) 1988. Die Anrechnung biologischer Quellen und Senken in Kyoto-Protokoll: Fortschritt oder Rückschlag für den globalen Umweltschutz Sondergutachten 1988. Bremerhaven, Germany, 76pp, (available in English).
- Wigley**, T.M.L., Richels, R., and Edmonds, J.A., 1996: Economic and environmental choices in the stabilization of  $\text{CO}_2$  concentrations: choosing the "right" emissions pathway. *Nature*, **379**, 240-243.
- Wigley**, T.M.L., A. K. Jain, F. Joos, B. S. Nyenzi, and P.R. Shukla, 1997: *Implications of Proposed  $\text{CO}_2$  Emissions Limitations. IPCC Technical Paper 4*. [Houghton, J.T., L.G. Meira Filho, D.J. Griggs and M. Noguer (eds)]. Intergovernmental Panel on Climate Change, Bracknell, UK, 41 pp.
- Williams**, S.N., S.J. Schaefer, M.L. Calvache, and D. Lopez, 1992: Global carbon dioxide emission to the atmosphere by volcanoes. *Geochimica et Cosmochimica Acta*, **56**, 1765-1770.
- Winguth**, A.M.E., M. Heimann, K.D. Kurz, E. Maier-Reimer, U. Mikolajewicz, and J. Segschneider, 1994: El-Niño-Southern oscillation related fluctuations of the marine carbon cycle. *Global Biogeochemical Cycles*, **8**, 39-63.
- Winn**, C.D., Y.H. Li, F.T. Mackenzie, and D.M. Karl, 1998: Rising surface ocean dissolved inorganic carbon at the Hawaii Ocean Time-series site. *Marine Chemistry*, **60**, 33-47.
- Wofsy**, S.C., Goulden, M.L., Munger, J.W., Fan, S.M., Bakwin, P.S., Daube, B.C., Bassow, S.L., Bazzaz, F.A., 1993: Net exchange of  $\text{CO}_2$  in a mid-latitude forest. *Science*, **260**, 1314-1317.
- Wong**, C.S., Y.H. Chan, J.S. Page, G.E. Smith, and R.D. Bellegay, 1993: Changes in equatorial  $\text{CO}_2$  flux and new production estimated from  $\text{CO}_2$  and nutrient levels in Pacific surface waters during the 1986/87 El-Niño. *Tellus Series B*, **45**, 64-79.
- Woodward**, F.I., 1987: Stomatal Numbers Are Sensitive to Increases in  $\text{CO}_2$  From Preindustrial Levels. *Nature*, **327**, 617-618.
- Woodward**, F.I., and F.A. Bazzaz, 1988: The Responses of Stomatal Density to  $\text{CO}_2$  Partial-Pressure. *Journal of Experimental Botany*, **39**, 1771-1781.
- Woodward**, F.I., M.R. Lomas, and R.A. Betts, 1998: Vegetation-climate feedbacks in a greenhouse world. *Philosophical Transactions of the Royal Society of London B*, **353**, 29-38.
- Wu**, J., W. Sunda, E.A. Boyle and D.M. Karl, 2000: Phosphate depletion in the western North Atlantic Ocean. *Science*, **289**, 759-762.
- Yang**, X. and M.X. Wang, 2000: Monsoon ecosystems control on atmospheric  $\text{CO}_2$  interannual variability: inferred from a significant positive correlation between year-to-year changes in land precipitation and atmospheric  $\text{CO}_2$  growth rate. *Geophys. Res. Lett.*, **27**, 1671-1674
- Yamanaka**, Y., and E. Tajika, 1996: The role of the vertical fluxes of particulate organic matter and calcite in the oceanic carbon cycle: Studies using an ocean biogeochemical general circulation model. *Global Biogeochemical Cycles*, **10**, 361-382
- Zeng**, X.B., 1999: The relationship among precipitation, cloud-top temperature, and precipitable water over the tropics. *Journal of Climate*, **12**, 2503-2514.



# 4

---

## Atmospheric Chemistry and Greenhouse Gases

---

### **Co-ordinating Lead Authors**

D. Ehhalt, M. Prather

### **Lead Authors**

F. Dentener, R. Derwent, E. Dlugokencky, E. Holland, I. Isaksen, J. Katima, V. Kirchhoff, P. Matson, P. Midgley, M. Wang

### **Contributing Authors**

T. Berntsen, I. Bey, G. Brasseur, L. Buja, W.J. Collins, J. Daniel, W.B. DeMore, N. Derek, R. Dickerson, D. Etheridge, J. Feichter, P. Fraser, R. Friedl, J. Fuglestvedt, M. Gauss, L. Grenfell, A. Grubler, N. Harris, D. Hauglustaine, L. Horowitz, C. Jackman, D. Jacob, L. Jaeglé, A. Jain, M. Kanakidou, S. Karlsdottir, M. Ko, M. Kurylo, M. Lawrence, J.A. Logan, M. Manning, D. Mauzerall, J. McConnell, L. Mickley, S. Montzka, J.F. Müller, J. Olivier, K. Pickering, G. Pitari, G.J. Roelofs, H. Rogers, B. Rognerud, S. Smith, S. Solomon, J. Staehelin, P. Steele, D. Stevenson, J. Sundet, A. Thompson, M. van Weele, R. von Kuhlmann, Y. Wang, D. Weisenstein, T. Wigley, O. Wild, D. Wuebbles, R. Yantosca

### **Review Editors**

F. Joos, M. McFarland

# Contents

---

<b>Executive Summary</b>	241		
<b>4.1 Introduction</b>	243	4.3.2 Shifting Regional Emissions of NO <sub>x</sub> , CO and VOC in 2100	267
4.1.1 Sources of Greenhouse Gases	243	4.3.3 Projections of Natural Emissions in 2100	267
4.1.2 Atmospheric Chemistry and Feedbacks	245		
4.1.3 Trace Gas Budgets and Trends	246	<b>4.4 Projections of Atmospheric Composition for the 21st Century</b>	267
4.1.4 Atmospheric Lifetimes and Time-Scales	247	4.4.1 Introduction	267
<b>4.2 Trace Gases: Current Observations, Trends and Budgets</b>	248	4.4.2 The OxComp Workshop	267
4.2.1 Non-CO <sub>2</sub> Kyoto Gases	248	4.4.3 Testing CTM Simulation of the Current (Y2000) Atmosphere	268
4.2.1.1 Methane (CH <sub>4</sub> )	248	4.4.4 Model Simulations of Perturbed and Y2100 Atmospheres	271
4.2.1.2 Nitrous oxide (N <sub>2</sub> O)	251	4.4.5 Atmospheric Composition for the IPCC Scenarios to 2100	274
4.2.1.3 Hydrofluorocarbons (HFCs)	253	4.4.6 Gaps in These Projections - the Need for Coupled Models	275
4.2.1.4 Perfluorocarbons (PFCs) and sulphur hexafluoride (SF <sub>6</sub> )	254	4.4.7 Sensitivity Analysis for Individual Sectors	275
4.2.2 Montreal Protocol Gases and Stratospheric Ozone (O <sub>3</sub> )	255		
4.2.3 Reactive Gases	256	<b>4.5 Open Questions</b>	277
4.2.3.1 Carbon monoxide (CO) and hydrogen (H <sub>2</sub> )	256	4.5.1 Chemical Processes Important on the Global Scale	277
4.2.3.2 Volatile organic compounds (VOC)	257	4.5.1.1 Missing chemistry, representation of small scales, and changing emission patterns	277
4.2.3.3 Nitrogen oxides (NO <sub>x</sub> )	259	4.5.1.2 Aerosol interactions with tropospheric O <sub>3</sub> and OH	277
4.2.4 Tropospheric O <sub>3</sub>	260	4.5.1.3 Stratosphere-troposphere coupling	277
4.2.5 Stratospheric H <sub>2</sub> O	263	4.5.1.4 Uncertainties in the tropospheric O <sub>3</sub> budget	278
4.2.6 Tropospheric OH and Photochemical Modelling	263	4.5.2 Impacts of Physical Climate Change on Atmospheric Chemistry	278
4.2.6.1 Laboratory data and the OH lifetime of greenhouse gases	263	4.5.3 Feedbacks through Natural Emissions	278
4.2.6.2 Atmospheric measurements and modelling of photochemistry	264		
<b>4.3 Projections of Future Emissions</b>	266	<b>4.6 Overall Impact of Global Atmospheric Chemistry Change</b>	279
4.3.1 The Adjusted/Augmented IPCC/SRES Emission Scenarios	266	<b>References</b>	280

## Executive Summary

*Two important new findings since the IPCC WGI Second Assessment Report (IPCC, 1996) (hereafter SAR) demonstrate the importance of atmospheric chemistry in controlling greenhouse gases:*

Currently, tropospheric ozone ( $O_3$ ) is the third most important greenhouse gas after carbon dioxide ( $CO_2$ ) and methane ( $CH_4$ ). It is a product of photochemistry, and its future abundance is controlled primarily by emissions of  $CH_4$ , carbon monoxide ( $CO$ ), nitrogen oxides ( $NO_x$ ), and volatile organic compounds (VOC). There is now greater confidence in the model assessment of the increase in tropospheric  $O_3$  since the pre-industrial period, which amounts to 30% when globally averaged, as well as the response to future emissions. For scenarios in which the  $CH_4$  abundance doubles and anthropogenic  $CO$  and  $NO_x$  emissions triple, the tropospheric  $O_3$  abundance is predicted to increase by an additional 50% above today's abundance.

$CO$  is identified as an important indirect greenhouse gas. An addition of  $CO$  to the atmosphere perturbs the  $OH-CH_4-O_3$  chemistry. Model calculations indicate that the emission of 100 Mt of  $CO$  stimulates an atmospheric chemistry perturbation that is equivalent to direct emission of about 5 Mt of  $CH_4$ .

*A major conclusion of this report is that atmospheric abundances of almost all greenhouse gases reached the highest values in their measurement records during the 1990s:*

The atmospheric abundance of  $CH_4$  continues to increase, from about 1,520 ppb in 1978 to 1,745 ppb in 1998. However, the observed annual increase in  $CH_4$  has declined during the last two decades. This increase is highly variable; it was near zero in 1992 and as large as +13 ppb during 1998. There is no clear, quantitative explanation for this variability. Since the SAR, quantification of certain anthropogenic sources of  $CH_4$ , such as that from rice production, has improved.

The atmospheric burden of nitrous oxide ( $N_2O$ ) continues to increase by about 0.25%/yr. New, higher estimates of emissions from agricultural sources improve our understanding of the global  $N_2O$  budget.

The atmospheric abundances of major greenhouse gases that deplete stratospheric ozone are decreasing (CFC-11, CFC-113,  $CH_3CCl_3$ ,  $CCl_4$ ), or increasing more slowly (CFC-12), in response to the phase-out in their production agreed to under the Montreal Protocol and its Amendments.

HFC-152a and HFC-134a are increasing in the atmosphere. This growth is consistent with the rise in their industrial use. HFC-23, an unintended by-product of HCFC-22 production, is also increasing.

Perfluorocarbon (PFC) e.g.,  $CF_4$  (perfluoromethane) appears to have a natural background; however, current anthropogenic emissions exceed natural ones by a factor of 1,000 or more and are responsible for the observed increase.

There is good agreement between the increase in atmospheric abundances of sulphur hexafluoride ( $SF_6$ ) and emissions estimates based on revised sales and storage data.

There has been little increase in global tropospheric  $O_3$  since the 1980s at the few remote locations where it is regularly

measured. Only two of the fourteen stations, one in Japan and one in Europe, had statistically significant increases in tropospheric  $O_3$  between 1980 and 1995. By contrast, the four Canadian stations, all at high latitudes, had significant decreases in tropospheric  $O_3$  for the same time period. However, limited observations from the late 19th and early 20th centuries combined with models suggest that tropospheric  $O_3$  has increased from a global mean value of 25 DU (where 1 DU =  $2.7 \times 10^{16} O_3$  molecules/cm<sup>2</sup>) in the pre-industrial era to 34 DU today. While the SAR estimated similar values, the new analysis provides more confidence in this increase of 9 DU.

*Changes in atmospheric composition and chemistry over the past century have affected, and those projected into the future will affect, the lifetimes of many greenhouse gases and thus alter the climate forcing of anthropogenic emissions:*

The atmospheric lifetime relates emissions of a component to its atmospheric burden. In some cases, for instance for methane, a change in emissions perturbs the chemistry and thus the corresponding lifetime. The  $CH_4$  feedback effect amplifies the climate forcing of an addition of  $CH_4$  to the current atmosphere by lengthening the perturbation lifetime relative to the global atmospheric lifetime of  $CH_4$  by a factor of 1.4. This earlier finding is corroborated here by new model studies that also predict only small changes in this  $CH_4$  feedback for the different scenarios projected to year 2100. Another feedback has been identified for the addition of  $N_2O$  to the atmosphere; it is associated with stratospheric  $O_3$  chemistry and shortens the perturbation lifetime relative to the global atmospheric lifetime of  $N_2O$  by about 5%.

Several chemically reactive gases –  $CO$ ,  $NO_x$  (=  $NO+NO_2$ ), and VOC – control in part the abundance of  $O_3$  and the oxidising capacity ( $OH$ ) of the troposphere. These pollutants act as indirect greenhouse gases through their influence on atmospheric chemistry, e.g., formation of tropospheric  $O_3$  or changing the lifetime of  $CH_4$ . The emissions of  $NO_x$  and  $CO$  are dominated by human activities. The abundance of  $CO$  in the Northern Hemisphere is about twice that in the Southern Hemisphere and has increased in the second half of the 20th century along with industrialisation and population. The urban and regional abundance of  $NO_x$  has generally increased with industrialisation, but the global abundance of this short-lived, highly variable pollutant cannot be derived from measurements. Increased  $NO_x$  abundances will in general increase tropospheric  $O_3$  and decrease  $CH_4$ . Deposition of  $NO_x$  reaction products fertilises the biosphere, stimulates  $CO_2$  uptake, but also provides an input of acidic precipitation.

*The IPCC Special Report on Emission Scenarios (SRES) generated six marker/illustrative scenarios (labelled A1B, A1T, A1FI, A2, B1, B2) plus four preliminary marker scenarios (labelled here A1p, A2p, B1p, and B2p). These projected changes in anthropogenic emissions of trace gases from year 2000 to year 2100, making different assumptions on population development, energy use, and technology. Results from both sets of scenarios are discussed here since the preliminary marker scenarios (December 1998) were used in this report:*

Model calculations of the abundances of the primary greenhouse gases by year 2100 vary considerably across the SRES scenarios: in general A1B, A1T, and B1 have the smallest increases of emissions and burdens; and A1FI and A2 the largest. CH<sub>4</sub> changes from 1998 to 2100 range from -10 to +115%; and N<sub>2</sub>O increases from 13 to 47%. The HFCs – 134a, 143a, and 125 – reach abundances of a few hundred to nearly a thousand ppt from negligible levels today. The PFC CF<sub>4</sub> is projected to increase to between 200 and 400 ppt; and SF<sub>6</sub> to between 35 and 65 ppt.

SRES projected anthropogenic emissions of the indirect greenhouse gases (NO<sub>x</sub>, CO and VOC) together with changes in CH<sub>4</sub> are expected to change the global mean abundance of tropospheric OH by -20 to +6% over the next century. Comparable, but opposite sign, changes occur in the atmospheric lifetimes of the greenhouse gases, CH<sub>4</sub> and HFCs. This impact depends in large part on the magnitude of, and the balance between, NO<sub>x</sub> and CO emissions.

For the SRES scenarios, changes in tropospheric O<sub>3</sub> between years 2000 and 2100 range from -4 to +21 DU. The largest increase predicted for the 21st century (scenarios A1FI and A2) would be more than twice as large as that experienced since the pre-industrial era. These O<sub>3</sub> increases are attributable to the concurrent, large (almost factor of 3) increases in anthropogenic NO<sub>x</sub> and CH<sub>4</sub> emissions.

*The large growth in emissions of greenhouse gases and other pollutants as projected in some SRES scenarios for the 21st century will degrade the global environment in ways beyond climate change:*

Changes projected in the SRES A2 and A1FI scenarios would degrade air quality over much of the globe by increasing background levels of O<sub>3</sub>. In northern mid-latitudes during summer, the zonal average increases near the surface are about 30 ppb or more, raising background levels to nearly 80 ppb, threat-

ening attainment of air quality standards over most metropolitan and even rural regions, and compromising crop and forest productivity. This problem reaches across continental boundaries since emissions of NO<sub>x</sub> influence photochemistry on a hemispheric scale.

*A more complete and accurate assessment of the human impact on greenhouse gases requires greater understanding of sources, processes, and coupling between different parts of the climate system:*

The current assessment is notably incomplete in calculating the total impact of individual industrial / agricultural sectors on greenhouse gases and aerosols. The IPCC Special Report on Aviation demonstrates that the total impact of a sector is not represented by (nor scalable to) the direct emissions of primary greenhouse gases alone, but needs to consider a wide range of atmospheric changes.

The ability to hindcast the detailed changes in atmospheric composition over the past decade, particularly the variability of tropospheric O<sub>3</sub> and CO, is limited by the availability of measurements and their integration with models and emissions data. Nevertheless, since the SAR there have been substantial advances in measurement techniques, field campaigns, laboratory studies, global networks, satellite observations, and coupled models that have improved the level of scientific understanding of this assessment. Better simulation of the past two decades, and in due course the upcoming one, would reduce uncertainty ranges and improve the confidence level of our projections of greenhouse gases.

Feedbacks between atmospheric chemistry, climate, and the biosphere were not developed to the stage that they could be included in the projected numbers here. Failure to include such coupling is likely to lead to systematic errors and may substantially alter the projected increases in the major greenhouse gases.

## 4.1 Introduction

This chapter investigates greenhouse gases whose atmospheric burdens<sup>1</sup> and climate impacts generally depend on atmospheric chemistry. These greenhouse gases include those listed in the Kyoto Protocol – methane ( $\text{CH}_4$ ), nitrous oxide ( $\text{N}_2\text{O}$ ), hydrofluorocarbons (HFCs), perfluorocarbons (PFCs), sulphur hexafluoride ( $\text{SF}_6$ ) – and those listed under the Montreal Protocol and its Amendments – the chlorofluorocarbons (CFCs), the hydrochlorofluorocarbons (HCFCs), and the halons. A major focus of this assessment is the change in tropospheric ozone ( $\text{O}_3$ ). Stratospheric water vapour ( $\text{H}_2\text{O}$ ) is also treated here, but tropospheric  $\text{H}_2\text{O}$ , which is part of the hydrological cycle and calculated within climate models, is not discussed. This chapter also treats the reactive gases carbon monoxide (CO), volatile organic compounds (VOC), and nitrogen oxides ( $\text{NO}_x = \text{NO} + \text{NO}_2$ ), termed indirect greenhouse gases. These pollutants are not significant direct greenhouse gases, but through atmospheric chemistry they control the abundances<sup>1</sup> of direct greenhouse gases. This chapter reviews the factors controlling the current atmospheric abundances of direct and indirect greenhouse gases; it looks at the changes since the pre-industrial era and their attribution to anthropogenic activities; and it calculates atmospheric abundances to the year 2100 based on projected emissions of greenhouse gases and pollutants. Carbon dioxide ( $\text{CO}_2$ ) is treated in Chapter 3; and aerosols in Chapter 5. The atmospheric abundances of greenhouse gases and aerosols from all chapters are combined in Chapter 6 to calculate current and future radiative forcing. This chapter is an update of the IPCC WGI Second Assessment Report (IPCC, 1996) (hereafter SAR). For a review of the chemical processes controlling the abundance of greenhouse gases see the SAR (Prather *et al.*, 1995) or Ehhalt (1999). More recent assessments of changing atmospheric chemistry and composition include the IPCC Special Report on Aviation and the Global Atmosphere (Penner *et al.*, 1999) and the World Meteorological Organization / United Nations Environmental Programme (WMO/UNEP) Scientific Assessment of Ozone Depletion (WMO, 1999).

### 4.1.1 Sources of Greenhouse Gases

Substantial, pre-industrial abundances for  $\text{CH}_4$  and  $\text{N}_2\text{O}$  are found in the tiny bubbles of ancient air trapped in ice cores. Both gases have large, natural emission rates, which have varied over past climatic changes but have sustained a stable atmospheric abundance for the centuries prior to the Industrial Revolution (see Figures 4.1 and 4.2). Emissions of  $\text{CH}_4$  and  $\text{N}_2\text{O}$  due to human activities are also substantial and have caused large relative

increases in their respective burdens over the last century. The atmospheric burdens of  $\text{CH}_4$  and  $\text{N}_2\text{O}$  over the next century will likely be driven by changes in both anthropogenic and natural sources. A second class of greenhouse gases – the synthetic HFCs, PFCs,  $\text{SF}_6$ , CFCs, and halons – did not exist in the atmosphere before the 20th century (Butler *et al.*, 1999).  $\text{CF}_4$ , a PFC, is detected in ice cores and appears to have an extremely small natural source (Harnisch and Eisenhauer, 1998). The current burdens of these latter gases are derived from atmospheric observations and represent accumulations of past anthropogenic releases; their future burdens depend almost solely on industrial production and release to the atmosphere. Stratospheric  $\text{H}_2\text{O}$  could increase, driven by *in situ* sources, such as the oxidation of  $\text{CH}_4$  and exhaust from aviation, or by a changing climate.

Tropospheric  $\text{O}_3$  is both generated and destroyed by photochemistry within the atmosphere. Its *in situ* sources are expected to have grown with the increasing industrial emissions of its precursors:  $\text{CH}_4$ ,  $\text{NO}_x$ , CO and VOC. In addition, there is substantial transport of ozone from the stratosphere to the troposphere (see also Section 4.2.4). The effects of stratospheric  $\text{O}_3$  depletion over the past three decades and the projections of its recovery, following cessation of emissions of the Montreal Protocol gases, was recently assessed (WMO, 1999).

The current global emissions, mean abundances, and trends of the gases mentioned above are summarised in Table 4.1a. Table 4.1b lists additional synthetic greenhouse gases without established atmospheric abundances. For the Montreal Protocol gases, political regulation has led to a phase-out of emissions that has slowed their atmospheric increases, or turned them into decreases, such as for CFC-11. For other greenhouse gases, the anthropogenic emissions are projected to increase or remain high in the absence of climate-policy regulations. Projections of future emissions for this assessment, i.e., the IPCC Special Report on Emission Scenarios (SRES) (Nakićenović *et al.*, 2000) anticipate future development of industries and agriculture that represent major sources of greenhouse gases in the absence of climate-policy regulations. The first draft of this chapter and many of the climate studies in this report used the greenhouse gas concentrations derived from the SRES preliminary marker scenarios (i.e., the SRES database as of January 1999 and labelled ‘p’ here). The scenario IS92a has been carried along in many tables to provide a reference of the changes since the SAR. The projections of greenhouse gases and aerosols for the six new SRES marker/illustrative scenarios are discussed here and tabulated in Appendix II.

An important policy issue is the complete impact of different industrial or agricultural sectors on climate. This requires aggregation of the SRES scenarios by sector (e.g., transportation) or sub-sector (e.g., aviation; Penner *et al.*, 1999), including not only emissions but also changes in land use or natural ecosystems. Due to chemical coupling, correlated emissions can have synergistic effects; for instance  $\text{NO}_x$  and CO from transportation produce regional  $\text{O}_3$  increases. Thus a given sector may act through several channels on the future trends of greenhouse gases. In this chapter we will evaluate the data available on this subject in the current literature and in the SRES scenarios.

<sup>1</sup> Atmospheric abundances for trace gases are reported here as the mole fraction (molar mixing ratio) of the gas relative to dry air ( $\text{ppm} = 10^{-6}$ ,  $\text{ppb} = 10^{-9}$ ,  $\text{ppt} = 10^{-12}$ ); whereas the burden is reported as the total mass of that gas in the atmosphere (e.g.,  $\text{Mt} = \text{Tg} = 10^{12}$  g). For most trace gases in this chapter, the burden is based on the total weight of the molecule; for the N-containing gases, it includes only the mass of the N; and for some VOC budgets where noted, it includes only the mass of the C.

**Table 4.1(a):** Chemically reactive greenhouse gases and their precursors: abundances, trends, budgets, lifetimes, and GWPs.

Chemical species	Formula	Abundance <sup>a</sup> ppt		Trend ppt/yr <sup>a</sup> 1990s	Annual emission late 90s	Life- time (yr)	100-yr GWP <sup>b</sup>
		1998	1750				
Methane	CH <sub>4</sub> (ppb)	1745	700	7.0	600 Tg	8.4/12 <sup>c</sup>	23
Nitrous oxide	N <sub>2</sub> O (ppb)	314	270	0.8	16.4 TgN	120/114 <sup>c</sup>	296
Perfluoromethane	CF <sub>4</sub>	80	40	1.0	~15 Gg	>50000	5700
Perfluoroethane	C <sub>2</sub> F <sub>6</sub>	3.0	0	0.08	~2 Gg	10000	11900
Sulphur hexafluoride	SF <sub>6</sub>	4.2	0	0.24	~6 Gg	3200	22200
HFC-23	CHF <sub>3</sub>	14	0	0.55	~7 Gg	260	12000
HFC-134a	CF <sub>3</sub> CH <sub>2</sub> F	7.5	0	2.0	~25 Gg	13.8	1300
HFC-152a	CH <sub>3</sub> CHF <sub>2</sub>	0.5	0	0.1	~4 Gg	1.40	120
Important greenhouse halocarbons under Montreal Protocol and its Amendments							
CFC-11	CFCl <sub>3</sub>	268	0	-1.4		45	4600
CFC-12	CF <sub>2</sub> Cl <sub>2</sub>	533	0	4.4		100	10600
CFC-13	CF <sub>3</sub> Cl	4	0	0.1		640	14000
CFC-113	CF <sub>2</sub> ClCFCl <sub>2</sub>	84	0	0.0		85	6000
CFC-114	CF <sub>2</sub> ClCF <sub>2</sub> Cl	15	0	<0.5		300	9800
CFC-115	CF <sub>3</sub> CF <sub>2</sub> Cl	7	0	0.4		1700	7200
Carbon tetrachloride	CCl <sub>4</sub>	102	0	-1.0		35	1800
Methyl chloroform	CH <sub>3</sub> CCl <sub>3</sub>	69	0	-14		4.8	140
HCFC-22	CHF <sub>2</sub> Cl	132	0	5		11.9	1700
HCFC-141b	CH <sub>3</sub> CFCl <sub>2</sub>	10	0	2		9.3	700
HCFC-142b	CH <sub>3</sub> CF <sub>2</sub> Cl	11	0	1		19	2400
Halon-1211	CF <sub>2</sub> ClBr	3.8	0	0.2		11	1300
Halon-1301	CF <sub>3</sub> Br	2.5	0	0.1		65	6900
Halon-2402	CF <sub>2</sub> BrCF <sub>2</sub> Br	0.45	0	~ 0		<20	
Other chemically active gases directly or indirectly affecting radiative forcing							
Tropospheric ozone	O <sub>3</sub> (DU)	34	25	?	see text	0.01-0.05	—
Tropospheric NO <sub>x</sub>	NO + NO <sub>2</sub>	5-999	?	?	~52 TgN	<0.01-0.03	—
Carbon monoxide	CO (ppb) <sup>d</sup>	80	?	6	~2800 Tg	0.08 - 0.25	— <sup>d</sup>
Stratospheric water	H <sub>2</sub> O (ppm)	3-6	3-5	?	see text	1-6	—

<sup>a</sup> All abundances are tropospheric molar mixing ratios in ppt ( $10^{-12}$ ) and trends are in ppt/yr unless superseded by units on line (ppb =  $10^{-9}$ , ppm =  $10^{-6}$ ). Where possible, the 1998 values are global, annual averages and the trends are calculated for 1996 to 1998.

<sup>b</sup> GWPs are from Chapter 6 of this report and refer to the 100-year horizon values.

<sup>c</sup> Species with chemical feedbacks that change the duration of the atmospheric response; global mean atmospheric lifetime (LT) is given first followed by perturbation lifetime (PT). Values are taken from the SAR (Prather *et al.*, 1995; Schimel *et al.*, 1996) updated with WMO98 (Kurylo and Rodriguez, 1999; Prinn and Zander, 1999) and new OH-scaling, see text. Uncertainties in lifetimes have not changed substantially since the SAR.

<sup>d</sup> CO trend is very sensitive to the time period chosen. The value listed for 1996 to 1998, +6 ppb/yr, is driven by a large increase during 1998. For the period 1991 to 1999, the CO trend was -0.6 ppb/yr. CO is an indirect greenhouse gas: for comparison with CH<sub>4</sub> see this chapter; for GWP, see Chapter 6.

**Table 4.1(b): Additional synthetic greenhouse gases.**

Chemical species	Formula	Lifetime (yr)	GWP <sup>b</sup>
Perfluoropropane	C <sub>3</sub> F <sub>8</sub>	2600	8600
Perfluorobutane	C <sub>4</sub> F <sub>10</sub>	2600	8600
Perfluorocyclobutane	C <sub>4</sub> F <sub>8</sub>	3200	10000
Perfluoropentane	C <sub>5</sub> F <sub>12</sub>	4100	8900
Perfluorohexane	C <sub>6</sub> F <sub>14</sub>	3200	9000
Trifluoromethyl-sulphur pentafluoride	SF <sub>5</sub> CF <sub>3</sub>	1000	17500
Nitrogen trifluoride	NF <sub>3</sub>	>500	10800
Trifluoroiodomethane	CF <sub>3</sub> I	<0.005	1
HFC-32	CH <sub>2</sub> F <sub>2</sub>	5.0	550
HFC-41	CH <sub>3</sub> F	2.6	97
HFC-125	CH <sub>2</sub> CF <sub>3</sub>	29	3400
HFC-134	CHF <sub>2</sub> CHF <sub>2</sub>	9.6	1100
HFC-143	CH <sub>2</sub> FCHF <sub>2</sub>	3.4	330
HFC-143a	CH <sub>3</sub> CF <sub>3</sub>	52	4300
HFC-152	CH <sub>2</sub> FCH <sub>2</sub> F	0.5	43
HFC-161	CH <sub>3</sub> CH <sub>2</sub> F	0.3	12
HFC-227ea	CF <sub>3</sub> CHFCF <sub>3</sub>	33	3500
HFC-236cb	CF <sub>3</sub> CF <sub>2</sub> CH <sub>2</sub> F	13.2	1300
HFC-236ea	CF <sub>3</sub> CHFCHF <sub>2</sub>	10.0	1200
HFC-236fa	CF <sub>3</sub> CH <sub>2</sub> CF <sub>3</sub>	220	9400
HFC-245ca	CH <sub>2</sub> FCF <sub>2</sub> CHF <sub>2</sub>	5.9	640
HFC-245ea	CHF <sub>2</sub> CHFCHF <sub>2</sub>	4.0	
HFC-245eb	CF <sub>3</sub> CHFCH <sub>2</sub> F	4.2	
HFC-245fa	CHF <sub>2</sub> CH <sub>2</sub> CF <sub>3</sub>	7.2	950
HFC-263fb	CF <sub>3</sub> CH <sub>2</sub> CH <sub>3</sub>	1.6	
HFC-338pcc	CHF <sub>2</sub> CF <sub>2</sub> CF <sub>2</sub> CF <sub>2</sub> H	11.4	
HFC-356mcf	CF <sub>3</sub> CF <sub>2</sub> CH <sub>2</sub> CH <sub>2</sub> F	1.2	
HFC-356mff	CF <sub>3</sub> CH <sub>2</sub> CH <sub>2</sub> CF <sub>3</sub>	7.9	
HFC-365mfc	CF <sub>3</sub> CH <sub>2</sub> CF <sub>2</sub> CH <sub>3</sub>	9.9	890
HFC-43-10mee	CF <sub>3</sub> CHFCHFCF <sub>2</sub> CF <sub>3</sub>	15	1500
HFC-458mfcf	CF <sub>3</sub> CH <sub>2</sub> CF <sub>2</sub> CH <sub>2</sub> CF <sub>3</sub>	22	
HFC-55-10mcff	CF <sub>3</sub> CF <sub>2</sub> CH <sub>2</sub> CH <sub>2</sub> CF <sub>2</sub> CF <sub>3</sub>	7.7	
HFE-125	CF <sub>3</sub> OCHF <sub>2</sub>	150	14900
HFE-134	CF <sub>2</sub> HOCH <sub>2</sub> H	26	2400
HFE-143a	CF <sub>3</sub> OCH <sub>3</sub>	4.4	750
HFE-152a	CH <sub>3</sub> OCHF <sub>2</sub>	1.5	
HFE-245fa2	CHF <sub>2</sub> OCH <sub>2</sub> CF <sub>3</sub>	4.6	570
HFE-356mff2	CF <sub>3</sub> CH <sub>2</sub> OCH <sub>2</sub> CF <sub>3</sub>	0.4	

#### 4.1.2 Atmospheric Chemistry and Feedbacks

All greenhouse gases except CO<sub>2</sub> and H<sub>2</sub>O are removed from the atmosphere primarily by chemical processes within the atmosphere. Greenhouse gases containing one or more H atoms (e.g., CH<sub>4</sub>, HFCs and HCFCs), as well as other pollutants, are removed primarily by the reaction with hydroxyl radicals (OH). This removal takes place in the troposphere, the lowermost part of the atmosphere, ranging from the surface up to 7 to 16 km depending on latitude and season and containing 80% of the mass

of the atmosphere. The greenhouse gases N<sub>2</sub>O, PFCs, SF<sub>6</sub>, CFCs and halons do not react with OH in the troposphere. These gases are destroyed in the stratosphere or above, mainly by solar ultraviolet radiation (UV) at short wavelengths (<240 nm), and are long-lived. Because of the time required to transport these gases to the region of chemical loss, they have a minimum lifetime of about 20 years. CO<sub>2</sub> is practically inert in the atmosphere and does not directly influence the chemistry, but it has a small *in situ* source from the oxidation of CH<sub>4</sub>, CO and VOC.

Tropospheric OH abundances depend on abundances of NO<sub>x</sub>, CH<sub>4</sub>, CO, VOC, O<sub>3</sub> and H<sub>2</sub>O plus the amount of solar UV (>300 nm) that reaches the troposphere. As a consequence, OH varies widely with geographical location, time of day, and season. Likewise the local loss rates of all those gases reacting with OH also vary. Because of its dependence on CH<sub>4</sub> and other pollutants, tropospheric OH is expected to have changed since the pre-industrial era and to change again for future emission scenarios. For some of these gases other removal processes, such as photolysis or surface uptake, are also important; and the total sink of the gas is obtained by integrating over all such processes. The chemistry of tropospheric O<sub>3</sub> is closely tied to that of OH, and its abundance also varies with changing precursor emissions. The chemistry of the troposphere is also directly influenced by the stratospheric burden of O<sub>3</sub>, climatic changes in temperature (T) and humidity (H<sub>2</sub>O), as well as by interactions between tropospheric aerosols and trace gases. Such couplings provide a “feedback” between the climate change induced by increasing greenhouse gases and the concentration of these gases. Another feedback, internal to the chemistry, is the impact of CH<sub>4</sub> on OH and hence its own loss. These feedbacks are expected to be important for tropospheric O<sub>3</sub> and OH. Such chemistry-chemistry or climate-chemistry coupling has been listed under “indirect effects” in the SAR (Prather *et al.*, 1995; Schimel *et al.*, 1996).

This chapter uses 3-D chemistry-transport models (CTMs) to integrate the varying chemical processes over global conditions, to estimate their significance, and to translate the emission scenarios into abundance changes in the greenhouse gases CH<sub>4</sub>, HFCs, and O<sub>3</sub>. An extensive modelling exercise called OxComp (tropospheric oxidant model comparison) – involving model comparisons, sensitivity studies, and investigation of the IPCC SRES scenarios – was organised to support this report.

Stratospheric circulation and distribution of O<sub>3</sub> control the transport of the long-lived greenhouse gases to regions of photochemical loss as well as the penetration of solar UV into the atmosphere. At the same time, many of these gases (e.g., N<sub>2</sub>O and CFCs) supply ozone-depleting radicals (e.g., nitric oxide (NO) and Cl) to the stratosphere, providing a feedback between the gas and its loss rate. Another consequence of the observed stratospheric ozone depletion is that tropospheric photochemical activity is expected to have increased, altering tropospheric OH and O<sub>3</sub>. Climate change in the 21st century, including the radiative cooling of the stratosphere by increased levels of CO<sub>2</sub>, is expected to alter stratospheric circulation and O<sub>3</sub>, and, hence, the global mean loss rates of the long-lived gases. Some of these effects are discussed in WMO (1999) and are briefly considered here.

The biosphere’s response to global change will impact the atmospheric composition of the 21st century. The anticipated changes in climate (e.g., temperature, precipitation) and in chemistry will alter ecosystems and thus the “natural”, background emissions of trace gases. There is accumulating evidence that increased N deposition (the result of NO<sub>x</sub> and ammonia (NH<sub>3</sub>) emissions) and elevated surface O<sub>3</sub>

abundances have opposite influences on plant CO<sub>2</sub> uptake: O<sub>3</sub> (>40 ppb) inhibits CO<sub>2</sub> uptake; while N deposition enhances it up to a threshold, above which the effects are detrimental. In addition, the increased N availability from atmospheric deposition and direct fertilisation accelerates the emission of N-containing trace gases (NO, N<sub>2</sub>O and NH<sub>3</sub>) and CH<sub>4</sub>, as well as altering species diversity and biospheric functioning. These complex interactions represent a chemistry-biosphere feedback that may alter greenhouse forcing.

#### 4.1.3 Trace Gas Budgets and Trends

The “budget” of a trace gas consists of three quantities: its global source, global sink and atmospheric burden. The burden is defined as the total mass of the gas integrated over the atmosphere and related reservoirs, which usually include just the troposphere and stratosphere. The global burden (in Tg) and its trend (i.e., the difference between sources and sinks, in Tg/yr) can be determined from atmospheric measurements and, for the long-lived gases, are usually the best-known quantities in the budgets. For short-lived, highly variable gases such as tropospheric O<sub>3</sub> and NO<sub>x</sub>, the atmospheric burden cannot be measured with great accuracy. The global source strength is the sum of all sources, including emissions and *in situ* chemical production. Likewise, the sink strength (or global loss rate) can have several independent components.

The source strength (Tg/yr) for most greenhouse gases is comprised of surface emissions. For synthetic gases where industrial production and emissions are well documented, the source strengths may be accurately known. For CH<sub>4</sub> and N<sub>2</sub>O, however, there are large, not well-quantified, natural emissions. Further, the anthropogenic emissions of these gases are primarily associated with agricultural sources that are difficult to quantify accurately. Considerable research has gone into identifying and quantifying the emissions from individual sources for CH<sub>4</sub> and N<sub>2</sub>O, as discussed below. Such uncertainty in source strength also holds for synthetic gases with undocumented emissions. The source strength for tropospheric O<sub>3</sub> includes both a stratospheric influx and *in situ* production and is thus derived primarily from global chemical models.

The sink strength (Tg/yr) of long-lived greenhouse gases can be derived from a combination of atmospheric observations, laboratory experiments, and models. The atmospheric chemistry models are based on physical principles and laboratory data, and include as constraints the observed chemistry of the atmosphere over the past two decades. For example, stratospheric loss rates are derived from models either by combining observed trace gas distributions with theoretically calculated loss frequencies or from the measured correlation of the respective gas with a trace gas of known vertical flux. In such analyses there are a wide range of self-consistency checks. Mean global loss rates based on *a priori* modelling (e.g., the CH<sub>4</sub>-lifetime studies from OxComp described later) can be compared with empirically-based loss rates that are scaled from a gas with similar loss processes that has well-known emissions and atmospheric burden (e.g., the AGAGE (Advanced Global Atmospheric Gases Experiment) calibration of mean tropo-

spheric OH using methyl chloroform ( $\text{CH}_3\text{CCl}_3$ ); Prinn *et al.*, 1995). Our knowledge of the current budget of a greenhouse gas provides a key constraint in modelling its future abundance. For example, in both the IS92a and SRES projected emissions of  $\text{CH}_4$  and  $\text{N}_2\text{O}$ , we apply a constant offset to each set of emissions so that our calculated burden is consistent with the observed budget and trend during the 1990s.

#### 4.1.4 Atmospheric Lifetimes and Time-Scales

The global atmospheric lifetime (yr) characterises the time required to turn over the global atmospheric burden. It is defined as the burden (Tg) divided by the mean global sink (Tg/yr) for a gas in steady state (i.e., with unchanging burden). This quantity was defined as both “lifetime” and “turnover time” in the SAR (see also Bolin and Rodhe, 1973). Lifetimes calculated in this manner are listed in Table 4.1. A corollary of this definition is that, when in steady state (i.e., source strength = sink strength), the atmospheric burden of a gas equals the product of its lifetime and its emissions. A further corollary is that the integrated atmospheric abundance following a single emission is equal to the product of its steady-state lifetime for that emission pattern and the amount emitted (Prather, 1996). This latter, new result since the SAR supports the market-basket approach of aggregating the direct emissions of different greenhouse gases with a GWP (Global Warming Potential) weighting.

The atmospheric lifetime is basically a scale factor relating (i) constant emissions (Tg/yr) to a steady-state burden (Tg), or (ii) an emission pulse (Tg) to the time-integrated burden of that pulse (Tg/yr). The lifetime is often additionally assumed to be a constant, independent of the sources; and it is also taken to represent the decay time (e-fold) of a perturbation. These latter assumptions apply rigorously only for a gas whose local chemical lifetime is constant in space and time, such as for the noble gas radon, whose lifetime is fixed by the rate of its radioactive decay. In such a case the mean atmospheric lifetime equals the local lifetime: the lifetime that relates source strength to global burden is exactly the decay time of a perturbation.

This general applicability of the atmospheric lifetime breaks down for those greenhouse gases and pollutants whose chemical losses vary in space and time.  $\text{NO}_x$ , for instance, has a local lifetime of <1 day in the lower troposphere, but >5 days in the upper troposphere; and both times are less than the time required for vertical mixing of the troposphere. In this case emission of  $\text{NO}_x$  into the upper troposphere will produce a larger atmospheric burden than the same emission into the lower troposphere. Consequently, the definition of the atmospheric lifetime of  $\text{NO}_x$  is not unique and depends on the location (and season) of its emissions. The same is true for any gas whose local lifetime is variable and on average shorter than about 0.5 year, i.e., the decay time of a north-south difference between hemispheres representing one of the longer time-scales for tropospheric mixing. The majority of greenhouse gases considered here have atmospheric lifetimes greater than 2 years, much longer than tropospheric mixing times; and hence their lifetimes are not significantly altered by the location of sources

within the troposphere. When lifetimes are reported for gases in Table 4.1, it is assumed that the gases are uniformly mixed throughout the troposphere. This assumption is unlikely for gases with lifetimes <1 year, and reported values must be viewed only as approximations.

Some gases have chemical feedbacks that change their lifetimes. For example, the increasing  $\text{CH}_4$  abundance leads to a longer lifetime for  $\text{CH}_4$  (Prather *et al.*, 1995; Schimel *et al.*, 1996). A chemical feedback with opposite effect has been identified for  $\text{N}_2\text{O}$  where a greater  $\text{N}_2\text{O}$  burden leads to increases in stratospheric  $\text{NO}_x$  which in turn depletes mid-stratospheric ozone. This ozone loss enhances the UV, and as a consequence  $\text{N}_2\text{O}$  is photolysed more rapidly (Prather, 1998). Such feedbacks cause the time-scale of a perturbation, henceforth called perturbation lifetime ( $PT$ ), to differ from the global atmospheric lifetime ( $LT$ ). In the limit of small perturbations, the relation between the perturbation lifetime of a gas and its global atmospheric lifetime can be derived from a simple budget relationship as  $PT = LT / (1 - s)$ , where the sensitivity coefficient  $s = \partial \ln(LT) / \partial \ln(B)$  and  $B$  = burden. Without a feedback on lifetime,  $s = 0$ , and  $PT$  is identical to  $LT$ . The product,  $PT$  times a sustained change in emission, gives the resulting change in the burden. The ratio of  $PT/LT$  adopted here for  $\text{CH}_4$ , 1.4, is based on recent model studies (see Section 4.4) and is consistent with the SAR results.

To evaluate the total greenhouse effect of a given gas molecule, one needs to know, first, how long it remains in the atmosphere and, second, how it interacts chemically with other molecules. This effect is calculated by injecting a pulse of that gas (e.g., 1 Tg) into the atmosphere and watching the added abundance decay as simulated in a CTM. This decay is represented by a sum of exponential functions, each with its own decay time. These exponential functions are the chemical modes of the linearised chemistry-transport equations of the CTM (Prather, 1996). In the case of a  $\text{CH}_4$  addition, the longest-lived mode has an e-fold time of 12 years, close to the perturbation lifetime ( $PT$ ) of  $\text{CH}_4$ , and carries most of the added burden. (This e-fold time was called the adjustment time in the SAR.) In the case of a CO addition, this same mode is also excited, but at a reduced amplitude (Prather, 1996; Daniel and Solomon, 1998). The pulse of added CO, by causing the concentration of OH to decrease and thus the lifetime of  $\text{CH}_4$  to increase temporarily, causes a build-up of  $\text{CH}_4$  while the added burden of CO persists. After the initial period of a few months defined by the CO photochemical lifetime, this built-up  $\text{CH}_4$  then decays in the same manner as would a direct pulse of  $\text{CH}_4$ . Similarly, an addition of  $\text{NO}_x$  (e.g., from aviation; see Isaksen and Jackman, 1999) will excite this mode, but with a negative amplitude. Thus, changes in the emissions of short-lived gases can generate long-lived perturbations as shown in 3-D CTMs (Wild and Prather, 2000; Derwent *et al.*, 2001). Changes in tropospheric  $\text{O}_3$  accompany the  $\text{CH}_4$  decay on a 12 year time-scale as an inherent component of this mode, a key example of chemical coupling in the troposphere. Thus, any chemically reactive gas, whether a greenhouse gas or not, will produce some level of indirect greenhouse effect through its impact on atmospheric chemistry.

## 4.2 Trace Gases: Current Observations, Trends, and Budgets

### 4.2.1 Non-CO<sub>2</sub> Kyoto Gases

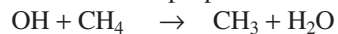
#### 4.2.1.1 Methane (CH<sub>4</sub>)

Methane's globally averaged atmospheric surface abundance in 1998 was 1,745 ppb (see Figure 4.1), corresponding to a total burden of about 4,850 Tg(CH<sub>4</sub>). The uncertainty in the burden is small ( $\pm 5\%$ ) because the spatial and temporal distributions of tropospheric and stratospheric CH<sub>4</sub> have been determined by extensive high-precision measurements and the tropospheric variability is relatively small. For example, the Northern Hemisphere CH<sub>4</sub> abundances average about 5% higher than those in the Southern Hemisphere. Seasonal variations, with a minimum in late summer, are observed with peak-to-peak amplitudes of about 2% at mid-latitudes. The average vertical gradient in the troposphere is negligible, but CH<sub>4</sub> abundances in the stratosphere decrease rapidly with altitude, e.g., to 1,400 ppb at 30 km altitude in the tropics and to 500 ppb at 30 km in high latitude northern winter.

The most important known sources of atmospheric methane are listed in Table 4.2. Although the major source terms of atmospheric CH<sub>4</sub> have probably been identified, many of the source strengths are still uncertain due to the difficulty in assessing the global emission rates of the biospheric sources, whose strengths are highly variable in space and time: e.g., local emissions from most types of natural wetland can vary by a few orders of magnitude over a few metres. Nevertheless, new approaches have led to improved estimates of the global emissions rates from some source types. For instance, intensive studies on emissions from rice agriculture have substantially improved these emissions estimates (Ding and Wang, 1996; Wang and Shangguan, 1996). Further, integration of emissions over a whole growth period (rather than looking at the emissions on individual days with different ambient temperatures) has lowered the estimates of CH<sub>4</sub> emissions from rice agriculture from about 80 Tg/yr to about 40 Tg/yr (Neue and Sass, 1998; Sass *et al.*, 1999). There have also been attempts to deduce emission rates from observed spatial and temporal distributions of atmospheric CH<sub>4</sub> through inverse modelling (e.g., Hein *et al.*, 1997; Houweling *et al.*, 1999). The emissions so derived depend on the precise knowledge of the mean global loss rate and represent a relative attribution into aggregated sources of similar properties. The results of some of these studies have been included in Table 4.2. The global CH<sub>4</sub> budget can also be constrained by measurements of stable isotopes ( $\delta^{13}\text{C}$  and  $\delta\text{D}$ ) and radiocarbon ( $^{14}\text{CH}_4$ ) in atmospheric CH<sub>4</sub> and in CH<sub>4</sub> from the major sources (e.g., Stevens and Engelkemeir, 1988; Wahlen *et al.*, 1989; Quay *et al.*, 1991, 1999; Lassey *et al.*, 1993; Lowe *et al.*, 1994). So far the measurements of isotopic composition of CH<sub>4</sub> have served mainly to constrain the contribution from fossil fuel related sources. The emissions from the various sources sum up to a global total of about 600 Tg/yr, of which about 60% are related to human activities such as agriculture, fossil fuel use and waste disposal. This is consistent with the SRES estimate of 347 Tg/yr for anthropogenic CH<sub>4</sub> emissions in the year 2000.

The current emissions from CH<sub>4</sub> hydrate deposits appear small, about 10 Tg/yr. However, these deposits are enormous, about  $10^7$  TgC (Suess *et al.*, 1999), and there is an indication of a catastrophic release of a gaseous carbon compound about 55 million years ago, which has been attributed to a large-scale perturbation of CH<sub>4</sub> hydrate deposits (Dickens, 1999; Norris and Röhl, 1999). Recent research points to regional releases of CH<sub>4</sub> from clathrates in ocean sediments during the last 60,000 years (Kennett *et al.*, 2000), but much of this CH<sub>4</sub> is likely to be oxidised by bacteria before reaching the atmosphere (Dickens, 2001). This evidence adds to the concern that the expected global warming may lead to an increase in these emissions and thus to another positive feedback in the climate system. So far, the size of that feedback has not been quantified. On the other hand, the historic record of atmospheric CH<sub>4</sub> derived from ice cores (Petit *et al.*, 1999), which spans several large temperature swings plus glaciations, constrains the possible past releases from methane hydrates to the atmosphere. Indeed, Brook *et al.* (2000) find little evidence for rapid, massive CH<sub>4</sub> excursions that might be associated with large-scale decomposition of methane hydrates in sediments during the past 50,000 years.

The mean global loss rate of atmospheric CH<sub>4</sub> is dominated by its reaction with OH in the troposphere.



This loss term can be quantified with relatively good accuracy based on the mean global OH concentration derived from the methyl chloroform (CH<sub>3</sub>CCL<sub>3</sub>) budget described in Section 4.2.6 on OH. In that way we obtain a mean global loss rate of 507 Tg(CH<sub>4</sub>)/yr for the current tropospheric removal of CH<sub>4</sub> by OH. In addition there are other minor removal processes for atmospheric CH<sub>4</sub>. Reaction with Cl atoms in the marine boundary layer probably constitutes less than 2% of the total sink (Singh *et al.*, 1996). A recent process model study (Ridgwell *et al.*, 1999) suggested a soil sink of 38 Tg/yr, and this can be compared to SAR estimates of 30 Tg/yr. Minor amounts of CH<sub>4</sub> are also destroyed in the stratosphere by reactions with OH, Cl, and O(<sup>1</sup>D), resulting in a combined loss rate of 40 Tg/yr. Summing these, our best estimate of the current global loss rate of atmospheric CH<sub>4</sub> totals 576 Tg/yr (see Table 4.2), which agrees reasonably with the total sources derived from process models. The atmospheric lifetime of CH<sub>4</sub> derived from this loss rate and the global burden is 8.4 years. Attributing individual lifetimes to the different components of CH<sub>4</sub> loss results in 9.6 years for loss due to tropospheric OH, 120 years for stratospheric loss, and 160 years for the soil sink (i.e.,  $1/8.4 \text{ yr} = 1/9.6 \text{ yr} + 1/120 \text{ yr} + 1/160 \text{ yr}$ ).

The atmospheric abundance of CH<sub>4</sub> has increased by about a factor of 2.5 since the pre-industrial era (see Figure 4.1a) as evidenced by measurements of CH<sub>4</sub> in air extracted from ice cores and firn (Etheridge *et al.*, 1998). This increase still continues, albeit at a declining rate (see Figure 4.1b). The global tropospheric CH<sub>4</sub> growth rate averaged over the period 1992 through 1998 is about 4.9 ppb/yr, corresponding to an average annual increase in atmospheric burden of 14 Tg. Superimposed on this long-term decline in growth rate are interannual variations in the trend (Figure 4.1c). There are no clear quantitative explanations for this variability, but understanding these variations in

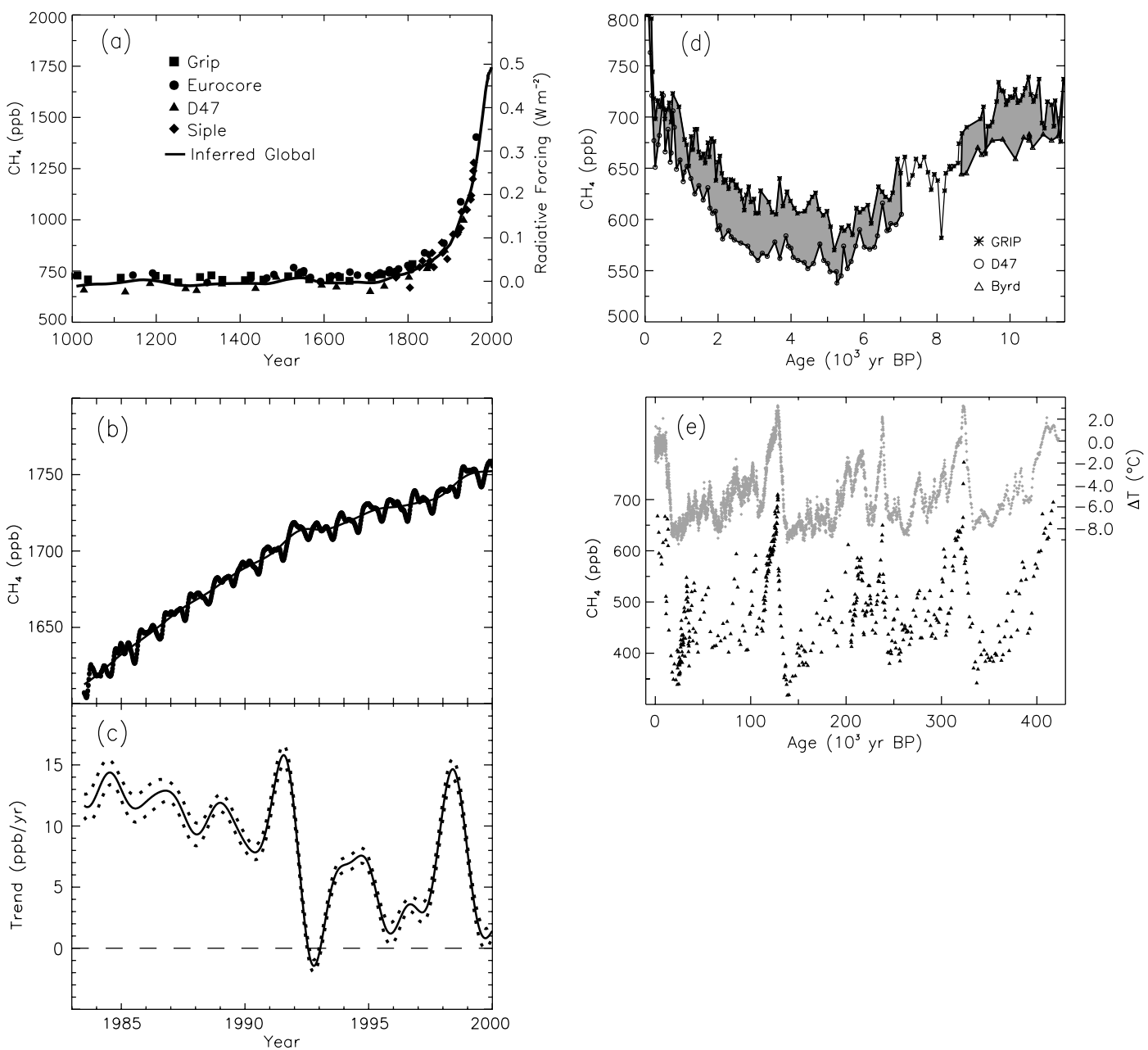


**Figure 4.1:** (a) Change in CH<sub>4</sub> abundance (mole fraction, in ppb = 10<sup>-9</sup>) determined from ice cores, firn, and whole air samples plotted for the last 1,000 years. Data sets are as follows: Grip, Blunier *et al.* (1995) and Chappellaz *et al.* (1997); Eurocore, Blunier *et al.* (1993); D47, Chappellaz *et al.* (1997); Siple, Stauffer *et al.* (1985); Global (inferred from Antarctic and Greenland ice cores, firn air, and modern measurements), Etheridge *et al.* (1998) and Dlugokencky *et al.* (1998). Radiative forcing, approximated by a linear scale since the pre-industrial era, is plotted on the right axis. (b) Globally averaged CH<sub>4</sub> (monthly varying) and deseasonalised CH<sub>4</sub> (smooth line) abundance plotted for 1983 to 1999 (Dlugokencky *et al.*, 1998). (c) Instantaneous annual growth rate (ppb/yr) in global atmospheric CH<sub>4</sub> abundance from 1983 through 1999 calculated as the derivative of the deseasonalised trend curve above (Dlugokencky *et al.*, 1998). Uncertainties (dotted lines) are  $\pm 1$  standard deviation. (d) Comparison of Greenland (GRIP) and Antarctic (D47 and Byrd) CH<sub>4</sub> abundances for the past 11.5 kyr (Chappellaz *et al.*, 1997). The shaded area is the pole-to-pole difference where Antarctic data exist. (e) Atmospheric CH<sub>4</sub> abundances (black triangles) and temperature anomalies with respect to mean recent temperature (grey diamonds) determined for the past 420 kyr from an ice core drilled at Vostok Station in East Antarctica (Petit *et al.*, 1999).

trend will ultimately help constrain specific budget terms. After the eruption of Mt. Pinatubo, a large positive anomaly in growth rate was observed at tropical latitudes. It has been attributed to short-term decreases in solar UV in the tropics immediately following the eruption that decreased OH formation rates in the

troposphere (Dlugokencky *et al.*, 1996). A large decrease in growth was observed, particularly in high northern latitudes, in 1992. This feature has been attributed in part to decreased northern wetland emission rates resulting from anomalously low surface temperatures (Hogan and Harriss, 1994) and in part to

**Table 4.2:** Estimates of the global methane budget (in Tg(CH<sub>4</sub>/yr) from different sources compared with the values adopted for this report (TAR).

Reference:	Fung <i>et al.</i> (1991)	Hein <i>et al.</i> (1997)	Lelieveld <i>et al.</i> (1998)	Houweling <i>et al.</i> (1999)	Mosier <i>et al.</i> (1998a)	Olivier <i>et al.</i> (1999)	Cao <i>et al.</i> (1998)	SAR	TAR <sup>a</sup>
Base year:	1980s	–	1992	–	1994	1990	–	1980s	1998
Natural sources									
Wetlands	115	237	225 <sup>c</sup>	145				92	
Termites	20	–	20	20					
Ocean	10	–	15	15					
Hydrates	5	–	10	–					
Anthropogenic sources									
Energy	75	97	110	89		109			
Landfills	40	35	40	73		36			
Ruminants	80	90 <sup>b</sup>	115	93	80	93 <sup>b</sup>			
Waste treatment	–	–	25	–	14				
Rice agriculture	100	88	–	–	25-54	60	53		
Biomass burning	55	40	40	40	34	23			
Other	–	–	–	20	15				
<b>Total source</b>	<b>500</b>	<b>587</b>	<b>600</b>					<b>597</b>	<b>598</b>
Imbalance (trend)									
Sinks									
Soils	10	–	30	30	44			30	30
Tropospheric OH	450	489	510					490	506
Stratospheric loss	–	46	40					40	40
<b>Total sink</b>	<b>460</b>	<b>535</b>	<b>580</b>					<b>560</b>	<b>576</b>

<sup>a</sup> TAR budget based on 1,745 ppb, 2.78 Tg/ppb, lifetime of 8.4 yr, and an imbalance of +8 ppb/yr.

<sup>b</sup> Waste treatment included under ruminants.

<sup>c</sup> Rice included under wetlands.

stratospheric ozone depletion that increased tropospheric OH (Bekki *et al.*, 1994; Fuglestvedt *et al.*, 1994). Records of changes in the <sup>13</sup>C/<sup>12</sup>C ratios in atmospheric CH<sub>4</sub> during this period suggest the existence of an anomaly in the sources or sinks involving more than one causal factor (Lowe *et al.*, 1997; Mak *et al.*, 2000).

There is no consensus on the causes of the long-term decline in the annual growth rate. Assuming a constant mean atmospheric lifetime of CH<sub>4</sub> of 8.9 years as derived by Prinn *et al.* (1995), Dlugokencky *et al.* (1998) suggest that during the period 1984 to 1997 global emissions were essentially constant and that the decline in annual growth rate was caused by an approach to steady state between global emissions and atmospheric loss rate. Their estimated average source strength was about 550 Tg/yr. (Inclusion of a soil sink term of 30 Tg/yr would decrease the lifetime to 8.6 years and suggest an average source strength of about 570 Tg/yr.) Francey *et al.* (1999), using measurements of <sup>13</sup>CH<sub>4</sub> from Antarctic firn air samples and archived air from Cape Grim, Tasmania, also concluded that the decreased CH<sub>4</sub> growth rate was consistent with constant OH and constant or very slowly increasing CH<sub>4</sub> sources after 1982. However, other analyses of the global methyl chloroform (CH<sub>3</sub>CCl<sub>3</sub>) budget (Krol *et al.*, 1998) and the changing chemistry of the atmosphere (Karlsdottir and Isaksen, 2000) argue for an increase in globally averaged OH of +0.5%/yr over the last two decades (see Section 4.2.6 below) and hence a parallel increase in global CH<sub>4</sub> emissions by +0.5%/yr.

The historic record of atmospheric CH<sub>4</sub> obtained from ice cores has been extended to 420,000 years before present (BP) (Petit *et al.*, 1999). As Figure 4.1e demonstrates, at no time during this record have atmospheric CH<sub>4</sub> mixing ratios approached today's values. CH<sub>4</sub> varies with climate as does CO<sub>2</sub>. High values are observed during interglacial periods, but these maxima barely exceed the immediate pre-industrial CH<sub>4</sub> mixing ratio of 700 ppb. At the same time, ice core measurements from Greenland and Antarctica indicate that during the Holocene CH<sub>4</sub> had a pole-to-pole difference of about 44 ± 7 ppb with higher values in the Arctic as today, but long before humans influenced atmospheric methane concentrations (Chappelaz *et al.*, 1997; Figure 4.1d). Finally, study of CH<sub>4</sub> ice-core records at high time resolution reveals no evidence for rapid, massive CH<sub>4</sub> excursions that might be associated with large-scale decomposition of methane hydrates in sediments (Brook *et al.*, 2000).

The feedback of CH<sub>4</sub> on tropospheric OH and its own lifetime is re-evaluated with contemporary CTMs as part of OxComp, and results are summarised in Table 4.3. The calculated OH feedback,  $\partial \ln(\text{OH}) / \partial \ln(\text{CH}_4)$ , is consistent between the models, indicating that tropospheric OH abundances decline by 0.32% for every 1% increase in CH<sub>4</sub>. The TAR value for the sensitivity coefficient  $s = \partial \ln(\text{LT}) / \partial \ln(\text{CH}_4)$  is then 0.28 and the ratio PT/LT is 1.4. This 40% increase in the integrated effect of a CH<sub>4</sub> perturbation does not appear as a 40% larger amplitude in the perturbation but rather as a lengthening of the duration of the perturbation to 12 years. This feedback is difficult